UNIVERSIDAD COMPLUTENSE DE MADRID
FACULTAD DE CIENCIAS GEOLÓGICAS

TESIS DOCTORAL

The sedimentary record of the Albian-Cenomanian transgression in the Cuenca Basin (Iberian Ranges, Spain) :palaeogeographical evolution and paleoflora

El registro sedimentario de la transgresión del Albiense-Cenomaniense en la Serranía de Cuenca (Cordillera Ibérica, España): evolución paleogeográfica y paleoflora

MEMORIA PARA OPTAR AL GRADO DE DOCTOR

PRESENTADA POR

Carlos Alberto Bueno Cebollada

Directores

María Antonia Frenegal
Eduardo Barrón López
Nieves Meléndez Hevia

Madrid

UNIVERSIDAD COMPLUTENSE DE MADRID

FACULTAD DE CIENCIAS GEOLÓGICAS

TESIS DOCTORAL

THE SEDIMENTARY RECORD OF THE ALBIAN-CENOMANIAN TRANSGRESSION IN THE CUENCA BASIN (IBERIAN RANGES, SPAIN): PALAEOGEOGRAPHICAL EVOLUTION AND PALAEOFLORA.

EL REGISTRO SEDIMENTARIO DE LA TRANSGRESIÓN DEL ALBIENSE-CENOMANIENSE EN LA SERRANÍA DE CUENCA (CORDILLERA IBÉRICA, ESPAÑA): EVOLUCIÓN PALEOGEOGRÁFICA Y PALEOFLORA.

MEMORIA PARA OPTAR AL GRADO DE DOCTOR

PRESENTADA POR

CARLOS ALBERTO BUENO CEBOLLADA

DIRECTORES

Dra. MARIA ANTONIA FREGENAL

Dr. EDUARDO BARRÓN LÓPEZ

Dra. NIEVES MELÉNDEZ HEVIA

FACULTAD DE CIENCIAS GEOLÓGICAS, UNIVERSIDAD COMPLUTENSE DE MADRID - INSTITUTO GEOLÓGICO Y MINERO DE ESPAÑA, CONSEJO SUPERIOR DE INVESTIGACIONES CIENTÍFICAS.

THE SEDIMENTARY RECORD OF THE ALBIAN-CENOMANIAN TRANSGRESSION IN THE CUENCA BASIN (IBERIAN RANGES, SPAIN): PALAEOGEOGRAPHICAL EVOLUTION AND PALAEOFLORA.

EL REGISTRO SEDIMENTARIO DE LA TRANSGRESIÓN DEL ALBIENSE-CENOMANIENSE EN LA SERRANÍA DE CUENCA (CORDILLERA IBÉRICA, ESPAÑA): EVOLUCIÓN PALEOGEOGRÁFICA Y PALEOFLORA.

Ph.D. thesis/Tesis doctoral

Programa de doctorado en Geología e Ingeniería Geológica de la Facultad de Ciencias Geológicas, Universidad Complutense de Madrid.

CARLOS ALBERTO BUENO CEBOLLADA

Supervised by/Dirigida por:

Dra. MARIA ANTONIA FREGENAL MARTÍNEZ

Departamento de Geodinámica, Estratigrafía y Paleontología. Facultad de Cc. Geológicas, Universidad Complutense de Madrid.

Dr. EDUARDO BARRÓN LÓPEZ

Instituto Geológico y Minero de España (CN IGME-CSIC)

Dra. Mª NIEVES MELÉNDEZ HEVIA

Dra. en Geología por la Universidad Complutense de Madrid

"*When you eliminate the impossible, whatever remains, however improbable, must be the truth*".

Sir Arthur C. Doyle

Agradecimientos/Acknowledgements:

Quiero dar las gracias a la Dra. Marian Fregenal Martínez, al Dr. Eduardo Barrón López y a la Dra. Nieves Meléndez Hevia por su ayuda y por enseñarme tanto durante estos cinco años. Sin ellos no hubiese sido posible esta tesis. En particular, quiero agradecer a la Dra. Nieves Meléndez Hevia por darme esta oportunidad, proponerme este tema tesis y enseñarme como trabajar con "las Utrillas" en el campo. Al Dr. Eduardo Barrón por enseñarme el mundo de la paleobotánica del Cretácico y acogerme en el IGME de la mejor manera posible. A la Dra. Marian Fregenal por ayudarme a entender los pormenores tectono-sedimentarios de la Serranía de Cuenca y por darme su visión de conjunto, lo cual ha ayudado mucho al desarrollo de esta tesis doctoral.

Quiero agradecer a mis padres por su apoyo tanto moral como económico durante todos estos años, porque siempre estáis ahí. A mi madre por una logística que ha marcado la diferencia. A mi padre también quiero agradecerle el apoyo informático, que no ha sido poco. A mis hermanas por aguantarme en casa, especialmente los últimos meses de la tesis, cosa que no ha debido de ser fácil. A mis abuelos (los que están y lo que por desgracia ya no). A mis tíos, en especial a mi tío Federico por su escepticismo y por sacarme al monte de vez en cuando.

Quiero agradecer al Dr. Raúl de la Horra del Barco y al Dr. José María Fernández Barrenechea de la Facultad de Ciencias Geológicas de la UCM, su ayuda prestada a la hora de realizar los estudios geoquímicos y mineralógicos llevados a cabo en esta tesis. También al Dr. Daniel Peyrot de University of Western Australia por su valiosa ayuda en la identificación de quistes de dinoflagelados.

Quiero dar las gracias a toda la gente del IGME-CSIC, de la Facultad de Ciencias Geológicas de la UCM que de una manera u otra me ha ayudado estos años. Also, I would like to say thank you to all those that, one way or the other, helped me by offering advice and sharing their knowledge during my academic stays at the Arctic Geology Department of the University Centre in Svalbard – UNIS (Longyearbyen, Norway) these years.

Quiero dar las gracias a mis amigos del barrio y a los de bailes latinos, por los buenos ratos que me han ayudado a desconectar cuando parecía imposible.

Quiero dar las gracias a Iván, Egidio y Marco por esos cafés por las mañanas en el IGME, que han ayudado a sobrellevar la parte más dura de la tesis, y el madrugar, también muy duro.

I would also like to thank Fernando and Ulla for our wee talks over coffee and tea in the mornings.

Finalmente, como no podía ser menos, gracias a Caroline por siempre estar ahí, por aguantarme, por darme tan buenos consejos y por siempre apoyarme en todo lo que hago. Tack så mycket!

INDEX OF CONTENTS

PART V: CONCLUDING REMARKS.

ABSTRACT

This Ph.D. thesis presents a high-resolution palaeogeographical study of the onset and evolution of the largest ever recorded marine transgression, the "mid" Cretaceous transgression, in an exceptional setting located in the Western Tethys, at the eastern margin of Iberia: the Cuenca Basin (Spain). The study of the Cuenca Basin allows the accurate reconstruction of the time-space evolution of the transgressive event due to:

(1) The Albian to early Cenomanian sedimentary succession represents the sedimentary record of that major transgressive event. This succession is composed of the siliciclastic deposits of the Utrillas Gr, interpreted as an arid braidplain system, and the mixed shallow marine deposits of the La Bicuerca Mb (Aras de Alpuente Fm).

(2) The basin is located at the interface between those areas entirely dominated by marine sedimentation during the "mid" and Late Cretaceous, and the areas that were dominated mainly by continental sedimentation until the transgression reached its climax during the Cenomanian-Turonian boundary.

Additionally, the Albian to early Cenomanian time in Iberia was characterised by: (a) representing the transition from the Late Jurassic-Early Cretaceous syn-rift stage to the Late Cretaceous post-rift stage, and (b) being an extremely prolific time span regarding the deposit of amber-bearing successions.

This Ph.D. thesis addresses these topics by carrying out a palaeogeographical study based on a multidisciplinary and integrative approach comprising stratigraphic, sedimentological, palaeofloral and palaeoedaphological analyses.

In the Cuenca Basin, the Utrillas Gr and La Bicuerca Mb deposits represent a sedimentary succession largely understudied regarding biostratigraphy, palaeofloras and sedimentology. Overall, 12 outcrops have been logged and grouped into three geographic sectors: Northern, Eastern and Southern. The first step undertaken in this research involved a palynostratigraphic analysis of eight of the outcrops (obtaining 29 palynological samples) that permitted inferring a middle Albian to early Cenomanian age for the aforementioned deposits. Additionally, the scope of the palynostratigraphic study has allowed us to date the Aptian units, Contreras Fm and El Burgal Mb (Aras de Alpuente Fm) in some of the studied outcrops, which has helped to identify the base of the Utrillas Gr.

Following the biostratigraphic study, the palynological analysis of the samples was conducted. The studied middle Albian to early Cenomanian palynological assemblages from the Cuenca Basin conform with the characteristics of the early Cenophytic palynofloras and are dominated by lowland and nearshore evergreen vegetation adapted to arid conditions. Based on the palynological assemblages, the vegetation cover was mainly composed of conifers attributed to the families Cheirolepidiaceae and Cupressaceae. To a lesser extent, Araucariaceae is also represented in the studied palynofloras, which, together with the occurrence of low percentages of dinocysts found in most samples, indicates a relative closeness to the palaeocoast.

The analysis of the palaeofloras has been completed with the study of the macroflora collected from a fossil bed found in the Cañada del Hoyo outcrop. The studied macroflora is mainly dominated by taxa

attributed to Coniferales of the genera *Frenelopsis*, *Glenrosa* and *Dammarites*. Palaeoflora assemblages dominated by these taxa are interpreted as plant communities that developed in nearshore supratidal environments (i.e., salt marshes) and were typical during the Cenomanian in Western Europe.

The palaeoclimatic conditions that existed in the Cuenca Basin during the middle Albian to early Cenomanian have been inferred based on the petrographical, mineralogical, and geochemical analysis of three palaeosoils profiles from the Buenache de la Sierra outcrop. In this regard, the palaeoclimate conditions interpreted from the studied palaeosoils were markedly seasonal ones regarding rainfall and the climate is interpreted as that of a tropical savanna biome. The inferred seasonal climate allowed for the development of woodlands and alternated with more arid periods due to latitudinal shifting of the "mid"- Cretaceous climate belts.

The sedimentary facies analysis carried out in the 12 logged sections has permitted identifying eight facies associations ranging from proximal alluvial to shallow marine deposits that reflect the mid-Albian to early Cenomanian transgression. In this sense, three evolutionary stages representing the NW advance of the facies belts (middle Albian, middle Albian – late Albian, and late Albian – early Cenomanian) have been identified based on the facies analysis combined with the biostratigraphic framework.

In order to obtain a higher resolution, a sequence stratigraphic analysis has been conducted in two of the studied outcrops, Reíllo and Pajaroncillo, located in the distal part of the basin and defining an along-strike relative position. The main transgressive and regressive trends of the succession have been identified, along with several correlatable stratigraphic surfaces. This has permitted us to improve the sedimentological analysis, distinguishing five stages (T1-T5), which reflect more accurately the progressive advance of Western Tethys transgression in the Cuenca Basin. The stages are characterised by: (i) a continental aggradational stage (T1), dominated by alluvial deposition; (ii) an initial transgression stage (T2) dominated by an open coast setting in Reíllo and a restricted mudflat system in Pajaroncillo; (iii) a regressive stage (T3), during which continental alluvial to supratidal environments deposited; (iv) a resumption in transgression (T4), characterised by an array of inter- to subtidal environments, and (v) a deepening stage (T5), when the transgression advanced landward, giving rise to the most distal deposits of the studied succession. The studied outcrops have been integrated within the regional sequence stratigraphy framework, initially devised for the Valencia Basin and the Prebetic Domain. This regional approach has allowed the interpretation of the studied deposits as third-order depositional sequences and the identification of their respective system tracts in the studied succession.

The research conducted in this Ph.D. thesis has also enabled the assessment of the allocyclical factors that controlled sedimentation in the Cuenca Basin during the mid-Albian to early Cenomanian, reflecting the interplay between eustatism and tectonism. In that regard, tectonism seems to have been a paramount factor controlling sedimentation during the middle Albian (T1). Conversely, eustatism became the dominant control during the late Albian to early Cenomanian (mainly comprising T2-T5) in the Cuenca Basin, although still affected by tectonism.

Therefore, the results of this Ph.D. thesis present a significant contribution to the knowledge of the "mid"-Cretaceous transgression in Iberia based on the study of the middle Albian – early Cenomanian succession

and offers an accurate environmental picture of the palaeofloral communities and palaeoclimate conditions that existed in the Cuenca Basin. Additionally, this research casts new light on two of the major events that occurred during that period in Iberia:

(i) The supra-regional implications of this research are discussed within the broader geo-tectonic context of Iberia and the subtleties of its evolution during the Albian to Cenomanian times, providing new insight into the transition from the Late Jurassic-Early Cretaceous syn-rift stage to the Late Cretaceous post-rift stage in the southern part of the Iberian Basin Rift System (IBRS). In that regard, the occurrence of active faults during the sedimentation of the middle Albian to early Cenomanian succession demonstrates that extensional tectonism in the intraplate rift basins of Iberia lasted longer than initially suggested.

(ii) The comparison of the studied middle Albian to early Cenomanian succession with coeval amber-bearing strata from the Maestrazgo and Basque-Cantabrian Basins has permitted elucidating on the possible reason/s explaining the lack of amber deposits in the Cuenca Basin. Given the similarities of the palaeofloras (regarding Coniferales) among the compared basins, the absence of Albian amber-bearing strata in the Cuenca Basin might have been related to the lack of suitable taphonomic environments (mainly during the biostratinomic phase). In this sense, if the resin was produced in alluvial floodplain or supratidal settings in the Cuenca Basin, it would have been washed down by sandy ephemeral alluvial and estuarine channels with a marked seasonality, preventing its deposition under anoxic conditions and hampering its preservation in the fossil record.

RESUMEN

Esta tesis doctoral presenta un estudio de alta resolución sobre el comienzo y evolución de la mayor transgresión marina del Mesozoico, la transgresión del Cretácico "medio", en un contexto privilegiado, localizado al oeste del Océano del Tethys, en el margen este de Iberia: La Serranía de Cuenca (España). El estudio de esta cuenca sedimentaria ha permitido realizar una reconstrucción espacio-temporal precisa y pormenorizada del registro geológico de la transgresión debido a dos factores:

(1) La sucesión sedimentaria Albiense - Cenomaniense inferior representa el registro de la transgresión del Cretácico "medio". Esta sucesión comprende un cambio lateral de facies entre los depósitos siliciclásticos del Gr. Utrillas, interpretados como una llanura alluvial de tipo *braided*, y los mixtos del Mb. La Bicuerca (Fm. Aras de Alpuente), interpretados como depositados en un ambiente marino somero.

(2) La cuenca sedimentaria está localizada en una zona de transición entre las areas dominadas por sedimentación marina durante el Cretácico "medio" y Superior (hacia el SE de la zona de estudio), y las áreas que estuvieron dominadas por sedimentación continental (localizadas al NO de la zona estudiada) hasta que tuvo lugar el máximo de la transgresión durante el límite Cenomaniense-Turoniense.

Además, cabe destacar que el intervalo Albiense - Cenomaniense inferior en Iberia estuvo caracterizado por: (a) registrar la transición de la etapa sin-rift del Jurásico Superior - Cretácico Inferior a la etapa post-rift del Cretácico Superior, y (b) ser un periodo en cuyos depósitos se han descubierto numerosos yacimientos ambarígenos.

Esta tesis doctoral aborda estos temas mediante un enfoque pluridisciplinar e integrador que ha comprendido el análisis de datos estratigráficos, sedimentológicos, paleobotánicos y paleoedofológicos, que ha permitido mejorar notablemente el conocimiento sobre la transgresión marina del intervalo Albiense - Cenomaniense inferior en el área de la Serranía de Cuenca, y que refleja el progresivo avance del Tethys hacia noroeste de la cuenca.

En la Serranía de Cuenca, las unidades estudiadas forman una sucesión estratigráfica que, hasta la fecha, no había sido estudiada en detalle con respecto a su bioestratigrafía, registro paleobotánico y sedimentología. Durante el desarrollo de la tesis se han levantado columnas estratigráficas en un total de 12 afloramientos que han sido agrupados en tres sectores geográficos: norte, este y sur. Para conocer la edad relativa de las rocas estudiadas se ha realizado un análisis palinoestratigráfico (con un total de 29 muestras palinológicas) que ha permitido asignarlas al intervalo Albiense medio - Cenomaniense inferior. Además, este análisis ha permitido datar las unidades Aptienses, Fm. Contreras (Aptiense inferior) y Mb. El Burgal (Fm. El Caroch) (Aptiense superior) en algunos de los afloramientos estudiados, lo cual ha ayudado a situar la base del Gr. Utrillas.

Las asociaciones palinológicas descritas presentan las características propias de las del Cenofítico temprano. La vegetación identificada estuvo dominada por plantas leñosas perennifolias adaptadas a

condiciones de estrés hídrico que se desarrollaron en llanuras de inundación fluvial y zonas cercanas a la costa. La cubierta vegetal estuvo principalmente compuesta por coníferas de las familias Cherirolepidiaceae y Cupressaceae. En zonas cercanas a la costa crecieron árboles de la familia Araucariaceae. La presencia de polen de esta familia junto con quistes de dinoflagelados refleja la influencia de la paleocosta del Tethys.

El análisis de las paleofloras del Albiense medio – Cenomaniense inferior ha sido completado tras examinar la asociación macroflorística encontrada en el afloramiento de Cañada del Hoyo. Ésta se encuentra dominada numéricamente por restos de coníferas de los géneros *Frenelopsis*, *Glenrosa* y *Dammarites*. Las asociaciones de plantas fósiles integradas por estos géneros fueron típicas del Cenomaniense del oeste de Europa, y se han interpretado como correspondientes a comunidades vegetales con una alta tolerancia a la salinidad, que se desarrollaban en ambientes supramareales.

El análisis petrográfico, mineralógico y geoquímico de tres paleosuelos en el afloramiento de Buenache de la Sierra ha permitido inferir las condiciones paleoclimáticas que existieron en la Serranía de Cuenca durante el intervalo estudiado. En este sentido se interpreta que el clima debió de ser de tipo sabana tropical, presentando una marcada estacionalidad con respecto a las precipitaciones, y caracterizado por una estación seca seguida de otra húmeda con intensas lluvias. Este clima estacional permitió un mayor desarrollo y expansión de las comunidades vegetales y alternó con periodos áridos debido a la migración latitudinal de los cinturones climáticos durante el Albiense medio al Cenomaniense inferior.

Por otro lado, se han identificado un total de ocho asociaciones de facies sedimentarias que incluyen desde depósitos aluviales proximales hasta marinos someros. Este análisis, que se apoya en los datos bioestratigráficos obtenidos a partir del estudio palinológico, ha permitido identificar tres etapas evolutivas (Albiense medio, Albiense medio - superior y Albiense superior - Cenomaniense inferior).

A fin de obtener una mayor resolución, se ha realizado un análisis de estratigrafía secuencial en los afloramientos de Reíllo y Pajaroncillo, que presentan una posición relativa “along-strike” y están localizados en la zona distal de la cuenca. De esta manera, se ha identificado las tendencias transgresivas y regresivas, así como una serie de superficies estratigráficas que han permitido la correlación. Todo esto ha dado lugar a un análisis sedimentológico más preciso, identificando cinco etapas evolutivas (T1-T5), que describen la evolución detallada de la transgresión Albiense-Cenomaniense: (i) una etapa agradacional continental (T1), dominada por sedimentación aluvial; (ii) una etapa transgresiva inicial (T2) dominada por ambientes costeros y estuarinos; (iii) una etapa regresiva (T3), caracterizada por ambientes aluviales y supramareales; (iv) una nueva etapa transgresiva (T4), definida por ambientes inter- y supramareales, y (v) una etapa de profundización (T5), en la cual la transgresión progresó hacia el NO invadiendo áreas continentales y dando lugar a los depósitos más distales de la sucesión. Este análisis ha posibilitado la integración de la sucesión estudiada dentro del marco secuencial regional originalmente definido para la Cuenca de Valencia y el Dominio del Prebético, y por lo tanto la identificación de secuencias deposicionales de tercer orden y sus respectivos cortejos sedimentarios.

La investigación realizada en esta tesis doctoral también ha permitido estudiar los factores alocíclicos que controlaron la sedimentación en el área de estudio durante el Albiense medio - Cenomaniense inferior, que estuvo caracterizado por la interacción entre tectónica y eustatismo. En este sentido, la tectónica fue el principal control de la sedimentación durante el Albiense medio (etapa T1). Por el contrario, del Albiense superior al Cenomaniense inferior (etapas T2-T5) el eustatismo pasó a ser el principal control de la sedimentación, aunque matizado por la tectónica, que actuó en forma de pulsos dando lugar a subsidencia diferencial entre los afloramientos analizados. El clima, dominantemente árido, presentaba una marcada estacionalidad con estación seca de larga duración seguida de otra lluviosa de más corta duración.

Por lo tanto, los resultados de esta tesis doctoral constituyen una importante contribución al conocimiento de la transgresión del Cretácico "medio" dentro el contexto paleogeográfico de Iberia, que además ofrece una visión detallada de las comunidades vegetales y las condiciones paleoclimáticas que existieron en la Serranía de Cuenca durante el intervalo temporal estudiado. Además, esta investigación ha arrojado nuevos resultados sobre dos de los principales eventos que ocurrieron en Iberia durante el intervalo Albiense - Cenomaniense inferior:

(i) La integración de los resultados obtenidos en el contexto supra-regional ha permitido ahondar en las particularidades de la evolución geotectónica de Iberia durante el Albiense - Cenomaniense, proporcionando un mayor conocimiento de la transición de la etapa sin-rift (Jurásico Superior - Cretácico Inferior) a la etapa post-rift (Cretácico Superior) en la zona sur del Sistema de Cuencas de Rift de Iberia (IBRS). A este respecto, la presencia de fallas sin-sedimentarias controlando la sedimentación en la sucesión estudiada indica que la tectónica extensional permaneció activa durante el intervalo Albiense – Cenomaniense inferior, lo cual prueba que la influencia de la transición al periodo de post-rift abarcó un lapso temporal más largo que lo que inicialmente se había asumido.

(ii) La comparación de la sucesión sedimentaria Albiense medio - Cenomaniense inferior estudiada con los depósitos ambarígenos coetáneos de las cuencas del Maestrazgo y Vasco-Cantábrica ha permitido debatir sobre las causas que podrían explicar la ausencia de ámbar en la Serranía de Cuenca. Dada la similitud entre las asociaciones paleobotánicas (con respecto a las coníferas) entre las cuencas que se comparan, la ausencia de ámbar en la región estudiada debería de estar relacionada con las características de los ambientes tafonómicos en los que tuvieron lugar los procesos bioestratinómicos que afectaron a la preservación de los restos de resina. En este sentido, en la Serranía de Cuenca, la resina habría sido transportada hacia la paleocosta por canales fluviales de alta energía, que por su marcado carácter efímero y estacionalidad habrían contribuido a su oxidación y destrucción.

PREFACE

This Ph.D. thesis focuses on the sedimentological and palynological evolution of the Utrillas Group and La Bicuerca Mb stratigraphic successions (Albian to early Cenomanian) in the Cuenca Basin, Eastern central Spain. Similarly, it also deals with the study of the mid-Albian to early Cenomanian macrofloras and Aptian palynofloras of the studied area. This multidisciplinary approach includes very different datasets: sedimentological, tectono-sedimentary, palynological, biostratigraphic, palaeoedaphological, and macrofloral, and has delivered a comprehensive analysis allowing obtaining an accurate environmental, climatic, and ecological picture of the Albian to early Cenomanian succession in the Cuenca Basin.

The Ph.D. studies that resulted in the present thesis manuscript have been carried out at the Instituto Geológico y Minero de España (IGME-CSIC) and Facultad de Ciencias Geológicas of the Universidad Complutense de Madrid (UCM), Spain, within the Ph.D. Programme in Geology and Geological Engineering (Programa de doctorado en Geología e Ingeniería Geológica) during the academic years 2016-2017 to 2021-2022.

This research has been financed and carried out within the Projects AMBERIA ("*El ámbar de Iberia. Un excepcional registro de los bosques cretácicos en los albores de los ecosistemas terrestres modernos*") and CRE ("*Cretaceous Resin Event: Global bioevent of massive resin production at the initial diversification of modern forest ecosystems*") funded by the Spanish AEI/FEDER, UE Grants CGL2014-52163 and CGL2017-84419, respectively. Both projects dealt with the study of the Cretaceous amber from (mainly) Iberia and worldwide based on a multidisciplinary approach. Besides, this thesis has been granted with a Ph.D. scholarship of the Ministry of Science, Innovation and Universities of the Spanish Government (*Contratos para la formación de doctores de la convocatoria de 2018 del Ministerio de Ciencia, Innovacción y Universidades, Gobierno de España*) since the beginning of the academic year 2019-2020.

During the years that this research has been ongoing, some of its results have been published in three research papers that are attached at the end of this thesis manuscript (Appendix I). The results, figures, and any other extra materials of the three published research papers are included as a fundamental part of the results and discussion of this thesis.

Additionally, the Ph.D. candidate has done a total of three academic stays at the University Centre in Svalbard - UNIS (Longyearbyen, Norway) completing the Ph.D. courses AG 834 (Arctic Basin and Petroleum Provinces – 10 ECTS), AG 838 (Sedimentology Field Course: From Depositional Systems to Stratigraphic Architecture – 10 ECTS), and AG 823 (Sequence

Stratigraphy: A Tool for Basin Analysis – 10 ECTS) during the summers of 2016, 2017, and 2021, respectively. The completion of these academic stays in Svalbard (Norway) represented invaluable hands-on training in sedimentology fieldwork and the application of the concepts of Sequence Stratigraphy in outcrop studies, and it has contributed immensely to improving the quality of this Ph.D. thesis.

PART I: INTRODUCTION

1. Towards a preliminary scientific approach.

The Early to Late Cretaceous transition represents a time span characterised by the highest global sea levels of the Phanerozoic (Haq, 2014), giving rise to seaways that flooded large continental areas worldwide. It also coincided with a period of early diversification of angiosperms along with a decline in the diversity of gymnosperms and pteridophytes, likely associated with major oceanic and climatic changes (Crane and Lidgard, 1989; Crane et al., 1995; Heimhofer et al., 2005). This time interval is referred to as a global warmth period dominated by greenhouse conditions, presenting reduced equator-pole temperature gradients and an absence of polar ice caps. The global temperature was relatively lower during the Aptian and characterised by an increase during the Albian, leading to the Late Cretaceous thermal maximum during the Cenomanian/Turonian ages (Norris et al., 2002; Puceat et al., 2003; Forster et al., 2007). These conditions were supported by the occurrence of thermophilic floras and faunas at high latitudes. Likewise, the Cretaceous period (in particular the Aptian to Cenomanian time interval) also constitutes an extremely prolific time span with regard to the deposit of amber-bearing successions which have been recorded worldwide (i.e., Peñalver et al., 1999; Peñalver and Delclòs, 2010; Perrichot et al., 2010; Ross et al., 2010; Álvarez-Parra et al., 2021). During this time span, the Tethys Ocean, oriented east-west and located at an equatorial palaeolatitude, acted as a geographical barrier separating the northern (Laurasia) and southern (Gondwana) hemispheres landmasses (Huber and O´Brien, 2021).

The warm climate conditions prevailing during the Cretaceous have been related to massive volcanism due to seafloor spreading associated with the final break-up of Pangaea and the progressive formation of the Atlantic Ocean (Dallman et al., 2015). In this regard, the Early Cretaceous coincides with the beginning of seafloor spreading in the central North Atlantic Ocean and the separation of Iberia from Newfoundland, and its later continuation further north in the Labrador Sea and the Norwegian and East Greenland conjugate margins (Pe-Piper and Piper, 2004). Similarly, the (essentially Aptian) counterclockwise rotation of the Iberian Plate due to the opening of the Bay of Biscay in northern Iberia was contemporaneous with the opening of the North Atlantic Ocean (Gong et al., 2008).

This Ph.D. thesis deals with the analysis of some of these changes in the Early to Late Cretaceous transition based on the study of the Albian to Cenomanian sedimentary record of the

southwestern part of the Iberian Basin Rift System (IBRS), the Cuenca Basin, located in eastern central Spain. The Cuenca Basin represents a palaeogeographic domain of the IBRS (Aurell et al., 2019) in which the Albian to early Cenomanian time span remains understudied in terms of palynofloras, biostratigraphy, and sedimentology compared to other regions of Iberia (Najarro et al., 2011; Heimhofer et al., 2012; Barrón et al., 2015; Horikx et al., 2016); and the continental successions attributed to this interval commonly lack suitable age-diagnostic biostratigraphic markers.

During the Albian to Cenomanian, the studied region was located on the continental edge of the Western Tethys Sea and was subjected to conditions of i) eustatic sea-level rise (Haq, 2014), ii) syn-sedimentary tectonic activity evolving into post-rift conditions, and iii) continuous and high input of siliciclastic sediments (Sopeña et al., 2004; Aurell et al., 2019; Martín-Chivelet et al., 2019a). Such conditions resulted in a sedimentary succession consisting of a continental-coastal siliciclastic unit, the Utrillas Group. This siliciclastic unit laterally shifts and pinches out into a shallow marine mixed (siliciclastic-carbonate) unit, the La Bicuerca Mb (Aras de Alpuente Fm) (Vilas et al., 1982; Meléndez, 1983). This progressive lateral shift of facies of the Utrillas Gr into the shallow marine deposits of the La Bicuerca Mb reflects the effect of the marine incursions from the Western Tethys into the still continental areas of SE Iberia during Albian to early Cenomanian times, because of the global long-term eustatic sea-level rise that characterised the "mid"- Cretaceous period (spanning from the Aptian-Albian boundary to the Cenomanian-Turonian boundary [Bengston and Kakabadze, 2018] [see chapter 4.4 of this manuscript for further information]) (Sopeña et al., 2004; Martín-Chivelet et al., 2019a; Martín-Chivelet et al., 2019b).

Additionally, the sedimentary succession studied in this thesis is co-eval with some of the main "mid"- Cretaceous amber sites of Iberia, located in the Maestrazgo Basin (San Just, Barranco de la Pascueta and La Hoya/Cortes de Arenoso outcrops) and the Basque-Cantabrian Basin (Peñacerrada I and II outcrops) (Peñalver et al., 2007; Delclòs et al., 2007; Peñalver and Delclòs, 2002), which are rich in bioinclusions of fauna (and macroflora, to a lesser extent) (i.e., Arillo et al., 2009; Peñalver and Szwedo, 2010; Arillo et al., 2016; Kvaček et al., 2018). Therefore, the study of the Albian to early Cenomanian succession of the Cuenca Basin as an integrative approach (including sedimentology, palaeobotany, and palaeoedaphology) is a powerful tool to cast light on the environmental, climatological, and ecological constraints that affected the development and evolution of the plant communities where the resin-producer "mid"-Cretaceous floras thrived.

2. Objectives and scope of the Ph.D. thesis.

This Ph.D. thesis deals with the study of the Utrillas Gr and La Bicuerca Mb (Aras de Alpuente Fm) sedimentary succession in the Cuenca Basin (Eastern Spain) based on an integrative multidisciplinary approach including, sedimentological, palynological, palaeobotanical, and palaeoedaphological data.

The aims of this Ph.D. thesis are:

I) To constrain the age of the deposits of the Utrillas Gr - La Bicuerca Mb succession in the Cuenca Basin by carrying out a regional palynostratigraphic analysis.

II) To reconstruct the palaeoenvironmental and palaeoclimatic conditions of the Cuenca Basin during the deposit of the Utrillas Gr - La Bicuerca Mb succession based on an integrative approach that includes sedimentary facies, palynofloras, macrofloras, and palaeosoils analyses.

III) To reconstruct the stratigraphic record of the Albian to early Cenomanian transgression and carry out a sequence stratigraphic analysis to better understand the eustatic and tectonic factors that controlled the evolution of the Cuenca Basin during that time-span.

IV) To shed light on the palaeogeographic evolution of the Cuenca Basin and the integration of the results within the supra-regional tectono-sedimentary context of Iberia during the Albian to early Cenomanian times.

V) To provide information about the key constraints ruling the accumulation and preservation of “mid”-Cretaceous amber deposits in the sedimentary basins of Iberia based on the results of the multidisciplinary analyses carried out.

3. Materials and methods.

The following pages describe the materials and methods required to carry out this Ph.D. thesis. The methodology has been divided into four major sub-chapters which address literature review, fieldwork, laboratory-based and computer-based methods, respectively.

3.1. Literature review.

During the course of this Ph.D. thesis and the writing of the present manuscript, an extensive literature review has been carried out representing one of the cornerstones and foundational steps of the research process. This literature review has mainly been focused on the finding of publications and the gathering of information about (1) the (tectono-) sedimentary evolution of Eastern Iberia (and the Cuenca Basin in particular) during the early to late Cretaceous transition; (2) the (palyno- and macro-) floral communities that inhabited in the Western Tethys margin/Eastern Iberia during the Aptian to early Cenomanian times; (3) the suite of different sedimentary facies associations that develop in fluvial to coastal settings characterised by transgression as well as its sequence stratigraphic significance.

For that purpose, the literature review was carried out in the data bases of several libraries from different universities and public research centres, including both Spanish and overseas ones. More concretely, it included the libraries of the Facultad de Ciencias Geológicas of the Universidad Complutense de Madrid (UCM; Madrid, Spain), Instituto Geológico y Minero de España (IGME-CSIC; Madrid, Spain), Museo Nacional de Ciencias Naturales (MNCN; Madrid, Spain) and University Centre in Svalbard (UNIS; Longyearbyen, Norway).

All the references consulted during this study (including book chapters, research and review articles, unpublished Ph.D. theses, conference abstracts, monographs, etc) were duly listed in an EndNote database that has been used to compile the final reference list included at the end of this manuscript.

3.2. Fieldwork methodology.

The sedimentary fieldwork started after an extensive literature review of the study area based on previous geological mapping works. The regional geological mapping studies, Magna IGME 1:50000 (nº 610 [del Olmo Zamora, 1986], 611 [Berasategui and Ramírez, 1982], 635 [Ramírez del Pozo et al., 1972] and 636 [Portero et al., 1972]) carried out by the Instituto Geológico y

Minero de España (IGME-CSIC), and the Geological Map of Spain and Portugal 1:1000000 (Rodríguez et al., 2014) carried out by the Instituto Geológico y Minero de España (IGME-CSIC) and the Laboratório Nacional de Energia e Geologia of Portugal (LNEG). This literature review, in combination with satellite images from Google Earth (https://earth.google.com) and Iberpix 5.0 (https://ign.es/iberpix/visor), has allowed the construction of geological and structural maps and identifying the potential outcrops where the Albian to lower Cenomanian succession has been logged.

The distribution of the logged sections has been intended to cover most of the study area so that both lateral shifts of facies and the vertical evolution of the Albian to lower Cenomanian succession can be observed and studied more in detail.

Additionally, several rock samples have been collected during the fieldwork campaigns. The collected material was used to prepare samples for different purposes including granulometry studies, petrography, palynology, macroflora, mineralogical and geochemical analyses. The preparation of the rock samples using different laboratory methods is explained in this chapter.

3.3. Sedimentary facies analysis methods.

The sedimentary facies analysis has been performed based on the guidelines provided by Collinson and Thompson (1982), Dabrio and Hernando (2003), and Dalrymple (2010a). In order to carry out the analysis, several sedimentary sections have been logged, and different sedimentary parameters were measured in each of the study outcrop sections. The analysed parameters include lithology, grain size, texture, sedimentary structures, palaeocurrent directions, sedimentary body morphology, and biogenic structures. The identified facies have been grouped into facies associations based on their spatial-temporal distribution, and their overall depositional architecture has been studied.

Additionally, a sequence stratigraphic analysis has been performed in those outcrops where the resolution of the studied succession was high enough to recognise the stacking patterns of the identified facies associations. The stacking patterns of the facies associations permitted distinguishing correlatable stratigraphic units bounded by key surfaces, identified based on the concepts of sequence stratigraphy (i.e., Embry, 2009; Helland-Hansen and Martinsen, 1996 Catuneanu, 2019).

3.4. Laboratory-based methodology.

3.4.1. Thin sections.

Thin sections for the transmitted-light microscope have been prepared, mostly in samples with high carbonate contents and in those interpreted as palaeosoils, aiming at obtaining new insights into their petrographical structure. The preparation of the 30 µm thin sections has followed the standard procedure for petrographic samples (Gribble and Hall, 1985; Humphries, 1992).

All the thin sections studied in this thesis have been prepared in the facilities of the Stratigraphy Laboratory of the Facultad de Ciencias Geológicas of the Universidad Complutense de Madrid (UCM), Spain.

3.4.2. Granulometry samples

The preparation of the granulometry samples has been carried out by the Stratigraphy Laboratory of the Facultad de Ciencias Geológicas of the Universidad Complutense de Madrid (UCM), Spain. The procedure consisted of smashing and disaggregating mildly lithified sandstone samples, and, subsequently sieving them in up to 10 grain-size intervals (>2 mm; 2 – 1 mm; 1 – 0.5 mm; 0.5 – 0.25 mm; 0.25 – 0.10 mm; 0.10 – 0.05 mm; 50 – 20 µm; 20 – 8 µm; 8 – 2 µm; <2 µm).

Later, cumulative weight percentages were calculated and plotted in a semi-logarithmic sheet for each sample (Bueno-Cebollada and Meléndez, 2018).

3.4.3. Palynological samples (palynoflora).

The palynological samples of this thesis were prepared by the Geologischer Dienst NRW (Germany) (www.gd.nrw.de) following the standard procedure (Batten, 1999; Traverse, 2007; Brown, 2008), which involves macerations in HCl, HF and diluted HNO_3, and sieved with different grid sizes. The resultant palynological assemblages were characterised using an Olympus BX51 brightfield light microscope coupled to a ColorView IIIu camera.

The procedure for the preparation of the palynological samples aims at the elimination of (most of the) mineral fraction and the preservation of the palynomorphs, and included the following steps:

1- The physical disaggregation of the samples, crushing them into clay-sized particles.
2- Pre-HF treatment: the calcium and magnesium carbonates included in the samples were removed by being solubilised with heated HCl (35 %) for an hour using a laboratory fume hood. In order to remove the remaining HCl, the samples were centrifuged at 2000 r.p.m. for 5 minutes. After that, the samples were washed with distilled water and centrifuged at 2000 r.p.m. for 5 minutes. This procedure was repeated three times.
3- Silicate removal: the samples were introduced in 600 ml polypropylene beakers where HF (48 %) was added. The beakers were heated for 30 minutes (using a laboratory fume hood). Afterwards, the acid residue was removed using distilled water following the procedure previously explained in 2.
4- Oxidation of the organic matter: it is performed in order to transform at least partially decomposed organic matter into alkali-soluble "humic acids". The samples were immersed in HNO3 (60 %) for 3 to 5 minutes. After the reaction, the resulting residues were removed by centrifuging them at 2000 r.p.m. Afterwards, the samples were washed using distilled water following the procedure previously explained in 2.
5- In general, the previous procedures gave rise to fluorosilicates that needed to be removed to ensure the release of the organic matter. For that purpose, the samples were placed in beakers with HCl (35 %) and heated for about 30 minutes using a laboratory fume hood. Afterwards, the samples were washed in distilled water following the procedure previously explained in steps 2, 3, and 4.
6- Concentration of palynomorphs: the resultant materials after the previous "acid treatments" were sieved using different grid sizes (12, 50, 75, 250, and 500 µm).
7- Slide making: the obtained residues in the two smaller mesh sizes (75 µm - 12 µm) were collected in Eppendorf tubes. The remaining material in the tubes was collected with the aid of a micropipette, mounted in glass slides with glycerine jelly, and covered by a cover slip. The resulting slides were sealed with paraffin wax and labelled.

The studied slides and palynological residues are stored in the facilities of the Museo Geominero, Instituto Geológico y Minero de España (IGME-CSIC), Madrid, Spain. The museum inventory codes are: MGM-11171C to MGM-11279C. The full references are indicated in Appendixes II and III. Regarding the quantitative study, the number of palynomorphs identified per sample ranges from more than 300 to 1700, approximately, depending on their preservation in the samples (Appendix II). Therefore, the number of palynomorphs identified permits obtaining significant results from a statistical perspective.

3.4.4. Plant remains (macroflora).

The collected fossil plant samples consist of compressions. The preparation of the samples for the study under the microscope has followed the procedure described by Bather (1908). Firstly, it consisted of cleaning the cuticle samples, which were originally embedded in a clayish and silty matrix of sediment, by soaking them in water mixed with a small amount of hydrogen peroxide. The resultant muddy sediment was sieved, separating the disintegrated mud from the cuticles, which were re-immersed in distilled water to remove the remaining muddy fraction. Then, the plant fragments were air-dried at room temperature.

The next step was to immerse for 24 to 48 hours the plant fragments in a Schulze´s reagent preparation (which consists of a solution of 50 % of nitric acid with potassium chlorate). Afterwards, the samples were rinsed in distilled water and subsequently immersed in a solution of ammonia (approximately 20%) for about 2-3 hours, aiming at eliminating the humic substances. Then, the samples are rinsed in distilled water by immersion and dissected under the stereomicroscope using needles to open the cuticles.

The final step consists of the mounting of the cuticle preparation for the stereomicroscope on glass slides embedded with glycerine jelly.

The fossil plant samples studied in this thesis have been examined under an Olympus BX51 brightfield light microscope coupled to a ColorView IIIu camera. The fossil plant samples are stored in the Museo Geominero facilities of the Instituto Geológico y Minero de España (IGME-CSIC), in Madrid (inventory numbers MGM-11283C to MGM-11358C).

3.4.5. Palaeosoil analyses.

3.4.5.1. Palaeosoil thin sections.

The procedure followed for the preparation of the thin sections is the one explained in section 3.4.1. Additionally, for these samples, K-felspar staining has been used.

3.4.5.2. *Geochemical analysis*

For the geochemical analyses carried out in palaeosoil profiles, samples of approximately 100 g of rock were powdered. The determination of geochemical whole-rock composition is based on a pressure digestion system. The samples were powdered, dried, and sieved to < 53 µm for

homogenization. In each sample, 0.25 g were weighed out and mixed with 0.5 g of flux. Then, the mixture was fluxed and dissolved in HNO3. Afterwards, the resulting solutions were analysed with ICP-MS (inductively coupled plasma mass spectroscopy) and ICP-OES (inductively coupled plasma optical emission spectroscopy). The geochemical analyses were performed at the ALS Geochemistry facilities in Seville, Spain.

The measured elements include: Major elements (SiO2, Al2O3, Fe2O3, CaO, MgO, Na2O, K2O, Cr2O3, TiO2, MnO, P2O5, SrO, BaO, LOI) and Minor elements and REE (Ba, Co, Cr, Cu, Li, Ni, Sc, Zn, Cs, Ta, Th, Rb, Sr, Nb, Ga, Sn, Hf, U, V, W, Y, Zr, Pb, Ag, As, Cd, Mo, Tl, La, Ce, Pr, Nd, Sm, Eu, Gd, Tb, Dy, Ho, Er, Tm, Yb, Lu). By convention, Major element abundances are expressed as weight percentages of oxides (%) and minor element/REE abundances are expressed as ppm. All the geochemical ratios used in this study have been calculated by dividing the weight per cent of each oxide or element by its molar mass (g mol^{-1}).

For a thorough explanation of the geochemical methods used, the reader is referred to Retallack (2001) and Sheldon and Tabor (2009). Additionally, some of the most useful indexes for provenance and soil chemical processes (Titanium/Alumina, Barium/Strontium, Alumina/Silica, Iron and Magnesium content/Alumina, Silica/Sesquioxides, Alkali/Alumina) are listed over the next pages:

Provenance:

- Titanium / Alumina = TiO_2 / Al_2O_3; The index between the TiO2 and Al2O3 content is used to determine possible variations in the source area (Sheldon and Tabor, 2009). Both elements are considered geochemically immobile, and their relationship is constant in igneous-type rocks, thus the sediments from source areas of similar composition will present similar proportions between both elements.

Hydrolysis:

- Alumina / Bases = Al_2O_3 / ($CaO+MgO+K_2O+Na_2O$); In normal fertile soils this ratio is usually below 2. This ratio can reach 100 in strongly developed soils.

- Barium / Strontium = Ba/Sr. This index is generally used as an indicator of leaching of the sediments or hydrolysis, which is related to a high weathering of the materials. Both elements present similar geochemical characteristics, but Sr is significantly more soluble than Ba, which will be leached more readily. In most rocks, the Ba/Sr value is around 2, being able to reach 10 in soils of very acid type (Retallack, 2001).

- Alumina / Silica = Al_2O_3/SiO_2; this ratio evaluates the clayeyness of the soil and is related to the illuviation of clays. Al accumulates in clay minerals and could be taken as indicative of a Bt horizon.

Oxidation:

- Iron and Magnesium content / Alumina = $(FeO+Fe_2O_3+MgO)/Al_2O_3$**;** Usually, the reduced iron is lost in groundwater flow. However, the oxidised minerals are insoluble and accumulate in soils. Generally, this index is under 0.4. In Ferruginous horizons can reach 1.2, and in argillic horizons 1.9.

Hydration:

- Silica / Sesquioxides = SiO_2 / $(Fe_2O_3+Al_2O_3)$; High values are indicative of quartz-rich palaeosoils with few hydrated minerals as goethite and gypsum.

Salinisation:

- Alkali / Alumina = (K_2O+Na_2O) / Al_2O_3; Presence of salts such as halite or gypsum, pseudomorphs and breccias are good indicators of alkaline conditions. With this molecular weathering ratio, values greater than 1, increasing up-profile, are indicative of salinisation.

Based on the relationship between primary minerals and their secondary products such as clay minerals, there are other ratios frequently used to measure the degree of chemical weathering in a palaeosoil and have been calculated in this study:

- Chemical Index of Alteration (CIA) of Nesbitt y Young (1982). The CIA is a measurement of the weathering of feldspar minerals and their hydration to form clay minerals.

  $CIA = 100 \times Al_2O_3 / (Al_2O_3+CaO+Na_2O+K_2O)$

- Chemical Index of Alteration without Potassium (CIA-K). As Potassium is susceptible to diagenesis alteration Maynard (1992) proposed the CIA-K index.

  $CIA\text{-}K = 100 \times Al_2O_3 / (Al_2O_3+CaO+Na_2O)$

- Plagioclase Index of Alteration (PIA) of Fedo et al. (1995). The PIA is a measurement of the weathering of plagioclases.

  $PIA = 100 \times (Al_2O_3-K_2O) / (Al_2O_3+CaO+Na_2O-K_2O)$

- Bases / Alumina. CIA and CIA-K basically focus on the alteration of feldspars. Trying to evaluate other types of minerals, Retallack (2001) proposed this index.

  $(MgO+CaO+Na_2O+K_2O) / Al_2O_3$

Additionally, using a wide database composed of numerous geochemical analyzes, Sheldon et al. (2002) established several mathematical functions that relate chemical weathering indexes with precipitation and average annual temperature. These equations relating CIA-K and Bases to Alumina to precipitation are useful over a precipitation range of 200–1600 mm/yr.

These functions are:

- P1 = 259.34 Ln(B)-759.5; where B is the Bases to Alumina of Retallack (2001). This climofunction has a correlation index of R^2=0,66.

- P2= 14.265(CIA-K)-37.632; With an accuracy of R^2=0,73

- P3 = $221.12e^{0,0197(CIA-K)}$; with R^2 = 0,72

The functions P1, P2, and P3 have been calculated in this study for two palaeosoil profiles to quantitatively estimate the annual palaeorainfall.

3.4.5.3. Mineralogical analysis

The bulk mineral composition of the studied palaeosoil samples (10 samples) has been determined by an X-ray diffraction (XRD) analysis with unoriented powders, after grinding and homogenisation of the samples to <53 µm. The analyses were carried out at the Geochronology and Isotopic Geochemistry CAI (*Centro de Asistencia a la Investigación*) of the Facultad de Ciencias Geológicas of the Universidad Complutense de Madrid (UCM) with a Bruker D8 Advance diffractometer using Cu-Kα at 30 kV and 40mA, a step size of 0.02 (°2θ), and time per step of 1 s, between 2 and 65 (°2θ). Clay mineral composition was determined on oriented aggregates of the <2 µm fraction obtained by sedimentation from an aqueous suspension onto glass slides.
The oriented aggregates underwent heating (550 °C for 2 hours) and solvation with ethylene glycol (for at least 24 hours), aiming at achieving a more complete characterisation of the clay mineralogy of the samples. In this case, a time per step of 1 s, between 2 and 65 (°2θ) was used. The software DIFFRACplus has been used for the acquisition, processing and assessment of the data obtained from the samples. Besides, semi-quantitative analyses were performed following the method proposed by Schultz (1964).

3.4.5.4. SEM samples

The textural and compositional characterisation of the studied palaeosoil samples has been completed with the study of gold-coated chips of selected samples under the scanning electron microscope (SEM). To prepare the samples for the SEM study, small fragments of the samples were collected and dried on a stove at 50 °C for 48 hours. Then, the studied samples were mounted on a specimen holder made of copper and coated in gold. The SEM samples were prepared and studied at the Geochronology and Isotopic Geochemistry CAI (*Centro de Asistencia a la Investigación*) of the Facultad de Ciencias Geológicas of the Universidad Complutense de Madrid (UCM), Spain. The microscope used in this study was a JEOL JSM-820 model (with microanalysis). The software EDX Oxford ISIS-Link was used for the acquisition, processing, and appraisal of the obtained analysis data.

3.5. Computer-based methodology.

The sedimentary sections logged in the field (see 3.1. fieldwork methodology) have been constructed using the software SEDLOG 3.1. (Zervas et al., 2009) and Adobe Illustrator CS6 (www.adobe.com).

The geological maps of the study area and of some of the studied locations were constructed using the software Adobe Illustrator CS6 (www.adobe.com).

The palynological diagrams were constructed using the software Tilia/TGView 2.0.2 (Grimm,1992; 2004) in combination with the software Adobe Illustrator CS6 (www.adobe.com).

4. Geological, stratigraphic and biostratigraphic framework: a literature review.

4.1. Geological Setting

This chapter presents a summary of the geological setting of Iberia during the Mesozoic Era based on the literature review of previous research on the topic. In this manner, this chapter will allow the reader to better understand the fundamental tectono-sedimentary processes that took place in Iberia during the Mesozoic.

The chapter is organised into several sections going from the broader context of the Iberian Plate during the Mesozoic to the Mesozoic evolution of eastern Iberia and the specific stratigraphic and palaeogeographic constraints of sedimentation during the Albian – early Cenomanian in the Cuenca Basin.

4.1.1. The Iberian Plate during the Mesozoic.

After the Variscan Orogeny, the European, African, and Iberian plates were part of the Pangea supercontinent. In this regard, the NW of Africa, SE of Europe, and Iberia were located at the axis of the Variscan Orogenic System, which was rifted during the Permian-Triassic, giving rise to a transtensional corridor during the Early-Middle Jurassic times (i.e., Puga et al., 2017; Ramos et al., 2017).

The Iberian Plate was defined during the Permian to Middle Jurassic times due to a rifting cycle that took place during this time interval. The differentiation of Iberia as an independent plate started during the Late Triassic owing to the initial opening of the middle segment of the Central Atlantic Ocean (Vergés et al., 2019). This first extensional cycle preceded a second rifting cycle, which affected both the intraplate area and margins of the Iberian Plate during the Jurassic and Cretaceous (Sopeña et al., 2004; Vergés et al., 2019). These extensional processes caused the continental break-up during the Jurassic and Cretaceous times along the margins of the Iberian Plate, which were located at its southern/southeastern (Ligurian Tethys), western (Atlantic) and northern (Bay of Biscay-Pyrenees) boundaries (Vergés et al., 2019).

The south-southeastern margin of the Iberia Plate developed due to the Early-Middle Jurassic opening of the northern segment of the Central Atlantic Ocean, which caused the SE movement of Africa relative to Iberia (Schettino and Turco, 2011; Sibuet et al., 2012; Vergés et al., 2019).

The western margin of the Iberian Plate was created during the Early Cretaceous owing to the northern propagation of the southern segment of the North Atlantic Ocean. The northern

margin of the Iberian Plate evolved during the late Early Cretaceous (Aptian to Cenomanian) owing to the opening of the Bay of Biscay (Vergés et al., 2019).

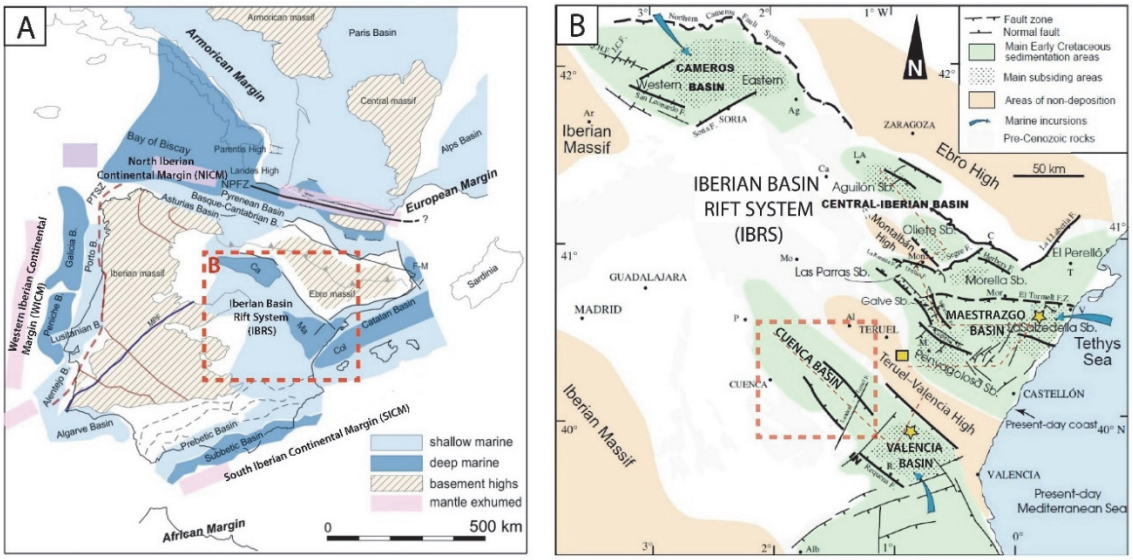

Fig. 1.1. (A) Map of Iberia during the Cretaceous where the location of the main basins can be observed. The area of the Iberian Basin Rift System (IBRS) is highlighted by a dashed red rectangle. Modified from Vergés et al. (2019); (B) Schematic map of the IBRS during the Lower Cretaceous including the different basins or domains and the main structural elements. The study area of this Ph.D. thesis is indicated by a red square. Modified from Martín-Chivelet et al. (2019a).

4.1.2. The sub-division of the Iberian Plate and the Iberian Basin Rift System (IBRS).

According to Martín Chivelet et al. (2019a) and Terrinha et al. (2019), the Iberian Plate can be divided into (Fig. 1.1A, B):

- The Western Iberian Continental Margin (WICM)
- The North Iberian Continental Margin (NICM), which includes the Pyrenean and Basque-Cantabrian Basins.
- The South Iberian Continental Margin (SICM), including the Prebetic and Subbetic Domains.
- The Iberian Basin Rift System (IBRS), which represents the intraplate area of Iberia and includes the Cuenca, Valencia, Central Iberian, Cameros, Maestrazgo and Garraf Basins.

The formation of these rift basins was associated with the first stages of the opening of the North Atlantic because of the separation of the Newfoundland and Iberia conjugate margins (Tucholke et al., 2007; Martín-Chivelet et al., 2019a). In this regard, several extensional episodes were recorded in the basins of Iberia during the Late Jurassic to late Early Cretaceous times where the

accommodation space for sediments was controlled by tectonic subsidence and eustatism (Martín-Chivelet et al., 2019a).

As a result of the opening of the Western Tethys and North Atlantic oceans during the Late Jurassic to Early Cretaceous times, a transtensional corridor oriented NW-SE was formed within the intraplate area of the Iberian Plate (hereafter referred to as the Iberian Basin Rift System [IBRS]; Martín-Chivelet et al., 2019a). Consequently, several major structural domains within the IBRS were individualised due to extensional tectonism, namely: the Cuenca, Valencia, Central Iberian (central-northern area), Cameros (in the northwest), Maestrazgo and Garraf (in the east) Basins (Sopeña et al., 2004; Martín-Chivelet et al., 2019a; Aurell et al., 2019) (Fig. 1.2A).

The Cuenca and Valencia Basins have traditionally been considered sub-basins or sub-domains of the so-called Southern Domain of the IBRS (previously referred to as the South Iberian Basin) (Sopeña et al., 2004; Martín-Chivelet et al., 2019a). However, more recent research (Aurell et al., 2019) points out their evolutionary structural and stratigraphic dissimilarities, particularly during the Jurassic and Cretaceous times, and considers the Cuenca and Valencia Domains as independent sedimentary basins within the IBRS. Therefore, in this Ph.D. thesis, the mentioned structural domains of the IBRS will be referred to as the Cuenca and Valencia Basins, according to the nomenclature given by Aurell et al. (2019).

The Cuenca and Valencia Basins and Maestrazgo Basin represent the structural domains that occupied the southern and eastern parts of the IBRS, respectively (Fig. 1.1B; Martín-Chivelet et al., 2019a). In these three basins, the main source of sediments was located in the Iberian Massif, a Variscan massif positioned to the west (Sopeña et al., 2004; Caja et al., 2007; Martín- Chivelet et al., 2019a). The Cuenca and Valencia Basins are separated from the Maestrazgo basin by a structural high (the Teruel-Valencia High; Fig. 1.1B), which might have also been one of the sediment sources of the basins (Martín- Chivelet et al., 2019a; Aurell et al., 2019).

During the Late Jurassic – Early Cretaceous rifting cycle, the Cuenca and Valencia Basins and the Maestrazgo basin formed two sedimentary troughs oriented NW-SE that respectively occupied the southern and eastern part of the IBRS (Fig. 1.1B; Martín-Chivelet et al., 2019a). The most northern trough (which corresponds to the Maestrazgo and Central Iberian Basins; Fig. 1.1B) recorded the highest tectonic subsidence, and therefore a greater thickness of sediment, during the rifting cycle (Fig. 1.2B; Martín-Chivelet et al., 2019a). Conversely, the southern trough which corresponds to the Cuenca and Valencia Basins (Fig. 1.2B; Martín-Chivelet et al., 2019a) recorded a lower thickness (approximately 2000 m in the depocenter of the Valencia Basin) due to a less intense tectonic subsidence (Martín-Chivelet et al., 2019a). The location of these Late

Jurassic – Early Cretaceous depocenters was influenced by those previously generated during the Late Permian – Triassic rifting cycle, although they do not always coincide (Martín-Chivelet et al., 2019a).

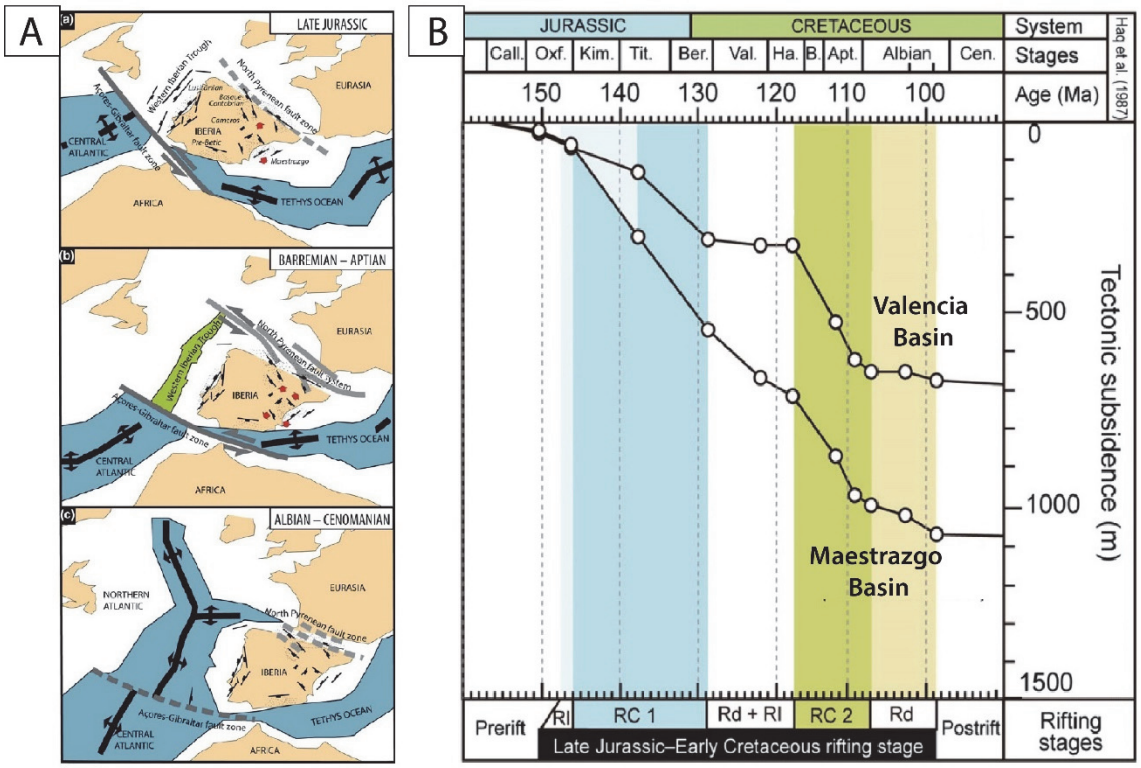

Fig. 1.2. (A) Plate tectonic configuration of Iberia during the Late Jurassic, Barremian-Aptian, and Albian – Cenomanian. The main subsidence areas and directions of extension are indicated. Modified from Martín-Chivelet et al. (2019a) after Sibuet et al. (2004) and Beltrando et al. (2015). (B) Subsidence curves for the Maestrazgo and Valencia Basins during the Late Jurassic to Early Cretaceous rifting cycle and the beginning of the Late Cretaceous post-rift. Two main rifting stages are distinguished (in blue and green, respectively). RC 1 (Rift Climax 1); RC 2 (Rift Climax 2); Rd (Rift subsidence deceleration phase); RI (Rift initiation phase). Modified from Martín-Chivelet et al. (2019) after Salas and Casas (1993) and Salas et al. (2001).

The geometry of the Cuenca, Valencia, and Maestrazgo Basins was determined by two sets of normal faults, respectively trending NNW-SSE (locally ranging from N-S to NNW-SSE) and E-W (locally it may range from E-W to ENE-WSW) (Martín-Chivelet et al., 2019a). These sets of faults are mostly the result of the reactivation of late and post-Variscan fault systems in an extensional setting (Álvaro et al., 1979; Liesa et al., 2006). Notwithstanding, new extensional syn-tectonic faults were also developed during the Late Jurassic – Early Cretaceous rifting giving rise to complex arrays of fault systems (Martín-Chivelet et al., 2019a).

The most relevant of these fault systems acted as barriers, separating important geographical regions, and showing different subsidence rates. Consequently, they defined the boundaries of the basins (Sopeña et al., 2004; Martín-Chivelet et al., 2019a). An example of one of these faults is the Teruel-Landete Fault (located in the Southern Domain of the IBRS) which is the

geographical feature that separates the Valencia and Cuenca Basins (i.e., Meléndez, 1983; Fregenal-Martínez and Meléndez, 1993; Fregenal-Martínez et al 2017; Aurell et al., 2019).

4.1.3. The tectono-sedimentary evolution of the IBRS.

The tectono-sedimentary evolution of the Iberian Basin is traditionally explained by two rifting cycles, followed by their respective post-rift stages during which sedimentation in passive margins took place:

- The first of these rifting cycles spanned Early Permian to Middle Triassic (i.e., Sopeña et al., 2004; Vargas et al., 2009; López-Gómez et al., 2019; Vergés et al., 2019).
- The second rift cycle lasted from the Late Jurassic to late Early ("mid") Cretaceous times. The development of this rifting cycle was intrinsically related to the separation of Africa and Europe, as well as to the anticlockwise rotation of the Iberian Plate (i.e., Sopeña et al., 2004; Martin-Chivelet et al., 2019a; Vergés et al., 2019).

4.1.3.1. The Permian-Triassic rifting cycle.

The Permian to Middle Triassic represents the first rifting cycle that has been recorded in the basins of the IBRS. The early phases of this Permo-Triassic rifting stage were linked to the break-up of the supercontinent Pangea (López-Gómez et al., 2019). In the Iberian Basin this first rifting cycle can be sub-divided into three tectono-sedimentary phases:

- A Latest Carboniferous to early Permian phase characterised by the creation of small extensional basins, representing the end of the Variscan cycle and the beginning of the Alpine cycle (López-Gómez et al., 2002, 2019).
- A Middle to Late Permian phase characterised by a change in the development of larger sedimentary basins dominated by normal faulting and half-graben structures which were infilled by continental successions (Arche and López-Gómez, 1996; Sopeña et al., 2004; López-Gómez et al., 2019).
- An Early to Middle Triassic phase related to the extensional development of the rift system, during which larger basins developed mainly in continental environments. This stage coincides with the deposits of the *Buntsandstein* facies (López-Gómez et al., 2019).

Finally, the Middle to Late Triassic times are characterised by a mature phase of rifting which implied an enlargement of the depositional area (López-Gómez et al., 2019). This phase meant

the onset of thermal subsidence, although tectonism still was playing a key role in the creation of accommodation (Arché and López-Gómez, 1996). This mature phase led to the deposit of a carbonate ramp during the Middle Triassic times (*Muschelkalk* facies), and the deposit of evaporite-dominated facies (*Keuper* facies) due to a regressive event during the latest Middle Triassic (López-Gómez et al., 2019). This event persisted until the end of the Triassic when a post-rift stage started and the basins of Iberia were dominated by thermal subsidence (Vargas et al., 2009; López-Gómez et al., 2019).

4.1.3.2. The Late Triassic to Middle Jurassic passive margin stage.

After the Permo-Triassic Rifting Cycle, Iberia was dominated by thermal subsidence that led to the development of a passive margin stage spanning Late Triassic to Middle Jurassic (Sopeña et al., 2004; Gómez et al., 2019). This phase was associated with the opening of the Central Atlantic and the Ligurian Tethys and it generated NW-SE trending fault systems.

During the beginning of this stage, passive margin conditions prevailed in most of the Iberian Plate but for the western and southern to eastern margins of Iberia, where there were still active rift systems. These rift systems were the precursors of the Central Atlantic and Tethys Oceans, respectively (Gómez et al., 2019). The creation of accommodation space was essentially controlled by thermal subsidence, together with eustatism. As a consequence, a thick laterally extensive succession dominated by shallow marine carbonates (which included environments ranging from outer ramps to sabkhas) deposited in the basins of Iberia and particularly extended across most of the eastern part of Iberia (Iberian Basin) (Gómez et al., 2019).

4.1.3.3. The Late Jurassic to Early Cretaceous rifting cycle.

During the Late Jurassic to Early Cretaceous Iberia experienced extensional and transtensional stresses that led to a new rifting phase that affected its basins (Sopeña et al., 2004; Martín-Chivelet et al., 2019a). During this time span, several rift-related basins were generated both along the margins and in the interior of the Iberian Plate due to its motion relative to the European and African plates (Martín-Chivelet et al., 2019a).

The transition from the Late Jurassic – Early Cretaceous rifting cycle into the Late Cretaceous post-rift started during middle to late Albian times when the tectonism ceased and the thermal subsidence became dominant in the IBRS (Sopeña et al., 2004; Martín-Chivelet et al., 2019a).

The second rifting cycle in the IBRS spanned middle Oxfordian to mid-Albian (Aurell et al., 2019; Martín-Chivelet et al., 2019a). There were two main rifting phases (syn-rift sequences 1 and 2) during the Late Jurassic – Early Cretaceous rifting cycle as indicated by the subsidence curves (Fig. 1.2B; Martín-Chivelet et al., 2019a), which in the southern part of the IBRS were better recorded in depocentral areas such as the Valencia and Maestrazgo Basins:

The *Syn-rift sequence 1* (Late Jurassic – earliest Cretaceous) (Fig. 1.3). This first phase of rifting (spanning middle Oxfordian to Berriasian) did not have a coeval onset across the different basins of the IBRS. In the Valencia Basin, it started during early Tithonian times, while in the Maestrazgo Basin the rift began during the latest Oxfordian (Martín-Chivelet et al., 2019a and references therein). Conversely, it started during the middle Oxfordian in the southern part of the Cuenca Basin (Aurell et al., 2019). It directly overlies the deposits of the Late Triassic to Middle Jurassic passive margin stage. The end of this first syn-rift sequence took place during the earliest Cretaceous times and it is reflected by a deceleration in the subsidence rate during the Berriasian and Hauterivian (Fig. 1.2B; Martín-Chivelet et al., 2019a).

The *Syn-rift sequence 2* spanned Early to "mid"-Cretaceous, more exactly from the Barremian (or even Hauterivian in some areas of the IBRS) to early Albian (Sopeña et al., 2004; Martín-Chivelet et al., 2019a). Since the Barremian times, there was an increase in tectonic subsidence in some areas of the Cuenca, Valencia, and Maestrazgo Basins, thus reflecting the beginning of a new phase of rifting (Martín-Chivelet et al., 2019a; Aurell et al., 2019). This phase of renewed tectonic subsidence favoured the development of isolated smaller sub-basins in both sedimentary basins and it is understood as the rifting initiation (Liesa et al., 2006; Martín-Chivelet et al., 2019a; Aurell et al., 2019). In the southern part of the IBRS, these periods are characterised by the development of two well-differentiated depocentres, separated by a structural high (the Landete-Teruel High), which coincide with the Valencia and Cuenca Basins (Aurell et al., 2019) (Fig. 1.1B).

The late Barremian to Aptian represents a time interval characterised by increased tectonic subsidence in the Southern Domain of the IBRS, which coincides with the climax of the second rift phase (Fig. 1.2B; Martín-Chivelet et al., 2019a). However, the subsidence rapidly decreased through the Aptian, reflecting the progressive homogenization of the sedimentary basins of the IBRS. During this time, continental to transitional siliciclastic systems developed in the Cuenca Basin (Meléndez 1983; Aurell et al., 2019) merging into shallow carbonate platforms toward the SE, in the Valencia Basin. However, marine conditions prevailed in the Maestrazgo Basin, characterised by the deposits of a thick carbonate platform successions (Peropadre, 2012;

Peropadre et al., 2013) previously known as “Urgonian Platforms”. The stratigraphic architecture of the Aptian deposits both in the Cuenca, Valencia, and Maestrazgo Basins was heavily influenced and controlled by transgressive-regressive cycles related to the advance and retreat of the Western Tethys Ocean (Meléndez and López-Gomez, 2003; Peropadre, 2012).

During the early Albian, towards the end of the Early Cretaceous rift phase, a major unconformity developed due to relative eustatic fall that generated incision of fluvial systems (Aurell et al., 2019; Martín-Chivelet et al., 2019a). The late Aptian to early Albian time-interval is considered the last pulse of crustal extension in the Cuenca, Valencia, and Maestrazgo Basins reflected by renewed tectonic subsidence which allowed the deposition of a fault-controlled sedimentary succession (Martín-Chivelet et al., 2019a). This sedimentary succession is thicker in the Maestrazgo, where it is represented by a coal-bearing siliciclastic deposits (Pardo, 1979; Querol, 1990; Rodríguez-López et al., 2009) (Fig. 1.1B).

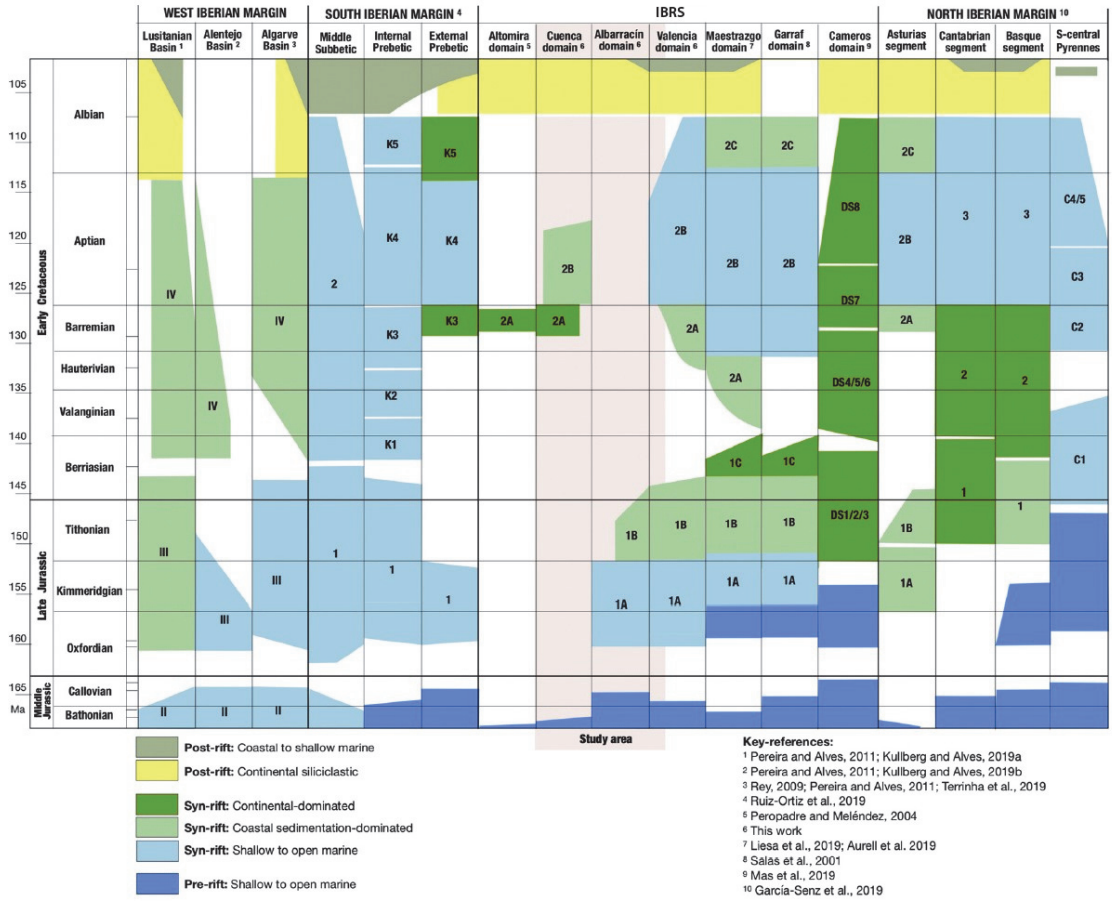

Fig. 1.3. Overall distribution and temporal variabilities of the Late Jurassic to Early Cretaceous syn-rift and the first Albian post-rift units in the different areas of Iberia and their subdomains or basins. In the IBRS the units in yellow colour correspond to the Utrillas Gr. Modified from Aurell et al. (2019).

The early to late Albian times (Fig. 1.2B; Martín-Chivelet et al., 2019a) were characterised by a marked decrease in the tectonic subsidence, which was progressively replaced by thermal subsidence, evincing the end of the second rifting cycle of the IBRS and the onset of the Late Cretaceous post-rift stage (Martín-Chivelet et al., 2019a, 2019b).

4.1.3.4. The Late Cretaceous Passive Margin stage.

During the Late Cretaceous, a passive margin stage with thermal subsidence, dominated by widespread marine carbonate successions, took place in the IBRS (Alonso et al., 1993; Sopeña et al., 2004; Martín-Chivelet et al., 2019b). The Late Cretaceous is characterised by the highest relative sea-level rise of the whole Mesozoic Era (Haq et al., 1988; Handerbol et al., 1998), and consequently, the marine carbonate platform systems reached their maximum landward extension across Iberia (Sopeña et al., 2004; Martín-Chivelet et al., 2019b).

In the IBRS, this passive margin stage is initiated by a transitional stage, which marks the transition from syn-rift into post-rift. The transitional stage is preceded by a stage of extension of the Tethys Ocean which eventually permitted the connection with the Proto-Atlantic realm during the Late Cretaceous (Sopeña et al., 2004; Martín-Chivelet et al., 2019b).

The basal contact and onset of the Late Cretaceous Passive Margin Stage is traditionally interpreted as an intra-Albian major unconformity in the IBRS (Sopeña et al., 2004; Rodríguez-López et al., 2009; Martín-Chivelet et al., 2019a). The Albian sedimentary succession is dominated by alluvial-aeolian sediments that interacted with the coeval shallow marine and transitional environments of the Western Tethys realm (Rodríguez-López, 2008; Rodríguez-López et al., 2009, 2012; Bueno-Cebollada et al., 2021) and it has traditionally been considered as the onset of the post-rift (Sopeña et al., 2004; Martín-Chivelet et al., 2019a, 2019b). The study of this Albian sedimentary succession is the aim of this Ph.D. thesis, and therefore a more detailed literature review of this sedimentary unit will be carried out in the next chapter of this manuscript.

The post-rift stage (or Late Cretaceous passive margin stage) is later characterised by the deposits of thick and widespread shallow marine carbonate successions, overlying the Albian continental to coastal deposits, in most basins of the IBRS (Sopeña et al., 2004; Martín-Chivelet et al., 2019b). These shallow marine carbonate deposits indicate the marine flooding of most areas of the IBRS during most of the Late Cretaceous.

A) Transitional stage:

During the early Albian, there is a generalised relative eustatic fall that affected the basins of the IBRS, giving rise to relative sea-level fall characterised by the increase of the erosional processes and subaerial exposure. The result of these processes is reflected by the large siliciclastic inputs arriving in the IBRS. However, a relative sea-level rise started in the early to middle Albian and lasted until Turonian times, which was eventually characterised by reaching the highest sea levels ever recorded in the Mesozoic Era (Haq et al., 1988). This transitional stage represents the initial transition from the syn-rift into the post-rift succession that will dominate the Upper Cretaceous and can be divided into three transgressive episodes recorded in Iberia (Sopeña et al., 2004).

i) A first transgressive episode, which is mainly recognised in the Prebetic Domain (South Iberian Continental Margin [SICM]). It is characterised by the deposit of a middle Albian limestone-dominated succession (Gimenez et al., 1993), which correlates with the cycle UZA-1.4 (Haq et al., 1988; Sopeña et al., 2004).
ii) A second transgressive episode represented by shallow marine carbonate deposits (Vilas et al., 1982), which are dated as late Albian (Schroeder et al., 1993; Cherchi et al., 1995). During this episode, sedimentation is mainly restricted to those areas with the highest subsidence rates (i.e., Valencia or Maestrazgo Basin). This episode correlates with the cycle UZA-1.5 (Haq et al., 1988; Sopeña et al., 2004). Likewise, a short regressive episode is recorded in the areas with the higher subsidence of the IBRS, which is represented by the deposits of a coastal low-energy succession (Vilas et al., 1982). This short-term regressive episode is related to a sea-level fall recorded between the UZA-1 and UZA-2 sequences of Haq et al. (1988) (Sopeña et al., 2004)
iii) A third transgressive episode represented by shallow marine carbonate deposits during the late Albian (Vilas et al., 1982; Sopeña et al., 2004). During this episode the marine carbonates advanced more landwards than in the two previous episodes, reaching the Cuenca Basin, in the Southern Domain of the IBRS (Meléndez, 1983). Likewise, the syn-sedimentary tectonics becomes progressively less significant along most basins of the IBRS (Sopeña et al 2004 and references therein). Toward the edges of the basin (i.e., Cuenca Basin), the shallow marine carbonates shift laterally into continental to coastal siliciclastic deposits (Meléndez, 1983; Chamizo-Borreguero et al., 2016; Bueno-Cebollada et al., 2021). This episode correlates with the cycle UZA-2.1 of Haq et al. (1988) (Sopeña et al., 2004).

B) Tethys extension and *Proto-Atlantic link stage*:

During the early Cenomanian, a relative eustatic fall took place giving rise to the sedimentation of a coastal succession characterised by the deposit of green marls in the Southern Domain of the IBRS (Vilas et al., 1982; Sopeña et al., 2004). However, by the late early Cenomanian times, a new eustatic rise took place, giving rise to the widespread development of carbonate platforms across the IBRS, due to the landwards expansion of the Western Tethys (Segura et al., 1983; Segura et al., 2004; Sopeña et al., 2004; Martín-Chivelet et al., 2019b). These marine conditions will dominate in the basins of the IBRS during most of the Late Cretaceous.

Likewise, a northward tilting of the Iberian Plate took place from the mid to late Cenomanian onwards, allowing the occurrence of repeated marine incursions from the Proto-Atlantic Ocean, which even permitted the connection between both palaeogeographic domains (Tethyan and Proto-Atlantic) for prolonged periods (Segura et al., 2004; Sopeña et al., 2004; Martín-Chivelet et al., 2019b).

The development of widespread carbonate platforms across the basins of the IBRS since the Cenomanian reflects the development of a new tectono-sedimentary framework at a supra-regional scale, dominated by thermal subsidence and deposition in a passive margin setting (Fig. 1.5.) (i.e., Segura et al., 2004; Sopeña et al., 2004; Martín-Chivelet et al., 2019b).

4.1.3.5. The Cenozoic Alpine Inversion.

The Alpine Orogeny will develop during the Cenozoic, and it will lead to the inversion of the Permian to Mesozoic extensional basins of the IBRS, eventually giving rise to the Iberian Ranges, due to the oncoming movement of the African and Eurasian plates (Sopeña et al., 2004).

From the latest Cretaceous to the Eocene the deformation was mainly transpressional and transmitted from the North Iberian Continental Margin (NICM) into the intraplate areas of Iberia (the IBRS). It affected the continental crust which had been previously thinned owing to the Mesozoic extensional tectonic cycles (Sopeña et al., 2004).

However, from the Eocene onwards, the NICM begins to accumulate all the compressional deformation due to the closer position of the African and Eurasian plates. These processes gave rise to the Pyrenean Orogen, and the subsequent inversion of the Permian-Mesozoic extensional structures of the intraplate areas of Iberia (Sopeña et al., 2004).

4.2. The Cuenca Basin.

4.2.1. The geographical extension of the Cuenca Basin and the Serranía de Cuenca region.

The Serranía de Cuenca is a geographical region in central Eastern Spain, a mountain range formed due to the Cenozoic Alpine inversion of the Mesozoic Iberian Basin, which is mainly located in the province of Cuenca (and Teruel and Guadalajara to a lesser extent).

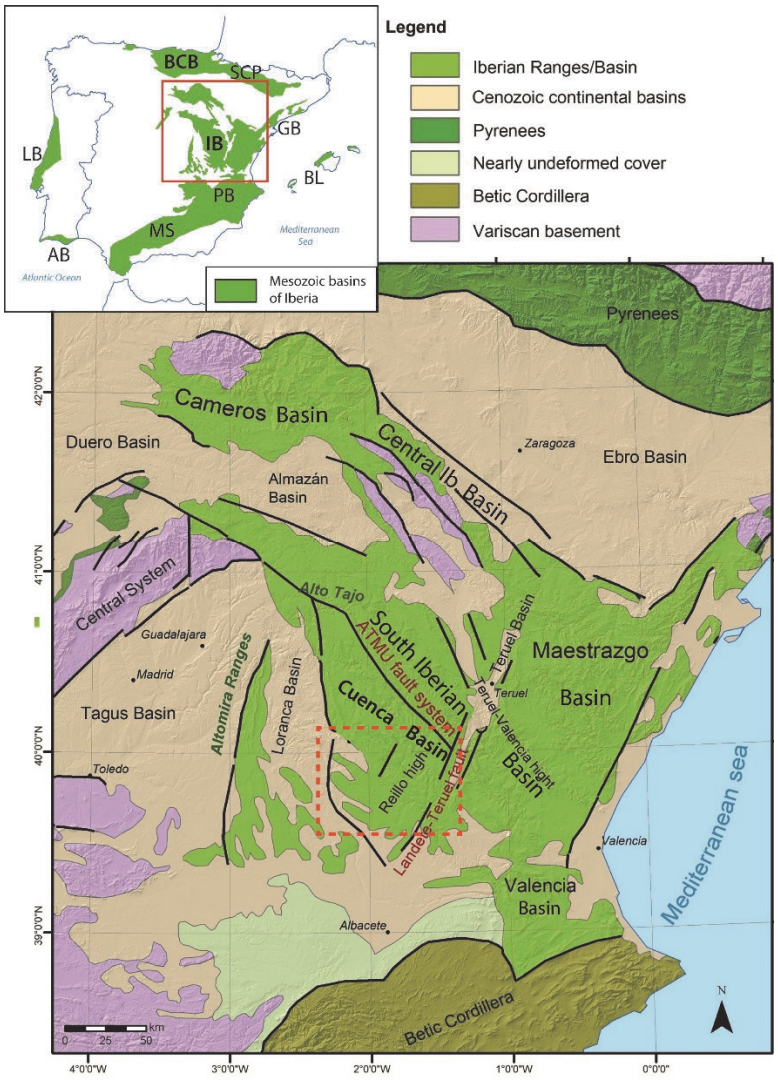

Fig 2.1. Location of the Mesozoic basins of the Iberian Peninsula showing the situation of the Iberian Basin Rift System (IBRS); and close-up of the IBRS indicating the location of the Cuenca Basin and the main tectonic structures bounding the Iberian Basin Rift System. ATMU (Alto Tajo-Montes Universales); BCB (Basque-Cantabrian Basin). The dashed red rectangle indicates the location of the Cuenca Basin, which represents the study area of this work. Modified from Aurell et al. (2019).

The Serranía de Cuenca region, as referred to herein in this work, is included within the Cuenca Basin (previously referred to as the Alto Tajo-Serranía de Cuenca region; Fregenal-Martínez et al. [2017]). In this sense, the Serranía de Cuenca region is here considered as the SE and central sectors of the Cuenca Basin (Fig. 2.1), which represent the main study area of this thesis. Conversely, the study of the most NW/N sector of the Cuenca Basin, referred to as the Alto Tajo region, is not the aim of this thesis, and therefore it has not been studied.

4.2.2. Tectono-sedimentary evolution of the Cuenca Basin during the Early to earliest Late Cretaceous.

The Late Jurassic – Early Cretaceous tectono-sedimentary evolution in the Cuenca Basin was controlled by two main fault systems: the ATMU (Alto Tajo - Montes Universales) Fault and the LT (Landete - Teruel) Fault (Fig. 2.1, 2.2).

- The ATMU Fault is a system of faults broadly oriented NW-SE, which separates the Cuenca Basin (and therefore the Serranía de Cuenca region), to the SW, from the so-called Albarracín Domain to the NE (Aurell et al., 2019).
- The LT Fault is a system of faults characterised by a NE-SW trend that defines the boundary between the Cuenca (to the NW) and Valencia (to the SE) basins.

Additionally, sedimentation was also influenced by associated smaller faults parallel to the ATMU and LT faults that were active during limited time intervals. Some of these smaller faults, particularly those parallel to the LT fault system, acted as palaeo-thresholds limiting the extent and type of sedimentation during the deposit of the Early Cretaceous syn-rift units (Aurell et al., 2019) and the upper Albian post-rift succession.

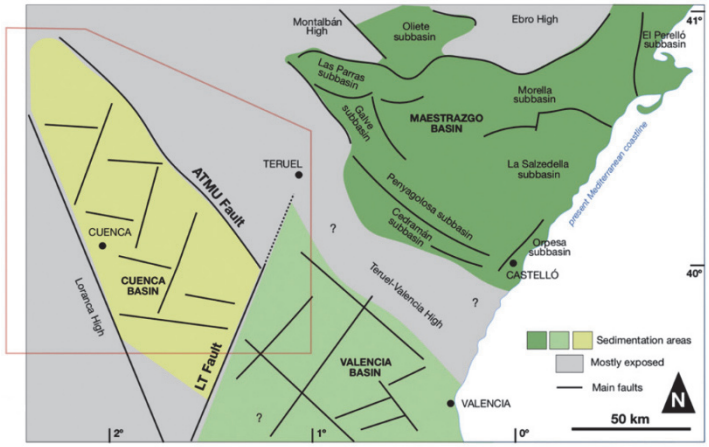

Fig. 2.2. Palaeogeographic reconstruction of the Cuenca, Valencia and Maestrazgo Basins during the Early Cretaceous (late Barremian). The subdivision of the Southern Domain of the IBRS into the Cuenca and Valencia Basins is shown as well as the main structural elements (i.e., ATMU and LT Fault systems). Figure from Aurell et al. (2019).

The Late Jurassic – Early Cretaceous rifting processes created very little accommodation space in the Cuenca Basin until the late Barremian times (Fregenal-Martínez et al., 2017; Aurell et al., 2019). The late Barremian in the Cuenca Basin was characterised by the main set of extensional faults trending N 110° with transfer faults trending NE-SW to N-S (Aurell et al., 2019). The deformation in the Cuenca Basin during the Early Cretaceous was very heterogeneously distributed, both regarding space and time, and is characterised by a reduced accommodation

of the syn-rift and early post-rift successions compared to that of the sedimentary domains developed to SE of the LT Fault System (Valencia Basin) (Aurell et al., 2019).

The late Barremian in the Cuenca Basin was characterised by the deposit of a continental carbonate to siliciclastic succession controlled by syn-sedimentary tectonics (Fregenal-Martínez et al., 2017). Its palaeogeographic and structural configuration largely consisted of small depocentres separated by local highs that generated variabilities in the depositional thicknesses. This configuration is characterised by a complex graben geometry with significant lateral variations at a basinal scale (Fig. 2.2) (Aurell et al., 2019). Likewise, the LT Fault acted as the boundary with the marine-influence area, since the upper Barremian succession in the Cuenca Basin is deposited in fresh-water environments (Fregenal-Martínez et al., 2017; Aurell et al., 2019).

The early Aptian meant a structural rearrangement of the sedimentation area, which was characterised by an increase in siliciclastic input and rising marine influence (Aurell et al., 2019). The Aptian sedimentation was constrained by the ATMU and LT fault systems and took place within a narrow trough bounded by NNW-SSE trending faults and stepped towards the SE by NNE-SSW faults. These faults acted as thresholds and controlled the distribution and extension of the facies belts and the landwards advance of sea level during the transgressive episodes (Meléndez, 1983; Aurell et al., 2019). The LT Fault system limited the maximum NW extension of the Aptian carbonate platforms (Urgonian Platforms), while a structure known as the Reíllo fault (parallel to the LT Fault) limited the NW extension of marine influence in the Cuenca Basin during the early Aptian transgression (Meléndez, 1983; Aurell et al., 2019). Likewise, the ATMU Fault system played a key role, since it marked the limit of the subsiding area to the west of the LT fault (Aurell et al., 2019).

The latest Aptian to late Albian is interpreted as a period of non-deposition and erosion in the Cuenca Basin represented by a regional unconformity (Aurell et al., 2019; Martín-Chivelet et al., 2019a), after which widespread continental siliciclastic sedimentation took place, during the late Albian, reflecting the onset of the post-rift stage (Sopeña, 2004; Martín-Chivelet et al., 2019a-b).

However, the occurrence of syn-sedimentary normal faults during the late Albian in most of the basins of the IBRS (i.e., Cuenca Basin) might have been related to far field stress effect due to the continuation of the rifting in the North Iberian Margin (Cadenas et al., 2018; Aurell et al., 2019). The late Albian initial post-rift is characterised by an enlargement of the sedimentation area compared to the late Barremian – Aptian (Fig. 2 in Aurell et al., 2019), which will lead to

more homogeneous sedimentation dominated by thermal subsidence and the deposit of marine carbonates in the Cuenca Basin during most of the Late Cretaceous.

4.2.3. Aptian to Cenomanian stratigraphy of the Cuenca Basin.

The Aptian in the Cuenca Basin is characterised by an increase in siliciclastic input compared to that of the late Barremian and by a progressively increasing marine influence (Aurell et al., 2019). During this time, two siliciclastic wedges, represented by the Contreras Fm and El Burgal Mb (El Caroch Fm), dominated sedimentation (i.e., Meléndez and López-Gómez, 2003).

The lower Aptian Contreras Fm (Fig. 2.3) (Vilas et al., 1982) is a siliciclastic unit which includes sandstones, mudstones, and conglomerates, and it is interpreted as deposited in alluvial plains (Meléndez, 1983). This unit unconformably overlies the upper Barremian deposits of the La Huerguina and Tragacete Fms (Fig. 2.3) (Meléndez, 1983; Vicente and Martín-Closas, 2013; Fregenal-Martínez et al., 2017). Towards the southeast, the Contreras Fm grades laterally into the Malacara Mb (lower member of the El Caroch Fm) (Vilas et al., 1982), which is a coastal to shallow marine mixed carbonate-siliciclastic unit that crops out in the SE of the Cuenca Basin (Fig. 2.3), and in the Valencia Basin (Meléndez, 1983; Aurell et al., 2019).

The upper Aptian El Burgal Mb (middle member of the El Caroch Fm) (Vilas et al., 1982) in the Cuenca Basin is characterised by (calcareous) sandstones and mudstones, which are interpreted as deposited in coastal plains (Meléndez, 1983; Meléndez and López-Gómez, 2003). The El Burgal Mb (Fig. 2.3) is separated from the underlying Contreras Fm by a sharp ferruginous surface, which reflects a short interruption in sedimentation (Meléndez, 1983; Fregenal-Martinez et al., 2017). Towards the SE, this unit grades laterally into the upper Aptian El Buseo Mb (upper member of the El Caroch Fm) (Vilas et al., 1982) which is a shallow marine carbonate unit well-recorded further to the SE, in the Valencia Basin (Fig. 2.3) (Vilas et al., 1982; Meléndez, 1983; Meléndez and López-Gómez, 2003).

The upper Aptian El Burgal Mb is traditionally considered the last syn-rift unit in the Cuenca Basin, and it is overlain by the deposits of the upper Albian deposits of the Utrillas group (Fig. 2.3) (Meléndez, 1983; Meléndez and López-Gómez, 2003). The base of the Utrillas Gr is considered the end of syn-rift sedimentation in the Cuenca Basin (as well as in most areas of the IBRS), and it is characterised by the occurrence of a widespread unconformity which includes an erosional gap (Meléndez, 1983; Aurell et al., 2019).

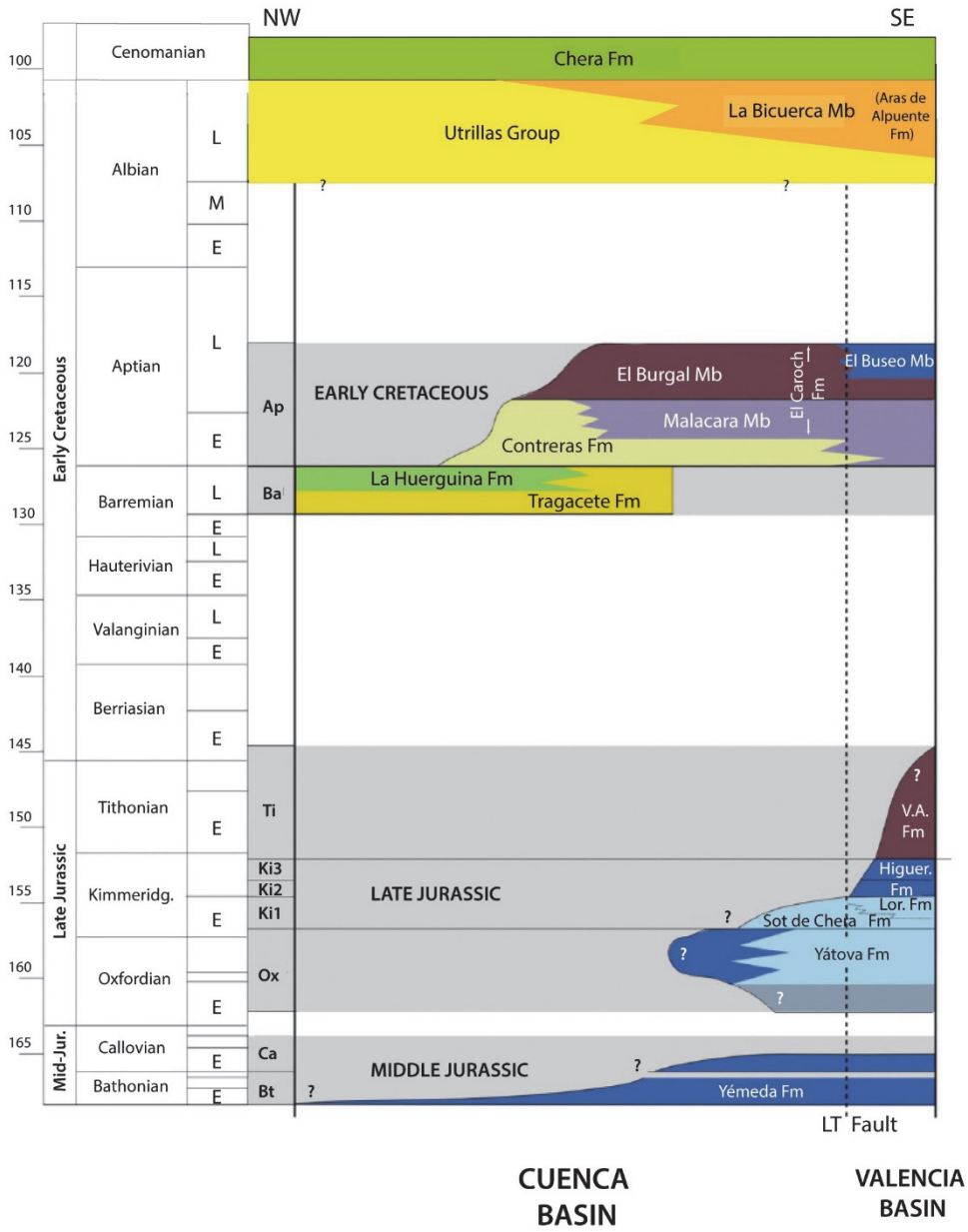

Fig. 2.3. Stratigraphic framework of the Cuenca Basin. After Aurell et al. (2019) and Chamizo-Borreguero et al. (2016).

The Utrillas Gr (Aguilar et al., 1971; Pardo, 1979) is a widespread unit observed across the different basins of the IBRS (Sopeña et al., 2004; Martín-Chivelet et al., 2019 a–b) which was deposited in continental to coastal environments (i.e., Pardo 1979; Pardo and Villena, 1979). Recent research on this unit in the Maestrazgo and Central-Iberian Basins have reinterpreted it as an erg system where aeolian dune facies dominated (i.e., Rodríguez-López, 2008; Rodríguez-López et al., 2008, 2009, 2010, 2012, 2013). This aeolian environments alternated with ephemeral alluvial facies in the proximal areas (back-erg), and with tidally influenced coastal deposits in the most distal areas (fore-erg) (i.e., Rodríguez-López et al., 2008, 2009, 2010, 2012, 2013).

In the Cuenca Basin, the Utrillas Gr has been interpreted as coastal arid braidplain system with local aeolian influence (Chamizo-Borreguero et al., 2016; Bueno-Cebollada and Meléndez, 2018). The Utrillas Gr grades laterally into the mixed carbonate-siliciclastic deposits of the La Bicuerca Mb (Aras de Alpuente Fm) (Vilas et al., 1982), toward the SE in the Cuenca Basin (Meléndez, 1983; Chamizo-Borreguero et al., 2016) (Fig. 2.3). Likewise, the Utrillas Gr succession shows an upwards transition from continental to coastal (tidally influenced) deposits, which, towards the SE of the Cuenca Basin, grade into the shallow marine deposits of the La Bicuerca Mb (Meléndez, 1983; Chamizo-Borreguero et al., 2008). The "sedimentary set" that comprises the Utrillas Gr and La Bicuerca Mb reflects one of the main transgressive pulses that took place in the IBRS because of the rise in sea level that started during the early–middle Albian and culminated during early Turonian times (Giménez et al., 1993; Sopeña et al., 2004).

The Utrillas Gr and La Bicuerca Mb successions are typically overlain by the green marls of the Chera Fm (Vilas et al., 1982), which represents the final marine incursion and homogenization of the basin during the early Cenomanian (Fig. 2.3). This unit is interpreted as deposited in coastal plain systems (Meléndez, 1983), representing a minor relative fall in sea level prior to the eustatic rise that led to the development of carbonate platforms in the Cuenca Basin during the Late Cretaceous. The Chera Fm is overlain by a thick Upper Cretaceous shallow marine carbonate succession in the Cuenca Basin (as well as in most areas of the IBRS), which represents the final instalment of carbonate platforms in the Southern Domain of the IBRS (Sopeña et al., 2004; Segura et al., 2004).

4.3. Biostratigraphy of the Aptian to lower Cenomanian succession of the Cuenca Basin

The Aptian to early Cenomanian time span in the Cuenca Basin is characterised by the deposit of a sedimentary succession that comprises three siliciclastic lithostratigraphic units (or clastic wedges) that were deposited in continental to coastal sedimentary environments: the Contreras Fm, the El Burgal Mb (El Caroch Fm), and the Utrillas Gr (Fig. 2.3). These three lithostratigraphic units grade laterally towards the SE into three mixed-carbonate coastal to marine units, respectively: the Malacara Mb, the El Buseo Mb (El Caroch Fm), and the La Bicuerca Mb (Aras de Alpuente Fm) (Fig. 2.3) (Vilas et al., 1982; Meléndez, 1983; Meléndez and López-Gómez, 2003; Sopeña et al., 2004; Aurell et al., 2019).

The identification, distinction, and dating of these three siliciclastic units have presented significant difficulties since they were initially defined. These difficulties are rooted in the similar

general aspect of the sedimentary facies and composition of the three siliciclastic units, which hampers their correct identification. Likewise, the general lack of fossils (biostratigraphic markers) together with the coarse sandstone-dominated composition (less likely to preserve fossil pollen or spores than mud-dominated successions) in the three units has hindered the possibility of obtaining sound biostratigraphic datings, which has been particularly difficult in the case of the Utrillas Gr. These three siliciclastic units have been dated based on biostratigraphic data collected in their coastal to marine laterally related units, in most cases to the SE of the study area of this thesis, in the Valencia Basin, where the more marine and distal position into the Western Tethys allowed obtaining a sounder biostratigraphic dating.

Early biostratigraphic works in the Valencia Basin suggest either a Barremian (Assens et al., 1973; Viallard, 1973) or early Aptian age (Meléndez, 1974; Ramírez del Pozo et al., 1974; Mas, 1981) for the Malacara Mb based on benthic foraminifera. In the Cuenca Basin, Meléndez (1983) alludes to the complexities of obtaining a sound biostratigraphic age in the strata attributed to the Contreras Fm due to the scarcity of biostratigraphic data. However, this author infers an early Aptian (Bedoulian) age for the laterally equivalent marine deposits of the Malacara Mb in the SE of the Cuenca Basin based on a benthic foraminifera association that includes *Palorbitolina lenticularis*, *Praeorbitolina cormyi*, *Praeorbitolina wiednansi*, *Nautiloculina bronnimanni*, *Choffatella decipiens*, *Pseudocyclamina* sp., and *Sabaudia* sp. Later works, essentially stratigraphic and sedimentological, consider the Contreras Mb as early Aptian age (Salas et al., 2001; Sopeña et al., 2004; Aurell et al., 2019) based on the previously mentioned earlier works and without adding any new biostratigraphic data. Therefore, a biostratigraphic study which allows obtaining a relative stratigraphic age for the deposits of the Contreras Fm in the Cuenca Basin remains to be done.

In the Cuenca Basin, the El Burgal Mb (El Caroch Fm) overlies the Contreras Fm on an unconformable ferruginous surface (Meléndez, 1983; Fregenal-Martínez et al., 2017). In the Valencia Basin, early works (Mas, 1981; Vilas et al., 1982) suggested a late Aptian (Gargasian-Clanseyesian) age for the deposits of the El Burgal Mb based on benthic foraminifera. In the Cuenca Basin, Meléndez (1983) studied a palynological assemblage in the deposits of the El Burgal Mb which included several trilete spores, dinocysts and gymnosperms pollen grains (but it lacked angiosperm pollen grains). That assemblage was dated as late Aptian based on a comparison with an early Albian palynological assemblage collected and studied by Arias and Doubinger (1980) in the sector of Mompichel (Albacete, Spain) in the southern margin of the IBRS. More concretely, Meléndez (1983) interpreted the pollen assemblage collected in the deposits of the El Burgal Mb as late Aptian due to the lack of angiosperm pollen, which is represented in Mompichel by the occurrence of the taxa *Clavatipollenites hughesii*, *C. minutus*,

Liliacidites textus, cf. *Senectotetradites amiantopollis* and *Palmaepollenites* sp. (Arias and Doubinger, 1980). Additionally, Fonolla Ocete and Fernández Marrón (2004) dated a pollen assemblage (dominated by abundant bisaccate pollen grains and trilete spores) from the Cuenca Basin as late Aptian, which was attributed to the El Burgal Mb.

Likewise, Meléndez (1983) dated the more biostratigraphically prolific El Buseo Mb, which represents the seaward lateral shift of facies of the El Burgal Mb, in the surroundings of Graja de Campalbo village, located to the SE of the Landete-Teruel Fault. This author identified a foraminifera association including age-diagnostic taxa such as *Orbitolina subconcava*, *Nautiloculina* sp., and *Pseudocyclamina* sp., which allowed inferring a late Aptian age for the El Buseo Mb.

In the Cuenca Basin, the Utrillas Gr succession remains hitherto understudied in terms of biostratigraphy compared to other areas of the IBRS. In this sense, there is a lack of reliable biostratigraphic data for this unit, as the ages obtained in the Valencia Basin (Vilas et al., 1982) have traditionally been extrapolated to the Cuenca Basin, falling into stratigraphic inaccuracies. Meléndez (1983) tentatively infers an Albian age for the Utrillas Gr deposits in the Cuenca Basin based on the ages of the underlying and overlying stratigraphic units (the El Burgal Mb and Chera Fm, respectively) and the age obtained from the seaward laterally equivalent unit (La Bicuerca Mb). However, she did not include any new biostratigraphic data and pointed out the scarcity of age-diagnostic biostratigraphic taxa in the Utrillas Gr, referring to the unit as "azoic". Notwithstanding, the La Bicuerca Mb has been dated as late Albian to early Cenomanian in the Cuenca Basin based on a foraminiferal association studied by Meléndez (1983), which included: *Orbitolina (Conicorbitolina)* gr. *conica*, *Orbitolina (Orbitolina)* gr. *concava*, *Orbitolina (Orbitolina) duranddelgai*, *Nautiloculina bronnimanni*, *Pseudocyclamina* sp., *Hensonina lenticularis*, *Valvulamina* sp., *Cuneolina* gr. *pavonia-parva*, and *Trocholina arabica*. In this sense, Meléndez (1983) considered that the top of the Utrillas Gr might have reached the base of the Cenomanian stage in the northwest areas of the Cuenca Basin, whilst the base of the Utrillas Gr is a regional-scale unconformity representing a hiatus between the Upper Aptian strata (El Burgal Mb) and the basal deposits of the Utrillas Gr. Consequently, both Aptian units (Contreras Fm and El Burgal Mb) crop out discontinuously throughout the Cuenca Basin (Aurell et al., 2019). This hiatus is thought to include (at least) the lower Albian strata (Meléndez, 1983; Meléndez and López-Gómez, 2003), but a more complete biostratigraphic study needs to be done in order to unravel the length of the time-span not represented by sediments at the base of the Utrillas Gr.

The Utrillas Gr - La Bicuerca Mb succession is overlain by green marls of the Chera Fm in the Cuenca Basin, which has been dated as early Cenomanian in age based on the occurrence of

Orbitolina (Conicorbitolina) gr. *conica*, *and Trocholina Arabica*, suggesting an age not younger than early Cenomanian for the Utrillas Gr and La Bicuerca Mb (Meléndez, 1983).

4.4. The "mid" – Cretaceous issue.

The Cretaceous period (d´Omalius d´Halloy, 1822) is the longest period of the Mesozoic Era and the Phanerozoic Eon, lasting for approximately 80 Myr (~ 145 – 66 Myr). The current subdivision of the Cretaceous system includes two series: Lower and Upper Cretaceous (Cohen et al., 2021). The current consensus about the scope of the Lower/Early and Upper/Late Cretaceous, adopted by the International Commission on Stratigraphy (IUGS), is that they spanned from Berriasian to Albian and Cenomanian to Maastrichtian, respectively (Cohen et al., 2021).

However, several early and current authors advocate for a three-fold division of the Cretaceous period (Bengtson and Kakabadze, 2018 and references therein), which would include a "middle"/"mid"-Cretaceous series, although the term has not been officially approved yet by the International Commission on Stratigraphy (IUGS). To date, there is no agreement about the boundaries and extension of the "mid"-Cretaceous since some authors consider that it may include the Barremian to Santonian time-interval (Föllmi, 1989), whilst others only include the Cenomanian (Bandy, 1967), to mention the most extreme examples.

The chronostratigraphic divisions are closely related to palaeontological turnover events recorded in the rock record. In the Cretaceous chronostratigraphy, the most important group is the ammonites (Bengtson and Kakabadze, 2018). The main causes triggering turnover events in ammonites are environmental changes related to tectonism, eustasy, and climate change. Among them, these turnover events are mainly taking place during major transgressive periods.

In this sense, Bengtson and Kakabadze (2018) studied the major ammonite turnover events of the base Barremian to base Santonian time span (an interval that covers the concept of "mid"-Cretaceous of most authors) trying to establish the first steps for a new proposal to define the "mid"- Cretaceous series, aiming at a three-fold subdivision of the Cretaceous system. The most pronounced ammonite turnover event identified by these authors occurred at the Aptian-Albian boundary, being the best candidate to establish the base of the "mid"-Cretaceous (Bengtson and Kakabadze, 2018). A potential upper boundary for the "mid"-Cretaceous can be placed at the Cenomanian-Turonian boundary, despite the ammonite turnover event was not as intense as at that of the Aptian-Albian boundary, since it coincides with an oceanic anoxic event (OAE 2) and mass extinction (Bengtson and Kakabadze, 2018).

Although there is not a formal proposal for the “mid”-Cretaceous series, this thesis manuscript will adopt hereinafter the term “mid”-Cretaceous *sensu* Bengtson and Kakabadze (2018) written with a lowercase letter and always including quotation marks. Therefore, the term “mid”-Cretaceous has been used in the present manuscript for those strata deposited during the time interval that spanned from the Aptian-Albian boundary to the Cenomanian-Turonian boundary. Consequently, those Cretaceous strata deposited earlier than the Aptian-Albian boundary or after the Cenomanian-Turonian boundary will be considered as Lower/Early Cretaceous or Upper/Late Cretaceous, respectively, and the words *Lower* and *Upper* will be written with an uppercase letter.

5. Outcrop descriptions.

As it is mentioned in chapter 4 of this manuscript, the sedimentary record of the Albian to lower Cenomanian succession in the Cuenca Basin corresponds to the Utrillas Gr and its progressive transition into the shallow marine mixed deposits of the La Bicuerca Mb (Aras de Alpuente Fm) (Meléndez, 1983). The Utrillas Gr- La Bicuerca Mb succession ends in the green marls of the Chera Fm (Vilas et al., 1982; Meléndez, 1983; Sopeña et al., 2004), a well-known and easily recognisable feature in most of the outcrops of the Cuenca Basin whose base represents the top of the studied strata in this thesis as well as a reliable datum for correlation.

However, the Lower Cretaceous sedimentary record of siliciclastic rocks in the Cuenca Basin includes two Aptian stratigraphic units, the Contreras Fm and the El Burgal Mb (Vilas et al., 1982; Meléndez, 1983), that can be difficult to distinguish from the Utrillas Gr strata at first glance. In this sense, the logged sedimentary sections of this Ph.D. thesis may include the Aptian strata (that overlay the Barremian deposits of the La Huerguina and Tragacete Fms (Fregenal-Martínez et al., 2017; Aurell et al., 2019) in those outcrops where their succession crops out in order to identify the lower boundary of the Utrillas Gr succession. Similarly, palynological samples have been collected and studied where possible (i.e., the Mina Pepita and Buenache de la Sierra outcrops), aiming at determining the base of the Utrillas Gr (Bueno-Cebollada et al., 2021). In those outcrops where sediments were not suitable for palynological sampling (i.e., lack of dark mudstone layers and predominance of barren coarse-grained sandstones), the main (lithostratigraphic) criteria for identifying the base of the Utrillas Gr is the occurrence of a distinct laterally traceable major erosional surface. This surface is heavily cemented with iron oxides, may contain quartzite pebbles and cobbles, and represents an unconformity that separates the Aptian units from the Albian strata of the Utrillas Gr in the Cuenca Basin (Meléndez, 1983). Additionally, another characteristic feature that may help in the identification of this unconformity is the occurrence of deposits with tidal signatures (i.e., the presence of double mud drapes or herringbone-like cross-bedding, attributed to the El Burgal Mb) right below the surface, and the development of an expansive coarse-grained sandstone alluvial succession with abundant pebble-cobble deposits interbedded immediately overlying the surface (attributed to the Utrillas Gr).

Consequently, the siliciclastic strata overlying the Barremian deposits of the La Huerguina and Tragacete Fms were logged during the first fieldwork stages of this Ph.D. thesis, which in some sections include either part or the whole extent of the two Aptian units. The main purpose of including Aptian strata has been the identification of the base of the Utrillas Gr-La Bicuerca Mb as well as obtaining a more complete record of the Albian to lower Cenomanian succession.

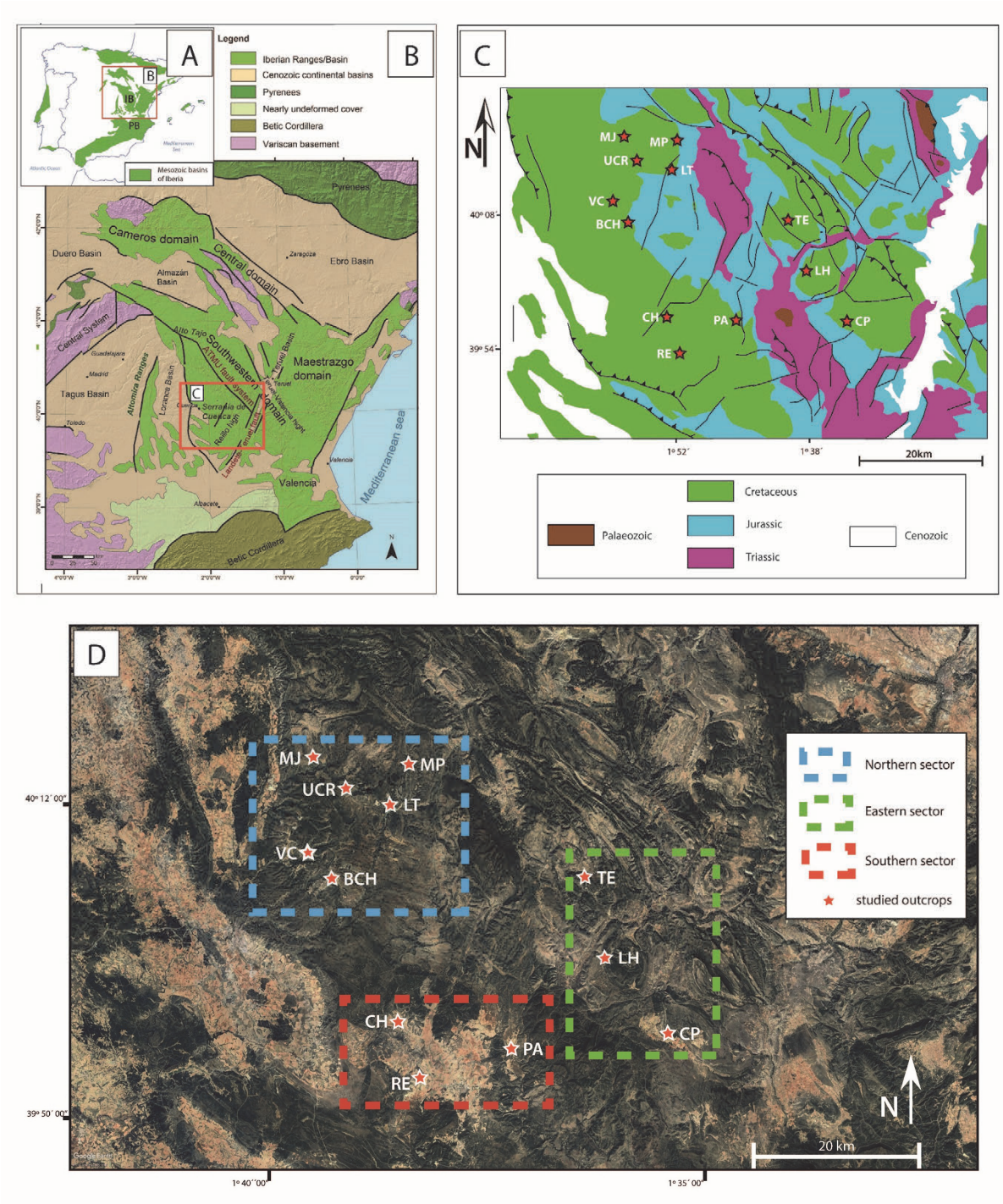

Fig. 5.1. (A-B) Location of the Mesozoic outcrops in the Iberian Peninsula, showing the situation of the Iberian Basin (IB); and close-up of the Iberian Basin/Ranges indicating the main sedimentary domains as well as the main tectonic structures bounding the Iberian Basin. ATMU (Alto Tajo-Montes Universales); BCB (Basque-Cantabrian Basin). Modified from Fregenal-Martinez et al. (2017) and Aurell et al. (2019). (C) Simplified geological map of the study area, where the sampled locations are indicated. Modified from Bueno-Cebollada et al. (2021). (D) Satellite map with the location of the 12 logged outcrops in the Cuenca Basin. The logged outcrops have been grouped into three geographical sectors (Northern, Eastern, and Southern sectors, respectively) highlighted with different colours. Image source: Google Earth. The location of the logged outcrops in C and D is pinpointed with a red star followed by the abbreviated name of the outcrop (MJ: Las Majadas; MP: Mina Pepita, UCR: Uña; LT: La Toba; VC: Valdecabras; BCH: Buenache de la Sierra; TE: Tejadillos; LH: La Huérguina; CP: Campillos-Paravientos; CH: Cañada del Hoyo; PA: Pajaroncillo; RE: Reíllo).

However, it is important to lay on the table that the study of the Aptian is not among the aims of this Ph.D. thesis, and as such their study in terms of sedimentology has not been included in this thesis.

Overall, this work includes the study of 12 Albian to lower Cenomanian outcrops located across the Serranía de Cuenca region (Cuenca Basin), corresponding to the Utrillas and La Bicuerca Mb succession, where at least one sedimentary section has been logged in each of the outcrops. The legend of symbols for the logged sections is included in Appendix IV (A).

The 12 studied outcrops have been grouped into 3 geographical sectors (Northern, Southern, and Eastern) that cover the whole study area of this thesis in the Cuenca Basin (Fig. 5.1):

- The Northern sector comprises six outcrops: the Buenache de la Sierra, Valdecabras, Uña, La Toba, Mina Pepita, and Las Majadas outcrops.
- The Eastern sector comprises three outcrops: the Campillos-Paravientos, La Huérguina and Tejadillos outcrops.
- The Southern sector includes three outcrops: the Reíllo, Pajaroncillo, and Cañada de Hoyo outcrops.

The following pages include the complete description and figures of the logged section(s) from each of the 12 studied outcrops. It also includes an explanation of the outcrops and figures with the exact location of the logged sections along with a succinct mapping of the Utrillas Gr-La Bicuerca Mb deposits at the outcrop scale.

5.1. Northern sector

5.1.1 Buenache de la Sierra outcrop.

The Buenache de la Sierra outcrop is located in the surroundings of the Buenache de la Sierra Village (40° 8′ 8″ N, 2° 0′ 3″ W; Cuenca Province, Spain). Overall, five uncomplete sedimentary sections have been logged in the several adjacent ravines in this location (Fig. 5.2).

In the study area, the Utrillas Gr overlies unconformably upper Aptian strata belonging to the El Burgal Mb (Fig. 5.2) (see chapter 6 in this manuscript) (Bueno-Cebollada et al., 2021), which in turn overlay lower Aptian, Barremian and Jurassic strata.

Likewise, the Utrillas is overlain by Upper Cretaceous deposits attributed to the green marls of the Cenomanian Chera Fm, which are in turn overlain by marine carbonate units (Fig. 5.2). In

this regard, the contact between the Utrillas Gr and the Chera Fm is observed towards the top of the studied ravines and represents the top surface of the studied sections as well as the datum for correlation.

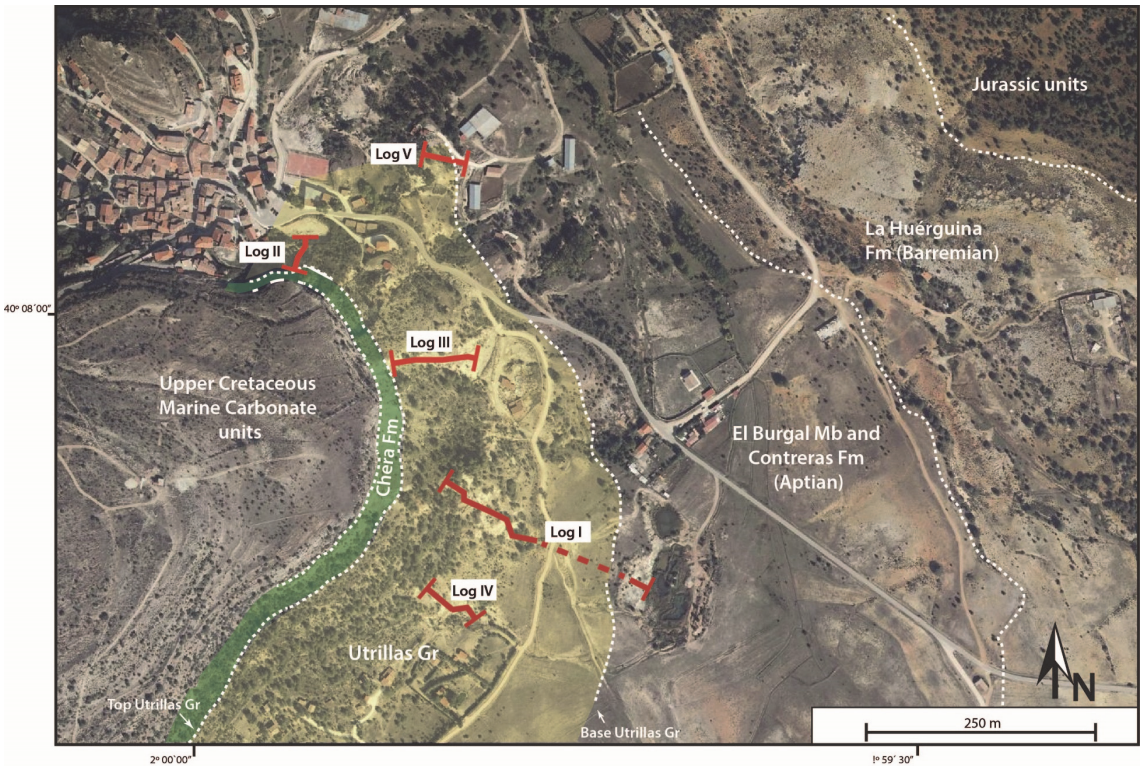

Fig. 5.2. Satellite image corresponding to the studied outcrop in Buenache de la Sierra. The extension of the Utrillas Gr succession, as well as that of the underlying and overlying stratigraphic units, has been drawn. The location and extension of the five logged sections (logs I to V) are also included (red lines). A correlation among the five logged sections is included in Appendix IV. Image source: Google Earth.

As previously mentioned, five partial sedimentary sections have been logged, due to the relatively good preservation of the outcrop, aiming at obtaining a better comprehension of its peculiarities as well as a better understanding of the horizontal distribution and stacking patterns of the sedimentary bodies. Besides a synthetic full logged section has been drawn, based on the partial studied sections, covering the full extent of the Utrillas Gr in the area (Fig. 5.3). The base of the composite logged section corresponds with the contact between the El Burgal Mb and the Utrillas Gr, while the top of the logged section (and datum for correlation) is the contact between the Utrillas Gr and the Chera Fm.

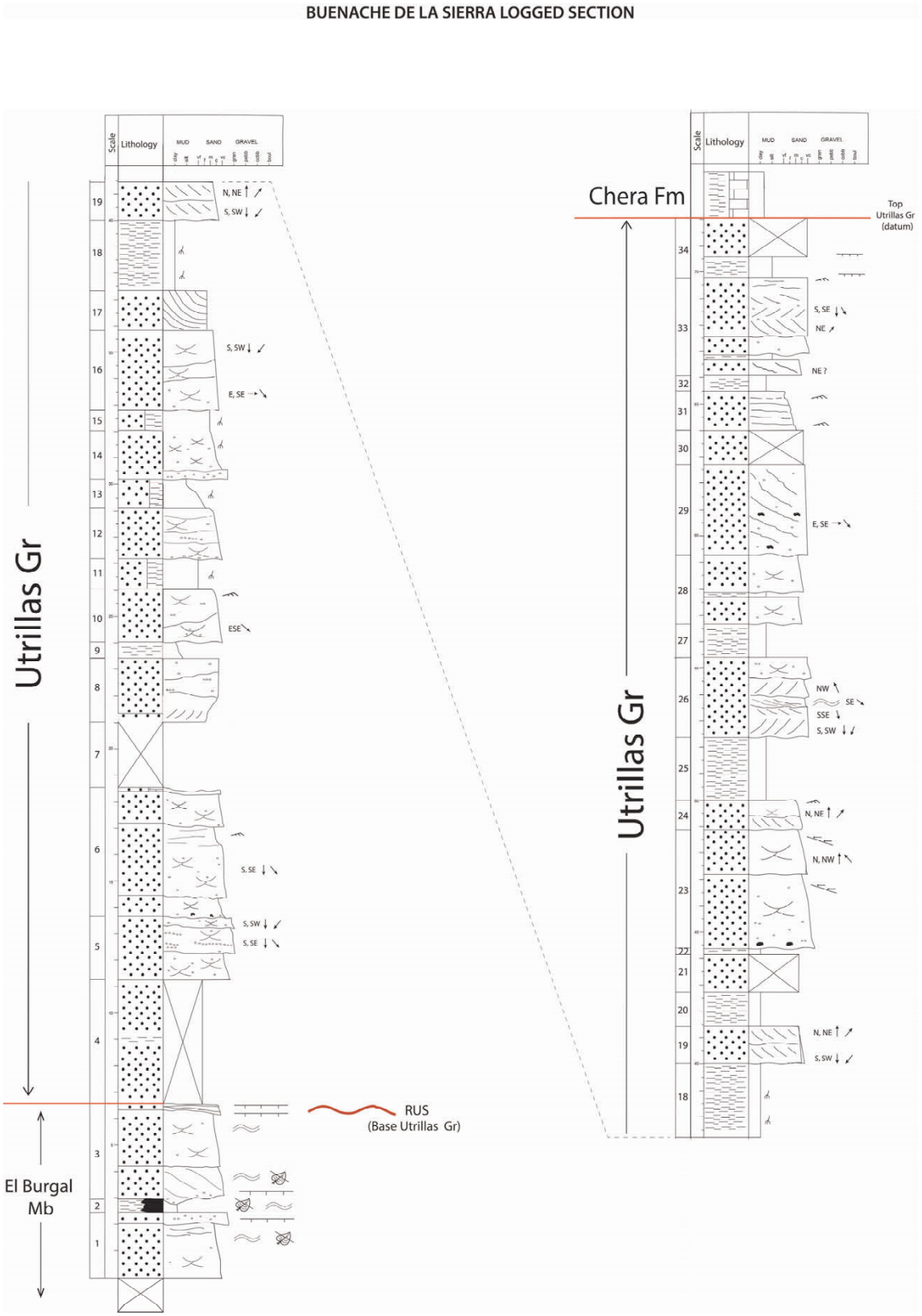

Fig. 5.3. Logged section at the Buenache de la Sierra outcrop. The explanation of the graphic symbols is included in appendix IV (A).

Description of the composite logged section (Figs. 5.3, 5.4, 5.5)**.**

The composite section drawn in the Buenache de la Sierra outcrop is a 72 m-thick section in which the intervals 1 - 7 correspond to section V, the intervals 8 – 24 correspond to logged section I, and the intervals 25 – 34 correspond to the logged section III (Fig. 5.3; Appendix IV).

Interval 1 (2.5 m): It consists of a coarse- to very coarse-grained sandstone body which shows trough cross-bedding, flaser to wavy heterolithic laminations and includes some scattered oxidised vegetal remains. The top of the interval is a gravel-grained size bed including pebbles and a ferruginous surface.

Interval 2 (0.4 m): Lignite to coaly shales with abundant plant fragments and, locally, pyrite framboids. This lignite-rich thin interval presents some sandy lenses and wavy laminations and crops out irregularly across the outcrop.

Interval 3 (3.6 m): It consists of coarse- to very coarse-grained sandstones showing a thinning upwards trend. The base is erosional and includes some scattered pebbles as well as plant remains and iron oxides. In general, and especially towards the base of the interval the bodies present an internal arrangement showing lateral accretion and amalgamation, depicting heterolithic wavy and flaser laminations (Fig. 5.4). The top of the interval is an erosional surface rich in iron oxides which can be laterally traced for a few meters across the outcrop, depending on the exposure conditions (Figs. 5.5A).

Fig. 5.4. Outcrop view of the lowermost levels of the logged succession at the Buenache de la Sierra outcrop, attributed to the El Burgal Mb, where two productive palynological samples have been collected. (A) Panoramic view of El Burgal Mb succession in the Buenache de La Sierra outcrop. The red dots in the picture represent the beds that were sampled in Buenache de la Sierra for palynological purposes. The blue backpack for scale to the left of the picture is 50 cm-long. (B) Lateral accretion channel observed towards the left-hand side of the picture. (C) The productive pollen samples studied in the Buenache de La Sierra outcrop were collected from several dark mudstone levels. Hammer for scale in (B) and (C) is 35 cm-long.

Interval 4 (5 m): Partly covered interval mostly composed of coarse-grained sandstones.

Interval 5 (2.3 m): It consists of very coarse-grained to gravel-grained arkose sandstones arranged into amalgamated bodies with lenticular morphologies which may extend laterally for more than 10 m. These bodies present sedimentary structures which comprise abundant internal scours, trough and planar cross-bedding, and abundant pebbles and cobbles (sizes are 3 to 4 cm in diameter on average, locally reaching up to 10 cm), both as scattered clasts and as matrix-supported accumulations. These pebble-cobble/sand accumulations may form planar and trough cross-bedded sets with imbricated clasts, unstratified beds, or one-pebble-thick laterally persistent flat surfaces creating lags. However, the bodies are dominated by trough and planar cross-bedded sets characterised by very coarse sandstones which show palaeocurrent directions that suggest bedform migration towards the S/SE, and occasionally towards the S/SW. The lenticular bodies present a slight fining upwards trend and irregular erosional base which "cannibalize" the underlying body (Fig. 5.5B).

Interval 6 (4.8 m): This interval consists of coarse- to very coarse-grained fining upwards arkose sandstone bodies, displaying lenticular shapes and erosive basal contacts. These bodies commonly present trough cross-bedded sets with palaeocurrents directions towards S/SE. Pebbles and cobbles are abundant, but in a lower proportion than in interval 5, and tend to be found as scattered clasts rather than producing matrix-supported accumulations. Towards the base of some of the bodies mud pebbles and cobbles (average diameter size of 4 – 5 cm) can be observed usually associated with their erosional bases, along with scattered quartzite pebbles and cobbles. These bodies, when duly preserved, tend to reduce the size of their sedimentary structures coupled with the grain size upwards, presenting current ripples in their upper part. The uppermost body is overlain by a 10 cm-thick irregular surface consisting of coarse-grained size sandstone cemented with calcite.

Interval 7 (~2.5 m): Fully covered.

Interval 8 (2.3 m): It consists medium- to (very) coarse-grained sandstone body depicting a coarsening upwards trend and dm-thick sets of planar cross-bedding. The body shows scattered pebbles and internal erosional scours.

Interval 9 (0.6 m): Reddish to purple mudstones to siltstones with minor yellowish mottling.

Interval 10 (2 m): This interval comprises a very coarse- to coarse-grained arkose sandstone body which presents an internal scour and is dominated by trough cross-bedding suggesting bedform migration towards ESE. Likewise, the body includes scattered pebbles (ranging from 2 - 3 cm in diameter on average). The body shows a fining upwards trend and presents current ripples towards its top. The lower contact is erosional, while the upper one is a flat non-erosional surface.

Interval 11 (1 m): Mudstone to siltstone with minor proportions of scattered sandstone grains, showing yellowish to reddish colours with mild mottling and poorly developed root traces. The transition from the underlying sandstone body into this interval is a sudden and abrupt one and it is represented by a sharp contact.

Interval 12 (2 m): The interval consists of a coarse- to very coarse-grained lenticular sandstone body which contains numerous internal scours and an erosional base. The sedimentary structures observed are dm-thick sets of trough cross-bedding and pebble lags. Towards the top of the interval, the size of the bedforms diminishes dramatically and cm-scale current ripple structures are observed (Fig. 5.3).

Interval 13 (1.1 m): Mudstone to siltstone with some scattered sand-sized grains towards the base, which displays a sharp non-erosional surface. This interval shows a poorly developed reddish mottling including traces of small roots and rootlets with some iron oxides which shift downwards in the interval into

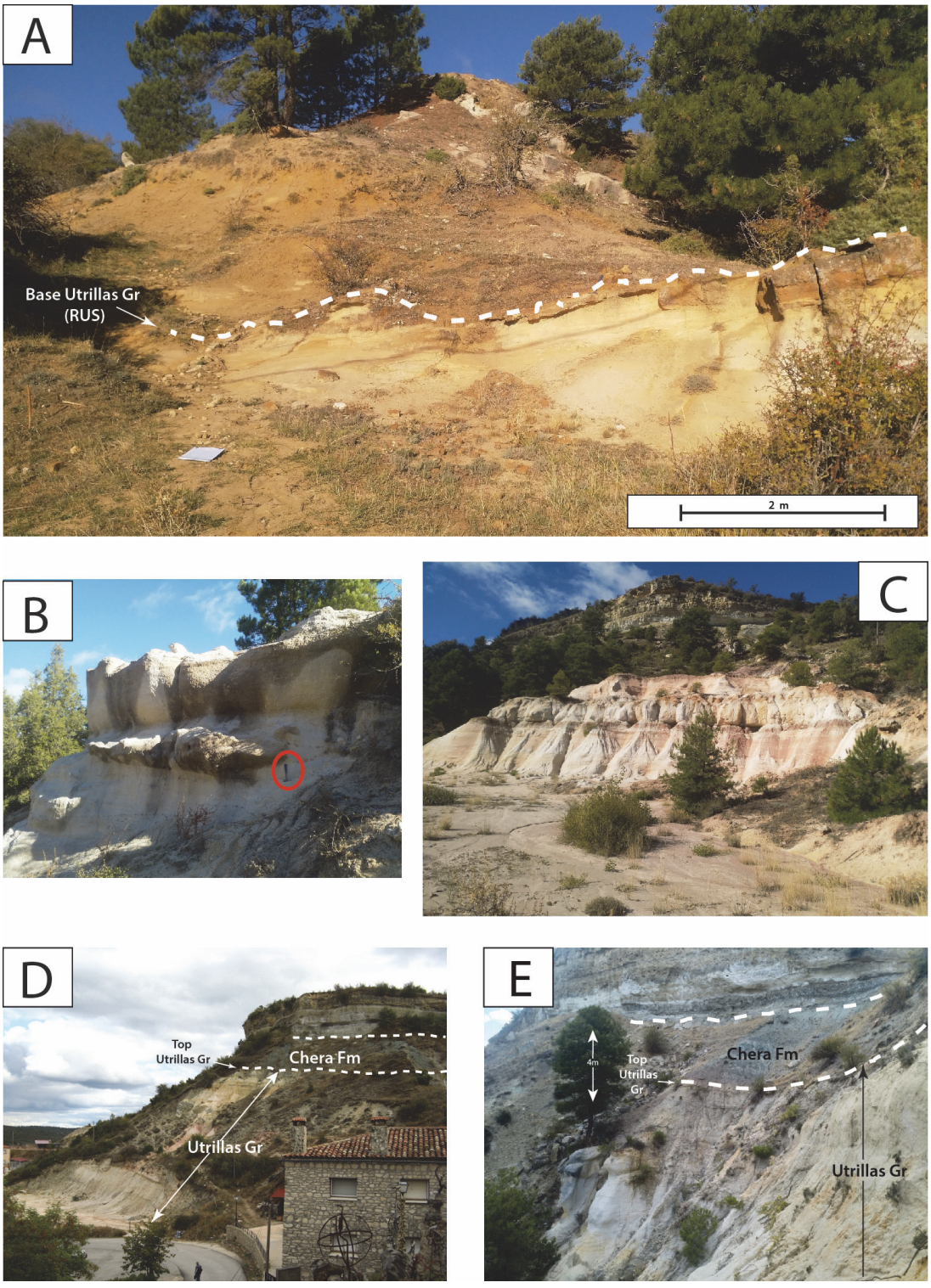

Fig. 5.5. (A) Contact between the El Burgal Mb (below) and the Utrillas Gr (above) at the base of the logged section V in the Buenache de la Sierra outcrop. The regional unconformity surface (RUS) that represents the base of the Utrillas group is highlighted by a white dotted line. (B) Amalgamated alluvial channels (FA I: Proximal alluvial) in the logged section V. Hammer for scale is 35 cm-long. (C) Alluvial channels overlain by rooted floodplain mudstones (FA II) and aeolian dunes interbedded (FA III) in the logged section III of the Buenache de la Sierra outcrop. (D) General view of the logged section II in the Buenache de la Sierra outcrop. The top surface of the Utrillas Gr and the green marls of the Chera formation overlying the sedimentary succession can be observed. (E) Close-up of the top surface of the Utrillas Gr and the overlying Chera Fm in the logged section III of the Buenache de la Sierra outcrop.

greyish-yellow mudstones and mottling with an increasing proportion of sand-size grains towards the base of the interval.

Interval 14 (2 m): It consists of a very coarse-grained lenticular arkose sandstone body displaying an erosional base, in which the lowermost 50 cm consist of gravel-size deposits including scattered (quartzite and mud) pebbles, pebble lags, and mud flakes. The sandstone body is dominated by abundant cm-thick trough cross-bedded sets, being the main sedimentary structure observed. In addition, this interval is heavily "bioturbated" by root traces, which taper downwards from the overlying interval (15) (Fig. 5.3). The root traces are cemented by iron oxides producing a dark reddish colour which contrasts with the "non-bioturbated" white sandstone.

Interval 15 (0.8 m): It comprises a very fine-grained sandstone and siltstone /claystone tabular body, showing abundant root traces which branch downwards, penetrating the underlying sandstone interval. Towards the upper part of this interval, a dark reddish colour can be noticed due to the cementation by iron oxides. Similarly, some iron nodules may be observed. However, downwards in this interval, the root traces branch and the iron oxide cementation remain mostly within them, producing a reddish mottled appearance. The lower contact of this interval is a sharp non-erosional one, despite the root traces taking place as a continuous feature between intervals 15 and 14 (Fig. 5.3).

Interval 16 (3 m): Coarse- to very coarse-grained arkose sandstone arranged into lenticular-shaped bodies commonly displaying internal scours and an erosive base, where scattered pebbles (less than 4 cm in diameter on average) may occur. Regarding sedimentary structures, this interval is dominated by dm-scale trough cross-bedding showing palaeocurrent directions ranging from E/SE to S.

Interval 17 (1.5 m): It consists of very well-sorted, homometric, medium-fine grained sandstones arranged into a tabular body. The body shows tangential cross-strata separated by several internal non-erosional surfaces displaying a hierarchical relationship among them. The base of this body is a flat non-erosional surface that mantles the underlying deposits. This sandstone body extends laterally for about 200 m, having been logged only in sections 1 and 3, and decreasing in thickness southwards (Appendix IV).

Interval 18 (2.6 m): Reddish mudstone and siltstone with yellowish to white mottling and moderate presence of root traces resembling the ones observed in intervals 15 and 14, although, less developed. The body displays a tabular shape with a flat base.

Interval 19 (1.4 m): Coarse-grained sandstone body displaying current bipolarity (herring bone-like cross-bedded sets) (Fig. 5.3), where the main palaeocurrent directions measured in two superimposed sets of cross-bedded strata are towards S/SW and N/NE, respectively.

Interval 20 (1.3 m): Partly covered interval consisting of reddish mudstones.

Interval 21 (1.4 m): Partly covered interval consisting of coarse-grained sandstone.

Interval 22 (0.4 m): It consists of grey to whitish mudstones with slight yellow-ochre mottling.

Interval 23 (4.5 m): Very coarse- to gravel-grained size sandstone arranged into laterally continuous tabular bodies showing large scale (foresets > 2 m) trough cross-bedded sets. Such cross-bedded strata essentially migrate in a N/NW direction, yet they are characterised by the presence of current ripples reworking the lee side of the main foresets in an opposite direction (SSE) to the main palaeocurrent direction measured (Fig. 5.3). Likewise, the bodies exhibit a highly erosive base that carves into the underlying mudstone deposits. Additionally, mud pebbles and cobbles (between 3 to 5 cm in diameter on average) and mud flakes can be observed in the

lower part of the interval in association with the erosional base (between 3 to 5 cm in diameter on average), as well as some scattered quartzite pebbles.

Interval 24 (1.2 m): Coarse- to very coarse-grained sandstone body displaying a lenticular shape and erosional base which cuts the deposits of the underlying interval. Regarding sedimentary structures, the body is dominated by dm-scale trough and planar cross-bedded sets which towards the top of the interval diminish in size and give way to current ripples. Measured palaeocurrents in this interval indicate a NNE bedform migration.

Interval 25 (2.4 m): Grey to light brown siltstones to mudstones which are massive in appearance, lacking any sedimentary structure.

Interval 26 (3 m): It consists of coarse- to very coarse-grained arkose sandstones arranged into two lenticular bodies with erosional base and a fining upwards trend. The first body is 2.2 m-thick and dominated by herringbone-like beddings and, locally, structures resembling mudstone bundles. Locally, the measured palaeocurrents indicate alternation between cross-bedded sets migrating towards the NW and S, SE and SW. The second body presents an erosional surface that erodes the former body. It shows a coarser grain size and poorer sorting, along with the occurrence of scattered pebble, and it is dominated by trough cross-bedding showing bedform migration towards SE.

Interval 27 (1.3 m): Light grey to brownish siltstones and mudstones arranged into a tabular body. Massive bedding and lacking any observable sedimentary structures.

Interval 28 (2.6 m): It consists of coarse- to very coarse-grained poorly sorted sandstone arranged in two fining upwards lenticular bodies with erosional bases, which are separated by a 10 cm-thick siltstone layer. Both bodies present dm-scale trough cross-bedding and scattered quartzite pebbles.

Interval 29 (3.4 m): The interval consists of a coarse- to very coarse-grained sandstone body with an erosional base and the presence of quartzite pebbles and abundant mudstone cobbles, which are more common towards the base. The body is lenticular in shape and may extend laterally for more than 80 metres. Regarding sedimentary structures, it is dominated by large-scale trough cross-bedding migrating toward the SE/S which are reworked by small asymmetrical ripples that migrate in an opposite direction (Fig. 5.3).

Interval 30 (1.3 m): Partly covered. Coarse-grained sandstone.

Interval 31 (1.5 m): It comprises medium- to fine-grained sandstones arranged into 40 to 10 cm-thick tabular layers separated by flat non-erosional surfaces which frequently show current (asymmetrical) ripples. The overall trend observed among the layers of this interval is a fining upwards one.

Interval 32 (0.5 m): Reddish-purple to yellowish mudstones with mottling. The base of this interval is dominated by yellow mudstones while the upper part consists of dark reddish ones. The transition between both mudstones is a diffuse contact, indicating a gradual transition.

Interval 33 (3.7 m): The interval consists of coarse- to very coarse-grained sandstones arranged into fining upwards lenticular bodies with erosional bases. The bodies display herringbone-like cross-bedding indicating the occurrence of foresets migrating to the S/SE and NE. Current ripples may be observed towards the top of the channelised bodies. Likewise, the upper contact of this interval is non-erosional and overlain by a ferruginous surface (Fig. 5.3).

Interval 34 (2.4 m): This interval consists of 0.7 m of grey to greenish (non-calcareous) mudstones, tabular in shape which lay on top of the ferruginous surface describe at the top of the previous interval (33). This mudstone layer is sharply overlain by a partly-covered

1.7 m-thick sandstone bed which presents bioturbation, minor ferruginous surfaces, and oxidised vegetal fragments. This sandy bed can be followed laterally for several tens of metres across the outcrop. However, the partially covered nature and the steepness of the slope of the outcrop in this interval do not allow for more accurate sedimentological observations. This interval is sharply (non-erosionally) overlain by a green marl succession attributed to the Cenomanian Chera Fm (Figs. 5.5D, E), which represents the top contact of the logged section as well as its datum for correlation.

5.1.2 Valdecabras outcrop.

The Valdecabras outcrop is located about 400 m to the ENE from Valdecabras village, Cuenca Province, Spain (Fig. 5.6). The logged section (coordinates: 40° 09´ 38", 2° 01´ 50") is located in a hill that is capped by the Upper Cretaceous marine carbonate succession (del Olmo Zamora, 1986). The logged section is approximately 36.5 m-thick and comprises a sedimentary succession that shows a horizontal to sub-horizontal dip. It consists of coarse-grained sandstones that alternate with reddish mudstones and siltstones lying below a 10 m-thick succession consisting of green marls, which in turn is overlain by the Upper Cretaceous marine carbonate succession.

Fig. 5.6. Satellite image corresponding to the studied outcrop in Valdecabras. The extension of the Utrillas Gr succession, as well as that of the overlying Chera Fm, have been mapped and coloured. The location and extension of the logged section are also included (red line). Image source: Google Earth.

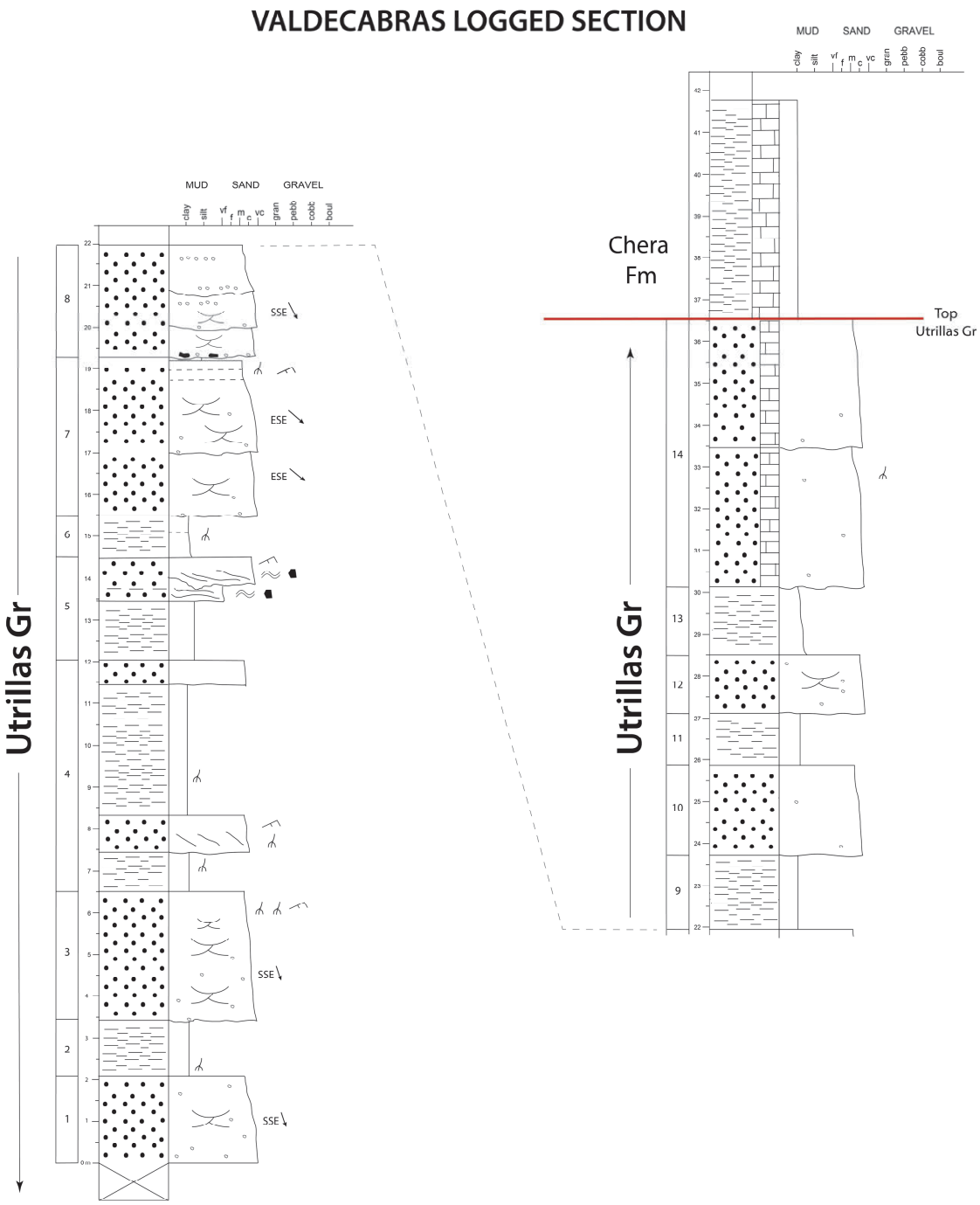

Fig. 5.7. Logged section at the Valdecabras outcrop. The explanation of the graphic symbols is included in appendix IV (A).

The logged section in the Valdecabras outcrop begins in the first sandstone bed at the bottom of the hill (Fig. 5.6) since the lowermost part of the Utrillas Gr succession is covered in the outcrop.

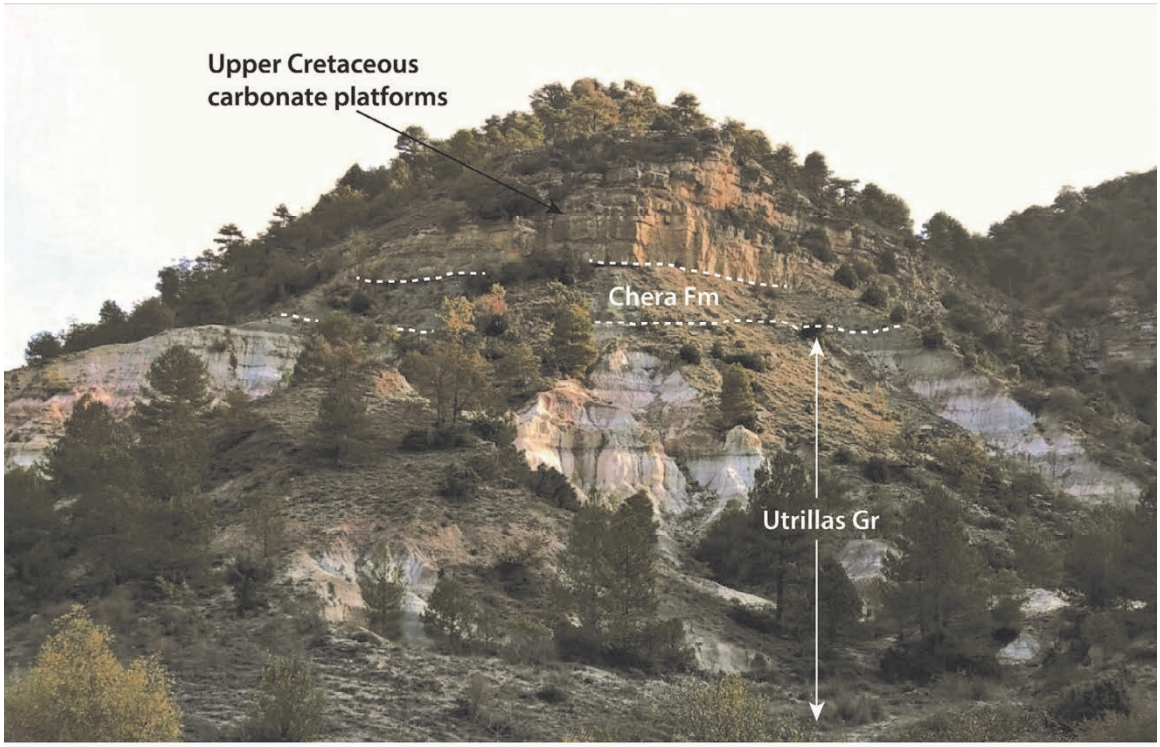

Fig. 5.8. General view of the logged ravine at the Valdecabras outcrop. The Utrillas Gr and the overlying units are interpreted. For scale, the thickness of the Chera Fm is approximately 10 m.

Description of the logged section (Fig. 5.7):

(Beginning at the bottom of the hill [Fig. 5.8])

Interval 1 (2 m): This interval consists of poorly sorted whitish coarse- to very coarse-grained sandstones arranged in a thinning upwards body. It presents scattered pebble-sized clasts (the pebbles range from 3 to 5 cm in diameter) with subangular morphologies. The main sedimentary structure observed is trough cross-bedding arranged in 30 cm-thick sets. The base of this interval is covered.

Interval 2 (1.3 m): This bed consists of reddish oxidised mudstone and siltstones, with scattered sand-sized particles, showing a massive appearance. Locally, and mainly towards the top, the mudstones may present root traces. The base of this interval is a flat, sharp, and non-erosional contact.

Interval 3 (3.6 m): The interval is composed of coarse- to very coarse-grained sandstones arranged into a fining upwards body. It presents an erosional contact at its base and scarce pebbles (about 4 cm in diameter on average). The main sedimentary structure observed is trough cross-bedding which is arranged in 30 cm-thick sets. As grain size decreases upwards in the interval, the size of the trough cross-bedding diminishes. The uppermost part of the interval presents current ripples and moderate development of root traces. The measured palaeocurrents indicate an SSE migration of the bedforms.

Interval 4 (5.5 m): This interval consists of an alternation of reddish mudstone-siltstones and medium- to coarse-grained sandstones. The lower layers of the interval comprise approximately 0.9 m

consisting of reddish mudstone with root traces overlain by a 0.7 m-thick poorly sorted sandstone body with erosional base, planar cross-bedding and root traces. The upper part of this interval consists mostly of 3.2 m of massive red mudstones with root traces at its base that are overlain by 0.6 m-thick poorly sorted sandstone bed.

Interval 5 (2.4 m): This interval consists of greyish to dark mudstones and siltstones which are overlain by a 50-70 cm-thick sandstone body. Towards the base, the mudstones show a massive appearance. However, upwards they are dominated by heterolithic wavy beddings, fusinite/charcoalified wood and coal fragments (smaller than 1 cm). The upper part of this interval consists of a 50-70 cm-thick medium-grained sandstone body with an erosional base, planar cross-bedding, coaly drapes and current ripples toward its top. This upper sandstone body shows a fining upwards trend and scattered coal and fusinite fragments (Fig. 5.7).

Interval 6 (1 m): It consists of reddish to grey mudstones and siltstones with a flat, sharp, and non-erosional base. The lower part of this interval comprises massive red oxidised mudstones with faint root traces, while the upper part consists of grey mudstones.

Interval 7 (3.8 m): It consists of coarse- to very coarse-grained sandstones arranged in two fining upwards sedimentary bodies with erosional bases. The bodies present cm- to dm-scale trough cross-bedding and scattered pebbles towards the base. The uppermost body is characterised by showing root traces and current ripple structures in its upper part. The measured palaeocurrents in both sedimentary bodies indicate an ESE migration of the bedforms.

Interval 8 (2.8 m): This Interval comprises a coarse- to very coarse-grained sandstone body composed of up to three smaller sandstone bodies separated by internal erosional scours. The bodies are dominated by cm-scale trough cross-bedding indicating an SSE transport direction. The lowermost body shows a pebble lag at its base, which includes abundant mud pebbles and cobbles. The upper bodies commonly show pebble lags, forming one-pebble-thick flat surfaces that extend laterally for a few metres.

Interval 9 (2.8 m): This interval is characterised by reddish mudstones and siltstones with yellowish mottling. No root traces have been observed.

Interval 10 (2.5 m): The interval consists of a coarse- to very coarse-grained sandstone body. It shows a fining upwards trend and erosional base. Locally, it may present scattered pebbles. It lacks sedimentary structures such as cross-bedding due to the poor preservation of the outcrop in this part of the succession.

Interval 11 (1.3 m): It consists of oxidised massive reddish mudstone and siltstone with yellowish mottling, in which no root traces have been observed.

Interval 12 (1.4 m): This interval comprises a coarse- to very coarse-grained sandstone body. It depicts a fining upwards trend and an erosional base. Locally, it presents scattered pebbles (3-4 cm in diameter on average). The only sedimentary structure identified is trough cross-bedding organised in cm-scale sets. However, the poor preservation of the outcrop in this part of the succession does not allow for measuring palaeocurrents.

Interval 13 (1.7 m): It consists of massive reddish mudstone and siltstone with yellowish mottling. No root traces are observed.

Interval 14 (6.4 m): This interval consists of slightly calcareous coarse-grained sandstones arranged in two fining upwards bodies with erosional bases. Scattered pebbles and root traces have locally been observed. Additionally, bivalve shell fragments may locally be observed. The steepness of the outcrop at this interval, along with its poor preservation, does not allow for the identification of any sedimentary structures or measuring the palaeocurrents (Fig. 5.7).

The previously described siliciclastic sedimentary succession (intervals 1 to 14) is sharply overlain with a flat non-erosional contact by a 10 m-thick sedimentary succession dominated by green marls with thin (10 to 30 cm) carbonate layers interbedded. These marls are overlain by a thick carbonate succession that tops the hill where the Valdecabras section has been logged (Fig. 5.8).

5.1.3. Uña outcrop.

The Uña outcrop is located approximately 600 m to the North of the Uña village on the slope of a hill (Fig. 5.9). The studied succession in the Uña outcrop is attributed to the Utrillas Gr based on the palynological assemblages identified. A complete description of the palynological samples collected in the Uña outcrop (UCR - 5 and UCR - 6) is included in the biostratigraphy and palynology chapters of this Ph.D. thesis manuscript, and in Bueno-Cebollada et al. (2021) (Appendix II).

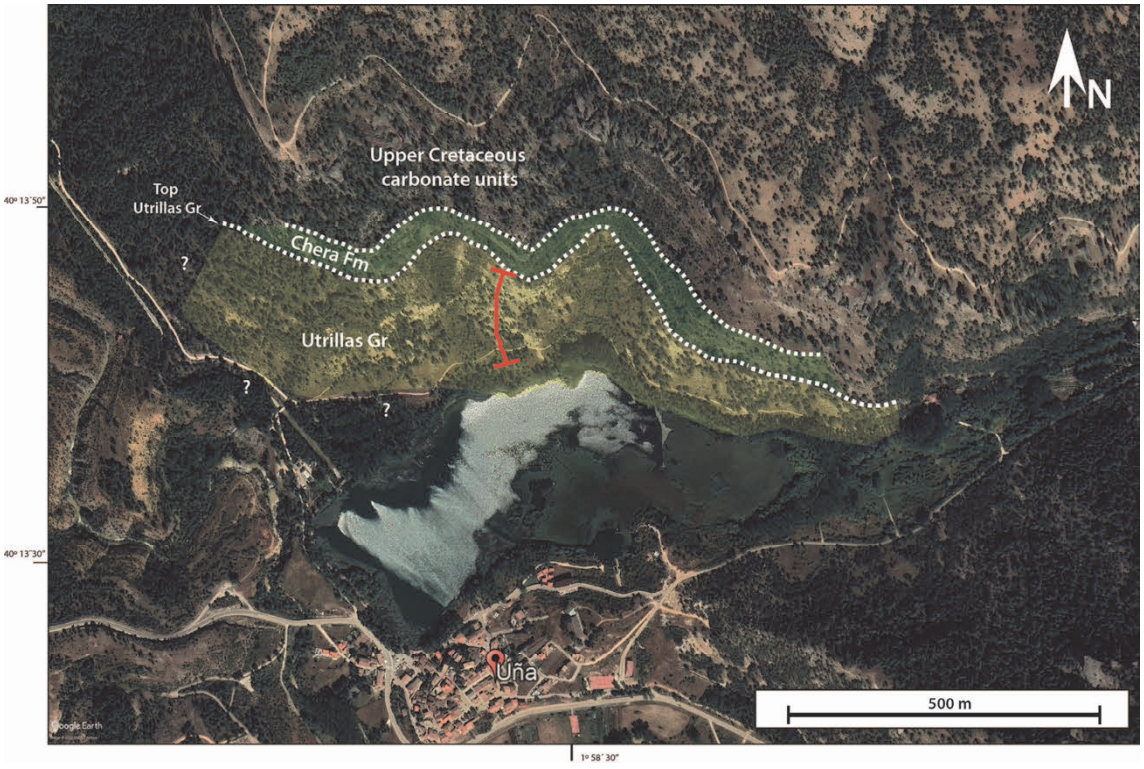

Fig. 5.9. Satellite image corresponding to the studied outcrop in Uña. The extension and location of the logged section are also represented in the picture (red line). The contact between Utrillas Gr and the Upper Cretaceous units (including the Chera Fm) has been drawn. Image source: Google Earth.

The Utrillas Gr sedimentary succession in the Uña outcrop was initially studied by Chamizo-Borreguero et al. (2016) who carried out a local facies analysis and correlation of several adjacents logged sections in the outcrop. In this thesis, the logged sections presented by

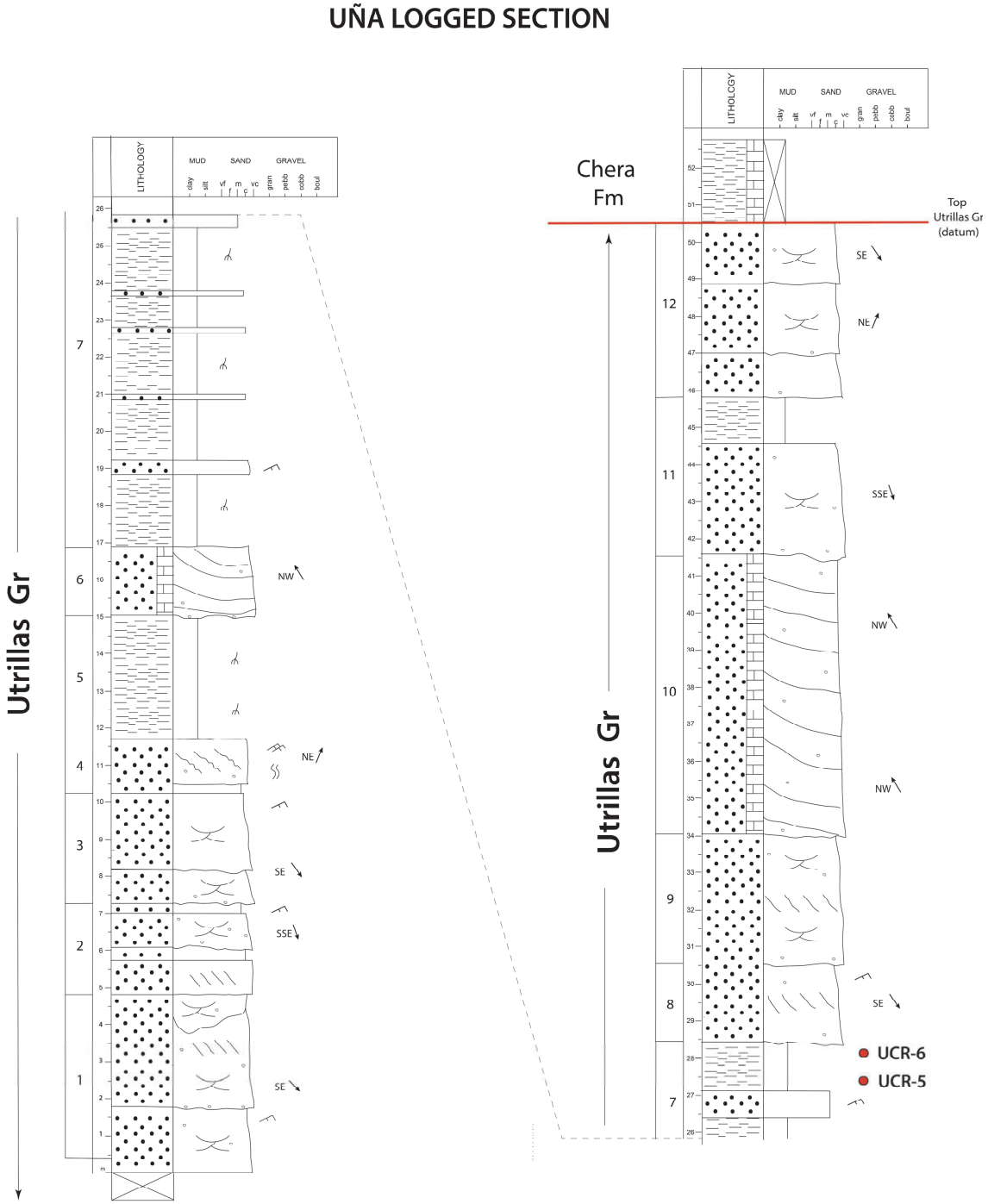

Fig. 5.10. Logged section at the Uña outcrop. The explanation of the graphic symbols is included in appendix IV (A).

Chamizo-Borreguero et al. (2016) have been revisited, and a ~50 m-thick composite logged section (Fig. 5.10) of the Uña outcrop has been constructed aiming at correlation purposes. Although partially covered, the upper contact of the logged succession is the top of the Utrillas Gr and is overlain by the Cenomanian Chera Fm and the Upper Cretaceous marine carbonate

units (Chamizo-Borreguero et al., 2016; Bueno-Cebollada et al., 2021). However, the lowermost strata of the Utrillas Gr succession are covered, and therefore its lower contact remains elusive in this location. Additionally, the Uña outcrop has also been revisited in sedimentological terms and facies analysis in this thesis.

Fig. 5.11. General view of the Uña outcrop with the top of the Utrillas Gr indicated by a dashed red line. The thickness of the Utrillas Gr succession, as indicated in the image, is approximately 50 metres. Photo courtesy of N. Meléndez.

The following pages include the complete description of the logged section in the Uña outcrop included in this thesis (Fig. 5.10).

Description of the logged section (Figs. 5.10, 5.11)

Interval 1 (4.7 m): This interval consists of coarse- to very coarse-grained sandstone arranged into two to three fining upward lenticular bodies with an erosional base. The bodies present 20 to 30 cm-thick sets of trough cross-bedding and include internal erosional scours and scattered quartzite pebbles, including faceted clasts. The base of the bodies may show pebble lags. The measured palaeocurrents indicate that bedform migration is towards the SE

Interval 2 (2.3 m): The interval consists of coarse- to very coarse-grained sandstones lithologically arranged in several bodies less than 1 m in thickness that show erosional bases. They present planar and trough cross-bedding describing 20 to 30 cm-thick

sets that migrate towards the SSE. Similarly, asymmetrical current ripples have also been observed.

Interval 3 (2.8 m): It comprises two coarse- to very coarse-grained sandstone bodies with lenticular, fining upwards trend, and an erosional base that may present lags of quartzite pebbles. The main sedimentary structure observed is trough cross-bedding arranged in sets similar to those of interval 1 along with local current ripples that are normally found in the upper part of the bodies. The measured palaeocurrents are toward the SE.

Interval 4 (1.9 m): It consists of medium- to coarse-grained sandstones arranged into a laterally continuous tabular body. The body is dominated by dm-scale planar cross-bedding that may present slightly deformed foresets migrating in a NE direction. Likewise, the body may present climbing ripples. Bioturbation is typically moderate to intense and consists of poorly preserved arenicolites-like trace fossils.

Interval 5 (3.3 m): Massive grey mudstones and, to a lesser extent, siltstones that are arranged into a laterally continuous tabular body. The present a scant reddish mottling that resembles poorly developed root traces.

Interval 6 (1.8 m): It consists of coarse-grained sandstones slightly cemented with calcite that present tangential tabular beds with low-angle planar bedding with transport directions to the NW. The body presents internal reactivation surfaces and an erosional base and fills a significant incision of the underlying deposits (Fig. 5.10).

Interval 7 (11.5 m): This interval comprises a lower part (8.5 m) dominated by massive red mudstones and siltstones with yellow mottling and root traces that alternate with subordinated thin (0.4 to 0.1 m-thick) layers of medium-grain sandstone with current ripples. Conversely, the upper part (3 m) of the interval is characterised by greyish mudstones with lenticular heterolithic lamination that alternate with medium-grained sandstone layers with mudstone bundles and wavy bedding. The upper part of this interval includes the beds where the samples UCR-5 and UCR-6 were collected (Bueno-Cebollada et al., 2021), which are described in the biostratigraphy and palynology chapters of this thesis manuscript.

Interval 8 (2.1 m): It consists of a coarse- to very coarse-grained sandstone body arranged with planar cross-bedded sets that show rhythmical alternations in grain size and bedform migration towards the SE.

Interval 9 (3.4 m): Coarse- to very coarse-grained sandstones arranged into a fining upwards body with internal scours and an erosional base. It comprises 20 to m-thick sets of trough and planar cross-bedding migrating toward the SSE that may present rhythmical alternations in the size of their foresets.

Interval 10 (7.6 m): It consists of coarse-grained slightly calcareous sandstones arranged into a lenticular body with an erosional base that forms a deep incision (reaching up to 9 m in depth in some areas of the outcrop) that erodes the underlying sandstone deposits. The sandstone body is arranged into tangential tabular beds with low-angle planar bedding and large-scale trough cross-bedding. Palaeocurrents indicate a NW transport direction, similar to those described in interval 6 of the logged section (Fig. 5.10). Laterally, the incision at the base of this interval may erode the strata of intervals 8 and 9. Therefore, in this case, the strata of interval 10 may directly overlie interval 7.

Interval 11 (4.2 m): This interval consists of a 2 to 2.5 m-thick coarse- to very coarse-grained sandstone body with an erosional base that carves into the strata of interval 10. The sandstone presents through cross-bedding with sets migrating toward the SSE and rhythmical alternations in the grain size of the foresets. The sandstone body is overlain by 1 to 1.5 m with greyish mudstones with mild mottling, which do not show root traces.

Interval 12 (4.7 m): It comprises three amalgamated coarse- to very coarse-grained sandstone bodies that show an erosional base and fining upwards trend. The sandstones present trough cross-bedding with palaeocurrents indicating transport directions toward the NE and SE. The foresets may show rhythmical alternations in the grain size.

The top of interval 12 represents the top of the Utrillas Gr and, therefore, it is the top of the logged section, which is overlain by a partially covered calcareous muddy succession attributed to the Cenomanian Chera Fm.

5.1.4. La Toba outcrop.

The La Toba outcrop is located on the road from the Uña village to the Huélamo village (km nº 41 of the CM – 2105 road), Cuenca Province, Spain (Fig. 5.12).

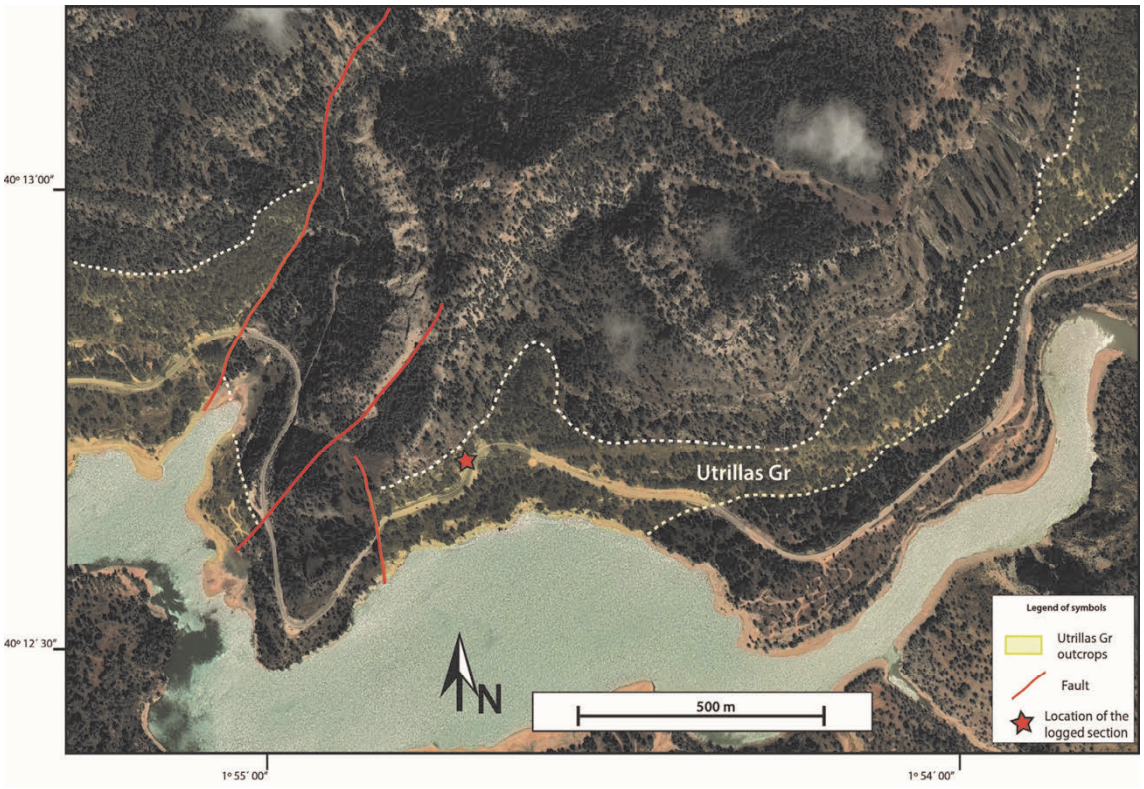

Fig. 5.12. Satellite image corresponding to the Utrillas Gr deposits in La Toba. The outcrops of the Utrillas Gr succession have been highlighted in yellow colour and yellow dotted lines. Several faults have also been detected to the west of the study area. The position of the studied outcrop, where the section is logged, is indicated by a red star. Image source: Google Earth.

The Utrillas Gr succession is covered in the La Toba outcrop but for the few meters logged in the section (Fig. 5.13) and some isolated outcropping areas (to the east of the logged section, following the road shoulder) (Fig. 5.12). Conversely, the area immediately to the west of the logged section has not been considered for the sedimentary analysis since it has been affected by an NNE-SSW trending fault system (Ramírez Merino, 1986) (Fig. 5.12).

The logged succession in the La Toba outcrop crops out on the shoulder of the CM-2105 road and it is a 6.6 m-thick partial section (Fig. 5.12, 5.13). However, this logged section has been very helpful in terms of biostratigraphy since four productive palynological samples (LT - 1, LT - 2, LT - 3, and LT - 4) have been collected in it and attributed to the Utrillas Gr based on the palynological assemblages studied by Bueno-Cebollada et al. (2021). The description of the palynological assemblages identified in the samples from La Toba is included in chapters 6 and 7 of this thesis manuscript (Appendix II).

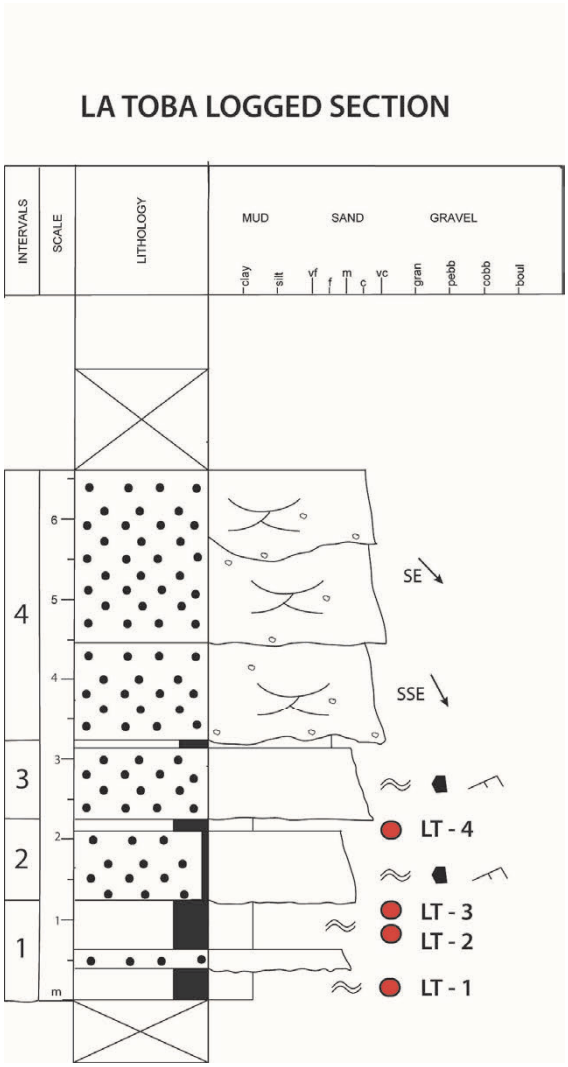

Fig. 5.13. Logged section in the La Toba outcrop. The explanation of the graphic symbols is included in appendix IV (A).

The lower part of the logged section (intervals 1 to 3; Fig. 5.13) consists of an alternation of coaly mudstones with wavy bedding interbedded with coarse- to medium-grained sandstones that may show coaly bundles and cementation by iron oxides. Conversely, the upper part of the logged section (interval 4; Fig. 5.13) is dominated by coarse- to very coarse-grained whitish to ochre arkose sandstones that are arranged into lenticular bodies with erosional base and internal erosional scours.

Description of the logged section (Fig. 5.13**).**

Interval 1 (1.25 m): This interval consists of grey mudstones/siltstones to coaly mudstones/siltstones that may present a thin (20 cm-thick) layer of medium-grained sandstone interbedded. The sandstone is cemented by iron oxides and presents wavy lamination. The palynological samples LT – 1, LT – 2, and LT – 3 were collected toward the base of this interval (Fig. 5.13).

Interval 2 (1 m): The interval is dominated by medium- to coarse-grained sandstones cemented by iron oxides and including coaly bundles, wavy lamination, and current ripples. The sandstones are arranged into a sigmoidal body that is laterally amalgamated with similar sigmoidal bodies. The sandstone body is overlain by an approximately 10 to 20 cm-thick layer of coaly mudstone in which the palynological sample LT – 4 was collected (Fig. 5.13).

Interval 3 (0.9 m): It consists of coarse-grained sandstones cemented by iron oxides which present coaly bundles, current ripples, and wavy heterolithic lamination. The bodies are fining upwards, laterally amalgamated, and show sigmoidal shapes. The sandstones are overlain by a thin layer of coaly mudstones.

Interval 4 (3.4 m): This interval consists of coarse- to very coarse-grained arkose sandstone arranged into 1 to 1.5 m-thick lenticular bodies. The bodies are amalgamated, showing a fining upwards trend and erosional bases, along with internal erosional scours. Regarding sedimentary structures, they present trough cross-bedding arranged into 40 to 50 cm-thick sets. The top of interval 4 represents the top of the logged section in La Toba as the overlying strata of the studied sedimentary succession are fully covered.

5.1.5. Mina Pepita outcrop.

The Mina Pepita outcrop is located approximately 8 km to the east of the Uña Village, Cuenca Spain (Fig. 5.14). The logged section is an 81 m-thick succession located on the hillside of a large hill (“Muela de Uña”), dipping horizontally to sub-horizontally. The base of the logged section is located at 40° 14´ 47”; 1° 53´ 12” and its top is located at 40° 14´ 51”; 1° 53´ 19”. The logged succession includes the siliciclastic strata that overlie the Barremian deposits of the La Huérguina Fm and is overlain by the green marls of the Chera Fm and Upper Cretaceous marine carbonate units (Ramírez Merino, 1986) (Fig. 5.14).

The logged section is mainly dominated by sandstones (and conglomerates). However, the lower intervals of the section comprise coaly layers in which five palynological samples (MP-I-2, MP-I-3, MP-II-1, MP-II-2, and MP-II-3) were collected (Figs. 5.15, 5.16A). Conversely, the uppermost part of the succession, although mostly covered, is dominated by relatively finer-grained sandstones and calcareous sandstones.

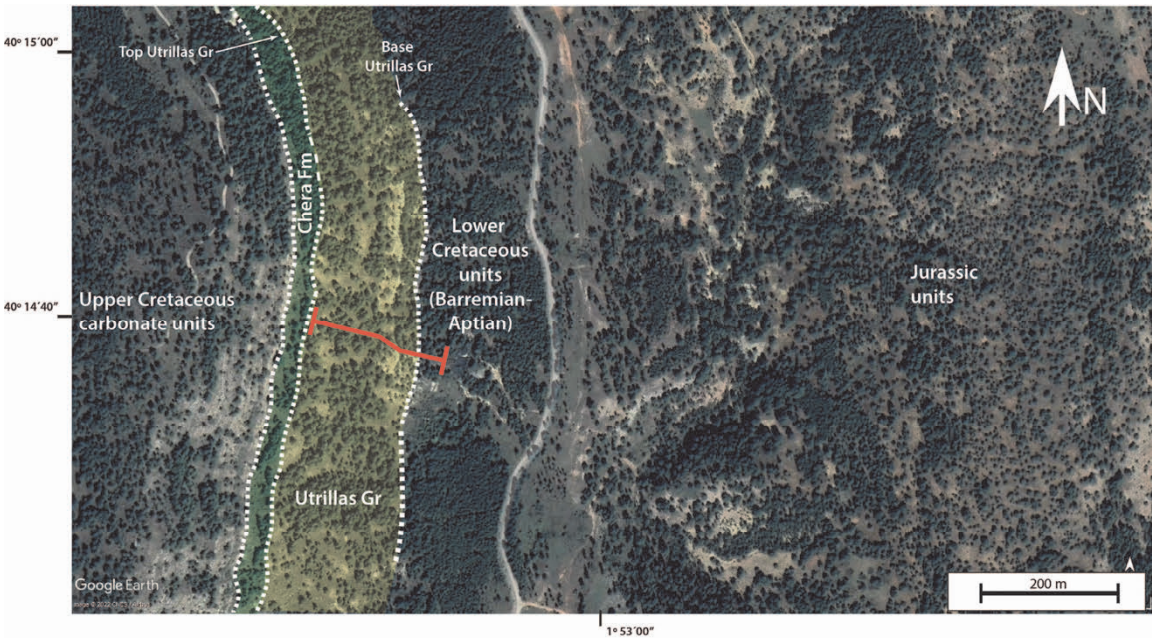

Fig. 5.14. Satellite image corresponding to the studied outcrop in Mina Pepita. The extension of the Utrillas Gr succession, as well as that of the underlying and overlying stratigraphic units, has been drawn. The location and extension of the logged section are also included (red line). Image source: Google Earth.

Description of the logged section (Figs. 5.15, 5.16, 5.17):

Interval 1 (1 m): The interval consists of medium-grained sandstones arranged in 30 to 40 cm-thick bodies with sharp bases. These bodies start on top of the entrance of the mine of Mina Pepita.

Interval 2 (0.5 m): Covered.

Interval 3 (2.1 m): It consists of lenticular sandstone bodies with erosional bases which are interspersed among mudstone and coaly mudstones. The coaly mudstones present coal layers (lignite), where the pollen samples, corresponding to the Mina Pepita outcrop, studied in this thesis were collected (Fig. 5.15, 5.16A, D) (samples MP-I-2, MP-I-3, MP-II-1, MP-II-2, and MP-II-3).

Interval 4 (0.7 m): This interval consists of a conglomerate bed composed of pebble- to cobble-size clasts (7-8 cm in diameter on average). The pebbles and cobbles are heavily cemented by iron oxides and form a major erosional surface overlying the underlying coaly deposits (Fig. 5.16A, B).

Interval 5 (2.6 m): The interval comprises two 100 to 140 cm-thick bodies consisting of medium-grained sandstone which show planar cross-bedding displaying opposite transport directions (NNW and SSW, respectively) and double mud drapes (tidal bundles) (Fig. 5.16C). Likewise, flat, and sharp reactivation surfaces can be observed between sets of the cross-beddings with opposite transport directions. This interval also shows plant compressions but their low degree of preservation has prevented their identification.

Interval 6 (1.7 m): The base of this interval consists of a 10 to 15 cm-thick surface of pebbles and cobbles (6-8 cm in diameter on average, reaching) cemented with iron oxides (Fig. 5.16B, 5.17A-C). This surface shows an undulating outline and can be traced laterally for tens of metres, depending on the outcrop

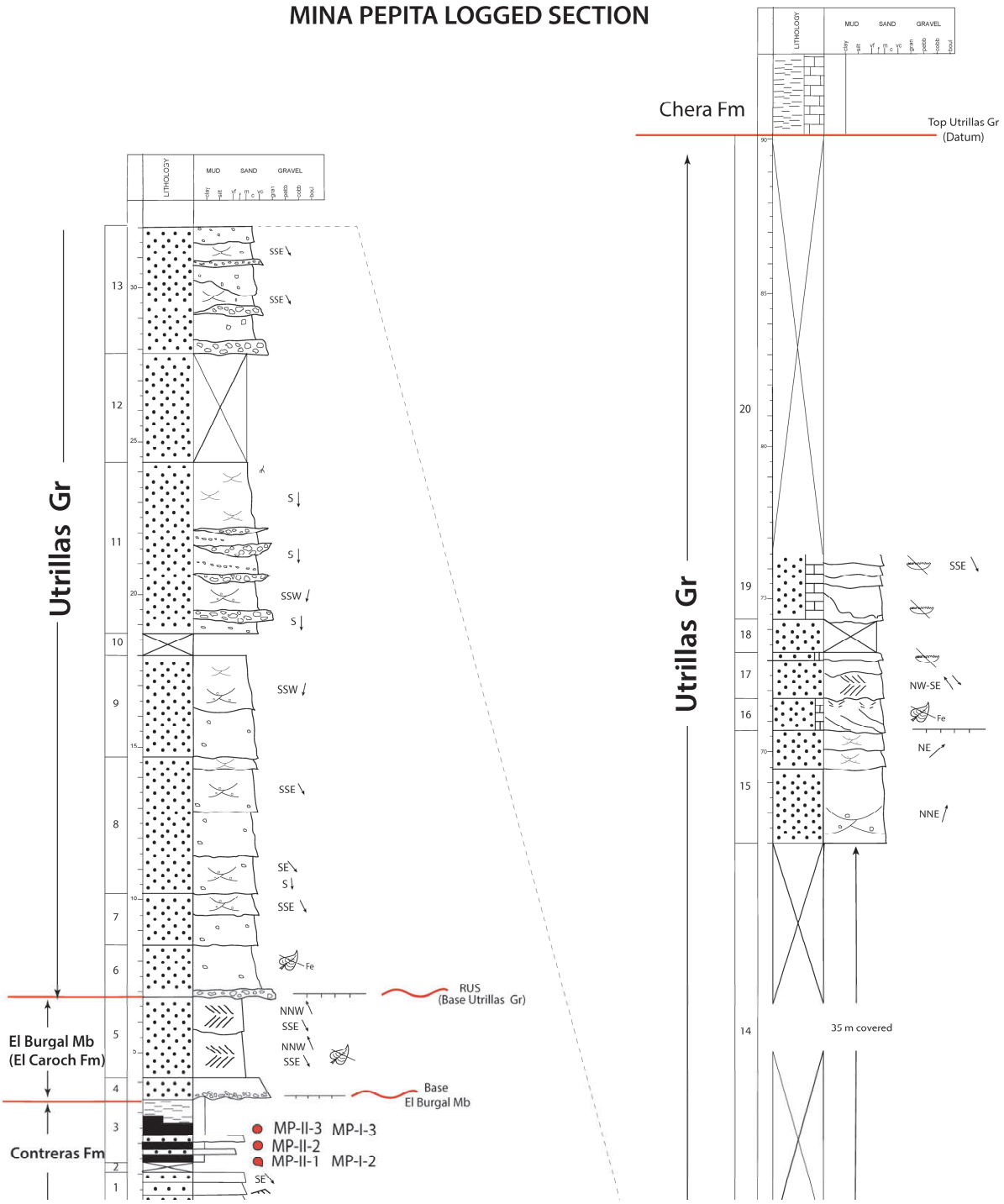

Fig. 5.15. Logged section at the Mina Pepita outcrop. The explanation of the graphic symbols is included in appendix IV (A).

conditions. It corresponds to a major erosional surface that separates the strata of interval 5 (below) from the strata of the overlying sedimentary succession, dominated by coarse sandstones and conglomerates. The surface is overlain by fining upwards 1.5 m-thick coarse- to very coarse-grained sandstone bodies with scattered pebbles and scarce oxidised plant remains.

Interval 7 (1.7 m): This interval comprises two fining upwards coarse-grained sandstone bodies, with scattered pebble-sized clasts, which show erosional bases. The upper body presents trough cross-bedding where the measured palaeocurrents indicate a SSE direction.

Interval 8 (4.5 m): It consists of several amalgamated coarse- to very coarse-grained sandstone bodies with scattered pebbles and cobbles. The bodies show a fining upwards trend and, in some cases, the palaeocurrent directions have been measured in the trough cross-bedded sets they present. The measured palaeocurrents indicate transport directions toward the S, SE, and SSE.

Interval 9 (3.3 m): It comprises two fining upward sandstone bodies with erosional bases. The grain size is coarse to very coarse and the bodies may present scattered pebbles. The main sedimentary structures identified are sets of trough cross-bedding that display a SSW palaeocurrent direction.

Interval 10 (0.7 m): Covered.

Interval 11 (5.7 m): Towards the base, it consists of very coarse-grained sandstones which include 20 to 50 cm-thick beds of cobbles and pebbles both forming clast- and matrix-supported conglomerates. Similarly, scattered within the sandstones (both as isolated pebbles-cobbles or forming wind deflation surfaces). The beds where the cobbles and pebbles accumulate tend to be massive (structureless). The clasts are 5 cm in diameter on average. However, the largest clasts may reach up to 90 to 10 cm. Some of the pebbles are arranged into one-pebble-thick flat surfaces that are laterally extensive throughout the outcrop. The main sedimentary structure observed is trough cross-bedding arranged into 20 to 30 cm-thick sets. The upper part of the interval consists of coarse-grained without pebbles or cobbles and shows smaller-scale trough cross-bedding (approximately 10 cm-thick sets) and, locally, weakly developed root traces. The main palaeocurrent directions measured in the interval indicate transport directions toward the S and SSW.

Interval 12 (3.5 m): Partly covered (coarse-grained sandstones).

Interval 13 (4.3 m): Very coarse-grained sandstone body with abundant cobbles and pebbles both forming matrix-supported conglomerate beds where they accumulate. Pebbles and cobbles are also found scattered within the sandstones (both as isolated pebbles-cobbles or forming one-pebble-thick flat surfaces). The conglomerate beds comprise clasts that are 4 to 6 cm in diameter on average towards the base, although they can reach up to 10 cm. However, the size of the clasts of the conglomerates in those beds located in the upper part of the interval is significantly smaller (1 to 2 cm in diameter on average).

This interval is composed of several amalgamated fining upwards sandstone bodies that commonly present internal erosional scours and trough cross-bedding with palaeocurrents directions toward the SSE.

Interval 14 (approximately 35 m): Covered.

Interval 15 (3.7 m): In its lower part, this interval consists of a coarse to very coarse-grained sandstone body with an erosional base with large scale trough cross-bedding (2 m-thick sets) indicating a NE direction of the palaeocurrents (Fig. 5.15). The foresets of the trough cross-bedding show rhythmical alternations in grain size. The upper part consists of two 0,5 to 0.7 m-thick coarse-grained sandstone bodies with smaller-scale trough cross-bedding (20 to 20 cm-thick sets). Scattered pebbles are also observed throughout the whole interval. Measured palaeocurrents indicate that the bedforms migrated toward the NE to NNE.

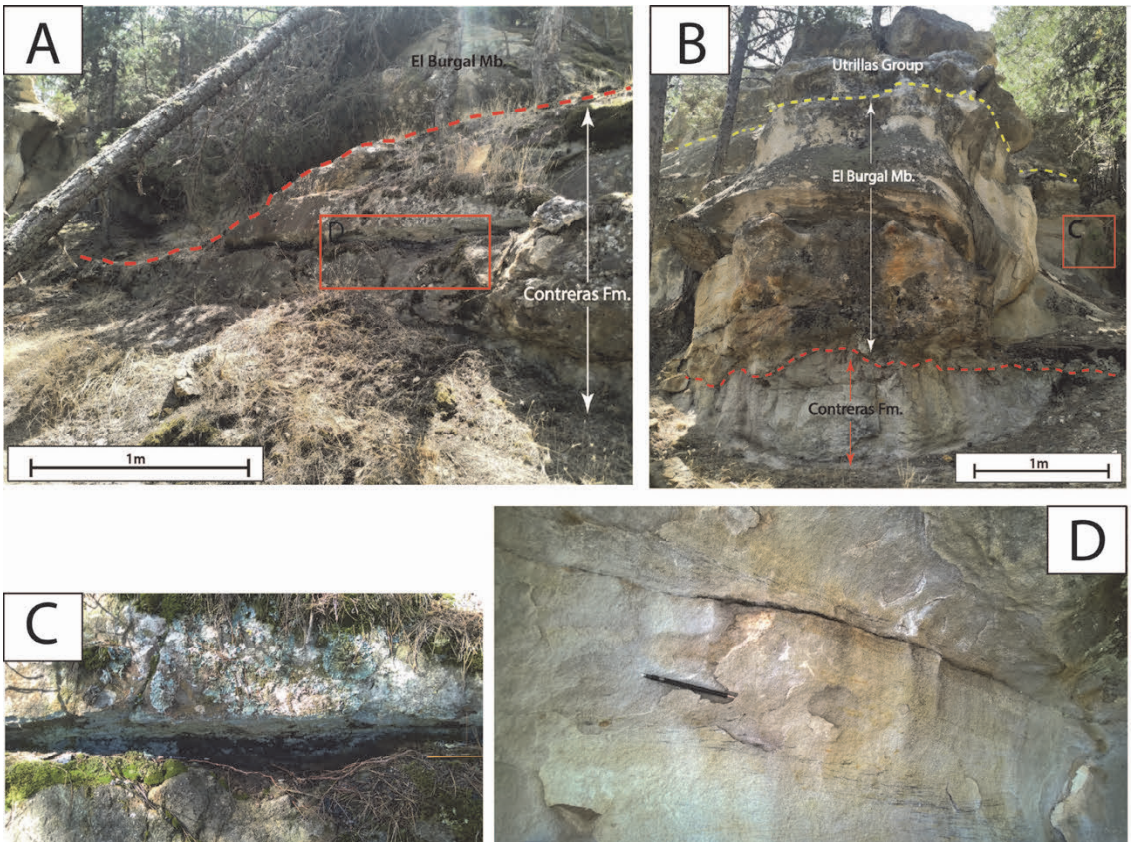

Fig. 5.16. (A) and (B) Erosional surface at the top of lower Aptian Contreras Fm. (red dotted line) and erosive surface at the top of the upper Aptian El Burgal Mb (yellow dotted line), representing the lowermost logged levels of the Mina Pepita outcrop. (C) Detail of one of the 10 cm-thick lignite-rich layers attributed to the Contreras Fm where a pollen sample has been collected. The pencil for scale is 15 m in length. (D) Double mud drape structures have been preserved forming foresets migrating towards the S in the lower part of the picture, while in the upper half of the picture the foresets migrate towards the N in the deposits of the El Burgal Mb (Mina Pepita outcrop). The pen for scale is 10 cm long.

Interval 16 (1.1 m): It consists of coarse-grained calcareous sandstones arranged into laterally amalgamated bodies (lateral accretion). The bodies present fining upwards trends and erosional bases, some of them cemented by iron. Towards the top, the bodies may present mud drapes. Locally, scarce oxidised plant remains may be observed.

Interval 17 (1.2 m): This interval consists of coarse-grained sandstones showing "Herringbone-like" cross-beddings, which consists of sets of trough cross-bedding migrating in opposite directions. The palaeocurrents measures in this bed indicate migration of the bedform towards the NW and SE. The upper part of this interval is slightly cemented by calcite and presents scarce bivalve shell fragments.

Interval 18 (1 m): Partly covered. Coarse-grained sandstone.

Interval 19 (2.1 m): This interval consists of coarse-grained calcareous sandstone arranged into 30 to 40 cm-thick laterally amalgamated sigmoidal bodies (lateral accretion bodies) with erosional bases. They present scattered bivalve shell fragments and detrital glauconite grains (Fig. 5.17E).

Interval 20 (approximately 14 m): Covered.

The studied succession is overlain by an approximately 10 to 15 m-thick succession, partly covered, consisting of green marls (Chera Fm) with thin whitish dolostone and limestone layers

interbedded, which are overlain by the Upper Cretaceous marine carbonate units (Ramírez Merino, 1986). The upper contact of the logged succession with the Chera Fm is covered, within interval 20, and has not been observed in the field (Fig. 5.15).

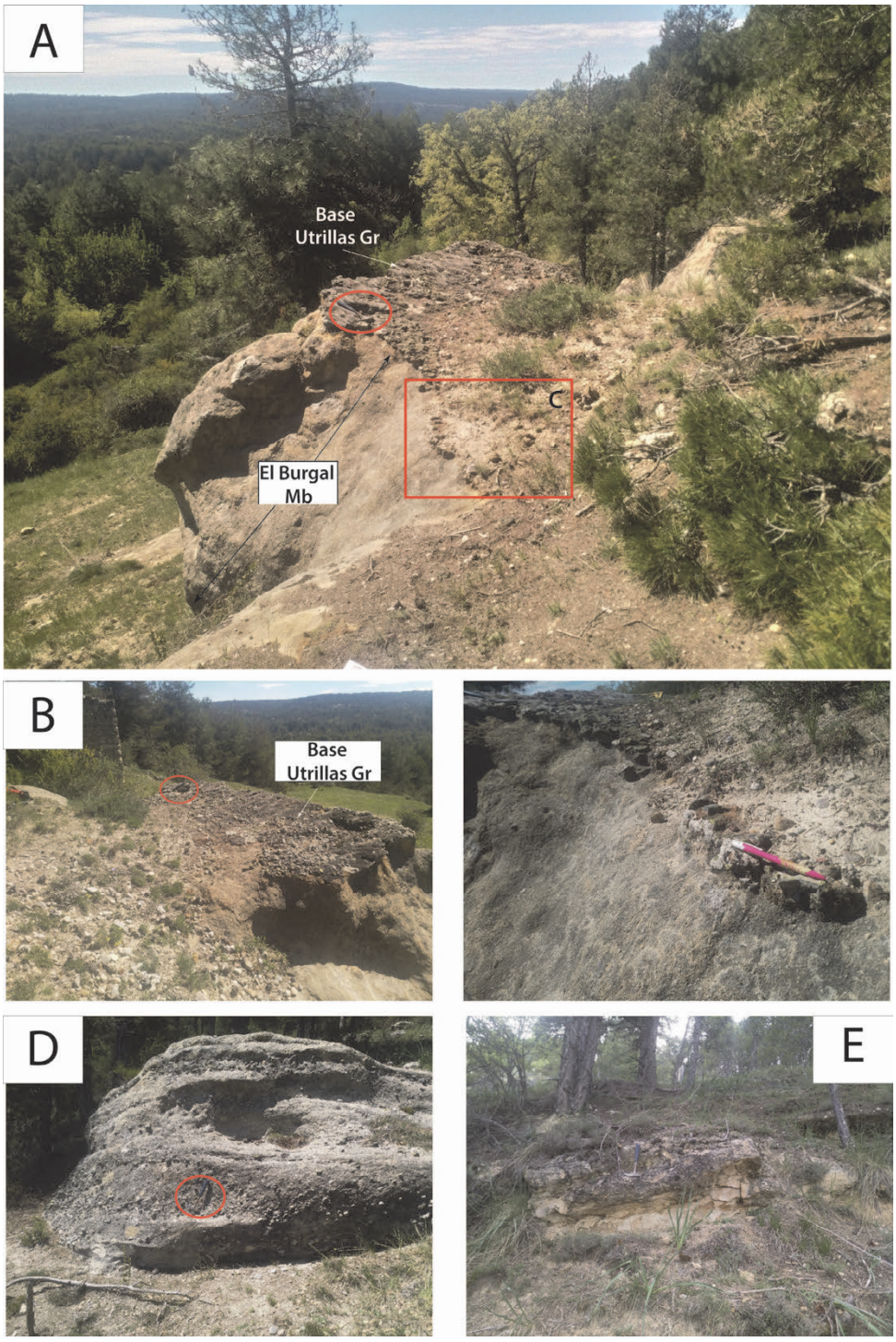

Fig. 5.17. (A) and (B) Base of the Utrillas Gr at the Mina Pepita outcrop, where a conspicuous erosional surface covered with pebbles and cobbles can be observed. This surface is interpreted as a regional unconformity surface (RUS). Hammer for scale is 35 cm-long (C) Close-up of (A). Pen for scale is 10 cm in length. (D) Aspect of the lower part of the logged section corresponding to the facies association I (FA I) (interval 13 of the logged section). (E) Calcareous sandstones arranged in lateral accretion bodies in the upper part of the logged section, representing a proximal estuarine succession and interpreted as the facies association IV (interval 19 of the logged section). See chapter 8 of this manuscript for the explanation of the facies associations.

5.1.6. Las Majadas outcrop.

The Las Majadas outcrop is approximately located 1 km to the southwest of the Las Majadas village, Cuenca Province (Fig. 5.18). The lower part of the measured section crops out in a ravine (intervals 1 to 16; Fig. 5.19), and the upper part has been logged on the roadside of the CUV-9113 road (intervals 17 to 26; Fig. 5.19). Both logged parts are in sedimentary continuity and form a 64 m-thick logged section (Fig. 5.19). The base of the logged section is located at the top of a continental limestone succession attributed to the Barremian La Huerguina Fm (Ramirez Merino, 1986, Fregenal-Martínez et al., 2017). The top of the logged section is a flat contact overlain by an approximately 10 m-thick succession consisting of green marls and thin layers of dolostones attributed to the Cenomanian Chera Fm (Ramirez Merino, 1986, Sopeña et al., 2004), which is in turn overlain by the Upper Cretaceous marine carbonate units (Fig. 5.18). A detailed description of the logged section is included in the following pages.

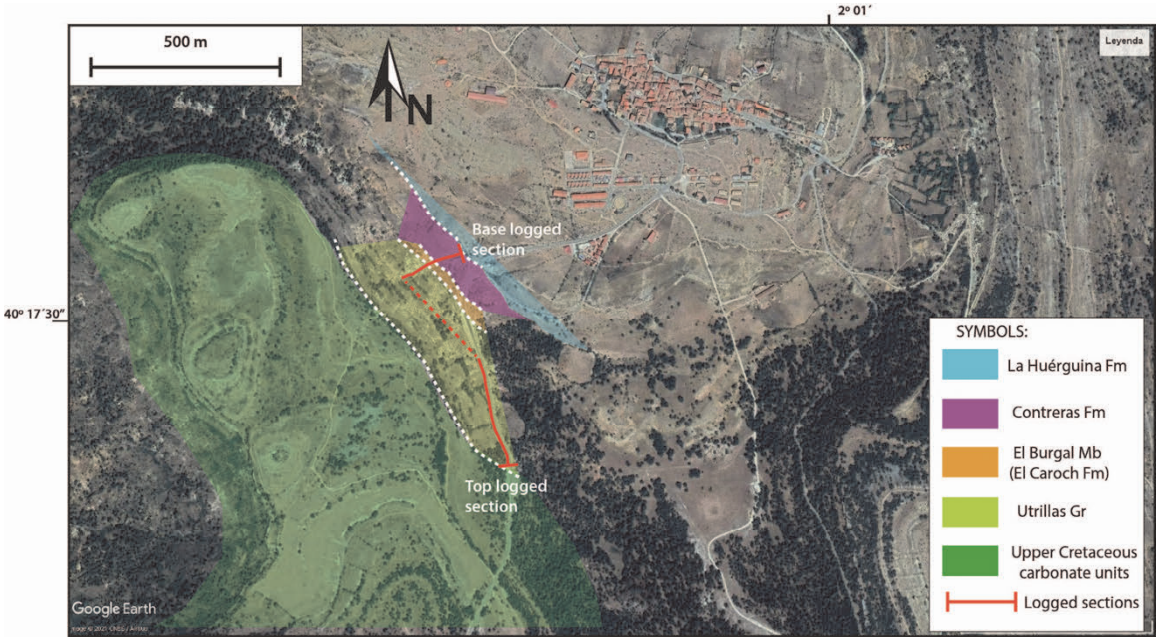

Fig. 5.18. Satellite image corresponding to the studied outcrop in Las Majadas. The extension of the Utrillas Gr succession (in yellow colour), as well as that of the underlying and overlying stratigraphic units, has been drawn. The location and extension of the logged section are also included (red line). Image source: Google Earth.

Description of the logged section (Fig. 5.19):

Interval 1 (5 m): One-meter-thick coarse-grained sandstone body overlying a carbonate succession (La Huerguina Fm; Figs. 5.18, 5.19, 5.20A). Sedimentary structures are not preserved due to the poor quality of the outcrop. The upper part of this interval consists of 4 m where the sedimentary succession is covered, but it is probably dominated by red mudstones.

Interval 2 (3 m): This interval consists of about 1.5 m of reddish coarse-grained sandstone (the basal contact is covered). The sandstone body is lens-shaped and presents poorly preserved planar cross-bedding and scattered pebbles of metamorphic rock. Measured transport direction indicates that bedforms migrated towards the SE.

Interval 3 (4.5 m): This interval consists of a 2.5 m-thick body of red sandstones with scattered pebbles (average size is 25 mm). The only sedimentary structure observed is planar cross-bedding, which is poorly preserved and arranged into 0.8 to 1 m-thick sets. The base of the sandstone body is erosional. This sandstone body is sharply overlain by an approximately 1 m-thick layer of red to brownish mudstone. The interval is overlain by an erosive surface.

Interval 4 (1.6 m): Coarse-grained whitish sandstone body with a prominent erosional base include a pebble lag, which erodes the deposits of interval 3. The body, in turn, consists of up to three smaller sandstone bodies separated by internal erosional scours with pebble lags. The main sedimentary structures observed are planar cross-bedding and current ripples towards the top of the interval. The measured palaeocurrents indicate a transport direction towards the NW.

Interval 5 (2 m): White coarse-grained sandstones arranged in 0.3 to 0.5 m-thick sets of planar cross-bedding, which include abundant pebble lags (Fig. 5.20B, C). Pebble sizes range between 10 and 40 mm on their longest axis, being the average pebble size observed is 30 mm. The morphology of the sedimentary body is tabular, and its base is erosional. The measured palaeocurrents are towards the SW and SSW.

Interval 6 (0.9 m): It consists of white coarse-grained sandstones arranged in an only body consisting of a sigmoidal set of planar cross-bedding (0.8 m-thick). The body has a tabular morphology and presents a flat sharp basal contact that overlies the deposits described in interval 5. The measured transport direction is toward the NNE, which strikingly contrasts with those of interval 4, showing opposite transport directions (Fig. 5.20B, C). The upper part of the interval shows a diminishment in grain size and locally weak palaeosol development. The interval is overlain by a marked erosional surface which incises into the underlying deposits (Fig. 5.19, 5.20A-D).

Interval 7 (1.6 m): The interval consists of ochre to yellowish coarse to very coarse-grained sandstone with scattered pebbles. The basal contact of this interval is a prominent erosional surface that incises into the underlying deposits of interval 6 (Fig. 5.20D). The body is lenticular in shape, shows a clear fining upwards trend, and presents dm-scale trough cross-bedding. The measured transport direction is toward the SE.

Interval 8 (2 m): It comprises trough cross-bedded (very) coarse-grained ochre sandstones arranged into three bodies with erosional base and finning upwards trend. Scattered pebbles may occur in this interval (average size is about 40 mm on their longest axis), although they are not very abundant. The uppermost body shows current ripples at its upper part and root traces (weakly developed palaeosol). The measured palaeocurrents indicate an ESE direction.

Interval 9 (0.4 m): Reddish to purple mudstone and siltstone with a very mild dark mottling, probably related to a weak palaeosol development.

Interval 10 (2.1 m): This interval consists of three bodies of coarse- to very coarse-grained sandstone with scattered pebbles and cobbles and an erosional base. The lowermost logged sandstone body does not show any sedimentary structures due to its poor preservation. The intermediate body shows a massive aspect and consists of pebbles-cobbles with sand-size particles (the average size of the pebbles is 50-60 mm, with their maximum size being about 80-90 mm in diameter in their longest axis). The uppermost body

shows trough cross-bedding and scattered pebbles. The measured palaeocurrents indicate a SSE transport direction.

a fining upwards trend. The lowermost body shows planar cross-bedding arranged in a set of 50 to 60 cm in thickness with transport directions towards the SE. Conversely, the uppermost body shows cm-scale

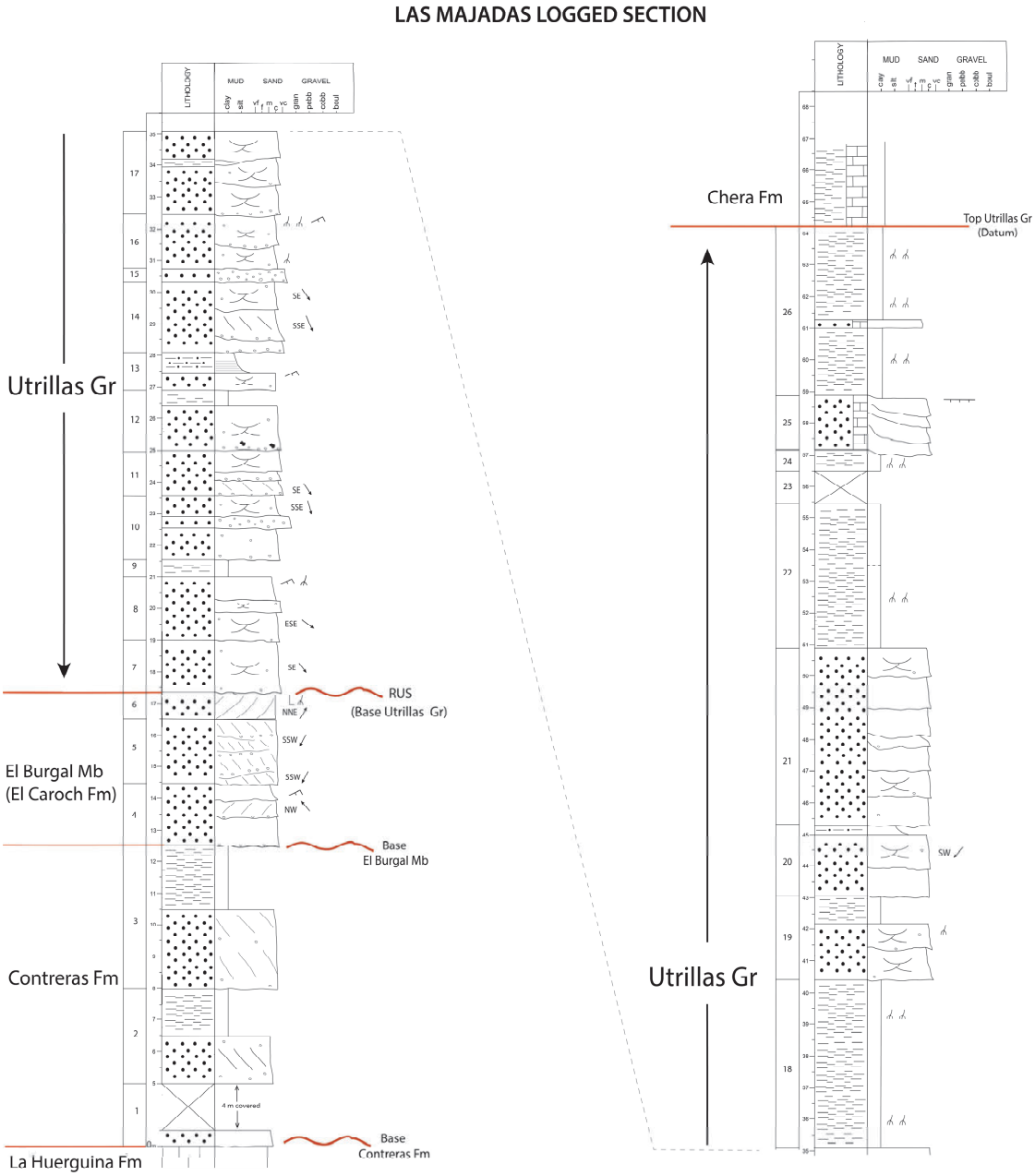

Fig. 5.19. Logged section at the Las Majadas outcrop. The explanation of the graphic symbols is included in appendix IV (A).

Interval 11 (1.4 m): It consists of very coarse- to coarse-grained sandstone bodies with erosional gravelly bases They are lenticular in shape and show trough cross-bedding.

Interval 12 (1.9 m): The interval consists of a 1.4 m-thick coarse-grained sandstone body with an

erosional base and trough cross-bedding. The base shows pebbles and cobbles (the average size of the clasts is 30 to 40 mm) and locally mud balls (up to 90 mm in diameter). The sandstone body is sharply overlain by a 0.5 m-thick layer that consists of dark red to purple mudstone (no root traces or mottling observed).

Interval 13 (1.3 m): This interval is composed of a coarse-grained sandstone body with an erosional base, small scale trough cross-bedding, and is dominated by current ripples towards the top. This body is overlain by laminated very fine-grained sandstones to siltstones lacking any mud drape structures. The interval shows a fining upwards trend.

Interval 14 (2.3 m): It comprises three lenticular amalgamated bodies with coarse- to very coarse-grained sandstone bodies with erosional base and a fining upwards trend. The erosional bases commonly present quartzite pebble and cobble lags (the quartzite pebbles-cobbles are on average 30 to 40 mm in diameter, and the maximum size measured is approximately 70 mm in diameter). The sedimentary structures observed are planar and trough cross-bedding with palaeocurrents indicating SE and SSE transport directions.

Interval 15 (0.4 m): The interval presents massive gravels (mostly pebble size but may locally include some cobbles) and very coarse-grained sandstone. The average diameter size of the pebbles-cobbles is about 50 mm, being the largest ones about 90 to 100 mm. They are arranged into a lenticular body with an erosional base. The body pinches out laterally into coarse-grained sandstone bodies with or without scattered pebbles.

Interval 16 (1.7 m): The interval consists of coarse- to very coarse-grained sandstone bodies with scattered gravel and pebble lags at their base. The basal contacts of the bodies are erosional and show a fining upwards trend and small-scale trough cross-bedding. The sandstone bodies show abundant and intense bioturbation by root traces owing to plant colonization. However, the upper body shows more intense bioturbation by roots than the overlying one. The interval 16 represents the top of the lower part of the logged section, located in a ravine (Fig. 5.18). The upper part of the stratigraphic section (interval 17 to 26; Fig. 5.19) has been measured in an outcrop located on an adjacent roadside approximately 200 m to the south (Fig. 5.18).

Interval 17 (2.7 m): This interval consists of coarse- to very coarse-grained sandstone bodies with erosional bases and some pebble lags towards the base. The sandstone bodies are lenticular in shape and show a fining upwards trend. The main sedimentary structures observed are trough cross-beddings, however, due to the poor preservation of their foresets, the transport directions of the bedforms have not been measured in this interval. Locally, thin accumulations of muddy deposits related to the sandstones may also occur. Root traces have not been observed in the sandstone bodies.

Interval 18 (5.3 m): This interval consists of reddish to purple mudstones with intense to moderate bioturbation by root traces and abundant yellowish mottling. Several pictures of this interval have been taken both on the roadside and in ravines corresponding to laterally equivalent beds.

Interval 19 (2.6 m): The interval is mainly composed of coarse-grained sandstone bodies (first 1.8 m of the interval) with a few scattered pebbles and trough cross-bedding. It shows finer grain size than that of similar facies in the lower part of the succession (i.e., sandstone bodies in intervals 10, 11, 12…). The sandstones are overlain by 0.8 m red mudstones with moderate bioturbation by root traces.

Interval 20 (2.2 m): It consists of coarse-grained lenticular sandstone bodies which may include a few scattered pebbles and trough cross-bedding (it includes the first 1.9 m of the interval). The measured

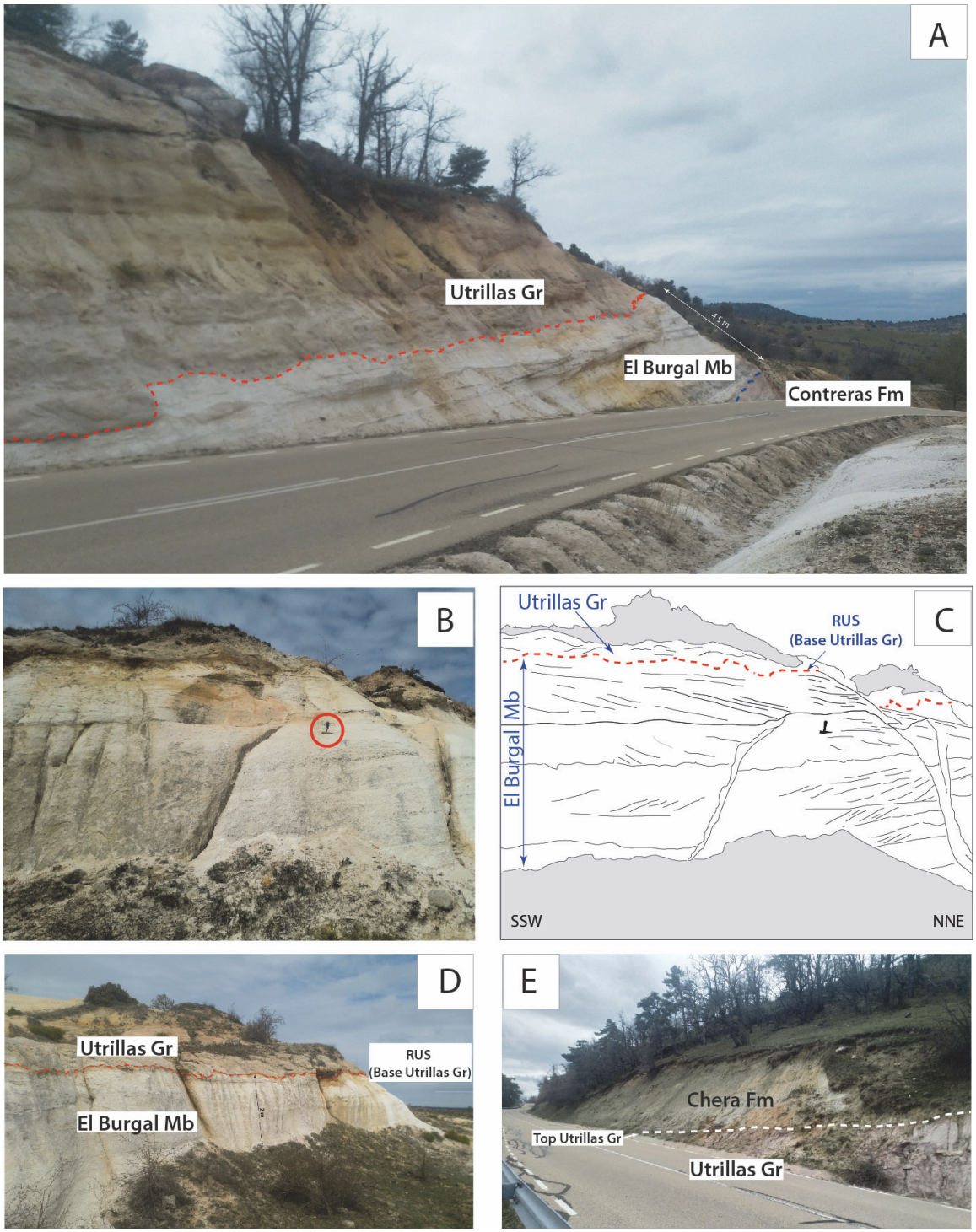

Fig. 5.20. Base and top of the Utrillas Gr succession in the Las Majadas outcrop. (A) Panoramic view of the lower part of the logged section in the Las Majadas outcrop. The lithostratigraphic contacts marking the base of the El Burgal Mb (dashed blue line) and the base of the Utrillas Gr (dashed red line) are drawn in the picture. (B) Detail of the strata of the El Burgal Mb overlaying by the Utrillas Gr succession at Las Majadas. Hammer for scale is 35 cm-thick. (C) Line drawing and interpretation of (B) where sets of planar cross-bedding showing palaeocurrent bipolarity (towards the SSW in the lower part and to the NNE in the upper part) are observed. The regional unconformity surface (RUS) that represents the base of the Utrillas Gr is also observed (dashed red line). (D) strata of the El Burgal Mb overlaying by the Utrillas Gr succession at Las Majadas. The RUS is also represented by a red line. **(E) Top surface of the Utrillas Gr in the Las Majadas outcrop. The marls of the Chera Fm overlay the succession with a sharp and non-erosional contact.**

palaeocurrents, when the outcrop preservation is good enough, allow inferring a SW transport direction. The sandstones are overlain by 0.3 m of massive fine-grained sandstone and siltstone.

Interval 21 (5.5 m): This interval consists of several amalgamated coarse-grained sandstone bodies with very few scattered pebbles, erosional bases, and lenticular morphology (channeled shape). A few trough cross bedding-like structures can be observed. Each individual sandstone body ranges between 0.4 and 1 m in thickness. The palaeocurrents have not been measured due to the poor quality of preserved stratigraphic structures in this interval.

Interval 22 (4.5 m): The interval consists of a 2.5 m-thick layer of reddish to purple mudstone and siltstone deposits, which may show yellowish mottling. Bioturbation by root traces is moderate. These deposits are overlain by a 2 m- thick succession composed of green and grey mudstones which do not show any signs of bioturbation. The transition between both layers is a diffuse contact.

Interval 23 (1.1 m): Partly covered interval. Most likely the interval consists of mudstones and siltstones.

Interval 24 (0.7 m): The interval consists of reddish to purple mudstones with moderate to intense bioturbation by root traces and frequent yellowish mottling.

Interval 25 (1.7 m): The interval consists of a coarse- to medium-grained calcareous sandstone body arranged in 0.3 to 0.6 m-thick smaller laterally amalgamated bodies. The bodies show erosional surfaces and sigmoidal morphology. The calcareous sandstones are overlain by a ferruginous surface describing a sharp contact (Fig. 5.19).

Interval 26 (5.6 m): This interval consists of reddish to purple mudstones which may include moderate bioturbation by root traces and yellowish mottling. They present a thin (approximately 30 cm-thick) slightly calcareous medium- to coarse-grained heterometric sandstone layers. The top of interval 26 is a sharp surface that coincides with the top of the logged sedimentary section (Fig. 5.18) and is overlain by a sedimentary succession that consists of approximately 10 m with dark green marls interspersed with thin (20 to 30 cm-thick) white dolomite and limestone layers. The green marls are in turn overlain by a thick carbonate succession (Fig. 5.20E).

5.2. Eastern sector.

5.2.1. Tejadillos outcrop.

The Tejadillos outcrop is located in the surroundings of the municipality of Tejadillos (Fig. 5.21), in a ravine located to the W of the village of Tejadillos. In order to study the sedimentary succession corresponding to the Utrillas Gr and the La Bicuerca Mb in the area, a stratigraphic section consisting of two parts has been logged (Fig. 5.22).

The lower part of the section (intervals 1 to 18; Fig. 5.22) is a 45 m-thick sedimentary succession characterised by sandstone-dominated siliciclastic strata with subordinate mudstone and siltstone layers. Conversely, the upper part of the section (intervals 19 to 27; Fig. 5.22) is a 28 m-thick sedimentary succession located approximately 100 m to the WSW of the lower part of the section (Figs. 5.21, 5.22). The upper part of the section was initially logged and succinctly studied by Chamizo-Borreguero et al. (2008); therefore, it has been revisited in the field and reinterpreted in this thesis. The upper part of the succession is essentially dominated by a

calcareous sandstone succession with bivalve shell fragments and minor calcareous mudstone layers interbedded.

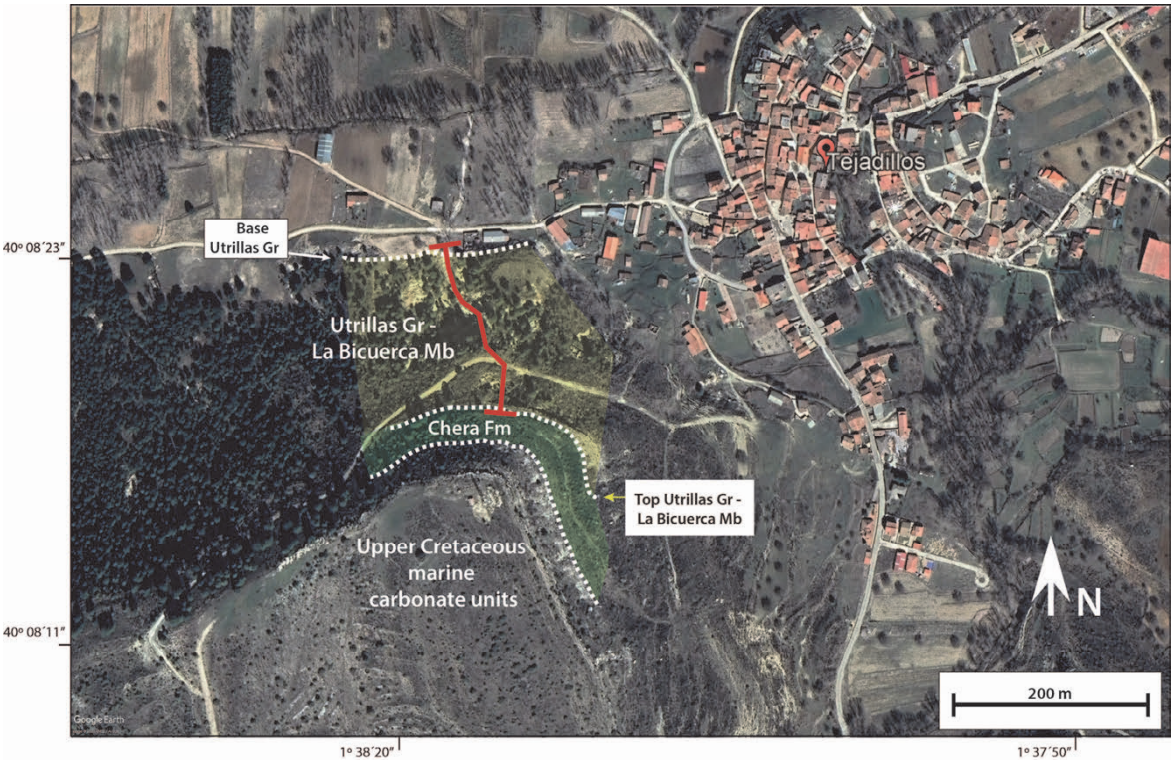

Fig. 5.21. Satellite image corresponding to the studied outcrop in Tejadillos. The extension of the Utrillas Gr - La Bicuerca Mb succession (between the yellow dotted lines), as well as that of the overlying Chera Fm, are included. The location of the logged section is also included (red line). Image source: Google Earth.

Description of the logged section (Fig. 5.22):

Interval 1 (3.7 m): The base of this first interval is covered and is located at the bottom of the ravine. It consists of a continuous coarse-grained heterometric sandstone body displaying ochre to yellowish colours. Regarding sedimentary structures, it presents ubiquitous cm-scale mostly planar cross-bedding, although locally trough cross-bedding has been locally observed. Likewise, current bipolarity may be locally observed at this interval. Such cross-bedded sets are punctuated by 10 to 20 cm-thick pebbles and, to a lesser extent, cobble-sized deposits. Pebbles and cobbles range from subangular to subrounded in shape, and they show an average size of about 2-3 cm in diameter, being the largest one around 7 cm in diameter. This interval is overlain by an erosional surface which truncates the succession (Fig. 5.23A-C). This surface commonly is paved with pebbles and cobbles, which usually range between 4 to 5 cm in diameter, yet the largest ones may reach up to 12 cm (Fig. 5.23B). Locally, this surface may be devoid of pebbles-cobbles, in which case it is characterised by a reddish iron-rich hardened surface.

Interval 2 (0.6 m): This interval consists of coaly fine to very fine-grained sandstones, which comprise 10 - 15 cm-thick interbedded lignite-rich accumulations including scarce plant fragments (Fig. 5.23D). The morphology and shape of the sedimentary body are

difficult to ascertain since it crops out irregularly due to it is heavily eroded by the base of the overlying sandstone bed.

Interval 3 (3.2 m): Coarse- and very coarse-grained white arkose sandstone with a very heterolithic nature, containing towards its base gravel-size deposits and abundant but scattered quartzite pebbles and cobbles. Towards its top, the grain size decreases notably, and it is characterised by medium-grained sandstones. Regarding sedimentary structures, the interval is dominated by cm-scale sets of trough cross-bedding, including some small pebbles and gravel-size grains in the foresets. Notwithstanding, the upper part of this interval is dominated by smaller-size (10 cm) planar cross-bedding and planar lamination, as well as current ripples in its uppermost part. The lower contact of the body is a highly erosive undulating contact that can be traced laterally across the outcrop, whilst the upper one is a flat and non-erosional contact. Regarding morphology, this sedimentary accumulation shows a lenticular shape and laterally amalgamates with morphologically similar sedimentary bodies.

Interval 4 (1.8 m): This interval comprises coarse-grained heterolithic arkose sandstones arranged into 0.8 to 1 m-thick tabular bodies. The bodies display sets (40 to 50 cm-thick) of planar cross-bedding with palaeocurrents indicating bedform migration towards SW. Additionally, mm- to 1 cm-thick current ripples can be observed towards the top of each tabular body. Although rare, the sandstone bodies may present local scattered pebbles. The base and top of this interval are sharp non-erosional contacts.

Interval 5 (2.0 m): It consists of a coarse-grained sandstone tabular body that displays m-scale planar cross-bedding whose palaeocurrents indicate bedform migration towards the SW and SE. This sedimentary body may also show current ripples at its base. Likewise, it is overlain by a 1.3 m-thick fine- to medium-grained sandstone body, which shows a gradational contact at its base. The body shows abundant parallel lamination, current ripples, and a clear fining upwards trend.

Interval 6 (3.3 m): This interval consists of an accumulation of mudstone and siltstone, which display reddish to purple colours with intense mottling. Likewise, it may present scattered fine- to coarse-grained sandstone grains, despite mainly being composed of mud- and silt-sized deposits. Regarding shape, it is a tabular body; however, the full lateral extension of the body cannot be ascertained since it is laterally eroded. It presents a gradual contact at its base and an erosional one at its top.

Interval 7 (4 m): Trough-cross bedded coarse- to very coarse-grained arkose sandstone body with a highly heterolithic nature and fining upwards trend. The basal contact is erosional with mud pebbles and scattered quartzite pebbles, while the upper contact is sharp flat contact. Laterally, the sandstone body extends for 3 to 5 m and amalgamates laterally with other similar bodies. Likewise, it shows one-pebble-thick laterally persistent flat pebble lags equally distributed along the body. The pebbles show subangular and faceted morphology.

Interval 8 (2.0 m): Purple to reddish mottled mudstone to siltstone deposits displaying a tabular morphology. The base of this interval is a sharp contact, whilst the top is erosional. The upper part (uppermost 0.5 m) of the mudstone deposits does not depict any mottling nor reddish to purple colours; instead, it is dominated by greyish to greenish mudstones.

Interval 9 (4.6 m): It consists of three amalgamated lenticular bodies that display erosional base and minor internal scours. The bodies are composed of coarse-grained arkose sandstones that present flat sub-horizontal quartzite pebble lags at their bases and a moderate number of scattered mudstone pebbles and cobbles. Likewise, they show a clear fining upwards trend regarding grain size. Among the sedimentary structures observed, there are abundant

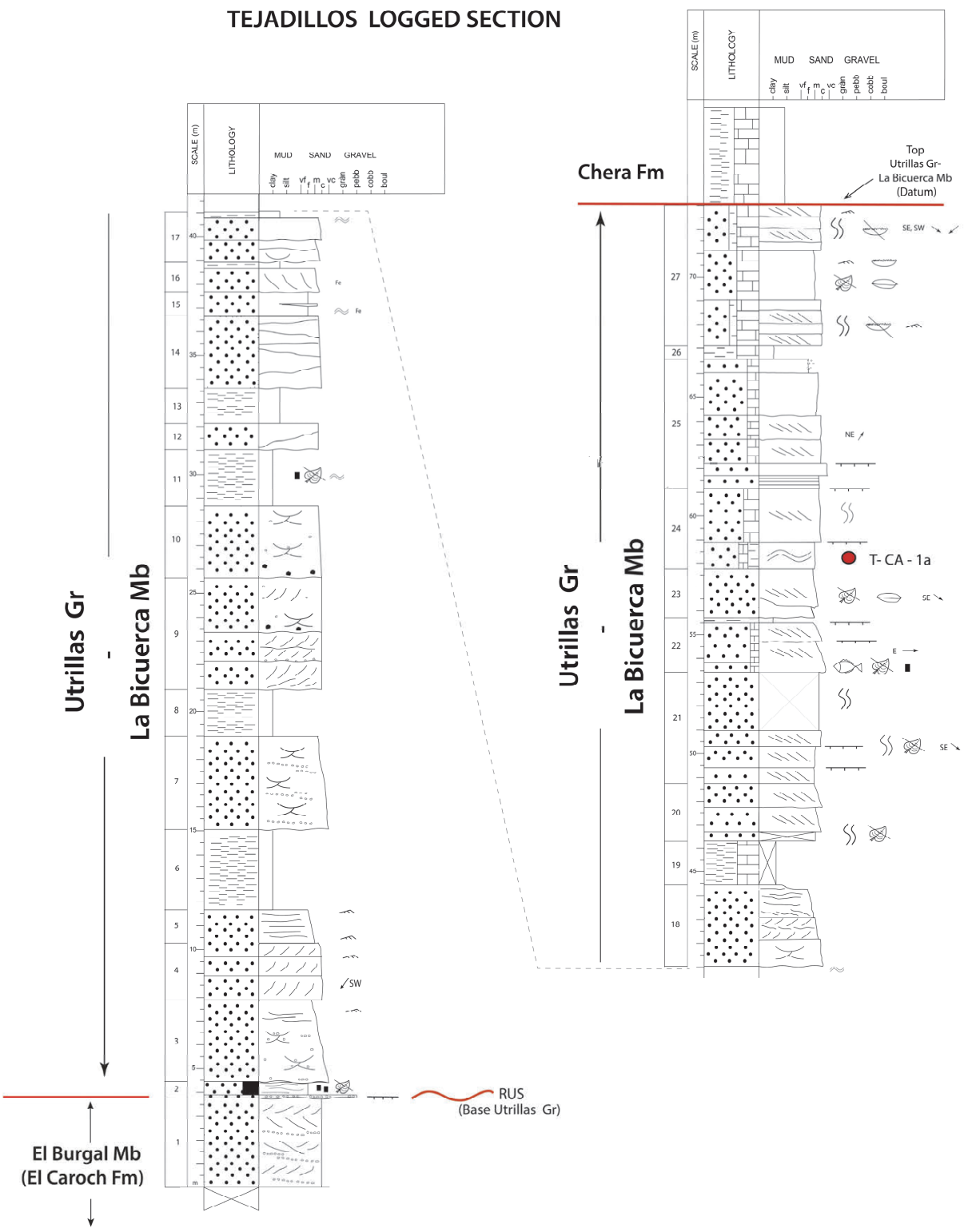

Fig. 5.22. Logged section at the Tejadillos outcrop. The explanation of the graphic symbols is included in appendix IV (A).

20-30 cm-thick sets of trough and planar cross-bedding (Fig. 5.22).

Interval 10 (2.9 m): Coarse- to very coarse-grained arkose sandstone body like the ones described in interval 9. It presents an erosional base, and the top is a flat sharp contact. This lenticular body includes scattered quartzite and mudstone pebbles, as well as some scarce highly oxidised plant fragments.

Interval 11 (2.4 m): Sandy mudstone to siltstone arranged into a tabular-shaped body. The two lowermost meters of the succession are dominated by grey mudstones; however, greyish sandy mudstones with double mud drape-like structures and tidal bundles characterise the top of the succession. Additionally, some charcoalified wood remains have also been found towards the top of this interval.

Interval 12 (1 m): Coarse- to medium-grained sandstones arranged into sigmoidal bodies which amalgamate laterally. Regarding sedimentary structures, they show dm-scale planar and trough cross-bedding.

Interval 13 (1.5 m): Greyish mudstones with fine-grained sandstone, depicting tabular morphology, which can be traced laterally throughout the outcrop for more than 5 m.

Interval 14 (3.0 m): This interval consists of laterally amalgamated sigmoidal coarse-grained sandstone bodies which show several internal scours similar to the ones described in interval 12. The sigmoidal bodies are laterally persistent for almost 10 metres until they eventually pinch out into similar sandstone bodies. Regarding sedimentary structures, the present trough or planar cross-bedding with mudstone pebbles. Locally, the sets of planar cross-bedding present rhythmical alternations of the grain size of their foresets.

Interval 15 (1 m): Fine- to medium-grained ferruginous sandstone displaying a tabular morphology. This sedimentary body shows planar heterolithic lamination including some wavy- and flaser-like laminations. Both contacts at its base and top are sharp and non-erosional ones.

Interval 16 (1.2 m): Coarse- to medium-grained sandstone arranged in a tabular body that displays dm-scale planar to sigmoidal cross-bedding. It contains moderate amounts of iron oxides and is defined by a sharp base and top contact. This interval of the sedimentary succession is overlain by approximately 0.2 m of greyish mudstones.

Interval 17 (2.1 m): It consists of two lenticular-shaped coarse-grained sandstone bodies displaying trough cross-bedding and an erosional base. Both bodies are overlain by 10 to 20 cm-thick layers, composed of heterolithic mudstones, which show wavy to lenticular heterolithic cm-scale lamination and mudstone bundles.

Interval 18 (3.4 m): Lenticular sandstone body with erosional base and a fining upwards trend which ranges from coarse-grained sandstone at its base to medium- to fine-grained sandstone in its upper part. The basal part is dominated by m- to dm-scale trough cross-beddings, whilst its upper part is characterised by planar cross-bedding ranging upwards into subhorizontal laminations with asymmetrical current ripples.

Interval 19 (1.5 - 2 m): Partly covered. Greyish to ochre marls with minor calcareous siltstone layers.

Interval 20 (2.4 m): Partly covered interval at its base. However, two fining upwards sandstone bodies are laterally observed towards the top of this interval. These bodies are lenticular in shape and show planar cross-bedding when preserved. Moderate bioturbation as well as some scattered and oxidised plant remains have also been observed.

Interval 21 (4.8 m): Partly covered interval towards its upper part. It consists of less than 1 m-thick coarse- to medium-grained sandstone bodies with planar cross-

bedding showing palaeocurrent directions towards the SSE. Moderate bioturbation, oxidised plant remains, and iron-rich surfaces may be observed.

Interval 22 (2.2 m): It consists of three coarse-grained slightly calcareous sandstone bodies commonly displaying planar cross-beddings and flat bases with ferruginous surfaces. The interval is topped by a thin mudstone accumulation (less than 0.4 m in thickness) that includes minor lignite amounts. Palaeocurrent directions measured (when possible) point towards an ENE direction. This interval is characterised by the occurrence of a vomerine dentition interpreted as belonging to an actinopterygian fish (Pycnodontiformes order) (Chamizo-Borreguero et al., 2008) (Fig. 5.22).

Interval 23 (2 m): It comprises a medium-grained fining upwards sandstone body with an internal erosional scour, displaying planar cross-bedding (palaeocurrent direction toward the SE), scattered plant remains, and bivalve shell fragments.

Interval 24 (3.5 m): The lower part of this interval consists of medium-grained calcareous sandstones with high clay contents that display abundant wavy and flaser heterolithic beddings and double mud drape structures. The pollen sample from the Tejadillos outcrop (T-CA-1a) studied in this Ph.D. thesis and by Bueno-Cebollada et al. (2021) was collected at this interval of the logged section. The former calcareous sandstone bodies are sharply overlain by coarse-grained calcareous sandstones displaying moderate bioturbation and scattered plant remains and bivalve shell fragments. Additionally, it shows conspicuous planar cross-bedding migrating in an SSE direction. Regarding morphology, this body consists of, at least, two amalgamated lenticular bodies that include an internal erosional scour and minor ferruginous surfaces.

Interval 25 (5.5 m): This interval shows an approximately 0.5 m-thick layer consisting of medium-grained sandstone with flaser heterolithic beddings which are overlain (with a sharp ferruginous contact) by lens-shaped calcareous sandstone bodies with planar cross-beddings and moderate bioturbation. The main palaeocurrents measured in the sandstone bodies indicate that the migration of the bedforms is toward the NE.

Interval 26 (0.5 m): Dark calcareous mudstones showing a laterally extensive tabular morphology.

Interval 28 (6 m): This interval consists of three calcareous sandstones to sandy limestone bodies which present flat base and top contacts, and tabular laterally extensive morphologies. The lowermost body consists of bioturbated marly limestones to calcareous sandstones which include ostreid shell fragments and asymmetrical ripple lamination. The former body is overlain by sandy limestones to calcareous sandstones with planar cross-beddings and bivalve and oyster shell fragments. The uppermost body is a marly limestone body arranged in 0.2 to 0.6 m-thick beds similar to the lowermost body described in this interval. The measured palaeocurrents indicate that the main transport direction was towards the SE and the subordinated direction towards the SW (Fig. 5.22). This interval marks the top of the logged section in the Tejadillos outcrop and is conformably overlain by the Cenomanian green marls and mudstones of the Chera Fm (Fig. 5.23E).

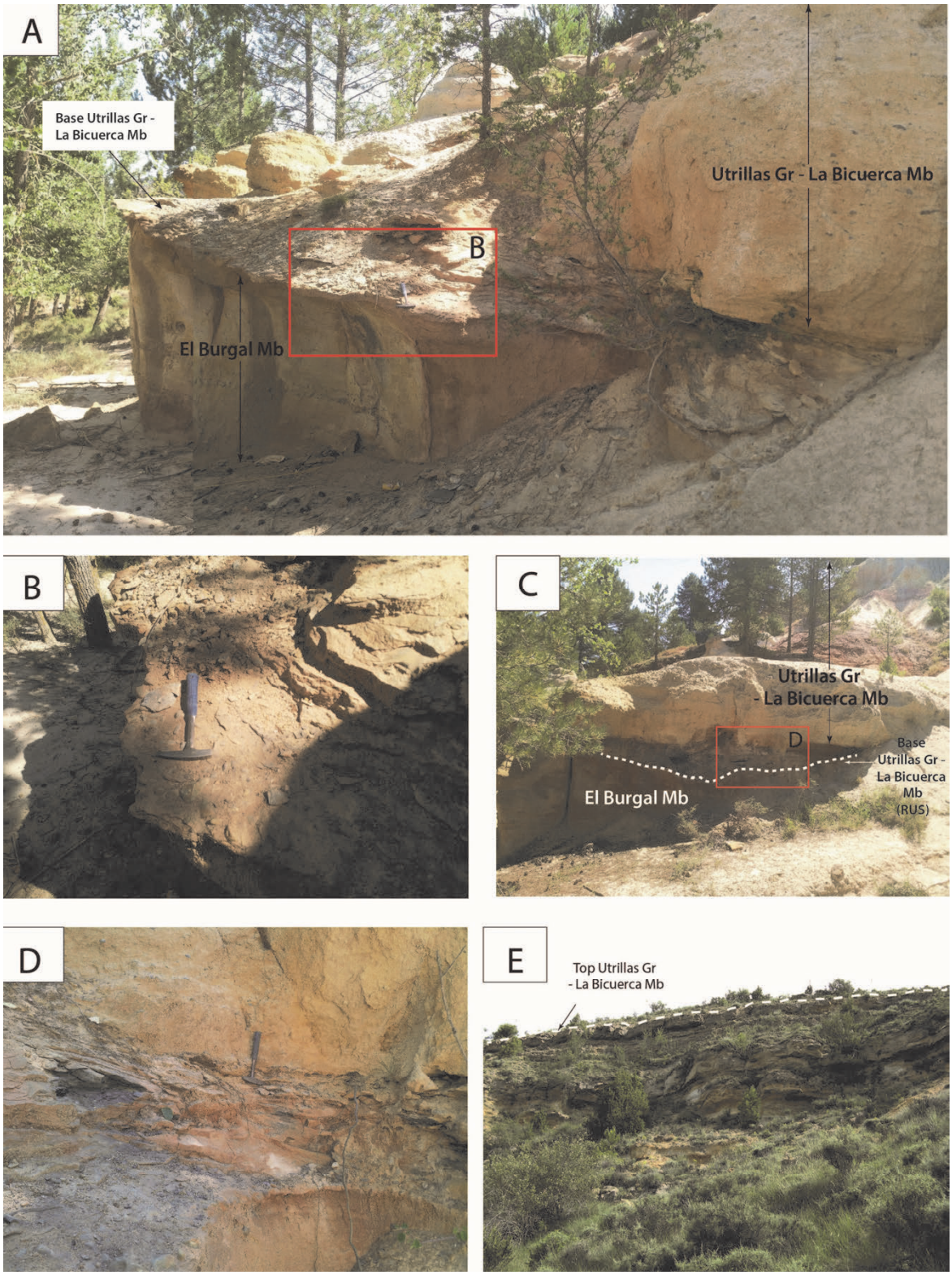

Fig. 5.23. (A) General view of the contact between the El Burgal Mb and the Utrillas Gr - La Bicuerca Mb succession at the Tejadillos outcrop. (B) Close-up of the erosional surface, covered by abundant pebbles and cobbles, that forms the base of the Utrillas Gr - La Bicuerca Mb succession in Tejadillos. This surface is referred to as the regional unconformity surface (RUS). (C) Picture showing the erosional character of the base of the Utrillas Gr - La Bicuerca Mb succession. (D) Fine-grained sandstone level with organic debris overlying the RUS. (E) Upper part of the Utrillas Gr - La Bicuerca Mb succession in Tejadillos. The dashed white line represents the top of the Utrillas Gr - La Bicuerca Mb in the outcrop that is overlain by the Chera Fm. Hammer for scale is 35 cm in length.

5.2.2. La Huérguina outcrop.

The La Huérguina outcrop is located in the surroundings of the La Huérguina village, Cuenca Province (Fig. 5.24). The study area is mainly located at the Cerro Pericón, a hill located to the North of the La Huerguina Village where a sedimentary section has been logged (Fig. 5.25). The lower part of the logged section (intervals 1 to 16; Fig. 5.25) in the La Huérguina outcrop has been logged in a ravine on the eastern side of the Cerro Pericón; while the upper part (intervals 17 to 30; Fig. 5.25) is logged in a ravine 150 meters to the south (Fig. 5.24).

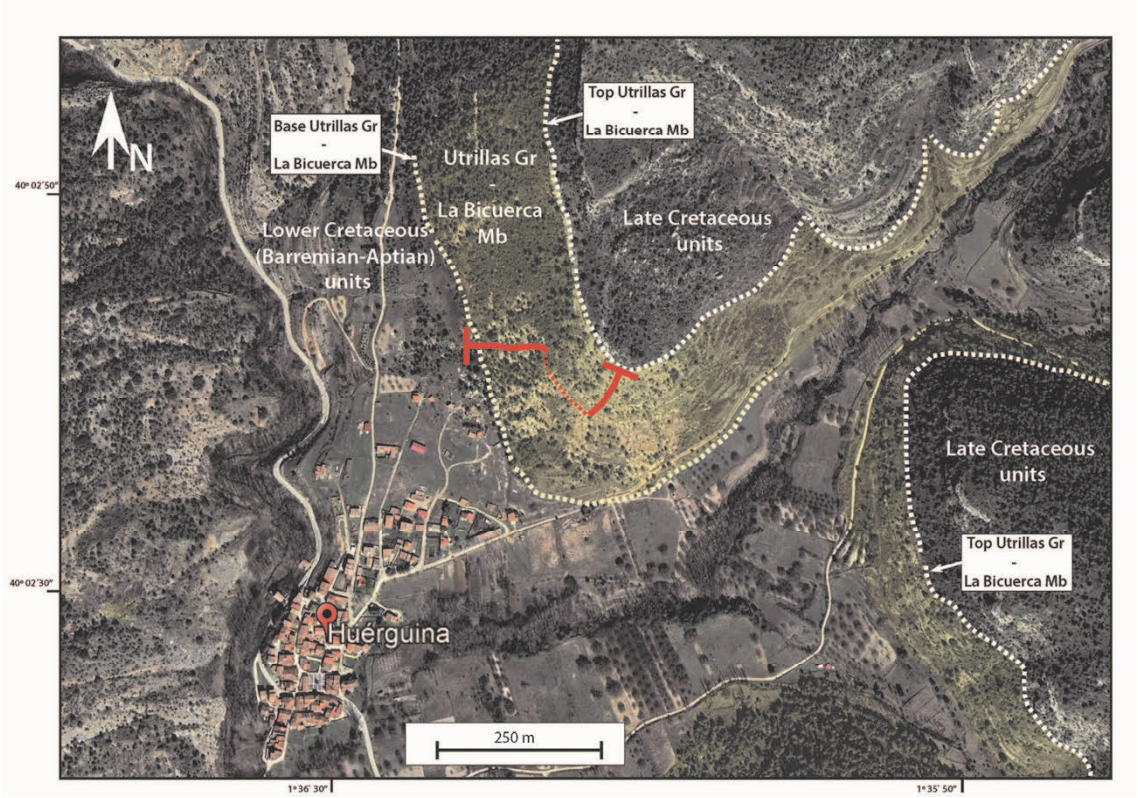

Fig. 5.24. Satellite image corresponding to the studied outcrop in La Huérguina. The extension of the Utrillas Gr - La Bicuerca Mb succession (between the yellow dotted lines and highlighted in yellow colour) is included. The location of the logged section is also included (red line). Image source: Google Earth.

The lower part of the logged section (intervals 1 to 16) is dominated by coarse-grained sandstones, with abundant pebbles towards the base, which alternate with reddish to greenish mudstones and siltstones. Conversely, the upper part (intervals 17 to 30) is dominated by calcareous sandstones interbedded with subordinate grey mudstones and marls (Fig. 5.25).

The upper part of the logged section was initially studied by Chamizo-Borreguero (2006), who logged three sedimentary sections in the Cerro Pericón (logged sections Cerro Pericón 1-3, respectively) comprising the upper half of the Utrillas Gr - La Bicuerca Mb succession and reaching the top contact with the Cenomanian Chera Fm. In this regard, the sections logged by

Chamizo-Borreguero (2006) have been revisited in the field during the fieldwork of this Ph.D. thesis and interpreted in a holistic approach, including the lower part of the Utrillas Gr - La Bicuerca Mb succession (Fig. 5.24, 5.25).

Fig. 5.25. Logged section at the La Huerguina outcrop. The explanation of the graphic symbols is included in appendix IV (A).

Likewise, the sedimentary succession studied in La Huérguina also includes a productive pollen sample (LH – CM (2) – 1a) that was collected on a hill, approximately 400 m to the ESE of the logged section (Fig. 5.24), in a bed that is laterally equivalent to interval 20 of the logged section. The palynological sample has been studied by Bueno-Cebollada et al. (2021) and in the chapters on palynology and biostratigraphy (6 and 7, respectively) of this Ph.D. thesis manuscript.

Description of the logged section (Figs. 5.25, 5.26).

Interval 1 (3 m): The lower part of this interval consists of a 1.3 m-thick body of gravel-size reddish sandstones with interbedded quartzite pebble and cobble beds. This lower body is overlain by a thin layer of red mudstone. The upper part of the interval is 1.7 m-thick and comprises a slightly fining upwards coarse-grained sandstone body with scattered pebbles that is sharply overlain by red mudstones.

Interval 2 (2.4 m): This interval comprises three 0.5 to 1 m-thick coarse-grained calcareous sandstone bodies with erosional bases. The base of the first body is particularly erosional and shows ferruginisation (Fig. 5.26B). The calcareous sandstone bodies show planar cross-bedding with sets migrating either in a SSE or NNW direction. They present a scarce palaeontological content that is represented by bivalve shell fragments (mainly poorly preserved ostreid fragments) and heavily oxidised, non-recognizable plant fragments.

Interval 3 (0.6 m): Partly covered coarse- to very coarse-grained arkose sandstone body with scattered quartzite pebbles and erosional base showing a conspicuous ferruginous surface (Fig. 5.26C-D). Regarding sedimentary structures, cm-scale trough cross-bedding has been observed.

Interval 4 (0.9 m): Partly covered. Coarse-grained sandstones.

Interval 5 (1.7 m): It consists of coarse- to very coarse-grained arkose sandstones arranged into 30 to 70 cm-thick bodies with erosional bases and fining upwards trends. The bodies present 20 to 50 cm-thick sets of planar and trough cross-bedding showing transport directions toward the SE. Additionally, asymmetrical ripples can locally be observed towards the top of the bodies along with oxidised plant fragments.

Interval 6 (3.4 m): This interval consists of massive red mudstones and siltstones that may show a mild yellowish mottling. Root traces have not been observed in this interval.

Interval 7 (0.8 m): Covered.

Interval 8 (3.3 m): The lower part of this interval comprises a 0.9 m-thick coarse-grained sandstone body with sets of trough cross-bedding migrating toward the East and oxidised plant remains that is overlain by a thin (10 cm-thick) layer of laminated mudstone. The upper part of this interval comprises a 2.4 m-thick body with very coarse-grained sandstones locally showing matrix-supported conglomerate (quartzite pebble) beds and oxidised plant remains. It presents an erosional base and a fining upwards trend. The main sedimentary structures observed are sets of trough and planar cross-bedding with foresets migrating to the NE and E. However, the uppermost beds present tabular plane parallel bedding and are dominated by medium-grained sandstones.

Interval 9 (2 m): It consists of coarse-grained arkose sandstones arranged into four tabular bodies with 30 to 40 cm-thick sets of planar cross-bedding that migrate in an E to SSE direction. They present flat

slightly erosional bases and scattered quartzite pebbles.

Interval 10 (3 m): The lower part of this interval consists of 2 m of massive reddish to purple mudstone and siltstone with weakly developed root traces and subordinate thin layers of fine- to medium-grained sandstone. Conversely, the upper part of the interval comprises a 1 m-thick body of coarse-grained sandstone with erosional base, internal scours, and planar cross-bedding with palaeocurrent directions toward the SSE.

Interval 11 (0.9 m): Partly covered, mainly mudstone.

Interval 12 (4.2 m): This interval comprises two coarse- to very coarse-grained sandstone bodies with fining upwards trends and erosional bases. The lower body is 3 m in thickness and comprises abundant internal erosional scours, scattered pebbles, and local ferruginous surfaces. It shows sets of planar cross-bedding with palaeocurrents towards the SSE and locally toward the NE, that are characterised by the occurrence of rhythmical alternations in the grain size of the foresets. The upper body is 1.2 m-thick and characterised by planar cross-bedding sets migrating toward the SSE and NE with rhythmical alternations in the grain size of the foresets.

Interval 13 (5.9 m): Massive red mudstone lacking root traces with 20 to 50 cm-thick beds of coarse-grained sandstones with planar cross-bedding and current ripples.

Interval 14 (2.1 m): It consists of coarse- to very coarse-grained sandstones depicting a fining upwards trend and showing an erosional base. They present planar cross-bedding arranged into sets indicating transport direction to the S and N/NW. The top of the interval presents asymmetrical ripples.

Interval 15 (2.6 m): This interval comprises three to four coarse- to very coarse-grained arkose sandstone bodies with erosional bases and cm-scale trough cross-bedding and oxidised plant fragments. The foresets of the trough cross-bedded sets show rhythmical alternations in the grain size of the foresets.

Interval 16 (1 m): It comprises a very coarse sandstone body with 1 m-thick planar cross-bedded sets with rhythmical alternations in the grain size of their foresets. The migration of the bedforms is toward the SE.

Interval 17 (2.7 m): The interval consists of coarse-grained calcareous sandstones arranged into three bodies with trough cross-bedding and internal erosional scours. The calcareous sandstones present scattered bivalve shell fragments and moderate bioturbation in the uppermost beds of the interval.

Interval 18 (3.3 m): Massive grey mudstones to marls.

Interval 19 (4.3 m): This interval comprises five to six coarse-grained sandstone bodies that show a slight fining upwards trend and erosional bases. The bodies present 30 to 50 cm-thick sets of planar cross-bedding dominated by palaeocurrents that migrate towards the SSE and SE and show rhythmical alternations in the grain size of the foresets. Oxidised plant remains along with quartzite pebbles may be locally found.

Interval 20 (3.4 m): Massive reddish mudstones with a mild grey mottling lacking root traces.

Interval 21 (1.6 m): Partly covered. it consists of coarse-grained calcareous sandstones which present moderate bioturbation (poorly preserved vertical tubes) and scattered bivalve shell fragments. The top of the interval is represented by a thin layer of calcareous mudstone.

Interval 22 (1.2 m): It consists of medium- to coarse-grained slightly calcareous sandstones with an erosional base that show a massive aspect and lenticular shape. However, large-scale planar cross-bedded sets can be locally observed, when preserved. The base of this body may present scattered quartzite pebbles and mud pebbles.

Interval 23 (3.2 m): This interval consists of medium- to coarse-grained calcareous sandstones whose base is erosional and may contain quartzite pebble lags. The interval shows a fining upwards trend being dominated by coarse-grained sandstones over the first 1.6 m and by medium-grained sandstones in the uppermost 1.6 m of the interval. The main sedimentary structure observed is planar cross-bedding arranged into 40 to 50 cm-thick sets in the lower part and 10 to 30 cm-thick sets in the upper part. The migration of the bedforms to the S and NE, respectively. Additionally, the upper beds of the interval seem to be moderately bioturbated.

Interval 24 (0.6 m): It consists of an alternation of slightly calcareous sandstone and grey mudstone with flaser and wavy heterolithic beddings and current ripples. The occurrence of bone fragments has been observed in a laterally equivalent bed (Chamizo-Borreguero, 2006).

Interval 25 (1.6 m): This interval consists of coarse-grained calcareous sandstones arranged into two 0.8 to 1 m-thick tabular bodies with flat bases. They present 0.8 to 1 m-sets of planar cross-bedding with their foresets migrating toward the NE. Locally, they present scarce bivalve shell fragments and organic debris.

Interval 26 (6.6 m): It comprises medium- to coarse-grained calcareous sandstones arranged into 10 to 20 cm-thick bodies with 10 cm-thick sets of planar cross-bedding showing current bipolarity. The calcareous sandstones present thin (10 cm-thick) dark mudstone layers interbedded. Additionally, wave ripples can be observed in the upper part of some sandstone bodies. This interval may present moderate to intense bioturbation, being dominated by vertical tubes. Similarly, it may present bivalve shells (ostreids) and echinoderms fragments.

Interval 27 (1.2 m): The interval comprises coarse-grained calcareous sandstones to sandy limestones (sandy packstone) that are arranged into 10 to 20 cm-thick tabular bodies dominated by planar cross-bedding with a NE transport direction and bioturbation (Fig. 5.25). Additionally, the sandstone bodies may present beds with wave ripples and interspersed calcareous dark mudstones.

Interval 28 (2.9 m): It comprises coarse-grained (slightly or non-calcareous) sandstones arranged in two 1.5 to 1.1 m-thick tabular bodies that show large-scale (more than 1 metre) planar cross-bedding with sigmoidal foresets that migrate toward the NE. The bodies show flat contacts both at their base and top surfaces and moderate to weak bioturbation.

Interval 29 (4.9 m): This interval consists of coarse-grained calcareous sandstones that form thin (10-20 cm-thick) bodies with planar cross-bedding, that show current bipolarity (palaeocurrents toward the SW and ENE) and wave ripples (Fig. 5.26E). Bioturbation in this interval is intense to moderate and dominated by vertical tubes.

Interval 30 (1.9 m): Coarse-grained slightly calcareous sandstones forming a lenticular body with an erosional base and moderate bioturbation. The only sedimentary structure observed is trough cross-bedding with palaeocurrents indicating a SW transport direction. The body shows a limited lateral extension, pinching out progressively toward the SE (Fig. 5.26E).

The top of interval 30 is overlain by a green marl succession, that is mostly covered in the La Huérguina outcrop and lies below the Upper Cretaceous marine carbonate units (Fig. 5.24, 5.25), interpreted as the Chera Fm. Therefore, its base represents the top of the Utrillas Gr - La Bicuerca Mb succession.

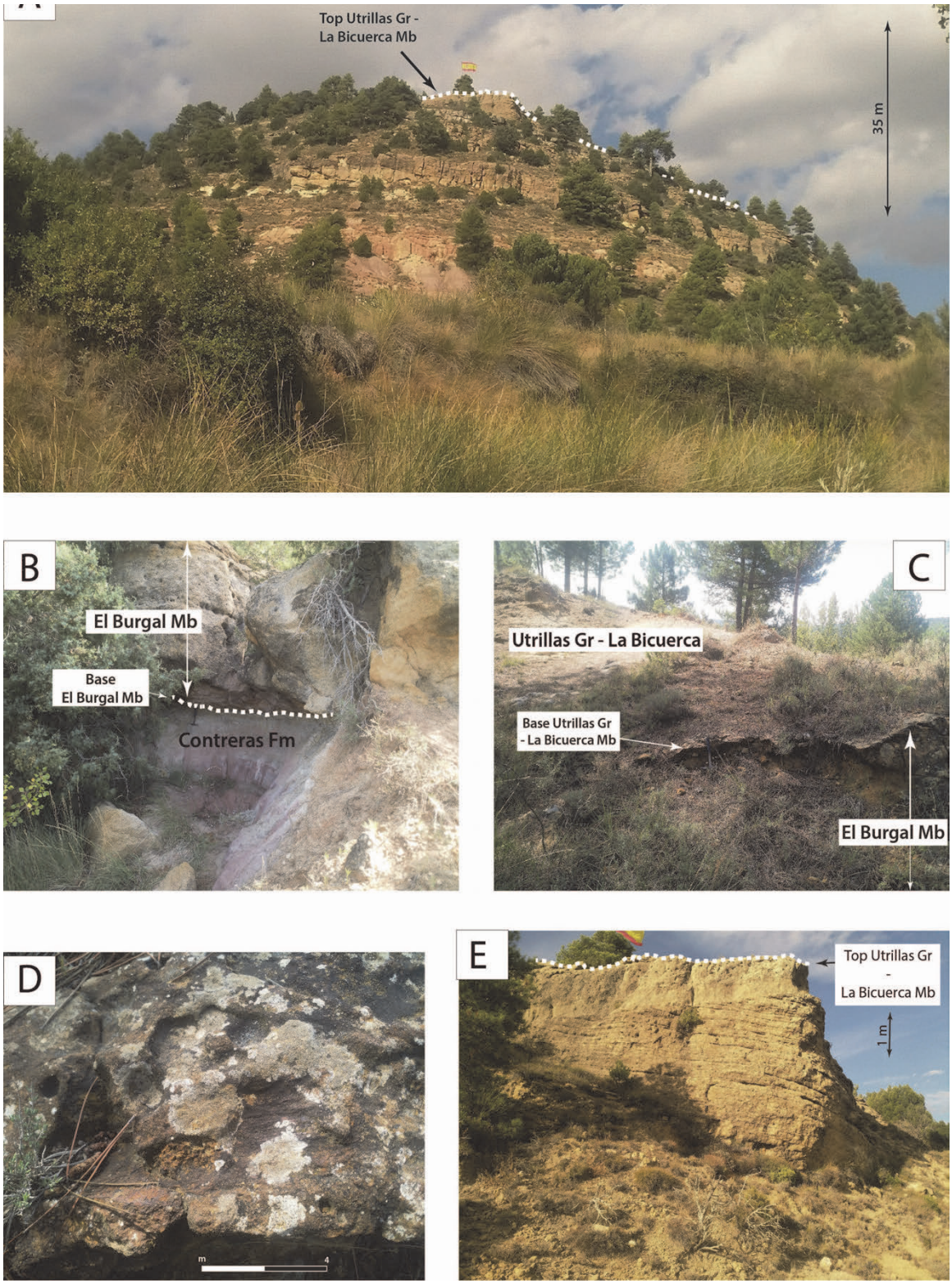

Fig. 5.26. (A) General view of the logged ravine at the La Huerguina outcrop (the lowermost logged levels cannot be seen in the picture). The dashed white line at the top of the outcrop marks the top of the Utrillas Gr - La Bicuerca Mb succession in La Huérguina. (B) Detail of the intervals 1 and 2 of the logged section in La Huérguina. The boundary between both intervals is an erosional surface (dashed white line) that represents the contact between the alluvial deposits of the lower Aptian Contreras Fm (below the surface) and the upper Aptian coastal succession of the El Burgal Mb (above the surface). (C) Contact between intervals 2 and 3 of the logged section in La Huérguina. The contact is a major ferruginous and erosional surface (regional unconformity surface - RUS) that represents the base of the Utrillas Gr - La Bicuerca Mb in the outcrop. (D) Close-up of the RUS at the base of the Utrillas Gr - La Bicuerca Mb succession, where poorly preserved moulds of tree bark can be observed. (E) Intervals 29 and 30 of the logged section in La Huérguina. The dashed white line indicates the top of the Utrillas Gr - La Bicuerca Mb succession. Hammer for scale in the pictures is 35 cm.

5.2.3. Campillos-Paravientos outcrop.

The Campillos-Paravientos outcrops is located in the surroundings of the Campillos-Paravientos village, Cuenca Province, Spain (Fig. 5.27). More concretely, the studied outcrop is located approximately 2 km to the ESE of Campillos-Paravientos.

The studied deposits in the Campillos-Paravientos outcrop correspond to the Albian to lower Cenomanian (C_{16}) and lower Cenomanian (C^{1}_{21}) units mapped by Portero et al. (1972). According to these authors, the Albian to lower Cenomanian unit is described as whitish to yellowish sandstones with kaolinite and interbedded with mudstones, interpreted as the Utrillas Gr deposits ("Utrillas-like facies"). The age of this unit was tentatively inferred based on the biostratigraphic ages of the overlying and underlying strata (Portero et al., 1972). Conversely, the lower Cenomanian unit is interpreted as calcarenite deposits with ostreids and orbitolinids.

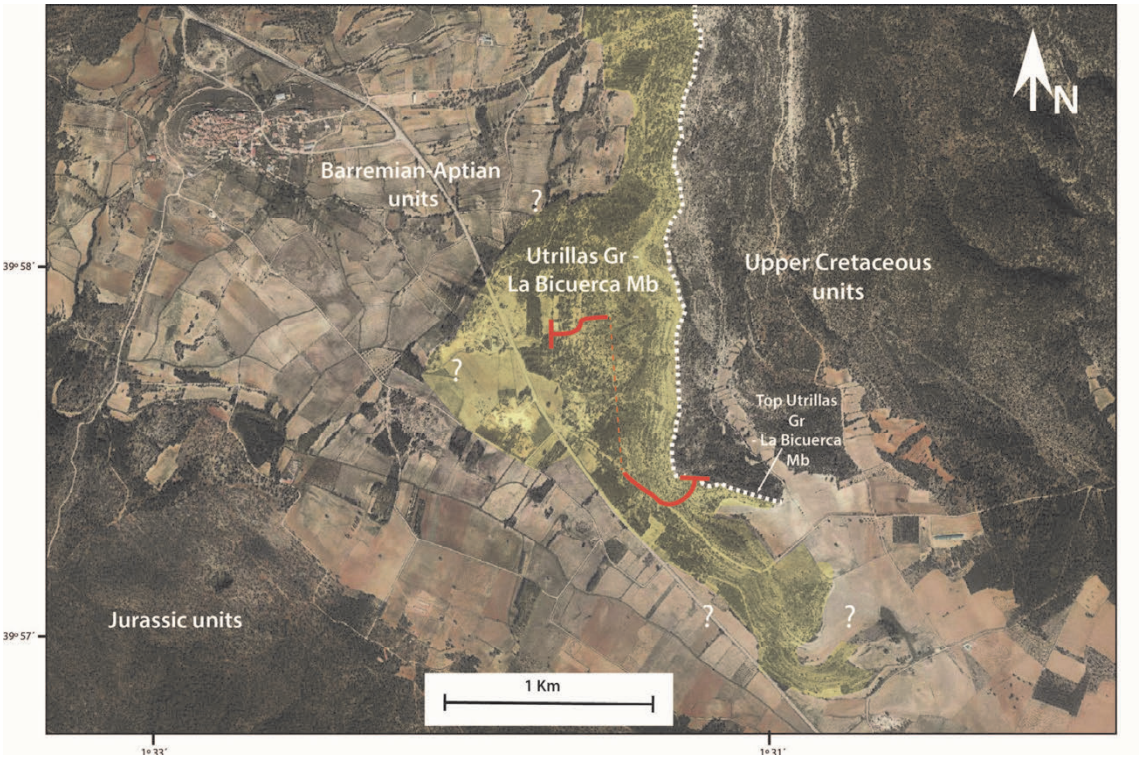

Fig. 5.27. Satellite image corresponding to the studied outcrop in Campillos-Paravientos. The extension of the Utrillas Gr - La Bicuerca Mb succession is highlighted in yellow colour and its top contact is indicated by a dashed white line. The location of the logged section is also included (red line). Image source: Google Earth.

These two stratigraphic units overlay shallow marine Aptian strata in the Campillos-Paravientos outcrop and are overlain by a Cenomanian green marl succession which is in turn overlain by the Upper Cretaceous marine carbonates (Portero et al., 1972).

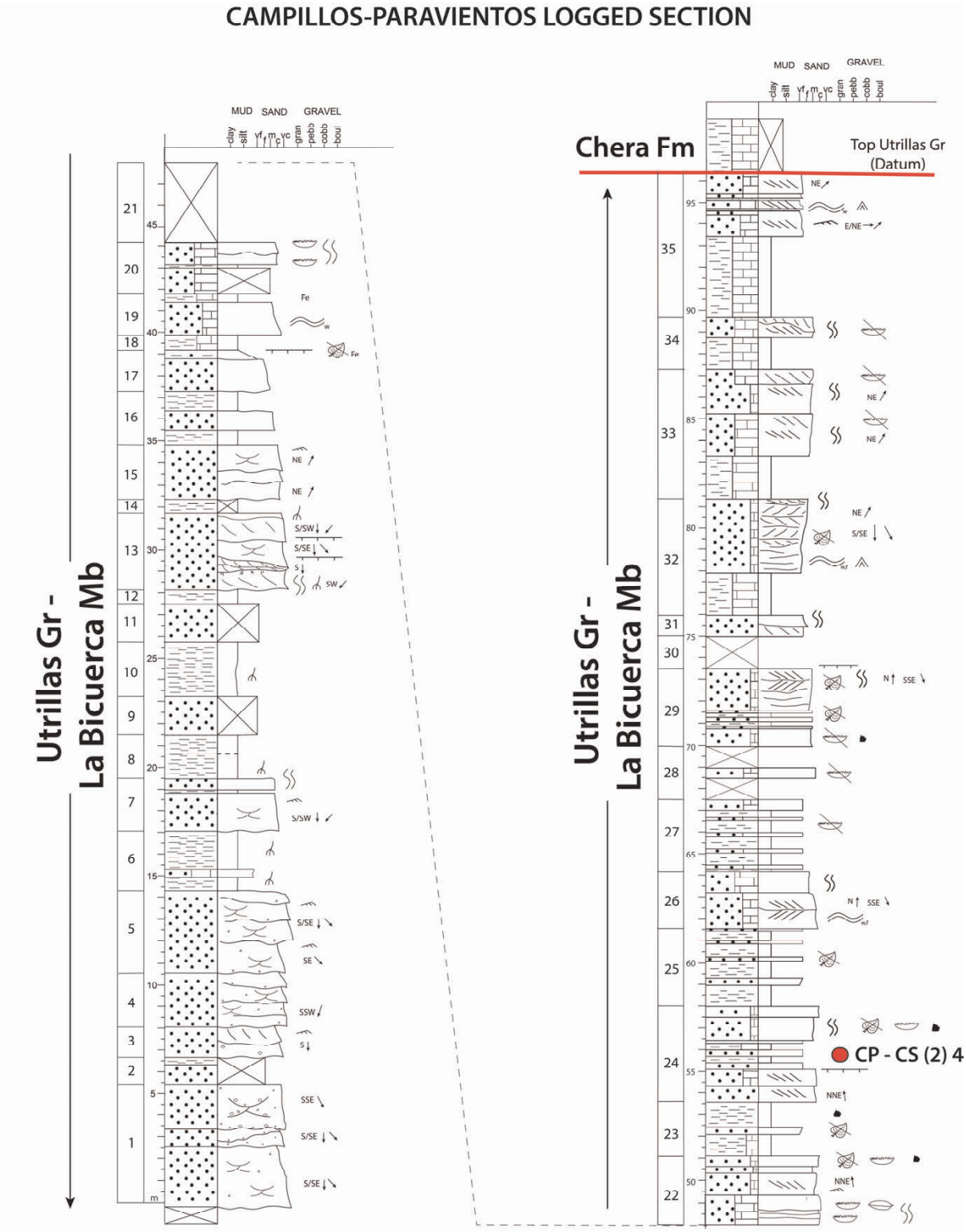

Fig. 5.28. Logged section at the Campillos-Paravientos outcrop. The explanation of the graphic symbols is included in appendix IV (A).

The logged section in the Campillos-Paravientos outcrop presented in this thesis is approximately 96 m-thick and comprises the deposits of the Utrillas Gr and La Bicuerca Mb. The top of the logged section represents the contact with the green marls of the Cenomanian Chera Fm, which has been used as the datum for local correlations at the scale of the Cuenca Basin (Fig. 5.28). The lower contact of the succession, with the Aptian strata, is covered in the area. However, it can be tentatively estimated that there are still 10 to 15 meters of Albian to lower Cenomanian strata covered until reaching the top of the Aptian strata.

In order to find the best-preserved levels of the outcrop, the logged succession has been divided into a lower (intervals 1 – 20 of the logged section) and an upper part (intervals 21 to 35 of the logged section) (Figs. 5.27, 5.28). The lower part comprises a sandstone succession consisting of amalgamated sandstone bodies towards the base that evolve into a sandstone succession with abundant red mudstones and siltstones interbedded. Conversely, the upper part is dominated by calcareous sandstones that alternate with mudstones and marls.

Description of the logged section (Figs. 5.27, 5.28)**:**

Interval 1 (5.4 m): This interval consists of coarse- to very coarse-grained sandstones arranged into three fining upwards bodies with erosional bases. The 2.5 m-thick lowermost body is dominated by 20 to 30 cm-thick sets of trough cross-bedding and scattered pebbles. The pebbles are mainly sub-angular in shape, although faceted ones can also be found. This body is overlain by a 0.5 m-thick body with scattered pebbles and internal erosional scours. The upper body shows larger-scale (50 to 60 cm-thick sets) trough cross-bedding and frequent pebbles and cobbles. The main palaeocurrent directions measured in these strata are towards S/SE and SSE.

Interval 2 (1.2 m): Partly covered. Mainly coarse-grained sandstones.

Interval 3 (1.3 m): It consists of a coarse- to very coarse-grained sandstone body with 20 to 30 cm-thick sets of planar cross-bedding migrating toward the south. The body is fining upwards and presents scattered pebbles and current ripples towards its top.

Interval 4 (1.5 m): It consists of amalgamated coarse- to very coarse-grained sandstone bodies which present 20 to 30 cm-thick sets of trough cross-bedding and current ripples. The bodies exhibit internal erosional scours and scattered quartzite pebbles. The measured palaeocurrents indicate a SSW transport direction.

Interval 5 (3.7 m): Amalgamated coarse to very coarse-grained sandstones with cm-scale trough cross-bedding showing a fining upwards trend similar to those described in interval 4. The measured palaeocurrents indicate that the bedforms migrate toward the S/SE.

Interval 6 (2.7 m): It consists of green and reddish-purple mudstones and siltstones which present a thin (0.3 m-thick) tabular body of poorly sorted calcareous sandstones. The occurrence of root traces is common in this interval.

Interval 7 (1.5 m): It comprises a fining upwards coarse-grained sandstone body with an erosional base. The sedimentary structures observed are cm-

scale trough cross-bedding and current ripples, the latter dominant towards the top of the body. The transport direction of the bedforms is toward the S/SW.

Interval 8 (2.7): Reddish to purple mudstones with yellowish mottling and root traces. Coarse-grained sandstone bodies with tabular morphology that pinch out in the mudstones are observed towards the lower part of the interval.

Interval 9 (1.7 m): Partly covered. Coarse-grained sandstones.

Interval 10 (2.6 m): Reddish to purple mudstones with weak palaeosoil development.

Interval 11 (1.8 m): Partly covered. Coarse-grained sandstones.

Interval 12 (0.5 m): Reddish to purple mudstones and siltstones with yellow mottling. Root traces have not been observed.

Interval 13 (3.6 m): It consists of amalgamated coarse to very coarse-grained sandstone bodies that exhibit fining upwards trends and erosional bases. The bodies are characterised by planar and trough cross-bedded sets with transport directions towards the SE, S and SW, which may show rhythmical alternations in grain size. Likewise, internal erosional scours and ferruginous surfaces are present in this interval. Regarding biogenic structures, this interval stands out by the occurrence of root traces and moderate bioturbation by vertical tubes.

Interval 14 (0.6 m): Covered. Mainly mudstones.

Interval 15 (2.4 m): The interval consists of amalgamated bodies of coarse- to very coarse-grained sandstones characterised by a mild fining upwards trend and erosional scours. Regarding sedimentary structures, they present 20 to 30 cm-thick sets of trough cross-bedding with transport directions toward the NE and current ripples towards the top of the bodies.

Interval 16 (2.6 m): Reddish to purple mottled mudstone with moderate bioturbation by root traces. The mudstones present a 0.7 m-thick coarse-grained sandstone body interbedded.

Interval 17 (1.9 m): It consists of 1.5 m of coarse-grained sandstone arranged into a lenticular body with an erosional base. The grain size fines upwards and gives rise to greenish siltstones with reddish mottling and root traces, showing ferruginisation at their top. The upper contact of this interval is a sharp and flat surface.

Interval 18 (0.8 m): This interval consists of dark marls that overlay the strata of interval 16 with a sharp and flat contact.

Interval 19 (1.5 m): It consists of coarse to medium-grained calcareous sandstones arranged in a lenticular body with fining upwards trend. It presents wavy heterolithic bedding and a ferruginous surface at its top which is overlain by a 30 cm marl bed.

Interval 20 (2.4 m): The lower part of this interval is partly covered and it mainly consists of calcareous sandstones. The upper part consists of a thin (10 cm-thick) layer with grey calcareous mudstone overlain by coarse-grained calcareous sandstones arranged into two 0.5 m-thick amalgamated bodies. These bodies show occasional ostreid shell fragments and moderate to intense bioturbation. No sedimentary structures have been observed.

Interval 21 (~ 4m): Covered.

Interval 22 (3.1 m): It consists of coarse- to medium-grained calcareous sandstones forming tabular bodies separated by flat surfaces. The sedimentary structures are not well-preserved and only, locally, current ripples and 20 to 30 cm-thick sets of planar cross-bedding may be observed, showing palaeocurrents directions to the NNE. Ostreid and bivalve other than ostreid shells can be found together with plant fragments and organic debris. Bioturbation is moderate to intense.

Interval 23 (2.5 m): The interval consists of a bed with green marls overlain by a thin (30 cm-thick) tabular layer of sandstone and approximately 1 m of greyish mudstones. Plant fragments and organic debris are present to a moderate extent.

Interval 24 (4.4 m): The lower part comprises two bodies with coarse- to medium-grained slightly calcareous sandstones with tabular morphology that exhibit planar cross-bedding (NNE palaeocurrent direction) and a ferruginous surface at their top. The middle part of the interval is characterised by a 1.2 m-thick bed with heterolithic (mudstone and sandstone alternations) deposits in which the palynological sample CP – CS (2) 4 was collected (Fig. 5.28). The upper part is dominated by coarse-grained calcareous bioturbated sandstones with ostreids, plant fragments, and organic debris.

Interval 25 (3.5 m): The interval consists of greyish mudstones and siltstones with thin tabular layers (10 to 20 cm) of non-calcareous sandstones interbedded. Rare, oxidised plant fragments may be found.

Interval 26 (2.5 m): It consists of two coarse- to medium-grained calcareous sandstone bodies with a slightly erosional base. The lower body shows cm-scale planar cross-bedding indicating that the migration of the bedforms was toward the N and SSE, together with wavy heterolithic lamination. Conversely, the upper body is intensely bioturbated and does not show any sedimentary structure. However, no identifiable trace fossils have been observed in this body.

Interval 27 (3.3 m): The interval comprises greyish mudstones and siltstones interbedded with thin tabular layers (10 to 20 cm) with non-calcareous sandstones. Plant fragments and organic debris can be found at this interval.

Interval 28 (2.5 m): Partly covered interval in which a thin, 0.4 m-thick, layer of calcareous sandstone with scattered bivalve shell fragments crops out.

Interval 29 (3.5 m): The lower part of the interval comprises a 0.7 m-thick body of coarse-grained calcareous sandstones with ostreid shell fragments and organic debris. It is overlain by approximately 0.7 m consisting of heterolithic (grey mudstone and sandstone) beds with scarce plant remains. The upper part of the interval comprises a 2 m-thick body of medium- to coarse-grained calcareous sandstones that show a coarsening upwards trend. The main sedimentary structure observed is planar cross-bedding showing an alternation in the direction of the palaeocurrents (N and SSE bedform migration directions). The body presents scattered plant debris, moderate bioturbation, and ferruginisation at its top.

Interval 30 (1.4 m): Covered.

Interval 31 (0.9 m): It consists of a 0.5 m-thick medium-grained calcareous sandstone body with planar cross-bedding sharply overlain by a 0.4 m-thick body with similar lithological characteristics but with intense bioturbation that has obliterated any sedimentary structures.

Interval 32 (5.4 m): Approximately 1.8 m consisting of dark marls (highly calcareous) which are overlain by a 3.6 m-thick body of medium- to coarse-grained calcareous sandstones showing a clear coarsening upwards trend. The lower part of the calcareous sandstone body is dominated by medium-grained sandstone with heterolithic wavy laminations showing double mud drapes and wave ripples. Upwards the grain size becomes coarser and the body is dominated by larger sets of planar and herringbone cross-bedding indicating migration of the bedforms towards the NE and S/SE in different superimposed sets. The uppermost bed (approximately 30 cm) presents bioturbation that has practically obliterated the sedimentary structures.

Interval 33 (5.9 m): It comprises 1.8 m of greenish to grey marls progressively overlain by two medium- to coarse-grained calcareous sandstone bodies with 30 to 50 cm-thick sets of planar to slightly sigmoidal

cross-bedding in which the measured palaeocurrents are towards the NE. The calcareous sandstones show ostreid shell fragments and intense to moderate bioturbation; plane horizontal tubular structures (*planolites*) have been observed among the identifiable trace fossils.

Interval 34 (2.3 m): This interval consists of 1.3 m of grey marls overlain by a 1 m-thick body consisting of medium-grain calcareous sandstone that presents planar cross-bedding and an internal erosional scour. The calcareous sandstone body is moderately bioturbated and presents ostreid fragments.

Interval 35 (6.6 m): It consists of a lower part with greyish to greenish marls (3.6 m) which are overlain by a 3 m-thick succession of medium-grained calcareous sandstones with 30 to 40 cm-thick sets of planar cross-bedding which present interbedded layers with wavy heterolithic laminations and wave ripples. The measured palaeocurrents indicate that the transport directions are toward the E/NE. The top of the interval 35 in the Campillos-Paravientos logged section is a sharp contact overlain by an approximately 20 m-thick green marl succession which is partly covered in the outcrop and interpreted as the Chera Fm. The green marl succession is overlain by the Upper Cretaceous marine carbonate units.

5.3. Southern sector.

5.3.1. Reíllo outcrop.

The Reíllo outcrop is located approximately 500 m to the north of Reíllo village, Cuenca, Spain (approximate coordinates: 39° 54’; 1° 52’) (Fig. 5.29). The outcrop studied here is in front of the village´s graveyard, and it can be reached by a secondary road parallel to the N-420 road.

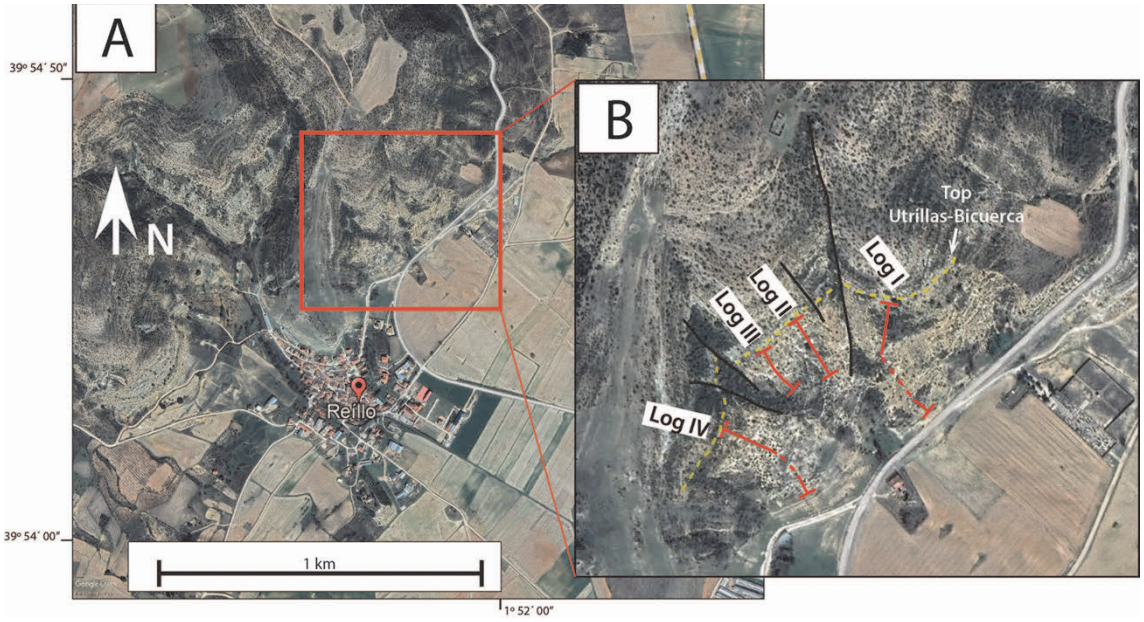

Fig. 5.29. Satellite image corresponding to the studied outcrop in Reíllo. (A) General view of the surroundings of Reíllo village. (B) Detail of the studied outcrop and logged section. The top of the Utrillas Gr - La Bicuerca Mb succession is marked by a dashed yellow line. The location of the logged section is also included and indicated by red lines, while the black lines represent faults interpreted in the outcrop. Image source: Google Earth.

Overall, four stratigraphic sections have been logged, correlated, and interpreted in this outcrop. The overall extension of the study area is approximately 400 m, and the adjacent logged sections are separated between 50 and 150 m (Figs. 5.29, 5.30).

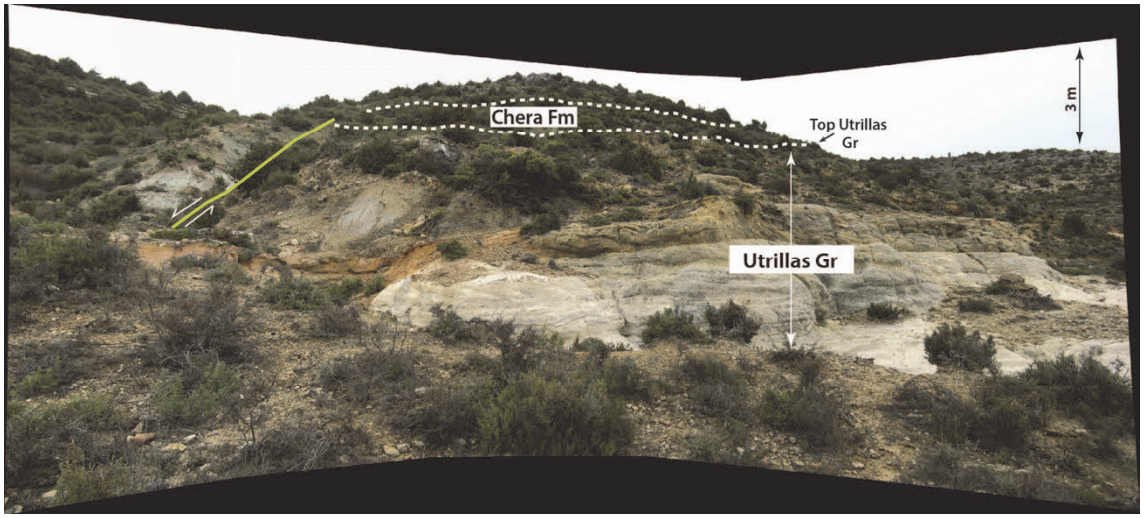

Fig. 5.30. Landscape picture of the studied outcrop at Reíllo. Photo courtesy of N. Meléndez.

The studied sections dip practically horizontal along the whole study area. However, the study area is affected by several fractures showing NNO-SSE and NO-SE trends. Such fractures (Fig. 5.29B) are interpreted as the result of Alpine faulting (Ramírez del Pozo et al., 1972). Therefore, the four stratigraphic sections are partial sections where the logged strata have not been affected by the fractures. Consequently, a correlation of the four logged sections has been carried out (Appendix IV), and a composite logged section has been constructed, which will be used for regional-scale correlation purposes and to better understand its vertical evolution (Fig. 5.31).

Description of the composite logged section (Fig. 5.31):

The logged section in the Reíllo outcrop is approximately 30 m-thick, but it is difficult to ascertain the exact thickness of the Utrillas Gr - La Bicuerca Mb succession in the area as the base of the logged section is completely covered. The intervals one to six of the composite logged section have been measured in the logged section I, while intervals seven to 14 are part of the logged section II (Fig. 5.31).

Interval 1 (>15 m): More than 15 m covered.

Interval 2 (2.5 m): It consists of coarse-grained to gravel-grain size arkose sandstones arranged in up to three amalgamated bodies that show 20 to 30 cm-thick sets of trough cross-bedding. Some scattered

pebbles up to 30 mm in diameter may also appear. The bodies are lenticular and show a slight fining upwards trend. The measured palaeocurrent direction is toward the SE. The upper part of the interval comprises green to yellowish mudstone with

of this manuscript and Bueno-Cebollada et al. [2021] for further information).

Interval 3 (2,1 m): Covered.

Interval 4 (1.7 m): It consists of coarse- to very coarse-

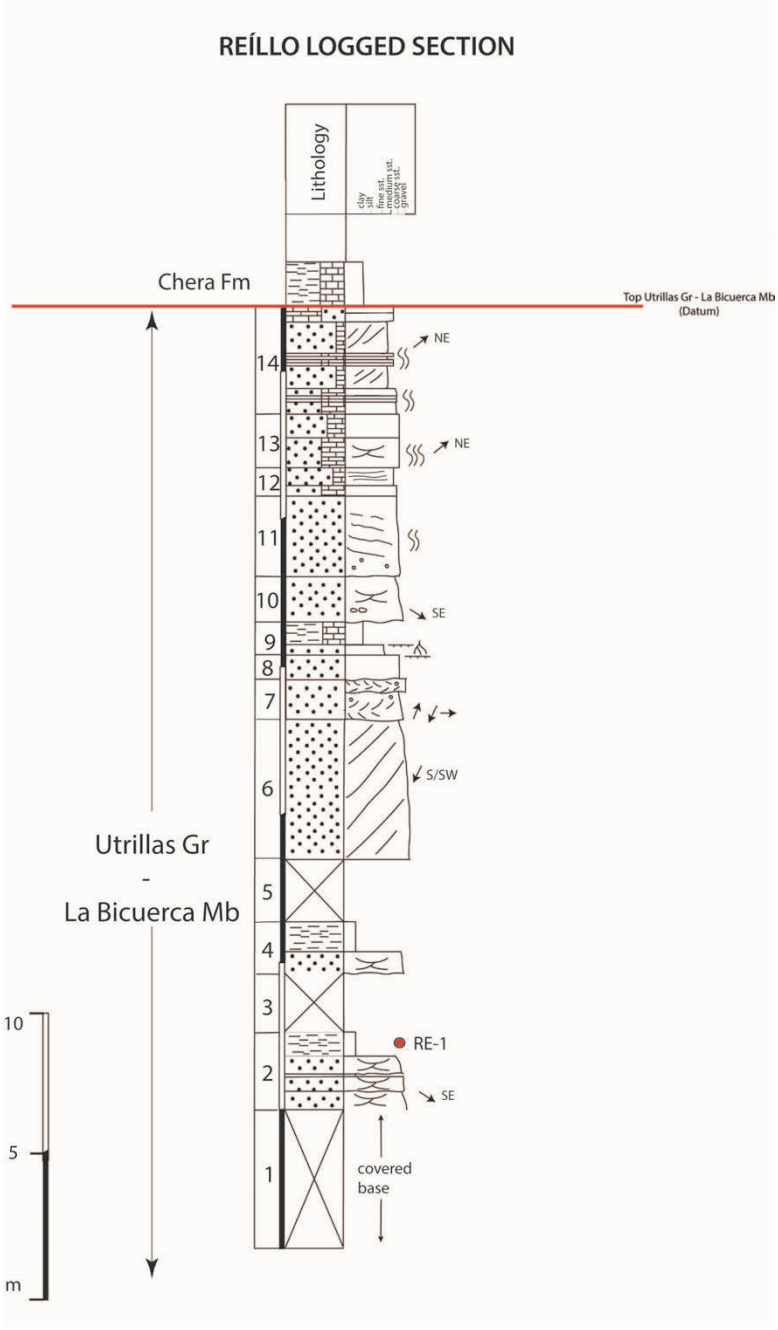

Fig. 5.31. Logged section at the Reíllo outcrop. The explanation of the graphic symbols is included in appendix IV (A).

scattered sand grains that sharply overlain the sandstone bodies. The pollen sample RE-1 was collected at this mudstone bed (see chapters 6 and 7

grained sandstones with trough cross-bedding and showing a fining upwards trend. The sandstone body (0.8 m-thick) also includes gravel-size siliciclastics

alternating with coarse sandstone-size grains. Locally, scattered pebbles may appear. The sandstone body is sharply overlain by a 1.1 m-thick reddish to greenish mudstone body. The lowermost part of this interval consists of green mudstones, which gradually change to reddish and purple mudstones upwards. The uppermost part of the interval consists of green mudstones.

Interval 5 (~3.5 m): Covered.

Interval 6 (5.5 m): The interval consists of coarse- to medium-grained sandstone arranged into a body with large foresets (two to four m-thick ones which can be traced downdip for approximately 10 m) of planar cross-bedding inclined towards the SW/S, dipping 10° on average. Its basal contact is covered in all the logged sections; however, its upper contact is a clear erosive surface. The bodies are wedge- to tabular-shaped.

Interval 7 (1.6 m): This interval consists of coarse-grained sandstones in which the prevailing sedimentary structure is trough cross-bedding arranged in 10 to 20 cm-thick sets that may show current bipolarity (herringbone-like beddings). The base of this unit is clearly an erosional one, and it may include encased mud pebbles and cobbles.

Interval 8 (0.8 m): It consists of yellowish to ochre coarse-grained arkose sandstone bodies, which display 40 to 50 cm-thick planar cross-bedding. The bodies show a sigmoidal morphology. Some scattered pebbles may appear towards the base, which is slightly erosional.

Interval 9 (1.2 m): Fine- to very fine-grained sandstone, poorly cemented and very well-sorted. It lacks any visible sedimentary structure but shows ferruginous surfaces and oxidised plant fragments that remain in a vertical position. The sandstone is arranged in lenticular bodies that crop out discontinuously across the outcrop, forming pods of sand that fill land depressions. This sandstone body is overlain by a bed with grey marls and calcareous siltstones whose colour may vary from greenish-grey to dark grey. Locally, reddish to yellowish colours may be found, indicating oxidation to some degree.

Interval 10 (1.6 m): It comprises a coarse- to very coarse-grained sandstone body with an erosional base that shows a fining upwards trend. It may have pebbles forming deflation lags that can be followed by more than 3 meters, laterally, throughout the outcrop. Regarding sedimentary structures, 10 to 20 cm-thick sets of planar cross-bedding are dominant, and minor through cross-bedding may also be observed. In the case of the planar cross beddings, the sets commonly display rhythmic grain size alternations. The bedforms migrate towards the SE.

Interval 11 (3.0 m): Coarse-grained sandstone showing large-scale horizontal to sub-horizontal bedding. The interval is fining upwards, consisting at its base of mostly gravel size deposits which fine upwards into coarse-grained sandstone. When observed closer, these horizontal to sub-horizontal beddings usually present crenulated surfaces that commonly contain abundant mud drapes. The lower contact of this interval is a sharp flat surface. Bioturbation is usually moderate in this interval; however, it is impossible to identify the observed trace fossils due to their poor preservation.

Interval 12 (1 m): The interval consists of a 30 cm-thick medium- to coarse-grained sandstone body heavily cemented with calcite. There are not any observable sedimentary structures. The body is overlain by a 70 cm-thick tabular sandstone body with lower contents of carbonate than the previously described one. Concerning sedimentary structures, the interval presents planar horizontal bedding, which extends laterally, and mud drapes.

Interval 13 (1.8 m): It consists of coarse-grained calcareous sandstones arranged into two amalgamated bodies that show flat sharp bases. The lowermost body is heavily bioturbated. It presents 30 to 40 cm-thick sets of trough cross-bedding that

migrate towards the NE. Scattered bivalve shell fragments can be observed.

Interval 14 (3.6 m): It consists of moderately bioturbated tabular bodies of medium to coarse-grained calcareous sandstones showing plane horizontal bedding overlain by medium-grained slightly calcareous sandstones with planar cross-bedding (arranged normally in 40 to 50 cm-thick sets). The planar cross-bedded sets show palaeocurrent directions towards the NE. Besides, the bodies may present scattered bivalve shell fragments. The uppermost beds comprise two 20 cm-thick sandy limestone layers whose upper contact is a flat and sharp surface overlain by the green marls of the Cenomanian Chera Fm (Fig. 5.30, 5.31).

5.3.2. Pajaroncillo outcrop.

The Pajaroncillo outcrop is located in the surroundings of Pajaroncillo Village, Cuenca Province. More concretely, it is on a small hill, to the west of a secondary road running from Carboneras de Guadazaón to Pajaroncillo villages (N-420 road) (Fig. 5.32).

In the Pajaroncillo outcrop, the studied stratigraphic succession is tilted, dipping about 30-35° towards NW and unconformably overlying Upper Jurassic strata (Fig. 5.32). The deposits of the logged succession in Pajaroncillo correspond to the Utrillas Gr, which presents calcareous sandstone beds in its upper part. The studied deposits are overlain by a thick marine carbonate succession which begins with the deposit of the green marls of the Chera Fm (Portero et al., 1972).

The logged section has an overall thickness of 79 m (including the covered areas) (Fig. 5.33). It begins in the structural contact (fault) with Jurassic (Fig. 5.32) and ends at the contact with the green marl of the Cenomanian Chera Fm, and it records the middle and upper parts of the Utrillas Gr - La Bicuerca Mb sedimentary succession. However, approximately 25 metres of the logged succession are covered by cultivated quaternary alluvial deposits.

The stratigraphic succession in the area is dominated by reddish to yellowish mudstones and siltstones and medium- to coarse-grained sandstones in its lower intervals. Locally, the sandstones display accumulations of pebble-sized quartzite clasts. This mudstone and sandstone succession is covered by approximately 25 m with cultivated quaternary deposits. Upwards in the logged section, the succession becomes progressively dominated by calcareous sandstones and greyish marls and mudstone, which progressively replace the sandstone and mudstone deposits.

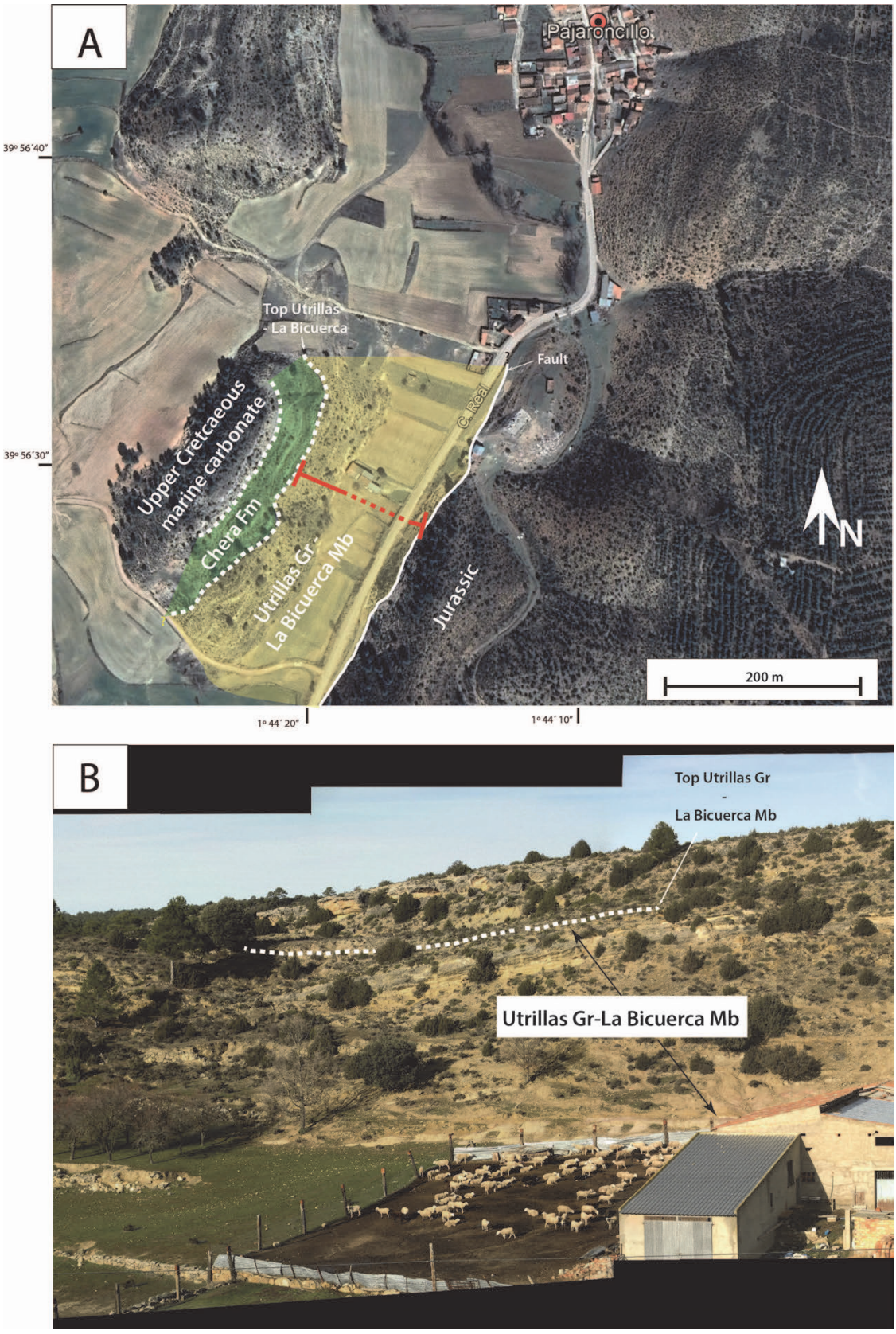

Fig. 5.32. (A) Satellite image corresponding to the studied outcrop in Pajaroncillo. The top of the Utrillas Gr - La Bicuerca Mb succession and the logged section are represented by a dashed yellow line and a solid red line, respectively. Image source: Google Earth. (B) Landscape picture of the studied outcrop at Pajaroncillo. The thickness of the succession indicated by the arrows is approximately 45 m (Modified from Bueno-Cebollada et al., 2022).

The following pages deal with a detailed description of the different intervals logged in the Pajaroncillo outcrop.

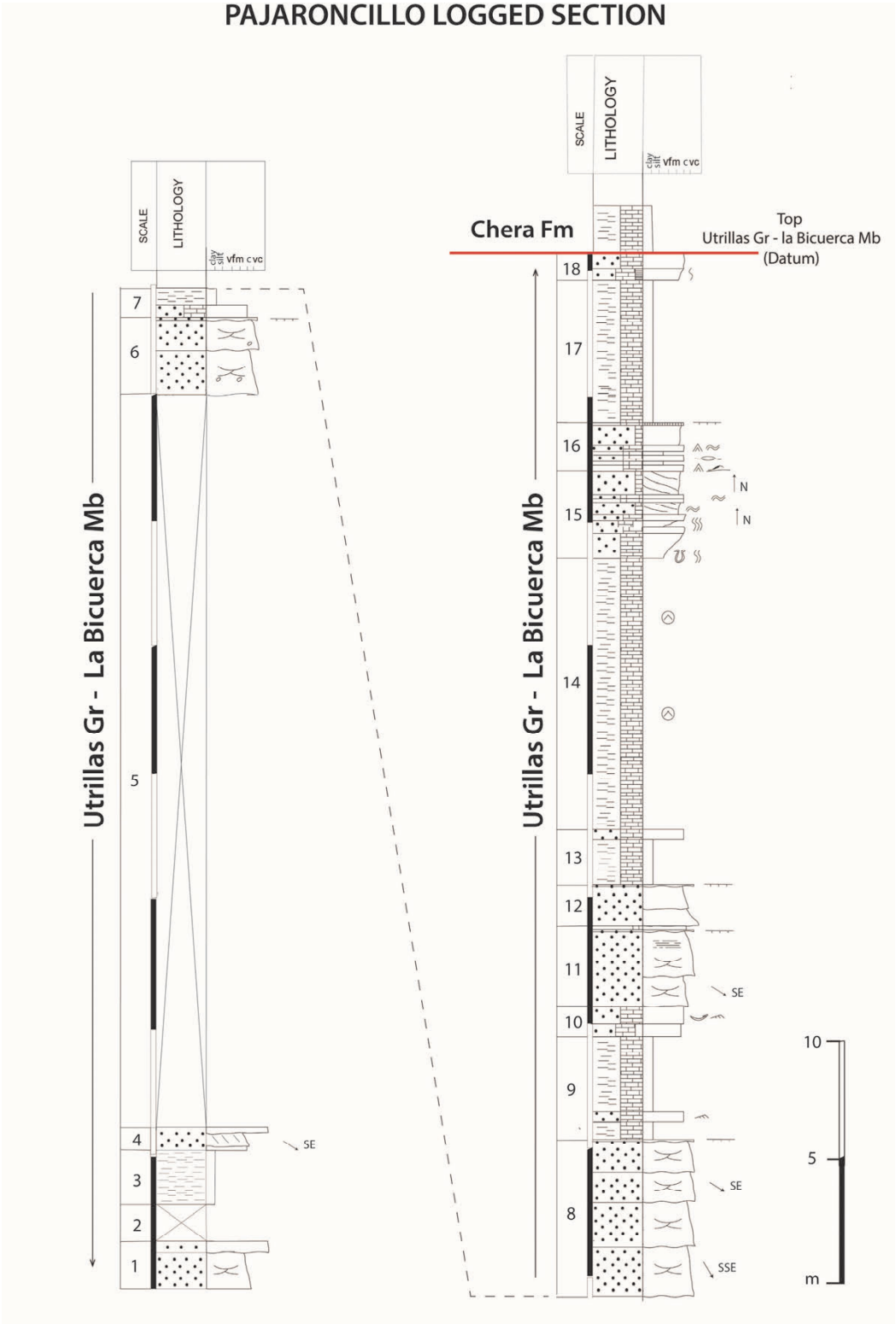

Fig. 5.33. Logged section at the Pajaroncillo outcrop. The explanation of the graphic symbols is included in appendix IV (A).

Description of the logged section (Fig. 5.33):

Base: The logged section begins in a structural contact (fault) between Jurassic strata and the Utrillas Gr succession.

Interval 1 (1.6 m): It consists of very coarse- to coarse-grained feldspar-rich sandstones. Some tiny pebbles (average size of 3 to 2 cm in diameter) can be observed but very locally and scattered across the outcrop. The general trend of the sandstone bodies is fining upwards. The sandstones are overlain by a 0.5 m-thick bed with matrix-supported conglomerates with a slightly erosive base. The clasts are quartzite clasts and pebble-size. It is important to mention that this conglomerate bed shows lenticular geometry and pinches out laterally in the outcrop.

Interval 2 (1.3 m): Covered.

Interval 3 (1.8 m): The interval consists of red mudstones to siltstones, with some fine-grained sand grains included within the mud- and silt-sized material. The base of this interval has not been observed since it is covered. No root traces have been observed.

Interval 4 (0.8 m): It consists of a very coarse- to coarse-grained yellowish feldspar-rich sandstone body, showing a finning upwards trend. Its base is flat and sharp, and it shows planar cross-bedding. This body is overlain by a flat-base thin layer (0.2 m-thick) that consists of matrix-supported conglomerates. The clasts are quartzite pebbles with sub-rounded morphologies.

Interval 5 (25 to 30 m): Covered.

Interval 6 (3.0 m): It consists of coarse- to very coarse-grained sandstone bodies; locally, the bodies may contain gravel-size sandstone and rare scattered pebbles. They usually are white to greyish ochre, although may locally present reddish to purple colours towards the top of the bodies. In general, sedimentary structures are poorly preserved, but cm- to dm-scale trough cross-bedded sets can be observed. Likewise, internal erosional scours within the bodies are observed throughout the outcrop, thus resulting in amalgamated sandstone bodies. The sandstone bodies are overlain by a reddish to orange coarse-grained to gravel-grained size sandstone body heavily cemented by iron oxides. It is arranged into a thin, tabular, and continuous layer which can be followed laterally throughout the outcrop.

Interval 7 (1.3 m): Thin layer (0.6 m) of ochre medium-grained calcareous sandstones that may show a slight nodular appearance. The layer is laterally continuous, and its geometry is tabular with a sharp upper contact. The calcareous sandstone is overlain by a 0.7 m-thick layer of light brown-yellowish to grey marls.

Interval 8 (5.9 m): Coarse- to very coarse-grained white to light greyish arkosic sandstone which locally presents gravel-size grains. The interval is arranged into four fining upwards bodies (1.2 to 2 m-thick) with an erosional base. Regarding sedimentary structures, trough cross-bedded sets can be observed. These sandy bodies show an amalgamated geometry and are overlain by a 10 cm-thick reddish gravel-size ferruginous level similar to the one mentioned at the top of interval 6.

Interval 9 (4.8 m): They consist of a 0.7 m-thick bed of grey marls with some sandstone and siltstone proportions that pinch out laterally towards the N-NE. This bed is overlain by a thin tabular layer (0.4 m-thick) of ochre to orange brownish calcareous sandstones, which locally show current ripple structures; its base is sharp to slightly erosional contact. The calcareous sandstone layer is overlain by a 3 m-thick bed consisting of greyish marls. A barren pollen sample was also collected at this interval.

Interval 10 (1.2 m): The first 0.5 m of this interval consists of a medium-grained calcareous sandstone

bed. Unlike its top, which is a slightly erosional contact, its base is a flat surface. The upper calcareous sandstone body, overlying the former, is approximately 0.7 m-thick and consists of medium-grained calcareous sandstones, which show current ripple structures and scarce bivalve fragments. These calcareous sandstones are heavily cemented by calcite cement. The body is tabular in geometry and can be followed laterally throughout practically the whole outcrop.

Interval 11 (3 m): The interval begins with 1.2 m of arkosic sandstone with some iron cementation towards its base. The grain size is coarse to medium showing a thinning upwards trend. The previous bed is overlain by 1.9 m of arkosic sandstones similar to the formerly described ones. However, this upper body shows coarse to very coarse grain size, and sedimentary structures are better preserved than in the underlying beds. Towards the base cm- to dm-scale trough cross-bedding can be observed, in which SE trending palaeocurrent directions have been measured. The top of this bed is a flat and sharp ferruginous surface. A 0.15 m-thick layer of whitish calcareous cemented coarse-grained sandstone can be observed on the top of the ferruginous surface.

Interval 12 (1.7 m): It consists of a 0.7 m-thick thinning upwards body of gravel-size arkosic sandstone that presents some small pebbles at its base and thins up to medium-grained sandstone size at its top. The top is an intense red coloured sandstone with a high content of iron oxides. A 0.9 m-thick medium- to fine-grained sandstone body overlies the previous body with a sharp contact, but unfortunately, no sedimentary structures have been observed. This bed is covered by a 10 cm-thick sandstone layer cemented by iron oxides, displaying an erosional contact.

Interval 13 (2 m): This interval begins with a 1.8 m–thick bed of greyish and yellow marls, which may locally present gypsum crystals. This bed is overlain by an approximately 20 cm-thick layer of calcareous sandstones. The calcareous sandstone is yellowish to ochre and shows an erosional base, and it can only be observed laterally in some areas of the outcrop since it is mainly covered by debris.

Interval 14 (10.8 m): This interval consists of grey to yellow marls with the occurrence of abundant weathered gypsum crystals observed laterally across the outcrop. However, in this interval, no gypsum layers have been found in situ, interbedded with the marls. Towards the top of the interval, this thick bed shows a gradual contact, presenting calcareous sandstone layers interbedded, becoming more heterolithic.

Interval 15 (5.1 m): The lower part of this interval consists of a 1 m-thick medium-grained calcareous sandstone body with thin marly layers interbedded that show a coarsening upwards trend. The lower contact is gradual, showing a coarsening upward succession from the marls described in interval 14; however, its upper contact is a sharp flat surface. Both symmetrical and asymmetrical ripples have been observed towards the middle of the bed regarding sedimentary structures. The bed shows tabular geometry throughout the whole outcrop. However, the most conspicuous feature of this bed is the presence of a laterally continuous bioturbated surface, which contains some exceptionally preserved vertical and u-shaped burrows.

The overlying bed consists of approximately 60 cm of calcareous sandstone which can show some variable marl contents towards its middle part. Likewise, bioturbation becomes more intense towards the middle of the bed. The main palaeocurrents measured indicate a northward transport direction. On top of the previous bed, a fine- to very fine-grained slightly calcareous sandstone body has been logged. The sandstone is white to ochre and shows 1 to 1.2 m-scale foresets of planar cross-bedding, depicting cm-scale small bundles. The bodies stack and pinch out towards the north. Regarding the observed sedimentary structures, small-scale planar cross-

bedding and heterolithic bedding (mostly wavy to flaser bedding) are the dominant features in this bed.

The top of this interval is a less calcareous sandstone body than the previously described one. It is a fine- to very fine-grained whitish sandstone body of about 95 cm in thickness. The main sedimentary structures observed in the outcrop are ~1 m-thick planar cross-bedded sets.

Interval 16 (2 m): The lower part of the interval comprises ~1.1 m of heterolithic layers where thin calcareous sandstone layers and marls alternate. The calcareous sandstone is medium-grained and more dominant than the marls; they usually depict thicknesses of about 15-20 cm, while the interbedded marl layers barely reach 10 cm in thickness. Regarding sedimentary structures, the whole spectrum of heterolithic bedding, ranging from flaser to wavy and lenticular beddings, has been observed in the outcrop. Likewise, asymmetrical (wave) ripple structures are also found in the strata.

The upper part of the interval consists of a 0.9 m-thick fine-grained sandstone body which is slightly calcareous. This sandstone shows similar appearance and characteristics as the ones described in interval 15 but lacks sedimentary structures. Hence, this sandstone body does not show any internal structure. The top of this body is crowned by a 15 cm-thick layer consisting of medium-grained calcareous sandstone heavily cemented by iron minerals. This surface can be traced laterally throughout the outcrop and presents irregularities and cavities (pot holes) 10 to 20 cm in diameter.

Interval 17 (5.7 m): Light grey to yellowish marls, which may present cm-scale calcareous sandstone layers that pinch out laterally in the outcrop.

Interval 18 (1.5 m): It consists of two heavily cemented calcareous sandstone beds, whose base is a flat surface. The lower body is 0.6 m-thick and the upper body is 0.9 m-thick. Its base is sharp non-erosional contact with the marls of the underlying interval 16, and its top is a sharp contact with the green marls of the Chera Fm, which represents the top of the Utrillas Gr - La Bicuerca Mb (Fig. 5.32, 5.33). The top of the Utrillas Gr - La Bicuerca Mb has been used as the main datum for correlation.

5.3.3. Cañada del Hoyo outcrop.

The Cañada del Hoyo outcrop is located in the surroundings of the Cañada del Hoyo village (Cuenca province) (Figs. 5.1, 5.34). More concretely, the logged section is on a small hill in the Centre of the Village which is topped by a castle (39°58´16” N, 1°54´07” W). The logged section (Fig. 5.35) is about 18 m in thickness and represents the uppermost intervals of the Utrillas- La Bicuerca Mb succession. The uppermost logged intervals coincide with the lithostratigraphic contact with the green marls of the Cenomanian Chera Fm, which are partly covered in the outcrop (Fig. 5.36A).

Despite the limited thickness of the sedimentary succession, the outcrop yielded abundant compressions of fossil plants towards the base of the logged section (Interval 2 of the logged section; Fig. 5.35). The fossil plant material was originally collected in the mid-1980s; however, it has been identified, classified, and interpreted for the first time in this Ph.D. thesis (see sub-chapter 7.2. of the manuscript for further information).

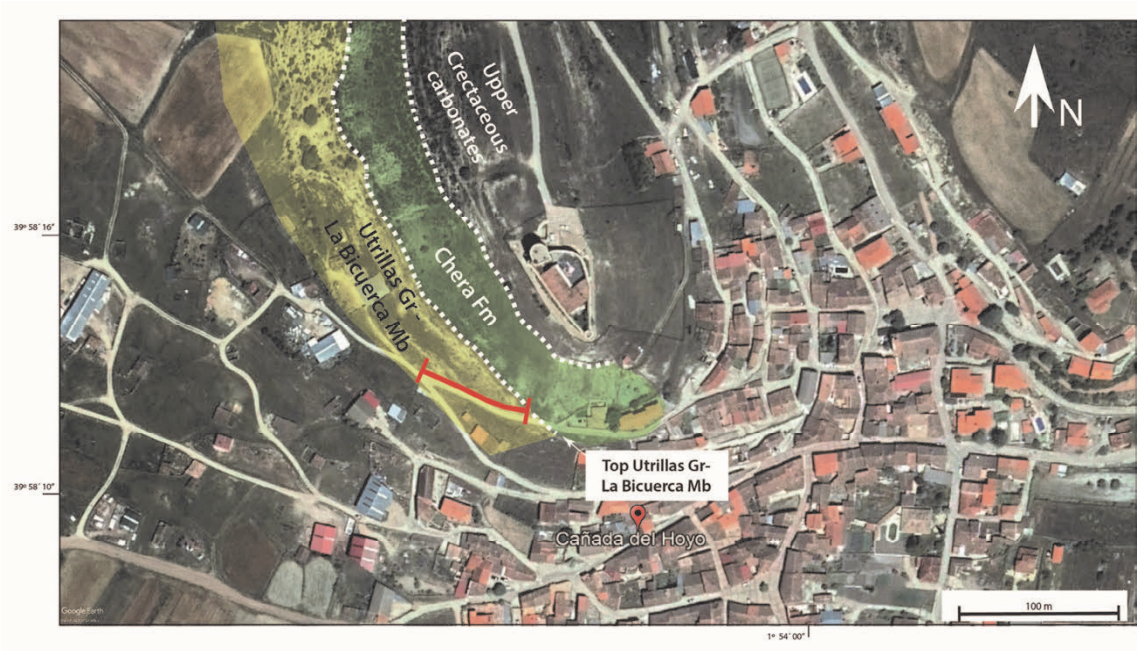

Fig. 5.34. Satellite image corresponding to the studied outcrop in Cañada del Hoyo. The top of the Utrillas Gr - La Bicuerca Mb succession is indicated. The location of the logged section is also included and indicated by a solid red line. Image source: Google Earth.

Description of the logged section (Fig. 5.35, 5.36)

Interval 1 (1.9 m): This interval lies on top of a covered sedimentary succession (Fig. 5.35). It consists of approximately 1.9 m of coarse- to very coarse-grained arkose sandstones showing planar cross-bedding in which the bedforms migrate in a SE direction. The planar cross-bedding is arranged in 30-40 cm-thick sets.

Interval 2 (0.4 m): This interval is approximately 50 cm thick and consists of a thin layer of dark mudstone (10 cm). On top of this layer of mudstone, there is a 40 cm-thick layer with slightly calcareous sandstones (Fig. 5.35), which are characterised by containing abundant fossil plant compressions, some of them showing a high degree of preservation. The collected fossil plant specimens from this layer have been identified and studied in the sub-chapter 7.2. of this thesis manuscript.

Interval 3 (3.3 m): The interval is characterised by a main 2.8 m-thick body with slightly coarsening upwards coarse-grained sandstones that are more than five meters in length showing a sub-horizontal to planar (2° to 3°) bedding (Fig. 5.36B). The foresets display abundant mud drapes which form undulated flaser-like heterolithic lamination structures. The main transport direction of the foresets is toward ESE (Fig. 5.35). The basal contact of the interval is slightly erosional. The upper part of this interval includes an approximately 0.5 m-thick layer of coarse-grained sandstones showing 40 to 30 cm-thick sets of planar cross-bedding with palaeocurrents indicating a WNW transport direction.

Interval 4 (0.4 m): The interval consists of coarse-grained calcareous sandstones arranged in a tabular body with a flat base. No sedimentary structures are observed. However, a moderate degree of bioturbation due to the action of non-identifiable biogenic structures can be noticed.

Interval 5 (0.8 m): It comprises coarse-grained ochre to light orange sandstones with abundant muddy bundles similar to the ones observed in interval 3 (Fig.

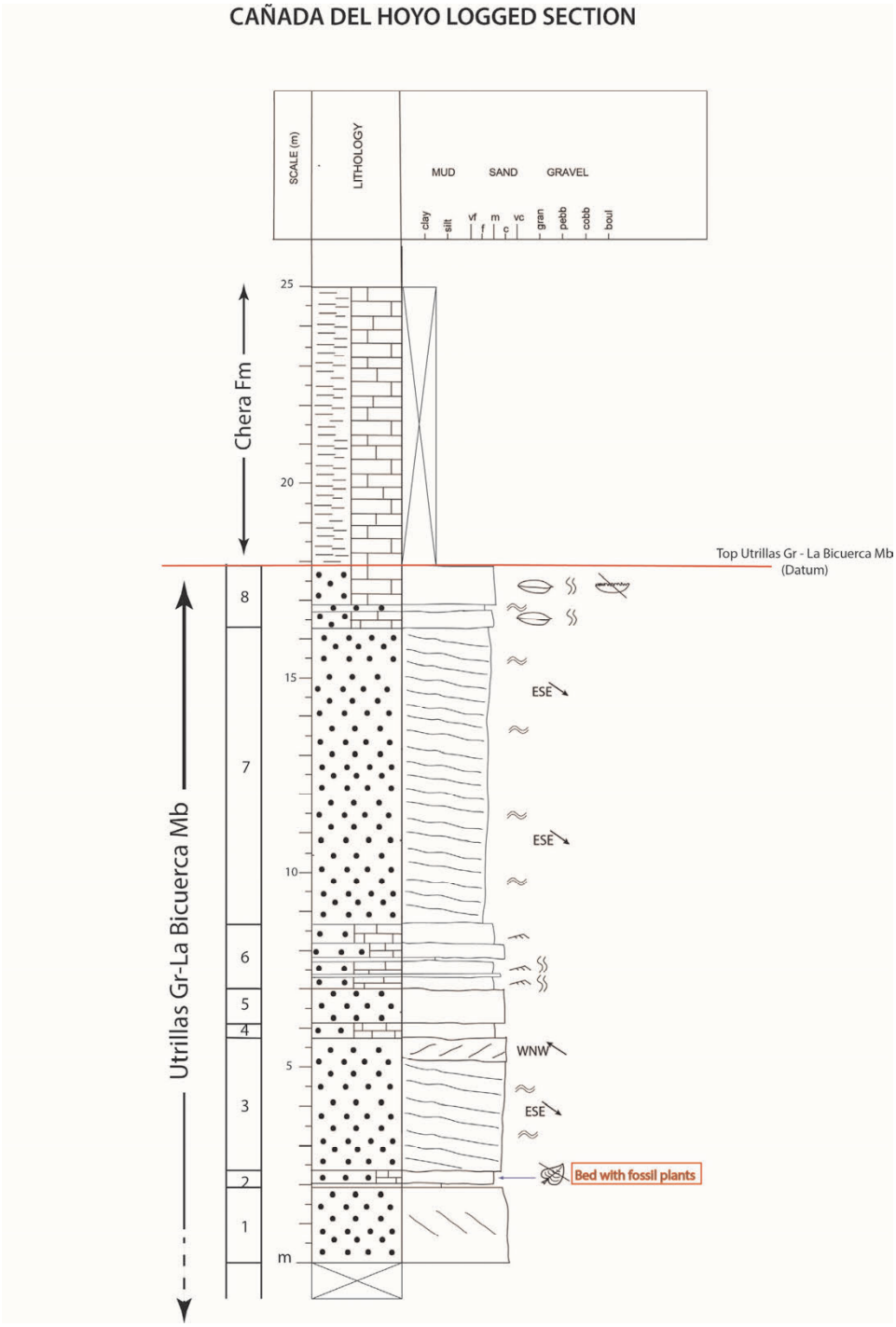

Fig. 5.35. Logged section at the Cañada del Hoyo outcrop. The explanation of the graphic symbols is included in appendix

5.35). The basal contact of this interval is slightly erosional.

Interval 6 (1.6 m): This interval consists of up to four 30 to 50 cm-thick beds of medium- to coarse-grained calcareous sandstone with moderate to highly bioturbation. The bodies are tabular and depict non-erosional flat-like bases. Regarding sedimentary structures, current ripples can be observed especially in the upper part of the bodies. Additionally, these bodies may present interspersed thin (less than 10 cm in thickness) layers of calcareous mudstones and siltstones.

Interval 7 (7.7 m): This interval consists of yellowish to light ochre non-calcareous sandstones characterised by long foresets (longer than 6 meters) of planar to sub-horizontal cross-bedding (Fig. 5.36D) with abundant flaser bedding. The foresets present an undulating outline (Fig. 5.36C), and the base of the interval is slightly erosional.

Interval 8 (2.6 m): This interval consists of three sedimentary bodies: (i) the lower sedimentary body is 50 cm-thick and consists of medium- to coarse-grained calcareous sandstones. The sandstones depict a flat to slightly undulating contact. They lack any observable sedimentary structure, probably obliterated due to the intense bioturbation. The occurrence of bivalve and ostreid shell fragments is scarce; (ii) the intermediate sedimentary body consists of coarse- to medium-grained slightly to non-calcareous whitish sandstones that present abundant silty to coaly bundles, giving rise to flaser-like laminations; (iii) The upper body is approximately 1 m-thick and consists of calcareous sandstones similar to those described in the lower body of this interval. However, the bioturbation is more intense and the occurrence of ostreids and other bivalve shell fragments is more frequent than in the first body logged. Interval 8 is overlain by green marls with a sharp, non-erosional contact that represents the boundary between the Utrillas Gr-La Bicuerca Mb succession and the Cenomanian Chera Fm, which in the outcrop is partly covered.

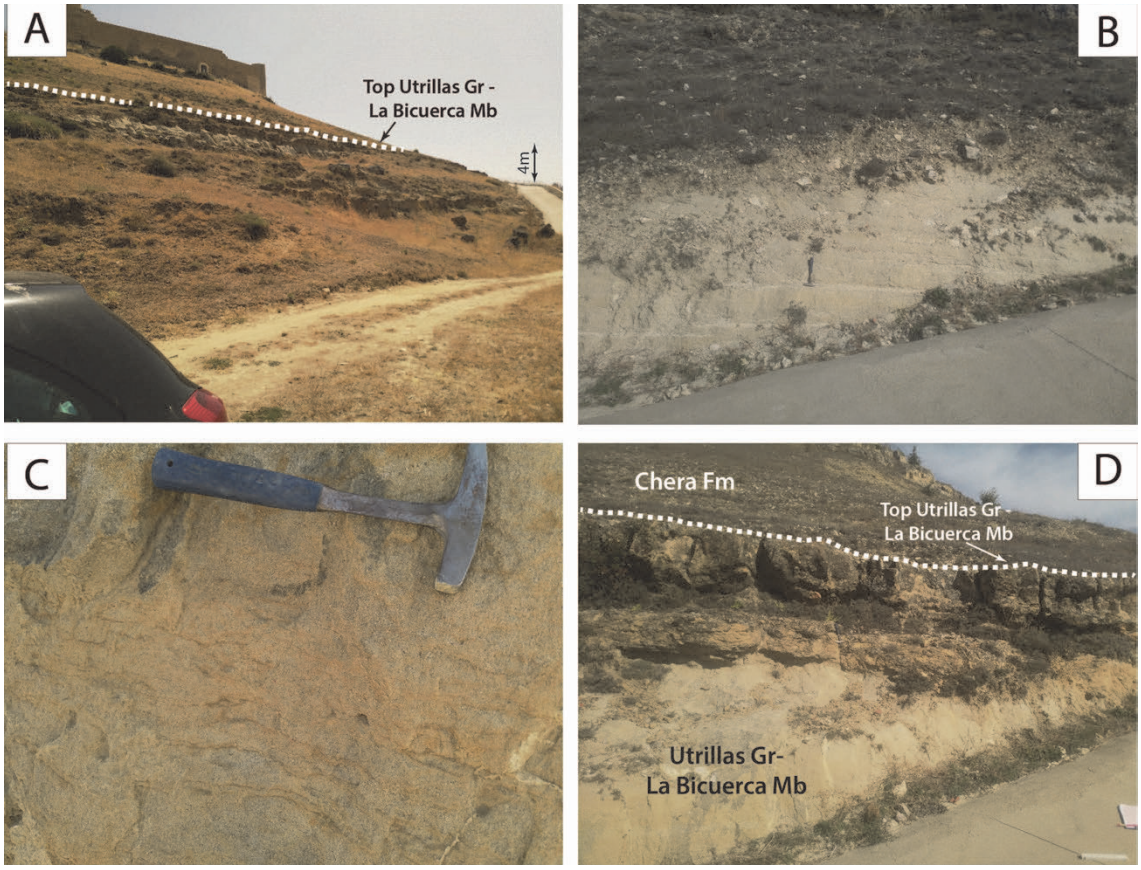

Fig. 5.36. (A) General view of the outcrop at Cañada del Hoyo. The dashed white line in the upper part of the picture represents the top of the Utrillas Gr - La Bicuerca Mb succession. (B) Horizontal to sub-horizontal bedding arranged in large foresets (facies Sh) deposited in a tidal flat environment (FA V) that characterises the studied outcrop in Cañada del Hoyo. (C) Close-up of (B) showing the aspect of the mud drapes found in the tidal flat deposits. (D) Detail of the uppermost levels of the Utrillas Gr - La Bicuerca Mb succession, where shallow marine mixed deposits (FA VIII) dominate. The dashed white line represents the top of the Utrillas Gr – La Bicuerca Mb. Hammer for scale is 35 cm. See chapter 8 of this manuscript for the explanation of the facies associations (FA).

6. Biostratigraphy. Aptian to early Cenomanian palynostratigraphy of the Cuenca Basin.

Palynomorphs include both plant and animal microscopic structures in the 5-500 µm size range and are composed of compounds (such as sporopollenin, chitin, and others) that are highly resistant to most forms of decay other than oxidation. In the strict sense, they are identified as microscopic structures abundant in most sediments and sedimentary rocks and are resistant to the routine pollen-extraction procedures including bases, strong acids acetolysis, and density separation (Traverse, 2007).

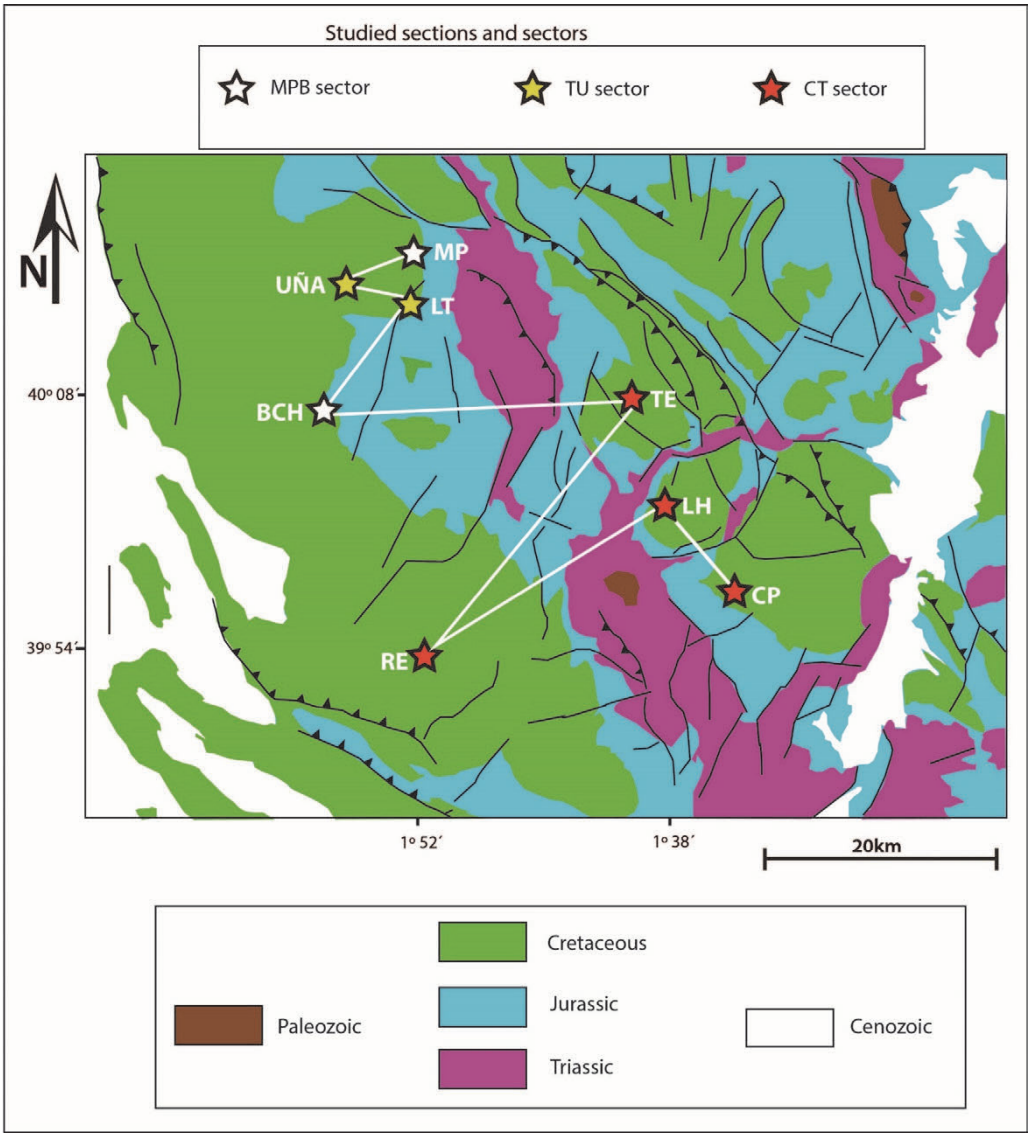

Fig. 6.1. Simplified geological map of the study area, where the sampled locations and the studied palynological sectors (MPB, TU, and CT) are indicated by coloured stars. The correlation path used by Bueno-Cebollada et al. (2021) is indicated by a white line. BCH: Buenache de la Sierra, CP: Campillos-Paravientos, LH: La Huerguina, LT: La Toba, MP: Mina Pepita, RE: Reíllo, TE: Tejadillos, UCR: Uña. Modified from the Geological Map of Spain and Portugal (Rodríguez et al., 2015) after Bueno-Cebollada et al. (2021). See figure 5.1A for the location of the study area within the Iberian Peninsula map.

Palynomorphs are part of the life cycle of some plants and animals that in most cases evolve rapidly, allowing defining narrow time spans, which makes them useful for age dating purposes. They occur in sedimentary rocks of all ages formed in many different sedimentary environments (Traverse, 2007). Besides, palynomorphs tend to be proportionally more abundant in the rocks than other groups of fossils and can be used for statistic and population studies better than any other microfossil. Their high abundance is mainly related to their small size and high presence in sediments since the spores and anemophilous pollen are part of the primary aerosol particle load of the atmosphere (Jaenicke, 2005; Traverse, 2007). Such features make them an excellent tool for the biostratigraphic dating and correlation of sedimentary deposits.

The data and interpretations presented over the next pages are the results of palynological research carried out in fulfillment of this Ph.D. thesis, and it is partly published in Bueno-Cebollada et al. (2021) (Appendix I [B]). The palynostratigraphic study has been carried out across the Cuenca Basin, where eight outcrops have been logged and sampled. The 8 studied outcrops are Mina Pepita (MP), Buenache de la Sierra (BCH), Reíllo (RE), Tejadillos (TE), La Huérguina (LH), Campillos-Paravientos (CP), Uña-Camino de la Raya (UCR), and La Toba (LT). In turn, these eight outcrops have been grouped into 3 sectors (Fig. 6.1) based on the palynostratigraphic similarities and biostratigraphic ages observed in the samples collected: the MPB sector (includes the MP and BCH outcrops), the CT sector (includes the RE, TE, LH and CT outcrops), and the TU sector (includes the UCR and LT outcrops).

Overall, 29 productive palynological samples (Appendix I [B]) have been collected in mudstone levels from sandstone-dominated successions located in a stratigraphic position between the Barremian deposits of the La Huerguina Fm and those of the lower Cenomanian Chera Fm.

The studied palynological assemblages include 191 palynomorphs identified (Appendix I [B]), which consist of gymnosperm (38 taxa) and angiosperm (37 taxa) pollen grains, spores of ferns and allies (98 taxa), freshwater algae (three taxa) dinoflagellate cysts (11 taxa), acritarchs (two taxa) and test linings of foraminifera. This chapter focuses on the identification of the age-diagnostic palynomorph assemblages and those with biostratigraphic importance and their distribution to cast light on the relative ages of the studied sedimentary successions. In general, the palynological assemblages identified in this Ph.D. thesis are of limited use as biostratigraphic markers, since most of the identified palynomorphs present widespread distributions through the Early and “mid”- Cretaceous.

Among the objectives of this chapter is to identify and stratigraphically constrain the Albian to early Cenomanian deposits in the Cuenca Basin (Utrillas Gr – La Bicuerca Mb), whose study is

the aim of this Ph.D. thesis. In this sense, this chapter aims to separate the Aptian succession from the Albian to lower Cenomanian one based on a palynostratigraphic approach. However, the Aptian palynostratigraphy and palynofloras identified in this study have also been included and discussed in the sub-chapters 6.1 and 6.2 of this manuscript since they are part of the palynological study carried out (Bueno-Cebollada et al., 2021).

6.1. Palynostratigraphy of the MPB sector: Mina Pepita (MP) and Buenache de la Sierra outcrops (BCH).

Overall, the MP outcrop has yielded five productive samples (MP-II-1, MP-I-2, MP-II-2, MP-I-3, and MP-II-3), while two productive pollen samples (BCH-3 and BCH-4) have been collected in the BCH outcrop (Fig. 6.2, Appendix II).

The palynological assemblages obtained in the samples from the Mina Pepita outcrop (Fig. 6.3) have produced two prolate, columellate, and reticulate pollen grains which resemble tricolpate pollen and would represent eudicot pollen grains (Figs. 6.2, 6.3K). These two specimens have been identified as cf. *Tricolpites* sp. (Appendixes II and III). The first consistent occurrence of triaperturate pollen grains in the fossil record is not well-constrained and remains under debate. The oldest triaperturate grains recorded in Europe were found in the uppermost Barremian to lowermost Aptian deposits of the Isle of Wight (UK) (Hughes and McDougall, 1990; Hughes, 1994), and lower Aptian deposits of England and the Cantabrian Basin (Northern Spain) (Hughes, 1994; Najarro et al., 2011).

However, the triaperturate pollen grains identified in the MP outcrop are different from the ones found in the Cantabrian Basin (Najarro et al., 2011), since the former pollen grains are like the Albian *Tricolpites parvus* Stanley identified in NW Alberta, Canada (Singh, 1971). Hence, the occurrence of true triaperturate pollen grains does not become consistent until the early Albian in the assemblages from England, Portugal, and North America (Tanrikulu et al., 2018 and references therein). Additionally, Heimhofer et al. (2007) studied an almost continuous sedimentary succession in western Iberia (Portugal) in which the first occurrences of reticulate and striate tricolpate pollen grains correspond to the earliest and early Albian, respectively. However, the occurrence of triaperturate pollen grain of angiosperm was already noticeable much earlier, during the Aptian, in Gondwana (Brazil and Africa) (Doyle et al., 1977; Penny, 1986; Doyle, 1992; Schrank and Ibrahim, 1995; Ibrahim, 2002; Heimhofer and Hochuli, 2010; Coiro et al., 2019), with their first occurrences dating back from the late Barremian (i.e., Zone C-VII of Gabon; Doyle et al., 1977; Doyle, 1992). The anecdotal occurrence of tricolpate pollen grains (cf.

Tricolpites sp.) in the MP outcrop might indicate that eudicots had become established in Iberia during the Aptian yet remained sporadic occurrences until the invasion from Gondwana during the earliest Albian.

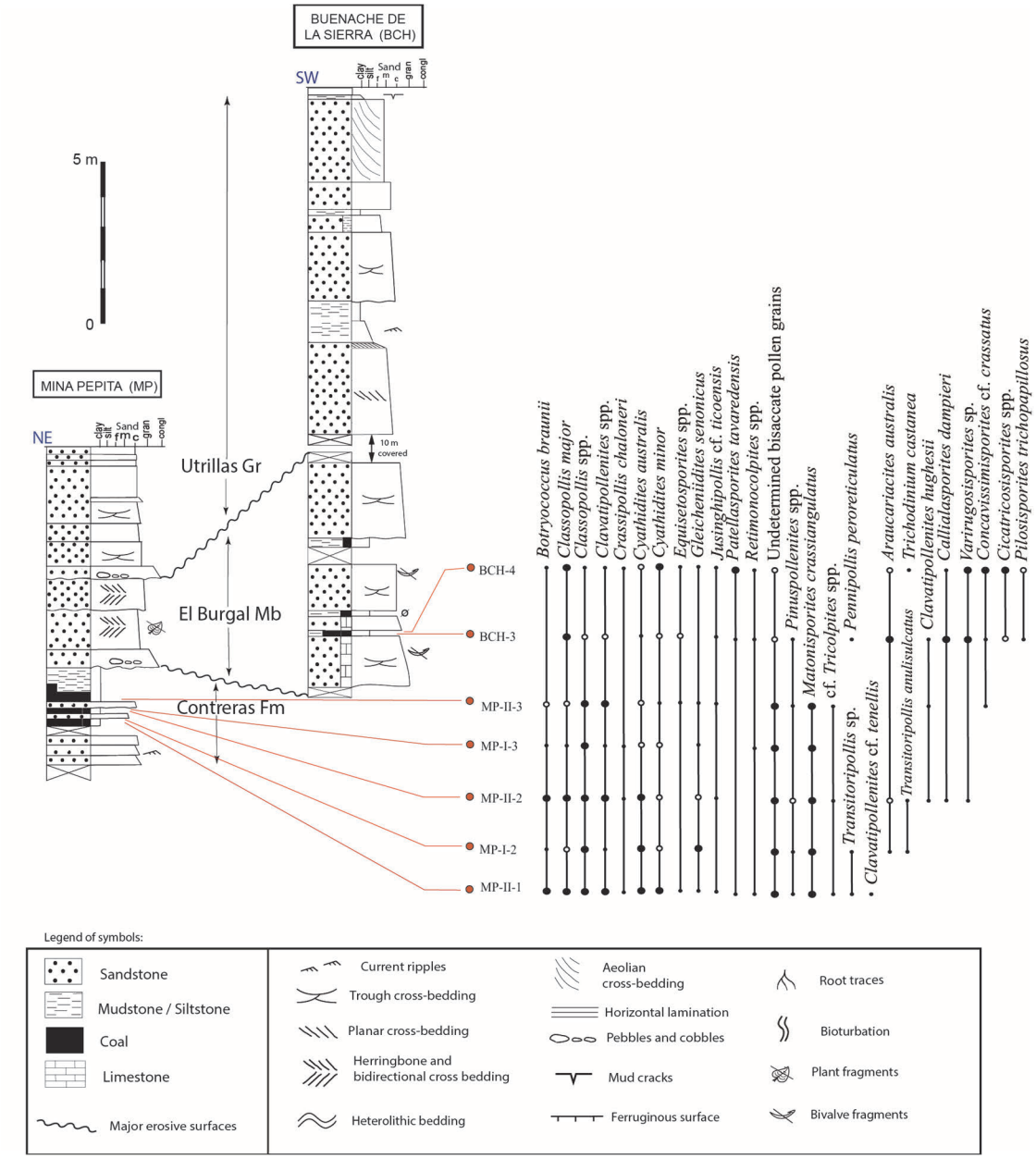

Fig. 6.2. Stratigraphic succession in the Mina Pepita/Buenache de la Sierra outcrops (MPB sector), showing the most abundant palynomorphs as well as those of biostratigraphic importance. • Present 1–10 specimens; ○ Common 11–30 specimens; ● Abundant >30 specimens. Lithostratigraphic units are indicated in the logged sections. Legend of symbols for Figs. 6.2, 6.6, and 6.8 is included. The overall number of identified taxa is indicated in Appendix II. Original image from Bueno-Cebollada et al. (2021).

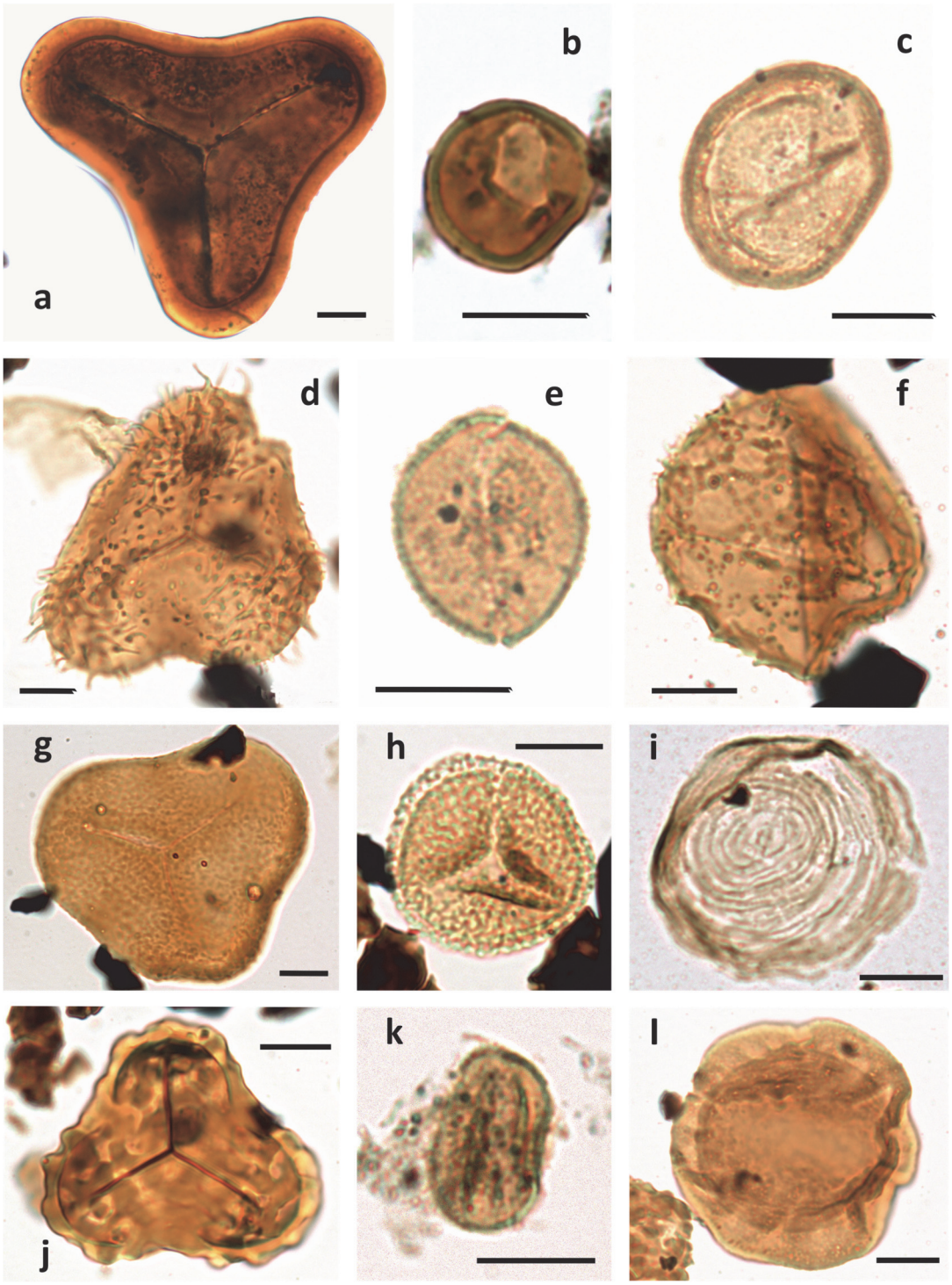

Fig. 6.3. Selected palynomorphs from the MPB sector: (A) *Matonisporites crassiangulatus* (Balme 1957) Dettmann 1963, level MP-II-2 (slide MGM-11183C, co-ord. F38/0), specimen MGM-11183C-1; (B) *Crassipollis chaloneri* (Brenner 1963) Góczán and Juhász 1985, level MP-II-2 (slide MGM-11183C, co-ord. Q39/3), specimen MGM-11183C-2; (C) *Classopollis major* Groot and Groot 1962, level MP-II-2 (slide MGM-11183C, co-ord. E30/0), specimen MGM-11183C-3; (D) *Pilosisporites trichopapillosus* Delcourt and Sprumont 1955, level BCH-3 (slide MGM-11203C, co-ord. L47/4), specimen MGM-11203C-1; (E) *Clavatipollenites* sp., level MP-II-3 (slide MGM-11191C, co-ord. D29/0), specimen MGM-11191C-1; (F) *Trichodinium castanea* Deflandre 1935 ex Clarke and Verdier 1967, level BCH-4 (slide MGM-11206C, co-ord. F34/0), specimen MGM-11206C-1; (G) *Concavissimisporites* cf. *granulatus* Pocock 1965, level BCH-3 (slide MGM-11203C, co-ord. S50/2), specimen MGM-11203C-2; (H) *Jusinghipollis* cf. *ticoensis* Llorens and Perez Loinaze 2016, level BCH-3 (slide MGM-11203C, co-ord. M45/0), specimen MGM-11203C-3; (I) *Chomotriletes minor* (Kedves 1961) Pocock 1970, level BCH-4 (slide MGM-11206C, co-ord. E49/3), specimen MGM-11206C-2; (J) *Trilobosporites* cf. *canadensis* Pocock 1962, level BCH-3 (slide MGM-11203C, co-ord. L47/4), specimen MGM-11203C-4; (K) cf. *Tricolpites* sp., level MP-II-2 (slide MGM-11183C, co-ord. N42/2), specimen MGM-11183C-4; (L) *Callialasporites dampieri* (Balme 1957) Dev 1961 emend. Norris 1969, level BCH-3 (slide MGM-11203C, co-ord. J46/1), specimen MGM-11203C-5. Scale bar: 10 µm. The location of the palynomorphs is indicated by England Finder slide coordinates. Original figure from Bueno-Cebollada et al. (2021).

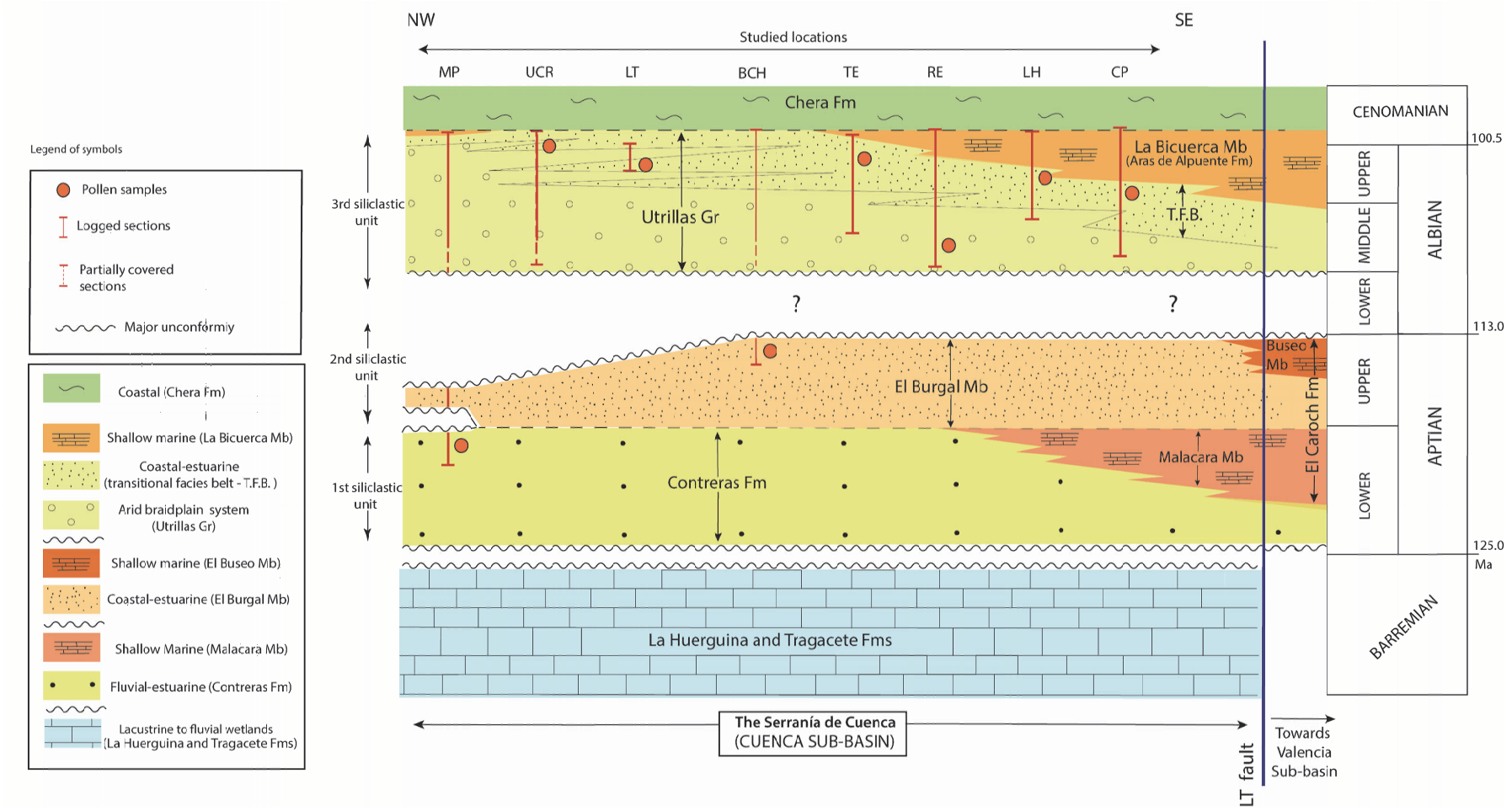

Fig. 6.4. Chronostratigraphic chart proposed based on the studied palynological samples and sedimentological data. Sampled locations have been included in the upper part of the chart and are arranged in accordance with the correlation depicted in Fig. 6.1. Likewise, the extension of each of the three mentioned siliciclastic units are included, to better clarify what is stated in the text. Pollen samples are indicated by red dots. BCH: Buenache de la Sierra, CP: Campillos-Paravientos, LH: La Huerguina, LT: La Toba, MP: Mina Pepita, RE: Reillo, TE: Tejadillos, UCR: Uña-Camino de la Raya. Lithostratigraphy is based on the units defined by Vilas et al. (1982) and Fregenal-Martínez et al. (2017). Original image from Bueno-Cebollada et al. (2021).

One of the peculiarities of the palynological assemblages studied in the MP outcrop is their high percentages of bisaccate pollen grains (Appendix II), accounting for approximately 30% out of the palynomorphs of the samples. These high percentages of bisaccate pollen grains conform with the early Aptian palynological assemblages from the Morella la Vella Mb of the Margas de Forcall Fm (Maestrazgo Basin, eastern Iberia), which was studied by Solé de Porta and Salas (1994). In this sense, these authors identified palynological assemblages where the percentages of bisaccates are as high as 46 %, whilst the spores only account for 20%. Additionally, this abundance in bisaccate pollen has also been reported in the early Aptian of the Sub-Betics (SE Spain) (Leereveld et al., 1989). These high percentages of bisaccate pollen might reflect the expansion of less xeromorphic plant communities during the early Aptian, than those existing during the Barremian in eastern Iberia (Diequez et al., 2010). Likewise, the abundance of *Classopollis* (Fig. 6.3C) together with the relatively high percentages of the spores of *Matonisporites crassiangulatus* (Fig. 6.3A) and Cyatheaceae/Dicksoniaceae/Dipteridaceae in the assemblages from the Mina Pepita outcrop (Appendix II), allows to compare them with the Barremian assemblages described in the Maestrazgo (Solé de Porta and Salas, 1994) and Valencia Basins (Doubinger and Mas, 1981) (E Iberia). However, the assemblages studied in the MP outcrop differ from the eastern Spanish Barremian ones in the occurrence of angiosperm pollen of the genera *Clavatipollenites*, *Crassipollis*, *Retimonocolpites*, *Jusinghipollis*, *Transitoripollis*, and cf. *Tricolpites*. The presence of the former angiosperm pollen in the studied assemblages of the MP outcrop allows comparing them with those of the early Aptian from the Cresmina and Luz sections in Portugal (Heimhofer et al., 2007).

Therefore, based on the previously mentioned data, an early Aptian age is inferred for the palynological assemblages studied in the Mina Pepita outcrop, which conforms with the stratigraphic data obtained from the outcrop (see chapter 5 of this thesis manuscript). Consequently, and based on previous early Aptian biostratigraphic research in the Cuenca Basin (Meléndez, 1983), the studied early Aptian succession in the MP outcrop is attributed to the Contreras Fm (Vilas et al., 1982).

The composition of the studied assemblages at the Buenache de la Sierra section resembles that described in Graja de Campalbo, Cuenca (Meléndez, 1983), which lacks pollen of Angiosperms and was attributed to the El Burgal Mb., implying a late Aptian age (Fig. 6.4). The assemblage from Graja de Campalbo (Meléndez, 1983) was in turn compared with the one described in the early Albian of Mompichel (eastern Spain) (Arias and Doubinger, 1980), which contained scarce angiosperm pollen but lacked dinocysts. Besides, the studied assemblages at the Buenache de la Sierra outcrop also show similarities with those from the upper Aptian of Montoria-La Mina

(Barrón et al., 2015); although the species *Schrankipollis microreticulatus* has not been recorded at Buenache de la Sierra. The occurrence of the *Pilosisporites trichopapillosus* (Figs. 6.2, 6.3) indicates an Aptian age in the BCH samples, even though this species has been identified in strata as young as Albian in North America (Brenner, 1963; Singh 1971; Ravn, 1995). However, *Pilosisporites trichopapillosus* has never been recorded in Albian deposits from Iberia (Leereveld et al., 1989). Therefore, the assemblages studied in the BCH outcrop are dated as Aptian. More concretely, they should be interpreted as late Aptian since they resemble late Albian to early Albian assemblage from other regions of Iberia. The samples from the BCH outcrop have been collected in a rock unit that is overlain by the deposits of the Utrillas Gr (Fig. 6.2) and therefore it is interpreted as the upper Aptian El Burgal Mb (El Caroch Fm) (Vilas et al., 1982).

6.2. Aptian palynofloras: Contreras Fm and El Burgal Mb (El Caroch Fm).

6.2.1. Early Aptian Palynofloras: Contreras Fm (MPB sector, Mina Pepita outcrop).

The sampled levels at the Mina Pepita outcrop (MPII-1, MP-2, MPII-2, MP-3, and MPII-3) are dated as early Aptian and attributed to the Contreras Fm (see Chapter 6.1. of this thesis). The palynological assemblages attributed to the Contreras Fm are dominated by gymnosperms (~59.5%) and spores of ferns and allied (~30.5%). To a lesser extent, they consist of angiosperm (~4.6%) and aquatic palynomorphs (~5.4%) (Appendix II).

Gymnosperms are mainly dominated by bisaccate pollen grains (representing ~57.4% of the identified gymnosperm pollen grains) mainly attributed to Pinaceae and/or Podocarpaceae (Appendix 1). Likewise, pollen grains of Cheirolepidiaceae are also significant in the samples from Mina Pepita accounting for ~36.6% of the identified gymnospermous pollen. Cheirolepidacean pollen is dominated by the genus *Classopollis*, being *Classopollis major* (Fig. 6.3C) and *Classopollis* spp. the main species identified (Appendix II). Additionally, gymnosperms belonging to groups other than Coniferales have been identified locally and in very small numbers (Appendix II).

Regarding spores, the samples are characterised by the conspicuous occurrence of *Matonisporites crassiangulatus* (Fig. 6.3A) and the frequent appearance of *Cyathidites australis*, *C. minor* and *Gleicheniidites senonicus*. The species *M. crassiangulatus* is present in all the samples attributed to the Contreras Fm and represents approximately 68% of the total of spores (and 20% out of all the palynomorphs) identified in the samples from Mina Pepita.

Angiosperms are dominated by *Clavatipollenites* spp. (Figs. 6.2, 6.3E). Additionally, other taxa such as *Crassipollis chaloneri* (Fig. 6.3), *Transitoripollis* spp., and cf. *Tricolpites* sp. (Fig. 6.3K) are present at the sampled levels in Mina Pepita, yet to a lesser extent.

Finally, the freshwater algae *Botryococcus braunii* (Fig. 6.2, Appendix II) was frequently observed in the Mina Pepita section, representing approximately 5% of the studied palynomorphs. Conversely, marine palynomorphs such as dinoflagellates or test lining of foraminifers are absent in the samples from the Mina Pepita outcrop, although a single undetermined acritarch was found in the sample MPII-1.

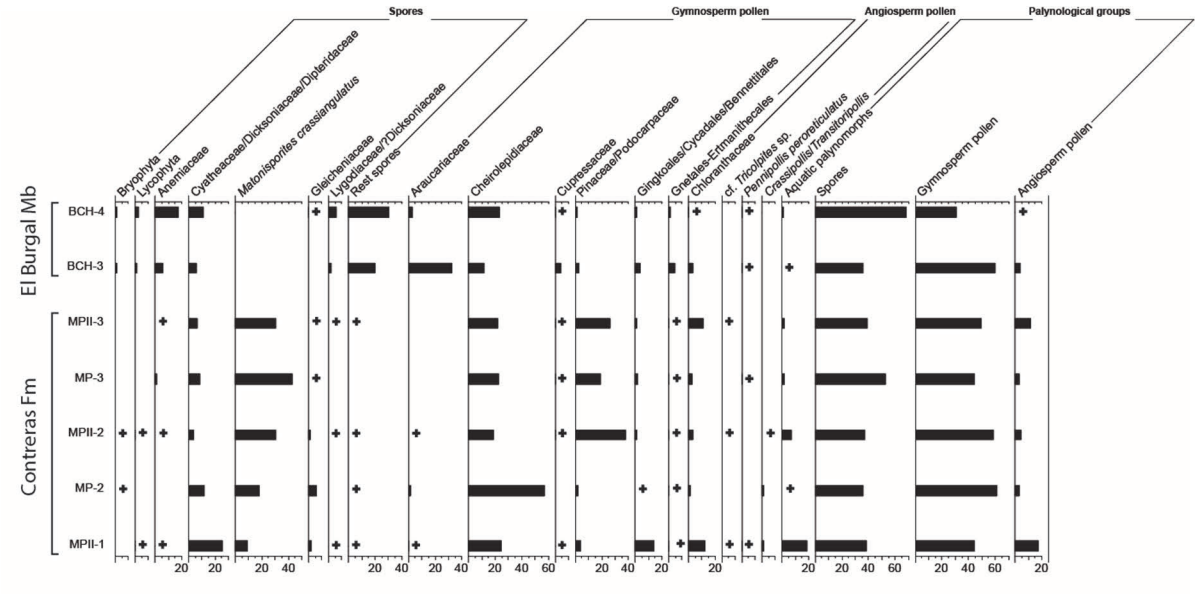

Fig. 6.5. Detailed palynological chart for the MPB sector (Contreras Fm and El Burgal Mb).

6.2.2. Late Aptian Palynofloras: El Burgal Mb (MPB sector, Buenache de la Sierra outcrop).

The palynoflora identified in the samples from the Buenache de la Sierra outcrop, attributed to the El Burgal Mb (upper Aptian), is dominated by trilete spores and gymnosperm pollen grains (Fig. 6.5) with the former being more diverse than in the early Aptian ones from the Mina Pepita outcrop (Appendix II).

The upper Aptian palynological assemblages from Buenache de la Sierra are dominated by spores of pteridophyte, representing approximately 54% of the identified palynomorphs. Gymnosperms are also abundant and represent 43.3% of the palynomorphs identified. Conversely, angiosperm pollen grains and aquatic palynomorphs represent only 1.9% and 0.9% of the identified palynomorphs, respectively (Appendix II).

Regarding pteridophyte spores, Dipteridaceae/Matoniaceae show decreasing abundances in the Buenache de la Sierra assemblages (Fig. 6.5) compared to those of the lower Aptian from Mina Pepita. This pattern is paralleled with increasing numbers of Anemiaceae (particularly, *Cicatricosisporites*), Lygodiaceae/?Dicksoniaceae (*Concavissimisporites* cf. *crassatus* [Fig. 6.3G]; *Trilobosporites* cf. *canadensis* [Fig. 6.3J]), *Patellasporites tavaredensis* and *Varirugosisporites* sp. Gymnosperms are dominated by Coniferales, in particular by the families Araucariaceae (*Araucariacites australis*), Cheirolepidiaceae (*Classopollis* spp.) and Cupressaceae (*Inaperturopollenites* spp.). Gymnosperms attributed to groups other than Coniferales, including *Cycadopites follicularis*, *Cycadopites* spp., *Equisetosporites* spp., *Exesipollenites tumulus*, *Eucommiidites minor*, *E. troedsonii*, *Monosulcites* spp. and *Steevesipollenites* sp., are also represented, but to a lesser extent (Fig. 6.3B, Appendix II).

Clavatipollenites spp. is the most abundant pollen of angiosperm identified in the Buenache de la Sierra samples. Although to a lesser extent, other angiosperm taxa such as *Jusinghipollis* (Fig. 6.3H), *Pennipollis* and *Retimonocolpites* (Fig. 6.2) are relatively dominant in the samples.

Regarding aquatic palynomorphs, the sampled levels at the Buenache de la Sierra outcrop stand out by the occurrence of *Chomotriletes minor, Schizosporis reticulatus,* and by the presence of the dinocyst *Trichodinium castanea* (Fig. 6.3F). Conversely, the main difference with the previously described lower Aptian assemblages from Mina Pepita is the lack or anecdotal occurrence of the freshwater algae *Botryococcus braunii.*

6.2.3. Remarks.

The Aptian palynofloras of the MPB sector (Mina Pepita and Buenache de la Sierra sections) represent a good example of early Cenophytic flora characterised by abundant spore producers gymnosperms and a low frequency of angiosperms (Fig. 6.2). Notwithstanding, the lower Aptian palynological assemblages studied in the Mina Pepita outcrop, attributed to the Contreras Fm (Fig. 6.5), show different characteristics from the upper Aptian ones from Buenache de la Sierra, attributed to the El Burgal Mb (Fig. 6.5).

The palynofloras from the Contreras Fm are characterised by abundant specimens of the green algae *Botryococcus braunii* that suggest the existence of fresh or brackish semi/permanent water bodies (Guy-Ohlson, 1992) and conform with the absence of dinoflagellate cysts in the studied samples. The spore *Matonisporites crassiangulatus* (Fig. 6.3A), which also includes a common component of the sporinite maceral (Fonolla Ocete and Fernández Marrón, 2004), represents one of the most common palynomorphs of the lower Aptian assemblages (Bueno-Cebollada et al., 2021). *M. crassiangulatus* has been found in situ associated with the fern *Weichselia reticulata* (Díez et al., 2005), associated with dry (Alvin, 1974; Dieguez and Meléndez,

2000) and/or frequently disturbed settings (Batten, 1974). According to Blanco-Moreno et al. (2018), its distribution conforms with the fern savanna biome, which existed during the Jurassic and Cretaceous. This biome probably became less important during the Aptian due to the increase in humidity (Coiffard et al., 2007). The co-occurrence of a high number of *Classopollis* pollen grains in the assemblages indicates that cheirolepids also formed a significant component of drought-adapted vegetation, possibly incorporating *W. reticulata* as ground cover.

However, the co-occurrence of hygrophyte taxa such as Cyatheaceae/Dicksoniaceae/Dipteridaceae, mainly represented by *Cyathidites*, and angiosperm pollen grains showing affinity to extant Chloranthaceae, points towards local humid conditions. These hygrophyte taxa might have thrived preferably in areas such as alluvial floodplains, more prone to be waterlogged at times. Besides, the high percentages of bisaccate pollen grains observed might be related to cooler conditions (Vakhrameyev, 1982; Hochuli et al., 1999). However, another plausible explanation for the conspicuous percentages of pollen grains with Pinaceae/Podocarpaceae affinities in the Contreras Fm is that the Mina Pepita outcrop was located in a proximal location, closer to the highland areas, where the input of bisaccate pollen grains was greater. This fact conforms with a previous palaeogeographical reconstruction for the Contreras Fm. proposed by Aurell et al. (2019). Additionally, the lack of dinocysts conforms with a low occurrence of araucariacean conifers (Fig. 6.5), reinforcing the continental alluvial nature of the deposits of the Contreras Fm (Meléndez, 1983).

Angiosperm pollen does not represent a significant part of the studied Aptian assemblages (Fig. 6.5). However, their representation in the vegetation might be skewed in the palynological assemblages due to possible insect pollination in the early representatives of the angiosperms (Taylor and Hu, 2010). The early Aptian of Portugal is characterised by several morphotypes of monoaperturate pollen belonging to *Clavatipollenites*, *Retimonocolpites*, *Asteropollis*, and *Pennipollis* groups (Heimhofer et al., 2005); however, tricolpate pollen is absent. Additionally, it is worth mentioning that the earliest appearance of eudicots in Iberian seems to be linked to the warming episode associated with OEA1a (early Aptian; Najarro et al., 2011). According to previous authors, this interval was related to a long-term warming period that began during the late Barremian times and reached its climax during the Cenomanian - Turonian thermal maximum (Clarke and Jenkyns, 1999; Puceat et al., 2003). Consequently, the appearance of tricolpate-producing eudicots in the lower mid-latitudes during the early Albian (Brenner, 1976) might reflect the migration from more equatorial areas of northern Gondwana, impelled by global warming (Heimhofer et al., 2005; Coiffard and Gomez, 2012; Coiro et al., 2019). This hypothesis is contrary to the opinion shared by other authors relating the bulk of early angiosperms to aquatic settings (Coiffard et al., 2006; Coiffard and Gomez, 2012; Zhang et al.,

2018), and suggests their diversification into groups with different ecological strategies since the early Aptian (Feild et al., 2004; Coiro et al., 2019).

The rise of the eudicots coinciding with the OAE1a would represent the initial step in the Early - "mid" Cretaceous radiation, which would eventually lead to the diversification of Fagales in the Northern Hemisphere, started during or in response to the Cenomanian-Turonian OAE2 (Heimhofer et al., 2018). However, this hypothesis remains highly speculative, especially given the fragmentary nature and poor calibration of the Aptian palynological record and the heterogeneity of the vegetation in Eurasia and North America. Additionally, the early Aptian palynofloras from the Cuenca Basin (Mina Pepita outcrop) are characterised by the occurrence of abundant bisaccate pollen grains (Appendix II), unlike other coeval palynological assemblages from NE Iberia (the Maestrazgo Basin) (Solé de Porta and Salas, 1994) and the UK (Kemp, 1970; Batten, 1974). As previously mentioned, the reason for this significant amount of bisaccate pollen grains might have been caused by climatic variabilities and/or the existence of topographic highs supporting mesic vegetation in the Cuenca Basin.

Conversely, the late Aptian palynofloras of the El Burgal Mb are characterised by a pronounced increase in pteridophyte spores (Fig. 6.5), however, they lack *M. crassiangulatus*, and are dominated by hygrophyte taxa if compared to the early Aptian palynofloras of the Contreras Fm. Therefore, a shift towards more humid climate conditions is inferred during late Aptian times in the Cuenca Basin. This transition towards more humid conditions during the late Aptian coincides with the occurrence of the coeval coaly deposits of the Escucha Fm in the Maestrazgo Basin (eastern Spain) (Rodríguez-López et al., 2009; Villanueva-Amadoz, 2009) and in the Basque-Cantabrian Basin (northern Spain) (Barrón et al., 2015), interpreted as a warm and humid sub-tropical environment (Rodríguez-López et al., 2009). In this sense, the Aptian palynofloras in the Cuenca Basin seem to conform with coeval palaeoclimatic data from Western Europe, where the existence of a relatively arid phase during the early Aptian and a transition towards more humid conditions during late Aptian times were recorded at mid-latitudes (Ruffell and Batten, 1990).

Additionally, the late Aptian palynofloras of the El Burgal Mb present dinocysts and relatively high percentages of *Araucariacites* and *Callialasporites* along with other palynomorphs with cheirolepidiacean and cupressacean affinities. The association between Araucariaceae and marine palynomorphs has also been observed in younger successions (Peyrot, 2011; Barrón et al., 2015; Peyrot et al., 2019), and it is related to the existence of coastal vegetation.

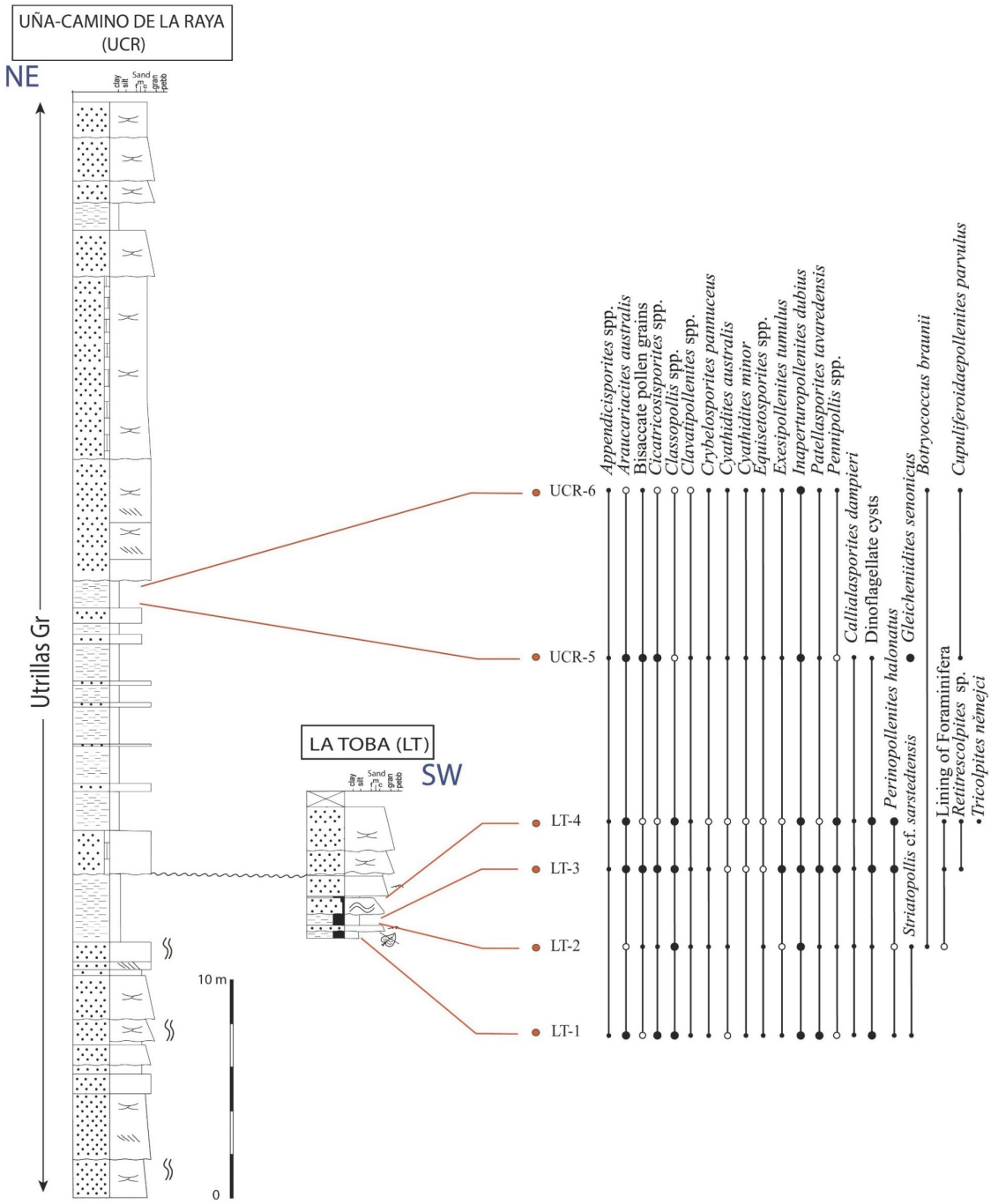

Fig. 6.6. Upper Albian to lower Cenomanian stratigraphic succession in the La Toba/Uña (TU sector) outcrops, showing the distribution of the most abundant palynomorphs identified, as well as those of biostratigraphic importance. • Present 1–10 specimens; ○ Common 11–30 specimens; ● Abundant >30 specimens. Lithostratigraphic units are indicated in the logged sections. Legend of symbols is included in Fig. 6.2. The overall number of identified taxa is indicated in Appendix II. Original image from Bueno-Cebollada et al. (2021).

6.3. Palynostratigraphy of the CT and TU sectors.

The palynological assemblages from the TU sector (Figs. 6.6, 6.7) are characterised by the occurrence of striato-reticulate or striate tricolpate pollen (*Striatopollis* cf. *sarstedtensis*). These morphotypes appeared during the late early Albian in Portugal (Galé and Porto de Mos Formations) (Heimhofer et al., 2007; Horikx et al., 2016) and southeastern North America

(Tanrikulu et al., 2018). Therefore, the occurrence of these morphotypes allows inferring an Albian age for the samples from the TU sector.

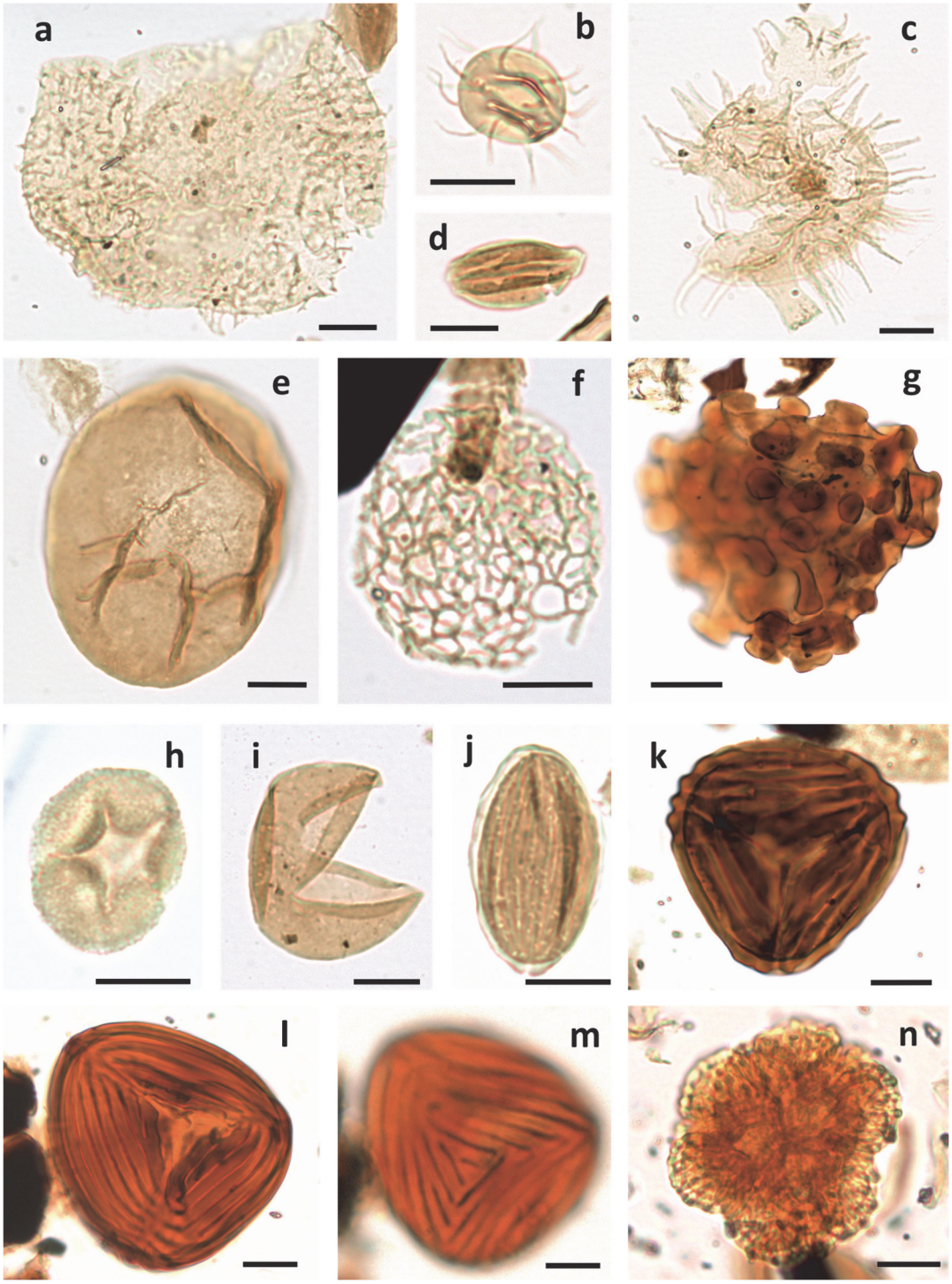

Fig. 6.7. Selected palynomorphs from the TU sector: (A) *Cyclonephelium vannophorum* Davey 1969, level LT-3 (slide MGM-11224C, co-ord. J28/1), specimen MGM-11224C-1; (B) *Michrystridium* sp., level LT-3 (slide MGM-11224C, co-ord. D41/4), specimen MGM-11224C-2; (C) ?*Coronifera oceanica* Cookson and Eisenak 1958, level LT-2 (slide MGM-11220C, co-ord. P34/2), specimen MGM-11220C-1; (D) *Cupuliferoidaepollenites* sp., level LT-2 (slide MGM-11220C, co-ord. K45/1), specimen MGM-11220C-2; (E) *Araucariacites australis* Cookson 1947, level LT-3 (slide MGM-11224C, co-ord. F36/1), specimen MGM-11224C-3; (F) *Afropollis jardinus* (Brenner 1968) Doyle, Jardiné and Doerenkamp 1982, level LT-3 (slide MGM-11224C, co-ord. N31/3), specimen MGM-11224C-4; (G) *Neoraistrickia robusta* Brenner 1963, level LT-1 (slide MGM-11216C, co-ord. F44/3), specimen MGM-11216C-1; (H)

Asteropollis asteroides **Hedlund and Norris 1968, level LT-1 (slide MGM-11216C, co-ord. M26/0), specimen MGM-11216C-2; (I)** ***Inaperturopollenites dubius*** **(Potonié and Venitz 1932) Thomson and Pflug 1953, level LT-3 (slide MGM-11224C, co-ord. F43/0), specimen MGM-11224C-5; (J)** ***Equisetosporites*** **sp., level LT-3 (slide MGM-11224C, co-ord. H45/2), specimen MGM-11224C-6; (K)** ***Cicatricosisporites angicanalis*** **Döring 1965, level LT-3 (slide MGM-11224C, co-ord. K27/3), specimen MGM-11224C-7; (L-M)** ***Cicatricosisporites recticicatricosus*** **Döring 1965, level UCR-5 (slide MGM-11239C, co-ord. C27/4), specimen MGM-11239C-1, (L) focus on proximal side, (M) same specimen, focus on distal side; (N)** ***Artiopollis indivisus*** **Agassie 1969, level UCR-6 (slide MGM-11244C, co-ord. H46/0), specimen MGM-11244C-1. Scale bar: 10 µm, except for (G) = 20 µm. The location of palynomorphs is indicated by England Finder slide coordinates. Original figure from Bueno-Cebollada et al. (2021).**

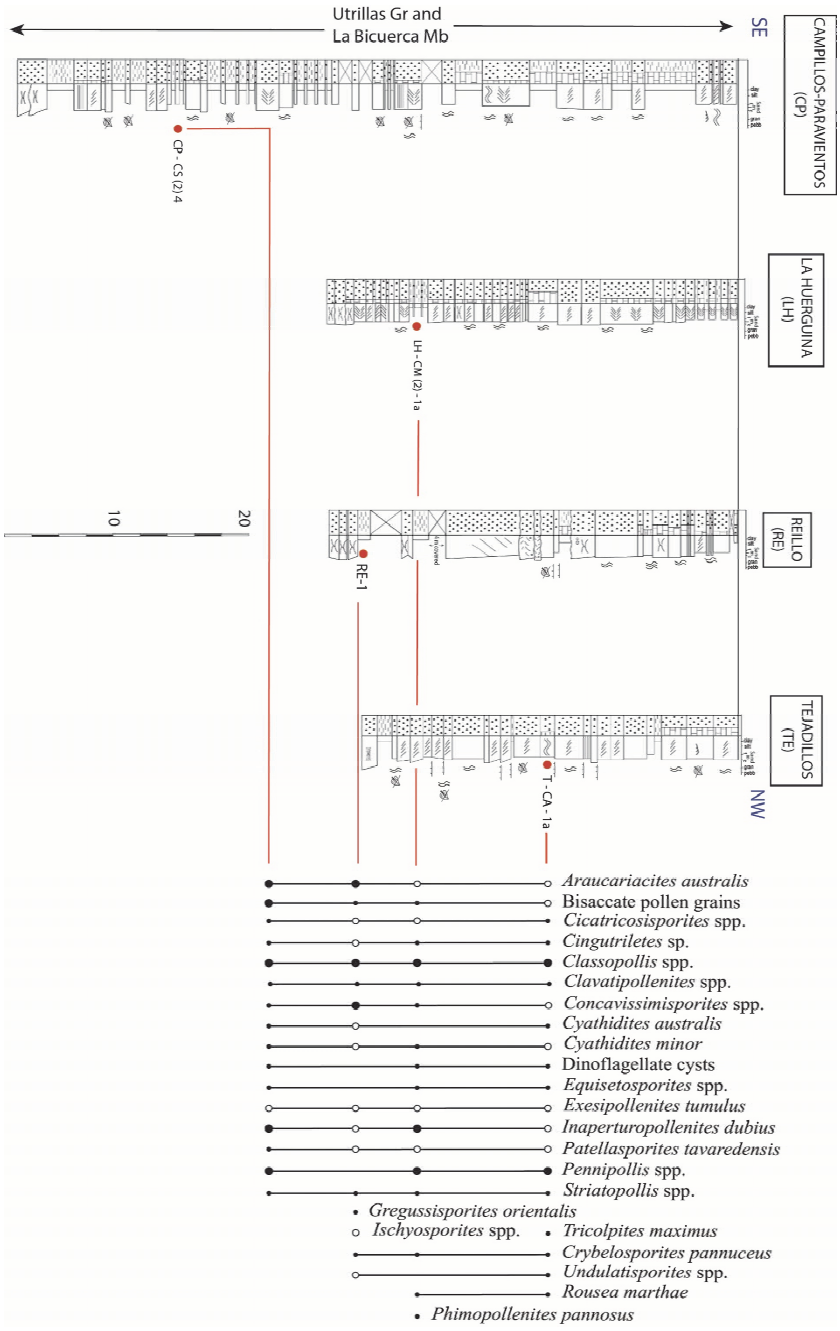

Fig. 6.8. Albian stratigraphic succession in the CT sector, showing the distribution of the most abundant palynomorphs identified, as well as those of biostratigraphic importance. • Present 1–10 specimens; ○ Common 11–30 specimens; ● Abundant >30 specimens. Lithostratigraphic units are indicated in the logged sections. Legend of symbols is included in Fig. 6.2. The overall number of identified taxa is indicated in Appendix II. Original figure from Bueno-Cebollada et al. (2021).

The occurrence of the angiosperm pollen *Hammenia fredericksburgensis* in the TU sector (level LT-2) indicates an age not older than middle Albian. This species has its oldest record in middle Albian strata from North America (Hedlund and Norris, 1968; Singh, 1983; Villanueva-Amadoz, 2009). However, in the Lusitanian Basin (Portugal), *Hammenia fredericksburgensis* does not occur before the late Albian (Horikx et al., 2016). The co-occurrence of *Tricolpites nemejci* and *Callialasporites dampieri* at the level LT-4 would suggest a younger late Albian age (Laing, 1975; Doyle and Robbins, 1977; Hasenboehler, 1981; Peyrot, 2011). However, the presence of *Callialasporites dampieri* becomes more inconsistent and local in strata younger than late Albian (Batten and Uwins, 1985; Burden and Hills, 1989; Schrank and Mahmoud, 1998), although it has been occasionally found in Cenomanian shales from the Outer Western Carpathians in Moravia (Svobodova et al., 2004).

Likewise, a younger early Cenomanian age has been tentatively attributed to the levels sampled in the Uña outcrop (UCR-5 and UCR-6) based on the occurrence of *Cupuliferoidaepollenites parvulus* since the stratigraphic record of this species spans from middle Albian to early Cenomanian times (Playford et al., 1975; Hochuli et al., 2006; Massoni et al., 2015), and because of the presence of *Artiopollis indivisus* in level UCR-6, whose stratigraphic record is essentially early Cenomanian (Fig. 6.7N) (Agasie,1969; Nichols et al., 1982; Singh, 1983; Peyrot et al., 2019).

In the samples collected in the CT sector (Figs. 6.8, 6.9), an age not older than middle Albian can be inferred (Fig. 6.4) based on the presence of the pollen grains *Tricolpites maximus* and *Tricolpites minutus,* and the spore *Gregussisporites orientalis* (Fig. 6.9A) (Singh, 1971; Doyle and Robbins, 1977; Juhasz and Smirnova, 1985; Burden and Hills, 1989; Leereveld et al., 1989). Therefore, a middle Albian to ?early Cenomanian age can be attributed to the sampled strata in the CT and TU sectors based on the studied palynological assemblages (Fig. 6.4). More precisely, the pollen assemblages from the CT sector seem to indicate a middle to late Albian age, while those from the TU sector most likely spanned the late Albian to ?early Cenomanian times. Consequently, the sampled sedimentary succession in the CT and TU sectors is attributed to the Utrillas Gr (Aguilar et al., 1971) and La Bicuerca Mb (Vilas et al., 1982).

Additionally, the lack of lower Albian strata between the upper Alptian (El Burgal Mb) and the middle Albian – ?lower Cenomanian (Utrillas Gr - La Bicuerca Mb) successions seems to indicate the existence of a hiatus comprising at least early Albian time, which in the field is represented by an unconformity at the base of the Utrillas Gr and conforms with previous research carried out by Meléndez (1983).

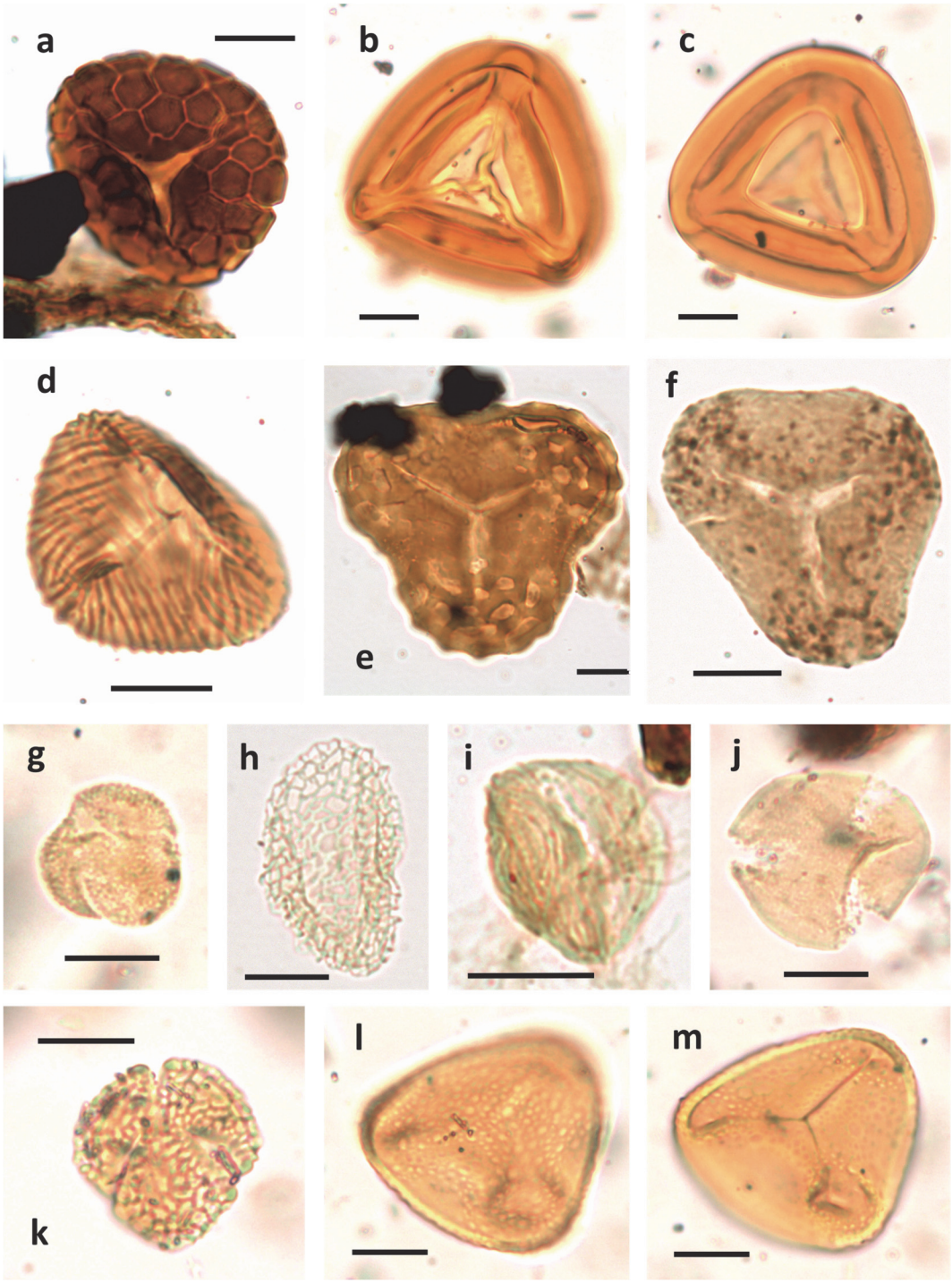

Fig. 6.9. Selected palynomorphs from the CT sector: (A) *Gregussisporites orientalis* Juhász and Smirnova 1985, level RE-1 (slide MGM-11264C, co-ord. F36/0), specimen MGM-11264C-1; (B–C) *Duplexisporites generalis* Deák 1962, level CP-CS(2)-4 (slide MGM-11252C, co-ord. H26/1), specimen MGM-11252C-1, (B) focus on proximal side, (C) same specimen, focus on distal side; (D) *Cicatricosisporites venustus* Deák 1963, level RE-1 (slide MGM-11264C, co-ord. K35/2), specimen MGM-11264C-2; (E) *Ischyosporites* cf. *crateris* Filatoff 1975, level RE-1 (slide MGM-11264C, co-ord. R42/1), specimen MGM-11264C-3; (F) *Concavissimisporites* cf. *irregularis* (Pocock 1970) Backhouse 1988, level RE-1 (slide MGM-11264C, co-ord. K41/4), specimen MGM-11264C-4; (G) *Tricolpites* cf. *micromunus* (Groot and Penny 1960) Burger 1971, level CP-CS(2)-4 (slide MGM-11252C, co-ord. N45/2), specimen MGM-11252C-2; (H) *Dichastopollenites* cf. *dunveganensis* Singh 1983, level RE-1 (slide MGM-11264C, co-ord. F46/1), specimen MGM-11264C-5; (I) *Striatopollis* cf. *sarstedtensis* Krutzsch 1959, level RE-1 (slide MGM-11264C, co-ord. D34/0), specimen MGM-11264C-6; (J) *Phimopollenites pannosus* (Dettmann and Playford 1968) Dettmann 1973, level LH-CM(2)-1a (slide MGM-11258C, co-ord. R37/1), specimen MGM-11258C-1; (K) *Rousea marthae* Ward 1986, level LH-CM(2)-1a (slide MGM-11258C, co-ord. R37/1), specimen MGM-11258C-2; (L–M) *Foveotriletes subtriangularis* Brenner 1963, level CP-CS(2)-4 (slide MGM-11252C, co-ord. J31/0), specimen MGM-11252C-3, (L) focus on distal side, (M) same specimen, focus on proximal side. Scale bar: 10 µm. The location of palynomorphs is indicated by England Finder slide coordinates. Original figure from Bueno-Cebollada et al. (2021).

7. Middle Albian to early Cenomanian palaeofloras of the Cuenca Basin.

The study of the mid-Albian to early Cenomanian palaeoflora presented in this manuscript has been tackled based on two different sorts of data: palynoflora and macroflora.

Plants include several morphological characters that reflect their contemporaneous climate and environmental conditions. Notwithstanding, this climatic signal tends to be distorted in fossil plants owing to transport, burial and diagenesis. Therefore, a good understanding of their taphonomy is paramount to correctly interpreting their palaeoclimatic and palaeoenvironmental conditions (Spicer, 1991).

A plant fossil assemblage is an accumulation of plant parts (i.e., pollen grains, seeds, branches, leaves, reproductive organs) that derives from either one or several individuals and is buried in sedimentary strata deposited under the same conditions (Spicer, 1989). As it was mentioned in the previous chapter, the main advantage of the study of palynofloras (and sporomorphs in particular) is that they tend to be proportionally more abundant in the rocks than other groups of fossils (Traverse, 2007). However, their high abundance may frequently lead to the mixing of palynological assemblages making it difficult to identify the different palaeoecological associations of their producing plants.

Conversely, the study of fossil macrofloras may offer a more accurate picture of the species that cohabited in a biocoenosis with less mixing than the study of fossil palynofloras may offer. In this sense, the study of macrofloras is typically less representative at the basin scale than palynological studies, and therefore it is always recommendable to combine both sources of palaeobotanical information when possible. Most fossil macrofloral assemblages have undergone (at least) some degree of transport before they deposit in their sites of burial and fossilization (Spicer, 1989). In this sense, processes as different as storms or riverbank undercutting (at the outside of the meander loops) may introduce whole branches and leaves of fresh plants into the aquatic system (Spicer, 1991). Rapid burial enhances the preservation of the plant remains, and therefore, their deposit in sedimentary environments with high rates of sedimentation, such as tidal flat systems, may help preserve the plant remains.

7.1. Middle Albian to early Cenomanian palynofloras (TU and CT sectors).

The middle Albian to early Cenomanian palynological assemblages, attributed to the Utrillas Gr - La Bicuerca Mb (see chapter 6.3 of this thesis manuscript) include terrestrial and marine

palynomorphs and are dominated by high proportions of gymnosperm pollen grains (75.8% out of the sum of palynomorphs identified) (Appendix II). Among the identified gymnosperm pollen, there is a dominance of those attributed to the families Cheirolepidiaceae (genus *Classopollis* consisting of ~20% of the identified palynomorphs) and Cupressaceae (~39.1% of the palynomorphs identified), dominated by the species *Inaperturopollenites dubius* (37.8%). In this regard, *Classopollis* and *I. dubius* account for ~60% (on average) of the identified specimens in the palynological assemblages attributed to the Utrillas Gr and La Bicuerca Mb (Appendix II). Additionally, the gymnosperm families Araucariaceae and Pinaceae/ Podocarpaceae are also represented in the assemblages, but to a lesser extent. In this sense, Araucariaceae represents 5.9% of the identified palynomorphs, being the main species identified *Araucariacites australis* (Appendix II). Bisacatte pollen of Pinaceae/Podocarpaceae affinities only represents ~2% of the assemblages.

Conversely, pteridophyte spores only account for a relatively small proportion (13.9%) of the identified middle Albian to early Cenomanian palynomorphs, despite being well-diversified (overall 76 taxa identified in both the TU and CT sectors).

Angiosperms only account for a small proportion of the palynomorphs identified (~7%). The dominant angiosperm taxa are attributed to the genus *Pennipollis* (mainly the species *Pennipollis peroreticulatus*) (Appendix II and III). In addition, other taxa such as *Transitoripollis anulisulcatus* become dominant in some samples (i.e., sample LT-4, TU sector). Aquatic palynomorphs only represent a small percentage of the studied samples and are primarily dominated by dinoflagellate cysts, accounting for 2.5% of the identified specimens on average.

7.1.1. Palynology of the Utrillas Gr – La Bicuerca Mb: the CT sector.

The samples studied in the CT sector were collected at nine different locations, out of which only four (samples RE-1, TE-CA-1a, LH-CM(2)-1a and CP-CS(2)-4) yielded well-preserved and diverse palynological assemblages (Fig. 6.8, Appendix II). The studied assemblages reflect the high percentages of gymnosperm pollen and small amounts of pteridophyte spores that characterised the palynofloras of the Utrillas Gr and La Bicuerca Mb.

Gymnosperms pollen grains represent 72.2% of the palynomorphs identified in the CT sector. In this sense, *Classopollis* is well-represented reaching 39% of abundance on average in the studied samples, being particularly high (54.6%) in the Reíllo outcrop (RE-1). Cupressaceae are the second best-represented conifer family in the CT sector and represents ~12% of the identified palynomorphs. Pollen grains attributed to this family are entirely dominated by the species *I.*

dubius, which can reach local dominance (i.e., sample LH-CM[2]-1a) (Fig. 7.1B). To a lesser extent, pollen grains of the family Araucariaceae and bisaccate pollen grains are also represented.

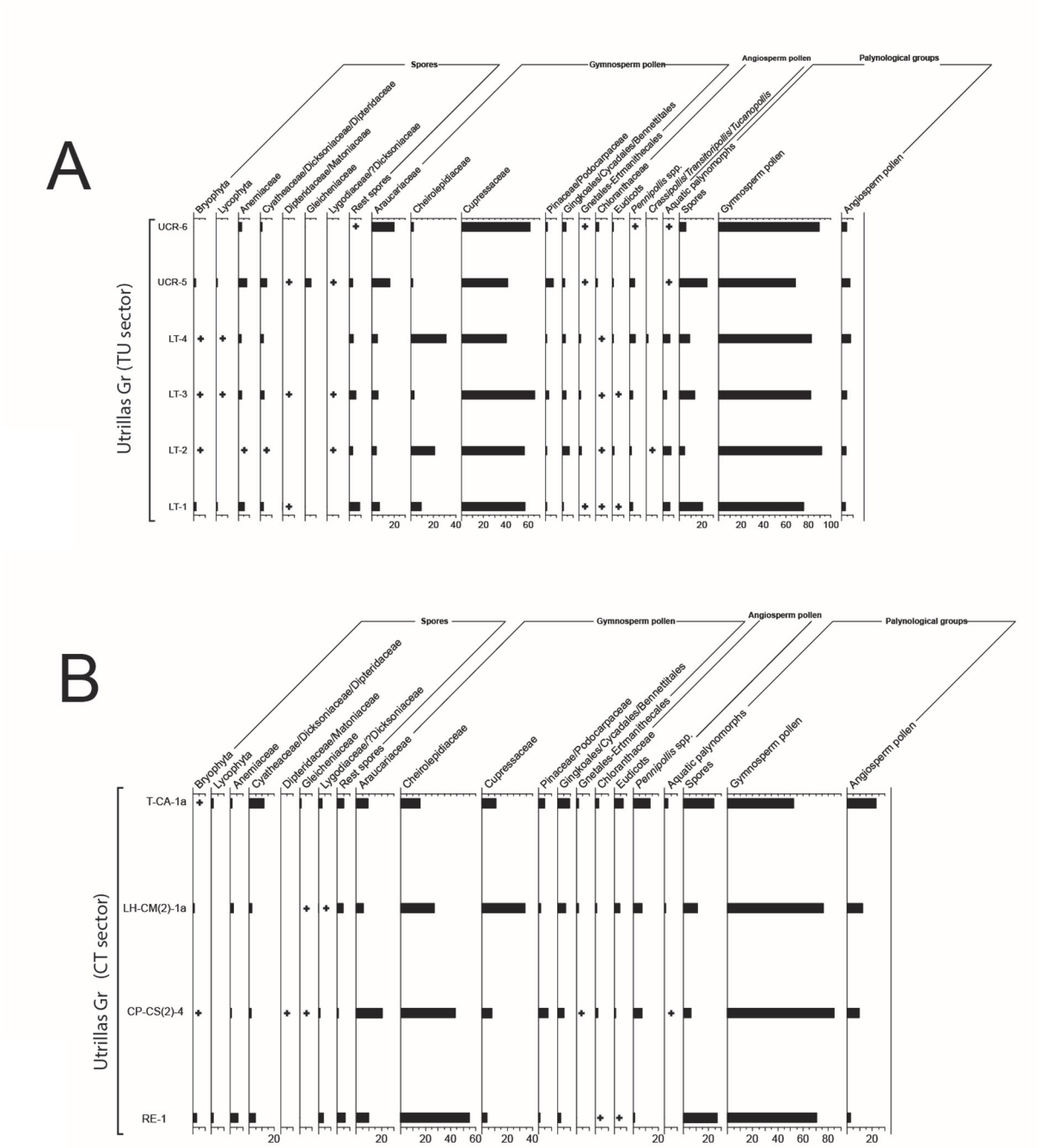

Fig. 7.1. Detailed palynological chart for (A) the TU sector (Utrillas Gr) and (B) the CT sector (Utrillas Gr - La Bicuerca Mb). Original figure from Bueno-Cebollada et al. (2021).

Spores are diverse (Fig. 6.8, 6.9B-F, L-M, Appendix II) and include *Cicatricosisporites* spp., *Cingutriletes* spp., *Concavissimisporites* cf. *crassatus*, *C.* cf. *irregularis* (Fig. 6.9F), *Cyathidites* spp., *Ischyosporites* spp. (Fig. 6.9E), *Patellasporites tavaredensis* and *Undulatisporites* spp. However,

their relative abundance among the identified palynomorphs is relatively low (~17.2%). Regarding angiosperms, monocolpate pollen types such as *Pennipollis* and *Clavatipollenites* are more abundant than types with more derived apertural systems. However, *Transitoripollis* has not been recorded in this sector (Appendix II). Additionally, undetermined dinocysts have been recorded in low numbers in all the studied samples except in the sample RE-1 (Reíllo outcrop) (Appendix II).

7.1.2. Palynology of the Utrillas Gr – La Bicuerca Mb: the TU sector.

The six samples from the TU sector (UCR-5, UCR-6, LT-1, LT-2, LT-3 and LT-4) correspond to the Uña and La Toba outcrops (Fig. 6.6). As it happened in the CT sector, the palynological assemblages of the TU sector are dominated by gymnosperm pollen grains (77.2%) being *Inaperturollenites dubius* the most abundant taxon (Fig. 6.7I). *I. dubius* represents ~50 % of the identified palynomorphs in the TU sector, on average in the six samples (this species is particularly abundant in the La Toba outcrop; Appendix II). Likewise, the occurrence of *Perinopollenites halonatus* is relatively frequent. Conversely, the abundance of pollen of the genus *Classopollis* only reaches 11% on average in the studied assemblages, reaching local dominance in the La Toba outcrop (sample LT-4; Appendix II). The highest gymnosperm diversity (27 species in level LT-3) is reached in an interval (comprising the levels LT-2 to LT-4) characterised by an impoverished spore element (Fig. 6.6, Appendix II). Additionally, gymnosperms of other affinities (Figs. 6.7F, J) are under-represented compared to Coniferales (Fig. 7.1A).

The spores of pteridophyte show a slight decrease (12.6% of the palynomorphs identified) if compared with the CT sector. However, they are the most diverse palynological group, with 61 species identified, despite their low relative abundance (Figs. 6.6, 6.7G, K-M, Appendixes II and III). However, their diversity fluctuates, and impoverished spore associations alternate with species-rich ones (Fig. 6.6: LT-2 and URC-6 compared with LT-1 and URC-5). Gleicheniaceae can be locally well-represented (UCR-5); however, Anemiaceae and Cyatheaceae/Dicksoniaceae/Dipteridaceae are the most diverse groups (Fig. 7.1A), and *Patellasporites tavaredensis*, *Cyathidites australis*, *C. minor*, *Cicatricosisporites venustus* and *Cicatricosisporites* spp. (Fig. 6.7K, M) are identified as the most frequent species in the spore record (Appendix II).

Angiosperms are represented by 28 species but do not constitute a conspicuous proportion of the palynofloras (Figs. 6.6, 7.1A, Appendix II). In this sense, monosulcate pollen grains are the

most frequently observed angiosperms (Appendix II). The genus *Pennipollis* is consistently recorded, while *Transitoripollis* presents a skewed distribution (LT-4) (Fig. 7.1A). These two genera have been related to Alismatales and Piperales, respectively (Friis et al., 2011). However, recent analyses carried out by Doyle and Endress (2014) indicate that they are more likely related to Chloranthaceae and/or Ceratophyllum. Eudicots are rare, but relatively diverse and include *Cupuliferoidaepollenites parvulus*, *Cupuliferoidaepollenites* sp. (Fig. 6.7D), *Retitrescolpites* spp., *Artiopollis indivisus* (Fig. 6.7N), *Striatopollis* cf. *sarstedtensis*, *Tricolpites* cf. *micromunus*, *Tricolpites nemejci* and *Tricolpites* cf. *vulgaris*.

Dinoflagellate cysts are more abundant in the TU sector than in the CT sector, particularly at the La Toba outcrop (Figs. 6.6, 6.7A, C, 7.1A). Similarly, acritarchs (Fig. 6.7B), prasinophytes, and foraminifera linings have also been identified. In this regard, the level at the La Toba section shows the highest diversity and abundance of dinocysts among the studied assemblages (Fig. 7.1A, Appendix II and III). This group is represented by the occurrence of *Subtilisphaera* spp., *Implestophaeridium* spp., *Cryboperidinium* spp., *Trichodinium castanea,* and *Cyclonephelium vannophorum* (Fig. 6.7A).

The palynostratigraphic analysis carried out in this chapter has allowed identifying the sedimentary record, corresponding to the Albian to early Cenomanian time interval (attributed to the Utrillas Gr and La Bicuerca Mb), and distinguishing it from the Aptian sedimentary succession in the studied outcrops across the Cuenca Basin. Consequently, the following chapters of this Ph.D. thesis only and exclusively deal with the analysis of the Utrillas Gr and La Bicuerca Mb (middle Albian to early Cenomanian) in the study area.

7.2. Middle Albian to early Cenomanian macroflora of the Cuenca Basin: the Cañada del Hoyo fossil bed.

This chapter of the manuscript focuses on the study of the macrofloral remains collected in the Cañada del Hoyo outcrop (Figs. 5.1, 5.34). The studied samples were collected by Dr. Meléndez in the mid-1980s during a fieldwork campaign. The macrofloral study in this Ph.D. thesis has only been carried out in Cañada del Hoyo since it is the only location where preserved plant remains were found, considering the 12 studied outcrops. The macroflora outcrop is located at the Cañada del Hoyo village (southern sector of the study area) and corresponds to a 40 to 50 cm-thick bed of slightly calcareous sandstones (interval 2 of the Cañada del Hoyo logged section) (Fig. 5.35). The macroflora site presents abundant fossil plant compressions yet the degree of preservation of most of the collected samples is poor. However, a few specimens present a higher degree of preservation and have been considered for their study and presented in this

chapter of the manuscript. Overall, 75 fossil plant samples were collected from the mentioned level out of which 10 have been studied in this Ph.D. thesis.

Most plant macrofossils are preserved as compressions where the vegetal material has been coated into a mineral layer (Spicer, 1989). The most common minerals coating the compressions are iron oxides/hydroxides that give rise to a red-brownish film due to biochemical alteration (Spicer, 1977). The study of compressions of fossil plant remains is a helpful tool in palaeoecology since it may reflect the existing floras during the time of burial of the now fossilised plant remains, which allows gaining a better understanding of the taphocoenosis from a palaeoenvironmental approach (Carrión, 2003). The primary value of the study of plant compressions is that they may show surface details of the part of the plant preserved (i.e., leaf shape, presence or absence of leaf stalks or petioles, or patterns of venation in some species) (Taylor, 1981).

In compressions with a high degree of preservation, the cellular microstructure of the original plant may be preserved in their cuticles, yet these cases are less commonly found in the fossil record. In these cases, the study of the preserved microstructure under the microscope allows observing the cellular details of the epidermis of a given species. More important, the microstructure of the plants presents distinctive epidermal features that are often helpful in the identification of some species (Taylor, 1981).

Unfortunately, the studied specimens from the Cuenca Basin are compressions that do not present preserved cuticles, and therefore their study in this Ph.D. thesis is more limited. Notwithstanding, this chapter also includes the study and identification of preserved cuticles (under the transmitted light microscope) from a coeval outcrop in the Maestrazgo Basin where similar palaeofloral assemblages have been identified. The studied plant cuticles were collected from the La Hoya Outcrop (Cortes de Arenoso, E Spain), where the sedimentary succession has been dated as late Albian and attributed to the Utrillas Gr (unpublished research). Including palaeoflora remains from the Maestrazgo Basin has allowed delving into the microstructural traits, given its better preservation. Similarly, it has permitted gaining a better understanding of some of the compressions collected from the Cañada del Hoyo outcrop that belong to the same genus.

Systematic palaeontology

The collected macroflora from the Cañada del Hoyo fossil bed (Fig. 5.35) consists of 75 collected samples stored in the facilities of the Geomining Museum (CN IGME-CSIC) in Madrid (Spain) with

the inventory numbers MGM-11283C to MGM-11358C. Overall, ten of these samples (MGM-11283C to MGM-11292C) of fossil plants have been studied in this Ph.D. thesis, corresponding to the best-preserved material found in the fossil bed. The following pages of this manuscript include the description and systematic classification of the different taxa found in the studied samples.

Order CONIFERALES sensu Farjon, 2010

Family CHEIROLEPIDIACEAE Takhtajan et al., 1963

Genus *Frenelopsis* (Schenk, 1869) emend. Watson, 1977

Frenelopsis sp.

(Figs. 7.2, 7.3)

Studied samples: MGM-11283C, MGM-11284C, MGM-11285C, and MGM-11286C.

Description: The specimens corresponding to this genus are characterised by shoots with thick cuticles, very abundant in the studied samples (Fig. 7.2).

The studied plant remains, corresponding to the samples MGM-11283C to MGM-11286C, are thin shoots divided into segments with nodes and internodes that separate them. The shoots consist of successive whorls of laterally fused leaves that comprise a proximal sheath and three distal triangular tips. The branching pattern cannot be ascertained due to the preservation of the samples (most of them consist of disjointed shoots; Fig. 7.2), yet it is observed that they may form a slight zig zag-like course (Fig. 7.2A).

Remarks: The genus *Frenelopsis*, which shows a widespread distribution through the Cretaceous period (Valanginian to Maastrichtian) (Mendes et al., 2010; Barral et al., 2019), is included within the Cherolepidiaceae family based on the discovery of *Classopollis* pollen in microsporangia cones attached to shoots of *Frenelopsis alata* (Hlustik and Konzalová, 1976). One of the main taphonomic characteristics of *Frenelopsis* is the occurrence of thick cuticles that are resistant to decay processes and preserved more easily than other plant remains. This genus (including around 20 species) was characterised by a widespread distribution in the low latitudes of the Northern Hemisphere and includes numerous highly specialised characteristics (i.e., the morphology of the shoots and leaves, cuticle anatomy, microsporangiate cone morphology or pollen morphology) (Watson, 1988; Kvaček, 2000; Gomez et al., 2002; Barral et al., 2019).

However, the here studied fossils do not allow for identification at the species level, and therefore they have been classified as *Frenelopsis* sp.

Additionally, shoots with preserved cuticles yet collected from the coeval (late Albian) La Hoya/Cortes de Arenoso outcrop (El Maestrazgo Basin, E Spain; Fig. 7.3) have been included in this manuscript to provide an example of the microscopic features observed in this genus. Under the microscope, the studied shoots show stomatal rows with single stomata per row, yet they may occasionally bifurcate. The stomatal rows are separated by (0 - 5) epidermal cells that are quadrangular to sub-rounded in shape (Fig. 7.3A). The stomata are usually surrounded by 4 or 5 epidermal cells and their stomatal pit is overlapped by four papillae that are usually sunken (Fig. 7.3B).

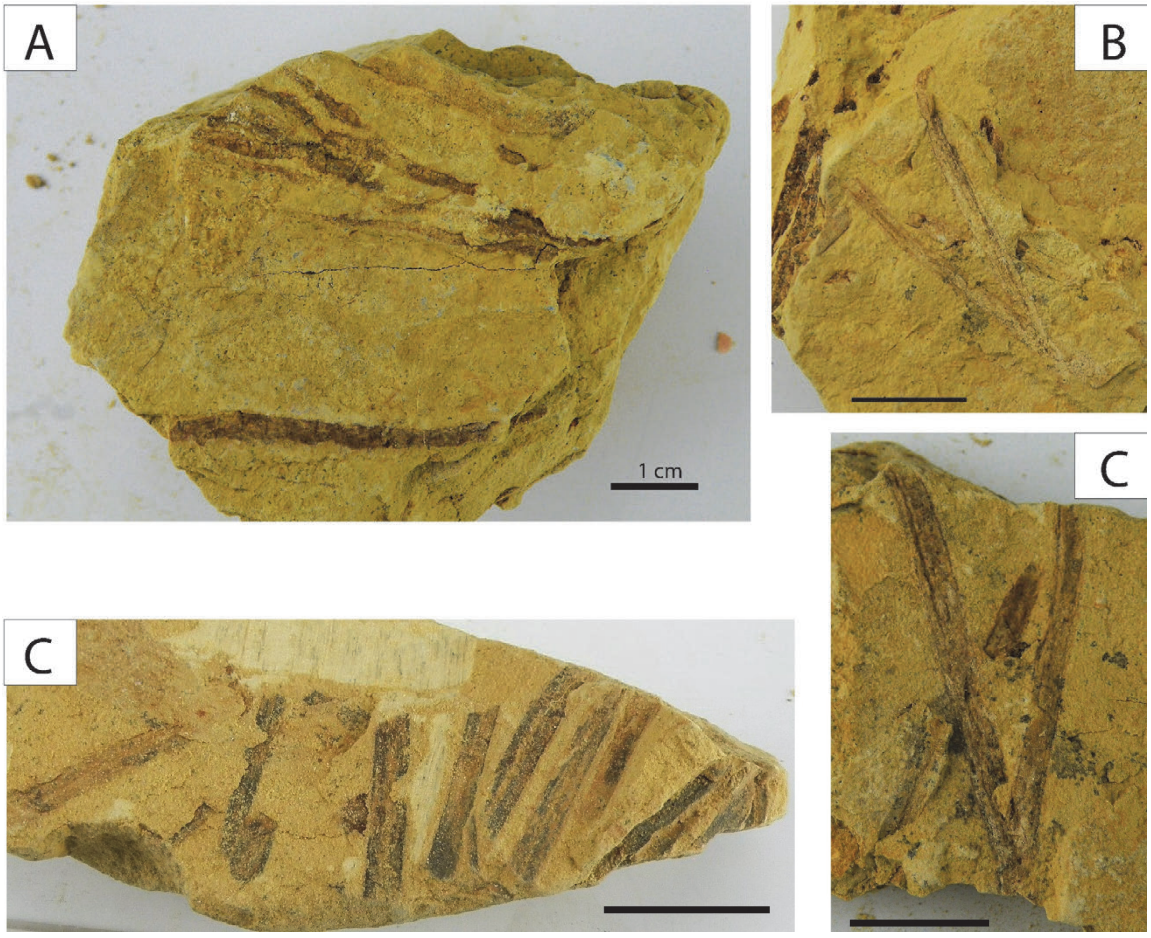

Fig. 7.2. Examples of compressions attributed to the genus *Frenelopsis* from the Cañada del Hoyo outcrop. (A) Sample with shoots of *Frenelopsis* sp. where the branching patterns can be observed (sample MGM-11283C). (B–D) Examples of compressions of cuticles of *Frenelopsis* sp. (samples MGM-11284C, MGM-11285C, and MGM-11286C). Scale bars are 1 cm long.

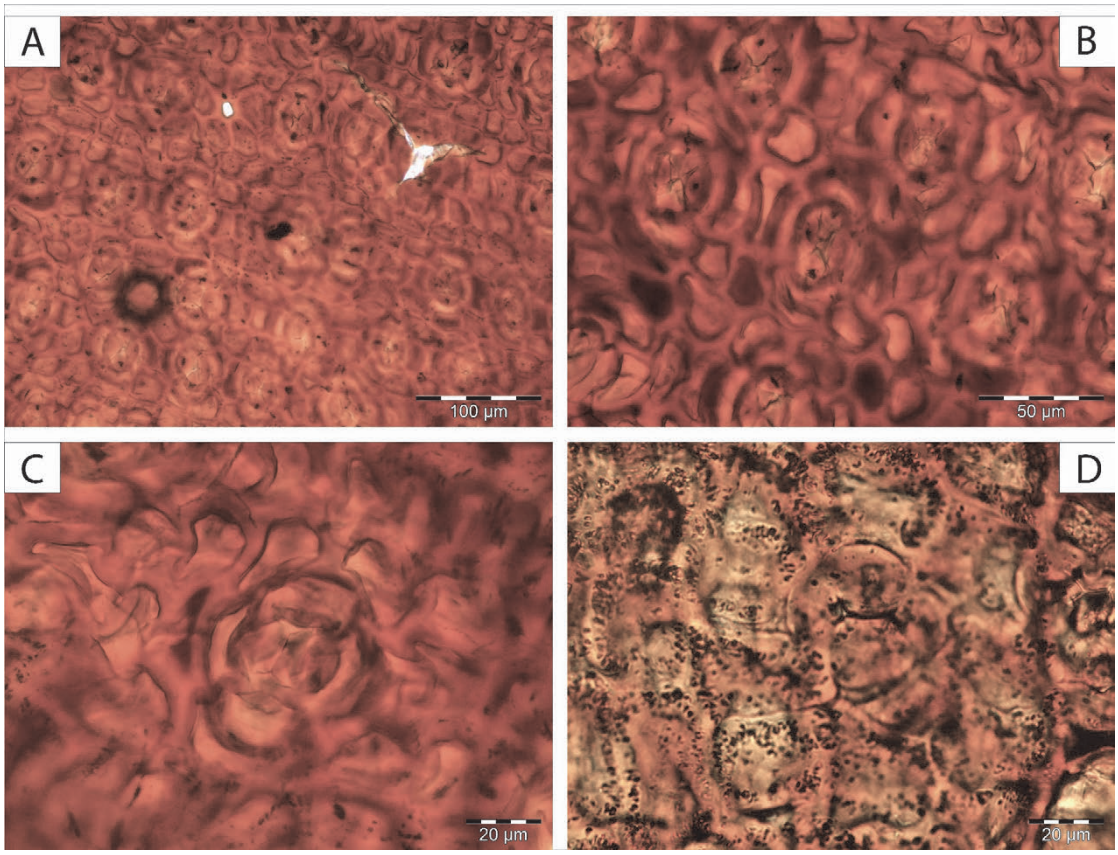

Fig. 7.3. Examples of cuticles of *Frenelopsis* sp. under the microscope. The samples were collected from the upper Albian La Hoya (Cortes de Arenoso) outcrop located in the Maestrazgo Basin (Eastern Spain). (A) and (B) stomatal apparatus arranged in rows. (C) and (D) Close-up of two stomata. Unpublished images.

Family INCERTAE SEDIS

Genus *Dammarites* Presl in Sternberg 1838

Dammarites sp.

(Fig. 7.4)

Studied samples: MGM-11287C, MGM-11288C, and MGM-11289C.

Description: Isolated ribbon-shaped leaves with a well-pronounced parallel venation (Fig. 7.4). The apical part of the leaves is acute (Fig. 7.4C), yet their apex tends to be oblong. The studied leaf compressions are 1 to 1.5 cm-thick fragments of leaves, reaching the longest ones 6 cm in length. The venation in the leaves is constituted by parallel-sided longitudinal veins less than 1 mm in width. The leaves present 20 to 15 veins per cm.

Remarks: The occurrence of fossil compressions with the previously described characteristics (Fig. 7.4) in the Cañada del Hoyo outcrop allows their interpretation as belonging to the genus *Dammarites*. However, the main difference with other species of the genus such as *D. albens*

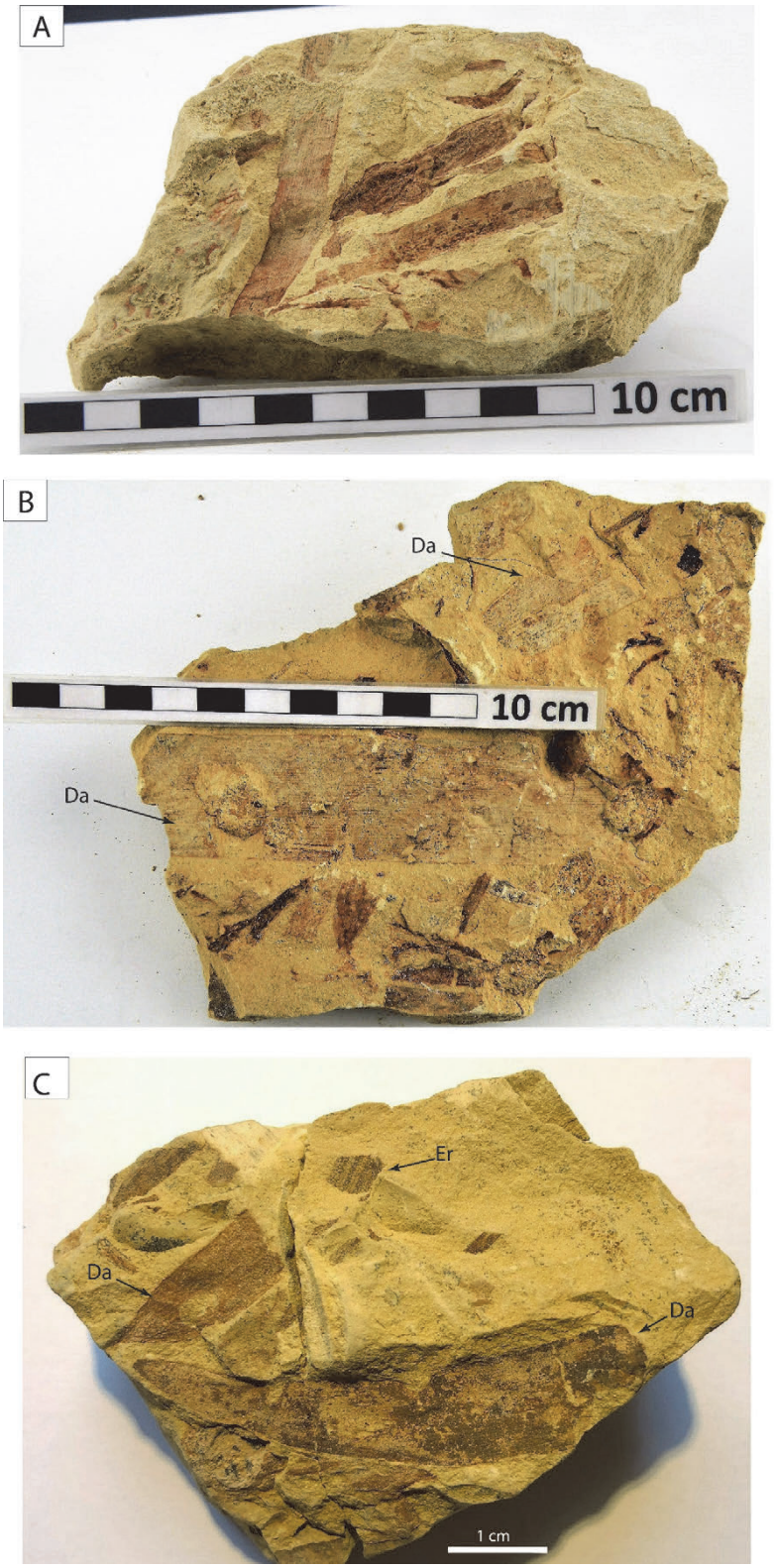

Fig. 7.4. Examples of leaves attributed to *Dammarites* sp. from the Cañada del Hoyo outcrop. (A) Fragments of leaves of *Dammarites* sp. where the venation can be observed (sample MGM-11287C). (B) Fragments of larger leaves than in (A), attributed to *Dammarites* sp., where the typical venation can be observed. This sample also presents a significant amount of poorly preserved undetermined plant compressions (sample MGM-11288C). (C) Examples of leaf compressions (sample MGM-11289C) attributed to *Dammarites* sp. (Da) (MGM-11289C) and a fragment tentatively attributed to the genus *Erethmophyllum* (Er) (MGM-11289C). The Dammarites leaf fragment to the left-hand side of the sample corresponds to the basal part of the leaf, while the leaf fragment to the lower part of the sample represents the apical part of a *Dammarites* sp. leaf.

or *D. coriaceous* (Barale, 1992; Kvaček and Lobitzer, 2010), is that the present species shows a considerably smaller size of the preserved leaves and their venations. Likewise, similar venations have also been observed in *Dammarophyllum*; however, this genus presents a proportionally broader and shorter leaf than *Dammarites* with an oval-shaped morphology (see Fig. 1 in Kvaček, 2003). Therefore, the fossil compressions from the Cañada del Hoyo outcrop attributed to *Dammarites* will be interpreted as *Dammarites sp.* due to the impossibility of their interpretation at the species level.

The genus *Dammarites* was considered a conifer with affinities to Cordaitales (Seward, 1917), although other authors suggested a cycadophyte affinity (Bayer and Petrbok, 1919). However, Barale (1992) attributed *Dammarites* (*D. coriaceous* from the Lower Cretaceous of NE Spain) to Araucariaceae based on the study of their leaves and microsporophylls. The occurrence of xerophytic adaptations has been reported from some species of Dammarites (i.e., *D. coriacea* in the Lower Cretaceous of NE Spain) based on the study of the anatomy of the mesophyll, despite the relatively great length observed in their leaves (Barale, 1992).

Genus *Glenrosa* Watson and Fisher, 1984 emend. Srinivasan, 1992

cf. *Glenrosa* sp.

(Fig. 7.5)

Studied samples: MGM-11290C, MGM-11291C, and MGM-11292C.

Description: The studied specimen (sample MGM-11290C) shows an alternate branching pattern characterised by shoots with spirally arranged leaves appressed basally against the shoot (Fig. 7.5A-C). The main branch in the specimen in sample MGM-11290C is 34 mm in length with 17 to 18 mm-long subsidiary shoots showing an alternate branching pattern (Fig. 7.5A). The leaf length may vary from 2.6 to 3.7 mm while its breadth ranges from 1.2 to 1.8 mm.

The free apical portion of the leaves is sharply incurved or spreading outwards, and their apex is sub-acute to acute in shape. The abaxial surface is keeled, and the leaf margin is entire. The specimen observed in sample MGM-11292C (Fig. 7.5D) is a compression of a probable seed cone attributable to *Glenrosa* sp. that has remained connected with leafy axes. Regarding morphology and size, the pollen or seed cone is oval-shaped to spherical and slightly wider than longer. The cone is approximately 80-82 mm in width.

Remarks: The previously described fossil plant compressions (Fig. 7.5) are tentatively interpreted as belonging to the genus *Glenrosa* based on the previously described leaf morphology. To date, *Glenrosa* presents seven species identified with a broad geographical distribution during the Cretaceous, being reported from the Barremian to the Cenomanian of America, Europe, and Asia (Moreau et al., 2015 and references therein). The different species that form the genus are characterised by having coniferous shoots with spirally arranged leaves that may range from scale-like and appressed (pressed close or lying flat against the shoot) to falcate (curved like a sickle) and spreading outwards (Srinivasan, 1992; Zhou et al., 2000; Gomez et al., 2012; Moreau et al., 2015).

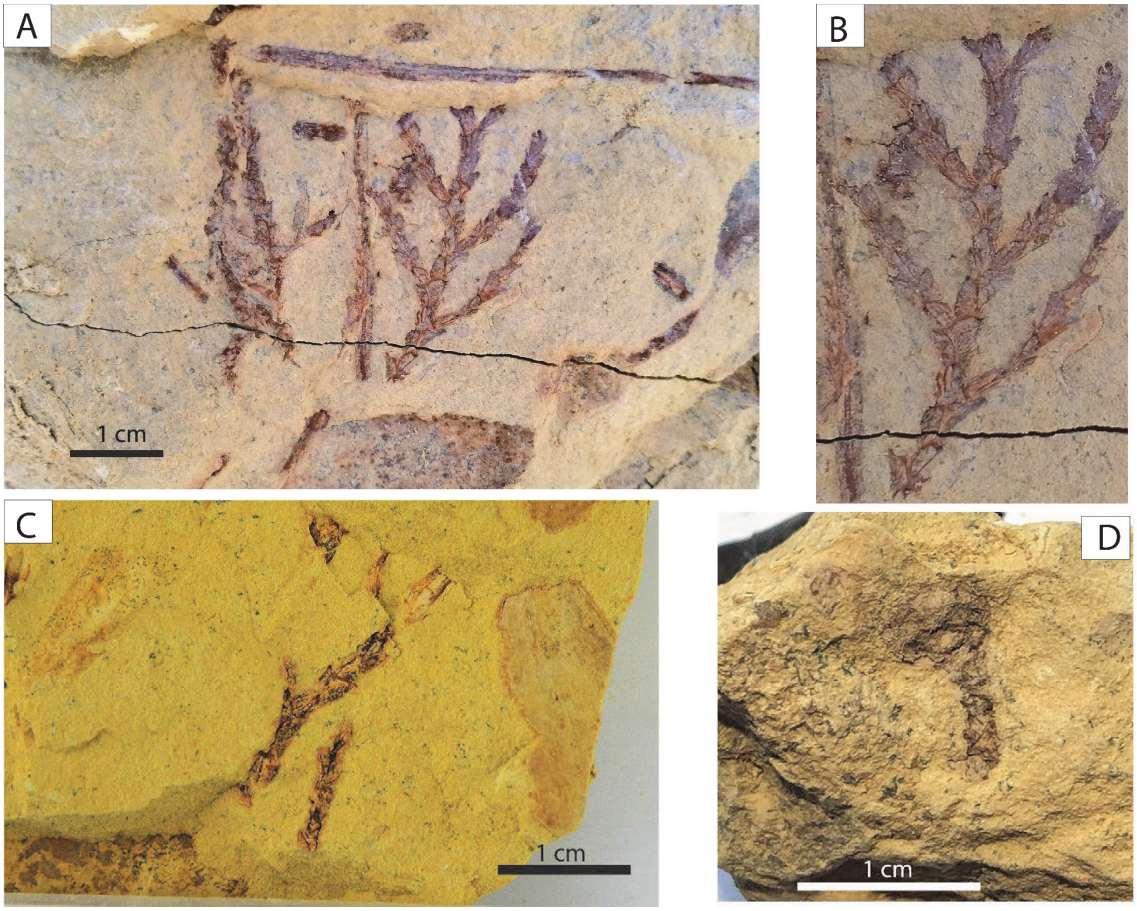

Fig. 7.5. Examples of compressions attributed to the genus *Glenrosa* from the Cañada del Hoyo outcrop. (A) Exceptionally preserved compression of *Glenrosa* sp. (sample MGM-11290C) where its branching pattern and leaf morphology can be observed. The sample also presents fragments of shoots attributed to *Frenelopsis* sp. (B) Close-up of (A) where a branch of *Glenrosa* sp. can be observed. (C) Shoot of *Glenrosa* sp. (sample MGM-11291C) where the same leaf morphology displayed in (A) is shown. (D) Possible ovuliferous cone attributed to *Glenrosa* sp. (sample MGM-11292C).

One of the main diagnostic features of the genus *Glenrosa* compared to other conifers is the presence of stomatal crypts, which is widely considered a xerophytic adaptation (Gomez et al.,

2012 and references therein). The studied specimens in the Cañada del Hoyo outcrop (Fig. 7.5A-B) resemble the species *G. falcata* and *G. virginiensis* (Fig. 7.6C) late Barremian and mid-Albian, respectively (Srinivasan, 1992; Gomez et al., 2012). However, the studied specimen presents a longer and straighter morphology of the leaves, being their free part significantly shorter and the adpressed part longer than in *G. falcata,* therefore resembling more the morphology of *G. virginiensis.* Likewise, they may also resemble *Watsoniocladus*, a genus established by Srinivasan (1995) for cheirolepidiacean conifers previously assigned to *Cupressinocladus*. The main characteristic of *Watsoniocladus* is the occurrence of leaves arranged in decussate pairs or forming whorls of three, with their stomata surrounded by large internal or external papillae producing a star-like pattern in the stomatal aperture (Kvaček and Mendes, 2021).

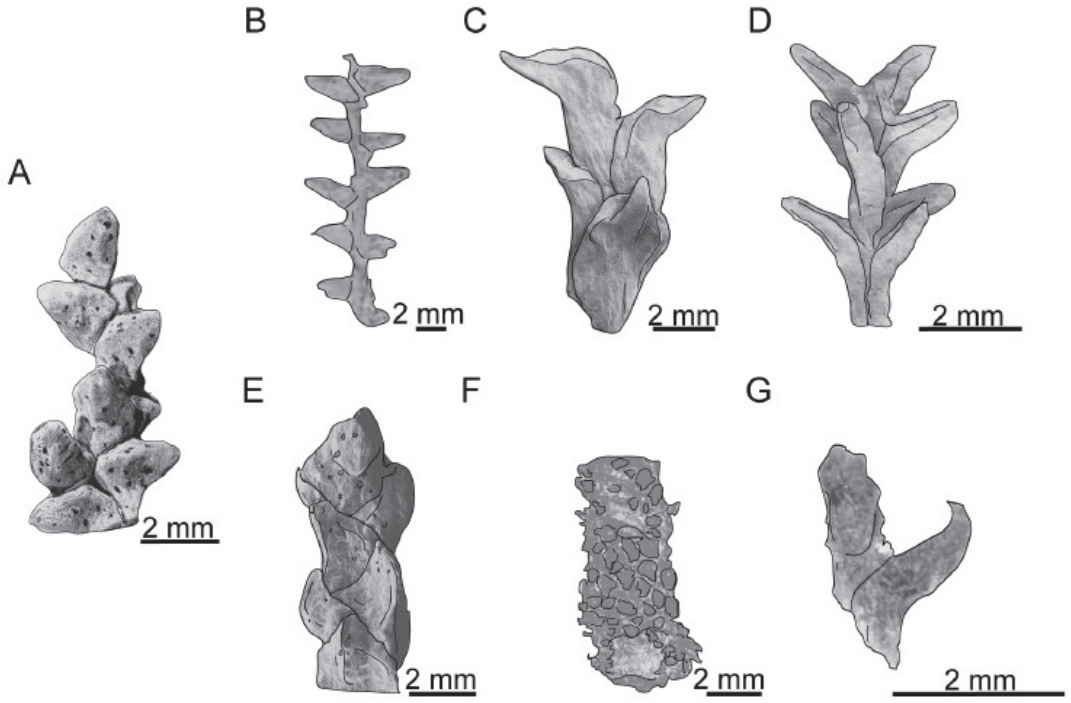

Fig. 7.6. Comparison of the morphology of the leaves in the seven different species of the genus *Glenrosa*. (A) *Glenrosa carentonensis* sp. nov. (B) *Glenrosa pagiophylloides*. (C) *Glenrosa virginiensis*. (D) *Glenrosa hopewellensis*. (E) *Glenrosa texensis*. (F) *Glenrosa nanjingensis*. (G) *Glenrosa falcata*. Original figure in Moreau et al., 2015.

Regarding its affinities, the genus *Glenrosa* was initially included within the Cheirolepidiaceae family due to its occurrence in association with other cheirolepidiacean conifers and its thick cuticles (Watson and Fisher, 1984). One of the main characteristics of the cheirolepidiacean conifers is the presence of *Classopollis*-type pollen (spheroidal asaccate pollen grains with a subequatorial furrow and a thickened striated equatorial band) (Alvin, 1982). However,

Classopollis-type pollen has not been found associated with the genus *Glenrosa* to date (Srinivasan, 1992).

Conversely, Srinivasan (1992) tentatively assigned *Glenrosa* to Cupressaceae based on the morphology of their reproductive organs (single structured cone scales that resemble those of some extant Cupressaceae) and the complete lack of *Classopollis*-type pollen associated with this genus. Similarly, Gomez et al. (2012) succinctly relate *Glenrosa* to modern Cupressaceae based on the sharing of subsidiary cells (Ewin, 2004). Following this hypothesis, Moreau et al. (2015) describe for the first time spherical to ovoid pollen cones attributed to *G. carentonensis,* approximately half the size of the cone studied here, which are borne apically, and present undetermined pollen grains preserved. The pollen grains reported by these authors (see Fig. 13) seem to resemble inaperturate pollen grains (i.e., *Inaperturopollenites*) that represent one of the most frequent pollen grains in the Cuenca Basin during the mid-Albian to early Cenomanian (Bueno-Cebollada et al., 2021) and would (tentatively) suggest a cupressacean affinity for *Glenrosa*.

Order GINKGOALES Gorozhankin (1904)

Family INCERTAE SEDIS

Genus *Erethmophyllum* Thomas (1913) emend. Harris and Millington (1974)

cf. *Erethmophyllum* sp.

(Fig. 7.4C)

Studied sample: MGM-11289C.

Description: the studied leaf fragment is a 4 mm broad fragment of the middle part of a blade with an entire margin and possible coriaceous texture. The leaf fragment is characterised by the occurrence of 1 mm-thick veins that present a prominent subparallel to parallel pattern (Fig. 7.4C).

Remarks: the studied leaf fragment (Fig. 7.4C) has tentatively been attributed to the genus *Erethmophyllum* based on the venation pattern and morphology of the blade. The genus *Eretmophyllum* belongs to the order Ginkgoales, consists of 20 species, and is restricted to the Mesozoic floras of Eurasia. However, its representation is less diverse during the Cretaceous (Li et al., 2018), and it became extinct after the mass extinction event at the end of the Cretaceous period (McElwain and Punyasena, 2007; Li et al., 2018). The genus *Erethmophyllum* presents

features in their leaf and cuticular morphologies (i.e., narrowly dichotomising veins and thick cuneate petioles in their leaves) that allow interpreting it as a Ginkgoal (Thomas, 1913; Li et al., 2018).

The leaves of *Erethmophyllum* are usually tongue-shaped, oblong to oblanceolate ones that taper towards their base. In most species, their apex tends to be rounded or obtuse, and the petiole shows a cuneate base (i.e., see Figs. 18 and 19 in Kvaček et al., 2005). The petiole typically contains two veins that dichotomously branch close to the base of the leaf. Then the veins are parallel (like those observed in the studied leaf fragment; Fig. 7.4C) and show 8 to 12 veins per cm (Kvaček et al., 2005; Li et al., 2018). In this regard, the genus *Nehvizdya* Hlùstik (1977) was erected to include this leaf morphology; however, this type of fossil leaf was transferred to the genus *Erethmophyllum* by Kvaček (2000) and Kvaček et al. (2005) after finding the ovuliferous organ *Nehvizdyella* associated with *Erethmophyllum*-type leaves. Additionally, Kvaček et al. (2005) reported the occurrence of *Cycadopites* sp. pollen grains associated with *Erethmophyllum* leaves, suggesting their affinity to this genus.

8. Sedimentary facies analysis of the middle Albian to lower Cenomanian succession.

The facies analysis carried out over the following pages represents a synthesis of the sedimentological information obtained based on the fieldwork data that represents one of the cornerstones of this Ph.D. thesis. Overall, 26 sedimentary facies have been identified in the 12 studied outcrops (Fig. 5.1), described and interpreted in terms of forming processes. The identified facies have been grouped into eight facies associations (FA) that represent the variability of sedimentary environments observed in the deposits of the Utrillas Gr and La Bicuerca Mb (Aras de Alpuente Fm) in the Cuenca Basin (Tables I and II).

Facies association	***Facies***	***Interpretation***	***References***
FA I: Proximal alluvial	*Gcm, Gt, St, Sp, Sr, Dl*	Ephemeral alluvial/braidplain environment (proximal zone).	Miall (1977, 2010); Bristow and Best (1993); Rodríguez-López et al. (2010).
FA II: Distal alluvial	*St, Sp, Sr, Fm1, Fm2, Fs, Dl, Tb*	Ephemeral alluvial/braidplain deposits (distal zone). Landwards from the limit of tidal influence.	Miall (1977, 2010); Bristow and Best (1993); Chamizo-Borreguero et al. (2016).
FA III: Aeolian dunes	*Sae1, Sae 2*	Aeolian dunes associated with the ephemeral alluvial setting.	Mountney and Thompson (2002); Rodríguez-López et al. (2008); Bueno-Cebollada and Meléndez (2018).
FA IV: Inner estuarine	*Sb1, Sb2, St_2, Sp_2, Sr, Ftb, Fm2, Smf, Ifc, Tb*	Proximal estuarine setting within the supratidal to the upper intertidal zone.	Dalrymple (2010b); Daidu (2012); Chamizo-Borreguero et al. (2016).
FA V: Tidal flat	*Sht, Sb, Sh, St, Sp, Sr, Ifc*	Open tidal sand flat. Middle to lower zone of an intertidal setting.	Daidu (2012); Daidu et al. (2013).
FA VI: Outer estuarine	*Scax, Scah, Fc, Fm2*	Distal part of a tide-dominated estuary.	Dalrymple (2010b); Olariu et al. (2012).
FA VII: High-gradient coastal deposits	*Shg, Ssc*	High-gradient foreshore to the upper zone of the upper shoreface. Non-protected open coast. Non-barred clastic shoreline.	Hart and Plint (1995); Clifton (2006); Isla et al. (2020).
FA VIII: Shallow marine mixed deposits	*Slc, Scax, Sbt, Lms, Fc*	Mixed siliciclastic-carbonate shallow marine environment. Mixed inner ramp.	Mount (1984); Clifton (2006); Schwarz et al. (2018).

Table I. Facies associations (FA) identified in the studied outcrops. See text for further explanations on the facies association and Table II for the description and interpretation of the identified facies.

The environments interpreted based on the facies associations identified range from purely continental alluvial (FA I and II) to shallow marine mixed deposit (FA VIII), showing a complex array of transitional continental to marine facies associations that will be tackled in the following pages. The eight facies associations identified in this thesis include: proximal alluvial (FA I), distal alluvial (FA II), aeolian dune (FA III), inner estuarine (FA IV), tidal flat (FA V), outer estuarine (FA VI), high-gradient coastal (FA VII), and shallow marine mixed (FA VIII) deposits.

Facies	Description	Forming process (es)	Environment (s)	References
Gcm. Clast-supported massive conglomerates	Clast-supported massive gravel beds, consisting of pebbles and cobbles. Locally, they can present matrix-supported terms, along with the presence of cm- thick sandstone lenses within the gravel. Generally, the average size of the pebbles is about 3 cm in diameter, reaching up to 5 – 6 cm locally. Regarding morphology, this facies is arranged in sheet-like cm-thick bodies. Flat base which may extend laterally for tens of meters depending upon the exposure conditions of the outcrop.	Sudden deposition of coarse-grained pebble to cobble deposits in unconfined high-energy plastic flows. Some of the pebbles observed in this facies are interpreted as ventifacts, therefore having been either originally modelled or reworked by wind action. Reactivation of the alluvial discharge after drier stages.	This facies is interpreted as pseudoplastic debris flow deposits, taking place in an ephemeral alluvial setting due to sudden sheet flood events.	Miall (2010); Rodríguez-López et al. (2010); Chamizo-Borreguero et al. (2016).
Gt. Stratified cross-bedded conglomerates	Stratified gravel beds showing pebble (to cobble) trough cross-bedding with clast imbrications, mainly appearing as isolated pockets. Matrix-supported. The matrix consists of coarse-grained sandstone. Erosional base usually presenting the larger clast sizes, when a gradation in grain size is noticeable. This facies is commonly arranged in lens-shaped bodies with sets ranging on average between 30 to 80 cm in thickness.	Deposition under high-energy subaqueous flows.	Minor channel fills as interspersed pockets among sandstone-prone deposits in an ephemeral alluvial setting. Transverse alluvial bedforms.	Miall (1977, 2010); Rodríguez-López et al. (2010).
St. Trough cross-bedded sandstone	Coarse to very coarse-grained heterometric sandstone, with some scattered pebbles/cobbles locally. Rip-up clasts. Trough cross-beddings are arranged in sets which can be cm- to dm- in thickness. Basal contacts are typically erosional and may present lags of pebbles. Common occurrence of reactivation surfaces. Locally, this facies may present bioturbation (roots).	The main process controlling the deposit of facies St is the downstream lee-face progradation of linguoid bed-forms (3D subaqueous dunes). Bed-load deposition from unidirectional flows.	Alluvial braided channels and bars.	Miall (1977, 2010); Rodríguez-López et al. (2010).
	(*Subfacies* St_2) Rhythmical alternation of grain size of the foresets. m-scale lenticular bodies with cm-scale foresets.	Similar processes as described in the facies St along with the modulation of the alluvial discharge by ebb and flood currents.	Estuarine or tidally-influenced alluvial channels.	Chamizo-Borreguero et al. (2016) and references therein.
Sp. Planar cross-bedded sandstone	Planar cross-bedded sandstones showing coarse- to very coarse-grained sandstones. Slightly better sorted than the facies St. Tabular bodies that range from cm- to dm-thick sets of planar cross-bedding. Flat or erosional bases. Usually associated with facies St. Locally, gradation in the grain size of the foresets may be observed. They may locally present bioturbation by root traces.	Linguoid bars or bedforms (2D dunes). Decrease in the energy of the discharge compared to three-dimensional dunes and trough cross-bedding (St). Downstream migration of sandy bedforms under unidirectional flows of the river channels.	Alluvial braided channels and bars.	Allen (1963); Miall (1977, 2010); Rubin and Carter (2006); Rodríguez-López et al. (2010).
	(Subfacies Sp_2) Rhythmical alternation of grain size in the foresets. m-scale lenticular bodies with cm-scale foresets.	Similar processes as described in the facies Sp along with the modulation of the alluvial discharge by ebb and flood currents.	Estuarine or tidally-influenced alluvial channels.	Chamizo-Borreguero et al. (2016) and references therein.
Sr. Current ripple cross-laminated sandstone	Ripple cross-laminated sandstones that range from very fine- to coarse-grained. Asymmetrical current ripples are arranged in solitary (or compound) ripple trains. It commonly overlies facies St and/or Sp by means of a sharp flat to diffuse contact. Local presence of root traces.	Small bedforms (ripples) deposited under lower flow regime conditions. Weak unidirectional subaqueous flows. Diminishment in the energy of the discharge represented by finer grain sizes and smaller bedforms compared to the facies St and Sp due to the progressive infill of an alluvial channel.	This facies represents the final infill of sandy channels in alluvial and tidally-influenced estuarine environments.	Miall (1978, 2010).
Fm1. Massive reddish-purple mudstone and siltstones	Massive (to faintly laminated) mudstones and siltstones including some disperse sand-sized grains. They generally present reddish-purple to dark yellow colours with intense mottling. Bioturbation root traces may be intense (in situ palaeosol development). Occasionally mud crack-like structures may be observed. Tabular sheet-like bodies that may laterally extend for several meters, showing thicknesses of up to 2 metres.	Low-energy deposits, settled by suspension. The reddish to purple colours of the mudstones and siltstones are the result of deposition in low-energy oxidizing environments where soils may develop due to plant colonisation or later oxidation. Reddish to purple colours in mudstone deposits are common evidence of subaerial exposure conditions and well-drained substrates and soils	Alluvial and tidally-influenced floodplain environments with plant colonisation at times. Oxidizing environment (well-drained soils)	Retallack (2001) and references therein; Spaletti and Colombo (2005); Marconato et al. (2014); Chamizo-Borreguero et al. (2016).
Fm2. Grey mudstones and siltstones	Massive mudstones and siltstones. Grey-black to greenish colours that may or may not include some mottling, although the latter is a rare feature compared to the facies Fm1. Tabular to lenticular bodies which expand laterally tens of meters and thicknesses of up to 1 m. Likewise, they may include some carbonate.	Low-energy events. Settling by suspension. Greenish to grey colours indicate a lack of oxidation and a reducing environment. Possible water-logged substrates. Darker colours indicate a greater content of organic matter	Tidally-influenced and distal alluvial floodplain environments (supratidal). Estuarine muds (upper intertidal zone). Reducing environment (water-logging).	Retallack (2001) and references therein; Spaletti and Colombo (2005); Chamizo-Borreguero et al. (2016).
Fs. Poorly sorted tabular sandstone	Very fine to very coarse, highly heterometric sandstone. Scattered pebbles. Massive, structureless or depicting faint beddings. Tabular to lenticular bodies, commonly less than 1 m in thickness. Either sharp or erosional bases. Minor and under-represented feature in the Buenache de la Sierra outcrop, which appear interspersed among facies Fm1 and Fm2 as sandy tabular intercalations. Locally bioturbation by roots may be observed.	Bedload transport within an overbank setting owing to floodwaters overcoming topographic levees and spilling from the parent feeder channels of the alluvial system into the floodplain. Proximal sectors of an alluvial crevasse splay are commonly either structureless or depict faint beddings, with sharp or erosional basal contacts.	Proximal crevasse splays deposits associated with the alluvial floodplain	Mjøs et al. (1993); Chamizo-Borreguero et al. (2016); Burns et al. (2017).
Dls. Flat pebble-cobble lags	Pebble and cobble linings that extend laterally for several meters depending upon the exposure conditions. Flat horizontal to sub-horizontal alignments or mildly inclined surfaces. Subangular to subrounded clasts alternating with some poly-faceted morphologies with concave shape faces, micro-impact features and polished surfaces. The average size of the clasts is about 2 to 3 cm in diameter, although locally sizes of up to 5 cm have been observed. Discrete lags interbedded between facies St and Sp or associated with facies Gcm.	Seasonally drier periods when the water table is low and the ephemeral alluvial system is dry, allowing wind deflation of the smaller grain sizes and leaving behind the coarser pebble and cobble size clasts. Wind reworking of gravelly alluvial facies Gmc or Gt generates these deposits.	Wind deflation lags (one pebble thick linings). Desert pavements (thicker accumulation of pebbles and cobbles) in an ephemeral braidplain system.	Glenie (1970); Fryberger (1993); Rodriguez- Lopez et al. (2010).
Sae1. Fine-grained homometric sandstone	Medium- to fine-grained homometric sandstones arranged into sets of planar cross-bedded strata. High (to moderate) angle (commonly ranging between 20° to 25°) planar cross-bedding with straight to sigmoidal foresets arranged in multiple superimposed sets that range from 0.4 – 1.2 m in thickness. Cross-bedded sets are abruptly separated by different order flat horizontal to sub-horizontal surfaces. Tabular geometry with flat bases and occasionally infilling previous topographic depressions.	Grainflow strata accumulated in the lee slopes of the dunes by sand avalanche processes. Planar cross-bedded sets truncated by flat surfaces represent the preserved lower parts of the foresets and the bottom sets of the aeolian accumulations. The surfaces that truncate cross-bedded sets are superimposition (2^{nd} order) and interdune (1^{st} order) surfaces.	Aeolian dunes and pods (lee faces).	Mountney and Thompson (2002); Rodríguez-López et al. (2008); Jordan and Mountney (2010); Chamizo-Borreguero et al. (2016); Bueno-Cebollada and Meléndez (2018).
Sae2. Low angle cross-bedded sandstone	Moderate to low angle fine- to medium-grained cross-bedded homometric sandstone with translatent strata. It may show sedimentary continuity with facies Sae1.	Migration of wind ripples across the lower flank of the dunes.	Aeolian dunes and pods.	Mountney and Thompson (2002) and references therein.
Tb Tangential tabular-bedded (calcareous) sandstone	Medium- to coarse-grained sandstones that may present carbonate cement. Gently tangential tabular beds (10 to 20 cm thick) with low-angle planar lamination and flat bases and tops. Foresets are continuous over 10s of metres with palaeocurrents towards the NW. Occasionally, faint reactivation surfaces. Bed contacts are erosional and continuous laterally across the outcrop. Infilling steep erosional incisions (up to 9 m deep and 65 m wide). Only reported from the Uña outcrop.	Upper stage plane bed deposits. Deposition under high-energy unidirectional (NW) currents. Currents progressing landwards. Frequent internal reactivation surfaces indicate different superimposed events.	Tidal bore deposits. Repeated surges of tidal bore events flooding upper estuarine and distal alluvial environments.	Chamizo-Borreguero et al. (2016) and references therein.
Sb1. Bidirectional cross-bedded sandstone	Medium- to very coarse-grained sandstone showing planar cross-bedding sets migrating in opposite directions (herringbone-like bedding). Commonly, this facies is associated with facies Sp and/or St. Water scape structures. Tabular to lenticular bodies commonly display either sharp or slightly erosional basal contacts. Bioturbation is scarce.	Subaqueous dunes and bars deposited under high energy conditions. The sand was reworked by bidirectional currents that generate the herringbone cross-bedding. Bed-load deposition from bidirectional flows. Additionally, liquefaction processes along with rapid burial of the sediments might have produced water scape structures.	Intertidal estuarine subaqueous bars and channels fill.	Dalrymple et al. (1992); Davis (2012). *This facies coincides with the facies Scb in Bueno-Cebollada et al. (2022).
Sb2. Ripple-reworked sandstone	Coarse- to very coarse-grained sandstone with large sets scale (> 1 m) of trough cross-bedding. The cross-bedded sets are reworked by rippled sand that migrates in the opposite direction than that of the main foresets. Lenticular-shaped bodies that extend laterally for more than 10 m and show erosional bases. Mudstone and quartzite pebbles.	High-energy deposition by downstream lee-face progradation. The direction of the main foresets represents the dominant current, while the rippled sand migrating in an opposite direction represent the subordinate current. Bed-load deposition from bidirectional flows	Tidally-influenced fluvial channels. Estuarine tidal channels	Dalrymple (2010b).

Sh. (Sub) Horizontally-bedded sandstone	Coarse grain-size siliciclastic sandstone (locally calcareous). Horizontal to very low angle beddings (laterally extensive across the outcrop). Undulated or crenulated surfaces which can present abundant mud drapes. Asymmetrical to symmetrical ripples. Low to moderate bioturbation. Tabular morphology with a sharp basal contact. 1 m-thick bodies and laterally extensive, for at least, 100 metres	Alternation between high energy, bed-load processes (tidal currents) and slack water periods when deposition by suspension dominates (mud drapes).	Middle to lower zone of an inter-tidal flat. Open coast tidal flat. Lower coastal plain	Shanley et al. (1992); Dalrymple (2010b); Daidu (2012); Daidu et al. (2013).
Sht. Heterolithic sandstone	Coarse- to fine-grained sandstones. Horizontal to planar cross-bedding. Mainly siliciclastic sandstones (locally calcareous). Commonly interbedded with grey and black mudstones and siltstones. Flaser and wavy laminations are common. Bioturbation may range from low to intense (i.e., Arenicolites). Vertebrate bone fragments, vegetal remains, mm-thick charcoal fragments. Water deformation structures.	Alternation of bedload and suspension deposition. Remobilisation levels may occur. Currents showing opposite transport directions.	Intertidal sand flat deposits (middle to lower intertidal zone)	Chamizo-Borreguero et al. (2008); Daidu et al. (2013), Dalrymple (2010b).
Ftb. Muddy heterolithic	Mudstones and siltstones interbedded with fine sands. Wavy to lenticular lamination. Double mud drapes. Bioturbation intensity is low to moderate. The mudstones and siltstones may be dark (high organic matter content). Scattered plant fragments and charcoalified wood (up to 15 cm fragments).	Alternation of suspension and bedload deposition. Dominance of suspension. Varying tidal current speeds with slack water periods in tidal environments (double mud drapes). Remobilisation levels (parautochtonous charcoalified wood fragments).	Tidally-influenced fluvio-estuarine mudflat/marsh. Supratidal to (upper) intertidal zone.	Daidu et al. (2013); Dalrymple et al. (2012).
Smf. Massive homometric fine-grained sandstone	Fine-grained siliciclastic sandstone. Massive appearance. Very well sorted. It can be interbedded with facies Ifc. Lenticular bodies or pods of sand filling land depressions. Very oxidized undifferentiated plant structures. Discontinuous bodies that can be traced laterally for a few 10s of metres.	Wind-blown sand accumulated and trapped by vegetation.	Nearshore air-borne accumulations. Supratidal environment.	Kuriyama et al. (2005).
Ifc. Ferruginous crust	Dark red to brown very heterometric coarse-grained sandstones and gravels. Heavily iron-cemented sandstone. Massive appearance and opaque under the petrographic microscope. Laterally extensive surfaces across the outcrop. 10 to 20 cm in thickness. Fining upwards gradations. Tabular to slightly dome-shaped. Slightly erosional to sharp contacts. Normally formed at the top of the sandstone beds.	Diagenetic products of replacement of carbonate components by iron oxyhydroxides. Iron precipitation induced by biological activity.	Post-sedimentary iron accumulation and ferruginous crust development Syn-depositional microbial activity.	Preston et al. (2011); Afify (2017); García-Hidalgo et al. (2018) and references therein.
Sbt. Bioturbated massive calcareous sandstone.	Ochre very calcareous medium- to coarse-grained sandstones. Occasionally they may present planar cross-bedding. Foraminifers, bivalves (oysters), gastropods and sponges. Very intense bioturbation. Occurrence of trace fossil *Planolites* (*Cruziana* Ichnofacies) in the Campillos-Paravientos outcrop.	Low-energy shallow marine setting that allows for colonisation (intense bioturbation). Change to low-energy conditions from originally high-energy deposition (relict planar cross-bedding when preserved). The occurrence of *Planolites* (*Cruziana* Ichnofacies) in the Campillos-Paravientos outcrop is characteristic of subtidal poorly sorted or heterolithic environments.	Abandoned subtidal dunes. Shallow marine environment.	MacEachern et al. (2010).
Scax. Calcareous cross-bedded sandstone	Coarse- to medium-grained calcareous sandstones. Planar to trough cross-bedding (50 cm to 1 m-thick). Coarsening upwards trend. Unimodal (N/NE) transport direction and, locally, bimodal (N/NE - S/SW). Scarce bivalve shell fragments. Karstified top bed surface. 1 to 1.5 m-thick and more than 200 m-long bodies that can be amalgamated. Bioturbation is moderate (vertical burrows).	Uni-directional (to bi-directional) tidal currents. Forward accretion architecture. Upper flow regime. Tidal asymmetry.	2-D and 3-D tidal dunes. Crest and lee sets of the tidal dunes. Amalgamated single bodies creating compound tidal dunes. Outer estuarine setting. Upper shoreface.	Dalrymple and Rhodes (1995); Dalrymple (2010b); Olariu et al. (2012); Schwarz et al. (2018).
Scah. Calcareous heterolithic sandstone	Medium- to fine-grained calcareous heterolithic sandstones with thin (mm- to cm-) interbedded calcareous mudstone laminae. Wavy to flaser heterolithic laminations and mud drapes. Locally, symmetrical ripples (2 cm in length). Highly bioturbated levels with U-shaped (*Arenicolites*) and vertical burrows (*Ichnogenus Skolithos*). Amalgamated, laterally persistent bodies (100 to 200 m depending on the outcrop conditions) in lateral continuity with the facies Scax. Pinching out in calcareous mudstones (facies Fc). Coarsening upwards trend with an upward increase in sandy terms.	Diminishment in the energy of tidal currents compared to facies Scax. Dominance of tidal currents over wave processes (relatively restricted environment). The decrease in the sedimentation rate favours more intense bioturbation.	Bottomsets of the 2-D and 3-D tidal dunes filling the troughs between adjacent dunes. Intertidal to subtidal outer estuarine environment.	Dalrymple (2010b); Olariu et al. (2012).
Shg. High-gradient inclined bedded sandstone	Coarse-grained heterometric sandstone arranged into inclined (high-gradient) large foresets of planar lamination. The beds are inclined towards the SE/S and show a maximum dip of 15° (10° on average). Two- to four-meter-thick sets which can be traced downdip for approximately 10 m depending on the outcrop conditions. Tabular to wedge geometries.	High-energy deposits (upper flow regime). Swash and backwash processes. Swash processes carry material ashore. Backwash processes remove the material. Oscillatory or combined currents.	Accretion of the foreshore and the most proximal part of the upper shoreface with a steep marine profile. Shoreline progradation. Non-barred siliciclastic shoreline.	Clifton (1969); Hart and Plint (1995); Schwartz and Birkemeier (2004); Plint et al. (2010); Isla et al. (2020); Bueno-Cebollada et al. (2022).
Ssc. Small-scale trough cross-bedded sandstone	Coarse- to very coarse-grained siliciclastic sandstones. Small-scale sets of trough cross-bedding (10 to 20 cm sets) and asymmetrical ripples. Polymodal (herringbone-like beddings) transport directions (NE, N, and SW). Erosional base locally with mudstone pebbles/cobbles (10 to 20 mm). Laterally extensive tabular, sheet-like bodies.	High-energy deposits (upper flow regime). Sediment is mainly reworked by wave action in onshore, along-shore, and offshore directions.	Distal portion of the upper shoreface. Non-barred siliciclastic shoreline	Schwarz et al. (2018); Isla et al. (2020).
Fc. Calcareous mudstone	Grey to greenish calcareous mudstones/marls with minor amounts of sand-sized grains. Massive to faintly laminated. Abundant gypsum crystals. Tabular sheet-like bodies that can be up to 10 m in thickness and may extend laterally for 100s of meters.	Low-energy shallow marine environment. Deposition by suspension.	Shallow marine low-energy deposits.	Dalrymple (2010b); Olariu et al. (2012).
Slc. Large-scale cross-bedded sandstone	Medium- to very coarse-grained sandstones. Siliciclastic or calcareous. Large-scale tangential cross-bedded sets. Reactivation surfaces. Presence of bivalve shell fragments and foraminifers. Low bioturbation. Transport direction is mainly unimodal (NE), but bimodal patterns are also possible.	High energy bedload transport and deposition which may alternate with reversal flows (reactivation surfaces).	Subaqueous subtidal dune foresets. Shallow marine environment. Sublittoral (shelf) talus. High energy (tidal action).	Dabrio (1989); Chamizo-Borreguero (2006).
Lms. Massive sandy limestone	Sandy limestone (grainstone) to medium-grain size calcareous sandstone. Calcite-cemented. Allochemical grains account for 40%. Quartz grains dominate. Moulds of mollusc shell fragments replaced by calcite. Tabular laterally extensive geometry in outcrop.	Mixing at the interface between nearshore siliciclastic sediments with migrating tidal bars and carbonate ramp deposits. High terrigenous input.	Background (shoreface) sedimentation in a mixed siliciclastic-carbonate inner ramp (shallow subtidal). Transition to a carbonate ramp setting.	Mount (1984); Jones (2010); Blomeier et al. (2011); Schwarz et al. (2018).

Table II. Sedimentary facies of the Utrillas Gr – La Bicuerca Mb succession identified in the studied outcrops.

8.1. Facies association I: proximal alluvial (Gcm, Gt, St, Sp, Sr and Dl)

Description: This facies association consists of the gravelly- and sandy-dominated Gcm, Gt, St, Sp, Sr, and Dls facies (Fig. 8.1). The facies association presents variabilities in the Northern sector compared to the Eastern sector. Conversely, it has not been identified in the outcrops of the Southern sector. This facies association is characterised by the occurrence of highly amalgamated lenticular-shaped sandy channelised bodies dominated by coarse- to very coarse-grained sandstones with trough and planar cross-bedding (facies St and Sp, respectively). The (trough and planar) cross-bedded sets are abundant in the sand-prone terms of the facies association and commonly range between 20 and 60 cm in thickness. Additionally, some of the amalgamated channelled bodies may present an upwards gradation into medium- to coarse-grained sandstones, dominated by asymmetrical ripples (Sr), showing a reduction in the size of the bedforms.

This facies association also includes pebble- to cobble-dominated deposits (Gcm, Gt, Dls facies) that can be either stratified and lenticular in shape (Gt; Fig. 8.1A) or massive, lacking any stratification, and with tabular morphologies (Gcm; Fig. 8.1A, C, F, G). Likewise, quartzite pebble linings may also be observed as part of this facies association (Dls; Fig. 8.1B, D). Such pebble linings are flat and sharp surfaces included within the amalgamated sandstone bodies, which are the main component of this facies association. The pebbles and cobbles are subangular to subrounded in shape, however, faceted morphologies depicting concave-up polished surfaces are also observed. The association is arranged into 1 to 4 m-thick amalgamated sandstone bodies with frequent internal erosional scours that either lack mudstones and siltstones, or present very limited accumulations of them. The palaeocurrents measured in the sets of the cross-bedded sandstones show a S/SE unimodal dominant direction in the outcrops of the Northern sector, although more locally SW directions have also been measured. In the Southern sector, more concretely in the Campillos-Paravientos outcrop, the main transport direction is towards the South, however, to a lesser extent some of the bodies may migrate to SSE or SE.

Interpretation: This facies association is interpreted as the proximal part of a braidplain system that presents the coarser grain size of the studied succession, and has been identified in the Northern (Buenache de la Sierra, Mina Pepita, and Las Majadas outcrops) and Eastern sectors (Campillos-Paravientos outcrops), representing the lowermost part of some of the logged sections (Fig. 5.3, 5.15, 5.28). It is characterised by a geometry of stacked amalgamated channels dominated by 2D and 3D subaqueous dunes (Sp and St facies, respectively), lacking overbank (mudstone and siltstone) deposits.

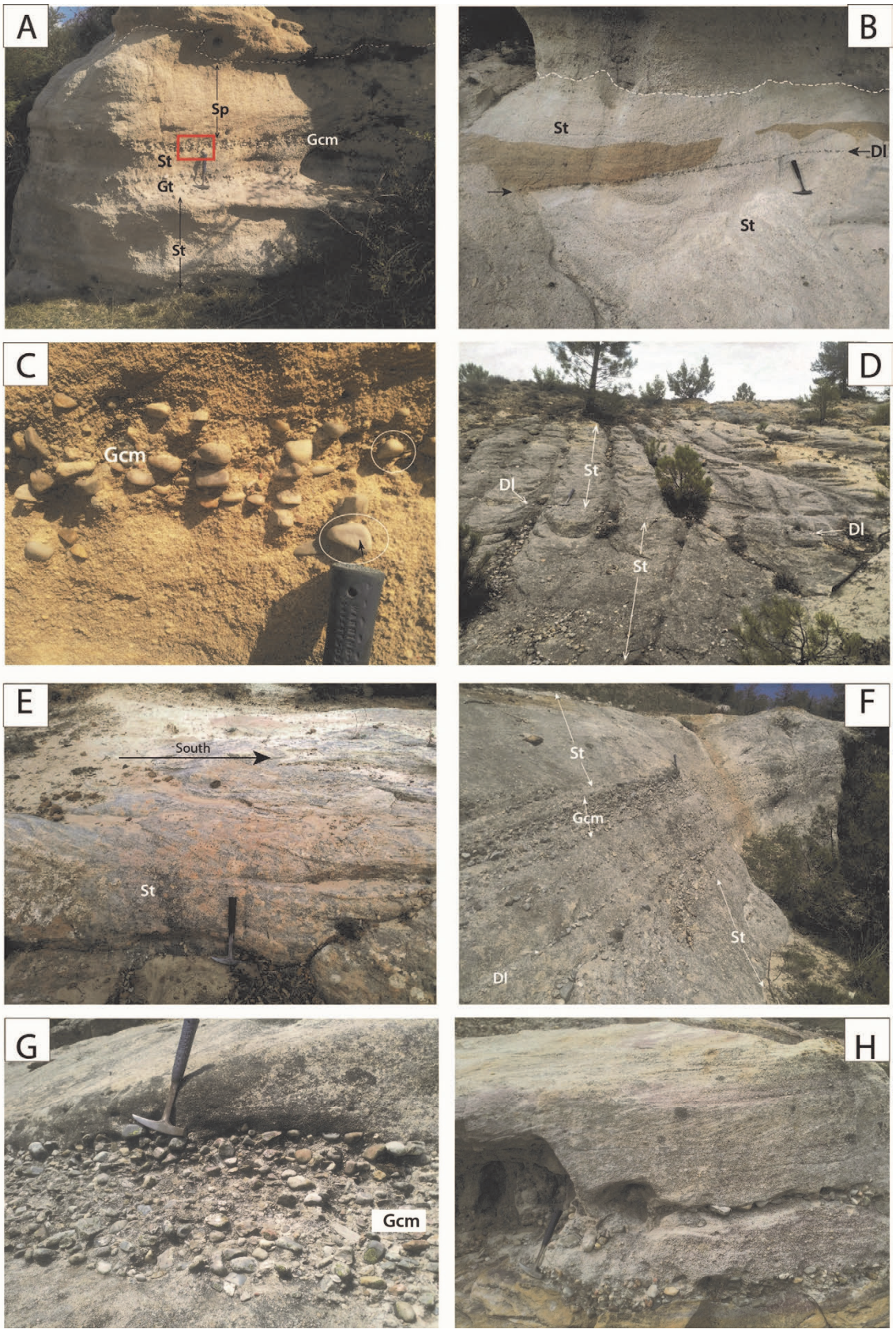

Fig. 8.1. (A) Proximal alluvial facies association (FA I). The facies Gcm, Gt, St, and Sp are indicated in the picture (Table II). This facies association dominates the lower part of the Utrillas Gr. succession in Buenache de la Sierra (Fig. 3). (B) Detail of the proximal alluvial facies association (FA I) where the interaction of the facies Dl with the facies St (Table II) is shown, indicating drier periods when there was no alluvial discharge in the system. (C) Detail of the facies Gcm, included within the proximal alluvial facies association (FA I). The occurrence of moderately faceted pebbles is indicated in the pictures by 145arto circles. (D) Proximal

alluvial deposits at the lower part of the logged section in the Campillos-Paravientos outcrop dominated by the facies St. In the figure, the architecture of the deposits is seen in a transversal section and is characterised by 30 to 50 cm-thick sets of trough cross-bedding that migrate to the South (towards the reader, in the picture). The deposits of the facies St are cut by deflation lags (facies Dl) that represent interruptions in the alluvial discharge and deflation during drier periods. (E) Detail of a set of trough cross-bedding from the lower part of the Campillos-Paravientos outcrop (same outcrop as in [D]) seen in a longitudinal section. The bedforms migrate to the South (right-hand side of the picture). (F) Proximal alluvial deposits in the lower part of the Mina Pepita section where the succession is dominated by the sand-prone facies St along with a significant proportion of the gravel-prone facies Gcm (and Gt to a lesser extent). (G) Close-up of the facies Gcm in the Mina Pepita outcrop where the facies is dominated by clast-supported terms. (H) Detail of the facies Sp arranged in small-scale sets included within fining upwards amalgamated bodies with erosional base and erosional lags of quartzite pebbles.

In the Campillos-Paravientos outcrop, the deposits of the facies association I are interpreted as the downstream lee face progradation of linguoid bedforms (3D dunes; facies St [Table II]) (Miall, 1977, 2010), which migrate in a seaward direction (towards the south, and the southeast, to a lesser extent) mainly showing the facies St, Gt and Dl (Fig. 8.1D, E). The local occurrence of facies Gt in several basal levels of the succession indicates higher energy deposits probably due to the reactivation of the alluvial discharge after drier periods. Facies Sp is anecdotal and represents a slight decrease in energy compared to facies St and Gt (Miall, 1977). The sandstone bodies of this facies association frequently present facies Sr at their top, which is characterised by smaller bedforms along with finer grain sizes compared to St, Gt or Sp. This fact indicates a diminishment in the energy conditions of the sedimentary environment (Miall, 2010).

The channelled bodies are characterised by the local occurrence of massive deposits of gravel (Gcm) interpreted as sheet flood events, which consist of surges of coarse-grained sediments due to the reactivation of the alluvial discharge after drier stages (Chamizo-Borreguero et al., 2016). The occurrence of faceted pebbles (interpreted as ventifacts) in this facies association reflects the reworking of the alluvial deposits by wind action, which is associated with drier stages during which the alluvial discharge was minimal or non-existent (Knight, 2008; Rodriguez-López et al., 2010). Additionally, the alluvial strata that dominate the proximal braidplain deposits may be punctuated by deflation lags that form by the action of wind deflation on alluvial deposits and are typical of arid settings (Fig. 8.1B, D) (Fryberger, 1993). In this sense, the lack of alluvial discharge during drier periods fostered wind deflation that blew away the finer particles of sediment leaving behind a pavement of pebble-cobble size clasts (a deflation lag) which prevented the underlying sandstone-size deposits from being blown away (Rodriguez-López et al., 2010).

Therefore, the sedimentological data obtained allows interpreting the facies association I as an ephemeral alluvial system whose deposits were reworked by wind action during more arid periods, giving rise to deflation lags or desert pavements. The migration of the bedforms is essentially toward the SE/S, which indicates a seaward direction, according to previous

palaeogeographic reconstructions in the study area (Chamizo-Borreguero et al., 2016; Bueno-Cebollada et al., 2021; Bueno-Cebollada et al., 2022).

8.2. Facies association II: distal alluvial (St, Sp, Sr, Fm1, Fm2, Fs, Tb and Dl)

Description: This facies association is composed of the (coarse-grained) sandstone (St, Sp and Sr) and mud rich (Fm1 and Fm2, and Fs to a lesser extent) facies, along with the local occurrence of facies Dl (Fig. 8.2). However, it lacks pebble- and cobble-dominated facies (Gcm and Gt) which are a common feature of the FA I, or if they develop, they tend to be a minor component of this facies association. In general, the ratio of sandstone versus mudstone-siltstone is approximately 40:60 in this facies association, and it can be better observed in the Northern and Eastern sectors of the study area (Fig. 5.1). The facies St and Sp usually represent the basal terms of the sandstone bodies of this facies association and are arranged into lenticular bodies, which typically show erosional surfaces at their base. The sandstone bodies present a fining upwards trend and range upwards into finer grain-sized sandstones with current ripples (facies Sr). However, the main problem that presents the facies Sr is the poor preservation of the current ripples due to the general coarse grain size of the deposits that tend to mask smaller-sized sedimentary structures. These sandstone successions are generally overlain by mudstone to siltstone (facies Fm1 and Fm2) showing a progressive transition into finer siliciclastic deposits. The facies Fm1 consists of massive reddish mudstone and siltstone (Fig. 8.2D, F, G, H), which may present yellowish to purple mottling and minor proportions of sandstone grains. The facies Fm2 consists of green to grey massive to faintly laminated mudstone and siltstone. This facies association locally presents moderate to intense vertical bioturbation primarily developed in facies Fm1 which may affect underlying sandstone facies and is interpreted as root traces (palaeosol development).

The facies Dl (Table II) can be observed in association with the mentioned facies (Sc and Sr), but it is much less frequently found than in the FA I. It consists of one-pebble-thick linings which may extend laterally for several metres showing flat horizontal to sub-horizontal surfaces. The pebbles observed range between 10 and 30 mm in diameter in their longer axis and showed both faceted and sub-angular morphologies.

The dominant palaeocurrent directions measured in this facies St and Sp of this facies association are toward the E and SE; however, locally some palaeocurrens indicating SW and S directions have also been observed. Additionally, this FA includes the facies Tb (Table II) which is described as medium- to very coarse-grained ochre sandstone, with a minor proportion of

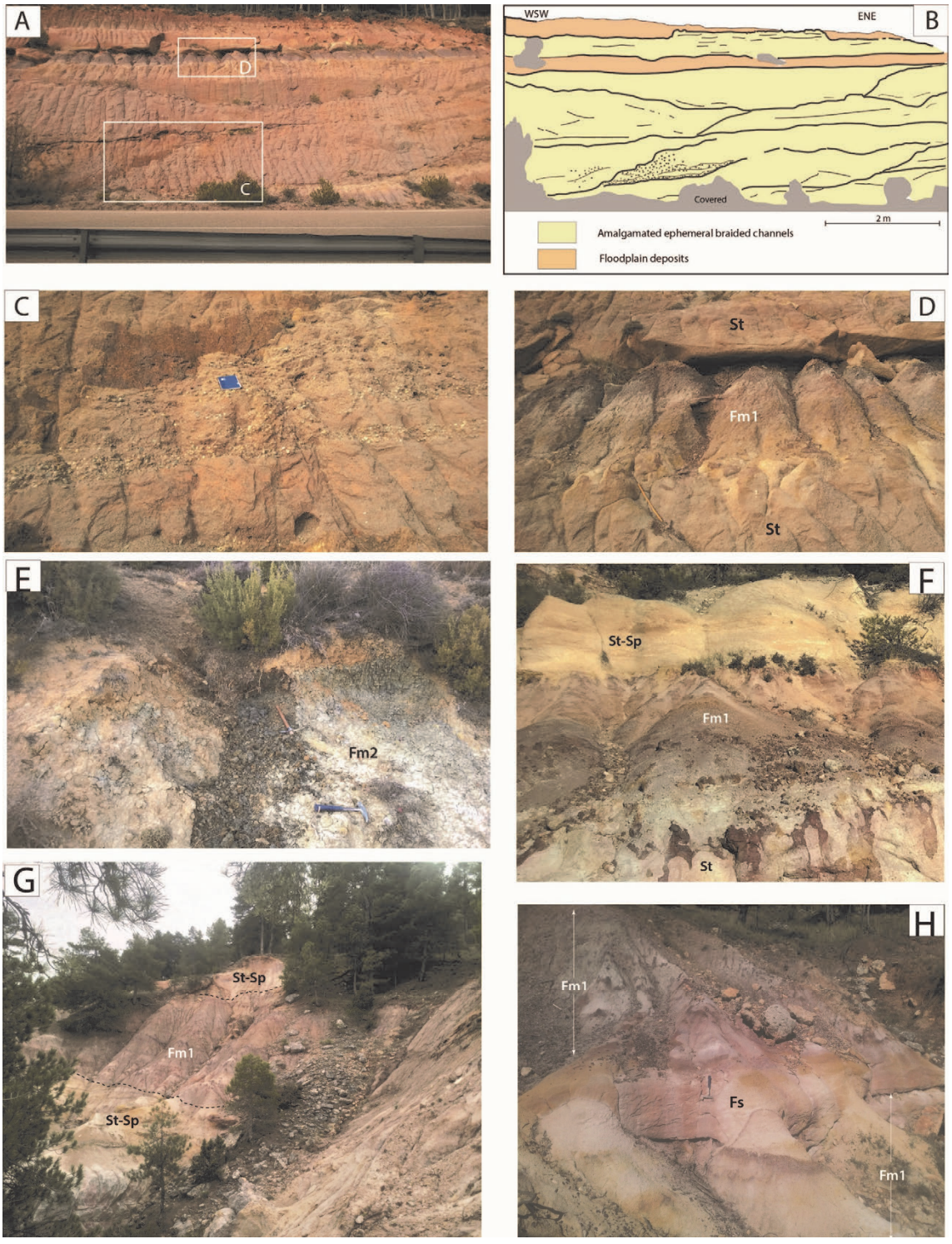

Fig. 8.2. Distal alluvial facies association (FA II). (A) The channelled bodies are composed of coarse-grained sandstone (dominated by the facies St and Sp) and may locally contain some gravel beds. Note that the channels are amalgamated, display conspicuous lenticular geometries with erosional, concave-up base contacts, and present fining upwards trends. (B) Line drawing and interpretation of (A). (C) Detail of some levels displaying gravel-prone sediments deposited due to higher energy events associated with the ephemeral alluvial deposits. (D) Reddish to purple mudstones deposited in the floodplain areas of the braided system. (E) Lower part of the logged section in the Reíllo outcrop showing the deposits of the facies Fm1. The palynological sample RE-1 was collected in this level. (F) Distal alluvial facies association (FA II) in the Buenache de la Sierra outcrop. This facies association is characterised by the occurrence of the low energy facies Fm1, which may present palaeosoil development, that alternate with channelled sandstone deposits. (G) View of the FA II in the Las Majadas outcrop where the typical architecture of alternating low sinuosity sandy channels (mainly facies St and Sp) and floodplain deposits (mainly facies Fm1) can be observed. The facies Fm1 presents palaeosoil development. (H) Detail of the floodplain deposits of the FA II in the Campillos-Paravientos outcrop. In the picture, they are dominated by the low-energy facies Fm1 which shows intense red mottling, probably related to

plant colonisation. It is also interbedded with tabular levels attributed to the facies Fs, that represents episodes of crevasse splay flooding the floodplain of the distal braidplain. Hammer for scale in the pictures is 35 cm in length.

feldspars; carbonate cement may be present. The facies Tb is typically arranged into gently tangential tabular beds (10 to 20 cm-thick) with low-angle planar lamination and flat bases and tops. Occasionally faint internal reactivation surface may occur. Bed contacts are erosive and characterised by slightly undulating erosive surfaces that continue through the outcrop. The very low-angle foresets are continuous over tens of metres and show a persistent NW palaeocurrent. The facies Tb is only found in the Uña outcrop infilling several steep erosive incisions (up to 9 m-deep and more than 65 m-wide) (Fig. 8.3). The morphology of the incision surfaces varies laterally, becoming deeper and narrower toward the W of the Uña outcrop. This surface erodes older sediments incising into alluvial deposits (facies St, Sp and Sr) and floodplain deposits (facies Fm1).

Interpretation: this association is represented by individual coarse grain-dominated sandstone channelled bodies with erosional basal contacts (facies St, Sp, and Sr) surrounded by mudstone to siltstone floodplain deposits (facies Fm1, Fm2, and Fs). The yellowish to purple mottling observed in the reddish mudstones of the facies Fm1 reflect oxidation and, locally, pedogenic processes, suggesting a temporarily moist ground that was occasionally colonised by plants (Spaletti and Piñol, 2005; Chamizo-Borreguero et al., 2016). Conversely, the deposits facies Fm2, dominated by green or greyish mudstones, indicate reducing conditions (Driese et al., 1995) that allowed the preservation of part of the organic matter of the floodplain. The main transport direction has been measured in the channelled coarse-grained sandstone bodies and indicates that the migration of the bedforms was towards the S and SE, and to a lesser extent toward the SW. Likewise, the absence of any tidal sedimentary structure along with the lack of marine or coastal ichnofacies suggests that the setting where the Facies Association II deposited was located landwards from the tidal limit. This assumption conforms with data obtained from a pollen sample (RE-1) collected in this facies association at the Reíllo outcrop (Bueno-Cebollada et al., 2021), which is also described in the chapter on palynology of this Ph.D. thesis (see Appendix II). The sample is dominated by pollen attributed to the genus *Classopollis* (Appendix II), whose producer might have been a xerophytic plant, and therefore reflects arid conditions in a continental environment (Abbink, 1998; Peyrot et al., 2019). Similarly, the occurrence of araucariacean pollen grains (*Araucariacites australis*) and lack of marine palynomorphs in this sample (Appendix II) might indicate that the depositional environment was continental yet located relatively close to the palaeocoast (Bueno-Cebollada et al., 2021).

A low sinuosity style of the alluvial channels of this facies association can be ascertained by the style of the sedimentary structures observed and by the lack of diagnostic sedimentary structures such as inclined heterolithic strata (Ihs), which is an indicator of lateral accretion of point bars in meandering rivers (i.e., Thomas et al., 1987; Dalrymple and Choi, 2007).

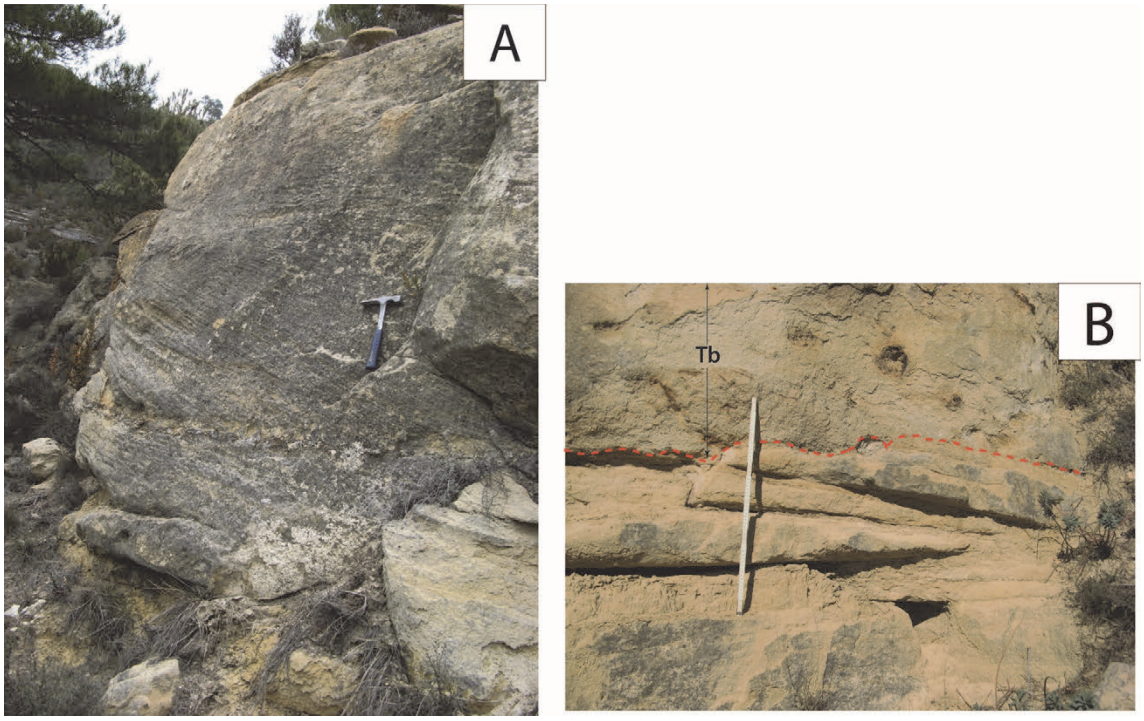

Fig. 8.3. (A) View of the tangential low-angle planar bedding of facies Tb in the Uña outcrop interpreted as tidal bore deposits. (B) Detail of the erosional surface (dashed red line) at the base of the tidal bore accumulation in the Uña outcrop. The erosional surface overlies tidal flat deposits (FA V) where two palynological samples (UCR-5 and UCR-6, respectively) were collected (Bueno-Cebollada et al., 2021).

Palaeosol development has been observed in this facies association, mainly in the Buenache de la Sierra outcrop (see Chapter about palaeosols in this Ph.D. thesis), but also in the Campillos-Paravientos, Uña, Valdecabras, and Las Majadas outcrops, and it reflects the colonisation of the floodplain areas by plants. In this regard, the occurrence of vegetal growth might, in turn, reflect more humid conditions than those of the facies association I. The interpretation of this facies association is that of a distal sector of the braided system where the tidal limit has not been reached yet and gravelly deposits typical of more proximal are almost absent and floodplain mudstones and siltstones (colonised by adapted plants) represent a significant component of the association.

The facies Tb, associated with this FA, is found in the Uña outcrop where it infills two deep incisions (Fig. 8.3) that have been interpreted as palaeovalleys. The accumulation of these low-angle planar-bedded strata with palaeocurrents advancing landwards (NW) and abundant reactivation surfaces is interpreted as successive tidal bore events that filled the incision of palaeovalley over periods of hundreds to thousands of years. This facies has originally been identified and studied in detail in the Uña outcrop by Chamizo-Borreguero et al. (2016). These authors reported the presence of dinoflagellate cysts in the tidal bore sandstones and ascribed the occurrence of tidal bore events in the Cuenca Basin to the amplification of the tides in a funnel-shape estuary due to tidal resonance during periods of diminished alluvial discharge.

8.3. Facies association III: aeolian dunes. (Sae1 and Sae2)

Description: This facies association consists of small-scale cross-bedded sets of aeolian cross strata which are the combination of two facies (Sae1 and Sae2) (Fig. 8.4). Sets generally range from 0.5 to 1.5 m in thickness approximately and can extend laterally for more than 5 meters, depending on the outcrop conditions. Foresets of cross-strata within the sets usually dip at high angles of 20° to 25°, and commonly lose steepness down dip towards their toe sets, displaying moderate to low angles (10° to 5°).

The facies Sae1 comprises three different types of aeolian surfaces that have been identified in the outcrop (Fig. 8.4A, B). These surfaces show a hierarchy of aeolian processes (Bueno-Cebollada and Meléndez, 2018) in the Buenache de la Sierra outcrop: first-order surfaces (IS) (Fig. 8.4B) can be laterally traced across the outcrop. They are represented by flat and sharp surfaces that literally cross the outcrop and cut any other higher-order surfaces. Second-order surfaces (S) are sub-parallel surfaces, usually describing low angle downwind dipping beddings and cut dune foresets and minor third-order surfaces (R) (Fig. 8.4B, D, E). Third-order surfaces (R) are surfaces bounded by either second or first order surfaces, which are concordant, but slightly steeper, with the cross strata of the dunes foreset (Fig. 8.4B).

Additionally, a granulometric analysis of the sandstones of the facies Sae1 and Sae2 was carried out as part of this Ph.D. thesis in the Buenache de la Sierra outcrop (Bueno-Cebollada and Meléndez, 2018). It shows that 90.6 % (mean cumulative percentage in weight) of the clasts from five samples collected is between $\phi = 1$ and $\phi = 4$, which corresponds to medium- to very fine-grained sandstones (Fig. 8.5). The mean cumulative percentage in weight of the clasts with $\phi > 4$ is 3.61 %, while that of the clasts with $\phi < 1$ is 5.79 % (Fig. 8.5).

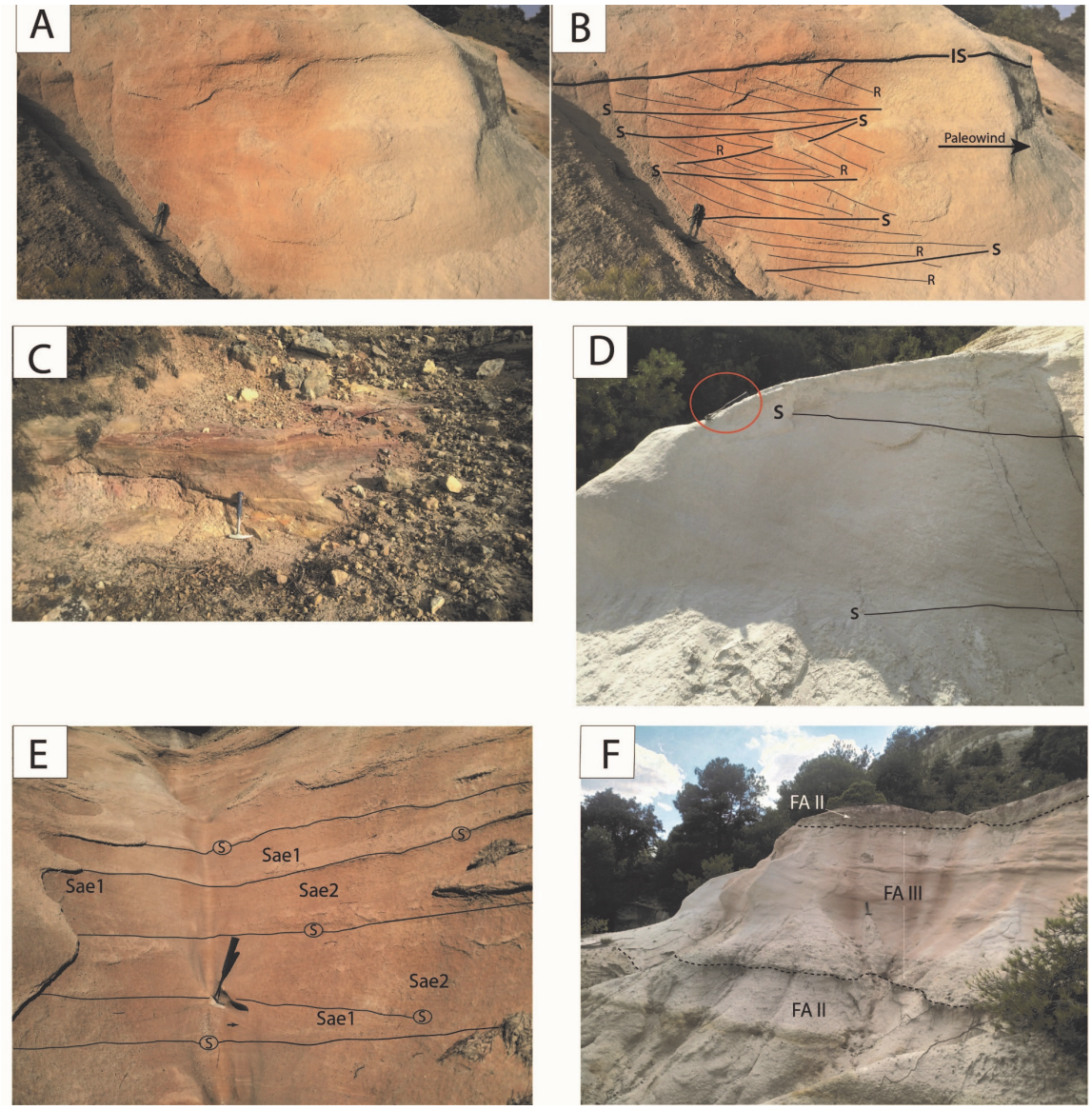

Fig. 8.4. (A) Photograph of complex aeolian dunes (FA III) in the Buenache de la Sierra outcrop. (B) Line drawing of A. The Hierarchy of bounding surfaces is highlighted (see text for explanation). Main palaeowind direction is towards the right (NNE). Figures (A) and (B) are published images from Bueno-Cebollada and Meléndez (2018). (C) Aeolian pod in the Uña outcrop. The local occurrence of aeolian dune facies in the Uña outcrop has been studied by Chamizo-Borreguero et al. (2016). (D) Aeolian dune foresets (facies Sae1) bounded by superimposition surfaces (s) in the Buenache de la Sierra outcrop. The red ellipsoid indicates the position of the hammer used as a scale (35 cm in length). (E) Detail of an aeolian dune body (FA III) including the facies Sae1 and Sae2 (Table II). The solid lines represent superimposition surfaces (s). (F) Interaction between aeolian (FA III) and distal alluvial deposits (FA II). The aeolian deposits overlain alluvial channel deposits and are overlain by mottled overbank deposits. Hammer for scale is 30 cm long.

The aeolian facies association has been identified in the middle part of the composite logged section in the Buenache de la Sierra and in the Uña outcrop (Chamizo-Borreguero et al., 2016; Bueno-Cebollada and Meléndez, 2018). The aeolian deposits are encased within the distal alluvial succession (braidplain deposits). They overlay alluvial deposits with flat non-erosional surfaces, depending on the roughness of the palaeotopography of the underlying deposits.

Interpretation: Based on the data obtained from the granulometric study (Bueno-Cebollada and Meléndez, 2018), 90.6 % of weight of the sampled sandstones consists of grains ranging between medium to very fine grain size. This fact conforms with previous studies of aeolian dune sands (Folk, 1971; Lancaster, 1986), but especially with Sharp (1966) since this author identified medium-grained sandstones in aeolian dunes in the Mojave Desert, California. The granulometric study allows deducing that the clasts in most of the samples were susceptible to transport within the field of saltation, and therefore wind transport would have been possible (Rodríguez-López et al., 2006; Bueno-Cebollada and Meléndez, 2018). Conversely, those grains with $\phi > 4$ represent the suspension load fraction (mud- and silt-sized particles) which is also transported by the wind in the facies Sae1 and Sae2. Conversely, the grains with $\phi < 1$ (5.79 %) represent the percentage of clasts transported by traction those clasts with $\phi < 1$ (5.79 %), which could not be transported by the wind and accumulate as aeolian dunes (Rodríguez-López et al., 2006, Bueno-Cebollada and Meléndez, 2018) (Fig. 8.5). The occurrence of a low percentage of coarse-grained sandstone clasts is interpreted as transported as bedload by the ephemeral alluvial systems (facies association I and II) which tend to interact with the local aeolian dunes in the study area (Bueno-Cebollada and Meléndez, 2018).

The first-order surfaces identified in facies Sae1 are interpreted as interdune surfaces (IS). They represent the migration of larger aeolian forms over the stoss slope of former aeolian dunes (Fig. 8.4). In the Buenache de la Sierra outcrop (Bueno-Cebollada and Meléndez, 2018), the lack of mudstone-siltstone in the interdune deposits is represented by an IS (Fig. 8.4A, B) and indicates a dry interdune (Mountney, 2004). Second-order surfaces are interpreted as superimposition surfaces (S) and have also been described in the Buenache de la Sierra outcrop (Bueno-Cebollada and Meléndez, 2018) (Fig. 8.4A, B, D, E). These surfaces are developed due to the migration of dunes over another larger dune body (Mountney, 2004). A regular recurrence in the occurrence of superimposition surfaces may indicate that bedform migration was taking place under equilibrium conditions (Mountney and Thompson, 2002). Third-order surfaces have been identified and interpreted as reactivation surfaces (R) (Fig. 8.4A). Reactivation surfaces are bounded by either second or first order surfaces, which are concordant (or slightly steeper) with the cross strata of the dunes foresets. They represent the erosion of the lee face of the dune owing to a change in the direction of the wind, and when sedimentation resumes the reactivation surface is generated (Rodríguez-López et al., 2008, Mountney and Thompson, 2002). This fact may be related to the occurrence of seasonally induced secondary winds leading to deflation of the lee slopes of the aeolian dunes, prior to the time when the main wind resumes (Mountney and Thompson, 2002 and references therein).

The aeolian bodies resemble the complex dune facies association described in the deposits of the Utrillas Gr in the Maestrazgo Basin (in the Eastern part of the IBRS) (Rodríguez-López et al., 2008), interpreted as deposited in a dry aeolian system. Likewise, this facies association can also be interpreted as compound sets of aeolian dune due to the migration of primary bedforms containing smaller, secondary wind-laid bedforms that migrated at a faster pace than the primary ones. This aeolian dune architecture has been described in the Triassic Helsby Sandstone of the Cheshire Basin, England (Mountney and Thompson, 2002), where it is referred to as "small-scale regularly repeating trough cross-bedding".

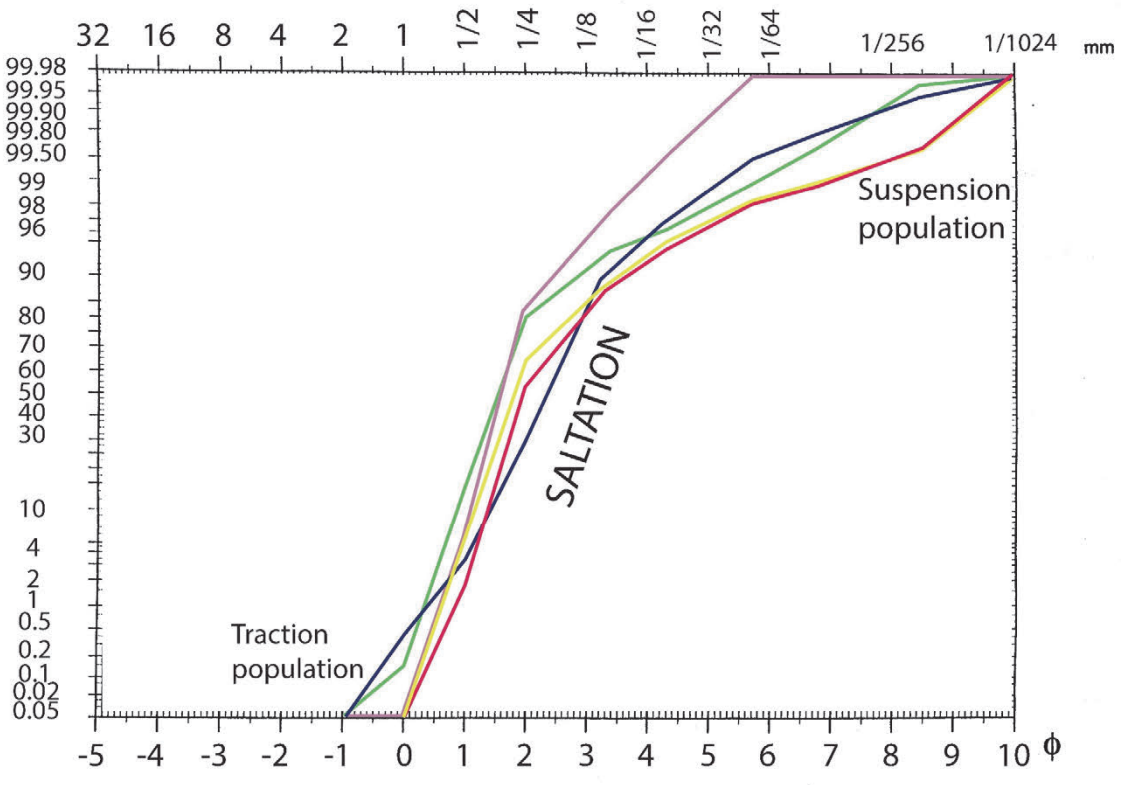

Fig. 8.5. Granulometric curve for the 5 collected samples from the aeolian dune deposits (FA III) (Appendix V). Traction, saltation and suspension populations are indicated. Original figure from Bueno-Cebollada and Meléndez (2018).

The sandstone bodies of this facies association are interpreted as complex aeolian dunes developed as a minor feature associated with the ephemeral alluvial deposits of a braidplain, considering the complex geometry of aeolian surfaces observed in the facies Sae1. The interaction of aeolian dune and ephemeral alluvial (braidplain) deposits has been reported in the literature in both modern (i.e., Skeleton Coast of Namibia) (Langford, 1989; Krapf et al., 2003; 2005) and ancient systems (i.e., Langford and Chan, 1989; Mountney and Thompson,

2002; Mountney and Jagger, 2004; Jordan and Mountney, 2010). In this sense, aeolian deposits in arid alluvial settings may fill topographic depressions due to aeolian dunes migrating over previous fluvial bedforms (Mountney and Thompson, 2002), giving rise to aeolian pods. The facies association III presents this geometry in the aeolian dune bodies identified in the Uña and Buencahe de la Sierra outcrops (Chamizo-Borreguero et al., 2016; Bueno-Cebollada and Meléndez, 2018).

Additionally, the occurrence of alluvial floodplain deposits (facies Fm1; Fig. 8.4F) overlying the aeolian dune deposits in the Buenache de la Sierra outcrop reflects the flooding of the dune. The lack of incision at the base of the overlying floodplain deposits is interpreted as the passive rise of the water table up to and above the sediment surface, even allowing for local plant colonisation.

8.4. Facies association IV: inner estuarine. (facies Sb1, Sb2, St_2, Sp_2, Sr, Ftb, Fm2, Smf, Tb and Ifc)

Description: This facies association is observed in the three sectors of the study area and consists of facies Sb1, Sb2, St_2, Sp_2, Sr, Ftb, Fm2, Smf, and Ifc (Table II) (Fig. 8.6). The sandstone facies St_2, Sp_2 and Sr represent unimodal transport directions (mainly towards the S and SE). The facies St_2 and Sp_2 are similar to the facies St and Sp but for the presence of rhythmical alternations in the grain size of the foresets. Likewise, this facies association includes facies Sb1 in the La Huerguina and Campillos-Paravientos outcrops, indicating the occurrence of sets of planar cross-bedding migrating in opposite directions, mainly NW/NNW and SE/SSE, respectively. The facies Sb2 is typically arranged into bodies with an erosional base, that display large-scale (50 to 80 cm) trough cross-bedded sets with the lee face of the foreset reworked by asymmetrical ripples migrating in an opposite direction to the main palaeocurrent of the trough cross-bedding (Fig. 8.6H).

The sandstone bodies included in this facies association (facies Sb1, Sb2, St_2, Sp_2, and Sr), may show lateral accretion sigmoidal morphologies (i.e, in the Tejadillos and Las Majadas outcrops) (Fig. 8.6A, B, E), interbedded with facies Fm2 and Ftb (Fig. 8.6C, E, F). The mudstone-dominated heterolithic facies Ftb is characterised by lamination mudstone-siltstone interbedded with sandstones that show wavy to lenticular heterolithic beddings and double mud drapes (Fig. 8.6C). The facies Ftb may also contain charcoalified wood fragments in the Tejadillos outcrop (Fig. 8.6D). The muddy facies Fm2 is also well-represented in this facies association and consist of massive beds that may present weakly developed root traces.

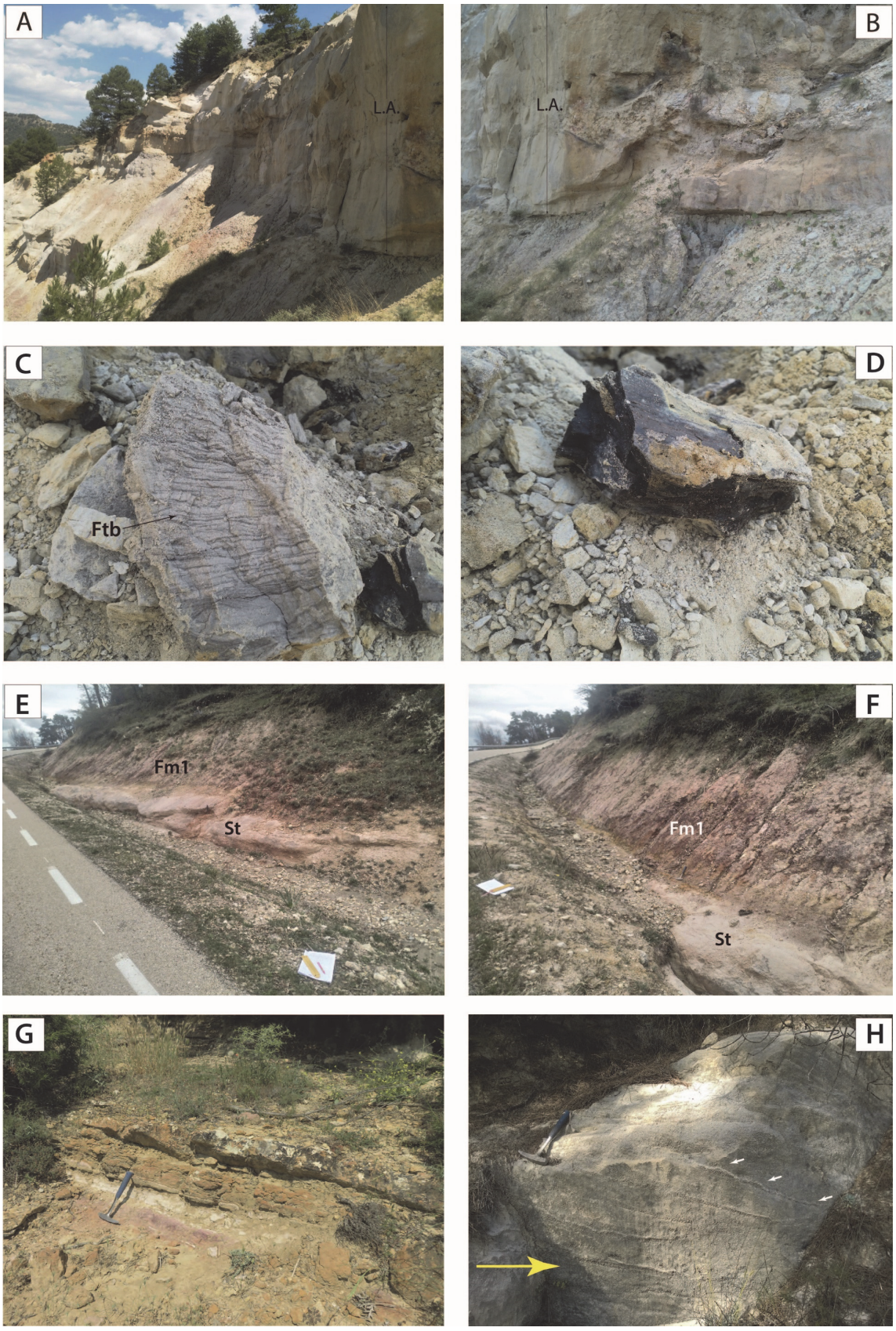

Fig. 8.6. (A) FA IV in the Tejadillos outcrop. It is dominated by the facies St, Sp and their subfacies, St2 and Sp2, that indicate a tidally-modulated fluvial to upper estuarine environment. The architectural style of the amalgamated channels indicates the occurrence of lateral accretion (L.A.) bodies, interpreted as tidal point bars, that characterise a high-sinuosity alluvio-estuarine environment. (B) Detail of a tidal point bar pinching out in upper estuarine mudstone-dominated heterolithic deposits (facies Ftb) in the Tejadillos outcrop. (C) Close-up of the facies Ftb in the Tejadillos outcrop showing mudstone and siltstone alternations

that form bundles indicating tidal influence. (D) Charcoalified wood fragments found within deposits attributed to the facies Ftb in the Tejadillos outcrop. (E) Lateral accretion amalgamated sandstone bodies observed in the uppermost levels of the Las Majadas section. The bodies pinch out laterally into floodplain mudstones with red mottling (facies Fm1). (F) Detail of the floodplain deposits (facies Fm1) observed in (E). The intense red mottling might have been related to the colonisation of a supratidal floodplain by plants. (G) Tidal creek associated with a tidal mudflat deposited in a supratidal environment in the Pajaroncillo outcrop (figure 9 from Bueno-Cebollada et al., 2022). (H) Detail of the facies Sb2 (Table II), included within the FA IV. The large yellow arrow indicates the main palaeocurrent direction that defines the foreset migration. The smaller white arrows indicate a subordinate palaeocurrent direction reworking the foresets due to tidal action. Hammer for scale in the pictures is approximately 35 cm long.

The facies Smf consists of very well-sorted fine-grained sandstones that crop out discontinuously, filling land depressions and is characterised by the occurrence of branching oxidised structures attributed to *in situ* plant growth and/or root traces (see Fig. 8 in Bueno-Cebollada et al. [2022]). The facies Smf has only been observed in Reíllo, and it is associated with ferruginous surfaces (facies Ifc; Table II) (Bueno-Cebollada et al., 2022).

Interpretation: The presence of the sandstone facies Sb1, Sb2, St2, Sp2, and Sr along with muddy and heterolithic facies Ftb and Fm2 (Table II) indicates the occurrence of sandy channelled laterally related to low-energy deposits. The occurrence of trough cross-bedded sets whose foresets are punctuated by rippled sand (facies Sb2) reflects the reworking of the lee faces in a subordinate opposite flow direction and may indicate fluvial currents influenced by the ebb and flood tidal currents as well as variations in the alluvial discharge (Shanley et al., 1992; Dalrymple, 2010b). Likewise, the occurrence of paired mudstone and siltstone drapes (facies Ftb), root traces, and charcoalified wood in association with the lateral accretion bodies (Fig. 8.6A-D), indicate the occurrence of a muddy plain within the tidal limit, typical of the upper intertidal zone (Shanley et al., 1992; Daidu, 2012). Likewise, the occurrence of massive grey to greenish and red mudstones (facies Fm1 and Fm2; Table II) together with high sinuosity channels and locally with weak root trace development seem to indicate that the depositional setting of this facies association might have been transitional between a supratidal salt marsh to the upper intertidal zone of a tidal flat or estuarine environment (Dalrymple, 2010b). The supratidal and upper parts of an intertidal flat are typically covered with vegetation and characterised by the occurrence of fine-grained deposits (mainly muddy and silty deposits with organic matter). The canopy may vary from mangrove communities in tropical areas to salt marsh vegetation in more temperate zones. Such supratidal to intertidal flats colonised by vegetation are usually cut by tidal channels (tidal point bars; Fig. 8.6A, B) and creeks characterised by lateral accretion bodies (Daidu, 2012). An example of the development of lateral accretion high-sinuosity (supra-) tidal creeks has been observed in the uppermost levels of the sedimentary succession logged in the Las Majadas outcrops (Fig. 8.6E).

In this sense, an increase in the sinuosity of the alluvial system represented by the FA I and II (Table I) seawards from the tidal limit is observed in this facies association and conforms with the previous environmental models for tide-dominated estuaries (i.e., Dalrymple, 2010b; Shiers et al., 2014). Therefore, this facies association is interpreted as a fluvial-estuarine or coastal plain environment influenced by tidal action, comprising the oscillations between distal fluvial setting influenced by tides and the upper-middle portion of an estuary or the sandy channels of the upper part of a coastal plain. Additionally, tidal bore deposits (facies Tb) can be related to this facies association since inner estuarine and distal alluvial are part of a continuum in the fluvioestuarine transition where tidal bore surges took place.

Finally, the occurrence of the facies Smf (Table II) in this facies association (Reíllo outcrop) represents air-borne sand accumulated in slightly sunken areas that were partially colonised by plants, acting as a baffle trapping the sand particles, producing minor coastal aeolian accumulations lacking the typical bedding and, therefore, they cannot be interpreted as aeolian dunes (see Fig. 8 in Bueno-Cebollada et al. [2022]). This interpretation also explains the presence of oxidised plant structures and moulds included in this facies, typical of coastal or estuarine supratidal environments (Kuriyama et al., 2005).

8.5. Facies association V: tidal flat. (facies Sht, Sb1, Sh, St, Sp, Sr, and Ifc)

Description: This facies association comprises the facies Sht, Sb1, Sh, St, Sp, Sr, and Ifc (Figs. 8.7, 8.8). Additionally, grey to dark mudstone deposits (Facies Fm2) can be part of this association, indicating the existence of low energy sub-environments, to a lesser extent. The facies Sh comprises siliciclastic to slightly calcareous coarse-grained sandstones showing horizontal to very low-angle beddings laterally extensive across the outcrop. The foresets defining the horizontal to low-angle beddings present crenulated irregular surfaces, which may contain mud drapes (Fig. 8.8C, D), and smaller symmetrical and asymmetrical ripples (facies Sr). Locally, the asymmetrical ripples of the facies Sr may amalgamate, and form superimposed ripple sets, giving rise to climbing ripples (i.e., Uña outcrop; see figure 3 in Chamizo-Borreguero et al. [2016]). Geometrically, the deposits of the facies Sh, Sht and Sr show a tabular shape with a flat base which defines a sharp contact (Fig. 8.8C, D).

The facies Sb1 is also part of this facies association and consists of very coarse- to medium-grained siliciclastic to slightly calcareous sandstones with sets of planar to trough cross-bedding (showing bipolarity in the palaeocurrents), which typically migrate towards the SSE/SE and N/NE (Fig. 8.8E-H). This facies is arranged in lenticular bodies extending laterally for up to 5 m and

showing erosional bases. In Reíllo outcrop, it may also present vegetal remains (featureless moulds of tree bark), which are usually ferruginous, with different states of preservation (Fig. 8.8G, H). Besides, to a lesser extent, this facies association may include facies St, Sp, Sr, and Ifc.

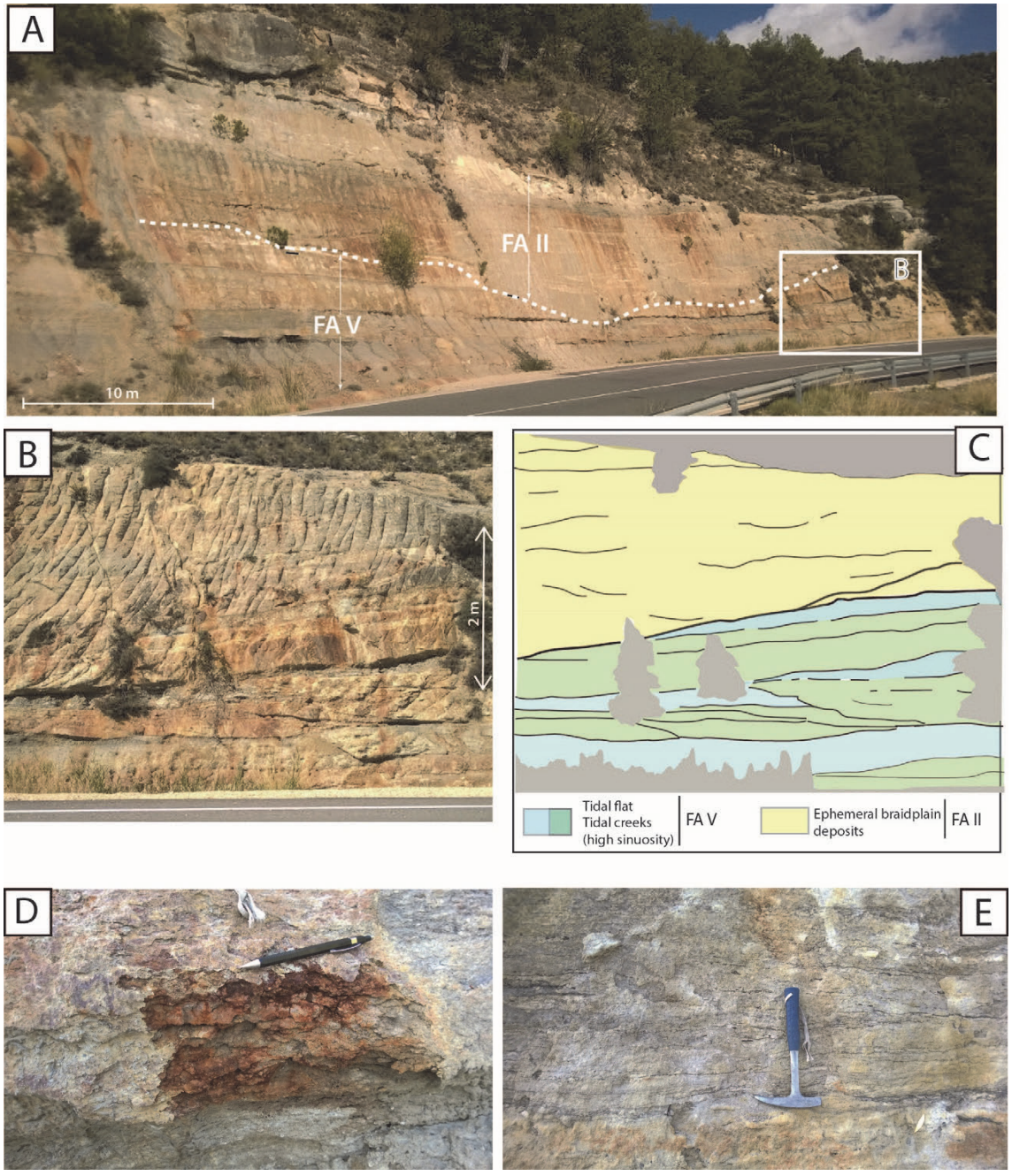

Fig. 8.7. (A) Outlook of the La Toba outcrop where tidal flat deposits (FA V) are sharply overlain by distal alluvial braided deposits (FA II) with a conspicuous erosional contact. (B) Detail of lateral accretion deposits interpreted as tidal channels-creeks interspersed among the tidal flat deposits. A conspicuous erosional surface erodes the former deposits, preceding the deposit of amalgamated alluvial deposits. (C) Line drawing and interpretation of (B). (D) Close-up of the lateral accretion bodies shown in (B) and (C) where the coarse-grained sandstones are cemented with iron oxides. (E) Draped silty sandstone in the La Toba outcrop interpreted as deposited in an intertidal flat setting. Hammer for scale is 35 cm.

The bioturbation of this facies, dominated by vertical tubes, is low to moderate; however, the type of trace fossil cannot be accurately ascertained due to the poor preservation of the sedimentary structures.

Interpretation: The occurrence of heterolithic deposits (facies Sht; Fig. 8.8A, B) with draped mudstones, reactivation surfaces and wavy and flaser beddings, and the presence of cross-bedded sets displaying opposite transport directions are indicative of tidal origin (Shanley et al., 1992; Dalrymple, 2010b). Heterolithic bedding or laminations are characteristic of intertidal environments, which may include flaser, wavy and lenticular beddings (Reineck and Singh, 1980; Daidu et al., 2013). In the Reíllo outcrop, the mud-draped crenulated surfaces (Fig. 8.8C, D) observed in the facies Sh reflect the slack-water periods when the tides were either at their highest or lowest level, allowing the settling of mud-sized particles by suspension (i.e., De Boer, 1998; Bueno-Cebollada et al., 2022). These structures represent small dunes or megaripples capped by mud drapes where ripple structures may be superimposed in the middle to lower zone of an intertidal setting (Daidu, 2012; Daidu et al., 2013). The ubiquitous presence of these mud drapes, along with the discrete occurrence of wave structures (symmetrical ripples), has enabled the interpretation of these deposits as the result of tidal action with the minor influence of wave processes (Bueno-Cebollada et al., 2022). Likewise, the co-occurrence of the channeled facies Sb1 (bimodal flow) and facies Sc and Sr (unimodal flow) indicates the existence of tidal channels cutting and crossing the tidal flat and draining from the coeval braidplain deposits, located to the N and NW of the studied outcrops, into the coast. (Fig. 8.8E-H).

The tidal channels identified in this facies association usually present the migration of their bedforms towards the SE (seawards) at their base, and towards the N/NE (landwards) later during their infill, which reflects the asymmetrical character of the tides (Fig. 8.8E, F) (De Boer, 1998; Daidu, 2012). The facies Ifc is interpreted as ferruginous crusts (Bueno-Cebollada et al., 2022) (Fig. 8.8H) developed owing to microbial activity that encrusted the iron minerals, generating microbial mats at the time of deposition in coastal siliciclastic environments (Retallack, 2012; Williams et al., 2012; Garcia-Hidalgo et al., 2018).

The local presence of mudstone-dominated deposits, such as those of facies Fm2, indicates areas where the settling of the sediment is dominated by suspension, and it is interpreted as mudflat deposits typical of the intertidal zone (Dalrymple, 2010b).

Therefore, this facies association is interpreted as an intertidal (to subtidal) system that may present associated tidal channels in its lower portion dissecting the deposits of the tidal flat. However, it is difficult to ascertain if part of the sediments found in this facies association were

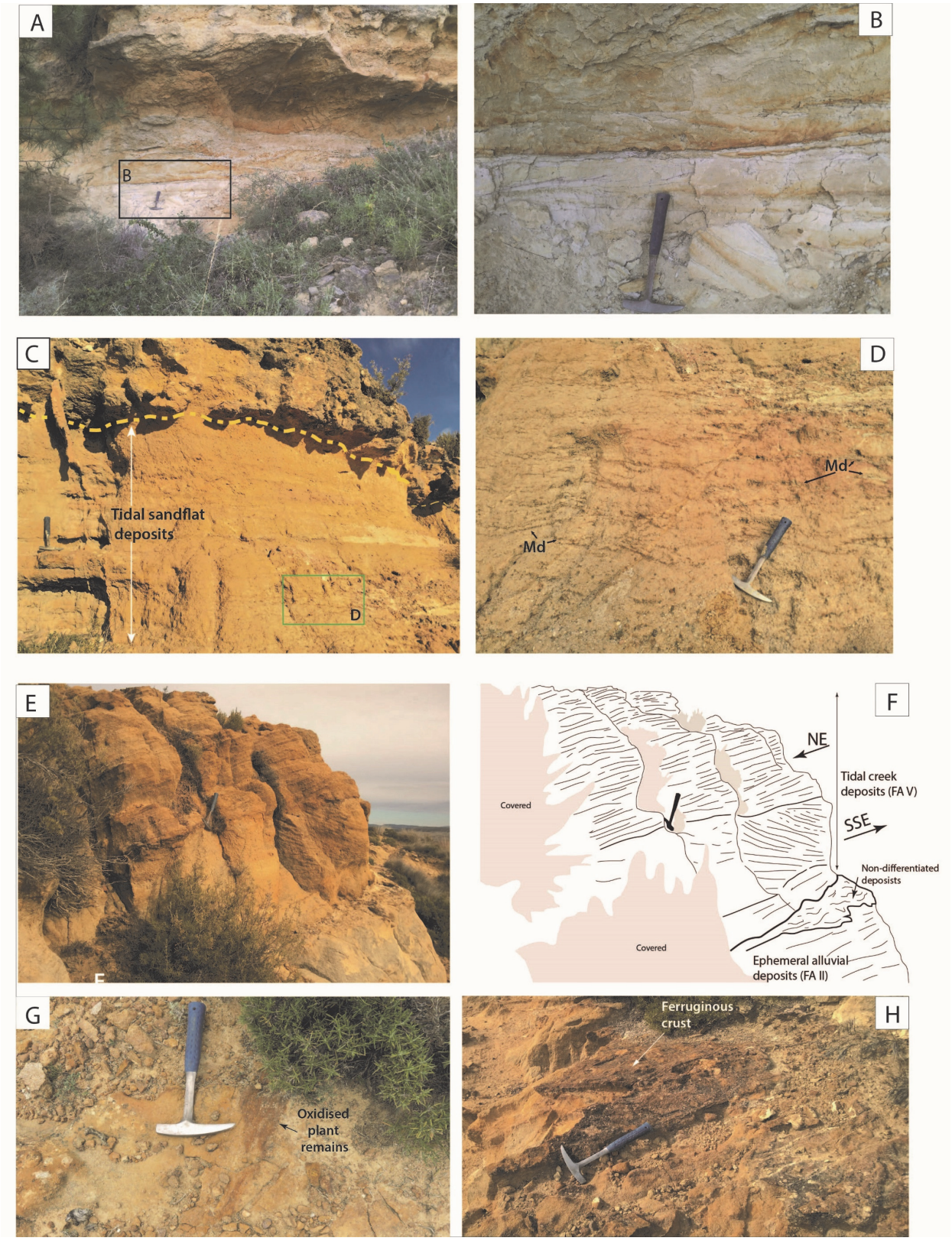

Fig. 8.8. (A) General view of the tidal flat deposits (FA V) observed in the Tejadillos outcrop. (B) Close-up of (A) where heterolithic sandstone-dominated deposits of the facies Sht can be observed. (C) Appearance of the tidal sand flat deposits (FA V) in the Reíllo outcrop. The dashed yellow line represents a subaerial exposure surface. The hollow green box highlights the ubiquitous presence of mud drapes in the outcrop. (D) Close-up and detailed view of the mud drapes (Md) observed in C. (E) Detail of a tidal channel overlying and eroding ephemeral alluvial deposits. Current bipolarity is also observed. (F) Line drawing interpretation of (E). The main measured palaeocurrent directions are indicated in the figure. (G) Oxidised tree bark remains in the tidal channels. (H) Ferruginous crust covering the tidal channel that is shown in (E). Hammer for scale is 35 cm.

deposited in the upper subtidal zone of the tidal flat. Commonly, the inter- to subtidal transition can be confusing or difficult to identify since they usually are sand-prone deposits, and the indicators are either rare or rather inconclusive (Dalrymple, 2010b).

8.6. Facies association VI: outer estuarine (facies Scax, Scah, Fc and Fm2)

Description: This facies association consist of a calcareous sandstone facies with scarce bivalve shell fragments (Scax), a heterolithic (Scah) facies with interbedded mudstone and sandstone laminations, and (calcareous) mudstone (Fc and Fm2) facies (Fig. 8.9) (Table II). The calcareous sandstone facies (Scah) is arranged into 0.5 to 1 m-thick sets of planar to trough cross-bedding, which normally show unimodal bedform migration toward the NE/N. However, they can also be bimodal, showing palaeocurrents toward the N/NE and S/SW. The facies Scax may contain scarce bivalve shell fragments and shows low to moderate bioturbation dominated by scattered vertical burrows. Regarding morphology, the facies Scax is arranged into 1 to 1.5 m-thick amalgamated bodies which may extend laterally for more than 200 m, parallel to the current direction.

The heterolithic facies (Scah) comprises fine- to medium-grained calcareous sandstones with interspersed calcareous mudstone laminae that display wavy, lenticular, flaser heterolithic laminations and mud drapes (Fig. 8.9B, D) (Table II). Although less abundant, this facies presents symmetrical (wave) ripples that are 2 cm in length on average (Fig. 8.9C). This facies is moderate to intensely bioturbated, depending on the level, and the main trace fossils observed are U-shaped and vertical burrows (Fig. 8.9F, G). The facies Scah shows a coarsening upward pattern, with more sand-prone terms increasing upwards and shifting into the facies Scax. Similarly, it shows lateral continuity with the facies Scax, and usually pinches out in the calcareous mudstones of the facies Fc (Bueno-Cebollada et al., 2022).

The facies Fc consists of faintly laminated to massive calcareous mudstones and siltstones that lack pedogenic processes. This facies may also include scattered gypsum crystals. Regarding morphology, it is characterised by forming up to 10 m-thick laterally persistent tabular-shaped bodies that extend across the outcrop for 100s of m.

This facies association is well-represented in the Pajaroncillo outcrop, where a gradual coarsening upwards trend can be observed in the transition from facies Fc into facies Scah and Scax. The top of this facies association in Pajaroncillo is a surface with high carbonate content showing signs of scouring and abrasion (Bueno-Cebollada et al., 2022).

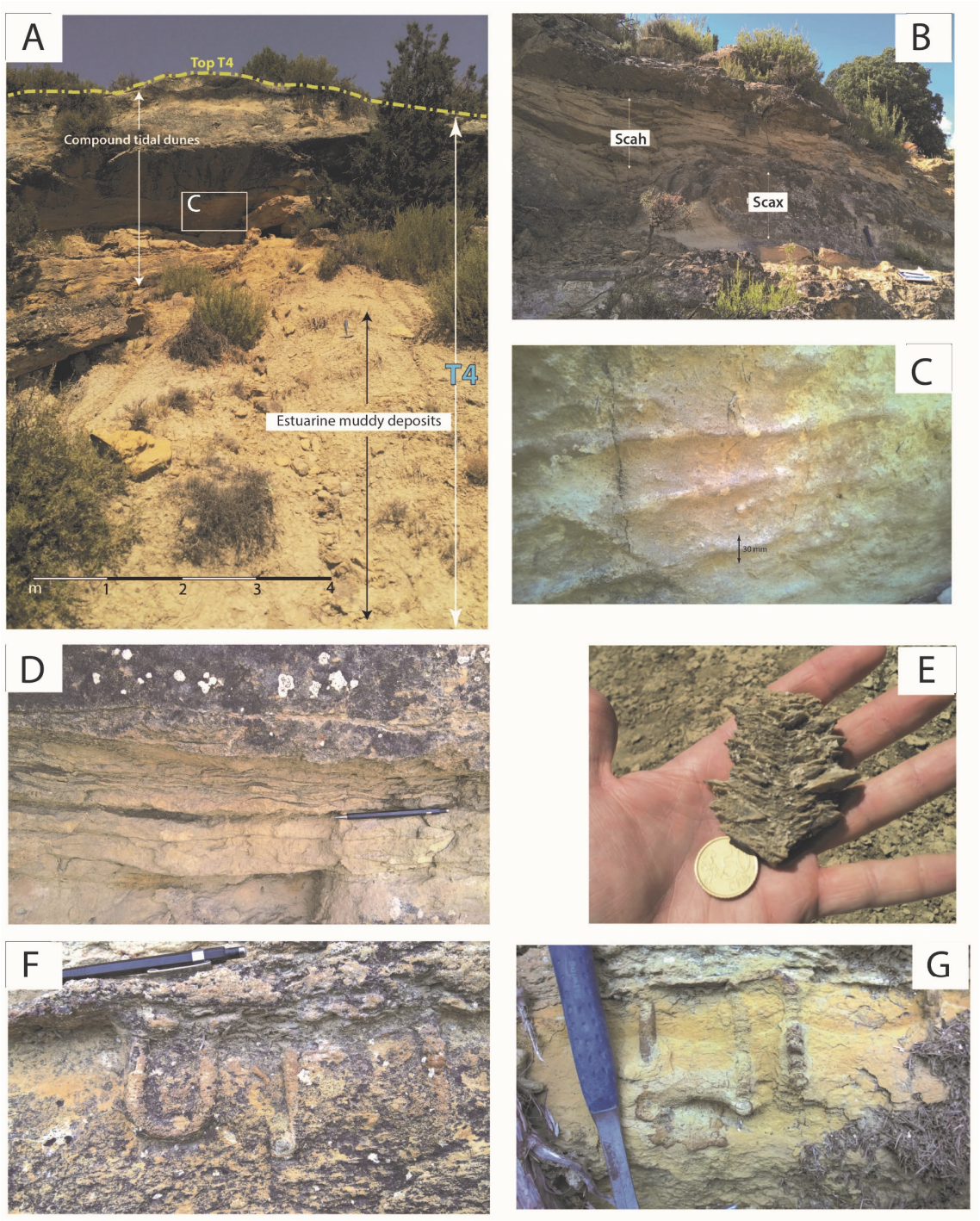

Fig. 8.9. (A) Outer estuarine muddy deposits showing a gradual transition into (inter-) tidal dunes (FA VI) in the Pajaroncillo outcrop. The yellow surface is interpreted as a subaerial exposure surface indicating the top of T4 in the studied succession. See chapter 11 in this manuscript for explanations about the sequence stratigraphic surfaces. (B) Detail of the intertidal deposits. Two types of body geometries are displayed: tabular heterolithic beds (facies Scah) (Table II) and cross-bedded calcareous sandstones (facies Scax) (Table II). (C) Detail of the symmetrical ripple structures interpreted as wave ripples. (D) Close-up of the heterolithic intertidal deposits (facies Scah) (Table II), where sand and calcareous mud alternations can be seen at different scales. (E) Gypsum crystal collected in the estuarine mudstones in Reíllo. (F and G) Detail of the trace fossil *Arenicolites*, as well as other vertical tube trace fossils, observed in intertidal deposits in Pajaroncillo. Hammer for scale is 35 cm.

Interpretation: The facies Scax represents the migration of 2-D and 3-D single tidal dunes bodies, which may give rise to stacked compound tidal dunes by overriding (Olariu et al., 2012). The facies Scax constitutes the main body and crest of the tidal dunes where the speed of the tidal currents is faster than in the troughs (Bueno-Cebollada et al., 2022). The facies Scah represents the bottomsets of tidal dunes (Dalrymple, 2010b; Olariu et al., 2012). The deposits attributed to the facies Scah fill the troughs between adjacent tidal dunes and eventually pinch out into coastal mudstones, such as those deposited in low-energy estuarine or lagoon settings (facies Fc). The heterolithic laminations (i.e., wavy and flaser beddings) (Fig. 8.9D) and mud drapes identified in the facies Scah reflect the diminishment in the energy of the tidal current and the current reversals taking place in the trough of the dunes, while the local occurrence of symmetrical ripples indicates the existence wave processes reworking the tidal dunes at times. The sedimentation of the calcareous mudstones of the facies Fc suggests the existence of a low-energy, relatively sheltered, coastal or estuarine environment across which tidal dunes of the facies Scax and Scah migrate. Therefore, facies Fc constitutes the low-energy fringes of the tidal dunes, where the bottomsets of the dunes pinch out into estuarine mudstones and marls (Bueno-Cebollada et al., 2022).

Bioturbation mainly occurs in the facies Scah and is dominated by U-shaped burrows interpreted as *Arenicolites* (Fig. 8.9F) (Bromley and Asgaard, 1991), a trace fossil commonly found in the *Skolithos Ichnofacies* (Hasiotis, 2004; MacEachern et al., 2010) and an indicator of coastal (inter- to sub-) tidal sedimentary environments (Gingras and MacEachern, 2012). The characteristic features of the *Skolithos Ichnofacies* include the occurrence of vertical and U-shaped burrows, low diversity of trace fossils, and the predominance of individual forms (MacEachern et al., 2010). The Skolithos Icnofacies usually develops in inter- to subtidal shifting or unstable substrates (i.e., migrating tidal dunes) in which erosion and abrupt changes in the depositional rate are common processes (MacEachern et al., 2010).

The transition from the mudstones of the facies Fc and Fm2 into the heterolithic deposits of the facies Scah, and, in turn, the transition of the latter facies into the calcareous sandstones of the facies Scax reflect a coarsening upwards trend that is interpreted as the migration of compound tidal dunes (stacked single dunes) bodies developed in a coastal tidal environment (Bueno-Cebollada et al., 2022). The deposits of this facies association are characterised by a forward accretional architecture and show a facies distribution similar to the one reported by Olariu et al. (2012) from the lower Eocene of NE Spain, where the deposits are interpreted as tidal dune complexes confined within a tidal seaway or a tectonically generated embayment.

8.7. Facies association VII: high-gradient coastal deposit. (Facies Shg and Ssc)

Description: This facies association consists of the facies Shg and Ssc. The facies Shg (Table II) (Figs. 8.10, 8.11) consists of coarse-grained arkose sandstones arranged into large (up to 3 m-thick) inclined tangential sets of planar bedding, dipping towards the SE/S. The foresets are long (over 8 m in length along the inclined surface: Fig. 8.10B) and inclined beds, characterised by high gradients, dipping about 14° in a SE/E direction. The average grain size is coarse to very coarse; however, this facies may locally contain even larger grain size particles (gravel size). The geometry of the facies Shg, which can only be observed at the Reíllo outcrop (Fig. 8.10A), is laterally extensive tabular to wedge-shaped, and it can be traced for more than 200 m throughout the outcrop. The facies Ssc consists of coarse- to very coarse-grained sandstones that locally may even reach gravel-grain sizes. Regarding sedimentary structures, this facies is dominated by small-scale trough cross-bedding (Fig. 8.10C, 8.11A) and asymmetrical ripples, which commonly show transport directions towards NE, N, and SW. Even though much less frequently, other sedimentary structures such as small-scale amalgamated sets of trough cross-bedding were observed in this facies in the Reíllo outcrop describing herringbone-like cross-beddings (Fig. 8.11C). This facies is characterised by an erosional base which may also present mud pebbles and cobbles (with an average size ranging between 30 and 40 mm) (Fig. 8.11A, B).

Interpretation: the facies Shg is interpreted as deposited in a nearshore (foreshore to upper shoreface) setting. The high gradient, inclined beds, which dip seawards (SE/S) with tangential geometries (Fig. 8.10), reflect the seawards accretion of a shoreline in a foreshore setting (Isla et al., 2020). The classic models for foreshore deposits attribute the occurrence of long inclined beds to swash and backwash processes in the swash zone of a beach profile, which typically includes a surf zone where longshore bars develop (i.e., Clifton, 1969; Plint et al., 2010). More recently, Isla et al. (2020) allude to coastal settings developed under steep marine profiles (i.e., reflective beaches; Sherman, 2019) where the surf zone tends to become a very narrow fringe, and longshore bars are less likely to form. These steeper beach profiles consist of high-gradient plane beds arranged into long tangential sets, which extend across the foreshore and the proximal portion of the upper shoreface (Isla et al., 2020). In this sense, there is a direct relationship between grain size and the steepness of the foreshore slope as mentioned in previous research, carried out both in field studies and in experimental tanks (i.e., Andrews and Van der Lingen, 1969; McLean and Kirk, 1969). This relationship directly relates to the permeability of sediment with coarser grain size, usually gravel size as it permits a significant diminishment of the energy of the backwash movement of the waves after breaking on the foreshore.

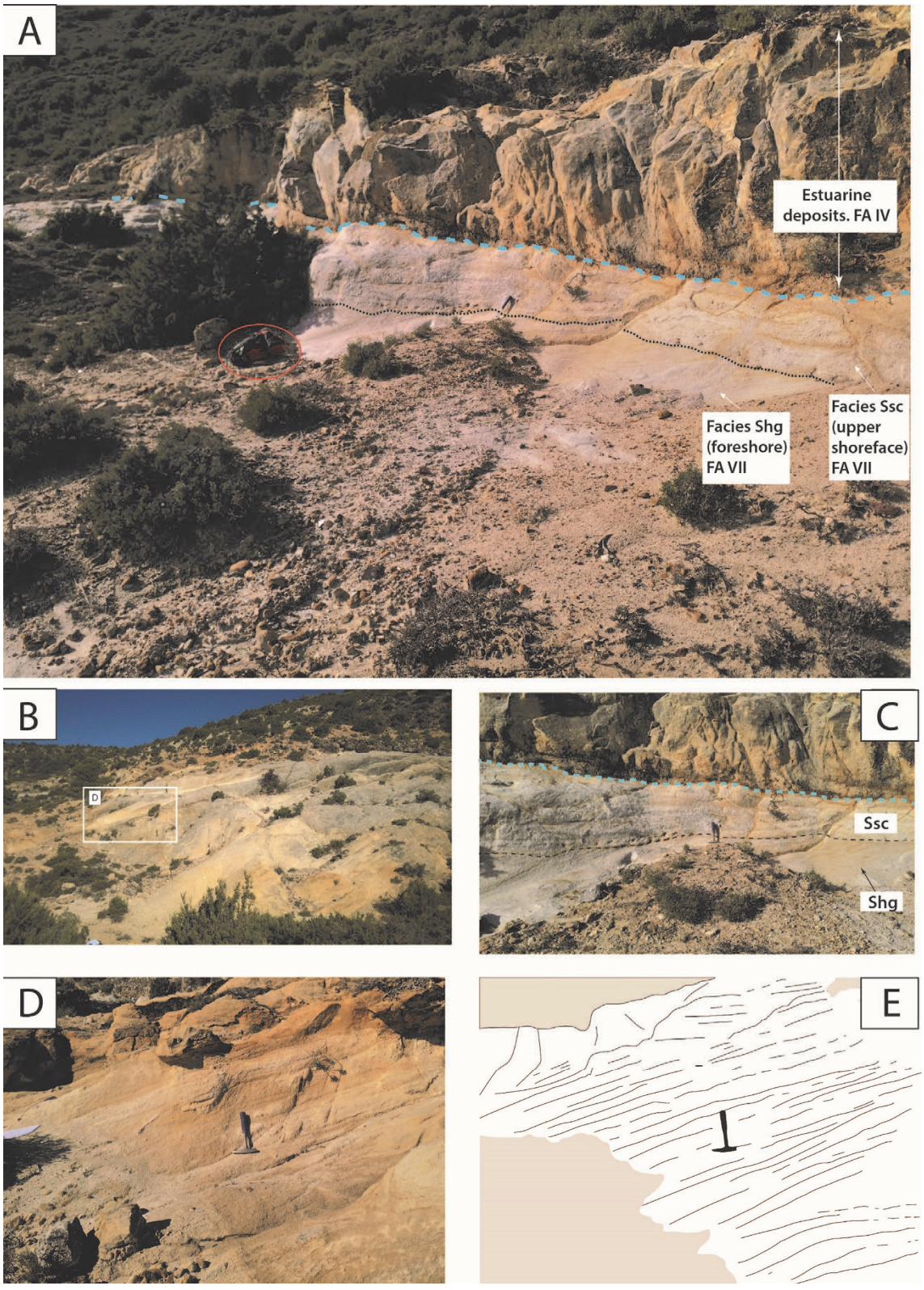

Fig. 8.10. FA VII in the Reíllo outcrop. (A) General view. The foreshore deposits (facies Shg) are overlain by upper shoreface deposits (facies Ssc) with an erosional contact interpreted as a ravinement surface (black dotted line). The dashed blue line mantling upper shoreface deposits is interpreted as a maximum flooding surface (MFS). (B) General overview of the long foresets interpreted as foreshore deposits (facies Shg) in the Reíllo outcrop. Hammer for scale is 35 cm. (C) View of the deposits of FA VII in Reíllo. Hammer for scale is 35 cm. (D) Close-up of (B) where the sedimentary architecture of the foreshore deposits can be observed at length. (E) Line drawing interpretation of (D). See chapter 11 of this manuscript for further explanation of the sequence stratigraphic surfaces.

This fact allows a coarse grain-dominated foreshore to establish a much steeper slope than those foreshore settings dominated by finer-grain size material by creating equilibrium between wave processes and gravity on the coast. Similarly, finer-grained foreshores with steepnesses ranging between 7.3° and 13°, with a mean value of 10° have been reported in the literature and possibly attributed to the presence of heavy mineral detrital grains in the sandstones (Dubois, 1972). The presence of heavy mineral grains might have diminished the strength of the backwash in a way similar to that of the aforementioned one for coarser grain sediments, according to this author.

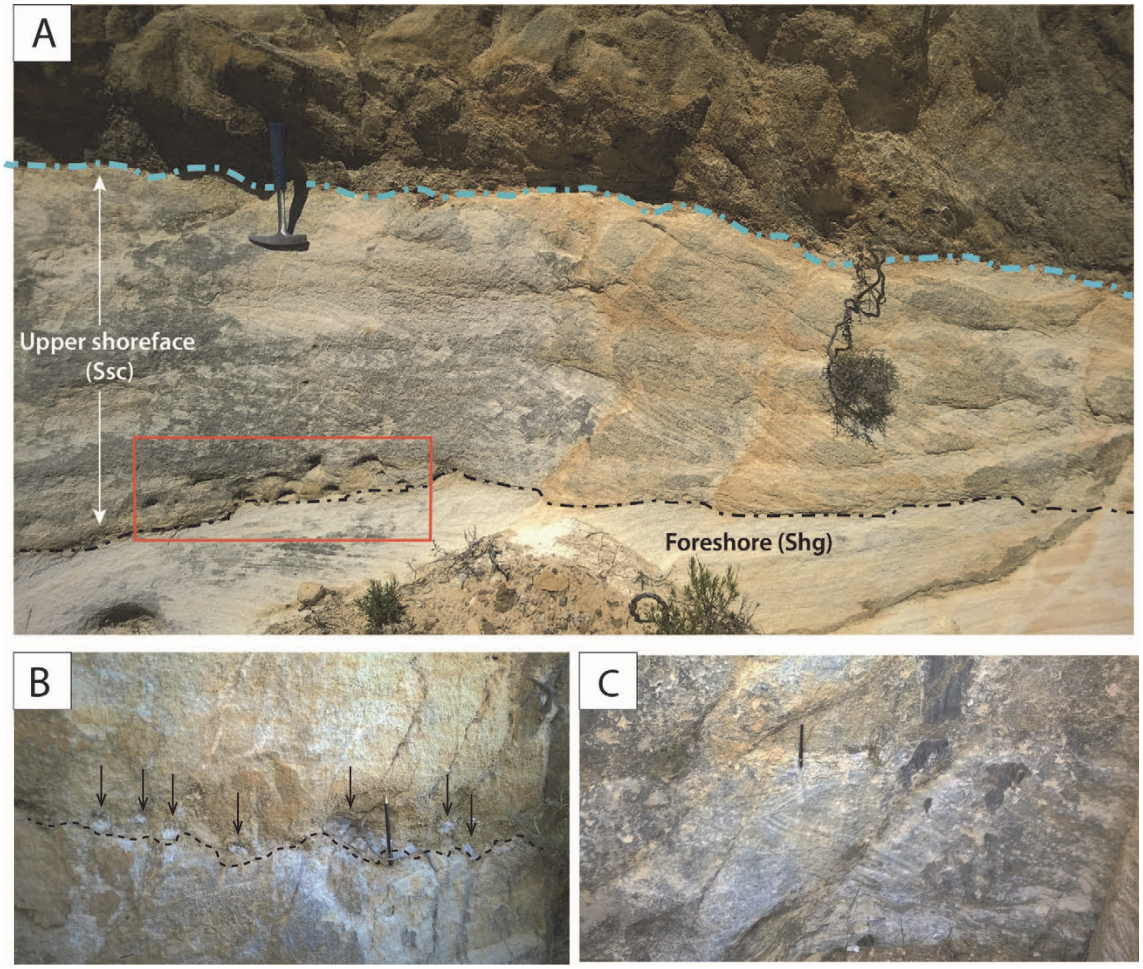

Fig. 8.11. High-gradient coastal deposits (FA VII) in the Reíllo outcrop. (A) Upper shoreface deposits (facies Ssc) overlying foreshore deposits (facies Shg) with an erosional contact interpreted as a ravinement surface (dashed black line). The upper shoreface deposits are topped by a maximum flooding surface (*MFS*, blue dotted thick line). The local occurrence of 2 to 8 cm in diameter moulds (solid red line box) are the result of either mud cobbles or pebbles at the erosive base of the shoreface deposits. Hammer for scale is 35 cm. (B) Detail of the erosional surface described in (A), separating foreshore deposits (below) and upper shoreface deposits (above). Black arrows point at preserved mud pebbles-cobbles (4 cm in diameter on average) associated with this erosive basal contact. (C) Detail of a herringbone cross-bedded sandstone (facies Ssc) (Table II) in the upper shoreface deposits. The pen for scale in (B) and (C) is 10 cm-long. This figure has been published as supplementary material in Bueno-Cebollada et al. (2022). See chapter 11 of this manuscript for further explanation of the sequence stratigraphic surfaces.

The facies Ssc, consisting of small-scale trough cross-bedding and asymmetrical ripples with polymodal transport directions directed onshore, offshore, or along-shore (Figs. 8.10C, 8.11A), is interpreted as upper shoreface deposits. Isla et al. (2020) interpreted a similar facies as deposited in the bottomsets of inclined high gradient tangential deposits that resemble those described in facies Shg. Trough and planar cross-beddings present different palaeocurrent directions, basically NE, N, and SW, due to the action of waves (being their energy at its maximum in the upper shoreface), rip currents, and longshore currents. Additionally, tidal currents might have also played an important role in the modelling of the upper shoreface, since they systematically move the swash zone onshore or offshore in the shoreline due to tidal oscillations, in a way that, when there is high tide, the upper shoreface will move landward and vice-versa (Hart and Plint, 1995; Clifton, 2006).

The association of small-scale trough cross-bedding (facies Ssc) with high gradient deposits (facies Shg), as observed in the Reíllo outcrop, is interpreted as a high-energy coastal environment where wave processes played a key role in the coastal dynamics. The sedimentary environment where they deposited consisted of steep beach profiles dominated by a wide swash zone and a very narrow surf zone, which is characteristic of non-barred clastic shorelines (Isla et al., 2020). This facies association has only been observed in the Reíllo outcrop and its deposition represents the transgression of the braidplain system and the development of a non-sheltered high-energy coastal fringe (Figs. 8.10A, C, 8.11A) (Bueno-Cebollada et al., 2022).

8.8. Facies association VIII: shallow marine mixed deposits. (Slc, Scax, Sbt, Lms, and Fc)

Description: This facies association consists of an array of mixed calcareous-siliciclastic deposits which include the facies Slc, Scax, Sbt, Sb1, Lms, and Fc (Fig. 8.12). The facies Slc consists of large-scale sets (up to two meters) of planar cross-bedded strata with sigmoidal foresets, where the main transport is usually towards NE (Fig. 8.12A, B, E). However, bimodal transport directions (NE-SW) are locally observed in this facies.

The facies Scax consists of medium- to coarse-grained tabular calcareous sandstones that typically show 0.5 to 1 m-thick sets of planar cross-bedding whose main transport direction is either unimodal (NE) or bimodal (NE-SW). In this sense, the facies Scax may develop a herringbone-like cross-bedding style in those cases where it shows a bimodal (NE-SW) transport direction. Likewise, this facies may also present associated wave ripples (symmetrical ripples). The facies Scax shows a finer grain size and smaller size of the sedimentary structures than facies Slc and it can be progressively overlain by the latter facies (Fig. 8.12A, B).

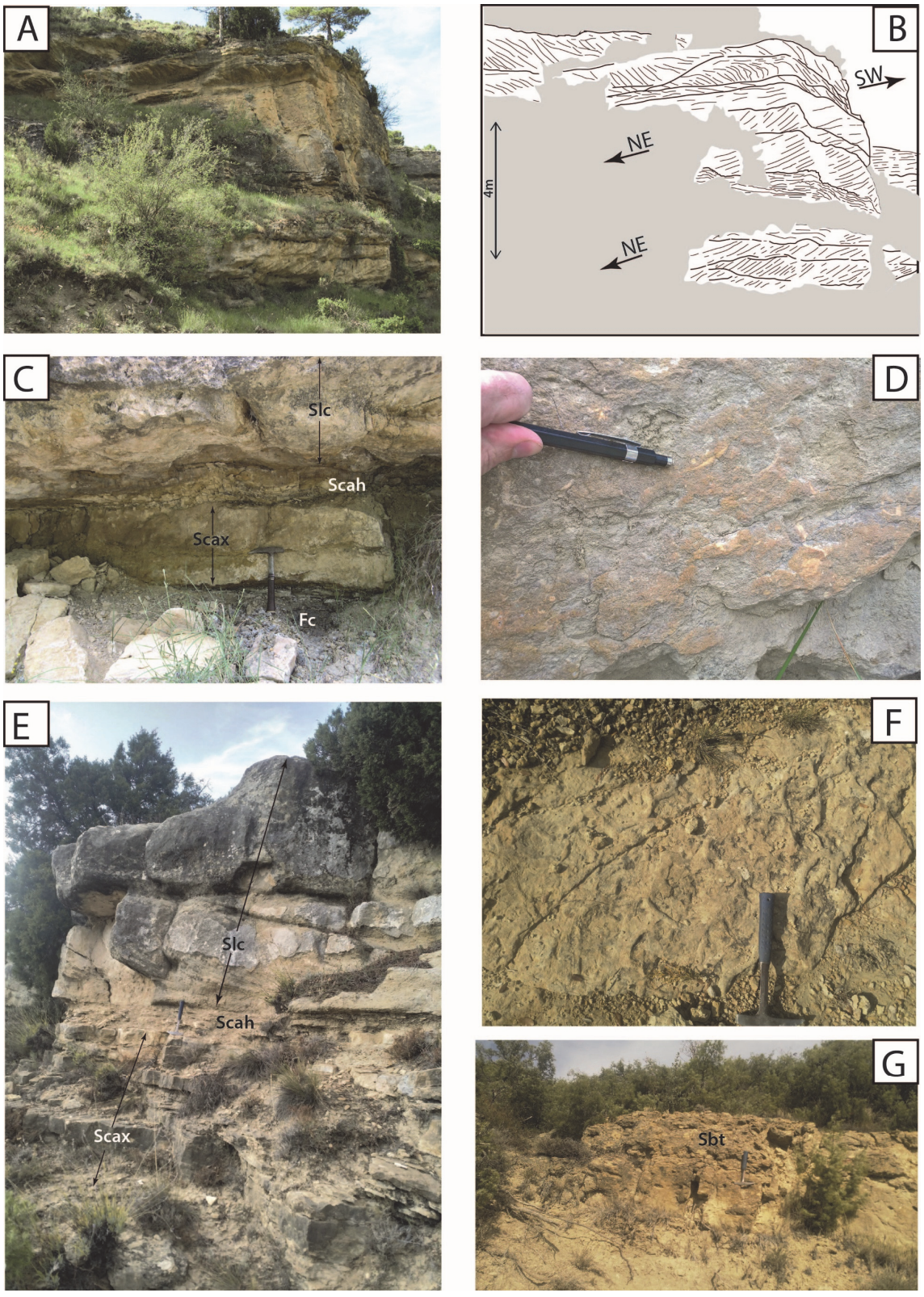

Fig. 8.12. Shallow to open marine facies mixed deposits (FA VIII). (A) Amalgamated proximal subtidal dunes (facies Slc and Scax) in the La Huérguina outcrop. They present ebb-directed currents (NE) in the lower parts and dominance of flood currents (SW) in the upper part of the channels, due to the tidal asymmetry. (B) Line drawing of (B). (C) Detail of the facies Scax, Scah, and Fc in the La Huérguina outcrop. Hammer for scale is 50 cm-long. (D) Detail of bivalve and gastropod shell fragments and undifferentiated moulds in the shallow marine deposits of the FA VIII (Campillos-Paravientos outcrop). The pen for scale is 10 cm-long. (E) Development of large sub-tidal dunes in a shallow marine setting in the La Huérguina outcrop. The distribution of the facies Slc, Scax, and Scah can be observed in the outcrop. (F) Detail of the trace fossil *Planolites* (*Cruziana* Ichnofacies) recognised

in the Campillos-Paravientos outcrop. (G) Facies Fbt, interpreted as the abandonment stage of the tidal dunes and its later colonisation by organisms. Hammer for scale (E-G) is 35 cm-long.

The facies Sbt consists of intensively bioturbated massive calcareous sandstones (Fig. 8.12G) that in some cases relict cross-bedded strata may be observed, almost obliterated by the intensity of the bioturbation. The observed bioturbation is a combination of vertical and horizontal burrows. This facies is well identified in the upper levels of the Campillos-Paravientos outcrop, where typically overlays the deposits of either facies Slc or Scax (Fig. 8.12G).

The facies Lms consists of medium- to coarse-grained highly calcareous sandstone to sandy limestones, arranged in 0,4 to 1 m-thick tabular body which may extend laterally for more than 300 m in the Pajaroncillo outcrop (see figure 12 in Bueno-Cebollada et al., 2022). The facies is dominated by single-crystal quartz grains and skeletal components, which mainly comprise mollusc (dominated by bivalves) shell fragment moulds replaced by calcite (Fig. 8.13) (Bueno-Cebollada et al., 2022). This facies has only been identified in the uppermost levels of the Pajaroncillo and Campillos-Paravientos outcrops.

Interpretation: This facies association is interpreted as shallow-marine tidal deposits, which may form in open mouth embayments and semi-enclosed epicontinental seas, where the tidal action is enhanced by resonance (Reynaud and Dalrymple, 2012). The occurrence of shallow-marine tidal deposits is sensitive to changes in sea level, as it happens in transgressive settings. The most frequent facies identified in this facies association are cross-bedded (calcareous) sandstones (i.e., facies Slc and Scax), which typically are part of tidal dunes, the most ubiquitous bedforms observed in tidal sandy shelves. The size and shape of the tidal dunes are controlled by the water depth, current speed, and grain size (Reynaud and Dalrymple, 2012). The tidal dunes observed in this facies association are typically compound dunes (that result from complex superimposition of simple dunes; Allen, 1980), whose vertical succession is usually a coarsening upwards one, regarding grain-size (Fig. 8.13E). Similarly, the thickness of the sedimentary bodies tends to thicken upwards within each tidal dune. This coarsening-upwards trend is the consequence of a stronger current at the crest of the dune than in the bottomsets, where finer deposits represented by the facies Fc accumulated (Reynaud and Dalrymple, 2012). The tidal dune bodies included in this facies association and observed in Campillos-Paravientos present a unimodal or main bedform migration path, which tends to be toward the NW. It indicates that the dunes might have been influenced by asymmetrical tidal currents, which gave rise to sets of cross-bedded strata either completely or mainly controlled by a unimodal transport direction (Reynaud and Dalrymple, 2012). Conversely, the great majority of the tidal

dunes observed in the La Huerguina outcrop (Fig. 8.12A, B, E) usually show sets of cross-bedded strata indicating bimodal transport direction (typically NW-SE; Fig. 8.12A, B). Although the main transport direction is still toward the NW, these bimodal orientations of the foresets reflect less asymmetrical tidal currents reworking the sediment (Reynaud and Dalrymple, 2012). The occurrence of asymmetrical tidal currents in the La Huerguina outcrop might be due to subordinate tidal currents that developed smaller dunes or mega ripples giving rise to herringbone-like beddings. Seasonal changes in ocean circulation and/or variabilities in the wind regime may produce master bedding planes in tidal dunes and current reversals (Reynaud and Dalrymple, 2012). Likewise, the migration of the tidal dunes (NE) at a low angle compared to the inferred orientation for the palaeocoast (ENE) reflects the effect of longshore currents reworking the deposits in the Reíllo outcrop (Bueno-Cebollada et al., 2022).

Tidal dunes developed in shallow marine to shelf (i.e., shoreface) settings may present tidal bundle structures produced by neap-spring tidal cycles (i.e., Longhitano and Nemec, 2005). However, they tend to be a rare feature since tidal dunes, in view of their large size, migrate too slow to properly record single tidal cycles (Reynaud and Dalrymple, 2012). In this sense, the tidal dune deposits observed in the Eastern sector (the La Huerguina and Campillos-Paravientos outcrops) may locally present tidal bundles recording neap-spring tidal cycles. The occurrence of tidal bundles in shallow marine to shelf settings is a much less significant feature than in intertidal settings (i.e., tidal flats or estuaries) since the former settings are normally characterised by rotary tides lacking the slack water period (Reynaud and Dalrymple, 2012).

In this facies association, the fact that some tidal dunes are capped by a massively bioturbated calcareous sandstone (facies Sbt; Fig. 8.12G) represents a stage of abandonment of the dune and the colonisation by organisms (Bueno-Cebollada et al., 2022). The intensity of bioturbation in tidal dunes is in inverse proportion to the speed at which they migrate across the shelf (Reynaud and Dalrymple, 2012). If the dunes migrate fast, the intensity of the bioturbation will tend to be lower than in those dunes which migrate more slowly, since slower currents allow the organisms to colonise the substrate more successfully. The main trace fossil found and identified in this facies association in the Eastern sector (Campillos-Paravientos outcrop) is *Planolites* (Fig. 8.13F), along with vertical structures, which belong to the *Cruziana* Ichnofacies (Seilacher, 1967; Mac Eachern et al., 2010). The *Cruziana* Ichnofacies is characteristic of subtidal environments where the depositional conditions range from long-term moderate-energy levels in shallow marine settings between fair-weather wave base and storm-weather wave base to lower energy levels in deeper settings (Mac Eachern et al., 2010). This ichnofacies is characterised by a combination of horizontal (i.e., *Planolites*) and vertical/sub-vertical (i.e.,

Diplocraterion) burrows of (semi-) dwellings produced by mobile structures, as well as deposit-feeding structures (Mac Eachern et al., 2010).

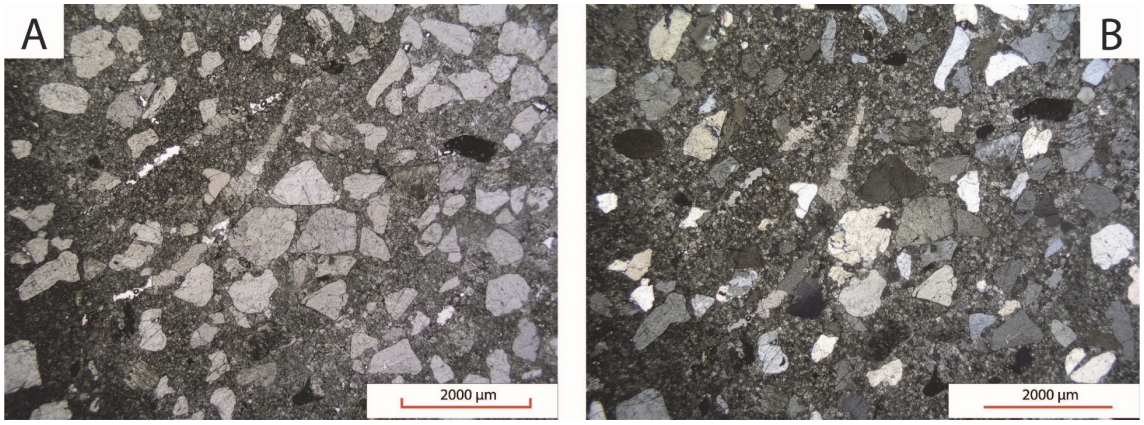

Fig. 8.13. (A) Thin-section of the mixed platform deposits (facies Lms; FA VI) where mostly monocrystalline quartz grains and calcite replaced bivalve shell moulds are cemented by carbonate cement, with plane-polarised light. (B) Thin-section of the mixed platform deposits (facies Lms), with cross-polarised light. Images published as supplementary material in Bueno-Cebollada et al. (2022).

The facies Lms is interpreted as a mixed carbonate-siliciclastic ramp system developed in a shallow marine setting. The generation of this mixed siliciclastic-carbonate platform system resulted from facies mixing (Mount, 1984). More concretely, it is the product of mixing at the interface between coastal to shallow marine siliciclastic deposits with migrating tidal dunes and the coeval (upper Albian to ?lower Cenomanian) subtidal carbonate deposits of the platforms, described towards the southeast of the study area (i.e., Valencia Domain), which belong to the Aras de Alpuente Fm (i.e., Vilas et al., 1982; Carenas et al., 1994; Sopeña et al., 2004; Martín-Chivelet et al., 2019b).

Therefore, this facies association is interpreted as deposited in a shallow marine mixed setting (above fair-weather wave base) dominated by a succession of tidal dunes, which migrated across a shoreface where tidal, longshore currents, and wave action played an important role in the sediment distribution, and by the later development of an embryonic mixed carbonate-siliciclastic ramp (Bueno-Cebollada et al., 2022).

9. Palaeoedaphological study.

A palaeosoil is a soil developed in a sedimentary environment of the geological past owing to the concomitant action of physical, chemical, and biological processes, and their formation is normally associated with prolonged periods of landscape stability (Yaalon, 1971, 1983; Kraus, 1999). Palaeosoils have been reported from many continental to transitional sedimentary environments, yet they are more frequently occurring in alluvial environments, typically associated with the overbank areas (Kraus, 1999), which remain undisturbed for periods, long enough to allow for (intense) plant colonisation. In the outcrop, palaeosoil successions may alternate with non-bioturbated sediments (i.e., floodplain mudstones with root traces alternating with coarse-grained sandstone channels) giving rise to palaeosoil-sediment sequences known as pedocomplexes (Morrison, 1977; Fedoroff et al., 2010).

According to Retallack (1988), there are three diagnostic features that are unequivocal when it comes to identifying a palaeosoil: (a) occurrence of branching and tapering down structures that are identifiable as root traces. Root traces are regarded as good indicators of the existence of soils during the geological past, as they are more easily preserved in the fossil record than other parts of the plants; (b) development of soil horizons since they reflect the complexity of the soils of the past, their vegetation, and the time for their formation. (c) existence of soil structures (i.e., soil peds) formed owing to bioturbation by plants and animals (trace fossils), wetting and drying cycles or other processes. The study of soil structures permits the interpretation of the drainage conditions of the palaeosoils.

Palaeosoils are insightful subjects of study in palaeoclimatology, particularly useful when it comes to estimating mean annual palaeotemperatures and palaeorainfall since they remained in the place where they were originally formed, and can be considered fossilised ecosystems (Kraus, 1999; Retallack, 2001; De la Horra et al., 2008). In this sense, palaeoclimates can be analysed by comparing ancient soils with the present-day ones and the climate conditions in which they develop (Mack, 1992; Kraus, 1999).

The occurrence of palaeosoils in the deposits of the Utrillas Gr is well-known in the literature (i.e., Platt, 1989; Marfil et al., 1992; Chamizo-Borreguero et al., 2008; Chamizo-Borreguero et al., 2016; Bueno-Cebollada and Meléndez, 2018). However, to date, there are no works dealing with the study of the subtleties of these palaeosoils and their palaeoclimatic implications.

The present chapter of this thesis manuscript addresses the study of three exceptionally preserved mid-Albian to lower Cenomanian sequences of palaeosoils (pedocomplexes sensu Morrison, 1977) from the Buenache de la Sierra outcrop (Figs. 5.1, 9.1).

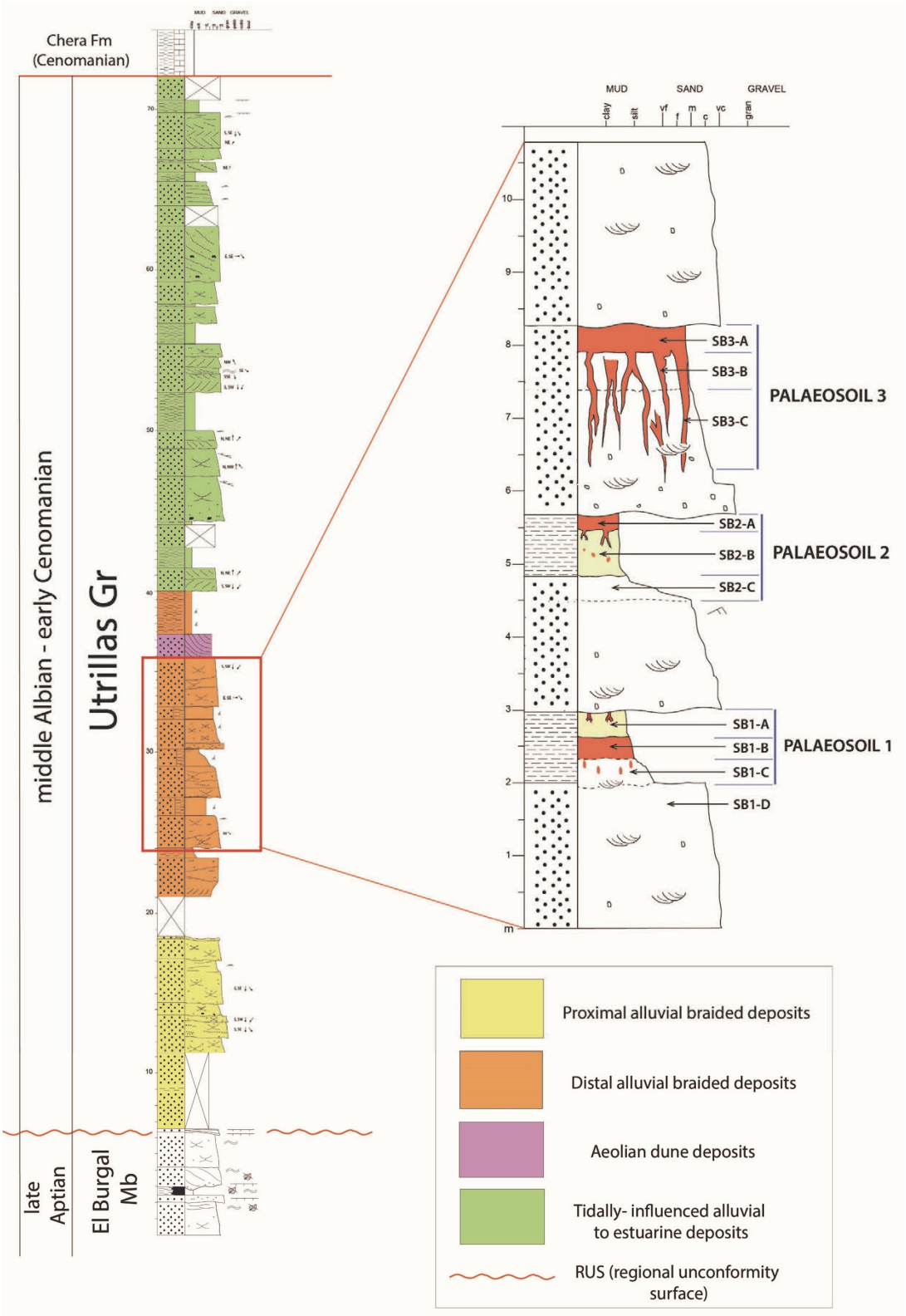

Fig. 9.1. Full logged section for the Utrillas Gr at the Buenache de la Sierra outcrop (to the left of the figure) where the distribution of the facies associations interpreted has been highlighted in different colours (see also Fig. 5.3). It includes a close-up and more detailed logged section (to the right of the figure) of the levels where the three studied palaeosoils are located. The position of the studied samples in each palaeosoil horizon is shown in the logged section. The full logged section in the Buenache de la Sierra outcrop is included in Fig. 5.3 (see chapter 5 of this manuscript).

The studied palaeosoils may present the characteristic sedimentary structures (root traces, soil structure and soil horizons [Retallack, 1988]) that allow them to be identified as such. These structures are mainly developed in the deposits of the facies association II (distal alluvial deposits) and, to a lesser extent, in those of the facies association III (inner estuarine).

The analysis of the palaeosoil sequences from the Buenache de la Sierra outcrop (herein referred to as Palaeosoils 1, 2 and 3, respectively) tackled in this chapter includes:

- Outcrop descriptions of the different soil horizons identified in the field.
- The study of petrographic samples corresponding to each of the soil horizons of the three palaeosoils under the transmitted light microscope.
- An X-ray diffraction analysis that has permitted identifying the different minerals that characterise the palaeosoils' horizons. Besides, SEM (scanning electron microscope) has been used to characterise the identified mineral phases when necessary.
- A geochemical analysis (using ICP-OES and ICP-MS) that includes major-element, minor-element, and REE determinations.

9.1. Outcrop description of the palaeosoil horizons. (Fig. 9.2)

Palaeosoil 1

-Horizon 1 (sample SB1-A*)*: this horizon is about 40 cm thick and consists of mudstone and siltstones with scattered sand-sized grains. They are dark yellowish to ochre in colour and may present reddish to purple mottling and vertical structures, which seem to indicate the presence of poorly developed roots (Fig. 9.2B)

The upper contact is an abrupt and erosional surface that corresponds with the base of an overlying alluvial channel. The lower contact is a clear sharp contact that shows lateral continuity.

-Horizon 2 (sample SB1-B): 20 cm-thick horizon consisting of light red reddish mudstones to siltstones slightly mottled with scattered sand-sized grains. The upper contact (with horizon 1) is a clear sharp one, whereas the lower contact is gradual and wavy to irregular regarding lateral continuity.

-Horizon 3 (sample SB1-C): 50 to 60 cm-thick siltstone to very fine-grained sandstone horizon depicting whitish-yellow colours. Locally, and especially towards the upper part of the horizon,

some reddish mottling can be observed. The upper contact (with horizon 2) is gradual, describing an irregular laterally continuous surface. The lower contact is a diffuse and irregular one.

-Horizon 4 (sample SB1-D): 2 m-thick horizon which consists of a coarse-grained arkose sandstone body. The body is lenticular in shape, fining upwards, and shows an erosional base. It may locally contain scattered pebbles, more numerous towards the base. The sample (SB1 – D) corresponds with the upper part of the sandstone body close to the contact with horizon 3.

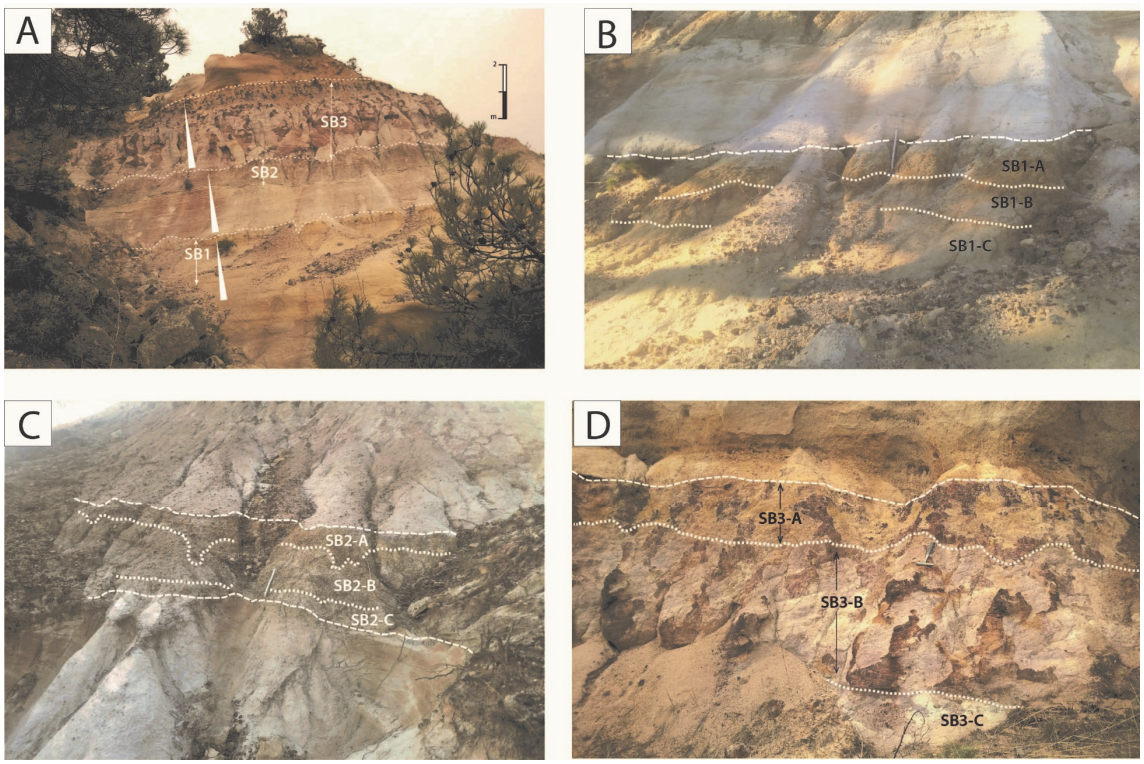

Fig. 9.2. General outcrop view of the studied palaeosoil succession in Buenache de la Sierra (see Fig. 9.1), where the extension of the three palaeosoils (SB1, SB2, and SB3) is indicated. The white elongated triangles indicate the trends in grain size in each of the studied palaeosoils. (B) Detail of the outcrop view of the palaeosoil SB1 including the three soil horizons identified (SB1-A, SB1-B, and SB1-C). (C) Detail of the outcrop view of the palaeosoil SB2 with the three soil horizons (SB2-A, SB2-B, and SB2-C) have been identified in the palaeosoil. (D) Detail of the outcrop view of the palaeosoil SB3. Three soil horizons (SB3-A, SB3-B, and SB3-C) have been identified in the palaeosoil. In figures (A), (B), and (C), the white dotted lines show the boundary among the horizons, while the dashed white line represents the upper boundary of the palaeosoil with the overlying alluvial sandstone body. The measuring stick for scale in (A) and (B) is 40 cm. Hammer for scale in (C) is approximately 35 cm long.

Palaeosoil 2

-Horizon 1 (sample SB2-A): 20 to 30 cm-thick horizon which consists of dark reddish mudstone and siltstone which may present a certain purplish hue in the outcrop. Mottles are “distinct”, yellow in colour, abundant and “fine” in size. They most probably represent small rootlets. The lower contact (with horizon 2) is gradual to diffuse and shows lateral continuity characterised

by wavy to irregular geometries of undulating pockets (Fig. 9.2C). Conversely, the upper contact (with an overlying channelised sandstone body) is an abrupt and erosional one (Fig. 9.2C).

-Horizon 2 (sample SB2-B): 40 to 60 cm-thick horizon consisting of mudstone and claystone with scattered sand-size grains. They are greenish-grey to ochre greenish in colour and present "distinct" mottles, although their abundance is rather low. The lower contact is a clear contact showing lateral continuity (Fig. 9.2C). However, its upper contact (with horizon 1) is a gradual one.

-Horizon 3 (sample SB2-C): interval of approximately 40 cm thick consisting of slightly altered white to pinkish fine-grained sandstone with high content of clay. The lower contact is a diffuse one. This horizon overlies a cross-bedded sandstone body which represents the non-weathered deposits of an alluvial channel.

Palaeosoil 3

-Horizon 1 (sample SB3-A): 40 cm-thick horizon which consists of dark red to purple coarse to medium-grained sandstones with significant clay contents. The horizon commonly presents abundant vertical structures, interpreted as roots as well as the occasional occurrence of iron concretions ((Fig. 9.2D). Likewise, this horizon may locally present a faint yellow mottling. The upper contact of this horizon is an abrupt erosional contact with an overlaying non-weathered arkose sandstone body showing abundant trough-cross bedding, which represents the deposits of an alluvial channel overlying palaeosoil 3 in the study area (Fig. X). Conversely, the lower contact can be classified as clear with an irregular lateral continuity, showing undulating pockets.

-Horizon 2 (sample SB3-B): 60 cm-thick horizon which consists of white coarse to medium-grained sandstones with a significant amount of clay. It presents abundant vertical dark red structures emanating from horizon 1, which branch and taper downwards. These structures are interpreted as the result of pervasive root development in the soil (Fig. 9.2D). Likewise, these vertical structures show a drab-haloed mottled appearance, which might have been the result of the dehydration of yellow and brown ferric oxyhydrates into red hematite during diagenesis (Retallack, 2001). However, according to this author drab-haloed roots may represent the last plant crops growing in a palaeosoil before its burial. The lower contact of this horizon is diffuse to gradual and irregular regarding lateral continuity.

-Horizon 3 (sample SB3-C): 120 cm-thick horizon which consists of coarse- to very coarse-grained white sandstone with abundant cm-scale trough-cross bedding showing abundant pebbles

towards the base. This horizon is also pervasively cut by the same vertical drab-haloed structures observed in horizon 2, interpreted as root traces, which taper downwards more than a metre in this horizon. The upper contact (with horizon 2) is diffuse to gradual. The lower contact of this horizon is a diffuse transitional one into the mostly non-weathered deposits of the lenticular fining upwards sandstone body with an erosional base, interpreted as an alluvial channel (Fig. 9.2A, D).

9.2. Palaeosoil petrography.

Overall, 10 petrographic samples have been prepared and studied under the transmitted light petrographic microscope, corresponding to each of the horizons of the three studied palaeosoils (Fig. 9.1): Palaesoil 1 (samples SB1 – A, SB1 – B, SB1 – C, and SB1 – D), Palaeosoil 2 (samples SB2 – A, SB2 – B, and SB2 – C), and Palaeosoil 3 (samples SB3 – A, SB3 – B, and SB3 – C).

Palaeosoil 1

Sample SB1 – A: The sample is dominated by feldspars and monocrystalline quartz, along with polycrystalline quartz grains, to a lesser extent (Fig. 9.3A). The matrix is characterised by illuvial clay. Although, the dark brown to black colour in the matrix is due to the occurrence of small percentages of iron minerals that precipitated after clay illuviation, as they impregnated the clayey matrix (Fig. 9.3B). The sample corresponds to a sandy argillic horizon whose original porosity consisted of simple pores, which were filled with illuvial clay. Likewise, the main porosity observed are channel-like elongated structures that tend to branch and taper across the sample and are not filled with illuvial clay or clay coatings (Fig. 9.3A). The elongated shape of this porosity suggests that they are the result of bioturbation by small roots or rootlets, and the complete lack of illuvial clays filling them seems to suggest that the growth of these rootlets was coeval with the illuviation of the horizon.

Sample SB1 – B: The primary minerals observed in the sample SB1-B are dominated by monocrystalline quartz and K-feldspar, as well as a smaller number of polycrystalline quartz grains (Fig. 9.3C). Compared with the sample SB1-A, this sample shows a slightly greater number of quartz grains at the expense of K-feldspar ones. The matrix consists of significant amounts of illuvial clay as in the sample SB1-A due to the chemical alteration of K-feldspar (Fig. 9.3D). Likewise, the dark colour of the matrix is due to the occurrence of small percentages of iron minerals, which most likely precipitated after clay illuviation, as they impregnated the clayey matrix.

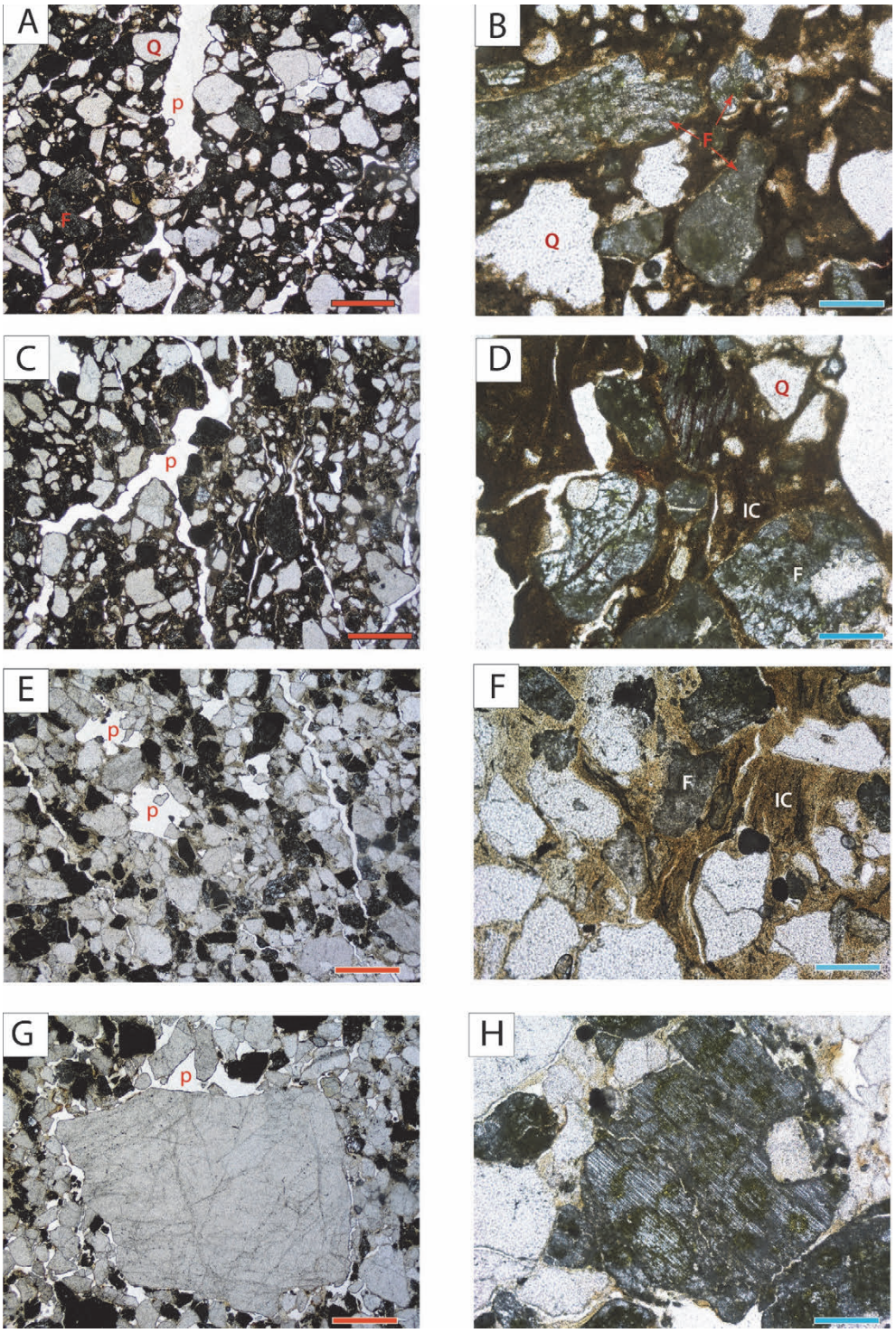

Fig. 9.3. Photomicrographs of palaeosoil 1. (A) Photomicrograph of the sample SB1-A under plane polarised light where the main mineral grains observed are K-feldspar (which show an intense alteration to clay minerals), polycrystalline and monocrystalline quartz. (B) Close-up of the sample SB1-A under plane-polarised light, where the alteration of the K-feldspar grains can be observed. Quartz grains are partly corroded, showing irregular edges, due to hydrolysis processes. (C) Photomicrograph of the sample SB1-B under plane-polarised light. The sample is dominated by altered K-feldspar grains and monocrystalline quartz. The matrix consists of illuvial clay. Channel-like porosities lacking any infill are most likely due to bioturbation by rootlets. (D) Detail of the partially dissolved K-feldspar and the illuvial clay matrix under plane-polarised light. (E) Photomicrograph of the sample SB1-C under plane-polarised light where abundant mono- and polycrystalline quartz grains are observed along with K-feldspar grains. The matrix consists of illuvial clay, and its amount is proportionally smaller than those of samples SB1-A and SB1-B. (F) Close-up of the sample SB1-C under plane-polarised light where an accumulation of illuvial clay can be observed. (G) Photomicrograph of sample SB1-D under plane-polarised light. Note the poor sorting and overall coarser grain size of quartz grains along with the lack of clay matrix. Q: quartz grains; F: feldspar grains; IC: illuvial clay; P: porosity. Red scale bars in (A, C, E, and G) are 1000 µm. Blue scale bars in (B, D, F, and H) are 200 µm.

Sample SB1 – C: The sample corresponding to this horizon is dominated by quartz and K-feldspars as the main skeletal grains. The quartz grains are mostly monocrystalline although polycrystalline ones may also be observed. The K-feldpars show signs of chemical alteration. In general, the grain size is coarser than those of the overlying horizons SB1-A and SB1-B (Fig. 9.3E).

Regarding the matrix, the amount of clay minerals observed is considerably smaller than that of both overlying horizons. However, small amounts of illuvial clay may be observed in sample SB1-C (Fig. 9.3F). The production of clay in a soil is due to the action of vegetation and chemical weathering. The lighter yellowish colour of the illuvial matrix may reflect little iron contents compared to the more reddish-brown colour observed in the samples SB1-A and SB1-B.

Sample SB1 – D: the skeletal components of the sample SB1-D are mainly grains of quartz (both mono- and polycrystalline) and K-feldspar to a lesser extent. The grains of this horizon depict a relatively coarser grain size as well as a much poorer sorting than those of the overlying horizons (Fig. 9.3G-H). The main difference with the horizon SB1-C is the absence of an illuvial clay matrix. Therefore, the sample shows high primary porosity. The amount of clay is considerably smaller than in the overlaying horizon and it was accumulated by forming clay coatings around quartz and feldspar grains.

Palaeosoil 2

Sample SB2 – A: The sample SB2-A is dominated by a groundmass that consists of mainly clay minerals, iron oxides, and hydroxides (Fig. 9.4A). The skeletal components represent a minor percentage of the horizon and are mainly very fine grain-size quartz grains. The groundmass may show alternations between opaque zones dominated by sesquioxides and hydroxides of iron and other zones where birefringent clay minerals are weakly oriented or even not showing a clear preferential orientation (Fig. 9.4A). Small mica flakes showing very weak orientation are commonly observed in the sample (Fig. 9.4B). Likewise, ferruginous nodules may develop owing to a moderate impregnation of the clayish matrix by iron oxides.

Sample SB2 – B: The sample SB2-B is dominated by a clayish matrix, which may locally show impregnations of iron oxides. The main skeletal grains are fine-grained quartz grains (Fig. 9.4C). The main difference between this horizon and the overlying one (SB2-A) is that quartz grains are slightly more abundant and coarser. Additionally, the horizon SB2-B also shows considerably smaller amounts of iron oxide.

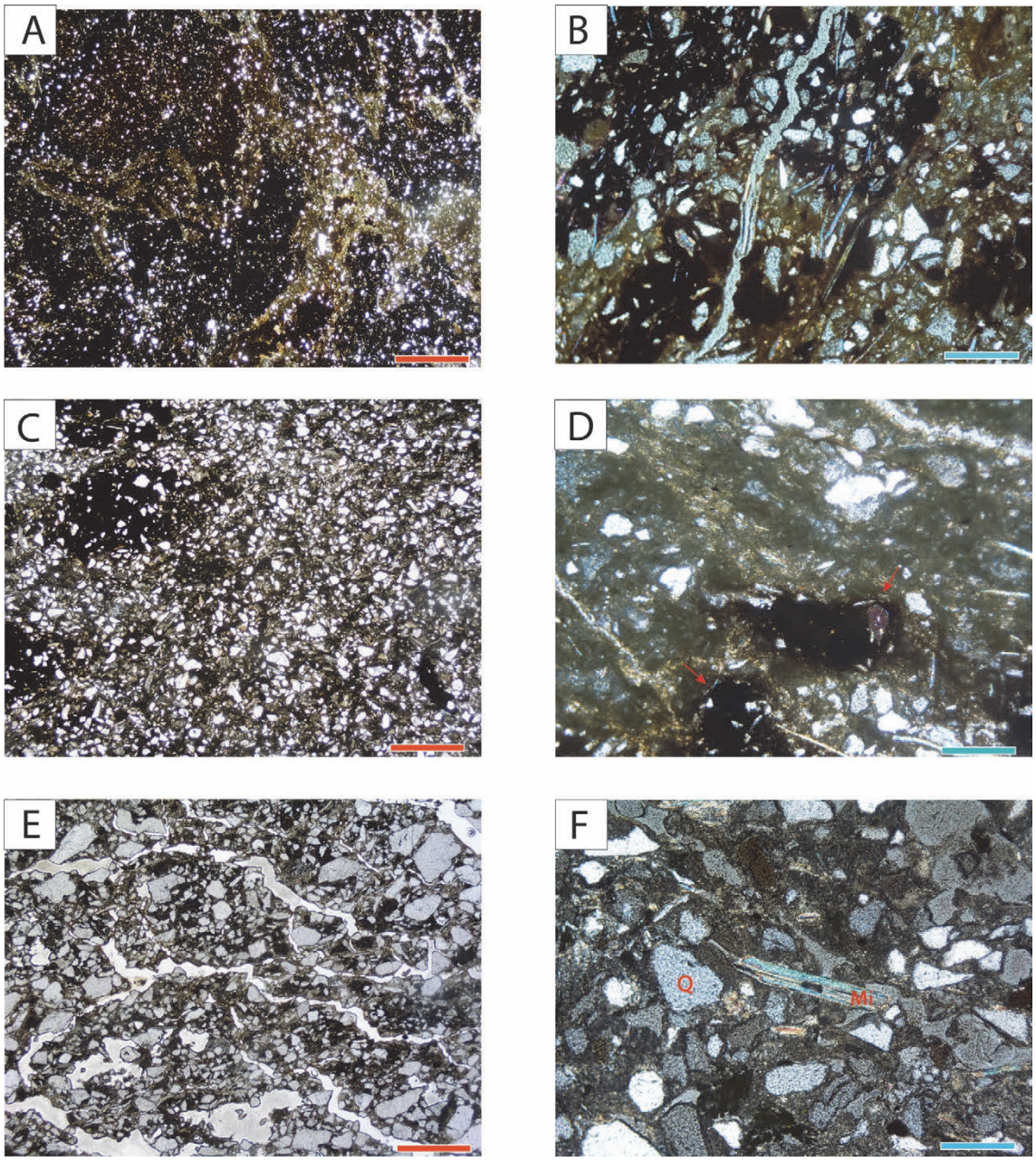

Fig. 9.4. Photomicrographs of palaeosoil 2. (A) Photomicrograph of the sample SB2-A under plane-polarised light. The sample is dominated by a groundmass of clay and iron oxides forming ferruginous hypocoatings. (B) Close-up of (A) under crossed-polarised light where the groundmass of clay can be observed together with scattered mica flakes. (C) Photomicrograph of the sample SB2-B under plane-polarised light. Note that the grain size of the quartz grains is notably larger than that of the sample SB2-A and the matrix proportionally smaller. (D) Close-up of the sample SB2-B under crossed-polarised light. Ferruginous hypocoatings can be observed in the matrix (indicated by red arrows). (E) Photomicrograph of the sample SB2-C under plane-polarised light. A larger amount, coarser grain size, and poorer sorting of the quartz grains can be observed compared with the overlying horizons (SB2-A and SB2-B). (F) Close-up of the sample SB2-C under crossed-polarised light. The sample is dominated by quartz grains and abundant illuvial clay and mica flakes. Q: quartz grains; Mi: mica flakes. Red scale bars in (A, C, E, and G) are 1000 µm. Blue scale bars in (B, D, F, and H) are 200 µm.

The groundmass is dominated by clay minerals in which some ferruginous hypocoatings may be observed (Fig. 9.4D). The hypocoatings arise due to the impregnation of the clayish groundmass with iron oxides and hydroxides (i.e., Hematite and Goethite), and their formation is usually

subject to alternations between wet and dry climate conditions (intense seasonal changes) (Retallack, 2001). Usually, periods of water saturation are needed to lead to Fe and Mn mobilization and periods of drought to produce their accumulation. Ferruginous hypocoatings are usually formed by intense drying which allows oxidation of iron minerals.

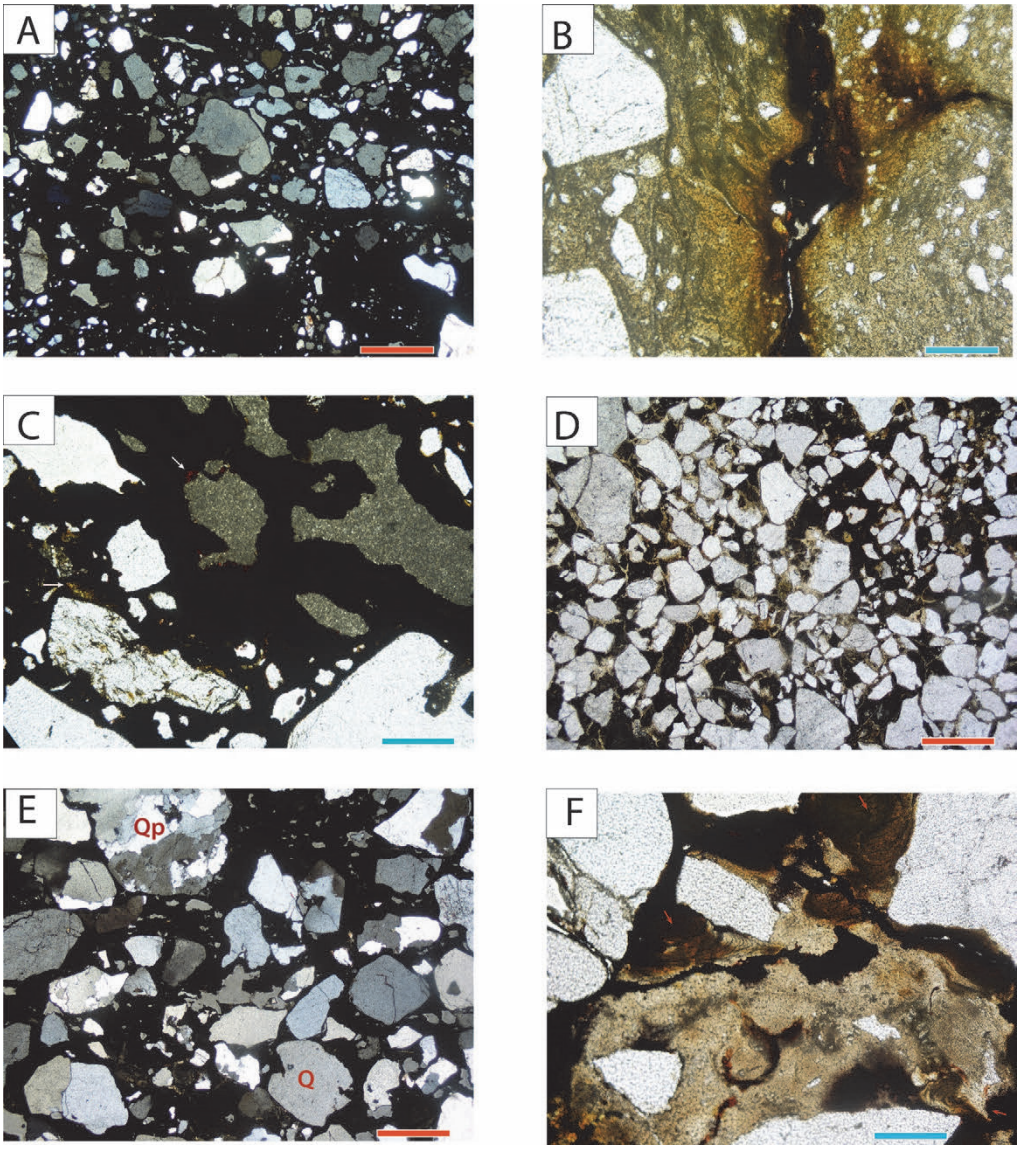

Fig. 9.5. Photomicrographs of palaeosoil 3. (A) General view under the petrographic microscope (plane-polarised light) of level SB3-A, where the skeletal components are dominated by monocrystalline quartz grains and, to a lesser extent, by polycrystalline ones. The conspicuous dark colour of the fine fraction is probably the result of the accumulation of iron oxides and hydroxides in the soil. (B) Detail of the illuvial clay accumulations where the yellowish to dark brown colours in the centre of the image represent variable amounts of iron impregnating the fine fraction and generating hypocoatings. (C) Sample SB3-A under plane-polarised light. Dark red colour spots seen in the upper central part of the picture (white arrow in the upper central part of the picture) are the result of impregnations of iron compounds (such as hematite) in the matrix. Light brownish to yellow-coloured spots (white arrow in the left-hand lower quarter) represent scattered hydrated iron compounds, most probably due to the presence of goethite. (D) Photomicrograph of the sample SB3-B under plane-polarised light. (E) Photomicrograph of the sample SB3-C under crossed-polarised light. The sample is dominated by quartz (poly- and monocrystalline) and K-feldspar grains with a matrix of illuvial clay. (F) Close-up of the sample SB3-C under plane-polarised light where examples of micro-laminated illuvial clays can be observed. Red arrows indicate the location of the micro-laminated clays. Red scale bars in (A, C, E, and G) are 1000 µm. Blue scale bars in (B, D, F, and H) are 200 µm.

Sample SB2 – C: This sample is mainly composed of monocrystalline quartz and K-feldspar grains (skeletal components). The grain size of the skeletal components is considerably coarser and poorly sorted than those of the overlying SB2-A and B horizons. The matrix consists of illuvial clay. The illuviation can be considered primary indicating good drainage conditions. Additionally, there is a lack of iron oxides/hydroxides in this horizon, unlike what happens in the overlying horizons (SB2-A and B). (Fig. 9.4E-F)

Palaeosoil 3

Sample SB3 – A: This level is dominated by monocrystalline quartz grains, although polycrystalline ones may also appear. Likewise, some heavily K-feldspar grains can be observed although their presence is rather anecdotal, showing partial alteration to clay minerals. The groundmass of the sample is dominated by a dark matrix which is characterised by the absence of interference colours (Fig. 9.5A) due to the presence of opaque or isotropic minerals such as iron sesquioxides (undifferentiated b-fabric; Bullock et al., 1985). Additionally, the groundmass may locally consist of illuvial clay accumulations which may present ferruginous hypo-coatings (Fig. 9.5B). Both the opaque groundmass and the occurrence of ferruginous hypo-coatings reflect the impregnation of the clayish matrix by iron compounds, which can be also noticed by the presence of red (hematite) and yellow (goethite) colours (Fig. 9.5C).

Sample SB3 – B: The skeletal fraction of the sample SB3-B consists of monocrystalline quartz grains and minor proportions of feldspar grains. Polycrystalline quartz grains are also observed in smaller amounts (Fig. 9.5D). The average grain size of this sample is slightly coarser, and the sorting is poorer than that of the sample SB3-A. The intergranular space is occupied by illuvial clay due to the alteration of feldspar grains. Dark colours in the matrix are due to the occurrence of opaque minerals such as iron sesquioxides similar to those of sample SB3-A (Fig. 9.5A).

Sample SB3 – C: The sample SB3-C shows similarities with the samples SB3-A and SB3-B. It is characterised by abundant quartz grains (mainly monocrystalline) and a smaller number of feldspar grains. However, the grain size in this sample tends to be coarser than those of the samples SB3-A and SB3-B (Fig. 9.5E). The matrix is dominated by an opaque groundmass that is almost ubiquitous in the sample. Likewise, abundant accumulations of illuvial clay are observed, which at times they may form microlaminated clays with bow-like distribution patterns (Fig. 9.5F). These crescentic coating fills normally grow among adjacent grains and consist of the alternation of limpid and speckled clay layers. This sort of textural pedofeatures most typically occurs in argillic horizons of soils and palaeosoils (Bullock et al., 1985).

9.3. Mineralogical analysis of the palaeosoils.

9.3.1. X-ray diffraction

Palaeosoil 1

Description: The sample/horizon SB1 – A is dominated by clay minerals that account for 72 % of the identified minerals. Illite (53 %) and kaolinite (43 %) are the main clay mineral identified in this horizon. Similarly, a small amount (3 %) of mixed-layer illite-smectite (I/S) has also been identified in the sample corresponding to this horizon. To a lesser extent, other minerals such as quartz (18 %) and K-feldspar (5 %) have been recognised in the analysis together with moderate amounts of the iron oxyhydroxide goethite (6 %) (Table III; Fig. 9.6A).

The sample/horizon SB1 – B is also characterised by the occurrence of conspicuous percentages of filosilicates (72 %) dominated by illite and kaolinite, accounting for 37 % and 32 %, respectively. Small percentages of I/S (3 %) are also represented among the identified clay minerals. Quartz, K-feldspar (microcline), and goethite are represented in similar amounts to the horizon SB1 – A (Table III; Fig. 9.6A).

The sample/horizon SB1 – C is dominated by quartz as the main mineral identified (43 %), together with conspicuous percentages of illite and kaolinite (23 % and 19 %, respectively). Additionally, a higher percentage of microcline (12 %) compared to those of the horizons SB1 – A and SB1 – B (Table III; Fig. 9.6A).

The sample/horizon SB1 – D is characterised by the highest percentages of quartz (65 %) observed in the palaeosoil 1 along with the lowest percentages of illite and kaolinite (10 % and 13 %). Regarding K-feldspar, the percentages are similar to those of the horizon SB1 – C (Table III; Fig. 9.6A).

Palaeosoil 2

Description: The sample/horizon SB2 – A is dominated by the clay minerals illite and kaolinite (38 % and 44 %, respectively) with subordinate amounts of I/S (2%) (Table III). Similarly, the percentages of quartz remain relatively high (Fig. 9.6B).

The sample/horizon SB2 – B is characterised by high percentages of clay minerals (illite and kaolinite), similar to the ones observed in horizon SB2 – A. Conversely, it is worth noting that the percentages of goethite are relatively high, reaching 11 % out of the overall weight of the

sample. Additionally, the analysis reveals a slight drop in the amount of quartz (13%) (Fig. 9.6B; Table III).

The sample/horizon SB2 – C presents high contents of clay minerals (74 %) dominated by kaolinite (57 %) and illite (18 %), to a lesser extent. Similarly, it presents slightly higher percentages of quartz (25 %), especially if compared with those of the horizons SB2 – A and SB2 – B (Table III; Fig. 9.6B).

Sample	Quartz	Microcline	Goethite	Illite	Kaolinite	I/S
SB1A	18	5	6	38	31	3
SB1B	18	5	5	37	32	3
SB1C	43	12	0	23	19	3
SB1D	65	11	0	10	13	1
SB2A	17	0	0	38	44	2
SB2B	13	1	11	35	40	0
SB2C	25	1	0	18	57	0
SB3A	18	1	12	14	55	0
SB3B	23	0	0	17	60	0
SB3C	28	1	11	13	48	0

Table III. Mineralogical composition of the studied samples obtained from X-ray diffraction data (Appendix VI). The abundances are expressed in weight percentages (%).

Palaeosoil 3

Description: The sample/horizon SB3 – A is dominated by clay minerals that represent 69 % of the weight of the sample. In this sense, kaolinite is the dominant clay mineral (55 %) while the percentage of illite remains comparatively lower (18 %). Additionally, goethite presents high percentages, reaching 12 % (Fig. 9.6C; Table III).

The sample/horizon SB3 – B presents an increase in the percentage of filosilicates, reaching 77 %, which is characterised by high values of kaolinite (60 %) and relatively low ones of illite (Fig. 9.6C; Table III).

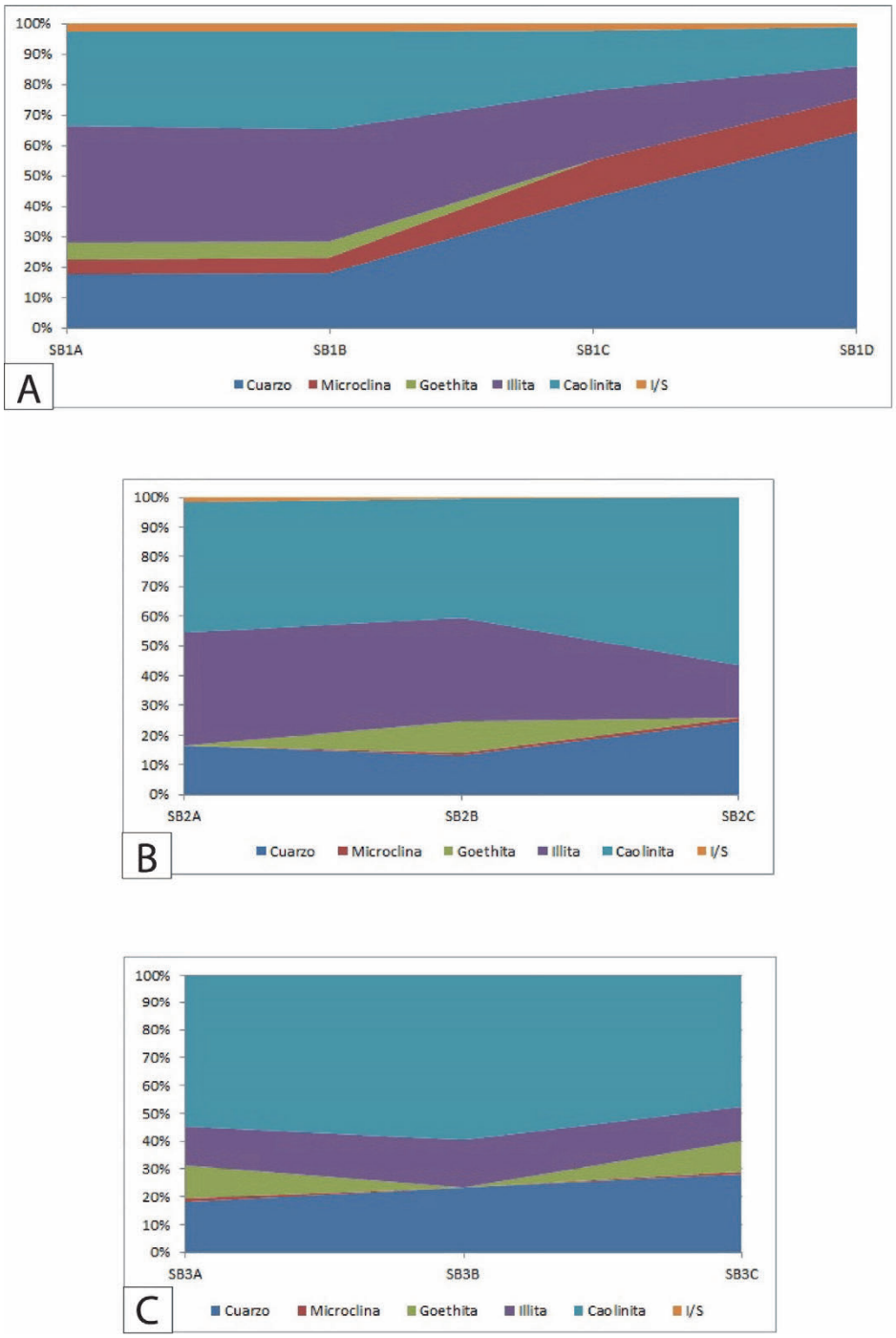

Fig. 9.6. Area charts showing the variation of the mineral compositions in each of the studied palaeosoil profiles. Y-axis represents the percentage value of the different minerals identified in the X-ray diffraction analysis of the different horizons sampled (X-axis) in the palaeosoils from Buenache de la Sierra. (A) Palaeosoil 1; (B) Palaeosoil 2; (C) Palaeosoil 3.

The sample/horizon SB3 – C is characterised by a slight diminishment in clay minerals compared to horizon SB3 – B. In this regard, the percentage of kaolinite is also higher than that of illite. Conversely, the percentage of quartz increases compared to that of horizon SB3 – B. Additionally, this horizon shows a conspicuous percentage of goethite, similar to the one observed on the horizon SB3 – A (Fig. 9.6C; Table III).

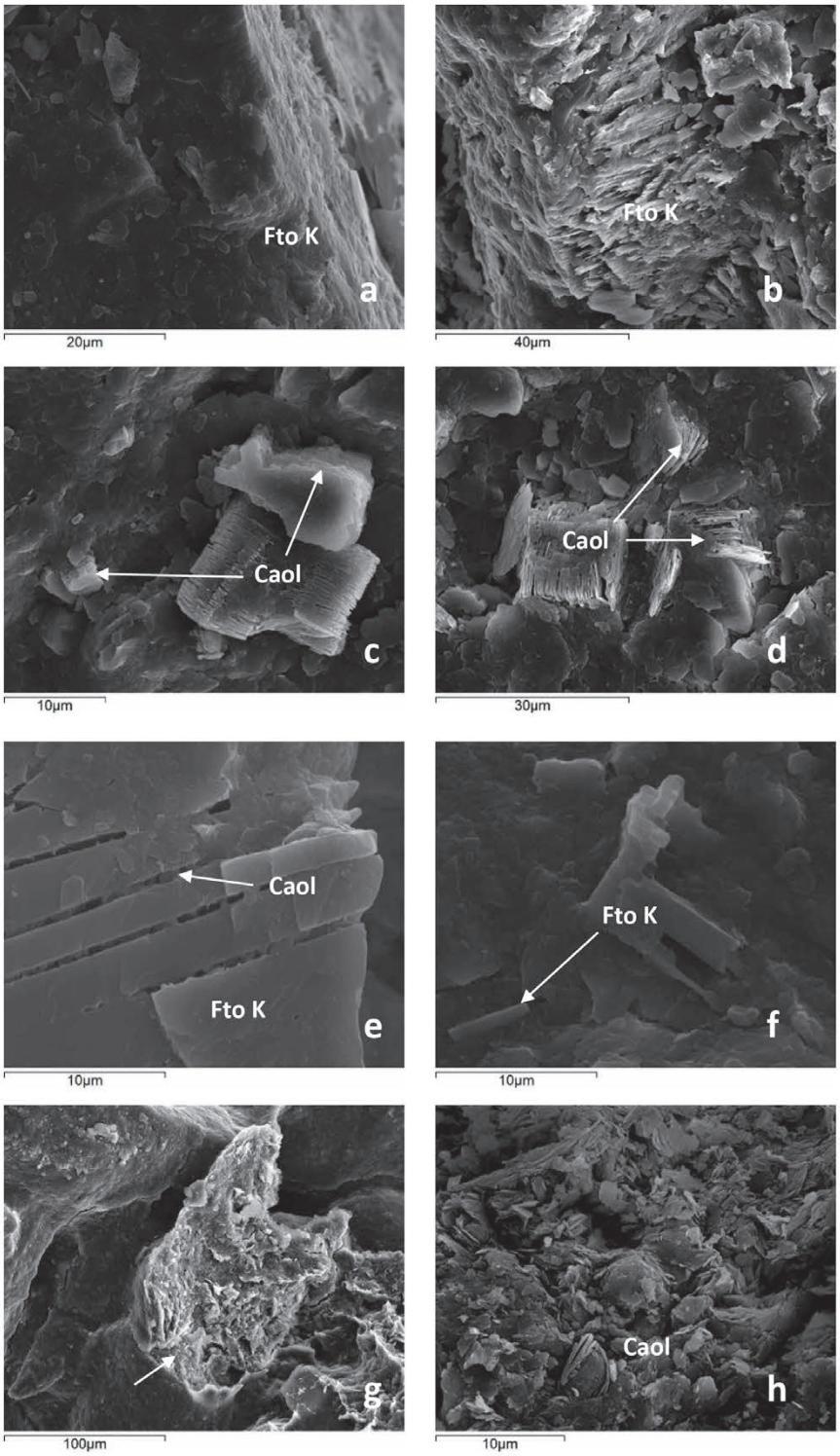

Fig. 9.7. Images of the palaeosoil 1 under the scanning electron microscope (SEM): (A) K-feldspar (Fto K) grain showing a low alteration degree in the sample SB1-D. (B) Example of another K-feldspar crystal (Fto-K) from the same sample (SB1-D) being slightly more altered than that of A. (C) and (D) hexagonal laminae aggregates of kaolinite (Caol) forming prisms with the typical "booklet" texture in sample SB1-D. (E) Detail of sample SB1-C showing a microcline (Fto K) crystal partially altered following parallel planes in which thin kaolinite laminae (Caol) develop. Kaolinite laminae are indicated by an arrow. (F) Small crystal of microcline in sample SC1-C showing a more intense alteration than in E. (G) Example of sample SB1-B where a few moulds of K-feldspar crystals can be seen (white arrow). The feldspars have been practically replaced by kaolinite. (H) General aspect of the sample SB1-B showing a texture dominated by clay minerals where kaolinite crystals prevail.

9.3.2. SEM analysis

In order to obtain a more complete textural and mineral characterization of the studied samples, Palaeosoil 1 has been considered for study under the SEM. The reason for only considering this soil profile is rooted in its more representative composition that allows to illustrate the progressive diminishment in K-feldspar and increase of kaolinite upwards in the soil profile, observed both in the thin sections and XRD analyses.

The sample SB1-D, corresponding to the lowermost sample of the soil profile shows a massive texture with low porosity in which abundant K-feldspar crystals can be identified. Some of these K-feldspar crystals are relatively well-preserved (Fig. 9.7A) while others are partly altered (Fig. 9.7B). The K-feldspars crystals are surrounded by kaolinite crystals that form laminar aggregates that give rise to pseudohexagonal prisms arranged into the classical booklet texture (i.e., Aróstegui et al., 2001) (Fig. 9.7C, D). The sample SB1-C, located on an upper horizon of the soil profile, shows K-feldspar crystals that are notably more altered and present a higher porosity developed along parallel planes, due to the alteration, where small kaolinite crystals grew (Fig. 9.7E, F). In the sample SB1-B, corresponding to an upper and more altered soil horizon, the porosity is more developed than in the lower horizons of the soil profile and most of the K-feldspar has been altered to kaolinite that occasionally may form pseudohexagonal aggregates, occasionally leaving behind some moulds of K-feldspar crystals (Fig. 9.7G, H).

These progressive variations in the proportion of kaolinite and K-feldspars seem to indicate that both mineral phases are closely related, given their compositional affinity. In this regard, the textural features observed in the SEM images conform with this pattern indicating the formation of authigenic kaolinite owing to the alteration of the feldspars (Fig. 9.7). Consequently, the SEM images obtained for the palaeosoil 1 reflect the progressive mineral alteration of sandstones with abundant feldspar crystals giving rise to authigenic kaolinite crystals.

9.4. Palaeosoil geochemistry.

The chemical processes of hydrolysis, oxidation, hydration, and dissolution, together with their opposite processes of alkalisation, reduction, dehydration, and precipitation constitute the basic reactions that take place during the development of a soil (Retallack, 2001). The geochemical characteristics of the soil are an important source of information that, treated with precautions, can help understand the basic reactions responsible for the development of soils, providing important palaeoenvironmental information. A common method to recognise chemical

processes in palaeosoils is to obtain numerical relationships between the molecular proportions of chemical elements and oxides and then observe their variations across the profile. These relationships between elements are known as indexes and are used to evaluate evidence of pedogenesis, the provenance of parental materials, or palaeoclimatic interpretations. In this study, seven representative samples of Palaeosoils 1 (samples SB1A to SB1-D) and 3 (samples SB3-A to SB3-C) were prepared for whole-rock analyses and performed by ICP-OES and ICP-MS. Major-element, minor-element, and REE determinations are provided in Tables IV and V. In this regard, Palaeosoils 1 and 3 have been selected for the geochemical analysis since they present greater differences in their mineralogical and geochemical compositions.

Sample	SiO2	Al2O3	Fe2O3	CaO	MgO	Na2O	K2O	Cr2O3	TiO2	MnO	P2O5	SrO	BaO	LOI	Total
	%	%	%	%	%	%	%	%	%	%	%	%	%	%	%
SB1-A	61.9	21.8	3.43	0.15	0.6	0.2	4.41	0.01	0.7	0.01	0.06	0.01	0.05	8.17	101.49
SB1-B	65.3	20.2	3.32	0.15	0.51	0.18	4.42	0.007	0.63	0.01	0.04	0.01	0.04	6.69	101.49
SB1-C	78.5	12.95	0.85	0.07	0.25	0.16	4.95	0.003	0.27	0.01	0.04	0.01	0.05	3.52	101.61
SB1-D	86.9	8.29	0.37	0.04	0.09	0.14	3.93	0.002	0.13	0.01	0.02	0.01	0.04	1.76	101.71
SB3-A	63.2	17.4	8.73	0.14	0.16	0.04	0.26	0.016	0.91	0.01	0.02	0.01	0.01	8.26	99.15
SB3-B	69.2	20.2	1.14	0.1	0.14	0.04	0.38	0.01	0.42	0.01	0.01	0.01	0.01	8.42	100.07
SB3-C	66	16.8	9.78	0.09	0.1	0.03	0.24	0.008	0.33	0.01	0.06	0.01	0.01	7.27	100.72

Table IV. Geochemical data of Major-elements of Palaeosoil 1 (samples SB1A to SB1-D) and 3 (SB3-A to SB3-C). LOI: loss on ignition.

Sample	Ba	Co	Cr	Cu	Li	Ni	Sc	Zn	Cs	Ta	Th	Rb	Sr	Nb	Ga	Sn	Hf	U	V	W	Y
	ppm	ppm	ppm	ppm	ppm	ppm	ppm	ppm	ppm	ppm	ppm	ppm	ppm	ppm	ppm	ppm	ppm	ppm	ppm	ppm	ppm
SB1-A	400	8	60	10	40	19	16	34	16.2	1.7	19.9	198.5	70.3	19.3	34.6	12	6.6	3.89	82	6	45.3
SB1-B	411	5	50	7	30	11	10	20	14.7	4.5	18.55	182.5	60.2	19.3	29.4	10	5.6	3.8	67	5	48.5
SB1-C	439	1	20	3	20	5	6	13	7.14	0.6	9.08	170	50.8	5.9	16.7	6	3.1	1.97	27	1	22.7
SB1-D	345	1	10	2	10	4	3	7	3.61	0.1	5.5	118	41.6	2.7	9.8	3	1.9	1.64	12	1	15.3
SB3-A	54.1	15	120	19	70	50	10	18	1.73	1.4	24.6	11.8	25.8	16.6	27	6	10.5	3.84	175	5	38.9
SB3-B	80.6	4	70	4	70	14	8	9	1.94	0.6	8.63	16.1	34.1	8	23.7	6	3.1	1.15	22	2	18.4
SB3-C	71	42	60	4	50	23	11	11	1.48	0.4	22	13.8	64.1	6.1	19.6	6	2.1	3.34	143	1	18.1

Sample	Zr	Pb	Ag	As	Cd	Mo	Tl	La	Ce	Pr	Nd	Sm	Eu	Gd	Tb	Dy	Ho	Er	Tm	Yb	Lu
	ppm	ppm	ppm	ppm	ppm	ppm	ppm	ppm	ppm	ppm	ppm	ppm	ppm	ppm	ppm	ppm	ppm	ppm	ppm	ppm	ppm
SB1-A	230	25	<0.5	<5	<0.5	<1	<10	43.8	92.2	12.05	47.5	11.1	2.07	10.15	1.69	8.39	1.59	4.48	0.61	4.16	0.53
SB1-B	211	25	<0.5	<5	<0.5	<1	<10	41.2	99	14.65	67.7	17.55	3.13	14.05	2.05	10.95	1.76	4.93	0.53	3.65	0.59
SB1-C	105	27	<0.5	<5	<0.5	1	<10	21.3	44.6	5.99	26.1	5.47	1.14	5.4	0.77	4.38	0.83	2.59	0.29	1.85	0.26
SB1-D	67	24	<0.5	<5	<0.5	<1	<10	15.9	34.6	4.04	17.5	3.86	0.75	3.12	0.51	2.71	0.5	1.66	0.24	1.38	0.21
SB3-A	368	12	<0.5	23	<0.5	1	<10	19.2	30.7	3.49	13	3.45	0.73	4.34	0.92	6.34	1.39	4.39	0.71	4.54	0.69
SB3-B	102	45	<0.5	<5	<0.5	<1	<10	33.1	41.1	3.57	9.9	1.85	0.34	2.14	0.48	2.97	0.61	1.88	0.27	1.76	0.28
SB3-C	77	63	<0.5	6	<0.5	<1	<10	147	229	17.9	43.5	5.38	0.77	3.79	0.6	3.35	0.68	1.79	0.23	1.8	0.22

Table V. Geochemical data of Minor-elements and REE of Palaeosoils 1 (samples SB1A to SB1-D) and 3 (SB3-A to SB3-C).

For a review of the geochemical methods used in the studied palaeosoils, the reader is referred to Retallack (2001) and Sheldon and Tabor (2009) (see further explanations in sub-chapter 3.4.5.2. of this thesis manuscript). All the geochemical ratios used in this study have been calculated by dividing the weight per cent of each oxide or element by its molar mass (g mol^{-1}). A summary of the most useful indexes for provenance and chemical processes in soils described

by Retallack (2001) and Sheldon and Tabor (2009) have been included in the methodology (see sub-chapter 3.4.5.2.). Similarly, several mathematical functions established by Sheldon et al. (2002) relating weathering indexes with rainfall (mm/yr) and mean average temperature per year are also included in the methodology chapter of this manuscript. These mathematical functions (P1, P2 and P3) relate Bases-to-Alumina (Table VI) and the chemical weathering indexes CIA-K (Table VII) to precipitation and are useful over a precipitation range of 200–1600 mm/yr.

Tables VI and VII show the indexes calculated in this work using the former mathematical functions.

Sample	Provenance	Hydrolysis			Oxidation	Hydration	Salinization
	Titanium / Alumina	Alumina / Bases	Barium / Strontium	Alumina / Silica	Iron+Magnesium / Alumina	Silica / sesquioxides	Alkali / Alumina
SB1-A	0,041	80,66	3,63	0,21	0,17	4,38	0,23
SB1-B	0,040	79,36	4,36	0,18	0,17	4,97	0,25
SB1-C	0,027	69,62	5,51	0,10	0,09	9,87	0,43
SB1-D	0,020	64,78	5,29	0,06	0,06	17,30	0,54
SB3-A	0,067	97,68	1,34	0,16	0,34	4,67	0,02
SB3-B	0,027	97,38	1,51	0,17	0,05	5,61	0,02
SB3-C	0,025	98,09	0,71	0,15	0,39	4,86	0,02

Table VI. Indexes used to evaluate pedogenesis and provenance of parental material.

Sample	Chemical weathering			Palaeoprecipitation		
	CIA	CIA-K	PIA	P1	P2	P3
SB1-A	80,66	97,96	97,40	1057,39	1359,73	1522,21
SB1-B	79,36	97,73	97,04	1047,21	1356,46	1515,36
SB1-C	69,62	97,79	96,28	942,44	1357,30	1517,11
SB1-D	64,78	97,02	94,07	901,47	1346,42	1494,50
SB3-A	97,68	99,25	99,24	1498,01	1378,16	1561,45
SB3-B	97,38	99,35	99,34	1534,74	1379,63	1564,64
SB3-C	98,09	99,60	99,60	1573,55	1383,18	1572,32

Table VII. Indexes used to evaluate chemical weathering and estimation of palaeoprecipitation in millimetres of MAP (Mean Annual Precipitation). See text for the formula used to obtain palaeoprecipitation P1, P2, and P3.

Based on the studied geochemical data (Tables IV and V), the mean differences between the two studied palaeosoils (1 and 3) can be summarised as follows:

From the uppermost (sample SB1-A) to the lowest horizon (SB1-D) of the profile, Palaeosoil 1 is characterised by contents of Silica (SiO_2) ranging between 62 to 87%, Alumina (Al_2O_3) from 22 to 8%, Iron (Fe_2O_3) from 3.5 to 0.4%, and Sodium (Na_2O) from 0.2 to 0.14. Potassium (K_2O) contents are around 4%. The main trend observed shows a progressive decrease in Silica at the expense of Alumina upwards in the soil profile. Regarding minor elements and REE, contents in ppm of Ba are 345 to 439, and Sr varies between 41 and 70.

Conversely, Palaeosoil 3 shows higher values in Alumina and Iron, but lower values in Potassium (K), Barium (Ba) and Strontium (Sr) than Palaeosoil 1. Values of Silica are between 63 and 69%, Alumina from 16 to 20%, Iron from 1 to 10%, Potassium from 0.24 to 0.38, Barium from 54 to 80, and Strontium from 25 to 64 ppm. In this sense, Palaeosoil 3 does not show a decrease in Silica and an increase in Alumina upwards in the soil profile as can be seen in Palaeosoil 1.

9.5. Interpretation of the palaeosoil profiles.

Three representative palaeosoil profiles have been studied in the field and sampled for subsequent laboratory analyses, consisting of the study of thin sections, clay-mineralogy identification, and whole-rock geochemistry. Field identification of palaeosoil profiles was based on the presence of vertical structures interpreted as root traces and differentiation of the profile into `palaeosoil horizons. The three profiles have common features such as their sandy texture, root traces, presence of sesquioxides and red mottling, and down-profile structuring on different horizons. However, these features seem to reflect different maturity degrees among the studied palaeosoils, being palaeosol 1 the least developed and palaeosoil 3 the most mature soil.

The palaeosoil 1 shows a conspicuous and progressive diminishment in clay minerals (kaolinite, illite, and mixed-layer illite-smectite [I/S]) from horizon SB1 – A to horizon SB1 – D (ranging from 72 % to 24 %). Conversely, an increase in quartz (and microcline, to a lesser extent) from horizon SB1 – A to horizon SB1 – D can be observed. Likewise, iron oxyhydroxide (goethite) has been observed in the two uppermost horizons of the palaeosoil (SB1 – A and SB1 – B), while it is not present in the two lowermost horizons (SB1 – C and SB1 – D) (Table III; Fig. 9.6A). These trends interpreted from the results of the X-ray diffraction analysis can be observed in thin section (Fig. 9.3). More concretely, the occurrence of abundant illuvial clay in samples SB1 – A and SB1 – B, and its progressive diminishment in samples SB1 – C and SB1 – D at the expense of quartz and K-feldspar reflects a palaeosoil profile where the K-feldspars are heavily altered into clay minerals (illuvial clay) in its uppermost horizons (SB1 – A and SB1 – B) (Fig. 9.3A, B). Conversely,

the diminishment in illuvial clay in horizon SB1 – C, and especially in horizon SB1 – D reflects the gradual transition into less altered horizons of the palaeosoil, where K-feldspar and quartz grains are progressively less affected by illuviation and hydrolysis processes than in the overlying soil horizons (Fig. 9.3C, D). Additionally, the presence of low amounts of iron oxyhydroxides such as goethite occurring as a cryptocrystalline constituent of the illuvial clay matrix (illite, kaolinite and mixed-layer illite-smectite) of the upper horizons of the palaeosoil 1 reflects an intense weathering of the soil due to the chemical process of ferrallisation, typical of well-drained tropical soils, whose higher intensity usually coincides with longer periods of soil formation, greater biomass, and stability in a given ecosystem (Nahon, 1991).

The palaeosoil 2 shows a greater accumulation of clay minerals and a finer grain size than the two other palaeosoils studied. The main characteristic observed in this palaeosoil is the gradual increase in kaolinite at the expense of illite downwards in the soil profile, and therefore the main chemical weathering process that affected the soil was illuviation (Figs. 9.4, 9.6B). The occurrence of comparatively high contents of goethite as ferruginous hypocoatings in horizon SB2 - B (Figs. 9.4, 9.6B) might have been related to periods when the soil remained waterlogged to a certain extent (Bullock et al., 1985).

In general terms, palaeosoil 3 shows similar characteristics to palaeosoil 1. However, the percentage of clay minerals and goethite tend to be higher, while quartz and K-feldspar are found in smaller amounts compared to palaeosoil 1 (Fig. 9.6). More concretely, palaeosoil 3 is characterised by very high contents of kaolinite (at the expense of illite and I/S) and moderately high ones of goethite in horizons SB3 – A and SB3 – C. The complete lack of goethite in horizon SB3 – B seems to be related to variabilities in the intensity of the chemical weathering within the horizon since the collected sample was less affected by the red mottling of the root traces (Fig. 9.2B) than those collected in the other two horizons of this palaeosoil.

The occurrence of sandstone-prone soils with abundant illuvial clay and moderate amounts of iron oxyhydroxide such as palaeosoils 1 and 3 indicates the existence of a well-drained substrate under tropical to subtropical conditions during the time of deposition. In this sense, mixed-layer clay minerals (I/S) reflect early stages of alteration in tropical soils, while conspicuous amounts of kaolinite are associated with tropical soils with good drainage conditions, and goethite is typical of leaching processes in tropical soils.

An increase in kaolinite and goethite together with a diminishment in illite and mixed-layer illite-smectite in palaeosoil 3 compared to palaeosoil 1 seem to indicate a longer period of soil formation in the former and an increase in the biomass and stability of the ecosystem (Bullock

et al., 1985; Nahon, 1991). This longer time of soil formation conforms with the field observations as palaeosoil 3 is pervasively affected by root traces and mottling compared to palaeosoil 3 (Fig. 9.2).

Conversely, the more mudstone-prone nature of palaeosoil 2 seems to suggest that it was subject to more waterlogged or, at least, it did not have the well-drained conditions that palaeosoils 1 and 2 seem to reflect. Therefore, palaeosoil 2 might have been tentatively related to the muddy floodplain areas of the distal part of the braidplain system (FA II) while palaeosoils 1 and 3 developed in more sand-prone substrates, probably related to the abandonment of alluvial channels, after they were filled with sediment, or the alluvial system migrates.

9.6. Palaeosoil classification.

To classify the type of palaeosoil into a known system, Retallack (2001) suggests the US classification system for soils (US Soil Survey Staff, 1992), which is subdivided into 12 orders. Mack et al. (1993) proposed a classification system specifically applied to palaeosoils. Considering the features of the three profiles studied and their state of development, they have been assigned here to the order Spodosols of the Retallack (2001) and Mack et al. (1993) classification systems.

The most superficial horizon of all the profiles shows a higher content of clays and it is considered an area of accumulation of clays and designated as a B horizon. However, the amount of clays, and the thickness of this horizon, which rarely exceeds 50 cm, prevents its classification as an argillic Bt horizon. The abundant vertical red mottling, clay coatings and presence of iron compounds forming opaque and amorphous zones observed in thin section, suggest its classification as a Bs horizon. The most plausible structuring of the palaeosoil profiles 1 and 3 from top to base is Bs-BC-C. Probably, the subsurface Bs horizon could be considered a spodic horizon, as most spodic horizons are levels in which organic matter, aluminium, and iron have accumulated (Soil Survey Staff, 1992). The amount of organic matter is most easily determined by dry combustion (LOI), following the suggestion of Mack et al. (1993) and references therein. As observed in the whole-rock geochemistry results, B horizons of the profiles show the highest LOI values (around 8%), suggesting more percentages of organic matter. Illuviation of iron, clays, and alumina are interpreted by observation of thin sections and variation of Hydrolysis indexes downwards in the soil profiles (Table VI). The identification of the three palaeosoil profiles as Spodosols is also based on their texture: most Spodosols have few clay-sized phyllosilicates and their particle-size class is mostly sandy and sandy-skeletal.

Spodosols are most extensive in areas of cool, humid or perhumid climates. However, they also formed in hot, humid tropical regions, mostly in areas of quartz-rich sands (Soil Survey Staff, 1992).

PART III. ANALYSIS OF THE CUENCA BASIN DURING THE MID-ALBIAN TO EARLY CENOMANIAN TIMES.

10. Palaeoenvironmental reconstruction and palaeogeographic evolution.

10.1. Sedimentary systems and stratigraphic architecture.

The mid-Albian to lower Cenomanian (Utrillas Gr – La Bicuerca Mb) sedimentary succession in the Cuenca Basin is characterised by a general transgressive trend that reflects the "mid"-Cretaceous global sea-level rise in the Western Tethys. This transgressive trend has been inferred by the sedimentological data and the occurrence of marine palynomorphs, indicating a palaeo-coastline migrating from the southeast towards the northwest (Figs. 5.1, 6.4) (Bueno-Cebollada et al., 2021). Consequently, the Northern sector of the Cuenca (Fig. 5.1) is characterised by a dominance of proximal facies associations compared to the Eastern and Southern sectors (Figs. 10.1, 10.2, 10.3).

The base of the Utrillas Gr in the studied basin is a regional unconformity represented by an erosional surface (regional unconformity surface - RUS) that overlays the upper Aptian coastal to shallow marine strata of the El Burgal Mb (El Caroch Fm) (Figs. 5.5A, 5.16B, 5.17A-C, 5.20A-D, 5.23A-C, 5.26C-D). Therefore, the regional unconformity surface at the base comprises (at least) the early Albian, not represented by sediments in the Cuenca Basin (Fig. 6.4) (Bueno-Cebollada et al., 2021). The RUS reflects the characteristics of the inherited palaeo-topography that existed during the early Albian time, which was tightly controlled by tectonism. Although the early Albian was characterised by partial erosion in the Cuenca Basin, the palaeo-topography that existed during the deposit of the Utrillas Gr was mainly controlled by the inherited tectonic structures that developed during the Late Jurassic – Early Cretaceous rifting episodes (Aurell et al., 2019; Bueno-Cebollada et al., 2022) (Fig. 10.4). In this sense, the mid-Albian to lower Cenomanian succession was deposited overlying strata of different ages (i.e., it overlays Jurassic strata in Pajaroncillo [Bueno-Cebollada et al., 2022], while in Buenache de la Sierra or Mina Pepita it overlays Aptian strata) due to non-deposition and partial erosion of pre-Albian sediments. The stratigraphic correlations carried out among the different outcrops studied in this thesis (Figs. 10.1, 10.2, 10.3) reflect the mentioned inherited structural patterns and features (i.e., faults, basement highs, etc).

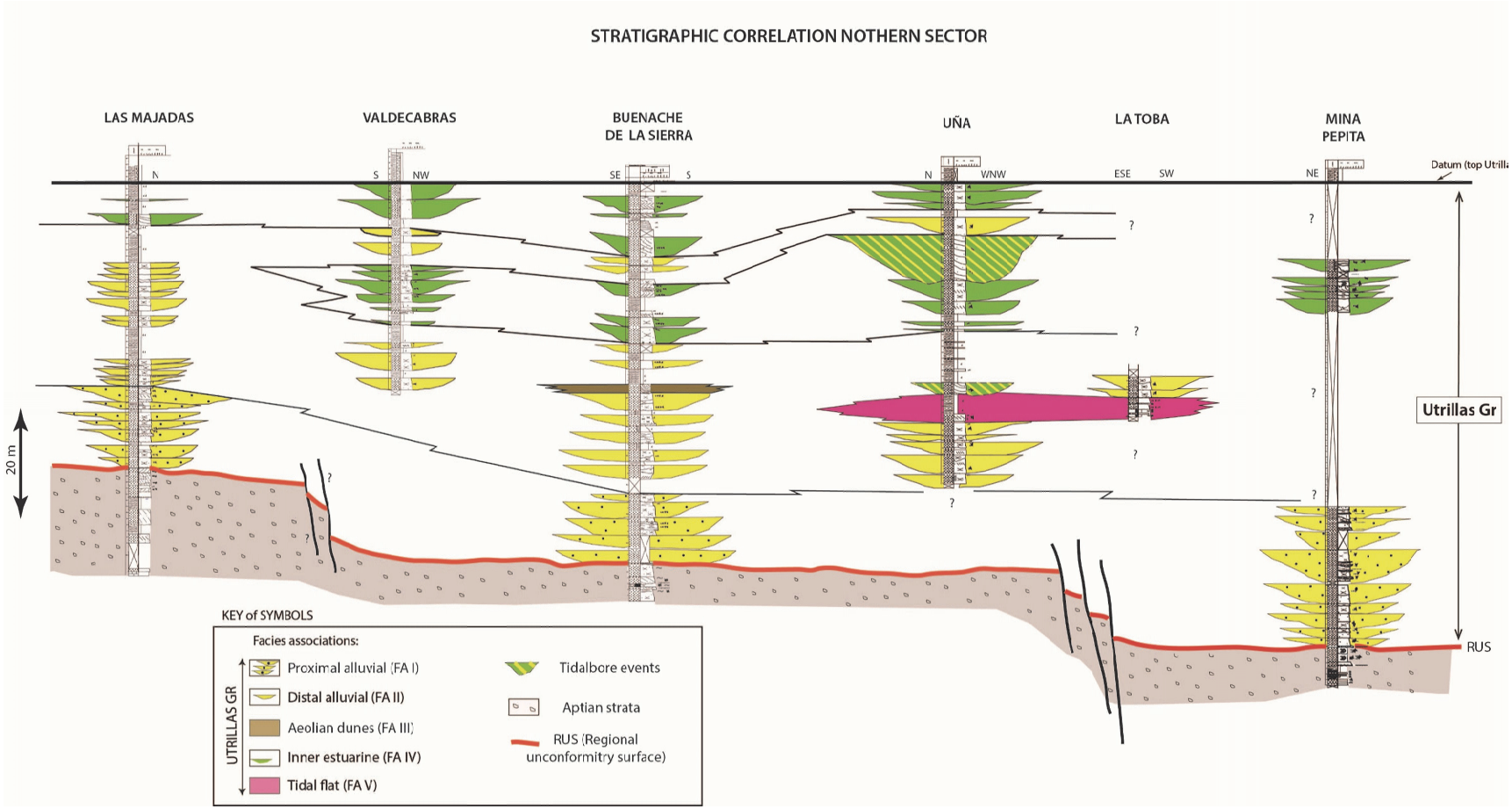

Fig. 10.1. Stratigraphic correlation of the outcrops of the Northern sector of the Cuenca Basin. See Fig. 5.1 for the relative position among the outcrops. The logged sections in high resolution are included in chapter 5 of this manuscript (Figs. 5.3, 5.7, 5.10, 5.13, 5.15, and 5.19).

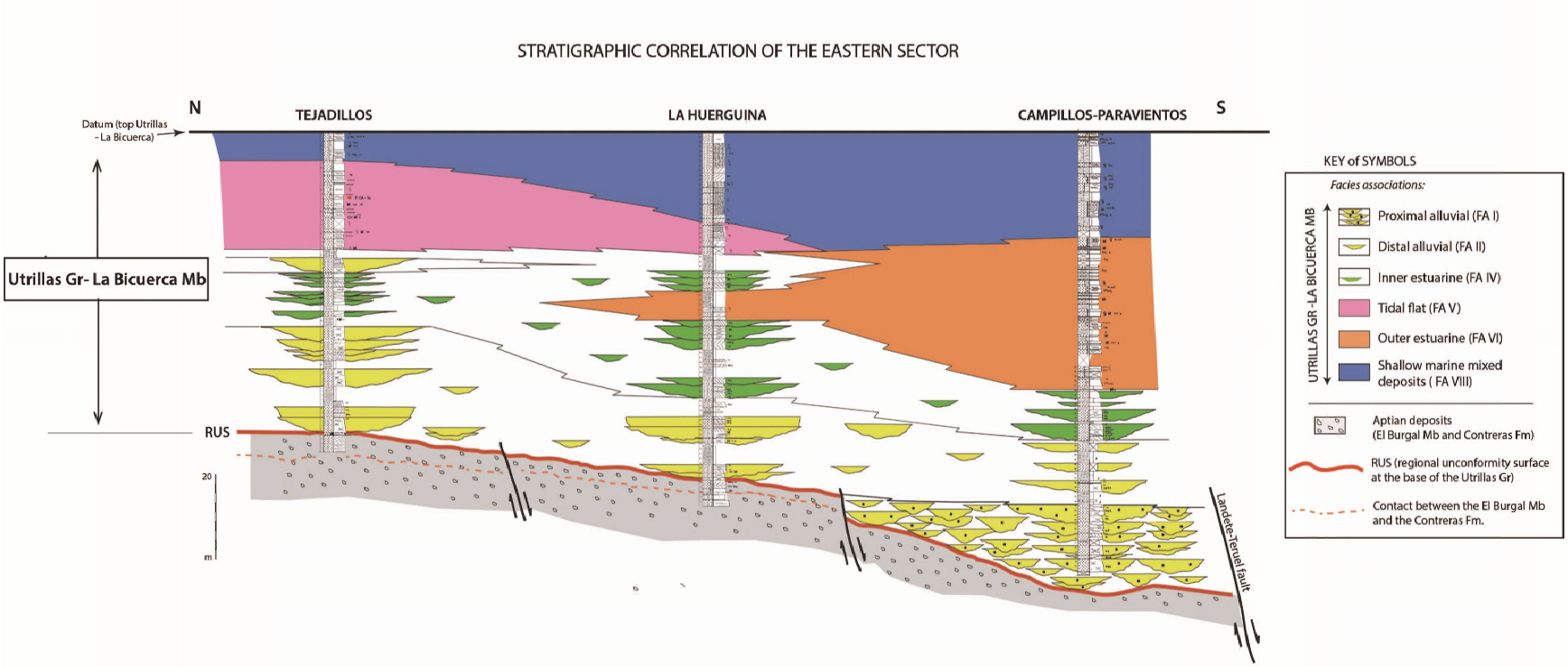

Fig. 10.2. Stratigraphic correlation of the outcrops of the Eastern sector of the Cuenca Basin. See Fig. 5.1 for the relative position among the outcrops. The logged sections in high resolution are included in chapter 5 of this manuscript (Figs. 5.22, 5.25, and 5.28).

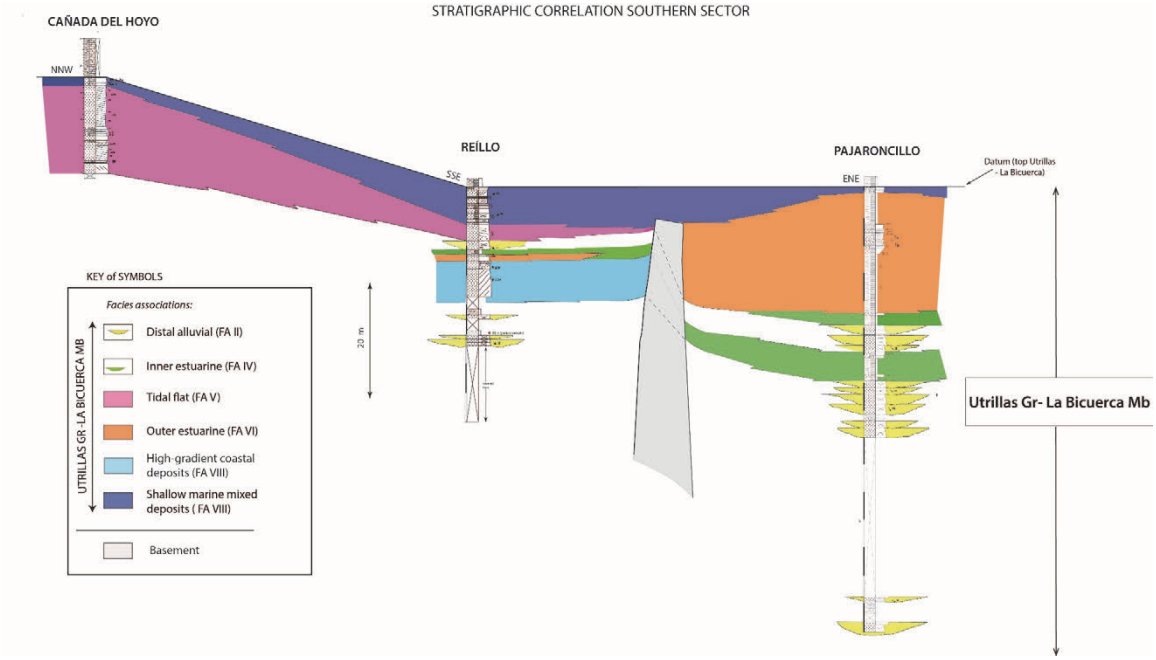

Fig. 10.3. Stratigraphic correlation of the outcrops of the Southern sector of the Cuenca Basin. See Fig. 5.1 for the relative position among the outcrops. The logged sections in high resolution are included in chapter 5 of this manuscript (Figs. 5.31, 5.33, and 5.35).

The Utrillas Gr - La Bicuerca Mb succession in the Cuenca Basin has been divided into three evolutionary stages based on the palynostratigraphic and sedimentary facies analyses performed (Fig. 10.5). The different stages correspond to the middle Albian, middle to late Albian, and late Albian to early Cenomanian times, respectively, and present marked differences in their tectonic and eustatic controls, sedimentary architecture and facies associations deposited. The three correlation panels (Figs. 10.1, 10.2, and 10.3) where the stratigraphic architecture has been reconstructed are based on the biostratigraphic dating carried out in this study and the analysis of the sedimentary trends regarding the marine influence, obtained from the sedimentary facies analysis.

- *First stage (middle Albian)* (Fig. 10.5A): the sedimentation of the Utrillas Gr in the Cuenca Basin began during the middle Albian (Bueno-Cebollada et al., 2021) and was initially characterised by the occurrence of a proximal braidplain succession (FA I). This proximal braidplain succession represents the initial infill of low-lying areas of the palaeo-topography (i.e., the lower part of the logged section in the Mina Pepita, Buenache de la Sierra, Las Majadas, or Campillos-Paravientos outcrops) owing to the activity of faults that generated local accommodation space in the basin (Figs. 10.1). In this sense, the occurrence of amalgamated components of the alluvial systems restricted to those specific geographical areas is attributed to the combination of high sediment inputs arriving in the basin from the source area (i.e., Iberian Massif), and reduced

accommodation space. Therefore, sedimentation is highly constrained by tectonics during the onset of the deposit of the Utrillas Gr, while eustatism plays a secondary role in generating (little) accommodation space. The occurrence of amalgamated sand bodies in the earlier stages of the infill reflects the deposits of migrating channels confined and unable to avulse outside the boundaries of a distinct valley, located upstream from backwater effects and being tributive in nature (Blum et al., 2013).

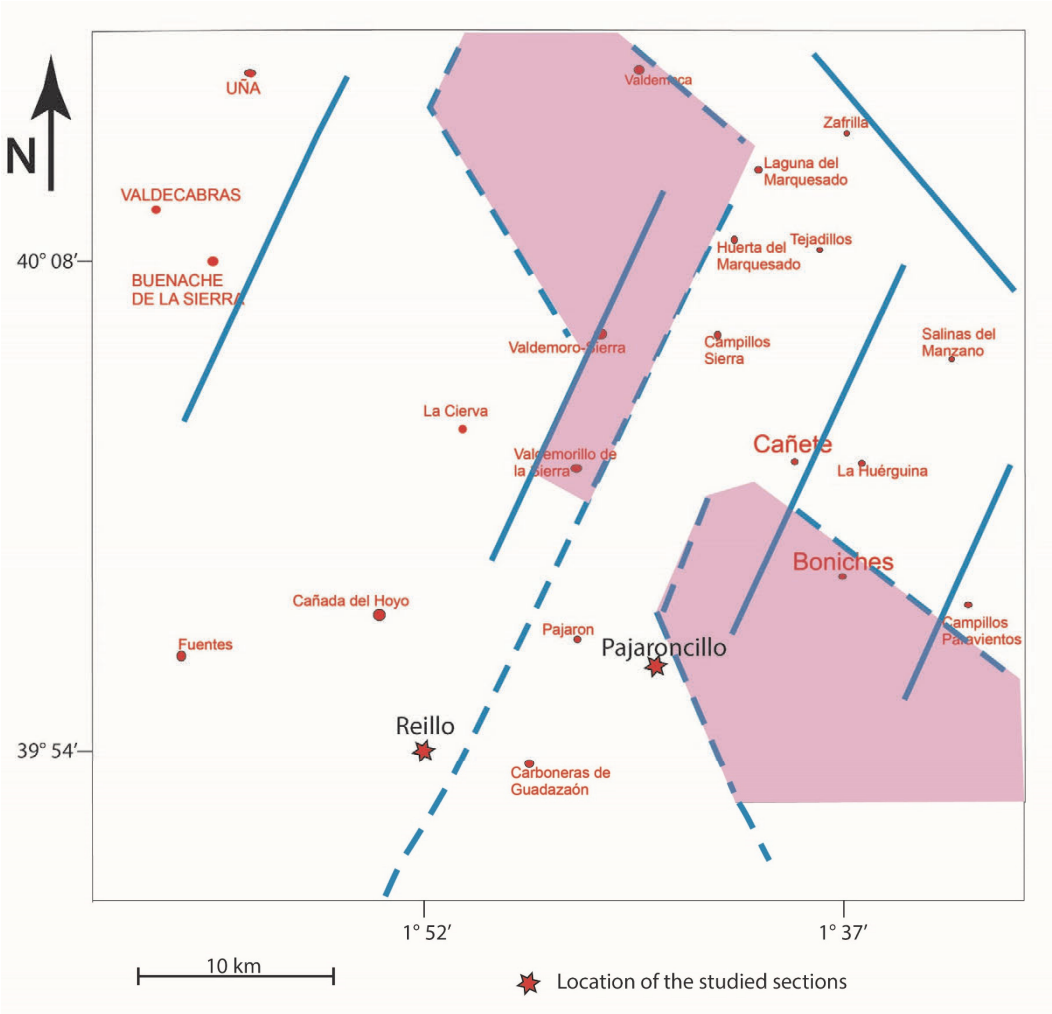

Fig. 10.4. Palaeostructural map of the Serranía de Cuenca region. The palaeotectonic guidelines corresponding to the main structural elements that existed in the area during the (post-Triassic) Mesozoic, which affected sedimentation in the study area during the Albian, are shown. Non-coloured areas in the map, represent those areas where the sedimentation of the Utrillas Gr - La Bicuerca Mb was mostly active and has been preserved, although it is not always outcropping. Shaded areas indicate eroded or non-depositional areas for the Lower to "mid"-Cretaceous succession. Blue lines represent the main syn-sedimentary faults interpreted. The geographical location of the measured sections (Reíllo and Pajaroncillo) is indicated by red stars. This map is based on the structural data presented by Aurell et al. (2019). Original figure from Bueno-Cebollada et al. (2022).

In the study area, the proximal braided deposits (FA I) evolve into distal braided deposits (FA II) upwards in the succession during the middle Albian (Figs. 10.1, 10.2, 10.3, 10.6A). Therefore, the distal braided deposits became widespread and were characterised by palaeosoil development such as, for instance, the ones studied in the Buenache de la Sierra outcrop (see chapter 9 of this manuscript). These mud-rich successions with less amalgamated bodies than those observed in the proximal part of the braidplain system reflect aggradation in continental areas in response to relative sea-level rise (Fig. 8.2). This change into a non-amalgamated alluvial architecture (from FA I into FA II) reflects the progressive increase in the accommodation space relative to the sediment input as the sea level rose due to the marine transgression during the middle Albian and indicates that the eustatic control has become more important. According to Blum et al. (2013), non-amalgamated mud-rich alluvial deposits form within the zone of backwater effects, are fundamentally avulsive and distributive, and occur as a landward-tapering wedge that onlaps the amalgamated components. The lack of marine palynomorphs and the presence of pollen of Araucariaceae in the distal braided deposits (FA II) in Reíllo (pollen sample RE-1) during the mid-Albian seem to reflect relative proximity to the sea (Bueno-Cebollada et al. [2021] and references therein) in continental deposits.

Consequently, it conforms with the hypothesis of them occurring near or within the zone of backwater effects, yet landwards from the tidal limit. These interpretations seem to agree with previous palaeo-geographic models for the middle and late Albian, which report the existence of coastal and marine coeval deposits in the Valencia Basin and reflect the expansion of the Western Tethys in Iberia (Segura et al., 2004; Sopeña et al., 2004; Bueno-Cebollada et al., 2021). Additionally, the occurrence of subordinate aeolian dune deposits (FA III) associated with the braidplain system (Bueno-Cebollada and Meléndez, 2018) reflects arid conditions in the Cuenca Basin during the middle Albian to early Cenomanian times. This fact agrees with the occurrence of a coeval well-developed erg system in the Maestrazgo Basin, where the sedimentary succession is dominated by aeolian dunes (Rodríguez-López et al., 2008, 2009, 2010, 2012, 2013). In this sense, ephemeral alluvial and aeolian deposits tend to spatially co-exist (to different degrees) in arid settings exhibiting a wide range of sedimentary interactions that give rise to considerable complexities in terms of stratigraphy and geomorphology (Al-Masrahy and Mountney, 2015).

- *Second stage (middle to late Albian)* (Fig. 10.5B): During the middle to late Albian, the braidplain system (FA I and FA II) was overlain by a transitional facies belt (Fig. 10.5B) characterised by

estuarine and coastal plain facies associations that dominated the palaeogeography of the Cuenca Basin because of the marine transgression, interacting with alluvial braidplain deposits (Fig. 10.6B). At this point, the sedimentary succession in the Northern sector is represented by an interaction of inner estuarine deposits (FA IV) that alternate in time and space with a distal braidplain succession (FA II). However, the most proximal outcrops of the Northern sector (i.e., Las Majadas outcrop) remained dominated by distal braidplain deposits (Figs. 10.1, 10.6B). Additionally, Chamizo-Borreguero et al. (2016) reported the existence of strong tides in the Cuenca Basin during the Albian that led to the development of tidal flats and the occurrence of tidal bore surges that reached the Uña outcrop, filling up deep erosional scours after relative sea-level falls within an overall transgressive setting. The occurrence of tidal bore events (only preserved as tidal bore deposits in Uña) might have been favoured by the funnel-shaped configuration (a narrow and long embayment) of the sedimentary basin, controlled by syn-sedimentary tectonism, together with the existence of strong semi-diurnal tides in the Western Tethys (Chamizo-Borreguero et al., 2016 and references therein).

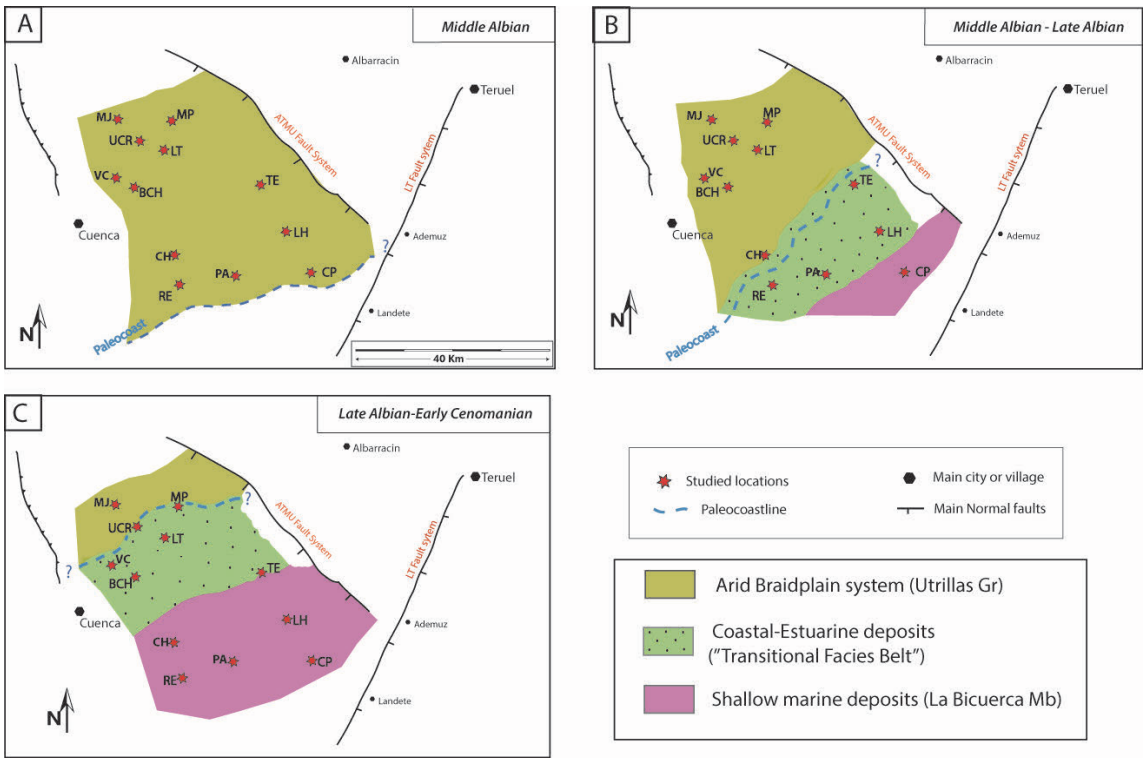

Fig. 10.5. Palaeogeographic reconstruction and palaeo-coastline location during the middle Albian to early Cenomanian transgression in the Cuenca Basin based on the palynological data analysed and the stratigraphy of the studied sections. (A) Middle Albian; (B) Latest middle Albian to late Albian; (C) Late Albian to early Cenomanian. Main fault systems bounding the study area are also represented (ATMU, Alto Tajo-Montes Universales Fault System; LT, Landete-Teruel Fault System). Modified from Bueno-Cebollada et al. (2021).

Conversely, the Eastern and Southern sectors show a very different picture during the late Albian due to their more distal location within the Cuenca Basin (Fig. 10.6B). In this way, the Eastern sector and Pajaroncillo outcrops are characterised by developing an estuarine setting dominated by supra- to intertidal environments in their proximal part (FA IV) and by a supratidal environment that presents migrating tidal dunes (FA VI). In the case of the Pajaroncillo outcrop, the succession at this point is dominated by mudflats developed in a protected environment. Conversely, the Reíllo outcrop is characterised by a high energy open coast environment (FA VIII) (Fig. 10.3) (Bueno-Cebollada et al., 2022). The main characteristic of this open coastal environment is the occurrence of high-gradient foreshore deposits and an upper shoreface dominated by small dunes and asymmetrical ripples, indicating a wave-dominated shoreline with predominantly nonbarred morphology (Isla et al., 2020) typical of reflective beaches (Asgaard et al., 2013). In this sense, the presence of coeval coastal sedimentary environments with very different energy regimes in the Cuenca Basin results from a highly compartmentalised basin that presented elevated basement areas, controlled by the activity of inherited syn-sedimentary faults (Fregenal-Martínez et al., 2017; Aurell et al., 2019). This compartmentalization resulted in a rugged coastal morphology which significantly conditioned the distribution and type of sediment and generated thresholds limiting the inland advance of the marine transgression (Bueno-Cebollada et al., 2022).

Additionally, the coastal to marine indicators (pollen assemblages including dinoflagellate cysts, along with high frequencies of Cheirolepidiaceae and Araucariaceae pollen grains) (Appendix II) identified in the samples collected in the Campillos-Paravientos, La Huérgina and Tejadillos outcrops, provide evidence that the palaeo-coastline was located at the Eastern and Southern sector during late Albian times (Figs. 10.5B, 10.6B) (Bueno-Cebollada et al., 2021). These palynological interpretations conform with the sedimentological data presented in this thesis manuscript and also agree with previous sedimentological studies carried out in the Tejadillos and La Huerguina outcrops (Chamizo-Borreguero 2006; Chamizo-Borreguero et al., 2008), which interpreted the succession as deposited in inter- to subtidal environments.

- *Third stage (Late Albian to early Cenomanian)* (Fig. 10.5C): During the late Albian to early Cenomanian times, the transgression became more generalised in the Cuenca Basin and the inception of a mixed shallow marine ramp began in the Southern and Eastern sectors while the Northern sector was dominated by a coastal plain alluvial to inner estuarine environment (Fig. 10.5C). The creation of accommodation space during the late Albian to early Cenomanian times was mainly ruled by eustatism; however, the occurrence of local tectonism is interpreted based

on variabilities in the depositional thicknesses of the logged sections (i.e., Reíllo and Pajaroncillo outcrops [Fig. 10.3]) (see chapter 13 of this manuscript for further explanation).

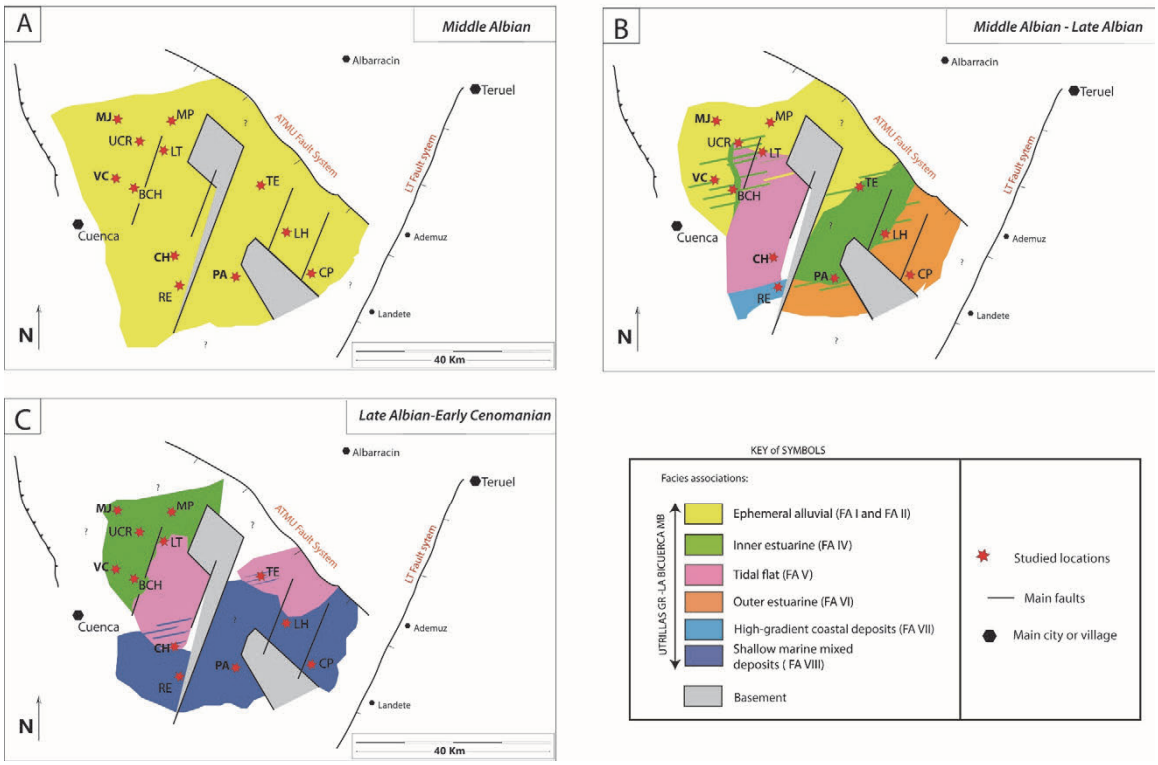

Fig. 10.6. Facies association distribution with the main structural elements during the middle Albian to early Cenomanian in the Cuenca Basin. (A) Middle Albian; (B) Latest middle Albian to late Albian; (C) Late Albian to early Cenomanian. Main fault systems bounding the study area are also represented (ATMU, Alto Tajo-Montes Universales Fault System; LT, Landete-Teruel Fault System). Modified from Bueno-Cebollada et al. (2021).

In the outcrops of the Northern sector of the study area (Fig. 10.1), the palynomorphs reflect the mixture of freshwater or brackish aquatic settings, including taxa such as *Tetraporina* sp. and *Botryococcus braunii* (Fig. 6.6; Bolkhovitina, 1953; Guy-Ohlson, 1992) and exclusively marine ones (i.e., dinocysts, linings of foraminifera) at level LT-2, as well as of acanthomorph acritarchs at the LT section (Fig. 6.6; Appendix II), suggesting the existence of a coastal plain to estuarine environment (Fig. 10.5C) (Bueno-Cebollada et al., 2021). The proliferation of acanthomorph acritarchs, mainly *Micrhystridium*, indicates a partly enclosed, shallow, inshore environment (Schrank, 2003). Tides represent the dominant process responsible for mixing fresh and marine water, controlling the sediment distribution and style. However, the effects of tides can be noticed at locations further landwards from the saline and brackish water limits (Shanley et al., 1992 and references therein). Although tides are the primary process controlling sedimentation in estuaries, their effects can be modified to a great extent by the alluvial discharge. In this sense,

when the alluvial discharge is reduced, marine and brackish water and tidal action may penetrate upstream in the estuary, giving rise to tidally-influenced alluvial deposits (Shanley et al., 1992). Additionally, a previous sedimentological study conducted in the Uña outcrop mentions the occurrence of supratidal to intertidal deposits in the upper intervals of the Utrillas Gr (Chamizo-Borreguero et al., 2016), which conforms with the results of this thesis. Therefore, all these data point to a coastline position either at or relatively close to the outcrops of the Northern sector during late Albian to ?early Cenomanian times (Fig. 10.6C) yet in any case located landwards relative to previous palaeo-coastline locations (Bueno-Cebollada et al., 2021).

Conversely, a tide-dominated (and wave-influenced) mixed shallow marine environment (FA VIII) took place in the Eastern and Southern sectors, mainly characterised by the development of tidal dunes, during the late Albian – early Cenomanian times (Figs. 8.12, 10.1, 10.2, 10.6C). Tidal currents are an effective sorting agent. The sediment usually becomes finer in the direction of sediment transport, in a way that the coarser sediment will be more present at the up-current end of the tidal transport path, where the current tends to be faster, passing into finer sandy and muddy deposits in more distal areas of the shelf (Reynaud and Dalrymple, 2012). This fact conforms with the occurrence of mudstones interbedded with tidal dune sandstones in the shallow marine deposits of the Campillos-Paravientos outcrop located in a more distal position, down-current in the tidal transport path (Fig. 5.28, 10.2). Conversely, the more amalgamated sedimentary architecture of the tidal dunes in the La Huérguina outcrop might have been related to its more proximal position within the tidal transport path. Besides, carbonate grains account for being one of the essential constituents of the shallow-marine deposits (at this point of the succession) in the Eastern and Southern sectors due to tidal current action enhancing the mixing of nutrients from the open sea and fostering carbonate production (Reynaud and Dalrymple, 2012). This fact would explain the increase in carbonate upwards in the succession of the Utrillas Gr – La Bicuerca Mb, which seems to reflect the Albian – Cenomanian transgression in the Cuenca Basin, as well as the existence of coeval open-sea carbonate platforms further S and SE in the Valencia Basin (Segura et al., 2004; Sopeña et al., 2004).

In this sense, the progressive northwestward migration of the coastal and marine facies associations highlights the “mid”-Cretaceous transgression in the Cuenca Basin (Figs. 10.5, 10.6), leading to the progressive drowning of an arid braidplain system. This process gave rise to an assortment of transitional coastal to estuarine environments and the later inception of a shallow marine mixed ramp that precluded the advent of the shallow marine platforms that dominated sedimentation in Eastern Iberia during the Late Cretaceous.

10.2. Palaeoflora and palaeoenvironmental constraints.

10.2.1. Middle Albian to early Cenomanian palynofloral evolution.

The middle Albian to early? Cenomanian palynofloras of the Utrillas Gr are characterised by low percentages of pteridophyte spores and dominated by pollen of conifers, mainly of cheirolepidacean (*Classopollis* spp.) and cupressacean (*Inaperturopollenites dubius*) affinities (Appendix II; Fig. 7.1B, C).

In both the TU and CT sectors, the pollen of cheirolepids and cupressacean may exhibit antagonistic percentage fluctuations in some of the studied levels (Fig. 7.1B, C). Although the most relevant cupressaceous taxon is by far *I. dubius*, the occurrence of pollen of taxodioids (*Perinopollenites halonatus* and *Taxodiaceaepollenites hiatus*) in the samples from the La Toba section (Appendix II), although scarce, might indicate the local existence of freshwater to brackish swamps or lagoons. Conversely, it is possible that *I. dubius* was produced by a drought-tolerant plant as it happens with some recent cupressaceous taxa such as *Cupressus*, *Juniperus* and *Tetraclinis* (Farjon, 2005). In this sense, Moreau et al. (2015) reported the occurrence of pollen grains that resemble inaperturate morphotypes within microsporophylls of the *Glenrosa carentonensis*, interpreted as a xerophytic shrub from the Cenomanian of France.

A higher proportion of Cheirolepidiaceae (*Classopollis* spp.) in the CT sector (Fig. 7.1C) could be related to marginally drier and/or saline environments (Alvin,1982; Vakhrameyev, 1991; Ulicný et al., 1997; Peyrot et al., 2019). However, the higher percentages of cheirolepidacean conifers (approximately 55%) in the sample RE-1 and the complete lack of marine palynomorphs indicate that this sample represents a more landwards area of the ecosystem. In this sense, the palynological data conforms with the sedimentological analysis that interpreted the strata where the sample RE-1 was collected as distal braidplain deposits lacking marine influence (FA II) (Fig. 10.3). Therefore, cheirolepidacean conifers might have constituted an essential part of the inland vegetation, suggesting more arid conditions than those of the coastal fringe where Cupresacceae become progressively more dominant. Similarly, a progressive increase in Cupressaceae at the expense of Cheirolepidiceae can be noticed in the TU sector (late Albian to early? Cenomanian) compared to the CT sector (mid- to late Albian), which might suggest a progressive replacement of the coastal vegetation during the time span of deposition of the Utrillas – La Bicuerca Mb succession. Consequently, cheirolepidacean conifers might have competed with cupressaceaen ones, occupying either the driest areas of the depositional

environments or water-stressed settings in saline to brackish nearshore sub-environments (Peyrot et al., 2019).

In addition, the conspicuous (but significantly lower) percentages of Araucariaceae in the TU and CT sectors may represent the local coastal vegetation due to the habitat preference of this conifer family (Abbink et al., 2004), also favoured by the limited dispersal potential of the araucariacean pollen (Peyrot et al., 2019). In this sense, the relationship between Araucariaceae and Cheirolepidiaceae and the exact nature of the Albian coastal assemblages of the Cuenca Basin is analysed more thoroughly based on the studied macrofloras from the Cañada del Hoyo outcrop (see chapter 10.2.2.).

In general, the Albian vegetation in the Cuenca Basin was composed of drought-tolerant arboreal and/or shrubby conifers associated with arid coastal environments that constituted the background vegetation of a braidplain system, dominated by ephemeral alluvial deposits within a transgressive setting (Chamizo-Borreguero et al., 2016; Bueno-Cebollada and Meléndez, 2018; Bueno-Cebollada et al., 2021, 2022). On the other hand, the presence of low percentages of spores of ferns and allies together with minor amounts of angiosperm pollen (Fig. 7.1B, C, Appendix II) might reflect vegetation growing in ponded areas of the floodplains where the water-table level was high, or in coastal marshes with relative freshwater input.

Additionally, the occurrence of small amounts of bisaccate pollen attributed to Pinaceae/Podocarpaceae affinities may reflect allochthonous flora growing in coeval highland areas, such as the Iberian Massif (Rodríguez-López et al., 2020). These bisaccate pollen grains might have been transported as air-borne particles and deposited in lowlands such as the study area due to the high (anemophilous) dispersal potential of these morphotypes of pollen. This hypothesis also seems to agree with the occurrence of slightly more significant amounts of bisaccate pollen in the TU sector than in the CT sector, as the former is located to the northwest of the Cuenca Basin in a position closer to the Iberian Massif.

The prevalence of arid climate conditions in Iberia during the Albian, as previously recorded in the Basque-Cantabrian Basin (Rodríguez-López et al., 2020) and the (eastern) Iberian Basin (Rodríguez-López et al., 2008, 2009, 2010, 2012), has been related to the northward migration of the climate belts. This movement of the climate belts left most of Iberia under the influence of the Northern Hot Arid belt (NHA belt) due to latitudinal shifts in the caloric equator and coinciding with the deposition of the Utrillas Gr succession at a palaeolatitude of 25° to 30° N (Chumakov et al., 1995; Rodríguez-López et al., 2009, 2012, 2020). Therefore, the studied mid-Albian to early Cenomanian palynofloras reflect a relative shift towards more arid conditions in

southern/southeastern Iberia based on the increase in xerophytic taxa, compared to the late Aptian palynofloras, and conforms with sedimentological studies that interpret the Utrillas Gr succession as an arid braidplain system in the Cuenca Basin (Chamizo-Borreguero et al., 2016; Bueno-Cebollada and Meléndez, 2018; Bueno-Cebollada et al., 2022).

Likewise, coeval palynofloras from the Algarve Basin, Western Iberia (Heimhofer et al., 2012), contrast with the mid-Albian to early Cenomanian palynofloras from the Cuenca Basin since the former palynofloras seem to record more oscillations in the proportion of xerophyte and hygrophyte taxa throughout the sedimentary succession. This fact might be attributed to the location of the Algarve Basin closer to the boundary between the NHA and the Northern Mid-latitude Warm Humid belt (NMWH belt), being more prone to oscillations in the position of this boundary (Chumakov, 1995; Heimhofer et al., 2012). Conversely, the Cuenca Basin, located toward the southeast of Iberia, might have been situated deeper within the NHA belt, recording fewer oscillations with the NMWH belt. Therefore, the climate would have remained comparatively drier in the Cuenca Basin, allowing the development of drought-adapted ecosystems dominated by cheirolepidiacean and cupressacean conifers and low percentages of hygrophyte taxa.

Regarding angiospermous palynofloras, it is not easy to compare the Albian taxa of the assemblages from the TU and CT sectors with those from the Albian assemblages from Portugal. In general, the Portuguese palynofloras are much more diverse in taxa since they comprise approximately 50 taxa identified in the Albian levels of the Cresmina and Luz sections (Heimhofer et al., 2007) and 80 in the São Julião section (Horikx et al., 2016). Additionally, some of the identified taxa, such as *Ajatipollis*, *Cretacaeiporites*, *Penetetrapites, Racemonocolpites* and *Senectotetradites,* are not found in the Cuenca Basin. Conversely, monoaperturate species of *Crassipollis* and *Transitoripollis* have been identified in the studied assemblages.

10.2.2. Palaeoecological and palaeoclimatic interpretations of the Cañada del Hoyo fossil plant bed.

In the studied fossil plant site in the Cañada del Hoyo outcrop, the conifer shoots identified as *Glenrosa* sp. (Fig. 7.5) are found in association with abundant compressions of shoots attributed to *Frenelopsis* (Fig. 7.2) and, to a lesser extent, to *Dammarites* and *Erethmophyllum*.

Several authors (i.e., Watson and Fisher, 1984; Srinivasan, 1992; Moreau et al., 2015) noted that plant remains assignable to the genus *Glenrosa* are frequently found in association with other

cheiroplepidiacean conifers, mainly *Frenelopsis* and *Pseudofrenelopsis* Nathorst emend. Watson. In this regard, Zhou et al. (2000) and Gomez et al. (2012) suggest that *Glenrosa* was a shrub-like plant that grew with stands of cheirolepideacean conifers in well-drained substrates.

The morphological features and microstructure that characterise the genus *Glenrosa* (for instance, small scale-like leaves, thick cuticles, or the occurrence of sunken stomata at the bottom of stomatal crypts) reflect extreme xeromorphic adaptations (Zhou et al., 2000; Gomez et al., 2012). Thus, the genus *Glenrosa* has been linked to environments with strong marine influence such as a lagoon or coastal depositional systems suggesting that they might have been highly tolerant to hyper-saline conditions (Upchurch and Doyle, 1981). Similarly, it has been associated with hot and dry climates with high evaporation rates (Zhou et al., 2000) and disturbed coastal environments (Moreau et al., 2015).

Additionally, some *Glenrosa* species (i.e., *G. Falcata*) inhabited continental freshwater environments subject to seasonally dry climates, suggesting that they were not necessarily restricted to nearshore hyper-saline environments. Therefore, the xerophytic features of *Glenrosa* are interpreted as an adaptation to seasonal drought and/or the abundance of salt or alkalis due to high evaporation rates (Gomez et al., 2012).

The common occurrence of the genus *Frenelopsis* has been associated with a broad spectrum of ecosystems ranging from alluvial floodplains and freshwater lakes to coastal plains and brackish swamps, where the most likely formed mangrove-like plant communities (i.e., Kvaček, 2000; Falcon-Lang et al., 2006; Mendes et al., 2010). In this sense, the species *F. alata* was a widespread Cenomanian species found in western Europe assemblages as part of the vegetation in nearshore environments (i.e., salt marshes) that in some cases grew together with *Erethmophyllum obtusum* and *Dammarites albens* (Kvaček, 2000). These plant communities probably formed marsh/mangrove hábitats (Kvaček, 2000). In this regard, some species that belong to the genus *Dammarites* (i.e., *D. albens* or *D. coriacea*) are considered halophytic plants, despite their broad leaves (Fig. 7.4), normally growing in salt marshes under brackish conditions (Barale, 1992; Ulicny et al., 1997; Kvaček and Lobitzer, 2010). In the Cañada del Hoyo outcrop, this araucariacean conifer is commonly found in assemblages dominated by *Frenelopsis* and scale-like leaf conifers (*Glenrosa*) associated with coastal deposits.

The leaf morphology of *Erethmophylum* (i.e., broadleaves) seems to conform with that of a less xeromorphic species (Kvaček et al., 2005; Li et al., 2018) than the rest of the taxa found in the assemblage from the Cañada del Hoyo outcrop (*Frenelopsis* sp., cf. *Glenrosa* sp. and *Dammarites* sp.). However, the epidermal characters of *Erethmophyllum* (i.e., sunken papillate stomata, enclosure of ovules in sterile tissues) may suggest xeromorphic adaptations (Kvaček et al., 2005).

The occurrence of *Erethmophyllum* has been related to mid-latitude seasonal climate with a moist rather than arid environment, associated with plant assemblages from humid and warm climates (Li et al., 2018). However, it has also been related to brackish, water-stressed conditions typical of salt marshes under a seasonally dry subtropical climate (Falcon-Lang et al., 2001; Kvaček et al., 2005).

In this sense, the dominance of thermophilic conifers with adpressed scale-like leaves (i.e., *Glenrosa*) and *Frenelopsis* with anecdotal occurrences of *Erethmophyllum* in the assemblages from the Cañada del Hoyo outcrop suggest a seasonally dry climate as the most plausible palaeoclimatological hypothesis. This hypothesis is reinforced by the lack of assemblages dominated by seasonally deciduous ginkgoaleans and czekanowskialeans (Li et al., 2018), together with low percentages of hygrophilous taxa (i.e., Pteridophyte spores) in the palynological assemblages at the scale of the Cuenca Basin (Bueno-Cebollada et al., 2021).

The palaeoecological implications of the plant assemblages from the Cañada del Hoyo outcrop conform with the sedimentological data obtained from the facies analysis. The studied compressions were found in strata that were interpreted as deposited in an open intertidal flat setting (FA V) (Fig. 5.36B, C) and given the disjointed nature of the studied plant remains, they should have been subject to transport and later deposition. Most likely, the studied plant community developed landwards in supratidal marshes, and their remains were transported seawards over short distances by tidal creeks until they were deposited in an intertidal flat setting. Thus, the studied plant remains can be considered parautochtonus.

Additionally, the study of this local plant community at the Cañada del Hoyo outcrop may shed new light on the regional basin-scale palynological study carried out as a part of this Ph.D. thesis (Bueno-Cebollada et al., 2021). The fact that the far more abundant two pollen taxa identified belong to the genus *Classopollis* (*Classopollis* Spp.) and *Inaperturopollenites* (*I. dubius*) and seem to be represented in the local scale of the Cañada del Hoyo outcrop by the dominance of the *Frenelopsis* sp. and conifers with adpressed scale-like leaves such as *Glenrosa* sp., respectively. In this regard, it is well-known that the producer of the *Classopollis*-type pollen belongs to the genus *Frenelopsis* (Hlustik and Konzalová, 1976; Srivastava, 1976). Conversely, the affinity between *Glenrosa* sp. and *Inaperturopollenites*-type pollen (*I. dubius*) is tentatively suggested in this thesis memoir based on the possible occurrence of inaperturate pollen morphotypes within the microsporophylls of *Glenrosa carentonensis* (Moreau et al., 2015) and the dominance of *Inaperturopollenites* in the mid-Albian to early Cenomanian palynological assemblages from the Cuenca Basin (Bueno-Cebollada et al., 2021). In addition, the less common occurrence of the

conifer *Dammarites* and the ginkgoal *Erethmophylum* among the compressions in Cañada del Hoyo seems to agree with the lower percentage of araucariacean and *Cycadophytes*-type pollen grains in the whole Cuenca Basin (Appendix II) (Bueno-Cebollada et al., 2021).

10.3. Palaeosoils and their palaeoclimatic implications.

The studied palaeosoils in the Buenache de la Sierra outcrop are developed in the distal part of an alluvial system dominated by multistorey channels among which aggradational floodplain mudstones and siltstones develop (Facies association II; Fig. 8.2) close to the palaeocoast, yet still landward from the tidal limit (Figs. 9.1, 9.2).

The occurrence of significant amounts of K-feldspars in the lower and less weathered horizons of the studied palaeosoils (i.e., horizons SB1 – C and SB1 – D; Table III) and the even higher amounts of the non-weathered alluvial sandstones seem to suggest that the feldspars arrived in this area of the basin in large amounts, indicating a lack or very weak chemical weathering processes in the source areas (or in more proximal areas of the basin). Therefore, it suggests that the alteration of the feldspars into clay minerals took place once the sediment was deposited in the distal part of the alluvial system where the palaeosoils developed.

This seems to indicate arid conditions in the source area and/or proximal areas of the basin that prevented the pervasive chemical weathering of the feldspars until they reached more distal areas of the braidplain system where annual rainfall was significantly greater due to the influence of the ocean. Under these conditions, the sediment would have been transported by the action of ephemeral channels and watercourses that were seasonally wet. In this sense, the lack of palaeosoil development, presence of ventifact pebbles and frequent deflation lags in the FA I (Fig. 8.1) in the study area (i.e., lower part of the Buenache de la Sierra, Mina Pepita, and Campillos-Paravientos outcrops) represent these more arid conditions of the proximal facies belt of the braidplain system. Conversely, the upwards transition of the deposits of the FA I into the palaeosoil-bearing FA II indicates an increase in the rainfall regime.

The existence of arid conditions during the mid-Albian to early Cenomanian in the Cuenca Basin is also supported by the palyno- and macroflora presented in this Ph.D. thesis (see chapter 7 of this manuscript) and in Bueno-Cebollada et al. (2021). The palynological assemblages are dominated by cheirolepidacean (mainly *Classopollis*) and cupressacean conifer pollen with low amounts of spores of pteridophyte and Araucariaceae or Pinaceae (Bueno-Cebollada et al., 2021). Similarly, the mid-Albian to early Cenomanian macrofloras from the Cuenca Basin are dominated by cupressoid (Cheirolepidiaceae and/or Cupressaceae) conifer taxa (*Frenelopsis*,

Glenrosa) characterised by presenting xerophytic features such as scale-like leaves (Fig. 7.5) or sunken stomata (Fig. 7.3).

The development of an ecosystem dominated by xerophytic taxa in the Cuenca Basin during mid-Albian to early Cenomanian agrees with previous works dealing with the sedimentology of the Utrillas Gr both in the study area (Chamizo-Borreguero et al., 2016; Bueno-Cebollada et al., 2018) and to the east of the study area, in the Maestrazgo Basin (Rodríguez-López et al., 2008, 2009, 2010, 2012). However, the intense chemical weathering conditions under which the studied palaeosoils formed indicate that palaeoprecipitation should have been intense. The results obtained from the studied palaeosoil profiles agree with the occurrence of well-drained soils affected by high-intensity seasonal rains (i.e., the presence of opaque fabrics of iron oxides and hydroxides, high values of chemical indices, and alteration of K-feldspars into kaolinite [Retallack, 2001; Sheldon and Tabor, 2009]). The estimation of palaeoprecipitation in millimetres of MAP (Mean Annual Precipitation), based on the CIA-K and Bases to Alumina of B horizons of the palaeosoil 1 and palaeosoil 3 profiles shows values between 1047 to 1515 (Palaeosoil 1) and 1534 and 1564 (Palaeosoil 3) (Table VII). These values agree with soils of tropical, alternating wet and dry climates (Retallack, 2001). It is important to emphasise that these equations are not precise and do not represent accurate values yet allow tentatively inferring an annual rainfall of around 1000 - 1500 mm. Additionally, it should be considered that the high mean temperatures that characterised most of the Cretaceous might have been the driver of very high evaporation rates leading to more arid environmental conditions, especially during drier seasons and periods (Haywood et al., 2004). Therefore, the information obtained should be calibrated with other palaeoclimatic criteria such as the mineralogy of the palaeosoil profiles and palaeofloras data.

The marked xerophytic character of the palaeoflora together with the intense rainfall conditions inferred analysis points out to a relatively arid climate with a pronounced seasonality, probably characterised by a wet season with monsoon-like climatic conditions, given the tropical palaeolatitude of Iberia during the “mid”- Cretaceous (25°- 30°N) (Rodríguez-López et al., 2008, 2010). The most plausible climatic model that conforms with these datasets is that of a tropical savanna biome typically characterised by two distinct seasons regarding rainfall, where the overall amount of evaporation is higher than that of precipitation. Tropical savannas differ from other tropical forest ecosystems (i.e., rainforests) in that they have less rainfall (normally it is around 800 to 1600 mm per year), which is markedly seasonal and typically unforeseeable within seasons (Alberts et al., 2014). Regarding temperature, however, they tend to be torrid and present slight variation across the year. Consequently, vegetal productivity in the current

tropical savanna biome exhibits a marked seasonality that is driven by rainfall seasonality rather than temperature (Alberts et al., 2014). The tropical savanna biome is currently dominated by plants (grasses, trees, and shrubs) with unique adaptations to thrive under the water stress conditions of the dry season. These drought adaptations include the development of taproots that reach the water table or trunks that can store water and thick bark capable of withstanding the often occurrence of wildfires (Solbrig, 1996).

10.4. Integrative palaeoenvironmental reconstruction: looking for the suitable modern analogue.

The palaeoenvironmental, palaeoecological, and palaeoclimatic approaches presented in the previous sub-chapters of the manuscript should be tackled together to obtain a more accurate "picture" of the landscape that existed during the "mid"-Albian to early Cenomanian and its evolution.

During the middle Albian, the study area was dominated by a braidplain system characterised by mainly unconfined channels, far from the ocean influence, that flowed towards the Western Tethys palaeocoast (Fig. 10.6A). The landscape was punctuated by bedrock areas (basement highs) that might have locally produced confined channels. The proximal braidplain system was ruled by ephemeral rivers (wadis) that remained dry for most of the year, favouring the reworking of the sediment by wind action. Conversely, alluvial discharge was high during the wet season. These conditions reflect the arid climate conditions existing during the middle Albian in the Cuenca Basin. The inland vegetation was dominated by xerophytic conifers attributed to Cheirolepidiaceae and Cupressaceae (Bueno-Cebollada et al., 2021), capable of enduring the existing water-stressed conditions (Alvin, 1982). Possible modern examples of a proximal braidplain system can be found in the Death Valley in California (USA) or the Huab River Valley in Namibia, where ephemeral alluvial systems are arranged into unconfined channels and the discharge is controlled by sheet flood events (North and Davidson, 2012) (Fig. 10.7).

The middle to late Albian was characterised by the development of a distal braidplain system in the proximal areas of the basin, evolving into estuarine and coastal plain environments towards the distal areas of the basin (Fig. 10.6B) (Bueno-Cebollada et al., 2021). In the most proximal areas of the basin, the distal braidplain was colonised by plant communities that thrived in the alluvial floodplains and abandoned alluvial channels located relatively close to the palaeocoast. In these locations, the climate was affected by the Tethys influence which contributed to the increase in the mean annual rainfall, giving rise to a marked seasonality. However, the mainly

xerophytic nature of the palaeofloras of the Cuenca Basin agrees with the existence of a long and dominant dry season and a shorter but intense wet season characteristic of savanna-like climates (Fox, 2001).

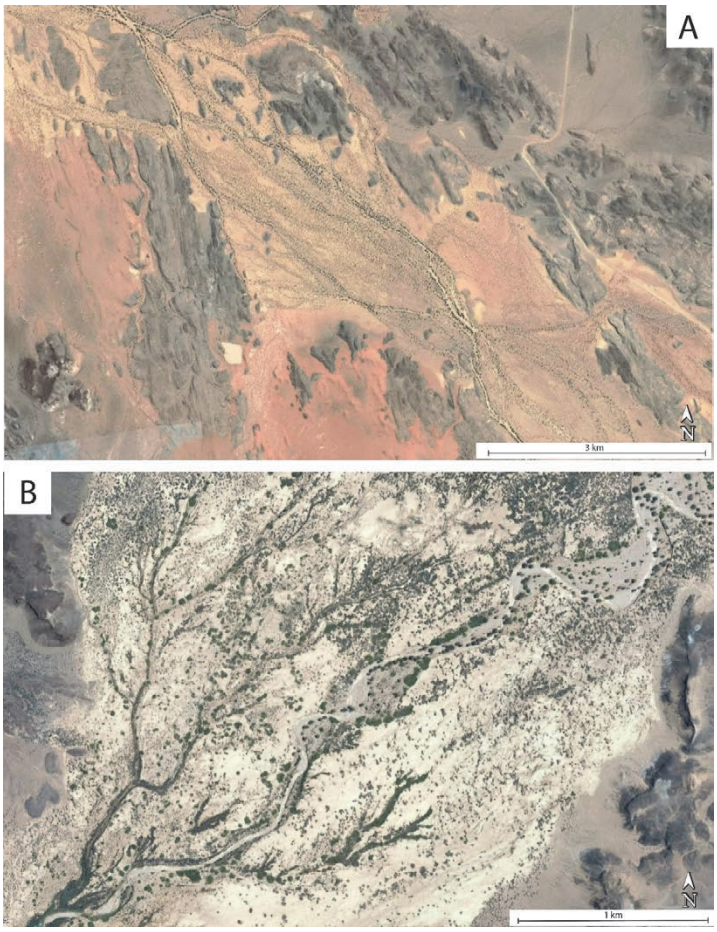

Fig. 10.7. Modern examples of ephemeral braided alluvial channels from the Huab River, Namibia. (A) General view of some of the channels that are seasonally flooded. (B) Close-up of several ephemeral alluvial channels in the same area where the development of sparse vegetation linked to the main water courses is observed. Image source: Google Earth.

The distal and central areas of the basin, dominated by coastal plain and estuarine environments (Fig. 10.6B), hosted ecosystems where mangrove communities thrived. These coastal plant communities developed in supratidal marshes, cut by tidal creeks, with generally brackish conditions, and were relatively common in "mid"-Cretaceous coastal areas of the Tethys (Falcon-Lang et al., 2001; Kvaček et al., 2005). In this sense, the Gulf of Carpentaria in Queensland (Australia) is a suitable modern climatic, ecological, and environmental analogue for the palaeoenvironments that developed in the coastal belt of the Cuenca Basin. The Gulf of Carpentaria is a broad coastal plain crossed by abundant tidal creeks where lush mangrove communities flourish under brackish conditions (Fig. 10.8A-C) (Asbridge et al., 2016). It presents a strongly seasonal climate, dry during most of the year and punctuated by heavy monsoon

rainfall during a few months (Fox, 2001), that becomes progressively drier with the distance from the coast (Fig. 10.8D).

During the latest Albian to early Cenomanian times, the transgression advanced, moving the coastal belts further landwards and giving rise to an estuarine to coastal plain setting in the proximal areas of the basin where supratidal marshes developed. Consequently, a tide-dominated (and wave-influenced) generalised shallow marine environment developed in the distal part of the Cuenca Basin (Fig. 10.6C). The widespread occurrence of a shallow marine environment dominated by mixed siliciclastic-carbonate sedimentation reflects the final marine flooding and shutdown of the "Albian" braidplain system in the Cuenca Basin due to the "mid"-Cretaceous transgression. This process eventually gave rise to the extensive marine carbonate platforms that dominated the basins of Eastern Iberia during the Late Cretaceous.

Regarding the palaeoclimate conditions existing during the mid-Albian to early Cenomanian times, there is an apparent mismatch in terms of palaeoprecipitation. On the one hand, the geochemical analysis of the studied palaeosoils reveals the occurrence of a seasonal tropical climate with alternating dry and humid seasons/periods, interpreted as that of a tropical savanna ecosystem. Conversely, the sedimentological (occurrence of deflation lags, ventifacts, or aeolian dunes) and palaeobotanical (dominance of xeric taxa) datasets indicate that significantly more arid conditions prevailed in eastern Iberia during the studied time span. In this sense, it is essential to mention that the occurrence of palaeosoils in the studied sections is rare within the overall Utrillas Gr succession. Therefore, it is essential to bear in mind the limitations of the studied datasets since the sedimentological and palaeobotanical data define a more complete representation of the mid-Albian to early Cenomanian stratigraphic record than the analysed palaeosoils, which represent a more limited time interval of the record.

The mid-Albian to early Cenomanian period has an approximate duration of 8-9 Ma (108-99 Ma) (Waite et al., 2007; Cohen et al., 2013); therefore, the sedimentation of the Utrillas Gr – La Bicuerca Mb succession in the Cuenca Basin would have lasted no more than 8-9 Ma or slightly less than that. Consequently, it can be expected that during time intervals spanning a few Ma, the climate showed variabilities, giving rise periodically to more humid and drier periods that alternate in time. In this sense, the development of palaeosoils, such as the ones studied here, within the Utrillas Gr – La Bicuerca Mb succession reveals the climate change periods where the arid climate, that dominated in eastern Iberia, turned into a more humid seasonal tropical savanna climate. Such changes toward more humid climate conditions allowed for the growth of more stable (xeric) woodlands due to the greater water availability as the water table rose.

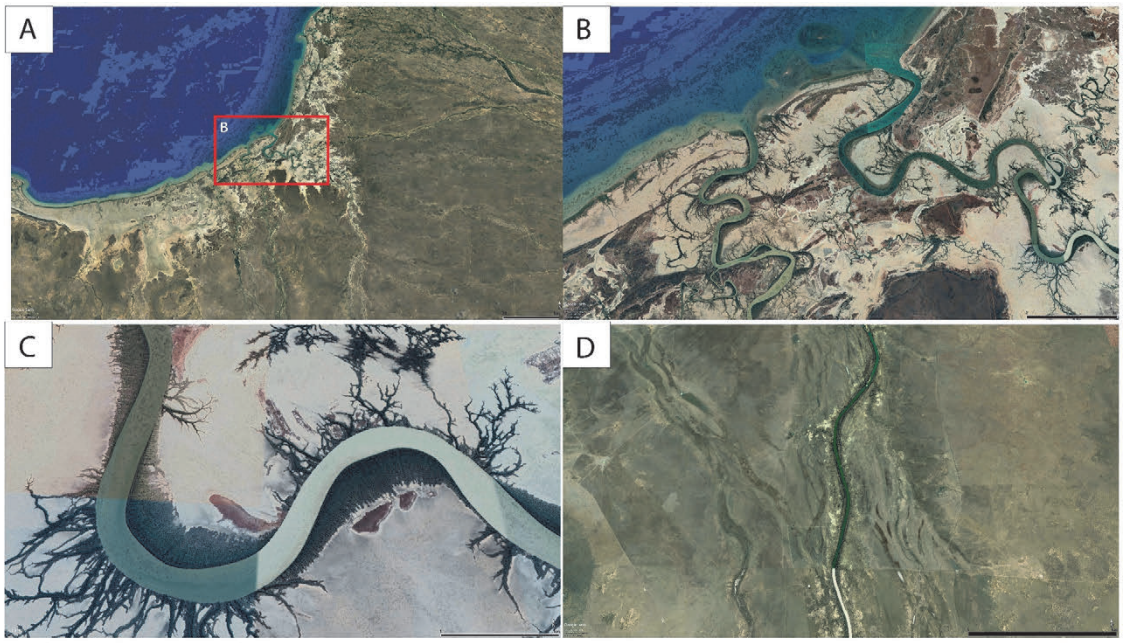

Fig. 10.8. (A) Satellite image of the Gulf of Carpentaria in Queensland, N Australia. (B) Detail of the tidal flats (see location in A) crossed by meandering tidal channels and creeks. (C) Close-up of the meander bends and creeks seen in B where lush marsh plant communities thrive. (D) Example of braided alluvial channels located approximately 60-70 km landwards from the coast where most of the vegetation thrives associated with the main (and more perennial) alluvial channels.

During the mid-Albian to early Cenomanian, the basins of the IBRS were located within the Northern Hot Arid (NHA) belt and close to the boundary with the Northern Mid-Latitude Humid (NMH) belt (Chumakov et al., 1995). Rodríguez-López et al. (2012) refer to the occurrence of climate forcing controlled by orbitally-induced latitudinal shifts as the main driver to explain the alternation of arid and more humid periods during the Albian to early Cenomanian in the Maestrazgo Basin. These latitudinal shifts, mainly controlled by the precession cycle (approx. 20 ka) and modulated by eccentricity at different scales (100 ka, 400 ka, 1.3 Ma, and 2 Ma), gave rise to the expansion and contraction of the boundaries of the NHA and NWM belts (Rodríguez-López et al., 2012). Therefore, this cyclical displacement of the low-latitude climatic belts might have accounted for the development of more humid periods when palaeosols developed, under a tropical savanna climate, and arid periods when water stress conditions did not allow a pervasive woodland development in the Cuenca Basin. Additionally, Skonieczny et al. (2019) and O´Mara et al. (2022) highlight that the precession of the Earth's axis as it rotates around the sun leads to changes in the location of the North African monsoon, and that these changes have produced the expansión of the savanna biome into the desert landscapes of the Sahara (and vice versa) in 20 ka-cycles during the Pleistocene.

Therefore, the Albian to lower Cenomanian succession in the Cuenca Basin seems to reflect the result of these latitudinal changes in the caloric equator, leading to more humid stages when savanna woodlands developed. These changes from an arid climate toward a seasonal tropical climate were repeated cyclically since the presence of palaeosoil beds similar to the ones analysed here can be found along the Utrillas Gr succession, which might conform with the occurrence of 20 ka precession cycles, as suggested by Rodríguez-López et al. (2012) in the Maestrago Basin.

However, this hypothesis is still tentative since the palaeosoil study carried out during this Ph.D. thesis, although insightful, is a preliminary one and has only analysed three palaeosoil levels in one location. Besides, this palaeoedaphological study should be extended in the future to the whole Utrillas Gr succession across the Cuenca Basin and even to coeval succession from other basins of Iberia in order to obtain palaeoclimatic results on a more regional scale.

11. Sequence stratigraphy.

Sequence stratigraphy is usually applied to marine strata where the development of depositional sequences can be easily attributed to fluctuations in eustatism (i.e., Embry, 2009). Conversely, applying the sequence stratigraphic concepts to continental strata is a more complex task (Wright and Marriot, 1993). In this sense, with increasing distance inland from the marine realm, the accommodation space is less influenced by the oscillations in relative sea level (Shanley and McCabe, 1994) and more related to climate and tectonic processes in the source area due to its proximity (Posamentier and James, 1993). However, in coastal plain environments or nearshore areas, the strata architecture is still strongly controlled by eustatic oscillations (Payton, 1977; Shanley and McCabe, 1994; Helland-Hansen, 1995; Embry, 2009; Catuneanu, 2019).

In the Cuenca Basin, the Utrillas Gr - La Bicuerca Mb succession is developed in three major facies belts ranging from continental alluvial (FA I and II) to shallow marine environments (FA VII and VIII) in space and time (Fig. 10.5) (See chapter 10.1. of this manuscript). Besides, the basin shows high compartmentalisation where basement highs alternated with depositional areas (Figs. 10.1, 10.2, 10.3).

This chapter deals with the sequence stratigraphic analysis of the Utrillas Gr - La Bicuerca Mb strata, after the study of two outcrops where the development of the coastal and shallow marine facies belts was thoroughly analysed: the Reillo and Pajaroncillo outcrops.

The location of these two outcrops in the coastal fringe (Southern sector; Figs. 5.1, 10.3) of the Albian to early Cenomanian braidplain system, their along-strike relative position, and good preservation of the strata have allowed the application of the sequence stratigraphic concepts identifying five evolutionary stages, corresponding to five “In-trend” stratigraphic units bounded by sequence stratigraphic surfaces (Fig. 11.1). These five evolutionary stages were later integrated within the regional sequence stratigraphic framework previously presented by Giménez et al. (1993). The discussion presented in this chapter is published in Bueno-Cebollada et al. (2022) (Appendix I [C]).

The five “in-trend” stratigraphic units and their bounding surfaces were identified by the study of the stacking patterns of the interpreted facies associations in both outcrops (Reíllo and Pajaroncillo), aiming at their later interpretation as system tracts. Each of the “in-trend” stratigraphic units consists of a succession of one or more facies associations that record either a transgressive or regressive trend.

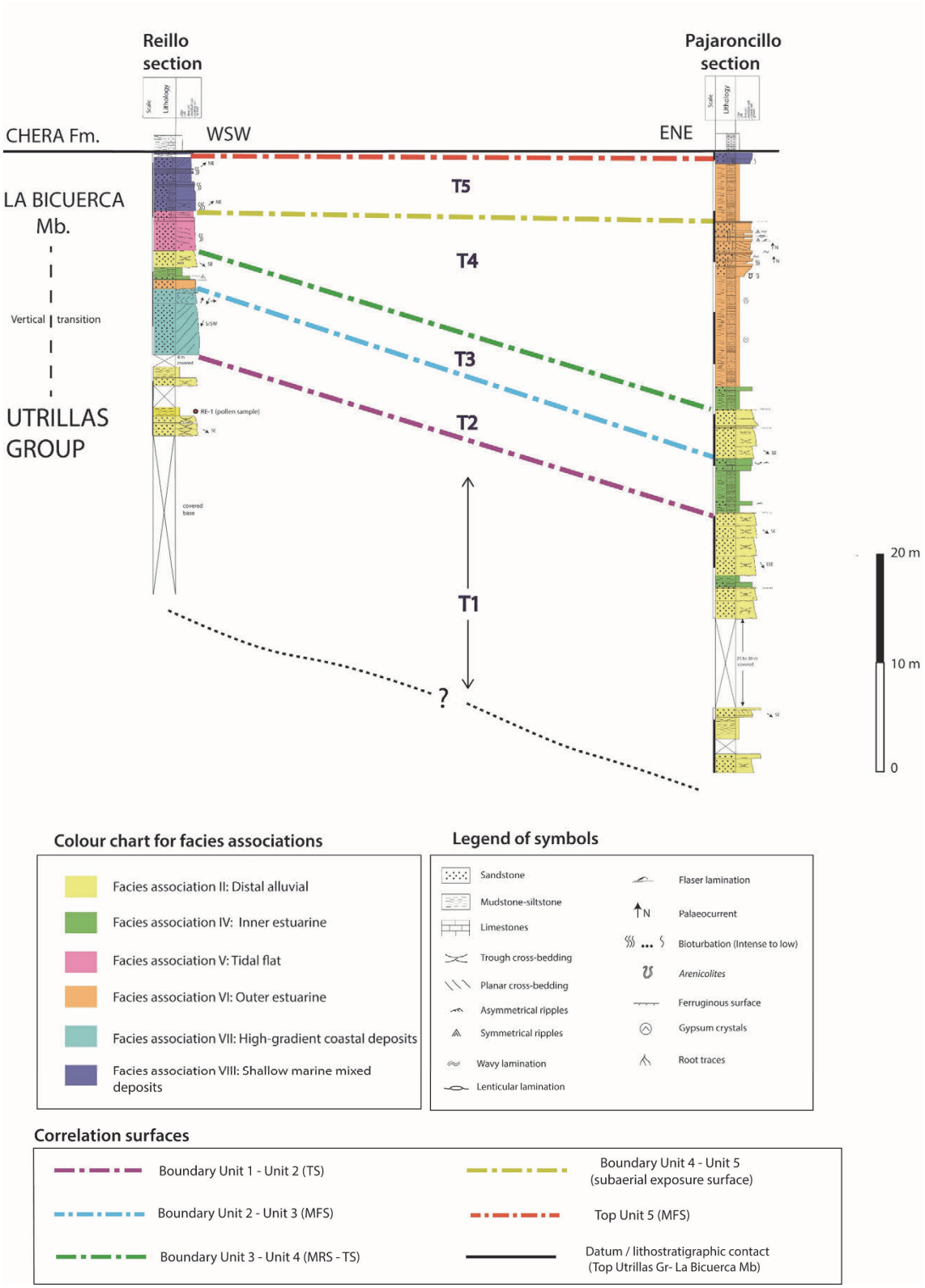

Fig. 11.1. Correlation of the two studied sections in an along-strike (WSW- ENE) direction. The datum for correlation is the boundary between the Utrillas Gr-La Bicuerca Mb and the Chera Fm, identified in both studied sections (solid black line). Evolutionary stages (T1- T5) representing the time intervals of each of the five "in-trend" units, respectively, are indicated. Key sequence stratigraphic surfaces used for correlation and separating the evolutionary stages/units are also included in the correlation. The higher resolution version of the logged sections is included in chapter 5 of this manuscript (see Figs. 5.31 and 5.33, respectively). Modified from Bueno-Cebollada et al. (2022).

The sequence stratigraphic surfaces that bound the five "in-trend" units have been analysed and interpreted, allowing a correlation between the two studied outcrops. The sequence stratigraphic surfaces must display low diachroneity to be suitable for correlation purposes (Embry, 1995). Despite some of the surfaces identified in this work being not synchronous, the proximity between both locations (12 km) and the along-strike path through which the correlation was set outweigh their diachronous nature. Besides, an additional surface (*Intra-Unit 2 surface*) has been identified and interpreted as a ravinement surface (wave ravinement surface - wRS). However, the latter surface has not been used as a correlation surface since it has only been identified in the Reíllo outcrop.

The five evolutionary stages or "In-trend" units (and the sequence stratigraphy surfaces bounding them) defined in Pajaroncillo and Reíllo have not been identified in the rest of the studied outcrops partially due to the marked compartmentalisation of the Cuenca Basin, but essentially because the succession is dominated by alluvial facies associations in the outcrops from the Northern sector (Figs. 5.1, 10.1). Therefore, they present a weaker eustatic signal which hampers identifying the five evolutionary stages observed in the Southern sector of the Cuenca Basin.

Notwithstanding, Sequence Stratigraphy concepts also provide useful tools of correlation that help develop a high-resolution time framework, within and beyond the chronostratigraphic framework provided by the biostratigraphic data. As it will be later discussed, the five evolutionary stages identified after the sequence stratigraphic analysis of Reillo and Pajaroncillo are controlled by a combination of eustatism and tectonics. Even if the effect of eustatism in the Northern sector is completely disregarded, the tectonic control should have exerted its influence in the whole area affecting both the continental and coastal facies belts (Fig. 10.5) deposited. In this sense, the development of these five evolutionary stages might have occurred in the entire study area, regardless of the difficulties of clearly identifying them in the alluvial-dominated areas. Thus, the sequence stratigraphic analysis presented over the following pages provides a more accurate time framework of the basin's evolution than the framework provided by the biostratigraphy study, which only consists of three evolutionary stages (Figs. 10.5, 10.6).

11.1. "In-trend" stratigraphic units: the Reíllo and Pajaroncillo outcrops.

The first unit defined (Unit 1) consists of more than 20 m (the base of this unit is covered in both logged sections) of distal alluvial deposits (FA. II), which include alluvial channels and overbank clays and silts (Fig. 11.1) lacking any tidal or marine influence and displaying an aggradational stacking pattern. Similar facies associations have been recognised in both sections. Therefore,

this first unit represents deposition in an arid braidplain system with minor associated floodplains and rare sheet flood events. Comparable sedimentary settings have previously been described in more proximal areas (towards NW) of the braidplain system (Chamizo-Borreguero et al., 2016; Bueno-Cebollada and Meléndez, 2018). The base of this unit is covered in both sections. Notwithstanding, the top surface corresponds to an erosive and sharp surface interpreted as a transgressive surface (dashed purple line) (Figs. 11.1, 11.2A), according to the trends of the underlying (alluvial braided deposits) and overlying (inner estuarine and high-energy coastal deposits in Pajaroncillo and Reíllo, respectively) sedimentary environments. The strata attributed to Unit 1 are dated as middle to early late Albian based on the co-occurrence of *Gregussisporites orientalis* and *Tricolpites minutus* (Bueno-Cebollada et al., 2021).

A second unit (Unit 2) has been described. This unit in Reíllo consists of 5 to 10 metres of foreshore deposits (facies Shg; FA. VII) overlain by upper shoreface deposits (facies Ssc; FA. VII). The contact between both facies is erosional, usually associated with the presence of mud pebbles, representing an erosive unconformity in Unit 2 (Figs. 8.11A, 11.2B). Conversely, Unit 2 in Pajaroncillo is dominated mainly by a five m-thick supra- to intertidal estuarine succession (FA. IV), which includes mudflat deposits cut by tidal creeks (Fig. 8.6G, 11.2B). The base and top boundaries of Unit 2 are the erosional surface located at the top of the first unit (transgressive surface – TS) and a slightly irregular contact (maximum flooding surface – MFS), respectively. Therefore, a clear transgressive trend can be deduced from the transition from Unit 1 into Unit 2, up until the top surface of the latter (dashed blue line) (Fig. 11.1), which marks the end of this transgressive pulse.

The third unit identified (Unit 3) starts on top of the previously mentioned MFS (Figs. 11.1, 11.2B, 11.3). In Reíllo, Unit 3 consists of approximately four to five m-thick inner estuarine succession developed within the supra- to the intertidal zone. It includes from base to top: tidal channels/creeks, coastal aeolian deposits (facies Smf), supratidal muddy deposits (facies Fm2), and tidally modulated alluvial deposits (facies Sp2/St2). Whereas in Pajaroncillo, it consists of a five m-thick succession comprising tidally-modulated alluvial deposits (facies Sp2/St2), which reflect the occurrence of a distal alluvial to supratidal estuarine environment located at or close to the tidal limit. Unit 3 represents a relapse towards more landward facies belts than the succession observed and interpreted for Unit 2. Therefore, it is characterised by a clear progradational depositional style, which reveals the regressive character of the succession during the time of its deposition. The top surface of Unit 3 (dashed green line) (Fig. 11.4) marks

the end of the progradation and the onset of a new recurrence towards transgression, and it is interpreted as a maximum regressive surface (MRS) and a transgressive surface (TS).

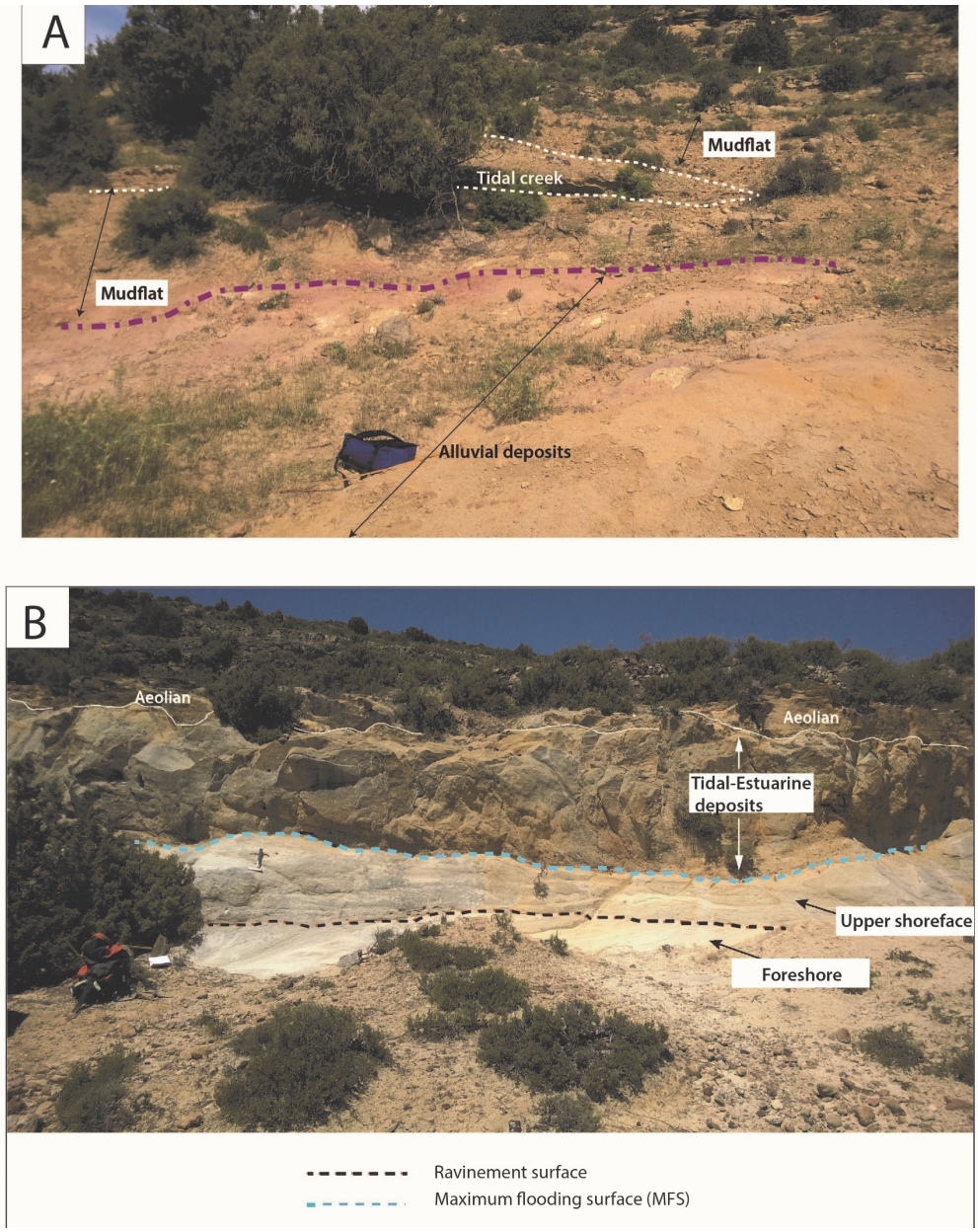

Fig. 11.2. (A) Mudflat facies association deposited in a supratidal environment (FA IV) in the Pajaroncillo outcrop. The mudflat is crossed by minor tidal creeks and underlaid by alluvial deposits (FA II). The basal surface of the supratidal deposits, represented by a dotted purple line, is interpreted as a transgressive surface/maximum regressive surface (TS/MRS). (B) Maximum flooding surface (MFS) in the Reíllo outcrop (dashed blue line). This surface separates upper shoreface deposits below from a tidal-estuarine succession above and is a key surface for correlation. The dashed black line is interpreted as a ravinement surface separating foreshore from upper shoreface deposits. See text for further explanation.

The fourth unit (Unit 4) identified comprises a five m-thick succession of tidal sand flat deposits developed in an inter- to subtidal zone (FA. V) in the Reíllo outcrop. Conversely, in the Pajaroncillo outcrop, this unit is represented by an approximately 18 m-thick succession,

interpreted as an outer estuarine environment (FA. VI). It consists of coastal to estuarine mudstones and marls (Fig. 11.1), which dominate approximately over the first 13 metres, with the occurrence of minor tidal creeks. Towards the top of the succession (approximately the uppermost 5 metres of the unit), intertidal to subtidal dunes deposits gradually migrated over the mentioned estuarine mudstones (Fig. 8.9). Unit 4 reflects the resumption of transgression in the basin after reaching the maximum regression at the top of Unit 3. This change is marked by the transition from supratidal to tidally-modulated alluvial facies associations, at the top of Unit 3, to intertidal deposits, during the sedimentation of Unit 4.

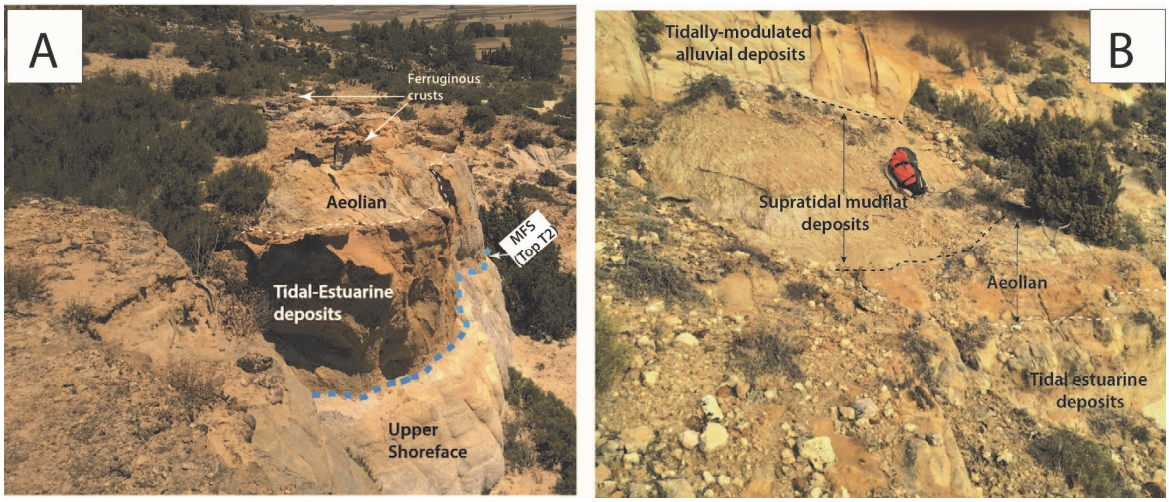

Fig. 11.3. (A) Detail of the maximum flooding surface in Reíllo where a suite of progradational deposits corresponding to a regressive phase (T3) can be observed overlying the surface. Hammer for scale is 35 cm. (B) Outcrop view showing an array of the different depositional environments that comprise the "in-trend" Unit 3 (T3) in Reíllo. The backpack for scale is approximately 80 cm long.

The last unit identified (Unit 5) entails a suite of subtidal facies (facies association VI) representing the most distal marine deposits interpreted in the studied outcrops. In the Reíllo outcrop, Unit 5 is a five to six m-thick succession that consists of subtidal dune deposits (Fig. 11.5). Conversely, a seven to eight m-thick succession dominated by outer estuarine mudstones and marls (FA. VI), which gives rise upwards to a mixed carbonate-siliciclastic inner ramp (FA. VIII), dominates the succession in the Pajaroncillo outcrop (Fig. 11.6). Unit 5 evinces a distinct transgressive character starting immediately after the subaerial exposure surface at its base, which reflects the deposition of seawards facies belts, in this case, deposited in a subtidal environment.

Units 2 to 5 correspond to strata dated as late Albian to early Cenomanian age based on pollen and spores assemblages. Although it is impossible to specify a more accurate biostratigraphic

age for each of these units, we can determine that Units 2 to 4 are late Albian in age. In contrast, Unit 5 reaches the early Cenomanian (Bueno-Cebollada et al., 2021).

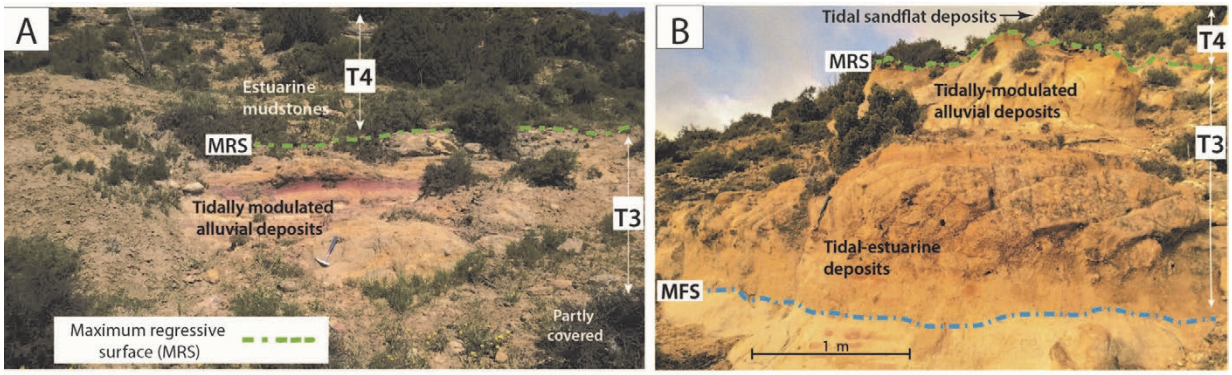

Fig. 11.4. (A) Top of the "in-trend" Unit 3 (T3) in the Pajaroncillo outcrop, where a maximum regressive surface (MRS) overlying tidally modulated alluvial deposits is indicated by a dashed green line. Hammer for scale is 35 cm long. (B) Outcrop picture of "in-trend" Unit 3 (T3) in Reíllo, where a maximum flooding surface (MFS; in blue colour) and a maximum regressive surface (MRS; in green), representing the base and top boundaries of T3, respectively.

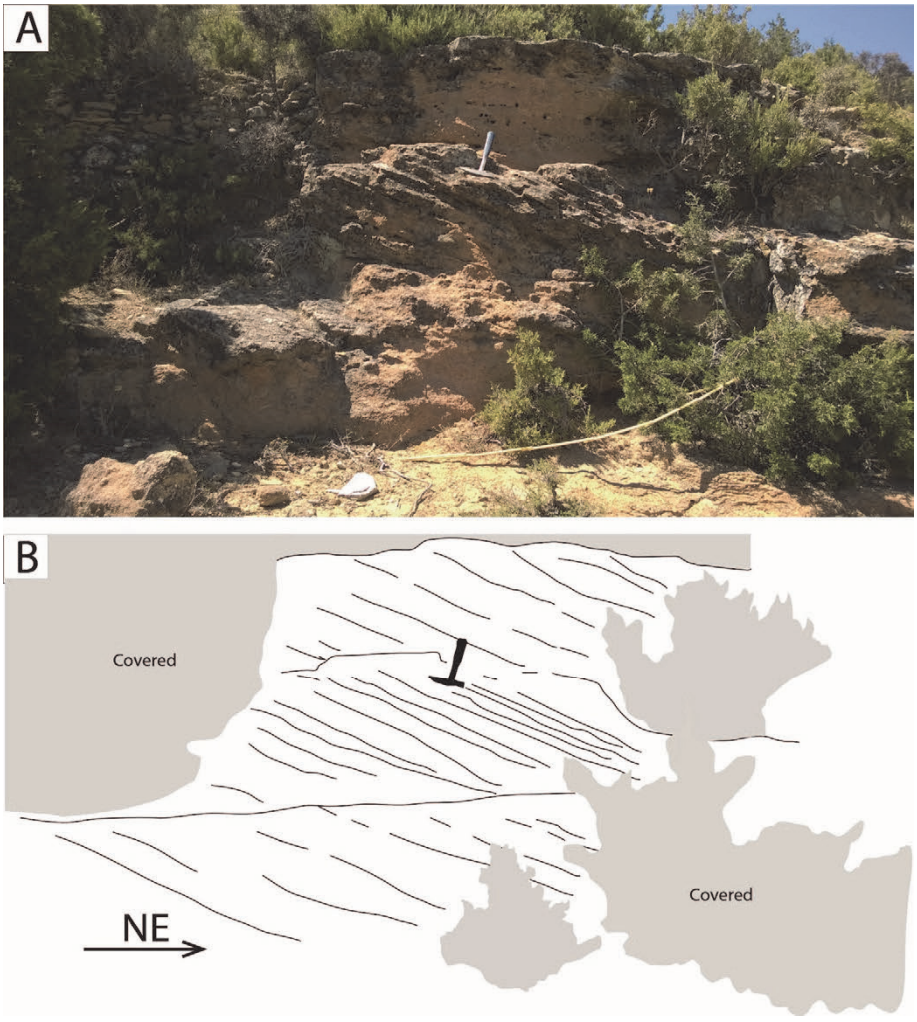

Fig. 11.5. (A) Appearance of the shallow marine deposits, consisting of amalgamated subtidal dunes, displaying cross-bedding in Reíllo (FA VIII). (B) Line drawing of (A). The main palaeocurrent direction is towards NE. Hammer for scale is 35 cm.

11.2. Sequence stratigraphic surfaces: description and interpretation.

Boundary Unit 1 – Unit 2 (transgressive surface): This surface has been observed in both studied sections, notwithstanding it separates very different facies associations in each case. In Reíllo, the transgressive surface (Fig. 11.1) separates continental alluvial deposits below (Unit 1) from foreshore deposits above (Unit 2). In Pajaroncillo (Fig. 11.1), the surface is represented by a clear contact that can be traced along the outcrop. It draws an abrupt sharp to erosive contact that separates Unit 1 below from Unit 2 above (Figs. 11.1, 11.2A). It must be mentioned that here the transgressive surface consists of a five to ten cm-thick accumulation of ferruginous sandstone (ferruginous crust; facies Ifc). Regarding geometry, the transgressive surface is a conformable contact that separates prograding beds below from the onset of a new transgressive interval (Embry, 1995; Cattaneo and Steel, 2003). Transgressive surfaces are diachronous (i.e., Embry and Johannensen, 1992), although their diachroneity is low, especially in along-strike sections. This surface is interpreted as a transgressive surface (TS) that represents the224haracterision of the strata of Unit 1.

Intra-Unit 2 surface (wave ravinement surface-WRS): This surface has only been identified in the Reíllo outcrop, within Unit 2 (Fig. 11.1). It is interpreted as a lower rank surface compared to the rest of the sequence stratigraphic surfaces described in this chapter. Therefore, it cannot be considered for the sequence stratigraphic analysis. The surface is described as an irregular one, presenting moulds of pebbles and mudballs (Fig. 8.11G), and therefore, it should be interpreted as an erosional contact. It overlies long and inclined foresets of foreshore deposits (facies Shg) and is always overlain by upper shoreface deposits (facies Ssc) (Figs. 8.10C, 11.2A). A shoreline ravinement surface is defined as a sharp or erosive contact with the occurrence of marine deposits depicting a transgressive trend, directly overlying the surface (Embry, 2002). This definition agrees with the field observations in the Reíllo outcrop.

Additionally, two different types of ravinement surface, wave ravinement and tidal ravinement, may be developed in settings where there is an interplay between tidal and wave currents (Embry, 2009). We interpret the surface observed in Reíllo as a wave ravinement surface (wRS), according to some of the previous descriptions of this type of surface (i.e., Swift, 1968; Cattaneo and Steel, 2003). In this regard, the surface here described lies above and erodes foreshore deposits in an open coast to embayment setting, where wave energy was moderate in strength and is overlain by transgressive marine deposits (Fig. 11.2B).

Boundary Unit 2 – Unit 3 (maximum flooding surface): A maximum flooding surface has been interpreted at the boundary between Units 2 and 3 (Fig. 11.1). This surface overlies deposits depicting a retrogradational trend in both studied locations and underlies deposits that show a

progradational pattern. These features conform with the definition and peculiarities that characterise a maximum flooding surface (Wagoner et al., 1990; Embry, 2009). In the Reíllo outcrop, this surface is characterised by a slightly undulating contact (Figs. 8.10C, 11.1*, 11.2B*), which separates upper shoreface deposits (below the surface) from an intertidal estuarine succession (above the surface) (Fig. 11.3A). However, in the Pajaroncillo outcrop, this surface is a sharper contact than the one observed in Reíllo. In Pajaroncillo, the surface is a boundary between a supra- to upper intertidal mudflat succession below and alluvial deposits above. From a genetic point of view, an MFS represents the time at which the base level is highest in a sedimentary basin, from which onwards it starts to drop. Therefore, it reflects a change from transgression into regression (Embry, 2002).

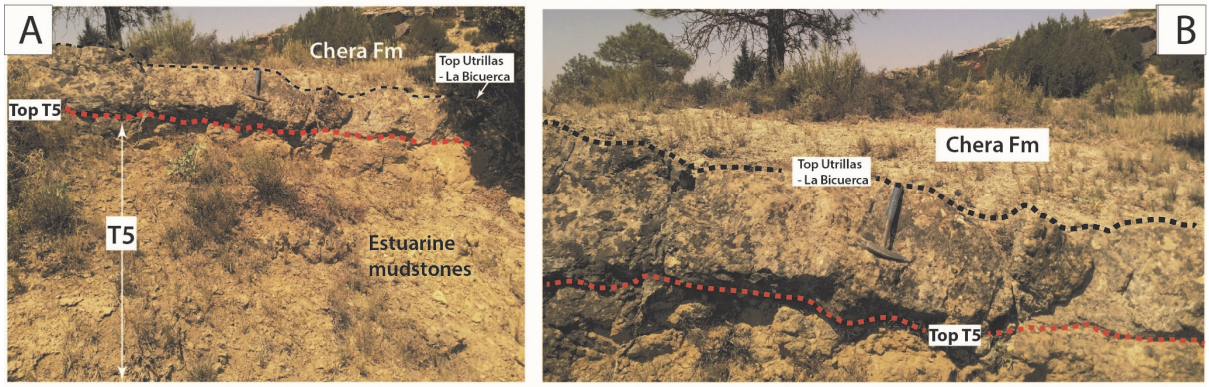

Fig. 11.6. (A) Mixed platform deposits (FA VIII) overlying distal estuarine sediments (FA V) at the top of the succession in the Pajaroncillo outcrop, just below the top of the Utrillas Gr - La Bicuerca Mb (dashed black line). A dashed red line represents the top of Unit 5 (MFS). (B) Detail of (A). Hammer for scale is 35 cm.

Boundary Unit 3 – Unit 4 (maximum regressive surface – transgressive surface): In the outcrop, this surface represents a conformable, non-erosive contact which essentially marks the moment when the increase in base level outweighs the sediment supplied by alluvial systems, giving rise to the sedimentation of estuarine and tidal flat depositional systems. Consequently, we may interpret that this surface reflects the end of the shoreline progradation (maximum regressive surface - MRS) and the resumption of a new transgressive pulse (transgressive surface - TS). In the Reíllo outcrop, the surface (Fig. 11.1) is characterised by a flat contact between alluvial deposits with minor tidal modulation features (below) and a tidal flat system developed in inter- to subtidal zone (above) (Fig. 11.4B). This contact represents a conspicuous transition from sedimentation in a continental environment (not directly affected by tides, but close enough to a theoretical tidal limit to show some tidal modulation features) into an inter- to subtidal environment. Besides, a laterally extensive surface (Fig. 11.1) can be identified in the Pajaroncillo outcrop (Fig. 11.2A). Here, the surface is a contact that overlies alluvial deposits with some tidal

modulation and is overlain by estuarine mudstones and marls interpreted as deposited in an inter- to a subtidal setting. Therefore, this surface reflects the transition from a progradational stage (or a secondary regressive pulse) into a new transgressive phase. The term maximum regressive surface (MRS; Helland-Hansen and Martinsen, 1996) should be used to emphasise the end of the regression. Conversely, the term transgressive surface (TS) refers to the same surface but places more emphasis on the onset of the transgression (Catuneanu et al., 2011).

Boundary Unit 4 – Unit 5 (Subaerial exposure surface): This surface presents a different expression in each of the two studied outcrops, based on the overlying and underlying sedimentary environments. The surface was initially identified in the Pajaroncillo outcrop (Fig. 11.1), where it consists of a prominent slightly undulating to sharp contact (Fig. 11.7A); a carbonate-cemented surface, easily observed thanks to the tectonic tilting of the outcrop, that presents abundant subcylindrical- or hemispheric-shaped holes with irregular outlines interpreted as potholes (Fig. 11.7B). Potholes (Sunamura, 1992) are erosional morphological features that form in exposed coastal settings, alluvial streams, or hillsides due to currents and/or rainwater flow scouring (Ji et al., 2018). Coastal potholes are developed by wave abrasion and scour in subaerially-exposed shore settings due to the hydrodynamic of wave motion in spray zones. They tend to occur between the high and low levels of the local tides and have also been associated with erosional processes due to changes in environmental conditions owing to slight tectono-eustatic changes that raise and lower the marine abrasion surfaces (De Pippo and Donadio, 1999; Ji et al., 2018).

In Pajaroncillo, the boundary between Units 4 and 5 separates tidal dunes deposited in an intertidal setting, below, from outer estuarine subtidal deposits and the development of incipient mixed carbonate-siliciclastic ramp deposits, above the surface. However, the common occurrence of potholes on the surface indicates the subaerial exposure and emersion of the tidal dune deposits identified at the top of Unit 4 in the Pajaroncillo outcrop (Fig. 11.7B).

The same surface has been extrapolated to the Reíllo outcrop (Fig. 11.1). Its identification in the Reíllo outcrop might seem more complex due to the outcrop characteristics (almost horizontal dip and similar calcareous sandstone lithology). However, an equivalent and potentially correlatable surface has been identified at the top of tidal sandflat deposits (Unit 4), prior to the deposition of a shallow marine succession (Unit 5). The boundary is characterised by a bioturbated undulating subaerial exposure surface overlain by heavily bioturbated strata (Fig. 8.8C).

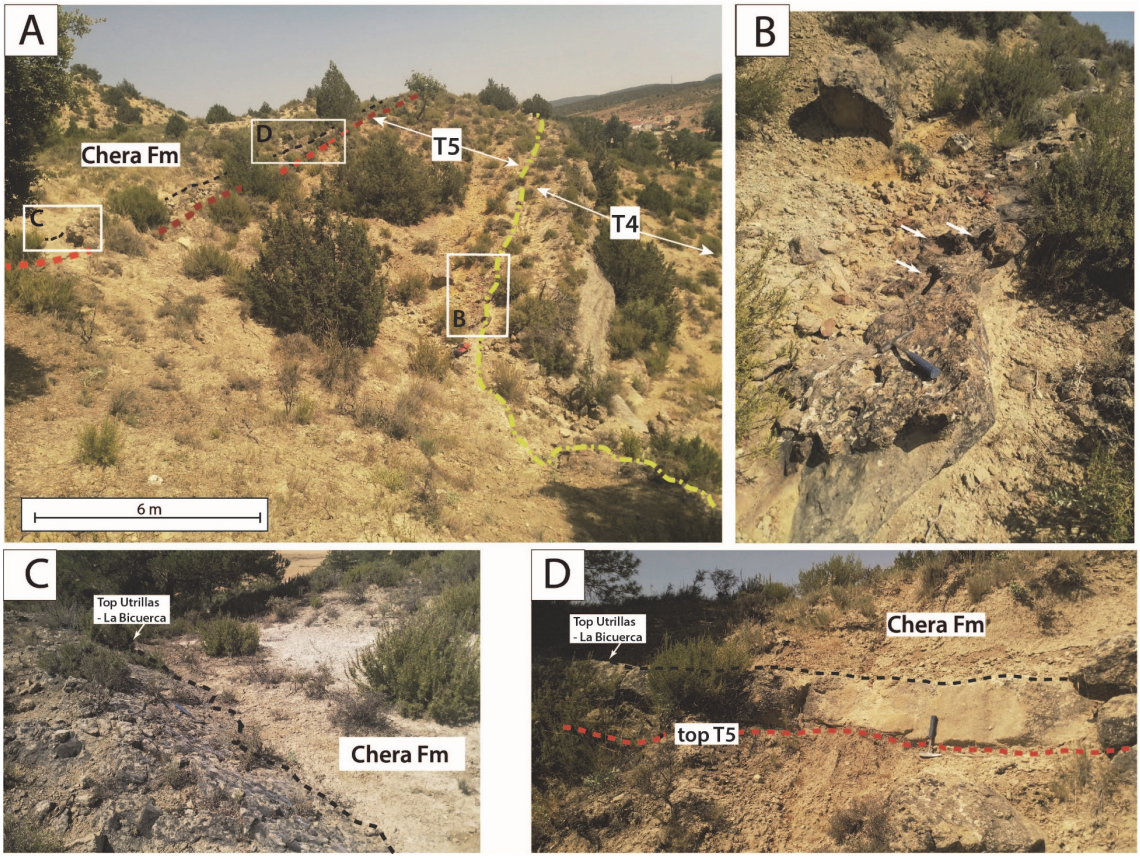

Fig. 11.7. (A) General view of the "in-trend" Unit 5 (T5) in the Pajaroncillo outcrop. The dashed yellow line represents a subaerial exposure surface located at the base of T5-top of T4. The dashed red line is interpreted as a maximum flooding surface (MFS). The dashed black line represents the top of the Utrillas Gr - La Bicuerca Mb, a lithostratigraphic contact that has been used as a datum for correlation. (B) Close-up of the subaerial exposure surface shown in (A). The white arrows indicate examples of potholes. (C and D) Close-up of picture (A) highlighting the maximum flooding surface (MFS), top of T5, and, consequently, of the studied succession. Hammer for scale is 35 cm long.

The origin of this surface is related to a drop in the relative sea level, which allowed for an emersion and the occurrence of erosional processes in formerly submerged areas of the basin. It is important to clarify that this surface is not understood as a subaerial unconformity, since the occurrence of the latter always entails a (third-order) depositional sequence boundary, commonly separating a progradational stratigraphic architecture below from a retrogradational one above, or a regressive trend from a transgressive trend (Embry, 2009). We, therefore, interpret this surface as a subaerial exposure surface, since it evinces either a eustatic fall or a tectonic uplift taking place in the middle of a transgressive trend, without evidence, in terms of facies associations, of a shallowing nor a progressive progradation, immediately below this surface.

Top Unit 5 (Maximum flooding surface - MFS): Additionally, the top surface of Unit 5, which is below the contact between the Utrillas Gr - La Bicuerca Mb and the lower Cenomanian Chera Fm (datum for correlation and represented by a black line) (Figs. 11.1, 11.7), is interpreted as a maximum flooding surface (MFS), according to Giménez et al., (1993). The top of Unit 5

corresponds with sedimentation in a mixed inner ramp setting, indicating the moment of maximum bathymetry in the studied succession (Fig. 11.7).

11.3. Along-strike correlation and sedimentary evolution.

The five "in-trend" stratigraphic units defined, and their bounding key stratigraphic surfaces have enabled an accurate reconstruction of the palaeogeography during five evolutionary stages (T1 to T5, corresponding to the deposition of each of the five "In-trend" stratigraphic units), recording the along-strike sedimentological evolution of a distal sector of an arid braidplain system that developed in a transgressive setting (Fig. 11.1). The palaeogeographic maps have been constructed based on the main Mesozoic palaeotectonic guidelines (Fig. 10.4) of the Cuenca Basin (Aurell et al., 2019). Combining the sedimentological analysis with the interpretation of the palaeotectonic guidelines of the basin has ultimately permitted carrying out the palaeographical maps and assessing the along-strike variability between both outcrops.

T1. Alluvial aggradational stage

It is important to mention that there is no clear variability regarding sedimentary environments between both outcrops during the development of this first stage since the continental alluvial deposits are ubiquitous in the study area (Fig. 11.8A) (Bueno-Cebollada et al., 2021). It is difficult to ascertain whether there is thickness variability during the deposition of this stage since the bases of both outcrops are either covered or eroded.

The first stage consists of a set of continental deposits which includes: high-energy deposits comprising major arid, ephemeral alluvial channels with minor sheet flows that alternate with floodplain deposits associated with the braidplain system. This set of continental deposits is equivalent, regarding sedimentary environments, to the one observed in more proximal areas of the Albian braidplain system (Chamizo-Borreguero et al., 2016; Bueno-Cebollada and Meléndez, 2018) located further north and northwest in the Cuenca Basin. It represents the stage before the onset of the marine transgression in the studied outcrops, during which neither coastal nor marine sediments were deposited. However, a previous palynological study carried out in the area (Bueno-Cebollada et al., 2021) alludes to the relatively high abundance of araucariacean pollen grains (*Araucariacites australis*) together with a complete absence of marine palynomorphs in the Reíllo outcrop, in strata that correspond to this first stage (T1). The presence of relatively abundant Araucariaceae pollen might be indicative of relative closeness to the coast (Abbink, 1998; Peyrot, 2019; Bueno-Cebollada et el., 2021), while the high percentages of cheirolepidacean pollen grains (genus *Classopollis)* reflect the arid climate

conditions of the braidplain system (Appendix II) (Bueno-Cebollada et al., 2021). The aggradational stacking pattern observed in these alluvial strata reflects the evolution of a succession located landward from the limit of tidal influence, resulting from an increase in the accommodation space in continental areas due to a rise in the relative sea level. Therefore, this aggradational trend represents the stratigraphic expression of a coeval marine transgression in areas away from the influence of the marine realm (Wright and Marriott, 1993; Shanley and McCabe, 1994).

T2. Initial transgression:

During the deposition of this second stage, significant variability between both sections regarding sedimentary environments occurred. In Reíllo, the succession consists of a high-energy open-coast coastal succession that comprises foreshore deposits, and it is transgressed by upper shoreface deposits upwards in the succession. The transition between both environments is represented by a disconformity, interpreted as a wave ravinement surface (wRS) and probably corresponds to a minor-order surface within Unit 2. In Reíllo, this stage is represented by a wave-dominated coastal system where tidal action should have played an important role.

Unlike in Reíllo, the Pajaroncillo outcrop is characterised by a different scenario regarding the sedimentary environment observed. It consists of a mud-dominated tidal flat environment located in an inter- to supratidal setting, which is locally crossed by minor tidal creeks (Fig. 11.2A). The Gulf of Carpentaria (Australia) (Rhodes, 1982) represents a possible modern outcropping analogue for the mudflat environment with tidal creeks described in Pajaroncillo. Another modern example of the facies associations described in Pajaroncillo is the intertidal system of the Westerchelde Estuary, in The Netherlands, where small-scale meandering tidal creeks transit throughout a mudflat environment (Kleinhans et al., 2009). However, this example differs in that the climate conditions are more humid than those expected for the Albian of the Cuenca Basin.

As can be observed in the palaeogeographical reconstruction of the second stage (Fig. 11.8B), the differences between both sections regarding environment distribution are conspicuous. We infer the existence of a tectonically-controlled elevated area or promontory as the trigger for such a variability (Fig. 10.3, 10.4) based on data from previous Mesozoic palaeographic reconstructions (Aurell et al., 2019). The promontory would have acted as an uplifted area where no sediments were deposited, limiting, and constraining the sedimentary processes occurring in the area. In this way, the location of the Reíllo outcrop with regards to the

promontory would have favoured the deposition of open coast to slightly embayed high-energy sedimentary environments typical of a wave-tidal dominated siliciclastic coasts, developed in a transgressive setting. The Reíllo outcrop during stage T2 can be interpreted as the transgressive retreat of a beach system because of the relative sea-level rise. Conversely, during the T2, the Pajaroncillo outcrop shows a more restricted and proximal environment, sheltered from wave currents in which there was no place for high-energy processes. Instead, tidal currents led to the development of a low-energy nearshore environment where settling from suspension dominated the sedimentation, except for the occurrence of minor tidal creeks, representing the distal portion of the braidplain system and located landwards. In the palaeographical reconstruction of T2 (Fig. 11.8B), it is also inferred that the mudflat deposits interpreted for the Pajaroncillo outcrop probably graded seawards into a tidal sand-dominated flat where, besides tidal currents, wave-current action would have played a key role in distributing sediments. Additionally, the lack of coarse sediment in Pajaroncillo is also related to the limited drainage of the braidplain system compared to Reíllo, where the coarse sediment delivered was conspicuously more significant. This fact was probably related to a better path for coarse sediment delivery in Reíllo, which connected proximal areas of the braidplain system to the palaeocoast and adjacent distal sectors during T2.

T3. A regressive phase:

The third stage is defined by a maximum flooding surface at the base, which marks a turnaround from transgression into (normal) regression, and a maximum regressive surface at its top, which indicates the transition again into a transgressive trend.

In the Reíllo outcrop, this regressive phase is represented by a complex array of different estuarine inter- to supratidal depositional environments (Figs. 11.3, 11.4). The succession started with the deposit of a sandy estuarine succession which prograded in a NE direction and was overlain by supratidal mudflat deposits. On top of these deposits, the succession grades into tidally-modulated alluvial deposits (De Boer et al., 1989; Chamizo-Borreguero et al., 2016) (see figure 4C in Bueno-Cebollada et al., 2022), which were located landward from the tidal limit, since they were not being directly affected by tidal action, but close enough to the tidal limit to produce the modulation of the alluvial discharge by the action of the ebb and flood currents.

The transition from estuarine inter- to supratidal deposits into a distal alluvial succession reflects the progradation and marine regression both within the succession of T3 and compared to T2 in Reíllo. This regressive transition of depositional environments is represented in the palaeogeographical reconstruction carried out in T3 (Fig. 11.8C).

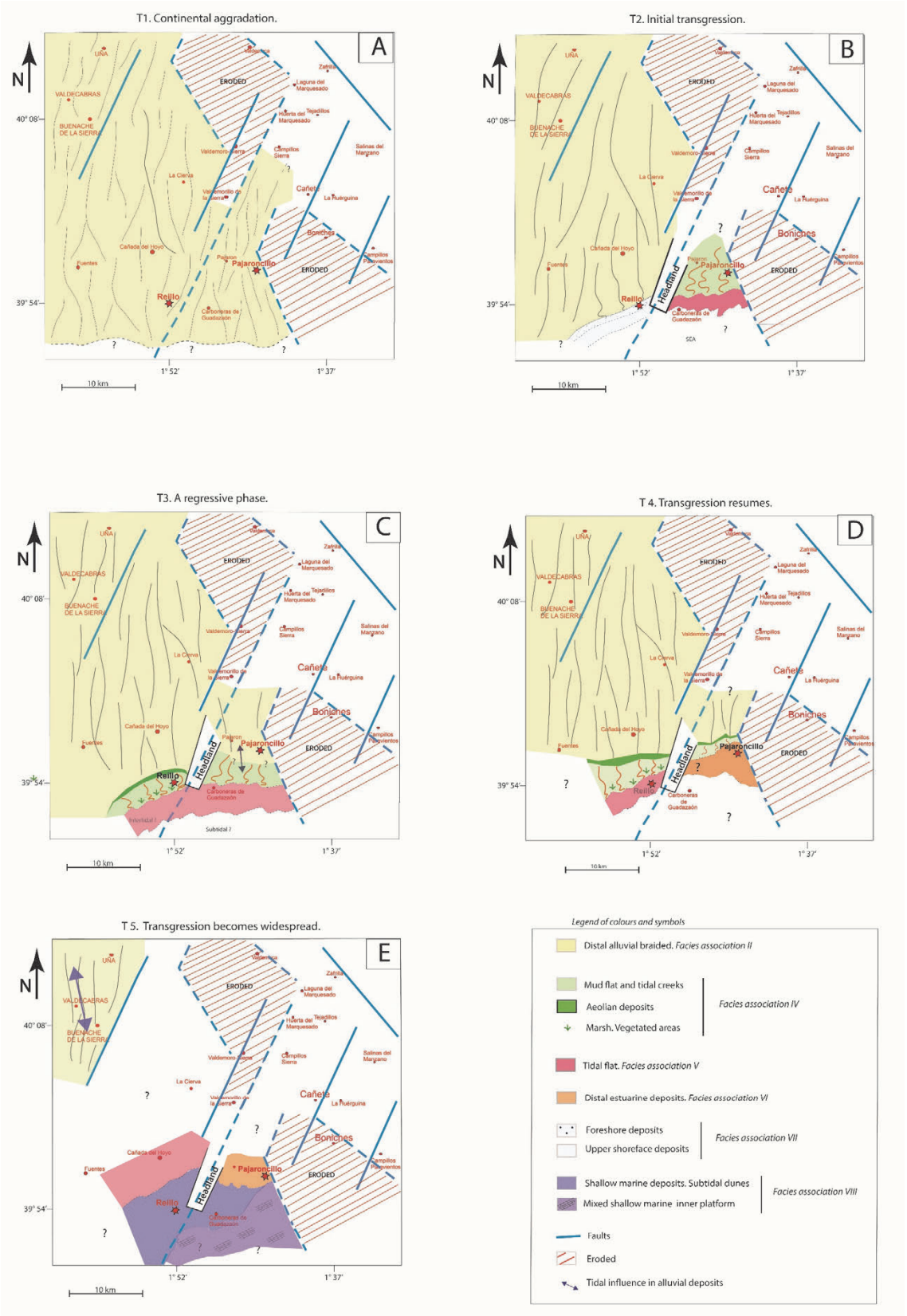

Fig. 11.8. Palaeogeographical maps showing the sedimentary evolution and the transgression in the Reíllo and Pajaroncillo outcrops at five evolutionary stages corresponding to the five in-trend stratigraphic units described. The figure includes palaeogeographical reconstructions during: (A) T1 ("in-trend" Unit 1), (B) T2 ("in-trend" Unit 2), (C) T3 ("in-trend" Unit 3), (D) T4 ("in-trend" Unit 4), and (E) T5 ("in-trend" Unit 5). After Bueno-Cebollada et al. (2022).

Conversely, the Pajaroncillo outcrop shows a much simpler situation regarding depositional environments during this third stage, as the succession only consists of tidally-modulated alluvial deposits which represent the seawards advance of the braidplain system during this regressive stage.

The occurrence of regressive episodes within a major transgressive pulse, like the one interpreted in T3, is not unusual in the sedimentary record. In this regard, the term punctuated transgression (Cattaneo and Steel, 2003) defines this style of transgressive shoreline migration. It is defined as the disruptions happening in a long-term transgressive system (such as the Utrillas Gr - La Bicuerca Mb succession) when the sediment supply inputs overcome the increase in accommodation rates for limited periods; therefore, leading to short-term regressive periods within an overall transgressive succession. Such an increase in sediment supply rates is materialised in a progradation of more proximal sedimentary environments.

T4. Transgression resumes:

This stage represents a new change in relative sea level, which is reflected by a new transgressive pulse (Fig. 11.8D). During this stage, the promontory between the two studied locations still acts as a geographic barrier and, therefore, it defines different sedimentary environments. The base of the unit that defines this stage (Unit 4) can be interpreted as an MRS (if the emphasis is placed on the end of the regressive episode of T3) or a TS (if the emphasis is placed on the new transgression during the onset of T4).

In the Reíllo outcrop, the stage T4 consists of tidal flat deposits developed in an inter- to subtidal environment which, compared to the supratidal sub-environment described in T3, shows the resumption of the transgression and a retrogradation as the tidal flat sub-environments migrate landward.

In the Pajaroncillo outcrop, T4 consists of an inter- to subtidal estuarine environment dominated by mudstone and marls over which compound tidal dunes migrate in a northward direction (Fig. 8.9). The sedimentary succession observed at T4 in Pajaroncillo resembles that of the lower Eocene Baronia Fm in the Ager Basin (NE Spain) (Olariu et al., 2012) in which successive series of compound tidal dunes were deposited in a tectonically controlled muddy coastal setting.

Strike variability in depositional systems depends on several factors: location of the sediment sources, coastal morphology, and local subsidence (Cattaneo and Steel, 2003). In the study area, these factors controlling along-strike variability were: i) the relative position of the braidplain system towards the north and northwest of the study area (i.e., Chamizo-Borreguero et al.,

2016; Bueno-Cebollada et al., 2021), concerning the sediment sources; ii) regarding coastal morphology, the main point to consider is the spatial relationship between open-sea areas versus embayed or restricted estuarine areas happening in a few kilometres in extent, as well as the existence of a promontory acting as a geographical barrier; and, iii) the local subsidence trends which were essentially controlled by the existing fault system between the Reíllo and Pajaroncillo outcrops (Fig. 10.3, 10.4). In this regard, during the T4 depositional stage, this fault system was active, producing significant differential subsidence, which is reflected by the conspicuous thickness variability observed between both studied sections (Fig. 11.1). The differential subsidence produced during the deposition of T4 was characterised by a much greater sinking eastern from the fault in the Pajaroncillo outcrop, which subsequently allowed for a greater space for the accommodation of sediment in this location than in Reíllo. The thickness of the successions is 5 and 20 m for Reíllo and Pajaroncillo, respectively. Examples of syn-sedimentary differential subsidence producing thickness variability in similar coastal-transitional environments have been previously reported in the literature: i.e., the Upper Cretaceous Cardium Fm, in Canada, is affected by a set of faults that determined its sedimentary style and thickness variability (Hart and Plint, 2003).

Additionally, the end of this palaeogeographic stage is characterised by subaerial exposure and emersion before the arrival of a last depositional stage of the Utrillas-La Bicuerca sedimentary succession. This subaerial exposure event is best noticed in the Pajaroncillo outcrop (Fig. 11.7B), where the occurrence of potholes in the top surface of Unit 4 reflects wave abrasion and scour in subaerially-exposed coastal settings (Ji et al., 2018), and therefore the emersion of the sedimentary succession.

T5. Transgression becomes widespread.

During this stage, the Reíllo outcrop consisted of a subtidal marine environment dominated by the deposit of a stacked tidal dune succession (Fig. 11.5), which migrated in a NE direction.

Conversely, the Pajaroncillo outcrop shows a different scenery. Here, the succession is dominated by strata deposited in a muddy outer estuarine environment (Fig. 11.6), which may locally present isolated tidal dunes migrating in a N/NNE direction. Additionally, the estuarine environment evolves into a mixed siliciclastic-carbonate inner ramp during this stage upward in the succession, as the transgression advances.

It is also noteworthy to mention that the migration pathway of the coastal sandy bedforms in Reíllo (NE) and Pajaroncillo (N) coincides to a great extent with the migration directions described for the Jurassic deposits in the study area (Aurell et al., 2019). This disparity between

the two studied outcrops is noticeable during the stages T4 and T5. During the deposition of the sediments that comprise the T5 stage, the transgression continued and advanced more landward than during any of the former palaeogeographic stages, and a shallow marine succession becomes more generalised all over the study area (Fig. 11.8E). The sedimentary environments and depositional styles in the studied localities are still different, though they show signs of some homogenisation. This fact essentially means that, during this stage, it should have still existed a tectonically-controlled promontory acting as a geographic obstacle between both outcrops. However, the lack of variability between both outcrops regarding thickness (differential subsidence), might reflect a possible relaxation of tectonic activity during T5. The end of the fifth stage precludes a regional-scale homogenisation in the sedimentary succession both regarding sedimentary environments, depositional style, and thickness of the succession 234eneralized234d by the deposit of the green marls of the lower Cenomanian Chera Fm (Giménez et al., 1993; Sopeña et al., 2004; Martín-Chivelet et al., 2019b). The sedimentation of the Chera Fm reflects the ultimate drowning and shutdown of the braidplain system in the Cuenca Basin (Bueno-Cebollada et al., 2021) and the advent of the widespread carbonate platform systems which existed in many areas of the Iberian basin during most of the Late Cretaceous times (Segura et al., 2004; Sopeña et al., 2004; Martín-Chivelet et al., 2019b).

11.4. Integration of the results within the regional sequence stratigraphic framework.

A sequence stratigraphic scheme for the upper Albian to middle Cenomanian record from the South Iberian Basin was originally developed for the Valencia Basin (located towards the SE of the study area of this work and representing a more seaward position in the Western Tethys) (Fig. 5.1), as well as for the Prebetic Domain, where the depocenter was located southwards (Giménez et al., 1993). However, this scheme has never been applied to the laterally equivalent and more proximal Albian to Cenomanian successions of the Cuenca Basin.

In general, the Cuenca Basin and, more specifically, the studied sections in Reíllo and Pajaroncillo present several difficulties in carrying out sequence stratigraphic interpretations. These complexities are due to several factors: i) the reduced thickness of the succession due to the position in a sedimentary basin edge (Cuenca Basin), compared to the hundred-metre-thick successions present in more depocentral areas (i.e., Valencia Basin). Ii) The stratigraphic record of the succession analysed in this work is predominantly siliciclastic, and it was deposited as a suite of sedimentary environments ranging from purely continental alluvial to transitional and shallow marine. Conversely, most of the Albian to lower Cenomanian succession is dominated

by extensive carbonate platform systems in more distal areas of the basin, such as the Valencia Basin (Giménez et al., 2004; Martín-Chivelet et al., 2019a). iii) It is generally accepted that the accommodation was greater and controlled mainly by eustasy in the Valencia Basin (Sopeña et al., 2004), which permitted the identification of sequence stratigraphic units. Conversely, in the Cuenca Basin, the result of our work reveals the influence of local tectonic activity affecting the mid-Albian to lower Cenomanian succession.

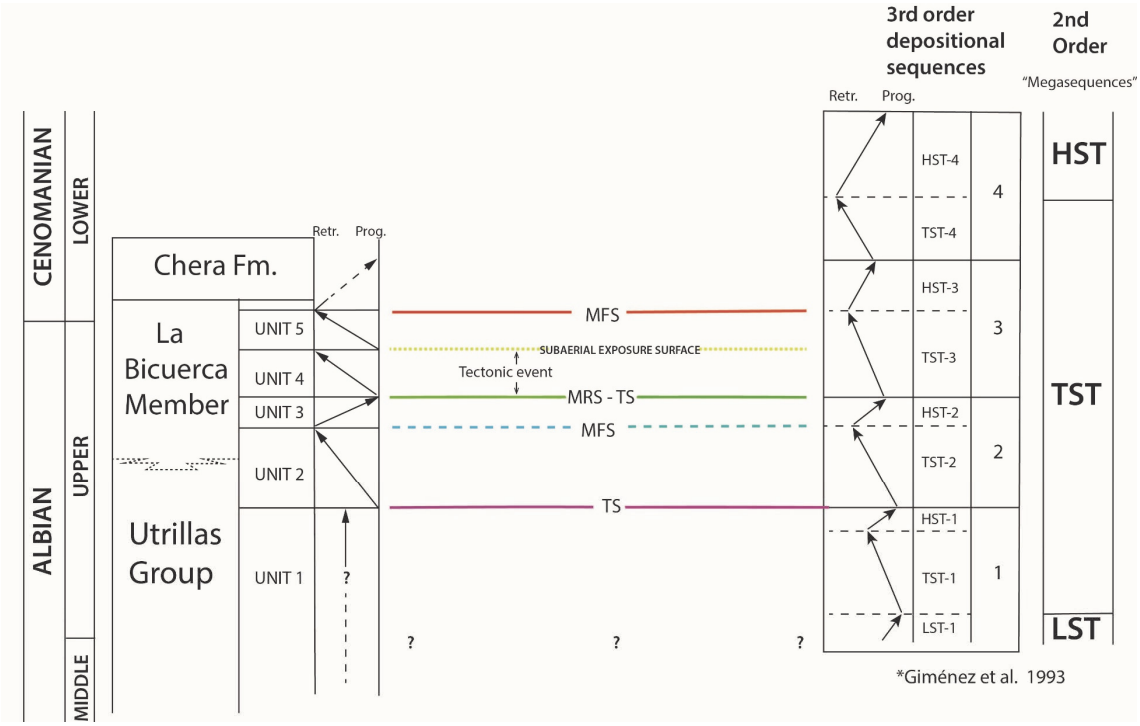

Fig. 11.9. Sequence stratigraphy chart for the Utrillas Gr - La Bicuerca Mb in the Serranía de Cuenca region showing the key sequence stratigraphy surfaces and "in-trend" stratigraphic units defined in this work and their position within the third-order sequences, and second-order "megasequences" originally defined by Gimenez et al. (1993) for the Valencia Domain (IBRS) and the Prebetic Domain (South Iberian Continental Margin). Original figure from Bueno-Cebollada et al. (2022).

Combining these three factors makes establishing a sequence stratigraphic interpretation in the study area challenging, being particularly difficult to identify formal sequence stratigraphic units and their hierarchy. Giménez et al. (1993) defined a second-order sequence spanning late Albian to middle Cenomanian times, which is composed of five third-order depositional sequences. The depositional sequences one to three as well as the TST (transgressive system tract) of sequence four of Gimenez et al. (1993) are upper Albian to lower Cenomanian and correspond to the "transgressive megasystem tract" of the second-order sequence. The HST (highstand system tract) of the fourth sequence and the whole fifth sequence are lower to middle Cenomanian and correspond to the "highstand megasystem tract" of the second-order sequence. The

“transgressive megasystem tract” of the second-order sequence defined by these authors reflects the maximum global eustatic transgression of the Cretaceous period (Haq, 2014). Each of the third-order depositional sequences defined by Giménez et al., (1993) consists of a TST and HST. It is noteworthy to mention that the sequence boundaries defined in these third-order sequences are not subject to extensive subaerial exposure since they are part of the TST of a second-order depositional sequence. Therefore, these sequence boundaries coincide with maximum regressive surfaces, which, in this case, are located at the transition between an HST of a given third-order depositional sequence and the TST of the overlying depositional sequence.

The mi—Albian to lower Cenomanian strata studied in this work correlates with sequences one to three of Gimenez et al. (1993), which show a 236eneralized transgressive trend (Fig. 11.9). To better understand this correlation, it is essential to bear in mind the eustatic trend corresponding to each of the five “in-trend” stratigraphic units described in this work. Considering that, we can establish the following sequence stratigraphic framework for the studied succession in the Cuenca Basin, based on the third-order depositional sequences defined by Giménez et al. (1993) (Fig. 11.9):

i) The sequence boundary of the third-order depositional sequence 1, correlates with the upper part of Unit 1, according to the eustatic trends observed (Fig. 11.9). The lack of record in the lowermost portion of the studied outcrops and the aggradational trend of Unit 1 prevents us from establishing a more accurate correlation in terms of third-order system tracts for the basal part of the succession (Fig. 11.9). However, a pollen sample collected in one of the lowermost outcropping levels of the Reíllo outcrop (corresponding to Unit 1) indicated a mid-Albian to early late Albian age (Bueno-Cebollada et al., 2021). In this regard, the contact between Units 1 and 2, interpreted as an MRS and TS, corresponds to the boundary between the HST of the first third-order depositional sequence (HST-1) and the TST of the second third-order depositional sequence (TST-2) (Fig. 11.9).

ii) The third-order sequence 2 correlates with Units 2 and 3. In this regard, Unit 2 is equivalent to the TST-2, while Unit 3 corresponds to the HST-2, based on the transgressive and regressive trends that these units respectively display (Fig. 11.9). The transgressive trend displayed by Unit 2 ends in an MFS (dashed blue line) (Figs. 11.1, 11.2B), which correlates with the MFS defined by these authors at the top of the TST-2 (Fig. 11.9). Additionally, the top of Unit 3, interpreted as an MRS that represents the maximum progradation of the regressive deposits of Unit 3 (green dotted line) (Fig. 11.4), correlates with the sequence boundary of the third-order depositional sequence 2 (Fig. 11.9).

iii) The transgressive system tract of the third-order depositional sequence 3 (TST-3) correlates with the Units 4 and 5 defined in this work (Fig. 11.9). These units have been distinguished based on their respective transgressive trends and the presence of a subaerial exposure surface (yellow line) (Figs. 11.7, 11.9) separating them, which is interpreted as an interruption of sedimentation. However, this disruption in sedimentation cannot be considered eustatic in origin since Units 4 and 5 correlate with the same transgressive system tract in the regional framework. Accordingly, the subaerial exposure surface indicates the conclusion or, at least, some attenuation of a minor tectonic event that led to the differential subsidence observed between the Reíllo and Pajaroncillo outcrops during the deposition of Unit 4 (Fig. 11.1). Finally, the contact between the TST-3 and HST-3 (third-order sequence 3), interpreted as an MFS, correlates with the top of Unit 5 (red line) (Figs. 11.7, 11.9). This MFS is considered as latest Albian in the Valencia Basin and the Prebetic Domain (Gimenez et al., 1993; Sopeña et al., 2004). However, in the Cuenca Basin, this contact is younger (early Cenomanian), showing a more marked diachroneity, particularly towards the NW of the study area of this work (Meléndez, 1983; Bueno-Cebollada et al., 2021).

12. Palaeogeographic evolution and allocyclical controls: a synthesis.

The palaeogeographical evolution of the Cuenca Basin during middle Albian to early Cenomanian times has been discussed, obtaining two complementary evolutionary models with different subdivisions (Fig. 12.1). These two models are originally included in Bueno-Cebollada et al. (2021) and Bueno-Cebollada et al. (2022), respectively.

The first model presented (Fig. 10.5) is based on the biostratigraphic data, later combined with data from sedimentary facies analysis (Fig. 10.6) and has permitted to divide the studied succession into three evolutionary stages, corresponding to three time spans: middle Albian, middle to late Albian, and late Albian to early Cenomanian. They reflect the landwards movement of the alluvial to shallow marine facies belts in the Cuenca Basin due to the marine transgression (Bueno-Cebollada et al., 2021).

Conversely, the second model proposed (Fig. 11.8) is rooted in the sequence stratigraphic analysis carried out in the Reíllo and Pajaroncillo outcrops and presents a higher resolution that has allowed the identification of five evolutionary phases (T1-T5) bounded by sequence stratigraphy surfaces (Bueno-Cebollada et al., 2022). Unfortunately, these five stages have not been identified in the rest of the studied outcrops owing to the strong compartmentalisation of the basin. Besides, the weaker eustatic signal in the proximal facies belts (due to their marked alluvial nature) has also contributed to hampering their identification.

This chapter includes a refined version of the palaeogeographical maps presented in Fig. 11.8 of this manuscript (Fig. 12.1) where the information obtained from sequence stratigraphy analysis has been combined with the information obtained from sedimentary correlations (Figs 10.1, 10.2, and 10.3) and the facies analysis. Despite the fact that the identification of the five stages in the studied outcrops (but for Reíllo and Pajaroncillo) is tentative, this has permitted obtaining a more accurate picture of the palaeogeographical evolution of the Cuenca Basin during the mid-Albian to early Cenomanian times.

In this sense, the sequence stratigraphy-based evolutionary model has permitted refining the three-stage model obtained by the biostratigraphic data and the facies analysis (Fig. 12.1) and delving into the nature of the allocyclic factors controlling the evolution of sedimentary succession.

During the middle Albian, the lower part of the Utrillas Gr succession was mainly controlled by tectonism since inherited faults generated accommodation space, and the sedimentation was mainly restricted to low-lying areas (Figs. 10.1, 10.2). Conversely, the eustatic control becomes

more important during the late Albian to early Cenomanian in the Cuenca Basin (mostly coinciding with the stages T2-T5). In the studied successions, this eustatic control is materialised by the aggradational stacking pattern of the deposits of alluvial and estuarine floodplain successions in the proximal areas due to the increase in accommodation space. Similarly, we can foreshadow that tectonism was still active, giving rise to significant thickness variabilities due to differential subsidence (i.e., the accommodation space during stage T4 is differentially increased in Pajaroncillo compared to Reíllo, creating an enhanced sink for sediments in the former, which can be identified by the thickness variability between both sections [Fig. 11.1]).

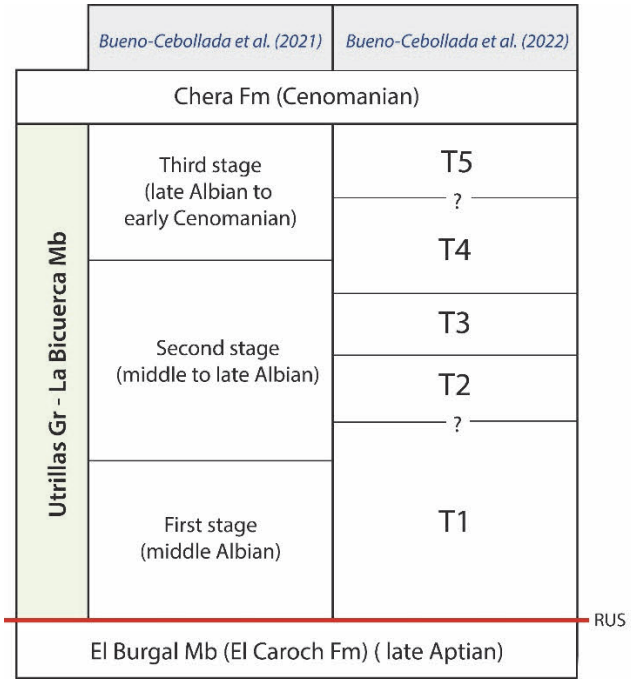

Fig. 12.1. Equivalences between the two subdivisions of the Utrillas Gr - La Bicuerca Mb succession in the Cuenca Basin, according to Bueno-Cebollada et al. (2021) and Bueno-Cebollada et al. (2022), respectively. RUS: regional unconformity surface.

Overall, the eustatic signal is strong during the deposition of the Utrillas Gr - La Bicuerca Mb (Bueno-Cebollada et al., 2021), coinciding with the global sea-level curve during the Albian to Cenomanian interval (Haq, 2014). The clear transgressive trend of the succession may be punctuated by regressive intervals (i.e., T3). Regressive episodes within an overall transgressive setting may be caused by independent accommodation/sediment supply variations during sea retreat (auto-cyclic shifting *sensu* Muto and Steel, 2000). In this sense, they may result from either a relative sea-level fall or a temporary slowdown in the eustatic rise in the basin, thus allowing sediment supply to overcome the rate of sea-level rise and leading to short progradational stages. Besides, tectonism seems to have played a key role, acting as one of the

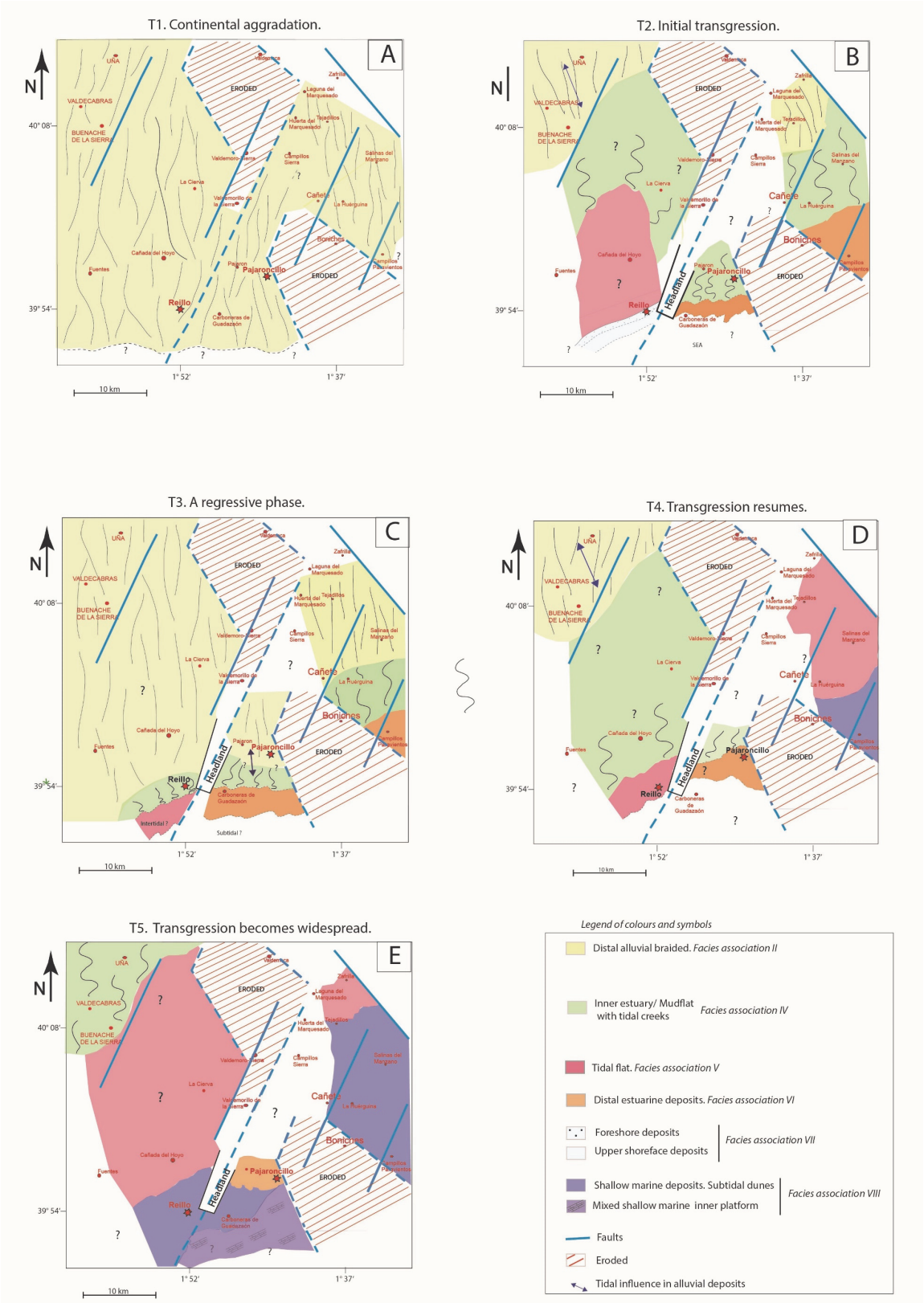

Fig. 12.2. Palaeogeographic evolution of the Cuenca Basin during the mid-Albian to early Cenomanian times. This final model is based on the correlations (Fig. 10.1, 10.2, 10.3) obtained after the combination of the evolutive stages revealed by biostratigraphic ages (Figs. 10).5, 10.6) and the sequence stratigraphic analysis (Fig. 11.8). Original model constructed for this thesis.

main palaeogeographical and depositional controls of the succession. In this sense, the variability of the thickness (particularly significant during T4) between the studied sections (and the subaerial exposure conditions observed in Reíllo during the T4-T5 boundary) reflects that the basin was more tectonically active than expected for the onset of a post-rift stage, as the Utrillas Gr–La Bicuerca Mb succession is traditionally considered in the southern part of the IBRS (Salas et al., 2001; Sopeña et al., 2004; Martín-Chivelet et al., 2019a, 2019b).

Finally, this chapter includes a final hypothesis of the palaeogeographical evolution of the studied area (Fig. 12.2) where the data obtained from sequence stratigraphy analysis has been combined with the information on the evolutive stages revelaed by the bioestratigraphic analysis (Figs. 10.1, 10.2, 10.3, 10.5 and 10.6) and the subsequent correlation of their facies association belts. Even though the identification of the five stages in the studied outcrops (but for Reíllo and Pajaroncillo) is tentative, this has permitted obtaining a more accurate picture of the palaeogeographical evolution of the Cuenca Basin during the mid-Albian to early Cenomanian times.

PART IV: FURTHER IMPLICATIONS TO THE KNOWLEDGE OF THE "MID"- CRETACEOUS PALAEOGEOGRAPHIC EVOLUTION OF IBERIA

This final part of the manuscript discusses two of the many possible larger-scale implications that might stem from the scientific breakthrough that this research entails. More concretely, the two lines discussed over the following pages deal with: (i) the syn-rift – post-rift implications of this research within the broader geo-tectonic context of Iberia (see chapter 13 of this manuscript); (ii) the comparison with the coeval upper Albian amber-bearing successions from other basins Iberia (Maestrazgo and Basque-Cantabrian Basins) aiming at explaining the reasons for the lack of amber deposits in the Cuenca Basin (see chapter 14 of this manuscript).

13. Integration within the geo-tectonic context of Iberia.

The widespread presence of the Utrillas Gr succession all over the intraplate basins of Iberia probably indicates the existence of supra-basinal scale controls in its deposition. During the Cretaceous, Iberia was characterised by a complex tectono-sedimentary evolution in its intraplate areas that was driven by the development of three major rift systems (the Alpine Tethys Ocean, the West Iberian margin rifting, and the North Iberian margin rifting), which eventually became ocean basins (Aurell et al., 2019). Besides, those diverse geotectonic scenarios evolved within the framework of the greatest global transgression in Earth's History (Hay, 2008). In such a situation, the global transgression was recorded differently depending on the interplay with the dominant tectonic processes developed in the different margins and the intraplate areas. Probably, the greatest contrasts occurred between the NW Atlantic margin of Iberia, which was undergoing breakup at that moment, and the eastern basins of Iberia facing the Alpine Tethys Ocean.

The "mid"-Cretaceous syn-rift to post-rift transition in the intraplate areas of Iberia (IBRS) is traditionally attributed to the deposit of the Utrillas Gr, which has been considered the first post-rift lithostratigraphic unit (Sopeña et al., 2004; Martin-Chivelet et al., 2019a, b). However, the subtleties of this transition are not well-understood yet.

The Aptian – Albian boundary in the intraplate basins of Iberia was marked by a eustatic fall that limited sedimentation to the most subsided areas (Sopeña et al., 2004), producing widespread erosion or non-deposition, and giving rise to an unconformity that represents the base of the Utrillas Gr. In the Cuenca Basin, this unconformity represents a hiatus that includes the lower

Albian strata, and it is overlain by the mid-Albian to lower Cenomanian Utrillas Gr succession (Bueno-Cebollada et al., 2021).

In the NW Iberian margin (Porto Basin) (Alves et al., 2009), the Aptian-Albian transition comprises an unconformity that represents the final lithospheric breakup between Iberia and Newfoundland and the emplacement of the oceanic crust due to the northward expansion of the rift in the Atlantic Realm (Soares et al., 2012; Soares et al., 2014; Alves and Cunha, 2018). This lithospheric breakup unconformity is overlain by a lower Albian to Cenomanian sedimentary sequence, the breakup sequence (*sensu* Soares et al., 2012), that represents the transitional period between the lithospheric breakup and the establishment of thermal subsidence as the main tectono-sedimentary control in NW Iberia (Soares et al., 2012; 2014; Alves et al., 2020). Therefore, the breakup sequence observed in the NW Iberian margin is partly coeval with the mid-Albian to lower Cenomanian strata from the Cuenca Basin and corresponds to the Utrillas Gr - La Bicuerca Mb succession.

The breakup sequence in the NW Iberian margin begins with a marked forced regression during the early Albian times, corresponding to the first stratigraphic unit identified by Soares et al. (2012). The occurrence of this forced regressive system tract is associated with a flexural rebound of the lithosphere after its breakup, which produced subsidence in the distal parts of the margin and uplift in the shoulder areas of the rift (Soares et al., 2012, 2014; Alves and Cunha, 2018; Alves et al., 2020).

Conversely, the early to middle Albian is marked by a generalised transgression in the intraplate IBRS (Sopeña et al., 2004), which in the studied outcrops is represented by the aggradational stacking pattern of the continental deposits observed during the stage T1 (Fig. 11.9) due to an increase in accommodation space as the transgression advanced landwards. We attribute the lack of lower Albian forced regressive strata to the concomitant effect of a rising relative sea level (Sopeña et al., 2004; Haq, 2014) and the eastwards tectonic tilting of Iberia due to the rift flank uplift that accompanied the northwards progression of the breakup of the western Iberian margin since the Jurassic – Cretaceous transition (Aurell et al., 2019). Therefore, the eastwards tectonic tilting favoured the Western Tethys transgression in the intraplate IBRS during the middle Albian, coinciding with the stage T1 identified in the Cuenca Basin. Likewise, it might explain the enhanced clastic input arriving in the IBRS from the uplifted areas of Iberia (Aurell et al., 2019), which characterised the sedimentation of the Utrillas Gr. This tectonic forcing enhanced the eustatic signal (marked by a relative sea-level rise), therefore favouring a faster transgression in Eastern Iberia.

During the late Albian to early Cenomanian, coinciding with stages T2-T5 identified in the present work, the NW Iberian margin was characterised by a succession dominated by a

generalised transgression punctuated by aggradation and regression (Units 2 to 4 of the breakup sequence *sensu* Soares et al., 2012). It is not possible to obtain a more accurate correlation between the breakup sequence from NW Iberia and the here studied "in-trend" units due to the limitations of the biostratigraphic dating, which do not allow constraining better their relative ages (Bueno-Cebollada et al., 2021). However, we can tentatively ascertain that the stages T2 to T5 (late Albian to early Cenomanian) identified in this work correspond to the Units 2 to 4 of the NW Iberian breakup sequence (see figure 5 in Soares et al., 2012) based on the comparison with their relative ages (Soares et al., 2012) and the similarities between the T-R trends observed (Fig. 11.9). These similarities seem to indicate that during the stages T2-T5 sedimentation in the Cuenca Basin was mainly controlled by eustasy, yet local tectonism was active at times (i.e., stage T4). The occurrence of local tectonic pulses in the intraplate areas of Iberia is related to far field extension induced by the coeval continuation of the rifting in the Northern Iberian margin (Cadenas et al., 2018; Aurell et al., 2019), eventually leading to the lithospheric breakup in the North Pyrenean Basins during the late Albian to early Cenomanian (Saspiturry et al., 2021).

To summarise, the syn-rift to post-rift transition in the Cuenca Basin is a gradual process, where tectonic and eustatic controls alternated and/or coexisted in time and space. These controls were defined by a robust eustatic signal, as can be expected owing to the generalised relative sea-level rise conditions that characterised the "mid"-Cretaceous, and active extensional tectonism related to far field necking phenomena. In this sense, the imprint of these controls should have been recorded in other intraplate basins of Iberia; therefore, future research should be extended to other areas of Iberia in order to cast light on this topic.

14. Key constraints of the accumulation and preservation of amber deposits: accounting for the lack of mid-Cretaceous amber-bearing strata in the Cuenca Basin.

The research carried out during this Ph.D. thesis also sheds light on the understanding of the upper Albian amber sites of Iberia. Despite the fact that amber-bearing strata have not been found in the studied outcrops from the Cuenca Basin, the multidisciplinary approach presented here provides insightful sedimentological, palaeoclimatic, and palaeoecological data that can be applied to the study of coeval amber-bearing succession from the Maestrazgo Basin (San Just, Arroyo de la Pascueta and La Hoya-Cortes de Arenoso amber-bearing outcrops [Delclòs et al., 2007; Peñalver et al., 2007; Peñalver and Delclòs, 2010]), eastern Spain, and the Basque-Cantabrian Basin (Peñacerrada amber-bearing outcrop [Alonso et al., 2000; Delclòs et al., 2007; Barrón et al., 2015]), northern Spain. In this sense, the palynostratigraphic study carried out in this Ph.D. thesis (Bueno-Cebollada et al., 2021) has been paramount since it has permitted establishing a sound biostratigraphic framework that allows carrying out this comparison.

The studied mid-Albian to early Cenomanian vegetal communities from the Cuenca Basin show similarities to those found in the mentioned coeval amber-bearing outcrops from the Maestrazgo (Peñalver et al., 2007) and Basque-Cantabrian Basins (Barrón et al., 2015). In this sense, the mid-Albian to early Cenomanian floral communities from (eastern and northern) Iberia were dominated by conifers belonging to Cheirolepidiaceae, Cupressaceae and Araucariaceae, which have been proposed as the possible conifer families that produced the resin in the mentioned Spanish amber-bearing outcrops (Menor-Salván et al., 2016).

According to Grimaldi (1996), there are four decisive factors in producing and preserving amber deposits in the sedimentary record: (i) the exudation of the right type of resin; (ii) the existence of nearshore plant communities as the source of large resin quantities; (iii) resins must become concentrated and lastly; and (iv) an appropriate burial in sediments. The first two factors are directly related to the existence of the resin-producer plant(s), which likely existed in the Cuenca Basin as it did in other coeval basins of Iberia where similar palaeofloras were identified. Conversely, the third and fourth factors have to do to a great extent with the dynamics of the sedimentary systems and the taphonomic processes that allow the preservation of the resin. Therefore, the absence of amber-bearing strata in the mid-Albian to lower Cenomanian deposits of the Cuenca Basin and its occurrence in coeval deposits of Iberia might be directly related to the biostratinomic processes that control the transport and accumulation of the resin, allowing for the formation of a deposit. This is closely linked to the sedimentary environments that existed when the resin was being produced and the transport paths for the sediments. Most of

the Albian amber deposits of Iberia are considered allochthonous accumulations where fluvial and estuarine watercourses transported the resin towards protected nearshore areas where it was deposited (Martínez-Delclòs et al., 2004; Seyfullah et al., 2018).

Late Albian sedimentation in the Maestrazgo Basin was dominated by an extensive fore-erg system where aeolian dunes interacted with the coastal deposits of the Western Tethys (Rodríguez-López, 2008; Rodríguez-López et al., 2008, 2009, 2012, 2013). Similarly, coeval sedimentation in the Basque-Cantabrian Basin was characterised by the deposit of a more geographically restricted fore-erg system that alternated in time and space with ephemeral alluvial/wadi (inland) and shallow marine (nearshore) deposits of the Proto-Atlantic (Rodríguez-López et al., 2020). The occurrence of aeolian dunes in these coastal areas, constantly flooded by the sea, produces low-energy restricted areas between the dunes prone to be waterlogged, giving rise to interdune coastal swamps or lagoons that provide the perfect conditions for the long-term preservation of the allochthonous resin. These waterlogged areas provide the anoxic conditions capable of inhibiting microorganism growth that slows down the breakdown of the resin (Wyse, 2012). Additionally, the relatively frequent migration of the aeolian dunes in coastal ergs would have ensured a rapid burial allowing for better preservation of the resin and formation of amber-bearing sedimentary successions.

Considering this line of thinking, the most plausible explanation for the lack of Albian amber-bearing strata in the Cuenca Basin seems to be related to the higher energy of the sedimentary system and its transport path, which is directly linked to the ephemeral nature of the braidplain system. If the resin was produced in the alluvial floodplain, it was (most likely) washed into channels and transported downstream by high energy streams that worked seasonally, preventing its deposition under anoxic conditions, and fostering its breakdown under oxidising conditions during the dry season. This hypothesis agrees with the highly oxidising nature of the taphonomic environments that dominate most of the distal alluvial to inner estuarine floodplain deposits (Fig. 8.2F-H, 8.6E, F), favoured by the well-drained conditions of the ground together with a marked seasonal climate characterised by a long dry season, typical of a savanna biome.

However, the presence of Albian amber-bearing strata in the Cuenca Basin should not be entirely disregarded, despite not finding any accumulations in the outcrops studied in this thesis. In this sense, more research needs to be done in the Cuenca Basin, paying particular attention to those facies deposited in nearshore areas under reducing conditions where the appropriate burial for the preservation of the resin might have happened.

PART V: CONCLUDING REMARKS.

(English version)

1. The results of the Ph.D. thesis presented in this manuscript have met the main objective of the research which is the study of the Utrillas Gr and La Bicuerca Mb (Aras de Alpuente Fm) sedimentary succession in the Cuenca Basin (Iberian Ranges, Eastern Spain) based on an integrative multidisciplinary approach that includes the analysis of stratigraphic, sedimentological, palynological, macroflora and palaeoedaphological datasets. This research sheds light on the Albian-Cenomanian marine transgression in the Cuenca Basin, reflecting the progressive landward expansion of Western Tethys in Iberia.
2. The first target of this research has been the obtention of a sound biostratigraphic dating that has allowed establishing a relative age for the studied succession based on palynostratigraphy. It has permitted us to infer a middle Albian to early Cenomanian palynostratigraphic age for the Utrillas Gr and La Bicuerca Mb sedimentary succession in the Cuenca Basin. Additionally, it has also enabled the identification and dating of the Aptian strata in some locations of the study area, corresponding to the Contreras Fm (early Aptian) and the El Burgal Mb (El Caroch Fm) (late Aptian), which has helped to identify the base of the Utrillas Gr.
3. The middle Albian to early Cenomanian palynofloras from the Cuenca Basin reflect that the vegetation was dominated by evergreen plants adapted to arid conditions in lowland and nearshore areas. It was mainly composed of cheirolepidiacean and cupressacean conifers, showing oscillations in their relative proportions through the succession. To a lesser extent, Araucariaceae also represents a certain proportion of the studied palynofloras, indicating a relative closeness to the palaeocoast. Additionally, bisaccate pollen grains of Pinaceae/Podocarpaceae affinities compose a small proportion of the palynofloras and likely represent allochthonous vegetation from coeval highland areas.
4. The mid-Albian to early Cenomanian floral communities of the Cuenca Basin have also been studied through the macroflora remains found in a fossil bed in the Cañada del Hoyo outcrop. The taxa identified are dominated by Coniferales that include specimens of the genera *Frenelopsis*, *Glenrosa* and *Dammarites* and, tentatively, it may also include leaf remains attributable to the genus *Erethmophyllum* (Ginkgoales). Palaeofloral assemblages dominated by these taxa were relatively common in western Europe during the Cenomanian and they are interpreted as floral communities that developed in nearshore supratidal environments (i.e., salt marshes).

5. The sedimentary facies analysis carried out in the mid-Albian to lower Cenomanian succession has permitted the identification of eight facies associations that range from proximal alluvial braidplain to shallow marine deposits: (FA I) Proximal alluvial, (FA II) Distal alluvial, (FA III) Aeolian dunes, (FA IV) Inner estuarine, (FA V) Tidal flat, (FA VI) Outer estuarine, (FA VII) High-gradient coastal deposits, and (FA VIII) Shallow marine mixed deposits. The study of the distribution of the facies associations both in time and space together with the palynostratigraphic data has permitted the identification of three stages (middle Albian, middle – late Albian, and late Albian – early Cenomanian) that reflect the progressive NW advance of the fluvio-estuarine and shallow marine facies belts in the Cuenca Basin due to the "mid"- Cretaceous marine transgression.
6. Three palaeosoil profiles have been analysed in the Buenache de la Sierra outcrop and interpreted as Spodosols based on petrographic, geochemical, and mineralogical datasets. The palaeoedaphophological study has permitted inferring that the palaeoclimate conditions during the depositional time of the Utrillas Gr - La Bicuerca Mb succession in the study area was a tropical one with a marked seasonality and an estimated palaeoprecipitation ranging from 1000 to 1500 mm per year. These palaeoclimatic inferences conform with a tropical savanna-type climate; however, they reflect more humid conditions than those inferred from palynological and sedimentological datasets. To explain this mismatch, the proposed climatic model is rooted in the cyclical latitudinal shifting of the "mid"-Cretaceous climatic belts, giving rise to an alternation of arid and more humid periods during the studied time span and explaining the discrepancies among the different datasets.
7. A sequence stratigraphic analysis carried out in the Reíllo and Pajaroncillo outcrops has allowed obtaining a more accurate picture of the mid-Albian to early Cenomanian transgression due to their location on the coastal fringe of the Cuenca Basin. This part of the study has permitted to divide the Utrillas Gr - La Bicuerca Mb succession into five units characterised by their stratigraphic tendencies ("in-trend" units) which are bounded by correlatable sequence stratigraphic surfaces, and correspond to five evolutive phases (T1-T5): (i) a continental aggradational stage (T1), dominated by alluvial deposition; (ii) an initial transgression stage (T2) dominated by an open coast setting in Reíllo and a restricted mudflat system in Pajaroncillo; (ii) a regressive stage (T3), during which continental alluvial to supratidal environments deposited; (iv) a resumption in transgression (T4), characterised by an array of inter- to subtidal environments; and (v) a deepening stage (T5), when the transgression advanced landward, giving rise to the most distal deposits of the studied succession.

8. The sequence stratigraphic analysis has permitted us to delve into the subtleties of the transgression identifying minor regressive pulses (T3) within the major transgressive trend of the succession. Additionally, the results of the analysis in the Cuenca Basin have been correlated and integrated within the regional framework proposed by Gimenez et al. (1993) for the Valencia Basin and the Prebetic Domain, identifying third-order depositional sequences and their respective system tracts in the studied succession. Likewise, the whole studied succession is part of a second-order transgressive system tract. Finally, the sequence stratigraphic analysis has provided an improved time framework for the reconstruction of the palaeogeographical evolution, allowing the identification of the five evolutive phases instead of the three stages identified by the sedimentological and palynostratigraphic analyses.
9. Sedimentation was mainly controlled by tectonism during the middle Albian (stage T1) since accommodation space was generated by the activity of extensional faults inherited from previous phases of basin infill, and being deposition restricted to low-lying areas of the basin. Conversely, the eustatic control becomes more important during the late Albian to early Cenomanian, mostly coinciding with the stages T2-T5. Notwithstanding, tectonism was still active in the basin, acting as discrete pulses, producing significant differential subsidence and, hence thickness variabilities in the succession among different localities.
10. Additionally, the integration of this research within the broader geotectonic context of Iberia has permitted shedding new light on the tectono-sedimentary evolution that characterised the Albian to early Cenomanian time-span in the supra-regional scale. This research provides a refined understanding of the middle Albian to early Cenomanian transition from the Late Jurassic-Early Cretaceous syn-rift stage to the Late Cretaceous post-rift stage in the southern part of the IBRS, proving that the influence of extensional tectonics lasted longer than initially thought.

CONCLUSIONES

(Versión en español)

1. El objetivo de esta Tesis Doctoral ha sido el estudio de la sucesión sedimentaria compuesta por el Grupo Utrillas y el Miembro La Bicuerca (Formación Aras de Alpuente) en la Serranía de Cuenca (Cordillera Ibérica, España). Se ha desarrollado siguiendo un enfoque multidisciplinar e integrador que ha incluido análisis estratigráficos, sedimentológicos, paleoflorísticos y paleoedafológicos. Esta tesis ha permitido avanzar en el conocimiento de la transgresión marina del Albiense-Cenomaniense, demostrando el progresivo avance del Tethys hacia noroeste en la región de la Serranía de Cuenca.
2. El estudio bioestratigráfico realizado a partir de asociaciones palinológicas ha permitido atribuir las sucesiones estudiadas al intervalo Albiense medio - Cenomaniense inferior. Además, ha posibilitado la identificación y datación de las unidades Aptienses que se corresponden con la Formación Contreras (Aptiense inferior) y el Miembro El Burgal (Formación El Caroch) (Aptiense superior). La identificación de estas unidades ha ayudado a situar la base del Grupo Utrillas en los afloramientos estudiados.
3. Las palinofloras del Albiense medio al Cenomaniense inferior reflejan la existencia de una vegetación perennifolia adaptada a condiciones de aridez que se desarrolló en zonas costeras y cercanas a éstas. La vegetación estuvo principalmente constituida por coníferas de las familias Cheirolepidaceae y Cupressaceae cuyos porcentajes polínicos muestran co-dominancia. En menor medida, éstas están compuestas por granos de polen de Araucariaceae y quistes de dinoflagelados, que reflejan cercanía a la paleocosta del Tethys. Por otro lado, debido a la presencia de pequeñas cantidades de polen bisacado de tipo Pinaceae/Podocarpaceae, que fue transportado por el viento desde zonas elevadas relativamente cercanas al área de estudio (Macizo Ibérico), se infiere la existencia de una vegetación coetánea de carácter montano.
4. El estudio macroflorístico del afloramiento Albiense superior-Cenomaniense inferior de Cañada del Hoyo, ha permitido reconocer una asociación dominada numéricamente por coníferas de los géneros *Frenelopsis*, *Glenrosa* y *Dammarites*, así como por restos que posiblemente se deban atribuir a *Erethmophyllum* (Ginkoales). Las asociaciones paleoflorísticas dominadas por estos taxones, que son relativamente frecuentes en el registro paleontológico del oeste de Europa durante el Cenomaniense, se interpretan como correspondientes a comunidades florísticas de ambientes costeros supramareales (p.ej. marismas).

5. El análisis de facies sedimentarias ha permitido identificar ocho asociaciones de facies en la sucesión Albiense medio – Cenomaniense inferior que incluyen: (FA I) Alluvial proximal, (FA II) Alluvial distal, (FA III) Dunas eólicas, (FA IV) Estuario interno, (FA V) Llanura de marea, (FA VI) Estuario externo, (FA VII) Depósitos costeros de alto gradiente y (FA VIII) Depósitos marinos someros mixtos. El estudio de la distribución temporal y espacial de estas asociaciones ha permitido, junto con los datos palinoestratigráficos, la identificación de tres etapas evolutivas (Albiense medio, Albiense medio - superior y Albiense superior - Cenomaniense inferior) que reflejan el avance de los cinturones de facies hacia el noroeste de la cuenca, como resultado de la transgresión marina del Albiense medio - Cenomaniense inferior.
6. Los tres paleosuelos analizados en el afloramiento de Buenache de la Sierra mediante observaciones *in situ* complementadas con un análisis petrográfico, geoquímico y mineralógico de los horizontes han sido interpretados como espodosoles. Su estudio ha permitido inferir que durante el Albiense medio - Cenomaniense inferior el clima era tropical y estaba caracterizado por una marcada estacionalidad con respecto a las precipitaciones. Se ha inferido que la precipitación acumulada anualmente de entre 1000 y 1500 mm que ha permitido interpretar un clima de tipo sabana tropical. Estas inferencias paleoclimáticas discrepan de las sedimentológicas y palinológicas, que indican una mayor aridez ambiental. Para explicar estas discrepancias, se propone una hipótesis basada en un modelo que explica las variaciones climáticas por medio de cambios cíclicos en la latitud de los cinturones climáticos durante el Cretácico medio. Dicha ciclicidad dio lugar a una alternancia de periodos más húmedos (al menos estacionalmente) que alternaron con periodos áridos, lo que ha permitido explicar las discrepancias entre los resultados obtenidos en esta tesis doctoral mediante diferentes conjuntos de datos.
7. El análisis estratigráfico secuencial llevado a cabo en los afloramientos de Reíllo y Pajaroncillo ha permitido obtener una mayor resolución de la transgresión del Albiense medio - Cenomaniense inferior en el área de estudio. Esto ha permitido dividir la sucesión del Grupo Utrillas y el Miembro La Bicuerca en 5 unidades caracterizadas por sus tendencias ("in-trend" units) y limitadas por superficies estratigráficas secuenciales, que corresponderían a 5 etapas evolutivas diferenciables (T1-T5): (i) una etapa agradacional continental (T1), dominada por sedimentación aluvial; (ii) una etapa transgresiva inicial (T2) dominada por ambientes costeros y estuarinos; (iii) una etapa regresiva (T3), caracterizada por ambientes aluviales y supramareales; (iv) una nueva etapa transgresiva (T4), caracterizada por ambientes inter- y supramareales; y, (v) una

etapa de profundización (T5), en la cual la transgresión progresó hacia el NO invadiendo áreas continentales y dando lugar a los depósitos más distales de la sucesión.

8. El análisis secuencial ha permitido la correlación e integración de la sucesión estudiada dentro del marco secuencial regional propuesto por Giménez et al. (1993) para la Cuenca de Valencia y el Dominio del Prebético, y por tanto la identificación de secuencias deposicionales de tercer orden y sus respectivos cortejos sedimentarios, formando parte la totalidad de la sucesión estudiada de un cortejo transgresivo de segundo orden. Por último, el análisis secuencial aporta una mejor definición temporal a la reconstrucción de la evolución paleogeográfica, permitiendo separar 5 etapas evolutivas frente a las tres que se deducen a partir del patrón de edades construido mediante el análisis palinoestratigráfico.
9. Los factores alocíclicos que controlaron la sedimentación de la Serranía de Cuenca durante el Albiense medio – Cenomaniense inferior han sido estudiados basándose en los datos de los análisis sedimentológico y secuencial, apoyados por el marco biostratigráfico. La sedimentación durante el Albiense medio (etapa T1) estuvo restringida a zonas deprimidas de la cuenca y fue principalmente controlada por la tectónica, ya que el espacio de acomodación se generó mayoritariamente por la actividad extensional de fallas heredadas de etapas previas de relleno de la cuenca. Por el contrario, del Albiense superior al Cenomaniense inferior (principalmente etapas T2 a T5) la acomodación estuvo principalmente controlada por el eustatismo. Sin embargo, la tectónica se mantuvo activa en la cuenca, actuando en forma de pulsos y dando lugar a subsidencia diferencial que se refleja en las notables variaciones que presenta el espesor de las sucesiones en distintas localidades.
10. La integración de los resultados dentro del contexto geotectónico de Iberia ha permitido mejorar el conocimiento de la evolutión tectono-sedimentaria del intervalo Albiense medio – Cenomaniense inferior en una escala supra-regional. Más concretamente, esta tesis doctoral proporciona una visión más precisa de la transición de la etapa sin-rift (Jurásico Superior-Cretácico Inferior) a la etapa post-rift (Cretácico Superior) en la zona sur del IBRS, demostrando que la influencia de la tectónica extensional abarcó un lapso temporal más largo del que tradicionalmente se ha asumido.

REFERENCES

Aagaard, T., Greenwood, B., and Hughes, M., 2013. Sediment transport on dissipative, intermediate and reflective beaches. Earth-Science Reviews 124, 32–50.

Abbink, O., 1998. Palynological Investigations in the Jurassic of the North Sea. Ph.D. Thesis, Universiteit Utrecht, The Netherlands.

Abbink, O.A., Van Konijnenburg-Van Cittert, J.H.A., Visscher, H., 2004. A sporomorph ecogroup model for the Northwest European Jurassic–Lower Cretaceous: concepts and framework. Geologie en Mijnbouw 83, 17–38.

Afify, A.M., 2017. Ironstone Occurrences in the Northern Part of the Bahariya Depression, Western Desert, Egypt: Geology, Mineralogy, Geochemistry and Origin. Ph.D. Thesis, Universidad Complutense de Madrid, Spain.

Agasie, J.M., 1969. Late Cretaceous palynomorphs from northeastern Arizona. Micropaleontology 15 (1), 13-30.

Aguilar, M.J., Ramírez del Pozo, J., Riba, O., 1971. Algunas precisiones sobre la sedimentación y paleontología del Cretácico inferior en la zona de Utrillas-Villarroya de los Pinares. Estudios Geológicos 27, 497–512.

Al-Masrahy, M.A., Mountney, N.P., 2015. A classification scheme for fluvial–aeolian system interaction in desert-margin settings. Aeolian Research 17, 67-88.

Alberts, S.C., Altmann, J., Hollister-Smith, J.A., Mututua, R.S., Sayialel, S.N., Muruthi, P.M., Warutere, J.K., 2005. Seasonality and long term change in a savannah environment. Emergence 16, 17.

Allen, J.R., 1963. The classification of cross-stratified units. With notes on their origin. Sedimentology 2, 93-114.

Allen, J.R.L., 1980. Sand waves: a model of origin and internal structure. Sedimentary Geology 26, 281-328.

Alonso, A., Floquet, M., Mas, R., Meléndez, A., 1993. Late Cretaceous Carbonate Platforms: Origin and Evolution, Iberian Range, Spain. In: Simó, J.A.T., Scott, R. W., Masse, J.P., (Eds.) Cretaceous Carbonate Platforms, AAPG Memoir 56, 297–313.

Alonso, J., Arillo, A., Barron, E., Corral, J.C., Grimalt, J., López, J.F., López del Valle, R., Martínez-Delclos, X., Ortuño, V., Peñalver, E., Trincao, P., 2000. A new fossil resin with biological inclusions in Lower Cretaceous deposits from Alava (Northern Spain, Basque-Cantabrian Basin). Journal of Paleontology 74, 158e178.

Álvarez-Parra, S., Pérez-De La Fuente, R., Peñalver, E., Barrón, E., Alcalá, L., Pérez-Cano, J., Martín-Closas, C., Trabelsi, K., Meléndez, N., López Del Valle, R., Lozano, R. P., Peris, D., Rodrigo, A., Sarto I Monteys, V., Bueno-Cebollada, C. A., Menor-Salván, C., Philippe, M., Sánchez-García, A., Peña-Kairath, C., Arillo, A., Espílez, E., Mampel, L., Delclòs, X. (2021): Dinosaur bonebed amber from an original swamp forest soil. eLife, 10, e72477

Álvaro, M., del Villar, R.C., Vegas, R., 1979. Un modelo de evolución geotectónica para la Cadena Celtibérica. Acta Geológica Hispánica 14, 172–177.

Alves, T.M., Cunha, T.A., 2018. A phase of transient subsidence, sediment bypass and deposition of regressive–transgressive cycles during the breakup of Iberia and Newfoundland. Earth and Planetary Science Letters 484, 168–183.

Alves, T.M., Moita, C., Cunha, T., Ullnaess, M., Myklebust, R., Monteiro, J.H., Manuppella, G., 2009. Diachronous evolution of Late Jurassic–Cretaceous continental rifting in the northeast Atlantic (west Iberian margin). Tectonics 28, TC4003.

Alves, T., Fetter, M., Busby, C., Gontijo, R., Cunha, T.A., Mattos, N.H., 2020. A tectono-stratigraphic review of continental breakup on intraplate continental margins and its impact on resultant hydrocarbon systems. Marine and Petroleum Geology 117, 104341.

Alvin, K. L., 1974. Leaf anatomy of *Weichselia* based on fusainized material. Palaeontology 17, 587–598.

Alvin, K.L., 1982. Cheirolepidiaceae: Biology, structure and paleoecology. Review of Palaeobotany and Palynology 37, 71–98.

Andrews, P.B., Van der Lingen, G.J., 1969. Environmentally significant sedimentologic characteristics of beach sands. New Zealand Journal of Geology and Geophysics 12, 119–137.

Arche, A., López-Gómez, J., 1996. Origin of the Permian-Triassic Iberian Basin, central-eastern Spain. Tectonophysics 266, 443–464.

Arias, C., Doubinger, J., 1980. La limite Aptien–Albien dans le secteur du Mompichel (Albacete). Cretaceous Research 1, 235–251.

Arillo, A., Penalver, E., Garcia-Gimeno, V.,2009. First fossil Litoleptis (Diptera: Spaniidae) from the Lower Cretaceous amber of San Just (Teruel Province, Spain). Zootaxa 2026, 33-39.

Arillo, A., Subías, L.S., Sánchez-García, A., 2016. New species of fossil oribatid mites (Acariformes, Oribatida), from the Lower Cretaceous amber of Spain. Cretaceous Research 63, 68-76.

Arostegui, J., Irabien, M.J., Nieto, F., Sangüesa, J., Zuluaga, M.C., 2001. Microtextures and the origin of muscovite-kaolinite intergrowths in sandstones of the Utrillas Formation, Basque Cantabrian Basin, Spain. Clays and Clay Minerals 49, 529-539.

Asbridge, E., Lucas, R., Ticehurst, C., Bunting, P., 2016. Mangrove response to environmental change in Australia's Gulf of Carpentaria. Ecology and Evolution 6, 3523-3539.

Assens, J., Ramírez del Pozo, J., Giannini, G., Riba, O., Vilena, J., Reguant, S., 1973. Hoja geológica nº 666 (Chelva). Mapa Geológico de España 1:50.000. 2ª serie, I.G.M.E., Madrid.

Aurell, M., Fregenal-Martínez, M., Bádenas B., Muñoz-García, M.B., Élez, J., Meléndez, N., De Santisteban, C., 2019. Middle Jurassic–Early Cretaceous tectono-sedimentary evolution of the southwestern Iberian Basin (central Spain): Major palaeogeographical changes in the geotectonic framework of the Western Tethys. Earth-Science Reviews 199, 1–33.

Bandy, O.L., 1967. Cretaceous planktonic foraminiferal zonation. Micropaleontology 3, 1e31.

Barale, G., 1992. De nouveaux restes fossiles attribués aux Araucariacées dans les calcaires lithographiques du Crétacé inférieur du Montsec (province de Lérida, Espagne). Review of Palaeobotany and Palynology 75, 53–64.

Barral, A., Gomez, B., Daviero-Gomez, V., Lécuyer, Mendes, M.M., Ewin, T.A.M., 2019. New insights into the morphology and taxonomy of the Cretaceous conifer *Frenelopsis* based on a new species from the Albian of San Just, Teruel, Spain. Cretaceous Research 95, 21–36.

Barrón, E., Peyrot, D., Rodríguez-López, J.P., Meléndez, N., López Del Valle, R., Najarro, M., Rosales, I., Comas-Rengifo, M.J., 2015. Palynology of Aptian and upper Albian (Lower Cretaceous) amber-bearing outcrops of the southern margin of the Basque-Cantabrian Basin (northern Spain). Cretaceous Research 52, 292–312.

Bather, F.A., 1908. VII.—Nathorst's Methods of studying Cutinised Portions of Fossil Plants. Geological Magazine 5, 454-459.

Batten, D.J., 1974. Wealden palaeoecology from the distribution of plant fossils. Proceedings of the Geologists' Association 85, 433–458.

Batten, D.J., 1999. Extraction techniques. Small palynomorphs. In: Jones T.P., Rowe, N.P. (Eds.), Fossil plants and spores: modern techniques. The Geological Society, London, UK, 15–19.

Batten, D.J., Uwins, P.J.R., 1985. Early–Late Cretaceous (Aptian–Cenomanian) palynomorphs. Journal of Micropalaeontology 4, 151–168.

Bayer, E., Petrbok, J., 1919. Příspěvek k fytopaleontologii českého cenomanu [A contribution to the phytopaleontology of the Bohemian Cenomanian]. Časopis Musea Království Českého 93, 74–83.

Beltrando, M., Stockli, D.F., Decarlis, A., Manatschal, G., 2015. A crustal scale view at rift localization along the fossil Adriatic margin of the Alpine Tethys preserved in NW Italy. Tectonics 34, 1927-1951.

Bengtson, P., Kakabadze, M.V., 2018. Ammonites and the mid-Cretaceous saga. Cretaceous Research 88, 90-99.

Berasategui, J., Ramírez, J.I., 1982. Mapa Geológico de España 1:50000, hoja nº611 (Cañete). IGME, Madrid, Spain.

Blanco Moreno, C., Gomez, B., Buscalioni, A., 2018. Palaeobiogeographic and metric analysis of the Mesozoic fern *Weichselia*. Geobios 51, 571–578.

Blomeier, D., Dustira, A., Forke, H., Scheibner, C., 2011. Environmental change in the Early Permian of NE Svalbard: from a warm-water carbonate platform (Gipshuken Formation) to a temperate, mixed siliciclastic-carbonate ramp (Kapp Starostin Formation). Facies 57, 493–523.

Blum, M., Martin, J., Milliken, K., Garvin, M., 2013. Paleovalley systems: insights from Quaternary analogs and experiments. Earth-Science Reviews 116, 128-169.

Bolkhovitina, N.A., 1953. Spores and pollen characteristic of the Cretaceous deposits of central regions of the U.S.S.R. Transactions of the Academy of Sciences of U.S.S.R. (Geological Institute, Ser. 6l) 145, 1–184 (in Russian).

Brenner, G.J., 1963. The spores and pollen of the Potomac Group of Maryland. Maryland Department of Geology, Mines and Water Resources Bulletin 27, 1–215.

Brenner, G.J., 1976. Middle Cretaceous floral provinces and early migrations of angiosperms. In: Beck, C.B. (Ed.), Origin and early evolution of angiosperms. Columbia University Press, New York, 23–47.

Bristow, C.S., Best, J.L., 1993. Braided rivers: perspectives and problems. Geological Society, London, Special Publications 75, 1–11.

Bromley, R.G., Asgaard, U., 1991. Ichnofacies: a mixture of taphofacies and biofacies. Lethaia 24, 153–163.

Brown, C.A., 2008. Palynological techniques. American Association of Stratigraphic Palynologists, Dallas, 137 pp.

Bueno-Cebollada, C.A., Meléndez-Hevia, N., 2018. Aeolian dune development in an Albian arid coastal braidplain system in Serranía de Cuenca (Iberian Basin, Spain). Geogaceta 64, 27–30.

Bueno-Cebollada, C.A., Barrón, E., Peyrot D., Meléndez, N., 2021. Palynostratigraphy and palaeoenvironmental evolution of the Aptian to lower Cenomanian succession in the Serranía de Cuenca (Eastern Spain). Cretaceous Research 128, 104956. https://doi.org/10.1016/j.cretres.2021.104956.

Bueno-Cebollada, C.A., Fregenal-Martínez, M., Meléndez, N., 2022. Along-strike sedimentological variability and architectural patterns of the transgression of a "mid"-cretaceous braidplain system (Iberian Basin, eastern Spain): A tool for depicting eustatic and tectonic signatures within the framework of a global transgression. Sedimentary Geology 429, 106082.

Bullock, P., Fedoroff, N., Jongerius, A., Stoops, G., Tursina, T., 1985. Handbook for soil thin section description. Waine Research Publications, England, 150 pp.

Burden, E.T., Hills L.V., 1989. Illustrated key to genera of Lower Cretaceous terrestrial palynomorphs (excluding megaspores) of Western Canada. American Association of Stratigraphic Palynologists Foundation Contribution Series 21, 1–147.

Burns, C.E., Mountney, N.P., Hodgson, D.M., Colombera, L., 2017. Anatomy and dimensions of fluvial crevasse-splay deposits: Examples from the Cretaceous Castlegate Sandstone and Neslen Formation, Utah, USA. Sedimentary Geology 351, 21-35.

Cadenas, P., Fernández-Viejo, G., Pulgar, J.A., Tugend, J., Manatschal, G., Minshull, T.A., 2018. Constraints imposed by rift inheritance on the compressional reactivation of a hyperextended margin: Mapping rift domains in the North Iberian margin and in the Cantabrian Mountains. Tectonics 37, 758–785.

Caja, M.A., Marfil, R., Lago, M., Salas, R., Ramseyer, K., 2007. Provenance discrimination of Lower Cretaceous syn-rift sandstones (eastern Iberian Chain, Spain): Constraints from detrital modes, heavy minerals, and geochemistry. In: Arribas J, Critelli S, Johnsson MJ (Eds.), Sedimentary Provenance and Petrogenesis: Perspectives from Petrography and Geochemistry. Geological Society of America Special Paper 420,181-197.

Carenas, B., Segura, M., García, A., García Hidalgo, J., Ruiz, G., Bravo, C., 1994. Revisión de la Formación Calizas de Aras de Alpuente en la Cordillera Ibérica suroccidental. Cuadernos de Geología Ibérica 18, 241–269.

Carrión, J., 2003. Evolución vegetal. DM, Diego Marín Librero-Editor, Murcia, Spain.

Cattaneo, A., Steel, R.J., 2003. Transgressive deposits: a review of their variability. Earth-Science Reviews 62, 187–228.

Catuneanu, O., 2019. Model-independent sequence stratigraphy. Earth-Science Reviews 188, 312-388.

Catuneanu, O., Galloway, W.E., Kendall, C.G.S.C., Miall, A.D., Posamentier, H.W., Strasser, A., Tucker, M.E., 2011. Sequence stratigraphy: methodology and nomenclature. Newsletters on Stratigraphy 44, 173–245.

Chamizo Borreguero, M., 2006. Análisis sedimentológico de un complejo mareal en el Mb. Calizas de La Bicuerca (Fm. Aras de Alpuente, Albiense–Cenomaniense). La Huérguina (Cuenca), Cordillera Ibérica. MSc Thesis, Universidad Complutense de Madrid, Spain.

Chamizo-Borreguero, M., Meléndez, N., Bermúdez, D. D., Poyato, F. J., 2008. Facies mareales con restos de vertebrados asociadas a un contexto transgresivo: Mb. Calizas de la Bicuerca, (Albiense-Cenomaniense) Serranía de Cuenca, Cuenca Ibérica. Geotemas 10, 195–198.

Chamizo-Borreguero, M., Meléndez, N., De Boer, P.L., 2016. Tidal-bore deposits in incised valleys, Albian, SW Iberian Ranges, Spain. Contributions to Modern and Ancient Tidal Sedimentology 304, 93–115.

Cherchi, A., García, A., Schroeder, R., Segura, M., 1995. Foraminíferos criptobióticos en el Albense superior-Cenomaniense inferior de la Cordillera Ibérica. Reflexiones sobre unas estructuras problemáticas en Lithocodium. Revista Española de Paleontología 10, 284-293.

Chumakov, N.M., Zharkov, M.A., Herman, A.B., Doludenko, M.P., Kalandadze, N.N., Lebedev, E.L., Ponomarenko, A.G., Rautian, A.S., 1995. Climatic belts of the mid-Cretaceous time. Stratigraphy and Geological Correlation 3, 42–63.

Clarke, L.J., Jenkyns, H.C., 1999. New oxygen isotope evidence for long-term Cretaceous climate change in the Southern Hemisphere. Geology 27, 699–702.

Clifton, H.E., 1969. Beach lamination: nature and origin. Marine Geology 7, 553–559.

Clifton, H.E., 2006. A re-examination of facies models for clastic shorelines. In: Posamentier, H.W., Walker, R.G. (Eds.), Facies Models Revisited. Society for Sedimentary Geology (SEPM), Special Publication 84, pp. 293–337.

Cohen, K.M., Finney, S.C., Gibbard, P.L., Fan, J.X., 2013 (updated). The ICS International Chronostratigraphic Chart. Episodes 36, 199-204. http://www.stratigraphy.org/ICSchart/ChronostratChart2021-05.pdf

Coiffard, C., Gomez, B., 2012. Influence of latitude and climate on spread, radiation and rise to dominance of early angiosperms during the Cretaceous in the Northern Hemisphere. Geologica Acta 10, 181–188.

Coiffard, C, Gomez, B., Kvaček, J., Thevenard, F., 2006. Early angiosperm ecology: evidence from the Albian–Cenomanian of Europe. Annals of Botany 98, 495–502.

Coiffard, C., Gomez, B., Thevenard, F., 2007. Early Cretaceous angiosperm invasion of Western Europe and major environmental changes. Annals of Botany 100, 545–553.

Coiro, M., Doyle, J.A., Hilton, J., 2019. How deep is the conflict between molecular and fossil evidence on the age of angiosperms? New Phytologist 223, 83–99.

Collinson, J.D., Thompson, D.B., 1982. Sedimentary Structures. London: George Allen & Unwin, 194 pp.

Crane, P.R., Lidgard, S., 1989. Angiosperm diversification and paleolatitudinal gradients in Cretaceous floristic diversity. Science 246, 675–678.

Crane, P.R., Friis, E. M., Pedersen, K.R., 1995. The origin and early diversification of angiosperms. Nature 374, 27–33.

d'Omalius d'Halloy, J.J., 1822. Observations sur un essai de carte geologique de la France, des Pays-Bas et des contr_ees voisines. Annales des Mines 7, 353e376.

Dabrio, C., 1989. Playas e isla barrera-lagoon. In: Arche, A. (Ed.) Sedimentología, Vol. 1. Consejo Superior de Investigaciones Científicas, Servicio de Publicaciones, Madrid, pp. 349-394 (in Spanish).

Dabrio, C.J., Hernando, S., 2003. Estratigrafía. Facultad de Ciencias Geológicas, Universidad Complutense de Madrid, Spain, 382 pp.

Daidu, F., 2012. Open-coast tidal flats. In: Davis, R.A., Dalrymple, R.W. (Eds.), Principles of Tidal Sedimentology. Springer, Dordrecht, pp. 187–229.

Daidu, F., Yuan, W., Min, L., 2013. Classifications, sedimentary features, and facies associations of tidal flats. Journal of Palaeogeography 2, 66–80..

Dalrymple, R.W., 2010a. Interpreting sedimentary successions: facies, facies analysis and facies models. In: James, N.P., Dalrymple, R.W. (Eds.), Facies Models 4. Geological Association of Canada, pp. 3-18.

Dalrymple, R.W., 2010b. Tidal depositional systems. In: James, N.P., Dalrymple, R.W. (Eds.), Facies Models 4. Geological Association of Canada, pp. 201–232.

Dalrymple, R.W., Rhodes, R.N., 1995. Estuarine dunes and bars. Developments in Sedimentology 53, 359–422.

Dalrymple, R. W., Choi, K., 2007. Morphologic and facies trends through the fluvial–marine transition in tide-dominated depositional systems: a schematic framework for environmental and sequence-stratigraphic interpretation. Earth-Science Reviews 81, 135-174.

Dalrymple, R.W., Zaitlin, B.A., Boyd, R., 1992. Estuarine facies models; conceptual basis and stratigraphic implications. Journal of Sedimentary Research 62, 1130-1146.

Dalrymple, R.W., Mackay, D.A., Ichaso, A.A., Choi, K.S., 2012. Processes, morphodynamics and facies in tide-dominated estuaries. In: Davis, R.A., Dalrymple, R.W. (Eds.), Principles of Tidal Sedimentology. Springer, Dordrecht, pp. 79–108.

Davis, R.A., 2012. Tidal signatures and their preservation potential in stratigraphic sequences. In: Davis, R.A., Dalrymple, R.W. (Eds.), Principles of Tidal Sedimentology. Springer, Dordrecht, pp. 35–55.

De Boer, P.L., 1998. Intertidal sediments: composition and structure. In: Eisma, D. (Ed.), Intertidal Deposits. River Mouths, Tidal Flats and Coastal Lagoons. CRC Press, pp. 345–361.

De Boer, P.L., Oost, A.P., Visser, M.J., 1989. The diurnal inequality of the tide as a parameter for recognizing tidal influences. Journal of Sedimentary Research 59, 912–921.

De La Horra, R., Benito, M.I., López-Gómez, J., Arche, A., Barrenechea, J.F., Luque, J., 2008. Palaeoenvironmental significance of Late Permian palaeosols in the South-Eastern Iberian Ranges, Spain. Sedimentology 55, 1849-1873.

De Pippo, T., Donadio, C., 1999. Morphology, genesis and evolution of rockpools along Italian coasts. Geografia Fisica e Dinamica Quaternaria 22, 129–141.

Del Olmo Zamora, P., 1986 Mapa Geológico de España 1:50000, hoja nº610 (Cuenca). IGME, Madrid, Spain.

Delclos, X., Arillo, A., Peñalver, E., Barrón, E., Soriano, C., Del Valle, R.L., Corral, E., Ortuno, V. M., 2007. Fossiliferous amber deposits from the Cretaceous (Albian) of Spain. Comptes Rendus Palevol 6, 135-149.

Diéguez, C., Meléndez, N., 2000. Early Cretaceous ferns from lacustrine limestones at Las Hoyas, Cuenca province, Spain. Palaeontology 43, 1113–1141.

Díez, J.B., Sender, L.M., Villanueva-Amadoz, U., Ferrer, J., Rubio, C., 2005. New data regarding *Weichselia reticulata*: soral clusters and the spore developmental process. Review of Palaeobotany and Palynology 135, 99–107.

Doubinger, J., Mas, J.R., 1981. Une microflore du Barrémien dans la Province de Valencia, Espagne. Cretaceous Research 2, 51–64.

Doyle, J.A., 1992. Revised palynological correlations of the lower Potomac Group (USA) and the Cocobeach sequence of Gabon (Barremian–Aptian). Cretaceous Research 13, 337–349.

Doyle, J.A., Robbins, E.I., 1977. Angiosperm pollen zonation of the continental Cretaceous of the Atlantic Coastal Plain and its application to deep wells in the Salisbury embayment. Palynology 1, 43–78.

Doyle, J.A., Endress, P.K., 2014. Integrating Early Cretaceous fossils into the phylogeny of living angiosperms: ANITA lines and relatives of Chloranthaceae. International Journal of Plant Sciences 175, 555–600.

Doyle, J.A., Biens, P., Doerenkamp, A., Jardine, S., 1977. Angiosperm pollen from the pre-Albian Cretaceous of Equatorial Africa. Bulletin des Centres de Recherches Exploration-Production Elf-Aquitaine 1, 451–473.

Driese, S.G., Simpson, E.L., Eriksson, K.A., 1995. Redoximorphic Paleosols in alluvial and lacustrine deposits, 1.8 Ga Lochness Formation, Mount Isa, Australia; pedogenic processes and implications for paleoclimate. Journal of Sedimentary Research 65, 675–689.

Dubois, R.N., 1972. Inverse relation between foreshore slope and mean grain size as a function of the heavy mineral content. Geological Society of America Bulletin 83, 871-876.

Embry, A.F., 1995. Sequence boundaries and sequence hierarchies: problems and proposals. In: Steel, R.J., Felt, V.L., Johannessen, E.P., Mathieu, C. (Eds.), Norwegian Petroleum Society Special Publications, Sequence Stratigraphy on the Northwest European Margin. Elsevier, pp. 1–11.

Embry, A.F., 2002. Transgressive-regressive (TR) sequence stratigraphy. Gulf Coast SEPM Conference Proceedings, Houston, USA, pp. 151–172.

Embry, A.F., 2009. Practical Sequence Stratigraphy. Canadian Society of Petroleum Geologists (CSPG), Canada.

Embry, A.F., Johannessen, E.P., 1992. T–R sequence stratigraphy, facies analysis and reservoir distribution in the uppermost Triassic–Lower Jurassic succession, western Sverdrup Basin, Arctic Canada. In: Vorren, T.O., Bergsager, E., Dahl-Stamnes, Ø.A., Holter, E., Johansen, B., Lie, E., Lund, T.B. (Eds.), Norwegian Petroleum Society Special Publications. Elsevier, pp. 121–146.

Ewin, T.A.M., 2004. Identification of conifer families using SEM analysis of fossil and extant conifer leaf cuticles. Ph.D. Thesis, University of Manchester, United Kingdom.

Falcon-Lang, H.J., Kvaček, J., Uličný, D., 2001. Fire-prone plant communities and palaeoclimate of a Late Cretaceous fluvial to estuarine environment, Pecínov Quarry, Czech Republic. Geological Magazine 138, 563–576.

Falcon-Lang, H.J., Kvaček, J., Uličný, D., 2006. Mesozoic mangroves. Geoscientist 16, 4–6.

Farjon, A., 2005. A monograph of Cupressaceae and *Sciadopitys*. Royal Botanic Gardens, Kew.

Farjon, A., 2010. A Handbook of the World's Conifers (2 vols.). Vol. 1. Brill, USA.

Fedo, C.M., Nesbitt, H.W., Young, G.M., 1995. Unravelling the effects of potassium metasomatism in sedimentary rocks and paleosols, with implications for paleoweathering conditions and provenance. Geology 23, 921–924.

Fedoroff, N., Courty, M.A., Guo, Z., 2010. Palaeosoils and relict soils. In: Stoops, G., Marcelino, V., Mees, F., (Eds.) Interpretation of micromorphological features of soils and regoliths. Elsevier, pp. 623-662.

Feild, T.S., Arens, N.C., Doyle, J.A., Dawson, T.E., Donoghue, M.J., 2004. Dark and disturbed: a new image of early angiosperm ecology. Paleobiology 30, 82–107.

Folk, R. L., 1971. Longitudinal dunes of the northwestern edge of the Simpson Desert, Northern Territory, Australia, 1. Geomorphology and grain size relationships. Sedimentology 16, 5-54.

Föllmi, K.B., 1989. Evolution of the Mid-Cretaceous triad. Lecture Notes in Earth Sciences 23, 1-153.

Fonollá Ocete, J.F., Fernández Marrón, M.T., 2004. Palinofacies de la sección Mina Pepita (Miembro El Burgal, Formación Caroch) Aptiense de la Cordillera Ibérica. Geotemas 6, 287–290.

Forster, A., Schouten, S., Baas, M., Sinninghe Damsté, J. S., 2007. Mid-Cretaceous (Albian–Santonian) sea surface temperature record of the tropical Atlantic Ocean. Geology 35, 919–922.

Fox, I.D.,2001. Vegetation of the Australian tropical savannas. Queensland Govt., Environmental Protection Agency.

Fregenal-Martínez, M.A., Meléndez, N., 1993. Sedimentología y evolución paleogeográfica de la cubeta de Las Hoyas (Cretácico inferior, Serranía de Cuenca). Cuadernos de geología ibérica 17, 231-256.

Fregenal-Martínez, M., Meléndez, N., Muñoz-García, M.B., Elez, J., De la Horra, R., 2017. The stratigraphic records of the Late Jurassic–Early Cretaceous rifting in the Alto Tajo-Serranía de Cuenca Region (Iberian Ranges, Spain): Genetic and structural evidences for a revision and a new lithostratigraphic proposal. Revista de la Sociedad Geologica de España 30, 113–141.

Friis, E.M., Crane, P.R., Pedersen, K.R., 2011. Early flowers and angiosperm evolution. Cambridge University Press, Cambridge.

Fryberger, S.G., 1993. A review of aeolian bounding surfaces, with examples from the Permian Minnelusa Formation, USA, in: North, C.P., Prosser, D.J. (Eds.), Characterization of Fluvial and Aeolian Reservoirs, Geological Society of America Special Paper 73, 167-197.

García-Hidalgo, J.F., Elorza, J., Gil-Gil, J., Herrero, J.M., Segura, M., 2018. Evidence of synsedimentary microbial activity and iron deposition in ferruginous crusts of the Late Cenomanian Utrillas Formation (Iberian Basin, central Spain). Sedimentary Geology 364, 24–41.

Giménez, R., Martín-Chivelet, J., Vilas, L., 1993. Late Albian–middle Cenomanian carbonate platforms of Betic and Iberian Basins, Spain: Chapter 22. In: Simó, J.A.T., Scott, R. W., Masse, J.P., (Eds.), Cretaceous Carbonate Platforms, AAPG Memoir 56, 271–281.

Gingras, M.K., Mac Eachern, J.A., 2012. Tidal ichnology of shallow-water clastic settings. In: Davis, R.A., Dalrymple, R.W. (Eds.), Principles of Tidal Sedimentology. Springer, Dordrecht, The Netherlands, pp. 57–77.

Glennie, K.W., 1970. Desert Sedimentary Environments. Elsevier, Amsterdam.

Gomez, B., Martín-Closas, C., Barale, G., Solé de Porta, N., Thévenard, F., Gignard, G., 2002. *Frenelopsis* (Coniferales; Cheirolepidiaceae) and related male organ genera from the Lower Cretaceous of Spain. Palaeontology 45, 997–1036.

Gomez, B., Ewin, T.A.M., Daviero-Gomez, V., 2012. The conifer *Glenrosa falcata* sp. nov. from the Lower Cretaceous of Spain and its palaeoecology. Review of Palaeobotany and Palynology 172, 21–32.

Gómez, J.J., Aguado, R., Azerêdo, A.C., Cortés, J.E., Duarte, L.V., O'Dogherty, L., da Rocha, R.B., Sandoval, J., 2019. The Late Triassic–Middle Jurassic Passive Margin Stage. In: Quesada, C., Oliveira, J.T. (Eds.), The Geology of Iberia: A Geodynamic Approach. Springer, Cham, pp. 113–167.

Gong, Z., Langereis, C. G., Mullender, T.A.T., 2008. The rotation of Iberia during the Aptian and the opening of the Bay of Biscay. Earth and Planetary Science Letters 273, 80-93.

Gorozhankin, I.N., 1904. Lektsii po morfologii i sistematike archegonialnykh rastenij. II, Pteridophyta, I, Archispermae. Moscú, AI Mamontov, 73e93.

Gribble, C.D. and A. J. Hall 1985 A Practical Guide to Optical Mineralogy, London.

Grimaldi, D., 1996. Amber: Window to the Past. Harry N. Abrams, Incorporated, New York, 216 pp.

Grimm, E.C., 1992. Tilia, Version 2. Springfield: Illinois State Museum, Research and Collection Center.

Grimm, E.C., 2004. TG View, Version 2.0.2. Springfield: Illinois State Museum, Research and Collections Center.

Guy-Ohlson, D., 1992. *Botryococcus* as an aid in the interpretation of palaeoenvironment and depositional processes. Review of Palaeobotany and Palynology 71, 1–15.

Haq, B.U., 2014. Cretaceous eustasy revisited. Global and Planetary Change 113, 44–58.

Haq, B.U., Hardenbol, J., Vail, P.R., 1988. Mesozoic and Cenozoic chronostratigraphy and cycles of sea-level change. In: Wilgus, C.K., Hastings, B.S., Kendall, C.G. St. C., Posamentier, H.W., Ross, C.A., and Van Wagoner, J.C. (Eds.) Sea-level Research: An Integrated Approach: SEPM Special Publication 42, 71-108.

Hardenbol, J.A.N., Thierry, J., Farley, M.B., Jacquin, T., De Graciansky, P.C., Vail, P.R., 1998. Mesozoic and Cenozoic sequence chronostratigraphic framework of European basins. In: Hardenbol, J.A.N., Jacquin, T., De Graciansky, P.C., Vail, P.R., (Eds.) Mesozoic and Cenozoic Sequence Stratigraphy of European Basins, SEPM Society for Sedimentary Geology, Special Publication 60, 3-13.

Harris, T.M., Millington, W., 1974. The Yorkshire Jurassic Flora, IV. I. Ginkgoales. British Museum of Natural History, London.

Hart, B.S., Plint, A.G., 1995. Gravelly shoreface and beachface deposits. Sedimentary facies analysis 22, 75–99.

Hart, B.S., Plint, A.G., 2003. Stratigraphy and sedimentology of shoreface and fluvial conglomerates: insights from the Cardium Formation in NW Alberta and adjacent British Columbia. Bulletin of Canadian Petroleum Geology 51, 437–464.

Hasenboehler, B., 1981. Étude paléobotanique et palynologique de l'Albien et du Cenomanien du "Bassin Occidental Portugais" au Sud de l'Accident de Nazare (Province d'Estremadure, Portugal). Sciences de la Têrre 6, 1–319.

Hasiotis, S.T., 2004. Reconnaissance of Upper Jurassic Morrison Formation ichnofossils, Rocky Mountain region, USA: paleoenvironmental, stratigraphic, and paleoclimatic significance of terrestrial and freshwater ichnocoenoses. Sedimentary Geology 167, 177–268.

Hay, W.W., 2008. Evolving ideas about the Cretaceous climate and ocean circulation. Cretaceous Research 29, 725–753.

Haywood, A.M., Valdes, P.J., Markwick, P.J., 2004. Cretaceous (Wealden) climates: a modelling perspective. Cretaceous Research 25, 303-311..

Hedlund, R. W., Norris, G., 1968. Spores and pollen grains from Fredericksburgian (Albian) strata, Marshall County, Oklahoma. Pollen et Spores 10, 129–159.

Heimhofer, U., Hochuli, P. A., 2010. Early Cretaceous angiosperm pollen from a low-latitude succession (Araripe Basin, NE Brazil). Review of Palaeobotany and Palynology 161, 105–126.

Heimhofer, U., Hochuli, P. A., Burla, S., Dinis, J. M. L., Weissert, H., 2005. Timing of Early Cretaceous angiosperm diversification and possible links to major paleoenvironmental change. Geology 33, 141–144.

Heimhofer, U., Hochuli, P. A., Burla, S., Weissert, H., 2007. New records of Early Cretaceous angiosperm pollen from Portuguese coastal deposits: Implications for the timing of the early angiosperm radiation. Review of Palaeobotany and Palynology 144, 39–76.

Heimhofer, U., Hochuli, P.A., Burla, S., Oberli, F., Adatte, T., Dinis, J.L., Weissert, H., 2012. Climate and vegetation history of western Portugal inferred from Albian near-shore deposits (Galé Formation, Lusitanian Basin). Geological Magazine 149, 1046–1064.

Heimhofer, U., Wucherpfennig, N., Adatte, T., Schouten, S., Schneebeli-Hermann, E., Gardin, S., Keller, G., Kentsch, S., Kujau, A., 2018. Vegetation response to exceptional global warmth during Oceanic Anoxic Event 2. Nature Communications 9, 3832.

Helland-Hansen, W., 1995. Sequence stratigraphy theory: remarks and recommendations. Norwegian Petroleum Society Special Publications (Elsevier) 5, 13-21.

Helland-Hansen, W., Martinsen, O.J., 1996. Shoreline trajectories and sequences; description of variable depositional-dip scenarios. Journal of Sedimentary Research 66, 670–688.

Hluštík, A., Konzalová, M., 1976. *Frenelopsis alata* (K.Feistm.) Knobloch (Cupressaceae) from the Cenomanian of Bohemia, a new plant producing *Classopollis* pollen. In: Novák, V.J.A., Pacltová, B. (Eds.), Evolutionary Biology: Proceedings of the International Conference, Liblice, June 2–6, 1975. Czechoslovak Biological Society, Praha, pp. 125–131.

Hochuli, P.A., Heimhofer, U., Weissert, H., 2006. Timing of early angiosperm radiation: recalibrating the classical succession. Journal of the Geological Society, London 163, 587–594.

Hochuli, P. A., Menegatti, A. P., Weissert, H., Riva, A., Erba, E., Silva, I. P., 1999. Episodes of high productivity and cooling in the early Aptian Alpine Tethys. Geology 27, 657–660

Horikx, M., Hochuli, P. A., Feist-Burkhardt, S., Heimhofer, U., 2016. Albian angiosperm pollen from shallow marine strata in the Lusitanian Basin, Portugal. Review of Palaeobotany and Palynology 228, 67–92.

Huber, B. T., O'Brien, C. L., 2021. Cretaceous Climate.

Hughes, N.F., 1994. The enigma of angiosperm origin. Cambridge University Press.

Hughes, N.F., McDougall, A.B., 1990. Barremian–Aptian angiospermid pollen records from southern England. Review of Palaeobotany and Palynology 65, 145–151.

Humphries, D.W. 1992 The preparation of thin sections of rocks, minerals, and ceramics, Royal Microscopical Society, Microscopy handbooks 24, Oxford.

Ibrahim, M.I.A., 2002. Late Albian–Middle Cenomanian palynofacies and palynostratigraphy, Abu Gharadig-5 well, Western Desert, Egypt. Cretaceous Research 23, 775–788.

Isla, M.F., Schwarz, E., Veiga, G.D., 2020. Record of a nonbarred clastic shoreline. Geology 48, 338–342.

Jaenicke, R., 2005. Abundance of cellular material and proteins in the atmosphere. Science 308, 73.

Ji, S., Li, L., Zeng, W., 2018. The relationship between diameter and depth of potholes eroded by running water. Journal of Rock Mechanics and Geotechnical Engineering 10, 818–831.

Jones, B., 2010. Warm water neritic carbonates. In: James, N.P., Dalrymple, R.W. (Eds.), Facies Models 4. Geological Association of Canada, pp. 341–370.

Jordan, O.D., Mountney, N.P., 2010. Styles of interaction between aeolian, fluvial and shallow marine environments in the Pennsylvanian to Permian lower Cutler beds, south-east Utah, USA. Sedimentology 57, 1357-1385.

Juhász, M., Smirnova, S.B., 1985. *Gregussisporites* a new spore genus from Albian sediments. Acta Biologica Szeged 31, 217–219.

Kemp, E.M., 1970. Aptian and Albian miospores from southern England. Palaeontographica Abteilung B 131, 73–143.

Kleinhans, M.G., Schuurman, F., Bakx, W., Markies, H., 2009. Meandering channel dynamics in highly cohesive sediment on an intertidal mudflat in the Westerschelde estuary, the Netherlands. Geomorphology 105, 261–276.

Knight, J., 2008. The environmental significance of ventifacts: A critical review. Earth-Science Reviews 86, 89–105.

Krapf, C.B., Stollhofen, H., Stanistreet, I.G., 2003. Contrasting styles of ephemeral river systems and their interaction with dunes of the Skeleton Coast erg (Namibia). Quaternary International 104, 41–52.

Krapf, C.B., Stanistreet, I.G., Stollhofen, H., 2005. Morphology and fluvio-aeolian interaction of the tropical latitude, ephemeral braided river dominated Koigab Fan, north-west Namibia. In: Blum, M., Marriott, S., Leclair, S. (Eds.), Fluvial Sedimentology VII, Vol. 35. John Wiley and Sons, pp. 99–120.

Kraus, M.J., 1999. Paleosols in clastic sedimentary rocks: their geologic applications. Earth-Science Reviews 47, 41-70.

Kuriyama, Y., Mochizuki, N., Nakashima, T., 2005. Influence of vegetation on aeolian sand transport rate from a backshore to a foredune at Hasaki, Japan. Sedimentology 52, 1123–1132.

Kvaček, J., 2000. *Frenelopsis alata* and its microsporangiate and ovuliferous reproductive structures from the Cenomanian of Bohemia (Czech Republic, Central Europe). Review of Palaeobotany and Palynology 112, 51–78.

Kvaček, J., 2003. Foliage of a broad leaved conifer Dammarophyllum from the Cenomanian of Bohemia. Časopis Národního muzea, Řada přírodovědná 172, 13-20.

Kvaček, J., Lobitzer, H., 2010. First records of *Dammarites albens* Presl in Sternberg (Pinopsida?) from the Cretaceous of Austria. Journal of the National Museum (Prague), Natural History Series 179, 131–137.

Kvaček, J., Mendes, M.M., 2021. A new Cheirolepidiaceae conifer *Watsoniocladus cunhae* sp. nov. from the Early Cretaceous (late Aptian–early Albian) of western Portugal. Review of Palaeobotany and Palynology 295, 104519.

Kvaček, J., Falcon-Lang, L., Dašková, J., 2005. A new late Cretaceous ginkgoalean reproductive structure *Nehvizdyella* gen. nov. from the Czech Republic and its whole-plant reconstruction. American Journal of Botany 92, 1958–1969.

Kvaček, J., Barron, E., Heřmanová, Z., Mendes, M.M., Karch, J., Žemlička, J., Dudak, J., 2018. Araucarian conifer from late Albian amber of northern Spain. Papers in Palaeontology 4, 643-656.

Laing, J.F., 1975. Mid-Cretaceous angiosperm pollen from Southern England and Northern France. Palaeontology 18, 775–808.

Lancaster, N., 1986. Grain-size characteristics of linear dunes in the southwestern Kalahari. Journal of Sedimentary Research 56, 395-400.

Langford, R.P., 1989. Fluvial-eolian interactions: Part I: modern systems. Sedimentology 36, 1023-1035.

Langford, R.P., Chan, M.A., 1989. Fluvial-aeolian interactions: Part II: ancient systems. Sedimentology 36, 1037-1051.

Leereveld, H., de Haan, P.J., Juhász, M., 1989. Stratigraphic evaluation of spore/pollen assemblages from the Lower Cretaceous of the Alpine–Mediterranean Realm. Laboratory of Palaeobotany and Palynology. Special Services Report 89/07, 1–253 + 1–98.

Li, Y.F., Sun, C.L., Wang, H., Dilcher, D.L., Tan, X., Li, T., Na, Y.L., 2018. First record of *Eretmophyllum* (Ginkgoales) with well-preserved cuticle from the Middle Jurassic of the Ordos Basin, Inner Mongolia, China. Palaeoworld 27, 188–201.

Liesa, C.L., Soria, A.R., Meléndez, N., Meléndez, A., 2006. Extensional fault control on the sedimentation patterns in a continental rift basin: El Castellar Formation, Galve sub-basin, Spain. Journal of the Geological Society 163, 487-498.

Longhitano, S.G., Nemec, W., 2005. Statistical analysis of bed-thickness variation in a Tortonian succession of biocalcarenitic tidal dunes, Amantea Basin, Calabria, southern Italy. Sedimentary Geology 179, 195-224.

López-Gómez, J., Arche, A., Pérez-López, A., 2002. Permian and Triassic. In: Gibbons, W., Moreno, T. (Eds.) The Geology of Spain. Geological Society of London, London, 185–212.

López-Gómez, J., Alonso-Azcárate, J., Arche, A., Arribas, J., Fernández, J., Borruel-Abadía, V., Bourquin, S., Cadenas, P., Cuevas, P., De la Horra, R., Díez, J., Escudero-Mozo, M.J., Fernández-Viejo, G., Galán-Abellán, B., Galé, C., Gaspar-Escribano, J., Gisbert Aguilar, J., Gómez-Gras, D., Goy, A., Gretter, N.,Heredia, N., Lago, M., Lloret, J., Luque, J., Márquez, L., Márquez-Aliaga, A., Martín-Algarra, A., Martín-Chivelet, J., Martín-González, F., Marzo, M., Mercedes-Martín, R., Ortí, F., Pérez-López, A., Pérez-Valera, F., Pérez-Valera, J.A., Plasencia, P., Ramos, E.,

Rodríguez-Méndez, L., Ronchi, A., Salas, R., Sánchez-Fernández, D., Sánchez-Moya, Y., Sopeña, A., Suárez-Rodríguez, A., Tubía, J. M., Ubide, T., Valero, B., Vargas, H., Viseras, C., 2019a. Permian–Triassic Rifting Stage (Chapter 3). In: Quesada, C., Oliveira, J. T. (Eds.), The Geology of Iberia: A Geodynamic Approach. Volume 3: The Alpine Cycle. Regional Geology Reviews, Springer, Cham, pp. 29–112.

Mac Eachern, J.A., Pemberton, S.G., Gingras, M.K., Bann, K.L., 2010. Ichnology and facies models. In: James, N.P., Dalrymple, R.W. (Eds.), Facies Models 4. Geological Association of Canada, Canada, pp. 19–58.

Mack, G.H., 1992. Paleosols as an indicator of climatic change at the early-late Cretaceous boundary, southwestern New Mexico. Journal of Sedimentary Research 62, 483-494.

Mack, G.H., James, W.C., Monger, H.C., 1993. Classification of paleosols: Geological Society of America Bulletin 105, 129–136.

McElwain, J.C., Punyasena, S.W., 2007. Mass extinction events and the plant fossil record. Trends in Ecology and Evolution 22, 548–557.

McLean, R.F., Kirk, R.M., 1969. Relationships between grain size, size-sorting, and foreshore slope on mixed sand – shingle beaches. New Zealand Journal of Geology and Geophysics 12, 138–155.

Marfil, R., Callaba, A., Gómez-Gras, D., 1992. Materia orgánica en la Fm. Arenas de Utrillas de Picofrentes (provincia de Soria): diagénesis mineral y orgánica. Geogaceta 12, 43-46.

Martín-Chivelet, J., López-Gómez, J., Aguado, R., Arias, C., Arribas, J., Arribas, M.E., Aurell, M., Bádenas, B., Benito, M.I., Bover-Arnal, T., Casas-Sainz, A., Castro, J.M., Coruña, F., de Gea, G.A., Fornós, J.J., Fregenal-Martínez, M., García-Senz, J., Garófano, D., Gelabert, B., Giménez, J., González-Acebrón, L., Guimerà, J., Liesa, C.L., Mas, R., Meléndez, N., Molina, J.M., Muñoz, J.A., Navarrete, R., Nebot, M., Nieto, L.M., Omodeo-Salé, S., Pedrera, A., Peropadre, C., Quijada, I.E., Quijano, M.L., Reolid, M., Robador, A., Rodríguez-López, J.M., Rodríguez-Perea, A., Rosales, I., Ruiz-Ortiz, P.A., Sàbat, F., Salas, R., Soria, A.R., Suárez-González, P., Vilas, L., 2019a. The Late Jurassic–Early Cretaceous Rifting (Chapter 5). In: Quesada, C., Oliveira, J.T. (Eds.), The Geology of Iberia: A Geodynamic Approach. Volume 3: The Alpine cycle. Regional Geology Reviews, Springer, Cham, pp. 169–249.

Martín-Chivelet, J., Floquet, M., García-Senz, J., Callapez, P.M., López-Mir, B., Muñoz, J.A., Barroso-Barcenilla, F., Segura, M., Soares, A.F., Dinis, P.M., Marques, J.F., Arbués, P., 2019b. Late Cretaceous Post-Rift to Convergence in Iberia (Chapter 7). In: Quesada, C., Oliveira, J.T. (Eds.), The Geology of Iberia: A Geodynamic Approach. Volume 3: The Alpine Cycle. Regional Geology Reviews, Springer, Cham, pp. 285–376.

Martínez-Delclòs, X., Briggs, D.E.G., Peñalver, E., 2004. Taphonomy of insects in carbonates and amber. Palaeogeography, Palaeoclimatology, Palaeoecology 203, 19–64.

Mas, J.R., 1981. El Cretácico inferior de la región noroccidental de la provincia de Valencia. Seminarios de Estratigrafía, Serie Monográfica 8, 1–476.

Massoni, J., Doyle, J., Sauquet, H., 2015. Fossil calibration of Magnoliidae, an ancient lineage of angiosperms. Palaeontologia Electronica 17, 1–25.

Maynard, J.B., 1992. Chemistry of modern soils as a guide to interpreting Precambrian paleosols. Journal of Geology 100, 279–289.

McLean, R.F., Kirk, R.M., 1969. Relationships between grain size, size-sorting, and foreshore slope on mixed sand-shingle beaches. New Zealand Journal of Geology and Geophysics 12, 138-155.

Meléndez, F., 1974. Correlación del Cretácico de la Serranía de Cuenca con el del sondeo de Villanueva de los Escuderos. In: I Symposio del Cretácico de la Cordillera Ibérica, 85–97.

Meléndez, N., 1983. El Cretácico de la región de Cañete-Rincón de Ademuz (provincia de Cuenca y Valencia). Seminarios de Estratigrafía 9, 1–242.

Meléndez, N., López-Gómez, J., 2003. Control eustático y tectónico durante una etapa regresiva de corta duración: Miembro El Burgal, Aptiense, Cordillera Ibérica, España. Journal of Iberian Geology 29, 29–54.

Mendes, M.M., Dinis, J.L., Gomez, B., Pais, J., 2010. Reassessment of the cheirolepidiaceous conifer *Frenelopsis teixeirae* Alvin et Pais from the Early Cretaceous (Hauterivian) of Portugal and palaeoenvironmental considerations. Review of Palaeobotany and Palynology 161, 30–42.

Menor-Salván, C., Simoneit, B.R., Ruiz-Bermejo, M., Alonso, J., 2016. The molecular composition of Cretaceous ambers: Identification and chemosystematic relevance of 1, 6-dimethyl-5-alkyltetralins and related bisnorlabdane biomarkers. Organic Geochemistry 93, 7-21.

Miall, A.D., 1977. A review of the braided river depositional environment. Earth-Science Reviews 13, 1–62.

Miall, A.D., 1978. Lithofacies types and vertical profile models in braided river deposits: a summary. In: Miall, A.D. (Ed.), Fluvial Sedimentology. Canadian Society of Petroleum Geologists, Memoir 5, pp. 597–604.

Miall, A.D., 2010. Alluvial deposits. In: James, N.P., Dalrymple, R.W. (Eds.), Facies Models 4. Geological Association of Canada, pp. 105–138.

Mjøs, R., Walderhaug, O., Prestholm, E., Marzo, M., Puigdefabregas, C., 1993. Crevasse splay sandstone geometries in the Middle Jurassic Ravenscar Group of Yorkshire, UK. In: Marzo, M., Puigdefabregas, C. (Eds.) Alluvial sedimentation 17, Special Publication of the International Association of Sedimentologists, pp. 167-184.

Moreau, J.D., Néraudeau, D., Tafforeau, P., Dépré, É., 2015. Study of the histology of leafy axes and male cones of *Glenrosa carentonensis* sp. nov. (Cenomanian Flints of Charente-Maritime, France) using synchrotron microtomography linked with palaeoecology. PLoS One 10, e0134515.

Morrison, R.B., 1977. Quaternary soil stratigraphy, concepts, methods and problems. In: Mahaney, W.C. (Ed.), Quaternary Soils. Geo-Abstracts, Norwich, pp. 77–108.

Mount, J.F., 1984. Mixing of siliciclastic and carbonate sediments in shallow shelf environments. Geology 12, 432–435.

Mountney, N.P., 2004. The sedimentary signature of deserts and their response to environmental change. Geology Today 20, 101–106.

Mountney, N.P., Thompson, D.B., 2002. Stratigraphic evolution and preservation of aeolian dune and damp/wet interdune strata: an example from the Triassic Helsby Sandstone Formation, Cheshire Basin, UK. Sedimentology 49, 805-833.

Mountney, N.P., Jagger, A., 2004. Stratigraphic evolution of an aeolian erg margin system: the Permian Cedar Mesa Sandstone, SE Utah, USA. Sedimentology 51, 713-743.

Muto, T., Steel, R.J., 2000. The accommodation concept in sequence stratigraphy: some dimensional problems and possible redefinition. Sedimentary Geology 130, 1–10.

Nahon, D.B., 1991. Self-organization in chemical lateritic weathering. Geoderma 51, 5-13.

Najarro, M., Rosales, I., Moreno-Bedmar, J.A., de Gea, G.A., Barrón, E., Company, M., Delanoy, G., 2011. High-resolution chemo- and biostratigraphic records of the Early Aptian oceanic anoxic event in Cantabria (N Spain): Palaeoceanographic and palaeoclimatic implications. Palaeogeography, Palaeoclimatology, Palaeoecology 299, 137–158.

Nathorst, A.G., 1893. Om en fossilförande leraflagring vid Skattmansö i Upland. Geologiska Föreningen i Stockholm Förhandlingar 15, 539–587.

Nesbitt, H.W., Young, G.M., 1982. Early Proterozoic climates and plate motions inferred from major element chemistry of lutites. Nature 299, 715.

Nichols, D.J., Jacobson, S.R., Tschudy, R.H., 1982. Cretaceous palynomorph biozones for the central and northern Rocky Mountain region of the United States. In: Powers, R. (Ed.), Geologic Studies of the Cordilleran Thrust Belt, Rocky Mountain vol. 2. Association of Geologists, Denver, USA, 721–733.

Norris, R. D., Bice, K. L., Magno, E. A., Wilson, P. A., 2002. Jiggling the tropical thermostat in the Cretaceous hothouse. Geology 30, 299–302.

North, C.P., Davidson, S.K. 2012. Unconfined alluvial flow processes: recognition and interpretation of their deposits, and the significance for palaeogeographic reconstruction. Earth-Science Reviews 111, 199-223.

O'mara, N.A., Skonieczny, C., McGee, D., Winckler, G., Bory, A. J.M., Bradtmiller, L.I., Malaizé, B., Polissar, P.J., 2022. Pleistocene drivers of Northwest African hydroclimate and vegetation. Nature communications 13, 1-11.

Olariu, C., Steel, R.J., Dalrymple, R.W., Gingras, M.K., 2012. Tidal dunes versus tidal bars: the sedimentological and architectural characteristics of compound dunes in a tidal seaway, the lower Baronia Sandstone (Lower Eocene), Ager Basin, Spain. Sedimentary Geology 279, 134–155.

Pardo, G., 1979. Estratigrafía y sedimentología de las formaciones detríticas del Cretácico inferior terminal del Bajo Aragón Turolense (Unpubl. Ph.D. thesis). Universidad de Zaragoza, Spain.

Pardo, G., Villena, J., 1979. Características sedimentológicas y paleogeográficas de la Formación Escucha. Cuadernos de Geología Ibérica, 5, 407–418.

Payton, C.E., 1977. Seismic stratigraphy—applications to hydrocarbon exploration. AAPG memoir 26, 502 pp.

Pe-Piper, G., Piper, D.J., 2004. The effects of strike-slip motion along the Cobequid–Chedabucto–southwest Grand Banks fault system on the Cretaceous–Tertiary evolution of Atlantic Canada. Canadian Journal of Earth Sciences 41, 799-808.

Penny, J.H.J., 1986. An Early Cretaceous angiosperm pollen assemblage from Egypt. Special Papers in Palaeontology 35, 119–132.

Peñalver, E., Martínez-DelClòs, X., 2002. Importancia patrimonial de Arroyo de la Pascueta, un yacimiento de ámbar cretácico con insectos fósiles en Rubielos de Mora. In: Meléndez, G., Peñalver, E. (Eds.) El patrimonio paleontológico de Teruel: I Jornadas sobre el Patrimonio de la provincia de Teruel, Paleontología: Rubielos de Mora, 24, 25 y 26 de septiembre de 1998. Instituto de Estudios Turolenses, 201-208.

Peñalver, E., Szwedo, J.,2010. Perforissidae (Hemiptera: Fulgoroidea) from the Lower Cretaceous San Just amber (Eastern Spain). Alavesia 3, 97-103.

Peñalver, E., Delclòs, X., 2010. Spanish amber. In: Penney, D. (Ed.), Biodiversity of fossils in amber from the major world deposits. Siri Scientific Press, Manchester, UK, 236–270.

Peñalver, E., Martínez-Delclòs, X., Arillo, A., 1999. Yacimientos con insectos fósiles en España. Revista Española de Paleontología 14, 231–245.

Peñalver, E., Delclòs, X., Soriano, C., 2007. A new rich amber outcrop with palaeobiological inclusions in the Lower Cretaceous of Spain. Cretaceous Research 28, 791-802.

Peropadre, C., 2011. El Aptiense del margen occidental de la Cuenca del Maestrazgo: controles tectónicos, eustático y climático de la sedimentación (Unpubl. Ph.D. thesis). Universidad Complutense de Madrid, Madrid (in Spanish).

Peropadre, C., Liesa, C.L., Meléndez, N., 2013. High-frequency, moderate to high-amplitude sea-level oscillations during the late Early Aptian: Insights into the Mid-Aptian event (Galve sub-basin, Spain). Sedimentary Geology 294, 233-250.

Perrichot, V., Néraudeau, D., Tafforeau, P., Penney, D., 2010. Charentese amber. Biodiversity of fossils in amber from the major world deposits, 192-207. In: Penney, D. (Ed.). Biodiversity of fossils in amber from the major world deposits. Siri Scientific Press, 192-207.

Peyrot, D., 2011. Late Cretaceous (Late Cenomanian–Early Turonian) dinoflagellate cysts from the Castilian Platform, northern Spain. Palynology 35, 267–300.

Peyrot, D., Barrón, E., Polette, F., Batten, D.J., Néraudeau, D., 2019. Early Cenomanian palynofloras and inferred resiniferous forests and vegetation types in Charentes (southwestern France). Cretaceous Research 94, 168–189.

Platt, N.H., 1989. Continental sedimentation in an evolving rift basin: the Lower Cretaceous of the western Cameros Basin (northern Spain). Sedimentary Geology 64, 91-109.

Playford, G., Haig, D.W., Dettmann, M.E., 1975. A mid-Cretaceous microfossil assemblage from the Great Artesian Basin, Northwestern Queensland. Neues Jahrbuch für Geologie und Paläontologie, Abhandlungen 149, 333–362.

Plint, A.G., James, N.P., Dalrymple, R.W., 2010. Wave-and storm-dominated shoreline and shallow-marine systems. In: James, N.P., Dalrymple, R.W. (Eds.), Facies Models 4. Geological Association of Canada, pp. 167–200.

Portero, J.M., Olivé, A., Ramírez, J., 1972. Mapa Geológico de España 1.50000, hoja nº636 (Villar del Humo). IGME, Madrid.

Posamentier, H.W., James, D.P., 1993. An overview of sequence-stratigraphic concepts: uses and abuses. In: Posamentier, H.W., (Ed.) Sequence stratigraphy and facies associations 18. International Association Sedimentologists, Special Publication, pp. 3-18.

Preston, L.J., Shuster, J., Fernandez-Remolar, D., Banerjee, N.R., Osinski, G.R., Southam, G., 2011. The preservation and degradation of filamentous bacteria and biomolecules within iron oxide deposits at Río Tinto, Spain. Geobiology 9, 233–249.

Pucéat, E., Lécuyer, C., Sheppard, S.M.F., Dromart, G., Reboulet, S., and Grandjean, P., 2003. Thermal evolution of Cretaceous Tethyan marine waters inferred from oxygen isotope composition of fish tooth enamels. Paleoceanography 18, 7.1–7.12.

Puga, E., Díaz de Federico, A., Fanning, M., Nieto, J., Rodríguez, Martínez-Conde, J., Díaz Puga, M., Lozano, J., Bianchini, G., Natali, C., Beccaluva, L., 2017. The Betic Ophiolites and the Mesozoic Evolution of the Western Tethys. Geosciences 7, 31.

Querol, X., 1990. Distribución de la materia mineral y azufre en los carbones de la Formación Escucha. Relación con los factores geológicos, sedimentológicos y diagenéticos. (Unpubl. Ph.D. thesis) Universidad de Barcelona, Spain (in Spanish).

Ramírez del Pozo, J., Portero, J.M., Olivé, A., 1972. Mapa Geológico de España 1.50000, hoja nº 635 (Fuentes). IGME, Madrid.

Ramírez del Pozo, J., Portero J.M., Olive, A., Meléndez, F., 1974. El Cretácico de la Serranía de Cuenca y de la región de Fuentes-Villar del Humo. Correlación y cambios de facies. I Symposium del Cretácico de la Cordillera Ibérica, Cuenca, 189–206.

Ramírez Merino, J.I., 1986. Mapa Geológico de España 1.50000, hoja nº587 (Las Majadas). IGME, Madrid.

Ramos, A., Fernández, O., Torne, M., Sánchez de la Muela, A., Muñoz, J.A., Terrinha, P., Manatschal, G., Salas, M.C., 2017. Crustal structure of the SW Iberian passive margin: The westernmost remnant of the Ligurian Tethys? Tectonophysics 705, 42–62.

Ravn, L. R., 1995. Miospores from the Muddy Sandstone (Upper Albian), Wind River Basin, Wyoming, USA. Palaeontographica Abt. B 234, 41–91.

Retallack, G.J., 1988. Field recognition of paleosols. Geological Society of America Special Paper 216, 1-20.

Retallack, G.J., 2001. Soils of the Past. Blackwell, Oxford. 404 pp.

Retallack, G.J., 2012. Criteria for distinguishing microbial mats and earths. In: Noffke, N., Chafetz, H.S. (Eds.), Microbial Mats in Siliciclastic Depositional Systems through Time. Tulsa, Oklahoma: SEPM (Society for Sedimentary Geology), pp. 139–153.

Reynaud, J.Y., Dalrymple, R.W., 2012. Shallow-marine tidal deposits. In: Davis, R.A., Dalrymple, R.W. (Eds.) Principles of tidal sedimentology Springer, Dordrecht, pp. 335-369.

Rhodes, E.G., 1982. Depositional model for a chenier plain, Gulf of Carpentaria, Australia. Sedimentology 29, 201–221.

Rodríguez, L.R., López, F., Oliveira, J.T., Medialdea, T., Terrinha, P., Matas, J., Martín-Serrano, A., Martín, L.M., Rubio, F., Marín, C., Montes, M., Nozal, F., 2014. Mapa Geológico de España y Portugal 1:1000000. IGME and LNEG.

Rodríguez-López, J.P., 2008. Sedimentología y evolución del sistema desértico arenoso (erg) desarrollado en el margen occidental del Tethys durante el Cretácico Medio, Cordillera Ibérica. Provincias de Teruel y Zaragoza (Unpubl. Ph.D. thesis). Complutense University of Madrid, Spain.

Rodríguez-López, J.P., De Boer, P.L., Meléndez, N., Soria, A.R., Pardo, G., 2006. Windblown desert sands in coeval shallow marine deposits: a key for the recognition of coastal ergs in the mid-Cretaceous Iberian Basin, Spain. Terra Nova 18, 314–320.

Rodríguez-López, J.P., Meléndez, N., Boer, P.L.D., Soria, A.R., 2008. Aeolian sand sea development along the mid-Cretaceous western Tethyan margin (Spain): erg sedimentology and palaeoclimate implications. Sedimentology 55, 1253–1292.

Rodríguez-López, J.P., Meléndez, N., Soria, A.R., De Boer, P., 2009. Reinterpretación estratigráfica y sedimentológica de las Formaciones Escucha y Utrillas de la Cordillera Ibérica. Revista de la Sociedad Geológica de España 22, 163–219.

Rodríguez-López, J.P., Meléndez, N., De Boer, P., Soria, A.R., 2010. The action of wind and water in a mid-Cretaceous subtropical erg-margin system close to the Variscan Iberian Massif, Spain. Sedimentology 57, 1315–1356.

Rodríguez-López, J. P., Melendez, N., De Boer, P. L., Soria, A. R., 2012. Controls on marine–erg margin cycle variability: aeolian–marine interaction in the mid-Cretaceous Iberian Desert System, Spain. Sedimentology 59, 466–501.

Rodríguez-López, J.P., Meléndez, N., de Boer, P.L., Soria, A.R., Liesa, C.L., 2013. Spatial variability of multi-controlled aeolian supersurfaces in central-erg and marine erg-margin systems. Aeolian Research 11, 141–154.

Rodríguez-López, J.P., Peyrot, D., Barrón, E., 2020. Complex sedimentology and palaeohabitats of Holocene coastal deserts, their topographic controls, and analogues for the mid-Cretaceous of northern Iberia. Earth-Science Reviews 201, 103075.

Ross, A., Mellish, C., York, P., Crighton, B., Penney, D., 2010. Burmese amber. Biodiversity of fossils in amber from the major world deposits. In: Penney, D. (Ed.). Biodiversity of fossils in amber from the major world deposits. Siri Scientific Press, 208-235.

Rubin, D.M., Carter, C.L., 2006. Bedforms and cross-bedding in animation. SEPM Atlas of Sedimentology. SEPM, Tulsa, Oklahoma.

Ruffell, A. H., Batten, D. J., 1990. The Barremian–Aptian arid phase in western Europe. Palaeogeography, Palaeoclimatology, Palaeoecology 80, 197–212.

Salas, R., Casas, A., 1993. Mesozoic extensional tectonics, stratigraphy, and crustal evolution during the Alpine cycle of the eastern Iberian basin. Tectonophysics 228, 33–55.

Salas, R., Guimerà, J., Mas, R., Martín-Closas, C., Melendéz, A., Alonso, A., 2001. Evolution of the Mesozoic central Iberian Rift System and its Cenozoic inversion (Iberian Chain). In: Ziegler, P.A., Cavazza, W., Robertson, A.H.F., Crasquin-Soleau, S. (Eds.), Peri-Tethyan Rift/Wrench Basins and Passive Margins. PeriTethys Memoir 6, 145–185.

Saspiturry, N., Issautier, B., Razin, P., Baudin, T., Asti, R., Lagabrielle, Y., Allanic, C., Serrano, O., Duretz, T., 2021. Review of Iberia–Eurasia plate-boundary basins: Role of sedimentary burial and salt tectonics during rifting and continental breakup. Basin Research 33, 1626–1661.

Schenk, A., 1869. Beiträge zur Flora der Vorwelt 3. Die fossilen Pflanzen der Wernsdorfer Schichten in den Nordkarpathen). Palaeontographica Abteilung 19, 1–34.

Schettino, A., Turco, E., 2011. Tectonic history of the western Tethys since the Late Triassic. Geological Society of America Bulletin 123, 89-105.

Schrank, E., 2003. Small acritarchs from the Upper Cretaceous: taxonomy, biological affinities and palaeoecology. Review of Palaeobotany and Palynology 123, 199–235.

Schrank, E., Ibrahim, M.I.A., 1995. Cretaceous (Aptian–Maastrichtian) palynology of foraminifera-dated wells (KRM-1, AG-18) in northwestern Egypt. Berliner Geowissenschaftliche Abhandlungen, Reihe A 177, 1–44.

Schrank, E., Mahmoud, M.S., 1998. Palynology (pollen, spores and dinoflagellates) and Cretaceous stratigraphy of the Dakhla Oasis, central Egypt. Journal of African Earth Sciences 26, 167–193.

Schroeder, R., García, A., Cherchi, A., Segura, M., 1993. El Albense-Cenomanense del puerto del Remolcador (Cordillera Ibérica, Maestrat, Castell.): secuencias deposicionales y biozonación con grandes foraminíferos. Geogaceta 14, 69-72.

Schultz, L.G., 1964. Quantitative interpretation of mineralogical composition from X-ray and chemical data for Pierce-Shale. Professional Papers, United States Geological Survey 391.

Schwartz, R.K., Birkemeier, W.A., 2004. Sedimentology and morphodynamics of a barrier island shoreface related to engineering concerns, Outer Banks, NC, USA. Marine Geology 211, 215–255.

Schwarz, E., Veiga, G.D., Álvarez Trentini, G., Isla, M.F., and Spalletti, L.A., 2018. Expanding the spectrum of shallow-marine, mixed carbonate siliciclastic systems: Processes, facies distribution, and depositional controls of a siliciclastic-dominated example. Sedimentology 65, 1558–1589.

Segura, M., García, A., Carenas, B., 1983. El Albiense superior-Cenomaniense de la Sierra de Albarracín (provincias de Teruel y Cuenca). Boletin de la Real Sociedad Española de Historia Natural (Geología) 81, 247-264.

Segura, M., García-Hidalgo, J. F., Carenas, B., Gil, J., García, A., 2004. Evolución paleogeográfica de la Cuenca Ibérica en el Cretácico Superior. Geogaceta, 36, 103–106.

Seilacher, A., 1967. Bathymetry of trace fossils. Marine Geology 5, 413-428.

Seward, A.C., 1917. Fossil plants. Vol. 3.: Cambridge University Press, Cambridge.

Seyfullah, L.J., Beimforde, C., Dal Corso, J., Perrichot, V., Rikkinen, J., Schmidt, A.R., 2018. Production and preservation of resins–past and present. Biological Reviews 93, 1684-1714.

Shanley, K.W., McCabe, P.J., 1994. Perspectives on the sequence stratigraphy of continental strata. AAPG Bulletin 78, 544–568.

Shanley, K.W., McCabe, P.J., Hettinger, R.D., 1992. Tidal influence in Cretaceous fluvial strata from Utah, USA: a key to sequence stratigraphic interpretation. Sedimentology 39, 905–930.

Sharp, R.P., 1966. Kelso Dunes, Mojave Desert, California. Geological Society of America Bulletin 77, 1045-1074.

Sheldon, N.D., Tabor, N.J., 2009. Quantitative paleoenvironmental and paleoclimatic reconstruction using paleosols. Earth-Science Reviews 95, 1–52.

Sheldon, N. D., Retallack, G. J., Tanaka, S., 2002. Geochemical climofunctions from North American soils and application to paleosols across the Eocene-Oligocene boundary in Oregon. The Journal of geology 110, 687-696.

Sherman, D.J., 2019. Reflective Beaches. In: Finkl, C.W., Makowski, C. (Eds.), Encyclopedia of Coastal Science. Encyclopedia of Earth Sciences Series. Springer, Cham, pp. 1393–1458.

Shiers, M.N., Mountney, N.P., Hodgson, D.M., Cobain, S.L., 2014. Depositional controls on tidally influenced fluvial successions, Neslen Formation, Utah, USA. Sedimentary Geology 311, 1-16.

Sibuet, J.C., Srivastava, S.P., Spakman, W., 2004. Pyrenean orogeny and plate kinematics. Journal of Geophysical Research: Solid Earth 109, B08104.

Sibuet, J.C., Rouzo, S., Srivastava, S., 2012. Plate tectonic reconstructions and paleogeographic maps of the central and North Atlantic oceans. Canadian Journal of Earth Sciences 49, 1395-1415

Singh, C., 1971. Lower Cretaceous microfloras of the Peace River Area, Northwestern Alberta. Research Council of Alberta Bulletin 28, 1–299.

Singh, C., 1983. Cenomanian microfloras of the Peace River area, northwestern Alberta. Research Council of Alberta Bulletin 44, 1–239.

Skarpe, C., 1992. Dynamics of savanna ecosystems. Journal of vegetation Science 3, 293-300.

Skonieczny, C., McGee, D., Winckler, G., Bory, A., Bradtmiller, L. I., Kinsley, C. W., Polissar, P.J., De Pol-Holz, R., Rossignol, L., Malaizé, B., 2019. Monsoon-driven Saharan dust variability over the past 240,000 years. Science advances 5, eaav1887.

Soares, D.M., Alves, T.M., Terrinha, P., 2012. The breakup sequence and associated lithospheric breakup surface: Their significance in the context of rifted continental margins (West Iberia and Newfoundland margins, North Atlantic). Earth and Planetary Science Letters 355, 311–326.

Soares, D.M., Alves, T.M., Terrinha, P., 2014. Contourite drifts on early passive margins as an indicator of established lithospheric breakup. Earth and Planetary Science Letters 401, 116–131.

Solé de Porta, N., Salas, R., 1994. Conjuntos microflorísticos del Cretácico Inferior de la Cuenca del Maestrazgo. Cordillera Ibérica Oriental (NE de España). Cuadernos de Geología Ibérica 18, 355–368.

Sopeña, A., Gutiérrez-Marco, J. C., Sánchez-Moya, Y., Gómez, J. J., Mas, R., García, A., Lago, M., 2004. Cordillera Ibérica y Costero Catalana. In: Vera, J.A. (Ed.), Geología de España. Sociedad Geológica de España–Instituto Geológico y Minero de España, Madrid, Spain, 465–528.

Spalletti, L.A., Colombo Piñol, F., 2005. From Alluvial Fan to Playa: An Upper Jurassic Ephemeral Fluvial System, Neuquén Basin, Argentina. Gondwana Research 8, 363–383.

Spicer, R.A., 1977. The pre-depositional formation of some leaf impressions. Palaeontology 20, 907–912.

Spicer, R.A., 1989. The formation and interpretation of plant fossil assemblages. Advances in Botanical Research 16, 96–191.

Spicer, R.A., 1991. Plant taphonomic processes. In: Allison, P.A., Briggs, D.E. (Eds.), Taphonomy: releasing the data locked in the fossil record. Plenum Press, New York and London, pp. 71–113.

Srinivasan, V., 1992. Two new species of the conifer *Glenrosa* from the Lower Cretaceous of North America. Review of Palaeobotany and Palynology 72, 245–255.

Srinivasan, V., 1995. Conifers from the Puddledock locality (Potomac Group, Early Cretaceous) in eastern North America. Review of Palaeobotany and Palynology 89, 257–286.

Srivastava, S.K., 1976. The fossil pollen genus *Classopollis*. Lethaia 9, 437–457.

Sternberg, G.K., 1838. Versuch einer geognostisch-botanischen Darstellung der Flora der Vorwelt: Skizzen zur vergleischenden Phytotomie vorund jeztweltlicher Pflanzen-Stämme (Vol. 2). F. Fleischer, Leipzig.

Sunamura, T., 1992. Geomorphology of Rocky Coasts. Wiley and Sons, UK.

Svobodová, M., Hradecká, L., Skupien, P., Švábenická, L., 2004. Microfossils of the Albian and Cenomanian shales from the Štramberk area (Silesia unit, Outer Western Carpathians, Czech Republic). Geologica Carpathica 55, 371–388.

Swift, D.J.P., 1968. Coastal Erosion and Transgressive Stratigraphy. The Journal of Geology 76, 444–456.

Takhtajan, A.L., Vakhrameev, V.A., Radtschenko, G.P., 1963. Gymnosperms and angiosperms. Osnovy Paleontologii 15, 1–743.

Tanrikulu, S., Doyle, J.A., Delusina, I., 2018. Early Cretaceous (Albian) spores and pollen from the Glen Rose Formation of Texas and their significance for correlation of the Potomac Group. Palynology 42, 438–456.

Taylor, T.N., 1981. Paleobotany: an introduction to fossil plant biology. McGraw-Hill, USA.

Taylor, D.W., Hu, S., 2010. Coevolution of early angiosperms and their pollinators: Evidence from pollen. Palaeontographica Abt. B 283, 103–135.

Terrinha, P., Kullberg, J. C., Neres, M., Alves, T., Ramos, A., Ribeiro, C., Mata, J., Pinheiro, L., Afilhado, A., Matias, L., Luis, J., Nuñoz, J.A., Fernández, Ó., 2019. Rifting of the Southwest and West Iberia continental margins. In: Quesada, C., Oliveira, J.T. (Eds.), The Geology of Iberia: A Geodynamic Approach. Volume 3: The Alpine cycle. Regional Geology Reviews, Springer, Cham, 251-283.

Thomas, H.H., 1913. On some new rare Jurassic plants from Yorkshire: *Eretmophyllum*, a new type of ginkgoalean leaf. Proceedings of the Cambridge Philosophical Society 17, 256–262.

Thomas, R.G., Smith, D.G., Wood, J.M., Visser, J., Calverley-Range, E.A., Koster, E.H., 1987. Inclined heterolithic stratification—terminology, description, interpretation, and significance. Sedimentary Geology 53, 123-179.

Traverse, A., 2007. Paleopalynology (2nd ed.). Springer, The Netherlands.

Tucholke, B.E., Sawyer, D.S., Sibuet, J.C., 2007. Breakup of the Newfoundland–Iberia rift. Geological Society, London, Special Publications 282, 9-46.

Uličný, D., Kvaček, J., Svobodová, M., Špičáková, L., 1997. High-frequency sea-level fluctuations and plant habitats in Cenomanian fluvial to estuarine succession: Pecínov quarry, Bohemia. Palaeogeography, Palaeoclimatology, Palaeoecology 136, 165–197.

Upchurch, G.R., Doyle, J.A., 1981. Palaeoecology of the conifers *Frenelopsis* and *Pseudofrenelopsis* (Cheirolepidiaceae) from the Cretaceous Potomac Group of Maryland and Virginia. In: Romans, R.C. (Ed.), Geobotany II. Plenum Publishing Corporation, New York, pp. 167–202.

Vakhrameyev, V.A., 1982. *Classopollis* pollen as an indicator of Jurassic and Cretaceous climate. International Geology Review 24, 1190–1196.

Vakhrameyev, V.A., 1991. Jurassic and Cretaceous floras and climates of the Earth. Cambridge University Press.

Vargas, H., Gaspar-Escribano, J.M., López-Gómez, J., Van-Wees, J., Cloetingh, S., De-La-Horra, R., Arche, A., 2009. Tectonophysics A comparison of the Iberian and Ebro Basins during the Permian and Triassic, eastern Spain: A quantitative subsidence modelling approach. Tectonophysics 474, 160-183.

Vergés, J., Kullberg, J.C., Casas-Sainz, A., Vicente, G. D., Duarte, L. V., Fernàndez, M., Gómez, J.J., Gómez-Pugnaire, M.T., Jabaloy-Sanchez, A., López-Gómez, J., Macchiavely, C., Martín-Algarra, A., Martín-Chivelet, J., Muñoz, J.A., Quesada, C., Terrinha, P., Torné, M., Vegas, R., 2019. An introduction to the Alpine cycle in Iberia. In: Quesada, C., Oliveira, J.T. (Eds.), The Geology of Iberia: A Geodynamic Approach. Volume 3: The Alpine cycle. Regional Geology Reviews, Springer, Cham, 1-14.

Viallard, P., 1973. Recherches sur le cycle alpin dans la chaîne ibérique sud-occidentale (Unpubl. Ph.D. thesis). Université de Toulouse, France.

Vicente, A., Martín-Closas, C., 2013. Lower Cretaceous charophytes from the Serranía de Cuenca, Iberian chain: Taxonomy, biostratigraphy and palaeoecology. Cretaceous Research 40, 227–242.

Vilas, L., Mas, R., García, A., Arias, C., Alonso, A., Meléndez, N., Rincón, R., 1982. La Cordillera Ibérica Suroccidental. In: García, A. (Ed.), El Cretácico de España. Universidad Complutense de Madrid, Spain, pp. 457–513.

Villanueva-Amadoz, U., 2009. Nuevas aportaciones palinostratigráficas para el intervalo Albiense–Cenomaniense en el Sector NE de la Península Ibérica. Implicaciones paleogeográficas y paleoclimáticas (Unpubl. Ph.D. thesis). Universidad de Zaragoza, Zaragoza, Spain.

Wagoner, J.V., Mitchum, R.M., Campion, K.M., Rahmanian, V.D., 1990. Siliciclastic Sequence Stratigraphy in Well Logs. Cores, and Outcrops: Concepts for High-Resolution Correlation of Time and Facies. AAPG Methods in Exploration Series 7, 3–55.

Watson, J., 1977. Some Lower Cretaceous conifers of the Cheirolepidiaceae from the USA and England. Palaeontology 20, 715–749.

Watson, J., 1988. The Cheirolepidiaceae. In: Origin and Evolution of Gymnosperms. Columbia University Press, New York, pp. 382–447.

Watson, J., Fisher, H.L., 1984. A new conifer genus from the Lower Cretaceous Glen Rose Formation, Texas. Palaeontology 77, 719–727.

Williams, A.J., Buck, B.J., Beyene, M.A., 2012. Biological Soil Crusts in the Mojave Desert, USA: Micromorphology and Pedogenesis. Soil Science Society of America Journal 76, 1685–1695.

Wright, V.P., Marriott, S.B., 1993. The sequence stratigraphy of fluvial depositional systems: the role of floodplain sediment storage. Sedimentary Geology 86, 203–210.

Wyse, S.V., 2012. Growth responses of five forest plant species to the soils formed beneath New Zealand kauri (Agathis australis). New Zealand Journal of Botany 50, 411–421.

Yaalon, D.H., 1971. Soil-forming processes in space and time. In: Yaalon, D.H. (Ed.), Paleopedology: Origin, Nature and Dating of Paleosols. Israel Universities Press, Jerusalem, pp. 29–39.

Yaalon, D.H., 1983. Climate, time, and soil development. In: Wilding, L.P., Smeck, N.E., Hall, G.F. (Eds.), Pedogenesis and Soil Taxonomy. I. Concepts and Interactions. Developments in Soil Science, Volume 11A. Elsevier, Amsterdam, pp. 233–251.

Zervas, D., Nichols, G.J., Hall, R., Smyth, H.R., Luthje, C., Murtagh, F., 2009. SedLog: A shareware program for drawing graphic logs and log data manipulation. Computer and Geosciences 35, 2151–2159.

Zhang, M., Dai, S., Du, B.-X., Ji, L., Hu, S., 2018. Mid Cretaceous hothouse climate and the expansión of early angiosperms. Acta Geologica Sinica (english edition) 92, 2004–2025.

Zhou, Z., Thévenard, F., Barale, G., Guignard G., 2000. A xeromorphic conifer from the Cretaceous of East China. Palaeontology 43, 561–572.

APPENDIXES – EXTRA MATERIALS.

APPENDIX I: Research papers.

APPENDIX II: Palynomorph abundances.

APPENDIX III: List of the identified taxa ordered according to their botanical affinity.

APPENDIX IV: Additional correlations.

APPENDIX V: Granulometry analysis (raw data).

APPENDIX VI: Difractograms.

APPENDIX I: Research papers.

A) Bueno-Cebollada and Meléndez (2018).

Bueno-Cebollada, C.A., Meléndez-Hevia, N., 2018. Aeolian dune development in an Albian arid coastal braidplain system in Serranía de Cuenca (Iberian Basin, Spain). Geogaceta 64, 27–30.

B) Bueno-Cebollada et al. (2021).

Bueno-Cebollada, C.A., Barrón, E., Peyrot D., Meléndez, N., 2021. Palynostratigraphy and palaeoenvironmental evolution of the Aptian to lower Cenomanian succession in the Serranía de Cuenca (Eastern Spain). Cretaceous Research 128, 104956. https://doi.org/10.1016/j.cretres.2021.104956.

C) Bueno-Cebollada et al. (2022).

Bueno-Cebollada, C.A., Fregenal-Martínez, M., Meléndez, N., 2022. Along-strike sedimentological variability and architectural patterns of the transgression of a "mid"-cretaceous braidplain system (Iberian Basin, eastern Spain): A tool for depicting eustatic and tectonic signatures within the framework of a global transgression. Sedimentary Geology 429, 106082. https://doi.org/10.1016/j.sedgeo.2022.106082.

Aeolian dune development in an Albian arid coastal braidplain system in Serranía de Cuenca (Iberian Basin, Spain)

Desarrollo de dunas eólicas en un sistema de braidplain *árido costero de edad Albiense en la Serranía de Cuenca (Cuenca Ibérica, España)*

Carlos A. Bueno-Cebollada[1] and Nieves Meléndez-Hevía[2]

[1] Dpto. de Geodinámica, Estratigrafía y Paleontología, Universidad Complutense, 28040, Madrid. cabueno@ucm.es
[2] Dpto. de Geodinámica, Estratigrafía y Paleontología, Universidad Complutense; IGEO (UCM, CSIC). 28040 Madrid. nievesml@ucm.es

ABSTRACT

The Utrillas Sandstone Group is an Albian to Cenomanian clastic succession which is widely spread along most areas in the Iberian Basin. In the Southwestern sector (Serranía de Cuenca) an arid braidplain was developed and connected to the Tethys towards SE, thus some facies associations present tidal features. Aeolian dune development within the arid braidplain system was possible, although as a minor feature. This paper aims: 1) to describe the facies associations of the arid braidplain regarding their different origin, and 2) to study and interpret aeolian dune accumulations based on the granulometric study of 5 samples and on the outcrop study of the geometry and surfaces hierarchy.

Key-words: *Utrillas Group, Iberian Basin, arid braidplain, Albian, aeolian dunes.*

RESUMEN

El Grupo Utrillas es una sucesión clástica Albiense-Cenomaniense la cual se encuentra ampliamente extendida en todo el contexto de la Cuenca Ibérica. En el sector Suroccidental (Serranía de Cuenca) un sistema de braidplain árido fue el principal paleoambiente. Este sistema de braidplain árido estuvo conectado con el Tethys hacia el SE. El desarrollo de dunas eólicas en el sistema de braidplain fue posible aunque no son una facies muy abundante. Este artículo tiene como objetivo: 1) describir las asociaciones de facies del sistema braided árido, y 2) estudiar e interpretar las dunas eólicas sobre la base del analisis granulométrico de 5 muestras y del estudio de la arquitectura estratigráfica del afloramiento.

Palabras clave: *Grupo Utrillas, Cuenca Ibérica, Braidplain árido, Albiense, dunas eólicas.*

Geogaceta, 64 (2018), 27-30
ISSN (versión impresa): 0213-683X
ISSN (Internet): 2173-6545

Recepción: 21 de enero de 2018
Revisión: 14 de abril de 2018
Aceptación: 25 de abril de 2018

Introduction

The Utrillas Sandstone Group is a well-known, mostly Albian to lower Cenomanian heterolithic but mainly detrital group, which is widely spread all over the Iberian Basin, Spain (Sopeña, 2004). This detrital group has paramount importance in the development of the second rifting stage of the Iberian Basin, which spanned from Upper Jurassic to latest Cretaceous (Sopeña, 2004), since its onset marks the transition from the syn-rift to the post-rift stage. Hence, the Utrillas Group can be considered the first unit of the second post-rift stage of the Iberian Basin in many localities (Rodríguez-López *et al.*, 2008).

The Utrillas Group was originally considered as a fluvial depositional system (Pardo, 1979). However it has been recently studied and reinterpreted as a subtropical erg system (Rodríguez-López *et al.*, 2010). In the Serrania de Cuenca area, the Utrillas Group overlies either the Aptian El Burgal Fm. or the Barremian La Huerguina Fm. (Fregenal-Martínez *et al.*, 2017).

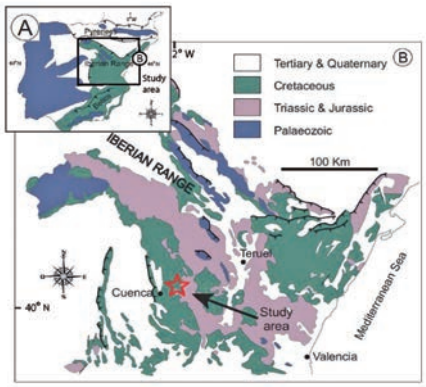

Fig. 1.- A) Location of the study area in the Iberian Basin. B) Close up of the Iberian Basin. A hollow red star indicates the study area (Modified from Sopeña, 2004). Ver figura en color en la web.

Fig. 1.- A) Localización del área de estudio en la Cuenca Ibérica. B) Detalle del área estudiada. Una estrella hueca roja indica la localización del área de estudio (Modificado de Sopeña, 2004). See color figure in the web.

This paper aims to study the Utrillas Group in the Serrania de Cuenca, Southwestern Iberian Basin, Spain (Fig. 1), an area where its sedimentological traits still remain little studied (Chamizo-Borreguero *et al.*, 2016). The present work comprises a granulometric analysis and outcrop study of 3 different aeolian accumulations within the context of a coastal arid braidplain in Serrania de Cuenca, Spain. Aeolian dune accumulations are not rare phenomena in arid braidplains (Mountney, 2004).

Methodology

5 sedimentary columns have been logged in several adjacent ravines in the surroundings of Buenache de la Sierra, a locality where the outcrops are well exposed. The logs were later digitalized by using a SED LOG 3.1 software (Zervas *et al.*, 2009). Figure 2 shows the most representative logged section.

By means of this procedure up to 9 facies associations (f.a.) have been identified, which are classified into 3 groups of facies associations according to their origin.

Likewise, 5 samples of aeolian dune sandstone were collected from the outcrops. Such samples were smashed and sieved in up to 10 grain size intervals. Later, cumulative weight percentages were calculated and plotted in a semi-logarithmic sheet for each sample.

Facies associations groups

Three groups of facies associations have been interpreted and described from the logged outcrops: alluvial, aeolian and coastal to shallow marine.

Alluvial Facies associations group: (EA, EO1, EO2 and EO3 f.a)

EA (Ephemeral alluvial): white to red heterometric sandstone, either bioturbated or not, with high feldspar content, medium-coarse to granule grain size, although medium-fine size can be locally found. Scattered faceted pebbles are common. The geometry of the bodies is generally tabular to lenticular, usually presenting erosive or sharp basal contacts. Main structures observed are dm- to dam- planar and trough cross beddings. This facies association is interpreted as ephemeral fluvial channels that remained dry and were occasionally flooded during the wet season. Indicators of a depositional arid climate are: high feldspar content, which indicates a lack of chemical weathering; and the presence of scattered ventifact pebbles (Knight, 2008).

EO1, EO2, EO3 (overbank deposits): EO1 consists of intense red mottled to yellowish mudstones and siltstones with some minor proportions of sand particles. EO2 is a grey to greenish color claystone to siltstone with minor sand proportions. In general EO2 and EO1 show similar geometrical and depositional characteristics. In both facies associations lower contacts are usually sharp, however upper contacts show some degree of transition in many cases, between EO1 and EO2.

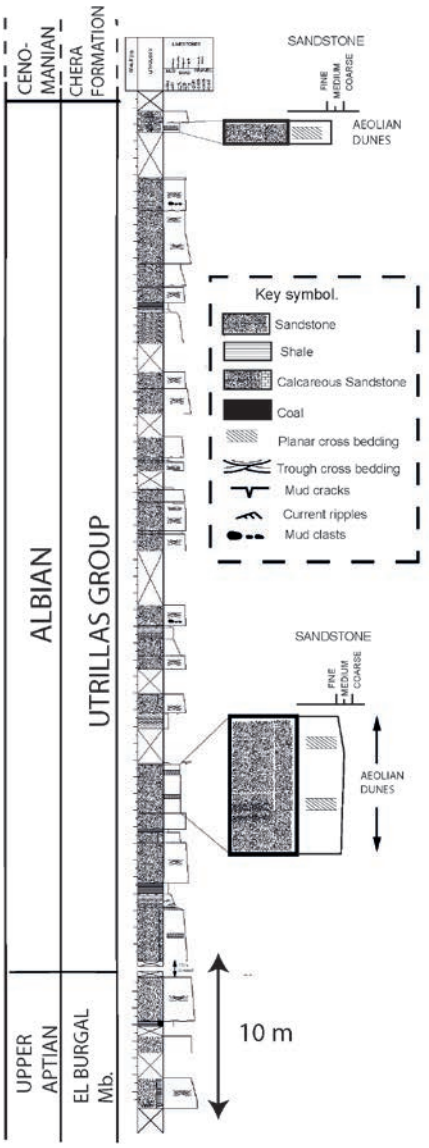

Fig. 2.-Compound logged section for the Utrillas Group in Buenache de la Sierra. Two sampled aeolian dune accumulations are enlarged.

Fig. 2.- Columna estratigráfica compuesta para el Grupo Utrillas en Buenache de la Sierra. Dos tramos de arenas eólicas muestreados han sido ampliados.

EO3 consists of poorly sorted sandstones with variable mud proportions, which are arranged in lenticular thin sand bodies. It appears encased in facies EO1 and EO2.

This three EO of facies associations are closely related to EA facies association and are interpreted as overbank deposits. EO1 and EO2 are interpreted as deposited in a flood plain. The difference between them lies in that EO1 indicates an oxidizing environment due to its intense red mottling and frequent soil development, whereas EO2 grey to greenish color is an indicator of reductive processes in the same depositional sub environment.

EO3 is interpreted as crevasse splays, which spread into the ephemeral flood plain as sandy lenses.

Aeolian Facies associations group: (AD1, AD2, ASS and DL f.a.)

AD1 and AD2 (aeolian dune and aeolian pods): both facies associations consist of fine to fine-medium grained sandstone. They are composed by cm- to dm- scale trough and planar cross bedding sets that stacked all over the facies. AD1 and AD2 are interpreted as complex aeolian dune sandstones due to its cross beddings, compositional and textural maturity and lack of coarser grains in a sedimentary setting where coarser material is predominant. AD1 represents well developed aeolian dunes whereas AD2 represents smaller aeolian dune bodies, which remained preserved encased within coarser fluvially or tidally influenced facies association.

ASS (aeolian sandsheet): fine to medium grained sandstones arranged in tabular sets (20 to 40 cm thick each set), with high clay contents. This facies association also can contain coarse to granule grain size particles. Yellow mottling is a common feature.

Therefore this facies association, which frequently appears associated with EA and EO deposits, is interpreted as an aeolian sandsheet, which keeps great resemblance with other sandstone bodies interpreted as aeolian sandsheets in the Utrillas Group (Rodriguez-Lopez *et al.*, 2010).

DL (Deflation lags): it consists of one flat-lying pebble thick layer that extends for several tens of meters. Pebbles are usually sub rounded and some ventifacts have been found as well. They are interpreted as lags of pebbles formed by wind deflaction when wind eject finer particles and pebble size or coarser particles remain *in situ* producing lags. It is a clear indicator of wind reworking in an arid environment (Rodríguez-López *et al.*, 2010).

Coastal Facies associations group: (TSF f.a.)

TSF (Tidal sandflat): coarse to very coarse grain sandstone, in some cases even granule size grains. Occasionally scattered pebbles and mud pebbles can be observed in this facies association. Although it is not very common, carbonate cement can be present. This

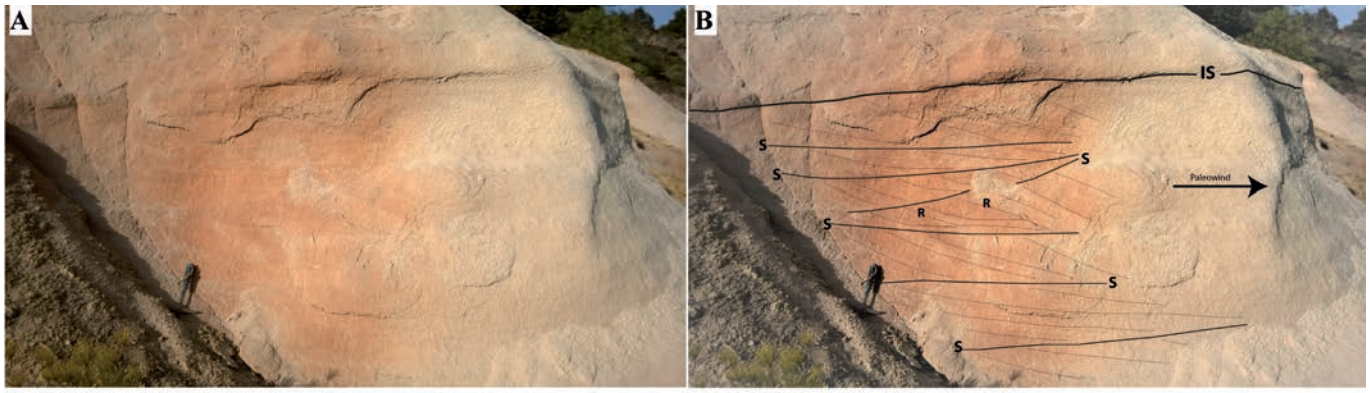

Fig. 3.- A) Photograph of complex aeolian dunes with dry interdunes. B) Line drawing of A. The hierarchy of bounding surfaces is highlighted (see text for explanation). Main paleowind direction is towards the right (NNE).Hammer for scale is 30 cm long. See color figure in the web.

Fig. 3.- A) Fotografía de dunas eólicas complejas con interdunas secas. B) Interpretación de A. En la fotografía se indica la jerarquía de las superficies eólicas (ver texto). La dirección de paleo-viento principal es hacia la derecha de la imagen (NNE). El martillo usado de escala mide 30 cm. Ver figura en color en la web.

f.a. consists of more or less tabular bodies of great lateral continuity (tens of meters). They present trough cross beddings and planar cross bedding although the latter is less common. The main feature is that the lee sides of the cross beddings are reworked in a direction opposed to the main current, showing a "curly" appearance. Therefore, we interpret this facies as a tidal facies in which the curly appearance would have been produced by the flow current (flood), while the main foresets correspond to the ebb current in a tidal sandflat setting.

Aeolian dune granulometry, geometry and interpretation

Granulometric analysis

The granulometry study shows that the population of clasts with ϕ between 1 and 4 is 90.6 % (mean cumulative percentage in weight of the five granulometries), which corresponds to medium to very fine grain size clasts (Fig. 4). Likewise, mean cumulative percentage in weight of clasts with $\phi > 4$ is 3.61% averaged for the five samples. In addition the mean cumulative percentage value for clasts with $\phi <$ 1 has also been included (5.79 %).

Hence 90.6 % of the weight of the sampled sandstones ranges between medium to very fine grain size, which agrees with previous studies of aeolian dune sands (Folk, 1971 ; Lancaster, 1986), but especially Sharp (1966), since this author identified medium grain size sandstones in aeolian dunes in the Mojave Desert, California. This allows us to deduce that the clasts in most of our samples are in the field of saltation, and therefore wind transport would have been possible (Rodríguez-López *et al.*, 2006).

Regarding grains with $\phi > 4$, they represent the suspension load fraction, which is wind laid in minor proportion in the aeolian system. On the other hand, those clasts with $\phi < 1$ (5.79 %) represent the traction load population, which could not be transported by the wind (Rodríguez-López *et al.*, 2006). The best explanation for this minor amount of coarser clasts is that they were incorporated by the action of ephemeral alluvial systems, fact that would have not been uncommon in arid braidplain system with associated aeolian dunes.

Dune geometry

3 aeolian outcropping accumulations have been found in the 5 sedimentary logs (both AD1 and AD2 facies associations are represented). The geometrical study of the dune bodies has been tackled based on the best preserved and exposed aeolian accumulations (Fig. 3).

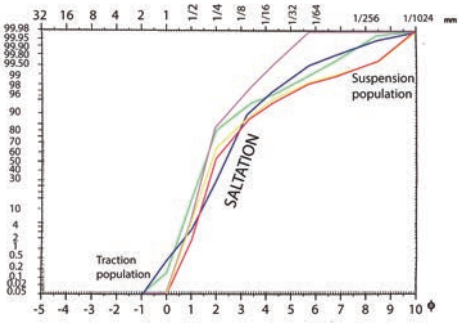

Fig. 4.- Granulometric curve for the 5 collected samples from the Aeolian dunes. Traction, saltation and suspension populations indicated. See color figure in the web

Fig. 4.- Curva granulométrica para las 5 muestras recogidas en las dunas eólicas. Se indican poblaciones de tracción, saltación y suspensión. Ver figura en color en la web.

The outcropping aeolian succession studied here is a 3 m thick well preserved aeolian body bounded at its base by coarse to granule size sandstones from EA facies associations and at its top by greenish to red clays, which belong to EO1 and EO2 facies associations, respectively. It spans laterally for 10 to 15 meters.

Geometrically, 3 different aeolian surfaces have been identified in the outcrop, which have been drawn in figure 3B. These surfaces depict the hierarchy of aeolian processes as follows:

First order surfaces (IS in figure 3B) represent interdune surfaces and can be traced all along the outcropping accumulation. These interdune surfaces represent the migration of larger aeolian forms over the stoss slope of former dunes. In this case the lack of interdune deposits in the IS (see figures 3 A and B) indicates a dry interdune and hence a dry aeolian system (Mountney, 2004). They are represented by flat and sharp surfaces that literally cross the outcrop and cut any other lower order surfaces.

Second order surfaces, interpreted as superimposition surfaces (S in figure 3B), have also been described in the outcrop. The observed superimposition surfaces are sub-parallel surfaces, which usually describe low angle downwind dipping beddings and cut dune foresets and minor third order surfaces (Fig 3B). Superimposition surfaces are the result of the migration of dunes over another larger dune body (Mountney, 2004).

Third order surfaces have been identified and interpreted as reactivation surfaces (R in figure 3B). They are surfaces bounded by either second or first order surfaces, which are more or less concordant, but slightly steeper, with the cross strata of the dunes foresets (see figure 3).

Reactivation surfaces are the result of erosion of the lee face of the dune as a consequence of a change in wind direction. When sedimentation resumes a reactivation surface is generated in the erosive surface (Rodríguez-López *et al.*, 2008, Mountney and Thompson, 2002).

Taking into account the complex geometry defined by the aforementioned surfaces, we identify the aeolian bodies as complex aeolian dunes in an arid braidplain aeolian system for the Utrillas Group. The present outcrop shows great similarity with the complex dune facies association described by Rodríguez-López *et al.*, 2008 (in his figure 14) in a dry aeolian system. The main difference resides in that in the Serrania de Cuenca area these dune bodies are minor and genetically associated with an arid braidplain, instead of being part of a proper erg as in Soria-Zaragoza-Teruel where they are much more abundant (Rodríguez-López *et al.*, 2006, 2010).

Conclusions

The Utrillas Group in the Serrania de Cuenca area has been interpreted as an arid coastal braidplain with minor aeolian record. The prevalence of ephemeral alluvial systems with occasional tidal influence reveals the existence of an arid braidplain, which was at some point affected by tides due to its nearness with the paleo-Tethys.

This work has allowed us to study how dunes develop, as minor features, in an arid braidplain from the Cretaceous (Albian) of the Southwestern sector of the Iberian Basin.

Both granulometric and outcrop studies were carried out. Granulometric studies show that 90.6 % of the grains sampled are in the field of saltation, hence it would have been possible their transport and deposition by wind, producing aeolian dunes.

Likewise an outcrop study reveals the existence of a typical aeolian dune bounding surface hierarchy, which includes: first order surfaces (IS), second order surfaces (S) and third order surfaces (R). The stacking pattern of the dune foresets and the way in which superimposition surfaces (S) cut them have led us to interpret them as complex aeolian dunes with dry interdunes acting as minor feature within an arid braidplain.

Acknowledgements

This paper is included in the research project CGL2014-52163 (MINECO, of the Spanish Government). This paper is part of an ongoing PhD thesis, which is being performed in the research group "*Paleoclimatología y cambio global*" of UCM. We are also grateful to the reviewers of this paper, Dr. A.R. Soria and Dr. J.M. Molina, for their helpful advice.

References

Chamizo-Borreguero, M., Meléndez, N. and De Boer, P.L. (2016). *Proceedings of the Tidalites 2012 Conference* IAS, 93-115.

Folk, R.L. (1971). *Sedimentology* 16, 5-54.

Fregenal-Martínez, M.A., Meléndez, N., Muñoz-García, M.B., Elez, J., and De la Horra, R. (2017). *Revista de la Sociedad Geológica de España* 30, 113-142.

Knight, J. (2008). *Earth-Science Reviews* 86, 89-105.

Lancaster, N. (1986). *Journal of Sedimentary Petrology* 56, 395–400.

Mountney, N. (2004). *Geology Today* 20, 101-106.

Mountney, N. and Thompson, D.B. (2002). *Sedimentology* 49, 805–833.

Pardo, G. (1979). *Estratigrafía y sedimentología de las formaciones detríticas del Cretácico inferior termial en el Bajo Aragón turolense.* PhD thesis, Universidad de Zaragoza, Spain.

Rodríguez-López, J.P., De Boer, P.L., Meléndez, N., Soria, A.R. and Pardo, G. (2006). *Terra Nova 18*, 314–320.

Rodríguez-López, J.P., Meléndez, N., De Boer, P.L. and Soria, A.R. (2008). *Sedimentology* 55, 1253–1292.

Rodríguez-López, J.P., Meléndez, N., De Boer, P.L. and Soria, A.R. (2010). *Sedimentology* 57, 1315–1356.

Sharp, R.P. (1966). *Geological Society of America Bulletin* 77, 1045–1074.

Sopeña, A. (2004). In: *Geología de España* (J.A. Vera, Ed.). SGE-IGME, Madrid, 465-527.

Zervas, D., Nichols, G.J., Hall, R., Smyth, H.R., Luthje, C. and Murtagh, F. (2009). *Computer and Geosciences* 35, 2151-2159.

Cretaceous Research 128 (2021) 104956

Contents lists available at ScienceDirect

Cretaceous Research

journal homepage: www.elsevier.com/locate/CretRes

Palynostratigraphy and palaeoenvironmental evolution of the Aptian to lower Cenomanian succession in the Serranía de Cuenca (Eastern Spain)

Carlos A. Bueno-Cebollada [a, *], Eduardo Barrón [a], Daniel Peyrot [b], Nieves Meléndez [c]

[a] Museo Geominero, Instituto Geológico y Minero de España – IGME-CSIC, Ríos Rosas 23, Madrid, 28003, Spain
[b] School of Earth and Environment, Centre for Energy Geoscience, University of Western Australia, Crawley, Western Australia, 6101, Australia
[c] Dpto. de Geodinámica, Estratigrafía y Paleontología, Facultad de Ciencias Geológicas, José Antonio Nováis 12, Madrid, 28040, Spain

ARTICLE INFO

Article history:
Received 24 June 2020
Received in revised form
7 June 2021
Accepted in revised form 8 July 2021
Available online 20 July 2021

Keywords:
Early Cenophytic palynofloras
Aptian–early Cenomanian
Serranía de Cuenca
Western Tethys
arid braidplain system

ABSTRACT

The Aptian to lower Cenomanian succession from the Serranía de Cuenca region (Eastern Iberia, Spain) comprises a time-span largely understudied regarding palynology and biostratigraphy. This research studies the deposits of three stratigraphic units that crop out in this region (the Contreras Formation, the El Burgal Member and the Utrillas Group), allowing identification, study and sampling of the palynofloras from the Aptian–?early Cenomanian time-interval. The studied sections are grouped into three sectors based on the palynostratigraphic ages obtained: the MPB, TU, and CT sectors, respectively. The palynoflora is dominated by gymnosperm pollen grains and diversified spores of ferns and allies. The palynofloral evidence and regional geology indicate that the sampled levels in the MPB sector are Aptian in age, whereas those levels sampled at the TU and CT sectors are dated as middle Albian–?early Cenomanian. The Aptian palynofloras of this sector differ from other contemporaneous sites of Europe and North America in the possible occurrence of tricolpate angiosperm pollen. In general, angiosperm pollen does not present high percentages; however, it becomes more diversified from the middle Albian in the TU and CT sectors, where more than 20 taxa were recorded on average. The studied pollen assemblages conform with the characteristics of the early Cenophytic palynofloras. Likewise, an increase in dinocysts towards the upper levels of the sedimentary succession in the TU and CT sectors is consistent with the transgressive nature of the deposits, documenting the progressive landward expansion of Western Tethys in Iberia during Albian to ?early Cenomanian times.

1. Introduction

The Aptian to Cenomanian interval represents a time-span characterized by the highest global sea-levels of the Mesozoic Era (Haq, 2014), coinciding with a period of early diversification of angiosperms along with a decline in the diversity of gymnosperms and pteridophytes, likely associated with oceanic and climatic changes (Crane and Lidgard, 1989; Crane et al., 1995; Heimhofer et al., 2005). This time-interval is referred to as a global warmth period dominated by greenhouse conditions, showing relatively lower temperatures during the Aptian and an increase in global temperatures during the Albian, leading to the Late Cretaceous thermal maximum during Cenomanian/Turonian times (Norris et al., 2002; Puceat et al., 2003; Forster et al., 2007).

The Aptian to early Cenomanian time-span has been studied at length in some regions of Iberia; namely, the Mesozoic Iberian Basin (i.e. El Maestrazgo Domain) and the Basque-Cantabrian Basin (Fig. 1). These two sedimentary basins are associated with the Western-Tethys and Proto-Atlantic realms, respectively. In this regard, recent works aiming at describing the palynological assemblages of these stratigraphic successions have been published in order to cast new light on their palaeonvironmental implications, as well as to obtain a more accurate biostratigraphic dating (i.e. Villanueva-Amadoz, 2009; Najarro et al., 2011; Barrón et al., 2015). Likewise, this period also constitutes an extremely prolific time-span with regard to the deposit of amber-bearing successions (i.e. Peñalver et al., 1999; Peñalver and Delclòs, 2010).

By contrast, there are other geographic regions in Iberia in which the Aptian to early Cenomanian time-span remains understudied in terms of palynofloras and biostratigraphy, and the continental successions attributed to this interval commonly lack suitable age-diagnostic biostratigraphic markers (Heimhofer et al.,

* Corresponding author.
E-mail address: c.bueno@igme.es (C.A. Bueno-Cebollada).

https://doi.org/10.1016/j.cretres.2021.104956
0195-6671/

Sedimentary Geology 429 (2022) 106082

Contents lists available at ScienceDirect

Sedimentary Geology

journal homepage: www.elsevier.com/locate/sedgeo

Along-strike sedimentological variability and architectural patterns of the transgression of a "mid"-Cretaceous braidplain system (Iberian Basin, eastern Spain): A tool for depicting eustatic and tectonic signatures within the framework of a global transgression

Carlos A. Bueno-Cebollada [a,*], Marian Fregenal-Martínez [b], Nieves Meléndez [b]

[a] Instituto Geológico y Minero de España – IGME-CSIC, Ríos Rosas 23, 28003 Madrid, Spain
[b] Dpto. de Geodinámica, Estratigrafía y Paleontología, Universidad Complutense, 28040 Madrid, Spain

ARTICLE INFO

Article history:
Received 29 September 2021
Received in revised form 5 January 2022
Accepted 9 January 2022
Available online 15 January 2022

Editor: Dr. Catherine Chagué

Keywords:
Braidplain coastal margin
Along-strike variability
Albian–Cenomanian Transgression
Tectono-eustatic control
Utrillas Group
Sequence stratigraphy

ABSTRACT

The mid-Albian to lower Cenomanian Utrillas Group is interpreted as an arid braidplain system in the Serranía de Cuenca region (Iberian Basin, Spain). In its proximal locations, it consists of an interaction of alluvial facies and subordinate aeolian deposits, with the occurrence of tidally-influenced deposits that reflect a general transgressive trend to the top of the succession. However, the distal areas of this braidplain system, where there was a more intense interaction with the Tethys Ocean, have remained understudied to date.

We present a sedimentological study of two outcrops (Pajaroncillo and Reíllo) located at the distal sector of the braidplain system and 12 km apart, defining an along-strike relative position. Both outcrops differ notably regarding the arrangement and distribution of the facies associations identified despite their relative closeness. Based on the sedimentological analysis, the main transgressive and regressive trends of the succession have been identified, along with several correlatable stratigraphic surfaces. This has permitted us to distinguish five stages (T1–T5), which reflect the overall transgressive evolution of the succession: a continental aggradational stage (T1), dominated by alluvial deposition; an initial transgression stage (T2) dominated by an open coast setting in Reíllo and a restricted mudflat system in Pajaroncillo; a regressive stage (T3), during which continental alluvial to supratidal environments deposited; a resumption in transgression (T4), characterised by an array of inter- to subtidal environments; and a deepening stage (T5), when the transgression advanced landward, giving rise to the most distal deposits of the studied succession.

The studied outcrops, located at the basin edge, have been integrated within the regional sequence stratigraphy framework, which was originally devised for more central areas of the Iberian Basin (Valencia Domain) and the Prebetic. This regional approach has allowed us to interpret the studied deposits as third-order depositional sequences. Besides, the supra-regional implications of this research are discussed within the broader context of Iberia and the subtleties of its tectono-sedimentary evolution during the Albian to Cenomanian times.

1. Introduction

Ephemeral alluvial systems are relatively common sedimentary environments linked to hyper-arid to semi-arid climate conditions. They are seasonally active, being perennially flooded only during a few days to a few weeks per year, depending on the aridity regime (Mountney, 2004). These flooding events may consist of sudden and violent surges of flash-flood events that, coupled with the occurrence of loose sand-prone substrates, transport high clastic inputs downstream. The generally reduced vegetated areas that characterise these environments lead to frequent channel instability and migration, ultimately resulting in the development of wide arid plains of migrating braided channels, known as braidplains (Mountney, 2004; Laronne and Shlomi, 2007). Arid braidplains have previously been addressed in the literature, although they are not among the most widely mentioned sedimentary environments, including both modern (Svendsen et al., 2003) and ancient (Mader and Laming, 1985) examples. However, most of the studied examples deal with inland cases (i.e., Turner, 1983; Mader and Laming, 1985; Mroczkowski and Mader, 1985), or if they are located at nearshore areas, they do not tackle their transition into coastal settings (i.e., Krapf et al., 2003, 2005; Svendsen et al., 2003). The interaction of these braidplains with the marine realm can generate a highly

* Corresponding author.
E-mail address: c.bueno@igme.es (C.A. Bueno-Cebollada).

https://doi.org/10.1016/j.sedgeo.2022.106082
0037-0738/

APPENDIX II: Palynomorph abundances.

A) MPB sector:

MPB sector - Taxa	Levels						
	BCH-4	BCH-3	MPII-3	MP-I-3	MPII-2	MP-I-2	MPII-1
Geominig Museum inventory numbers	MGM-11205C/MGM-11207C	MGM-11202C/MGM-11204C	MGM-11189C/MGM-11191C	MGM-11185C/MGM-11188C	MGM-11182C/MGM-11184C	MGM-11178C/MGM-11181C	MGM-11175C/MGM-11177C
Aquatic palynomorphs							
Botryococcus braunii	1	0	16	6	122	1	97
Chomotriletes minor	3	0	0	0	0	0	0
Schizosporis reticulatus	2	6	0	0	0	0	0
Trichodinium castanea	1	0	0	0	0	0	0
Undetermined acritarchs	1	0	0	0	0	0	1
Spores of ferns and allied							
Antulsporites distaverrucosus	0	1	0	0	0	0	0
Appendicisporites erdtmanii	1	0	0	0	0	0	0
Appendicisporites jansonii	1	0	0	0	0	0	0
Appendicisporites problematicus	9	0	0	0	0	0	0
Appendicisporites spp.	31	8	1	2	1	0	1
Biretisporites spp.	7	11	1	2	2	1	0
Camarozonosporites sp.	0	0	0	0	1	0	0
Cibotiumspora jurienensis	2	0	0	0	0	0	0
Cicatricosisporites apicanalis	2	0	0	0	0	0	0
Cicatricosisporites hughesii	4	1	0	0	0	0	0
Cicatricosisporites potomacensis	2	0	0	0	0	0	0
Cicatricosisporites venustus	6	6	0	0	0	0	0
Cicatricosisporites spp.	92	17	0	0	0	0	0
Cingutriletes sp.	4	2	0	0	0	1	0
Clavifera nigra	0	0	0	0	0	1	0
*Claviferas*p.	0	0	0	0	6	6	0
Concavissimisporites cf. *crassatus*	41	2	1	0	0	0	0
Concavissimisporites cf. *granulatus*	0	5	0	0	0	0	0
Concavissimisporites punctatus	0	0	0	0	0	0	2
Concavissimisporites spp.	4	3	1	0	0	0	1
Contignisporites cf. *cooksoniae*	1	0	0	0	0	0	0
Converrucosisporites spp.	0	26	0	0	1	0	0
Costatoperforosporites foveolatus	2	3	0	0	0	0	0
Cyathidites australis	29	9	24	11	31	54	46
Cyathidites minor	56	19	4	12	30	27	33
Deltoidospora spp.	5	2	2	2	0	1	30
Densoisporites velatus	1	0	0	0	0	0	0
Dictyophyllidites harrisii	0	0	0	0	1	0	2

Distaltriangulisporites spp.	1	0	0	0	0	0	0
Echinatisporites sp.	1	1	0	0	0	0	0
Foraminisporis sp.	1	0	0	0	0	0	0
Foveotriletes subtriangularis	8	2	0	0	0	0	0
Foveotriletes spp.	1	0	0	0	1	0	1
Gleicheniidites senonicus	2	0	4	2	15	36	9
Impardecispora cf. *apiverrucata*	0	1	0	0	0	0	0
Ischyosporites cf. crateris	1	2	0	0	0	0	0
Ischyosporites spp.	2	0	0	1	2	0	0
Kraeuselisporites sp.	0	1	0	0	0	0	0
Laevigatosporites sp.	1	0	0	0	0	1	0
Leptolepidites macroverrucosus	7	0	0	0	0	0	0
Leptolepidites spp.	11	4	0	0	3	0	1
Matonisporites crassiangulatus	0	0	143	135	489	127	37
Patellasporites tavaredensis	103	6	0	0	0	0	2
Pilosisporites trichopapillosus	26	7	0	0	0	0	0
Punctatisporites couperi	0	0	0	0	1	0	0
Retitriletes spp.	0	1	0	0	0	0	0
Ruffordiospora spp.	4	1	0	0	0	0	0
Stereisporites cf. antiquasporites	2	3	0	0	0	0	0
Stereisporites spp.	8	2	0	0	1	0	0
Todisporites sp.	3	1	0	0	0	0	0
Trilobosporites cf. *canadensis*	0	1	0	0	7	0	0
Trilobosporites cf. *hannonicus*	2	1	0	0	0	0	0
Trilobosporites spp.	5	0	1	0	0	0	1
Undulatisporites sp.	25	12	0	0	4	1	0
Vallizonosporites sp.	1	0	0	0	0	0	0
Varirugosisporites sp.	102	76	0	0	1	0	0
Verrucosisporites spp.	2	0	0	0	0	0	0
Pollen grains (gymnosperms)							
Alisporites bilateralis	0	0	0	0	1	0	2
Alisporites grandis	0	0	1	0	0	0	0
Alisporites spp.	0	1	2	0	1	7	7
Araucariacites australis	12	75	0	0	12	9	0
Callialasporites dampieri	3	30	0	0	1	0	0
Cedripites mesozoicus	0	0	0	0	1	0	0
Cedripites sp.	0	0	1	0	10	0	0
Cerebropollenites macroverrucosus	2	0	0	0	1	0	1
Classopollis major	198	59	16	10	223	29	32
Classopollis obidosensis	7	4	0	0	0	0	0
Classopollis spp.	2	15	87	62	74	373	73
Cycadopites follicularis	1	5	0	0	1	0	10
Cycadopites spp.	1	3	0	0	0	2	2
Equisetosporites spp.	2	13	1	0	0	0	1
Eucommiidites minor	6	8	0	1	0	2	0
Eucommidites troedsonii	4	9	0	0	1	1	0
Exesipollenites tumulus	7	7	0	0	2	0	0
Inaperturopollenites dubius	5	27	1	1	10	0	2

Inaperturopollenites spp.	10	100	0	0	0	0	0
Monosulcites minimus	0	1	0	0	2	0	22
Monosulcites spp.	3	10	4	4	3	2	23
Parvisaccites radiatus	0	0	0	0	2	0	0
Parvisaccites spp.	0	0	0	0	4	0	2
Perinopollenites halonatus	0	1	0	1	0	0	0
Phyllocladidites sp.	0	0	0	0	7	0	1
Pinuspollenites sp.	0	1	2	0	13	2	2
Podocarpidites sp.	0	1	0	0	6	5	4
Spheripollenites sp.	4	6	0	0	0	0	0
Steevesipollenites sp.	1	0	0	0	0	0	0
Taxodiaceaepollenites hiatus	0	0	0	0	0	0	1
Uesugipollenites sp.	2	10	0	0	0	0	1
Undetermined bisaccate pollen grains	15	15	116	61	569	450	275
Pollen grains (angiosperms)							
Clavatipollenites hughesii	0	1	1	0	1	0	0
Clavatipollenites cf. *tenellis*	0	0	0	0	0	0	2
Clavatipollenites spp.	2	21	49	8	53	10	50
Crassipollis chaloneri	1	0	0	1	7	0	5
Jusinghipollis cf. *ticoensis*	1	1	1	0	2	0	2
Retimonocolpites spp.	2	1	0	1	0	0	1
Pennipollis peroreticulatus	0	2	0	0	0	0	0
cf. Tricolpites sp.	0	0	1	0	1	0	1
Transitoripollis anulisulcatus	0	0	0	0	9	9	0
Transitoripollis spp.	0	0	0	0	0	2	5
Total	**918**	**670**	**481**	**323**	**1736**	**1160**	**791**

B) CT Sector:

CT sector - Taxa	Levels			
	T-CA-1a	LH-CM(2)-1a	RE-1	CP-CS(2)-4
Geominig Museum inventory numbers	MGM-11268C/MGM-11275C	MGM-11257C/MGM-11262C	MGM-11263C/MGM-11267C	MGM-11251C/MGM-11256C
Aquatic palynomorphs				
Botryococcus braunii	6	0	0	0
Chomotriletes minor	0	1	0	0
Michrystridium sp.	0	0	0	2
Undetermined Dinoflagellate cysts	4	5	0	6
Spores of vascular cryptogamma				
Acritosporites cf. *kyrtomus*	1	1	0	0
Antulsporites sp.	0	1	1	0
Appendicisporites aff. *dentimarginatus*	1	0	0	0
Appendicisporites potomacensis	0	1	0	0
Appendicisporites spp.	2	0	10	0
Baculatisporites sp.	0	0	3	0
Biretisporites potoniaei	1	0	0	0
Camarozonosporites sp.	2	0	0	0
Cicatricosisporites apicanalis	0	1	0	0
Cicatricosisporites patapscoensis	0	0	2	0
Cicatricosisporites venustus	0	4	6	0
Cicatricosisporites spp.	2	7	16	4
Cingutriletes sp.	3	5	17	1
*Claviferas*p.	0	4	0	0
Concavissimisporites cf. *crassatus*	0	0	15	0
Concavissimisporites cf. *irregularis*	0	0	15	0
Concavissimisporites punctatus	2	0	0	0
Concavissimisporites verrucatus	4	0	0	7
Concavissimisporites spp.	5	1	3	0
Contignisporites cf. *crenatus*	0	0	0	1
Converrucosisporites spp.	0	5	10	0
Costatoperforosporites fistulosus	0	0	1	0
Costatoperforosporites foveolatus	0	0	3	0
Crybelosporites pannuceus	1	1	1	0
Cyathidites australis	1	0	17	3
Cyathidites minor	30	7	22	3
Deltoidospora spp.	13	4	7	2
Densoisporites velatus	1	0	0	0
Dictyophyllidites harrisii	0	0	0	1
Duplexisporites generalis	0	0	0	1
Foveotriletes subtriangularis	0	0	0	1
Gleicheniidites senonicus	5	0	0	4
Ischyosporites spp.	0	0	17	0
Kraeuselisporites sp.	1	0	0	0
Laevigatosporites sp.	1	0	1	0
Leptolepidites macroverrucosus	1	0	0	0

Leptolepidites spp.	1	0	2	0
Patellasporites tavaredensis	13	15	14	1
Polycingulatisporites reduncus	0	0	1	0
Punctatisporites couperi	1	0	0	0
Retitriletes sp.	0	0	1	0
Stereisporites spp.	0	0	7	0
Gregussosporites orientalis	0	0	4	0
Taurucosporites sp.	0	0	1	0
Todisporites sp.	0	0	3	0
Trilobosporites cf. *aequiverrucosus*	0	0	0	1
Trilobosporites spp.	0	0	1	1
Triporoletes reticulatus	0	0	1	0
Undulatisporites sp.	1	0	14	0
Varirugosisporites sp.	0	0	9	0
Verrucosisporites rotundus	1	0	0	2
Verrucatosporites sp.	0	0	1	0
Pollen grains (gymnosperms)				
Afropollis jardinus	21	1	0	1
Alisporites bilateralis	1	1	0	11
Alisporites spp.	13	5	0	12
Araucariacites australis	28	26	50	113
Callialasporites dampieri	2	2	0	8
Classopollis major	62	133	151	253
Classopollis obidosensis	0	1	121	0
Classopollis spp.	0	0	193	0
Cycadopites follicularis	0	2	6	3
Cycadopites spp.	1	0	0	0
Equisetosporites cf. *multicostatus*	0	0	0	1
Equisetosporites spp.	3	5	0	1
Eucommidites troedsonii	3	3	0	0
Exesipollenites tumulus	15	18	15	21
Inaperturopollenites dubius	43	169	28	45
Inaperturopollenites spp.	7	1	29	1
Monosulcites minutus	10	7	0	0
Monosulcites spp.	10	5	2	3
Parvisaccites sp.	0	0	0	1
Pinuspollenites sp.	1	0	6	5
Podocarpidites sp.	0	0	0	1
Spheripollenites sp.	3	11	1	4
Undetermined bisaccate pollen grains	4	1	3	14
Pollen grains (angiosperms)				
Clavatipollenites spp.	8	2	4	5
Clavatipollenites hughesii	0	1	0	2
Clavatipollenites cf. *tenellis*	0	1	0	1
Clavatipollenites cf. *minutus*	1	0	0	0
Crassipollis chaloneri	1	0	0	0
Cupuliferoidaepollenites sp.	3	4	0	1
Dichastopollenites cf. *dunveganensi*	0	0	8	0
Dichastopollenites spp.	0	0	0	4
Jusinghipollis cf. *ticoensis*	1	1	0	1
Liliacidites spp.	1	1	0	2

Monocolpopollenites sp.	1	0	0	0
Pennipollis peroreticulatus	47	20	0	31
Pennipollis reticulatus	1	12	0	1
Pennipollis spp.	0	2	1	0
Phymopollenites pannosus	0	1	0	0
Retimonocolpites spp.	2	1	2	2
Rousea marthae	3	4	0	0
Striatopollis cf. *sarstedtensis*	3	8	2	1
Striatopollis sp.	4	0	0	2
Tricolpites cf. *hians*	0	0	1	0
Tricolpites maximus	1	0	0	0
Tricolpites cf. *micromunus*	1	2	0	1
Tricolpites minutus	0	0	1	0
Tricolpites spp.	13	2	2	2
Total	**422**	**516**	**852**	**595**

C) TU sector:

TU sector - Taxa	Levels					
	UCR-6	UCR-5	LT-4	LT-3	LT-2	LT-1
Geomining Museum inventory numbers	MGM-11243C/MGM-11248C	MGM-11239C/MGM-11242C	MGM-11227C/MGM-11229C	MGM-11223C/MGM-11226C	MGM-11219C/MGM-11222C	MGM-11215C/MGM-11218C
Aquatic palynomorphs						
Botryococcus braunii	1	0	0	0	1	0
Chichaouadinium arabicum	0	0	0	1	0	0
Criboperidinium spp.	0	0	12	0	0	0
?*Coronifera oceanica*	0	0	0	0	1	0
Cyclonephelium vannophorum	0	0	26	3	0	0
Cyclonephelium sp.	0	0	0	2	1	8
Exochosphaeridium phragmites	0	0	5	0	0	0
Florentinia clavigera	0	0	1	0	0	0
Implestosphaeridium spp.	0	0	0	13	3	0
Lining of Foraminifera	0	0	9	9	28	0
Michrystridium sp.	0	0	0	2	2	1
Odontochitina sp.	0	0	0	1	0	0
Schizosporis reticulatus	0	0	0	0	1	1
Subtilisphaera spp.	0	0	0	14	0	49
Tetraporina sp.	0	0	0	0	1	0
Trichodinium castanea	0	1	11	0	1	0
Undetermined acritarchs	0	0	0	0	1	1
Undetermined dinoflagellate cysts	0	2	18	5	4	11
Spores of vascular cryptogamma						
Acritosporites cf. *kyrtomus*	0	1	1	0	0	1
Aequitriradites spinulosus	0	0	0	0	0	1
Appendicisporites aff. *dentimarginatus*	0	2	0	0	0	0
Appendicisporites problematicus	0	0	0	0	0	1
Appendicisporites spp.	1	2	2	1	0	5
*Auritulinasporites*sp.	0	1	0	0	0	0
Biretisporites potoniaei	0	4	0	0	0	0
Biretisporites spp.	0	0	0	0	0	5
Camarozonosporites insignis	0	3	0	0	0	0
Camarozonosporites sp.	0	0	1	0	0	0
Cibotiumspora jurienensis	0	1	0	0	0	0
Cicatricosisporites angicanalis	0	0	0	3	0	0
Cicatricosisporites apicanalis	0	0	0	0	0	2
Cicatricosisporites recticicatricosus	0	3	0	0	0	0
Cicatricosisporites sinuatus	0	0	1	0	0	0
Cicatricosisporites venustus	13	9	12	22	3	25
Cicatricosisporites spp.	5	37	15	20	0	16
Cingutriletes sp.	0	5	3	3	0	19
*Claviferas*p.	0	1	0	0	0	0
Concavissimisporites cf. *crassatus*	0	0	0	0	1	0
Concavissimisporites cf. *irregularis*	0	0	0	1	0	0

Concavissimisporites punctatus	0	3	0	0	0	0
Concavissimisporites verrucatus	0	0	0	1	0	0
Contignisporites sp.	0	0	1	1	0	0
Converrucosisporites spp.	0	0	4	0	0	2
Costatoperforosporites fistulosus	0	0	0	0	0	1
Costatoperforosporites foveolatus	0	0	0	0	0	2
Crassitudisporites sp.	0	1	0	0	0	0
Crybelosporites pannuceus	1	7	11	9	9	5
Cyathidites australis	4	7	12	22	2	17
Cyathidites minor	2	6	19	14	0	9
Deltoidospora spp.	4	24	3	7	0	1
Dictyophyllidites harrisii	0	2	0	0	0	0
Distaltriangulisporites spp.	0	0	0	0	0	2
Echinatisporites sp.	0	0	0	1	0	0
Gleicheniidites senonicus	0	35	0	0	0	0
Ischyosporites variegatus	0	0	0	0	0	1
Ischyosporites spp.	0	1	0	0	1	2
Laevigatosporites sp.	0	1	0	1	2	0
Leptolepidites macroverrucosus	0	2	0	0	0	0
Leptolepidites spp.	0	1	1	2	0	6
Murospora mesozoica	0	1	0	0	0	0
Murospora sp.	0	1	0	0	0	0
Neoraistrickia robusta	0	0	0	0	0	1
Neoraistrickia truncata	0	2	0	0	0	0
Neoraistrickia sp.	0	0	0	0	0	1
Ornamentifera sp.	0	2	0	0	0	0
Patellasporites tavaredensis	1	7	17	56	4	75
Peromonolites allenensis	0	0	5	8	0	3
Phanerosorisporites cf. *surensis*	0	0	0	0	0	1
Phlebopterisporites cf. *norskatensis*	0	0	0	4	0	0
Phlebopterisporites sp.	0	0	0	0	0	1
Retitriletes sp.	0	0	0	0	0	1
Stereisporites psilatus	0	0	0	0	0	4
Stereisporites spp.	0	4	1	3	1	1
Todisporites sp.	0	0	1	0	0	1
Trilobosporites sp.	0	1	0	0	0	0
Undulatisporites spp.	0	2	2	3	0	10
Varirugosisporites sp.	0	0	0	5	0	1
Verrucosisporites rotundus	1	0	0	0	0	0
Verrucosisporites sp.	0	0	0	0	0	1
Pollen grains (gymnosperms)						
Afropollis jardinus	0	2	3	3	0	1
Alisporites bilateralis	0	7	0	0	0	0
Alisporites grandis	0	0	0	1	0	0
Alisporites spp.	2	6	0	1	0	0
Araucariacites australis	12	63	46	57	14	52
Balmeiopsis limbatus	0	0	0	0	0	2
Callialasporites dampieri	0	2	4	5	2	10
Cedripites cretaceous	0	0	0	3	0	0
Cerebropollenites macroverrucosus	0	0	0	0	1	0

Classopollis major	12	11	357	30	89	71
Classopollis obidosensis	0	0	0	0	0	1
Classopollis spp.	1	0	28	11	24	26
Cycadopites follicularis	0	1	4	3	7	2
Cycadopites spp.	8	12	0	2	2	2
Ephedripites cf. regularis	0	0	1	1	11	0
Equisetosporites cf. *multicostatus*	1	1	0	3	0	4
Equisetosporites spp.	1	0	10	12	0	2
Eucommiidites minor	0	0	4	1	1	0
Eucommidites troedsonii	0	1	3	3	0	1
Exesipollenites tumulus	3	3	11	32	16	9
Exesipollenites sp.	0	0	8	3	0	0
Inaperturopollenites dubius	359	302	408	855	285	621
Inaperturopollenites spp.	107	55	6	17	2	12
Monosulcites minutus	0	0	5	0	0	0
Monosulcites spp.	11	0	8	7	10	2
Parvisaccites radiatus	0	9	0	0	0	0
Parvisaccites spp.	2	0	0	0	0	0
Perinopollenites halonatus	0	0	82	56	15	3
Phyllocladidites sp.	0	0	1	0	0	0
Pinuspollenites sp.	1	4	4	8	0	0
Spheripollenites sp.	9	4	0	37	14	35
Steevesipollenites sp.	0	0	1	2	0	0
Taxodiaceaepollenites hiatus	0	0	4	2	1	0
Uesugipollenites callosus	0	0	9	2	3	0
Undetermined bisaccate pollen grains	5	25	14	34	6	13
Pollen grains (angiosperms)						
Artiopollis indivisus	1	0	0	0	0	0
Asteropollis asteroides	0	0	0	0	0	1
Clavatipollenites hughesii	2	0	0	0	0	0
Clavatipollenites cf. *minutus*	2	1	0	1	1	0
Clavatipollenites spp.	8	9	1	5	2	3
Crassipollis chaloneri	0	0	0	0	0	1
Cupuliferoidaepollenites parvulus	2	1	0	0	0	0
Cupuliferoidaepollenites sp.	0	0	0	0	1	0
Dichastopollenites cf. *dunveganensis*	0	0	0	1	0	0
Dichastopollenites spp.	0	0	5	0	1	1
Jusinghipollis cf. *ticoensis*	4	1	0	2	0	0
Liliacidites spp.	0	1	0	0	1	1
Monocolpopollenites sp.	1	0	1	0	0	0
Pennipollis escuchensis	0	0	7	3	1	0
Pennipollis peroreticulatus	0	20	5	2	4	2
Pennipollis reticulatus	0	6	30	31	0	13
Pennipollis spp.	3	0	11	0	0	6
Retimonocolpites dividuus	0	0	0	1	0	1
Retimonocolpites spp.	0	2	7	6	3	6
Retitrescolpites sp.	0	0	1	1	0	0
Stellatopollis cf. *baghornii*	0	6	0	1	0	1
Striatipollis cf. *sarstedtensis*	0	0	0	0	1	2
Transitoripollis anulisulcatus	0	0	20	0	0	0

Transitoripollis spp.	0	0	2	0	1	0
Tricolpites cf. *micromunus*	0	0	0	0	0	1
Tricolpites nemejci	0	0	1	0	0	0
Tricolpites cf. *vulgaris*	0	1	0	0	0	0
Tricolpites spp.	5	4	6	5	5	1
Tucanopollis crispolensis	0	0	3	1	0	2
Undetermined angiosperm pollen	13	20	5	7	1	9
Total	**608**	**762**	**1320**	**1495**	**592**	**1215**

Appendix III: List of the identified taxa ordered according to their botanical affinity.

Aquatic palynomorphs

Freshwater algae

Botryococcus braunii Kutzing 1849 (MP, BCH, LT, UCR and T-CA-1a outcrops)

Chomotriletes minor (Kedves 1961) Pocock 1970 (BCH and LH-CM(2)-1a outcrops; fig. 8i)

Tetraporina sp. (LT outcrop)

Prasinophytes

Schizosporis reticulatus Cookson and Dettman 1959 (BCH and LT outcrops)

Dinoflagellate cysts

Chichaouadinium arabicum Below 1981 (LT outcrop)

?Coronifera oceanica Cookson and Eisenak 1958 (LT outcrop; Fig. 9c)

Cribroperidinium sp. (LT outcrop)

Cyclonephelium vannophorum Davey 1969 (LT outcrop; Fig. 9a)

Cyclonephelium sp. (LT outcrop)

Exochosphaeridium phragmites Davey, Downie, Sarjeant and Williams 1966 (LT outcrop)

Florentinia clavigera (Deflandre 1937) Davey and Verdier 1973 emend. Davey and Verdier 1976 (LT outcrop)

Impletosphaeridium sp. (LT outcrop)

Odontochitina sp. (LT outcrop)

Subtilisphaera sp. (LT outcrop)

Trichodinium castanea Deflandre 1935 ex Clarke and Verdier 1967 (BCH, LT and UCR outcrops; Fig.8f)

Undetermined dinoflagellate cysts (LT, UCR, CP-CS(2)4, LH-CM(2)-1a and T-CA-1a outcrops)

Acritarchs

Micrhystridium sp. (LT and CP-CS(2)4 outcrops; Fig. 9b)

Undetermined acritarchs (MP, BCH and LT outcrops)

Other aquatic palynomorphs

Lining of Foraminifera (LT outcrop)

Spores

Bryophyta

Aequitriradites spinulosus (Cookson and Dettmann 1958) Cookson and Dettmann 1961 (LT outcrop)

Antulsporites distaverrucosus (Brenner 1963) Archangelsky and Gamerro 1966 (BCH outcrop)

Antulsporites sp. (RE-1 and LH-CM(2)-1a outcrops)

Cingutriletes spp. (MP, BCH, LT, UCR, CP-CS(2)4, RE-1, LH-CM(2)-1a and T-CA-1a outcrops)

Foraminisporis sp. (BCH outcrop)

Nevesisporites sp. (RE-1 outcrop)

Polycingulatisporites reduncus (Bolkhovitina 1953) Playford and Dettmann 1965 (RE-1 outcrop)

Stereisporites cf. *antiquasporites* (Wilson and Webster 1946) Dettmann 1963 (BCH outcrop)

Stereisporites psilatus (Ross 1949) Thomson and Pflug 1953 (LT outcrop)

Stereisporites spp. (MP, BCH, LT, UCR and RE-1 outcrops)

Taurucosporites sp. (RE-1 outcrop)

Triporoletes reticulatus (Pocock 1962) Playford 1971 (RE-1 outcrop)

Lycophyta

Camarozonosporites insignis Norris 1967 (UCR outcrop)

Camarozonosporites sp. (MP, LT and T-CA-1a outcrops)

Densoisporites velatus Weyland and Krieger 1953 (BCH and T-CA-1a outcrops)

Echinatisporites sp. (BCH and LT outcrops)

Foveotriletes subtriangularis Brenner 1963 (BCH and CP-CS(2)4 outcrops; Fig. 10l– m)

Foveotriletes spp. (MP and BCH outcrops)

Kraeuselisporites sp. (BCH and T-CA-1a outcrops)

Leptolepidites macroverrucosus Schulz 1967 (BCH, UCR and T-CA-1a outcrops)

Leptolepidites spp. (MP, BCH, LT, UCR, RE-1 and T-CA-1a outcrops)

Neoraistrickia robusta Brenner 1963 (LT outcrop; Fig. 9g)

Neoraistrickia truncata (Cookson 1953) Potonié 1956 (UCR outcrop)

Neoraistrickia sp. (LT outcrop)

Retitriletes sp. (BCH, LT and RE-1 outcrops)

Vallizonosporites sp. (BCH outcrop)

Pteridophyta Anemiaceae

Appendicisporites aff. *dentimarginatus* Brenner 1963 (UCR and T-CA-1a outcrops)

Appendicisporites erdtmanii Pocock 1964 (BCH outcrop)

Appendicisporites jansonii Pocock 1962 (BCH outcrop)

Appendicisporites problematicus (Burger 1966) Singh 1971 (BCH and LT outcrops)

Appendicisporites potomacensis Brenner 1963 (LH-CM(2)-1a outcrop)

Appendicisporites spp. (MP, BCH, LT, UCR, RE-1 and T-CA-1a outcrops)

Cicatricosisporites angicanalis Döring 1965 (LT outcrop; Fig. 9k)

Cicatricosisporites apicanalis Paden Phillips and Felix 1972 (BCH, LT and LH-CM(2)-1a outcrops)

Cicatricosisporites hughesii Dettmann 1963 (BCH outcrop)

Cicatricosisporites patapscoensis Brenner 1963 (RE-1 outcrop)

Cicatricosisporites potomacensis Brenner 1963 (BCH outcrop)

Cicatricosisporites recticicatricosus Döring 1965 (UCR outcrop; Fig. 9l–m)

Cicatricosisporites sinuosus Hunt 1985 (LT outcrop)

Cicatricosisporites venustus Deák 1963 (BCH, LT, UCR, RE-1 and LH-CM(2)-1a outcrops; Fig. 10d)

Cicatricosisporites spp. (BCH, LT, UCR, CP-CS(2)4, RE-1, LH-CM(2)-1a and T-CA-1a outcrops)

Costatoperforosporites fistulosus Deák 1962 (LT and RE-1 outcrops)

Costatoperforosporites foveolatus Deák 1962 (BCH, LT and RE-1 outcrops)

Distaltriangulisporites sp. (BCH and LT outcrops)

Duplexisporites generalis Deák 1962 (CP-CS(2)4 outcrop; Fig. 10b–c)

Ischyosporites cf. *crateris* Balme 1957 (BCH and RE-1 outcrops; Fig. 10e)

Ischyosporites variegatus (Couper 1958) Schulz 1967 (LT outcrop)

Ischyosporites spp. (MP, BCH, LT, UCR and RE-1 outcrops)

Ruffordiaspora sp. (BCH outcrop)

Pteridophyta Cyatheaceae/Dicksoniaceae/Dipteridaceae

Biretisporites potoniaei Delcourt and Sprumont 1955 (LT and T-CA-1a outcrops)

Biretisporites spp. (MP, BCH and LT outcrops)

Cibotiumspora jurienensis (Balme 1957) Filatoff 1975 (BCH and UCR outcrops)

Cyathidites australis Couper 1953 (MP, BCH, LT, UCR, CP-CS(2)4, RE-1, T-CA-1a outcrops)

Cyathidites minor Couper 1953 (MP, BCH, LT, UCR CP-CS(2)4, RE-1, LH-CM(2)-1a and T-CA-1a outcrops)

Deltoidospora spp. (MP, BCH, LT, UCR, CP-CS(2)4, RE-1, LH-CM(2)-1a and T-CA-1a outcrops)

Pteridophyta Dipteridaceae/Matoniaceae

Dictyophyllidites harrisii Couper 1958 (MP, UCR and CP-CS(2)4 outcrops)

Matonisporites crassiangulatus (Balme 1957) Dettmann 1963 (MP outcrop; Fig. 8a)

Phanerosorisporites cf. *surensis* Juhász 1979 (LT outcrop)

Phlebopterisporites cf. *harskutensis* Juhász 1979 (LT outcrop)

Phlebopterisporites sp. (LT outcrop)

Pteridophyta Gleicheniaceae

Clavifera nigra (Bolchovitina 1953) Juhász 1977 (MP outcrop)

Clavifera sp. (MP, UCR and LH-CM(2)-1a outcrops)

Gleicheniidites senonicus Ross 1949 emend. Skarby 1964 (MP, BCH, UCR, CP-CS(2)4 and T-CA-1a outcrops)

Ornamentifera sp. (UCR outcrop)

Pteridophyta Lygodiaceae/?Dicksoniaceae

Concavissimisporites cf. *crassatus* (Delcourt & Sprumont) Delcourt, Dettmann & Hughes 1963 (MP, BCH, LT and RE-1 outcrops)

Concavissimisporites cf. *granulatus* Pocock 1965 (BCH outcrop; Fig. 8g)

Concavissimisporites cf. *irregularis* (Pocock 1970) Backhouse 1988 (LT and RE-1 outcrops; Fig. 10f)

Concavissimisporites punctatus (Delcourt and Sprumont 1955) Brenner 1963 (MP, UCR and T-CA-1a outcrops)

Concavissimisporites verrucosus Delcourt & Sprumont 1955 emend. Delcourt, Dettmann and Hughes 1963 (LT, CP-CS(2)4 and T-CA-1a outcrops)

Concavissimisporites spp. (MP, BCH, RE-1, LH-CM(2)-1a and T-CA-1a outcrops)

Impardecispora cf. *apiverrucata* (Couper 1958) Venkatachala, Kar and Raza 1969 (BCH outcrop)

Trilobosporites cf. *aequiverrucosus* Dörhöfer 1977 (CP-CS(2)4 outcrop)

Trilobosporites cf. *canadensis* Pocock 1962 (MP and BCH outcrops; Fig. 8j)

Trilobosporites cf. *hannonicus* (Delcourt and Sprumont 1955) Potonié 1956 (BCH outcrop)

Trilobosporites spp. (MP, BCH, UCR, CP-CS(2)4 and RE-1 outcrops)

Pteridophyta Osmundaceae

Baculatisporites sp. (RE-1 outcrop)

Punctatisporites couperi Ravn 1995 (MP and T-CA-1a outcrops)

Todisporites sp. (BCH, LT and RE-1 outcrops)

Pteridophyta ?Polypodiaceae

Laevigatosporites sp. (MP, BCH, LT, UCR, RE-1 and T-CA-1a outcrops)

Pteridophyta Pteridaceae

Contignisporites cf. cooksoniae (Balme 1957) Dettmann 1963 (BCH outcrop)

Contignisporites cf. *crenatus* Varma and Ramanujam 1984 (CP-CS(2)4 outcrop)

Contignisporites sp. (LT outcrop)

Pteridophyta Salviniales/?Marsileaceae

Crybelosporites pannuceus (Brenner 1963) Srivastava 1977 (LT, UCR, RE-1, LH-CM(2)-1a and T-CA-1a outcrops)

Pteridophyta unknown affinities

Acritosporites cf. *kyrtomus* Juhász 1979 (LT, UCR, LH-CM(2)-1a and T-CA-1a outcrops)

Auritulinasporites sp. (UCR outcrop)

Converrucosisporites spp. (MP, BCH, LT, RE-1 and LH-CM(2)-1a outcrops)

Crassitudisporites sp. (UCR outcrop)

Gregussisporites orientalis Juhász and Smirnova 1985 (RE-1 outcrop; Fig. 10a)

Murospora mesozoica Pocock 1961 (UCR outcrop)

Murospora sp (UCR outcrop)

Patellasporites tavaredensis Groot and Groot 1962 (MP, BCH, LT, UCR, CP-CS(2)4, RE-1, LH-CM(2)-1a and T-CA-1a outcrops)

Peromonolites allenensis Brenner 1963 (LT outcrop)

Pilosisporites trichopapillosus Delcourt and Sprumont 1955 (BCH outcrop; Fig. 8d)

Undulatisporites spp. (MP, BCH, LT, UCR, RE-1 and T-CA-1a outcrops)

Varirugosisporites sp. (MP, BCH, LT and RE-1 outcrops; Fig. 8k)

Verrucatosporites sp. (RE-1 outcrop)

Verrucosisporites rotundus Singh 1964 (UCR, CP-CS(2)4 and T-CA-1a outcrops)

Verrucosisporites sp. (BCH and LT outcrops)

Gymnosperm pollen

Cycadales/Ginkgoales/Bennettitales

Cycadopites follicularis Wilson and Webster 1946 (MP, BCH, LT, UCR, CP-CS(2)4, RE-1 and LH-CM(2)-1a outcrops)

Cycadopites spp. (MP, BCH, LT, UCR, and T-CA-1a outcrops)

Exesipollenites tumulus Balme 1957 (MP, BCH, LT, UCR, CP-CS(2)4, RE-1, LH-CM(2)-1a and T-CA-1a outcrops)

Exesipollenites sp. (LT outcrop)

Monosulcites minimus Cookson, 1947 ex Couper 1953 (MP, BCH, LT, LH-CM(2)-1a and T-CA-1a outcrops)

Monosulcites spp. (MP, BCH, LT, UCR, CP-CS(2)4, RE-1, LH-CM(2)-1a and T-CA-1a outcrops)

Coniferales Araucariaceae

Araucariacites australis Cookson 1947 (MP, BCH, LT, UCR, CP-CS(2)4, RE-1, LH-CM(2)-1a and T-CA-1a outcrops; Fig. 9e)

Balmeiopsis limbata (Balme 1957) Archangelsky 1977 (LT outcrop)

Callialasporites dampieri (Balme 1957) Dev 1961 emend. Norris 1969 (MP, BCH, LT, UCR, CP-CS(2)4, LH-CM(2)-1a and T-CA-1a outcrops; Fig. 8l)

Uesuguipollenites callosus Dino 1996 (LT outcrop)

Uesuguipollenites sp. (MP and BCH outcrops)

Coniferales Cheirolepidiaceae

Classopollis major Groot and Groot 1962 (MP, BCH, LT, UCR, CP-CS(2)4, RE-1, LH-CM(2)-1a and T-CA-1a outcrops; Fig. 8c)

Classopollis obidosensis Groot and Groot 1962 (BCH, LT, RE-1 and LH-CM(2)-1a outcrops)

Classopollis spp. (MP, BCH, LT, UCR and RE-1 outcrops)

Coniferales Cupressaceae

Inaperturopollenites dubius (Potonié and Venitz 1932) Thomson and Pflug 1953 (MP, BCH, LT, UCR, CP-CS(2)4, RE-1, LH-CM(2)-1a and T-CA-1a outcrops; Fig. 9i)

Taxodiaceaepollenites hiatus (Potonié 1931) Kremp 1949 (MP and LT outcrops)

Perinopollenites halonatus Paden Phillips and Felix 1971 (LT outcrop)

Coniferales Pinaceae/Podocarpaceae

Cedripites cretaceous Pocock 1962 (MP and LT outcrops)

Cedripites sp. (MP outcrop)

Parvisaccites radiatus Couper 1958 (MP and UCR outcrops)

Parvisaccites spp. (MP, UCR and CP-CS(2)4 outcrops)

Phyllocladidites spp. (MP and LT outcrops)

Pinuspollenites spp. (MP, BCH, LT, UCR, CP-CS(2)4, RE-1 and T-CA-1a outcrops)

Podocarpidites sp. (MP, BCH and CP-CS(2)4 outcrops)

Erdtmanithecales

Eucommiidites minor Groot and Penny 1960 (MP, BCH and LT outcrops)

Eucommiidites troedsonii Erdtman 1948 (MP, BCH, LT, UCR, LH-CM(2)-1a and T-CA-1a outcrops)

Gnetales

Ephedripites cf. *regularis* van Hoeken-Klinkenberg 1964 (LT outcrop)

Equisetosporites cf. *multicostatus* (Brenner 1963) Norris 1967 (LT, UCR and CP-CS(2)4 outcrops)

Equisetosporites spp. (MP, BCH, LT, UCR, CP-CS(2)4, LH-CM(2)-1a and T-CA-1a outcrops; Fig. 9j)

Steevesipollenites sp. (BCH and LT outcrops)

Uncertain affinities

Afropollis jardinus (Brenner 1968) Doyle, Jardiné and Doerenkamp 1982 (LT, UCR, CP-CS(2)4, LH-CM(2)-1a and T-CA-1a outcrops; Fig. 9f)

Alisporites bilateralis Rouse 1959 (MP, UCR, CP-CS(2)4, LH-CM(2)-1a and T-CA-1a outcrops)

Alisporites grandis (Cookson 1947) Dettmann 1963 (MP and LT outcrops)

Alisporites spp. (MP, BCH, LT, UCR, CP-CS(2)4, LH-CM(2)-1a and T-CA-1a outcrops)

Cerebropollenites macroverrucosus (Thiergart 1949) Schulz 1967 (MP, BCH and LT outcrops)

Inaperturopollenites spp. (LT, UCR, CP-CS(2)4, RE-1, LH-CM(2)-1a and T-CA-1a outcrops)

Spheripollenites sp. (BCH, LT, UCR, CP-CS(2)4, RE-1, LH-CM(2)-1a and T-CA-1a outcrops)

Angiosperm pollen

Chloranthaceae

Asteropollis asteroides Hedlund and Norris 1968 (LT outcrop; Fig. 9h)

Clavatipollenites hughesii Couper 1958 (MP, BCH, UCR, CP-CS(2)4 and LH-CM(2)-1a outcrops)

Clavatipollenites cf. *minutus* Brenner 1963 (LT, UCR and T-CA-1a outcrops)

Clavatipollenites cf *tenellis* Paden Phillips and Felix 1971 (MP, CP-CS(2)4 and LH-CM(2)-1a outcrops)

Clavatipollenites spp. (MP, BCH, LT, UCR, CP-CS(2)4, RE-1, LH-CM(2)-1a and T-CA-1a outcrops; Fig. 8e)

Hammenia fredericksburgensis (Hedlund and Norris 1968) Ward 1986 (LT outcrop)

Chloranthaceae and/or *Ceratophyllaceae*

Crassipollis chaloneri (Brenner 1963) Góczán and Juhász 1985 (MP, BCH, LT and T-CA-1a outcrops; Fig. 8b)

Pennipollis escuchensis Villanueva-Amadoz, Pons, Díez, Ferrer and Sender 2010 (LT outcrop)

Pennipollis peroreticulatus (Brenner 1963) Friis, Pedersen and Crane 2000 (BCH, LT, UCR, CP-CS(2)4, LH-CM(2)-1a and T-CA-1a outcrops)

Pennipollis reticulatus (Brenner 1963) Friis, Pedersen and Crane 2000 (LT, UCR, CP-CS(2)4, LH-CM(2)-1a and T-CA-1a outcrops)

Pennipollis spp. (LT, UCR, RE-1 and LH-CM(2)-1a outcrops)

Transitoripollis anulisulcatus Góczán and Juhász 1984 (MP and LT outcrops)

Transitoripollis sp. (MP and LT outcrops)

Tucanopollis crisopolensis (Regali, Uesugui and Santos 1974) da Silva Pares-Regali 1989 (LT outcrop)

Probable monocots

Liliacidites spp. (LT, UCR, CP-CS(2)4, LH-CM(2)-1a and T-CA-1a outcrops)

Monocolpopollenites sp. (LT, UCR and T-CA-1a outcrops)

Eudicots

Cupuliferoidaepollenites parvulus (Groot and Penny 1960) Dettmann 1973 (UCR outcrop)

Cupuliferoidaepollenites spp. (LT, CP-CS(2)4, LH-CM(2)-1a and T-CA-1a outcrops; Fig. 9d)

Phimopollenites pannosus (Dettmann and Playford 1968) Dettmann 1973 (LH-CM(2)-1a; Fig. 10j)

Retitrescolpites sp. (LT outcrop)

Rousea marthae Ward 1986 (LH-CM(2)-1a and T-CA-1a outcrops; Fig. 10k)

Striatopollis cf. *sarstedtensis* Krutzsch 1959 (LT, CP-CS(2)4, RE-1, LH-CM(2)-1a and T-CA-1a outcrops; Fig. 10i)

Striatopollis sp. (CP-CS(2)4 and T-CA-1a outcrops)

Tricolpites cf. *hians* Stanley 1965 (RE-1 outcrop)

Tricolpites maximus (Singh 1971) Ward 1986 (T-CA-1a outcrop)

Tricolpites cf. *micromunus* (Groot and Penny 1960) Singh 1971 (LT, CP-CS(2)4, LH-CM(2)-1a and T-CA-1a outcrops; Fig. 10g)

Tricolpites minutus (Brenner 1963) Dettmann 1973 (RE-1 outcrop)

Tricolpites němejci Pacltová, 1971 (LT outcrop)

Tricolpites cf. *vulgaris* (Pierce 1961) Srivastava 1969 (UCR outcrop)

Tricolpites spp. (LT, UCR, CP-CS(2)4, RE-1, LH-CM(2)-1a and T-CA-1a outcrops)

cf. *Tricolpites* sp. (MP outcrop).

Uncertain affinities

Artiopollis indivisus Agassie 1969 (UCR outcrop; Fig. 9n)

Dichastopollenites cf. *dunveganensis* Singh 1983 (LT and RE-1 outcrops; Fig. 10h)

Dichastopollenites spp. (LT and CP-CS(2)4 outcrops)

Jusinghipollis cf. *ticoensis* Llorens and Perez Lozaine 2016 (MP, BCH, LT, UCR, CP-CS(2)4, LH-CM(2)-1a and T-CA-1a outcrops; Fig. 8h)

Retimonocolpites dividuus Pierce 1961 (LT outcrop)

Retimonocolpites spp. (MP, BCH, LT, UCR, CP-CS(2)4, RE-1, LH-CM(2)-1a and T-CA-1a outcrops)

Stellatopollis cf. *barghoornii* Doyle in Doyle, Van Campo and Lugardon 1975 (LT and UCR outcrops)

Undetermined angiosperm pollen grains (LT and UCR outcrops)

APPENDIX IV: Legend of symbols for the logged sections and additional correlations.

A) Legend of symbols for the logged sections (see chapter 5 of this manuscript):

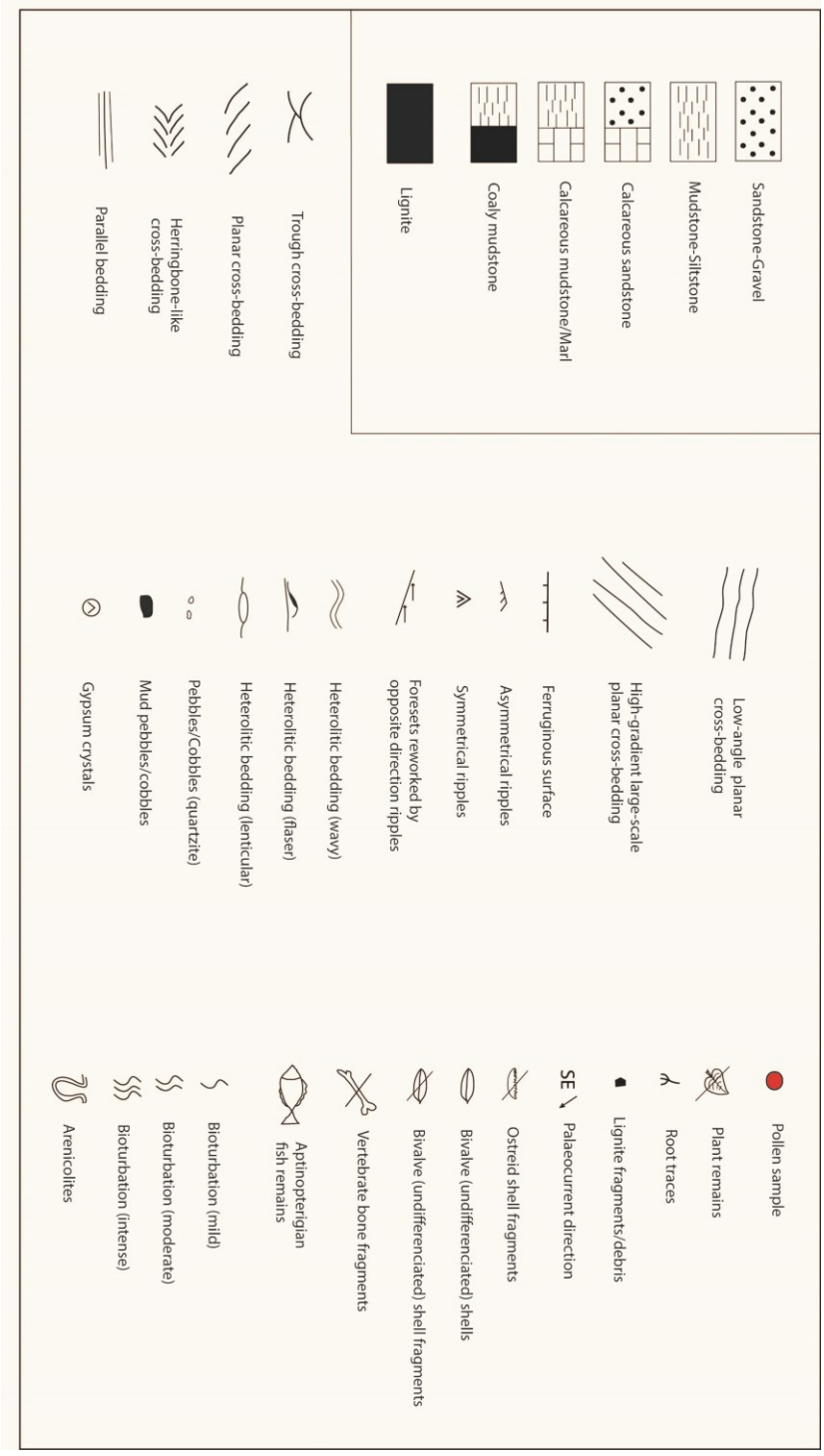

B) Buenache de la Sierra logged sections and their correlation:

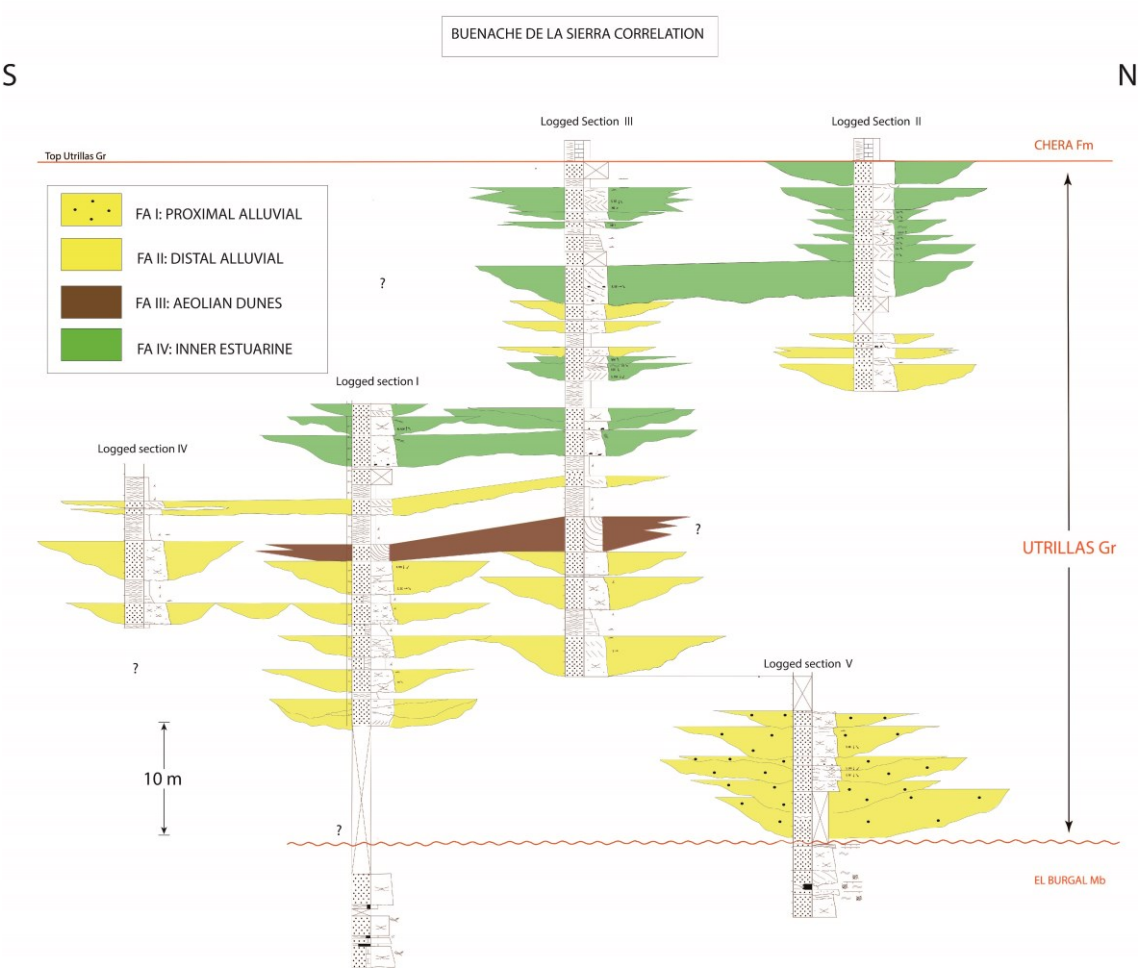

*See Figure 5.2 to know the exact location of the logged sections in the outcrop.

C) Reíllo logged sections and their correlation:

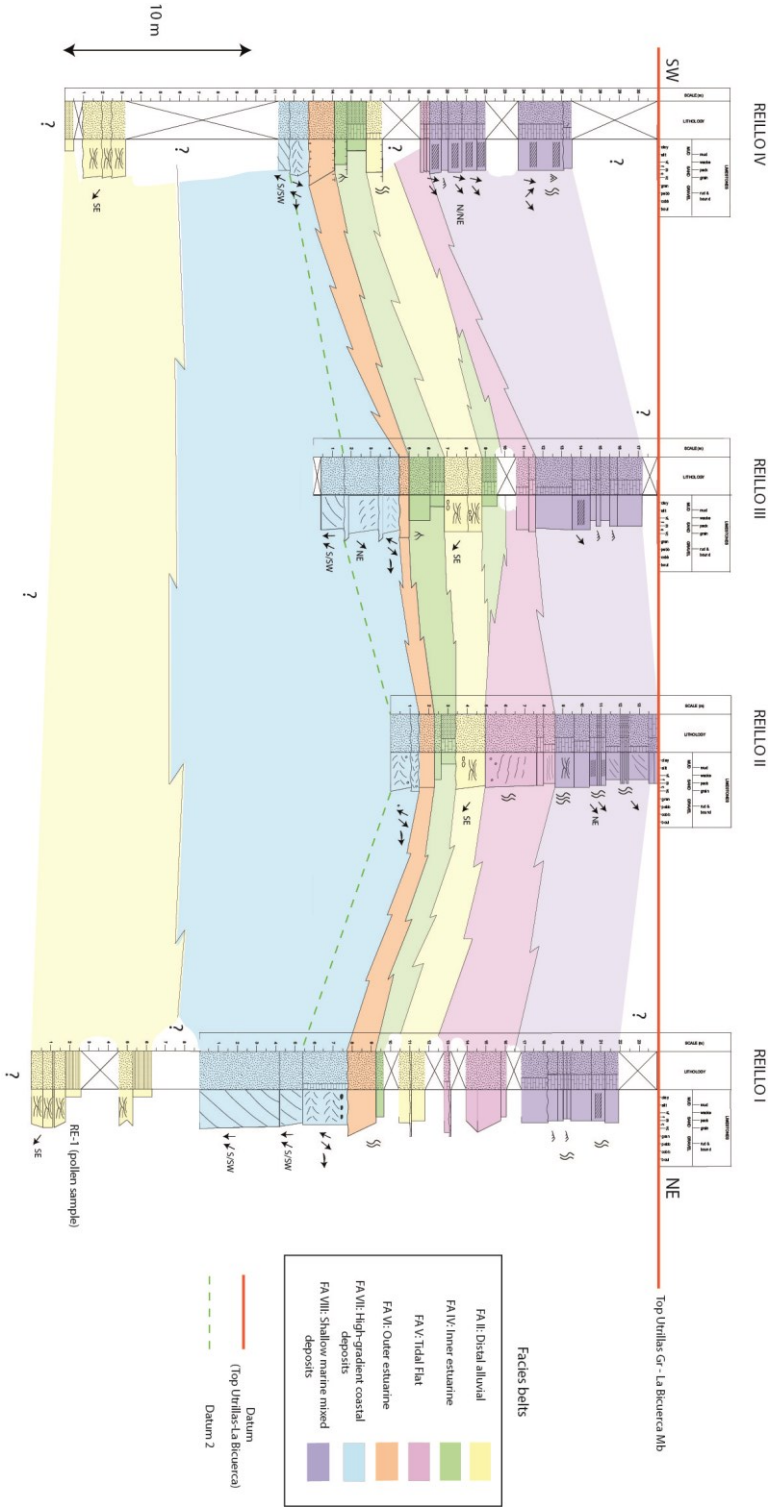

*See Figure 5.30 to know the exact location of the logged sections in the outcrop.

APPENDIX V: Granulometry analysis

		Grain size intervals (gr)									
Sample	Weight of the sample (gr)	>2 mm	2 – 1 mm	1 – 0.5 mm	0.5 – 0.25 mm	0.25 – 0.10 mm	0.10 – 0.05 mm	50 – 20 µm	20 – 8 µm	8 – 2 µm	<2 µm
BUE1-GR-1	233.54	0.03	0.96	7.25	61.20	138.90	17.17	5.92	0.63	0.34	0..18
BUE3-GR-2	375.10	0	0.1	22.67	223.50	86.61	24.80	10.29	2.23	2.16	1.42
BUE3-GR-1	328.76	0	0.008	5.65	168.86	111.80	22.70	11.03	2.33	2.25	0.98
BUE4-GR-1	139..17	0	0.03	7.69	106.19	21.43	2.27	0.76	0.05	0.01	0
BUE4-GR-2	181.26	0	0.26	27.80	119.22	23.83	4.05	4.46	0.56	0.44	0.15

* Raw data of the granulometry analysis conducted by Bueno-Cebollada and Meléndez (2018). It includes the amount of sample included in each of the 10 grain-size intervals sieved in the analysis. The amounts are expressed in grams (gr). The five studied samples were collected in the interval 17 of the Buenache de la Sierra logged section.

APPENDIX VI: Diffractograms

PALAEOSOIL 1

SB1-A

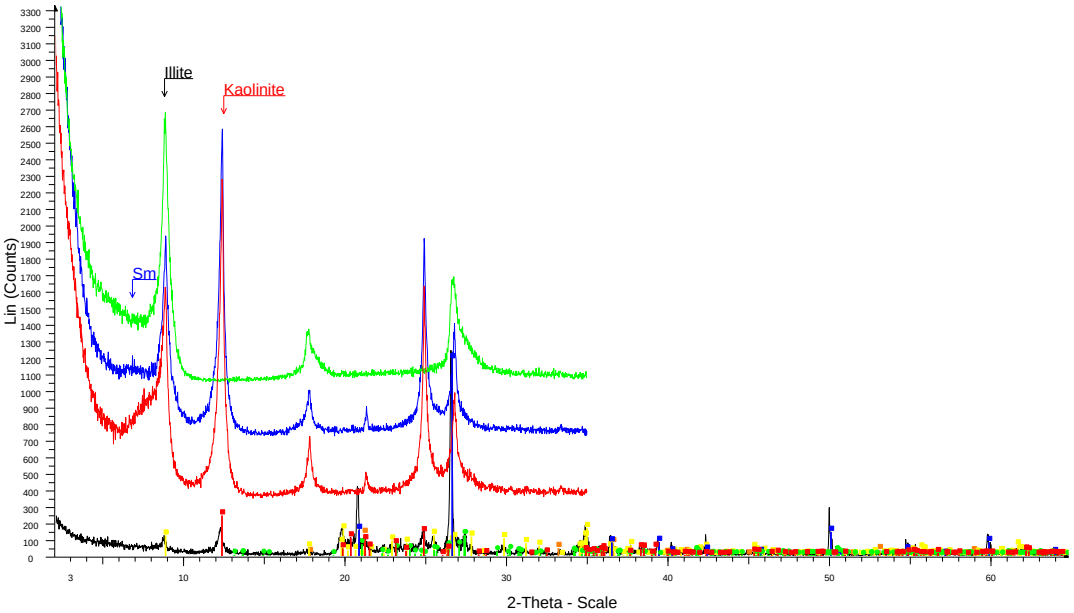

SB1-B

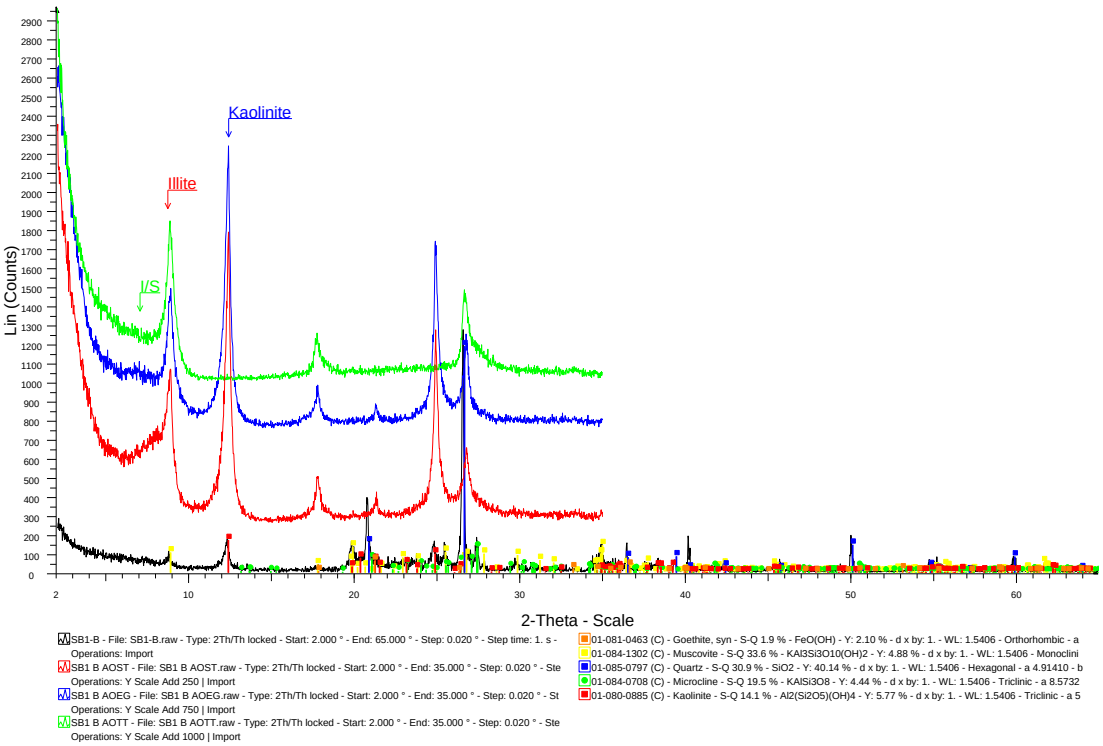

SB1-C

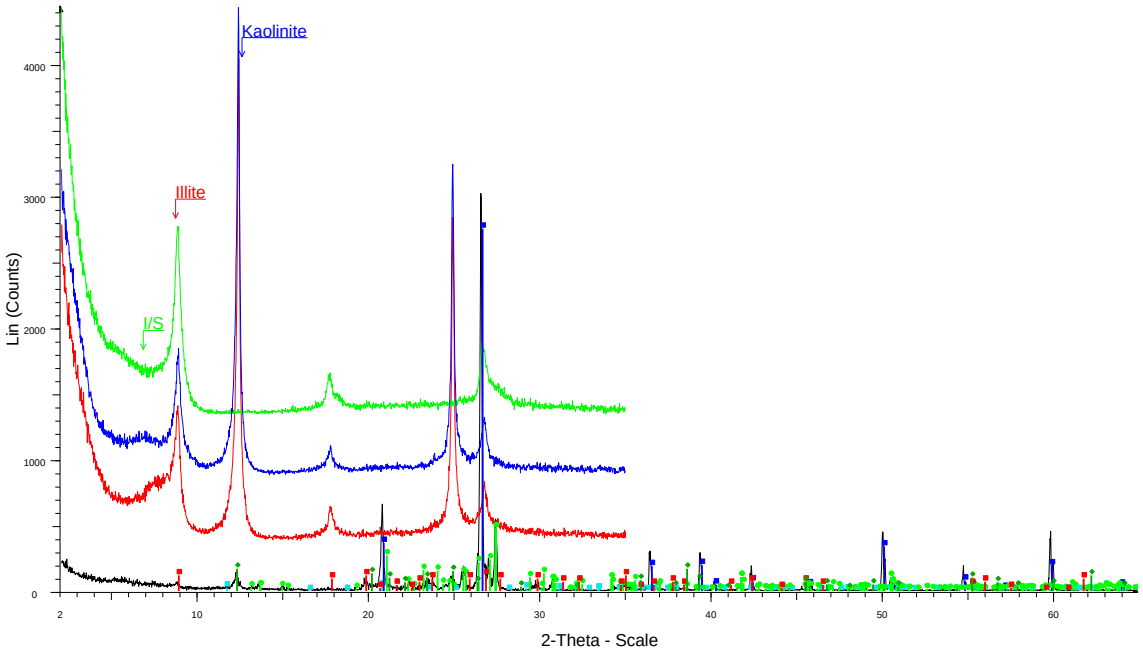

SB1-C - File: SB1-C.raw - Type: 2Th/Th locked - Start: 2.000 ° - End: 65.000 ° - Step: 0.020 ° - Step time: 1. s - Operations: Import

SB1 C AOST - File: SB1 C AOST.raw - Type: 2Th/Th locked - Start: 2.000 ° - End: 35.000 ° - Step: 0.020 ° - Ste Operations: Y Scale Add 375 | Import

SB1 C AOEG - File: SB1 C AOEG.raw - Type: 2Th/Th locked - Start: 2.000 ° - End: 35.000 ° - Step: 0.020 ° - St Operations: Y Scale Add 875 | Import

SB1 C AOTT - File: SB1 C AOTT.raw - Type: 2Th/Th locked - Start: 2.000 ° - End: 35.000 ° - Step: 0.020 ° - Ste Operations: Y Scale Add 333 | Y Scale Add 1000 | Import

01-072-0596 (C) - Gypsum - Ca(SO4)(H2O)2 - Y: 0.81 % - d x by: 1. - WL: 1.5406 - Monoclinic - a 10.47000 - b

01-085-0797 (C) - Quartz - SiO2 - Y: 61.72 % - d x by: 1. - WL: 1.5406 - Hexagonal - a 4.91410 - b 4.91410 - c

01-084-0708 (C) - Microcline - KAlSi3O8 - Y: 10.71 % - d x by: 1. - WL: 1.5406 - Triclinic - a 8.57320 - b 12.966

00-002-0056 (D) - Illite - KAl2Si3AlO10(OH)2 - Y: 2.69 % - d x by: 1. - WL: 1.5406 - Monoclinic - a 5.18000 - b 9

00-002-0105 (D) - Kaolinite - H4Al2Si2O9/Al2O3·2SiO2·2H2O - Y: 3.83 % - d x by: 1. - WL: 1.5406 - Triclinic - a

SB1-D

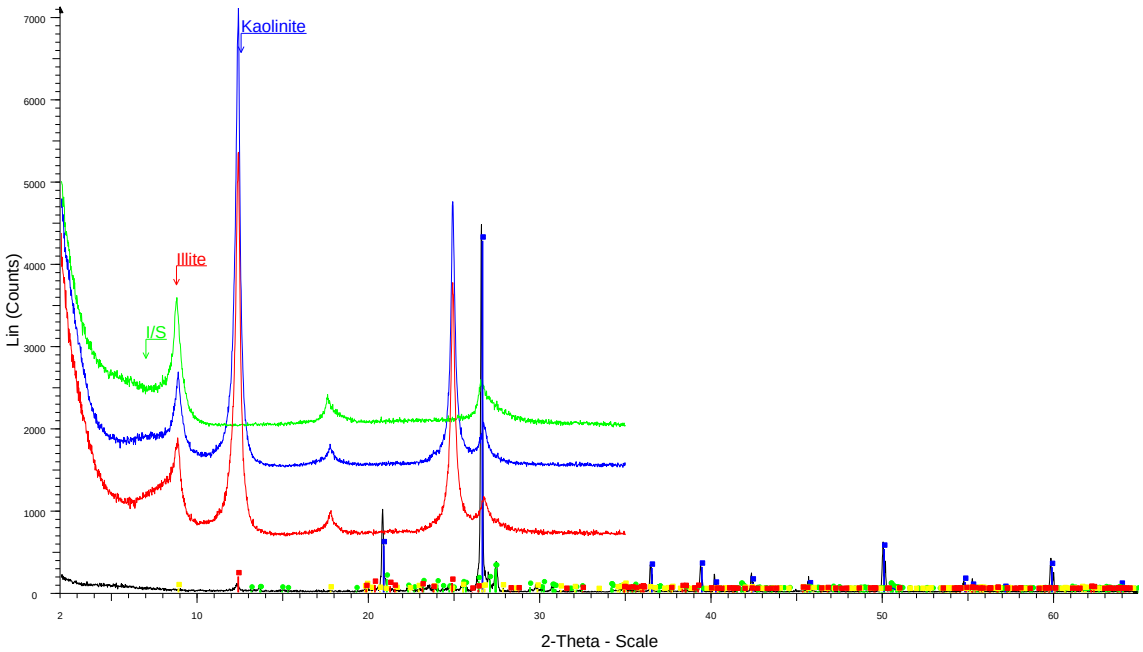

SB1-D - File: SB1-D.raw - Type: 2Th/Th locked - Start: 2.000 ° - End: 65.000 ° - Step: 0.020 ° - Step time: 1. s - Operations: Import

SB1 D AOST - File: SB1 D AOST.raw - Type: 2Th/Th locked - Start: 2.000 ° - End: 35.000 ° - Step: 0.020 ° - Ste Operations: Y Scale Add 667 | Import

SB1 D AOEG - File: SB1 D AOEG.raw - Type: 2Th/Th locked - Start: 2.000 ° - End: 35.000 ° - Step: 0.020 ° - St Operations: Y Scale Add -500 | Y Scale Add 1000 | Import

SB1 D AOTT - File: SB1 D AOTT.raw - Type: 2Th/Th locked - Start: 2.000 ° - End: 35.000 ° - Step: 0.020 ° - Ste Operations: Y Scale Add 1000 | Y Scale Add 1000 | Import

01-085-0797 (C) - Quartz - S-Q 60.4 % - SiO2 - Y: 60.14 % - d x by: 1. - WL: 1.5406 - Hexagonal - a 4.91410 - b

01-084-0708 (C) - Microcline - S-Q 23.0 % - KAlSi3O8 - Y: 4.01 % - d x by: 1. - WL: 1.5406 - Triclinic - a 8.5732

01-084-1302 (C) - Muscovite - S-Q 8.0 % - KAl3Si3O10(OH)2 - Y: 0.89 % - d x by: 1. - WL: 1.5406 - Monoclinic

01-080-0885 (C) - Kaolinite - S-Q 8.6 % - Al2(Si2O5)(OH)4 - Y: 2.69 % - d x by: 1. - WL: 1.5406 - Triclinic - a 5.

PALAEOSOIL 2

SB2-A

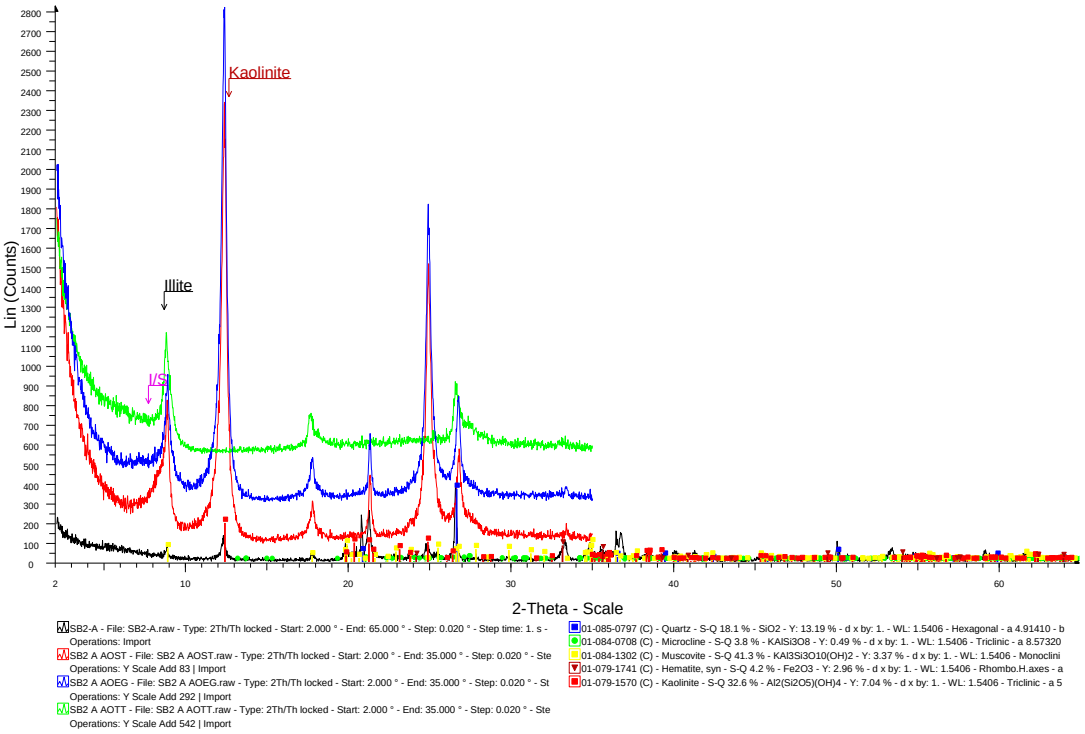

SB2-B

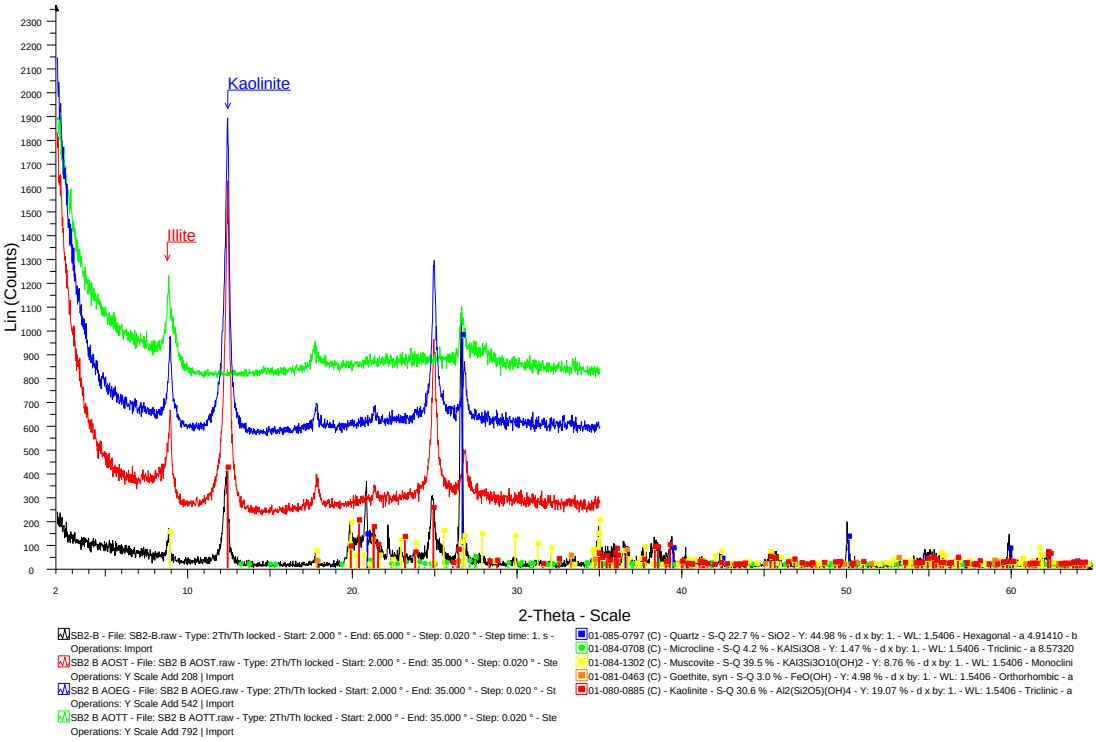

SB2-C

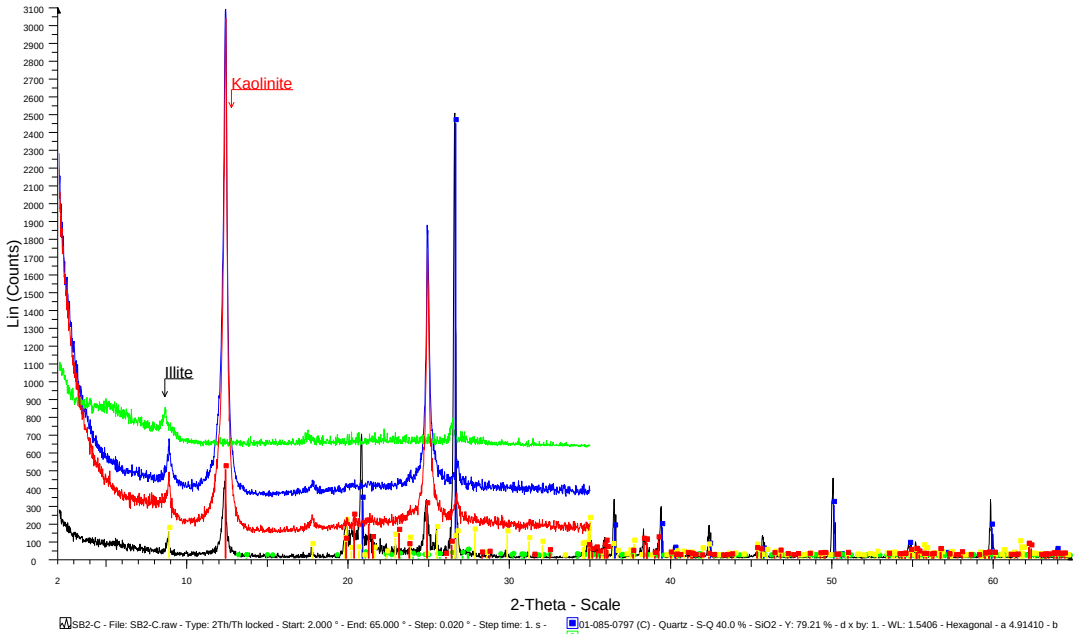

PALAEOSOIL 3

SB3-A

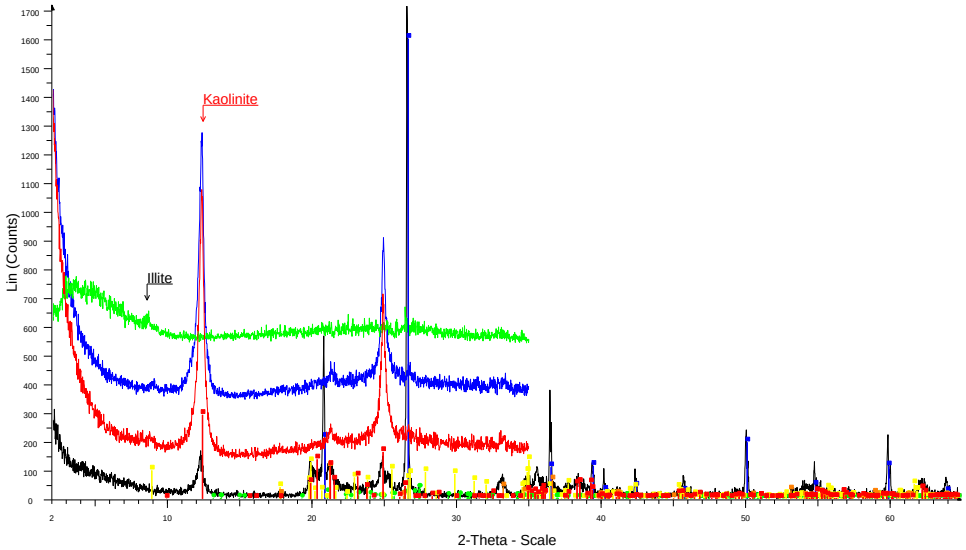

SB3-B

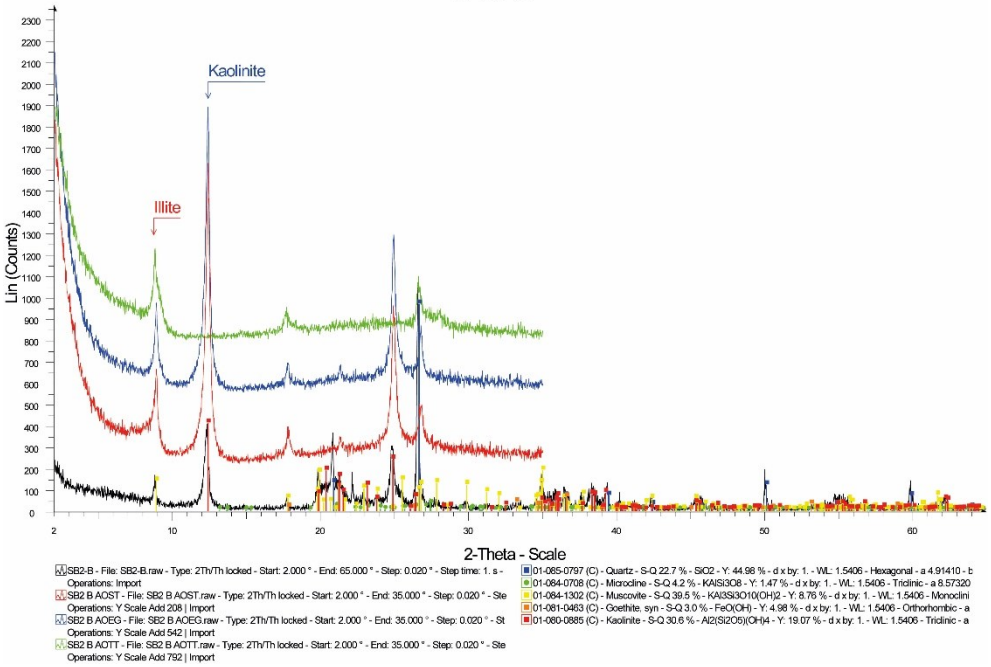
Kaolinite
Illite
Lin (Counts)
2-Theta - Scale
SB2-B - File: SB2-B.raw - Type: 2Th/Th locked - Start: 2.000 ° - End: 65.000 ° - Step: 0.020 ° - Step time: 1. s - Operations: Import
SB2 B AOST - File: SB2 B AOST.raw - Type: 2Th/Th locked - Start: 2.000 ° - End: 35.000 ° - Step: 0.020 ° - Ste Operations: Y Scale Add 208 | Import
SB2 B AOEG - File: SB2 B AOEG.raw - Type: 2Th/Th locked - Start: 2.000 ° - End: 35.000 ° - Step: 0.020 ° - St Operations: Y Scale Add 542 | Import
SB2 B AOTT - File: SB2 B AOTT.raw - Type: 2Th/Th locked - Start: 2.000 ° - End: 35.000 ° - Step: 0.020 ° - Ste Operations: Y Scale Add 792 | Import
01-085-0797 (C) - Quartz - S-Q 22.7 % - SiO2 - Y: 44.98 % - d x by: 1. - WL: 1.5406 - Hexagonal - a 4.91410 - b
01-084-0708 (C) - Microcline - S-Q 4.2 % - KAlSi3O8 - Y: 1.47 % - d x by: 1. - WL: 1.5406 - Triclinic - a 8.57320
01-084-1302 (C) - Muscovite - S-Q 39.5 % - KAl3Si3O10(OH)2 - Y: 8.76 % - d x by: 1. - WL: 1.5406 - Monoclini
01-081-0463 (C) - Goethite, syn - S-Q 3.0 % - FeO(OH) - Y: 4.98 % - d x by: 1. - WL: 1.5406 - Orthorhombic - a
01-080-0885 (C) - Kaolinite - S-Q 30.6 % - Al2(Si2O5)(OH)4 - Y: 19.07 % - d x by: 1. - WL: 1.5406 - Triclinic - a

SB3-C

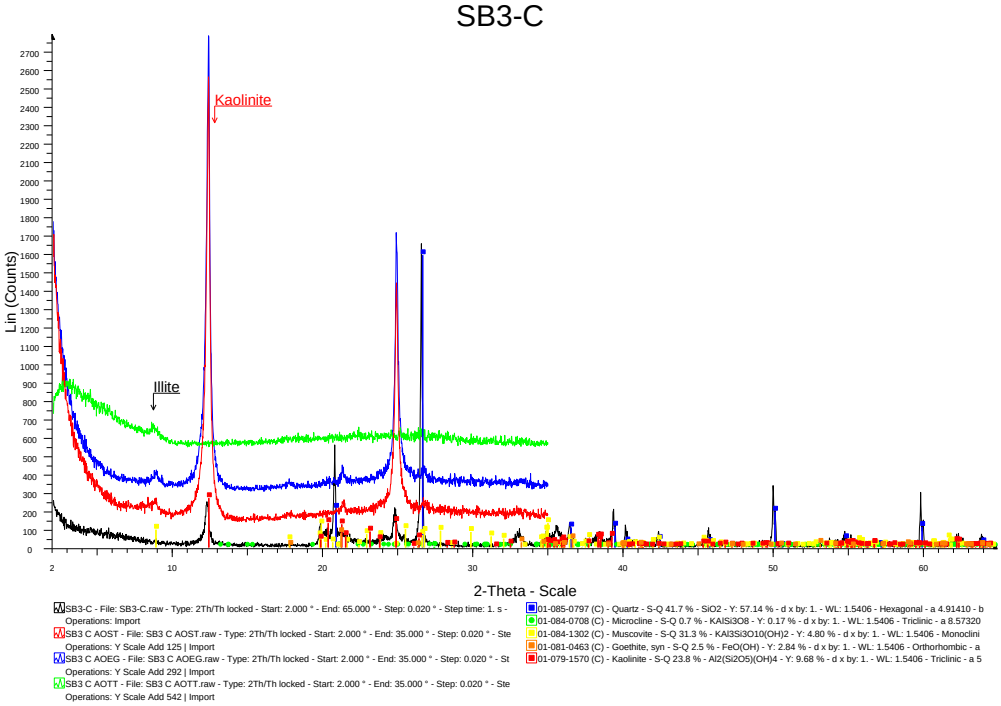
Kaolinite
Illite
Lin (Counts)
2-Theta - Scale
SB3-C - File: SB3-C.raw - Type: 2Th/Th locked - Start: 2.000 ° - End: 65.000 ° - Step: 0.020 ° - Step time: 1. s - Operations: Import
SB3 C AOST - File: SB3 C AOST.raw - Type: 2Th/Th locked - Start: 2.000 ° - End: 35.000 ° - Step: 0.020 ° - Ste Operations: Y Scale Add 125 | Import
SB3 C AOEG - File: SB3 C AOEG.raw - Type: 2Th/Th locked - Start: 2.000 ° - End: 35.000 ° - Step: 0.020 ° - St Operations: Y Scale Add 292 | Import
SB3 C AOTT - File: SB3 C AOTT.raw - Type: 2Th/Th locked - Start: 2.000 ° - End: 35.000 ° - Step: 0.020 ° - Ste Operations: Y Scale Add 542 | Import
01-085-0797 (C) - Quartz - S-Q 41.7 % - SiO2 - Y: 57.14 % - d x by: 1. - WL: 1.5406 - Hexagonal - a 4.91410 - b
01-084-0708 (C) - Microcline - S-Q 0.7 % - KAlSi3O8 - Y: 0.17 % - d x by: 1. - WL: 1.5406 - Triclinic - a 8.57320
01-084-1302 (C) - Muscovite - S-Q 31.3 % - KAl3Si3O10(OH)2 - Y: 4.80 % - d x by: 1. - WL: 1.5406 - Monoclini
01-081-0463 (C) - Goethite, syn - S-Q 2.5 % - FeO(OH) - Y: 2.84 % - d x by: 1. - WL: 1.5406 - Orthorhombic - a
01-079-1570 (C) - Kaolinite - S-Q 23.8 % - Al2(Si2O5)(OH)4 - Y: 9.68 % - d x by: 1. - WL: 1.5406 - Triclinic - a 5